Soil Moisture Monitoring with Ground-Based Gravity Data

Adam Brook Smith

Submitted in total fulfilment of the requirements
of the degree of Doctor of Philosophy

August 2013

Department of Infrastructure Engineering
The University of Melbourne

Abstract

Soil moisture is the key component of the terrestrial water cycle, controlling the partitioning of precipitation to evaporation, runoff, and groundwater recharge. Moreover, soil moisture regulates the weather and climate by providing land surface feedbacks to the atmosphere, thus influencing the onset and persistence of drought and floods. Despite the importance of soil moisture, it is not well understood as it is highly variable in space and time. Therefore there is a need for improved simulation of soil moisture and validation of these land surface models with field observations.

Traditional methods to measure in-situ soil moisture include probes or oven dried soil samples. These techniques are destructive, labour intensive, and measure a limited spatial extent of soil moisture. This thesis develops a new method to measure depth integrated soil moisture with ground-based gravity observations.

Gravity changes at the surface of the Earth due to the movement of the Moon and Sun, and rotation of the Earth. Smaller changes are due to change in mass and distribution of ocean tides and atmospheric pressure and the resultant loading of the Earth's crust. Gravity at the Earth's surface is approximately 9.8 m/s^2 and can be measured using a gravimeter, with a resolution of 10 nm/s^2 or 1 μGal. Change in mass due to terrestrial water storage (TWS) below the gravimeter increases gravity by around 1 μGal for 24 mm of TWS. Consequently TWS, including depth integrated soil moisture and groundwater, can be monitored with ground-based gravity, provided the larger signals can be removed from the gravity data, and a precision of less than 5 μGal is achievable for the observations of gravity change (corresponding to a change in soil moisture of 5 % vol/vol over the top 2 m of the profile).

This thesis investigates three key science questions that need to be addressed before gravity data can be used to routinely monitor soil moisture.

1. What gravity data precision is achievable in the field?

2. Is a terrestrial water storage signal detectable in gravity data?

3. Can the soil moisture profile be retrieved from depth integrated gravity data?

Methods to correct the geophysical signals in gravity were evaluated using the precise (stationary) superconducting gravimeter (SG) at Canberra, Australia. The Scintrex CG-3M relative gravimeter was selected as the most precise, portable gravimeter available to monitor soil moisture. The Scintrex CG-3M response to meteorological signals was assessed and a correction determined for atmospheric pressure. Corrections for instrumental artefacts in the relative gravity data were also developed. Two case studies involving small networks of three field sites were investigated and a precision of 1.4 μGal (34 mm TWS equivalent) achieved.

A network of 20 soil moisture monitoring sites was installed in the temperate 84000 km^2 Murrumbidgee River Catchment in Australia. Four sites and a hydrologically stable bedrock reference site in the 600 km^2 Kyeamba Creek Catchment (100 km west of Canberra) were monitored during dry and wet conditions. The precision of the gravity estimates at each site relative to the bedrock reference was 1.4-2.1 μGal, with a resultant gravity change precision of 3.6 μGal. The gravity change at each site corresponded with observed TWS changes, and a statistically significant change in gravity of 9.9±3.6 μGal was detected at a valley site.

A land surface model and variational data assimilation was used to retrieve the soil moisture profile from depth integrated gravity observations at one monitoring site. The temporal variability of the TWS and profile soil moisture was retrieved with a TWS and 60-90 cm soil moisture variance of 20 mm and 10.9 % vol/vol respectively, corresponding to an observed variance of 20 mm and 11.1 % vol/vol. However there was a (dry) bias in simulated soil moisture and TWS when assimilating gravity data alone. Jointly assimilating gravity anomalies and near-surface soil moisture improved the profile soil moisture retrieval with the 0-30 cm soil moisture bias reduced from -5.0 % vol/vol to -0.5 % vol/vol.

The methods developed in this thesis to monitor soil moisture with ground-based gravity data are quite general, using freely available software and public ancillary data. The soil moisture monitoring methods from this thesis should be applicable to other sites, climates, gravimeters, and data sets.

This is to certify that;

(i) the thesis comprises only my original work towards the PhD,

(ii) due acknowledgement has been made in the text to all other material used,

(iii) the thesis is less than 100,000 words in length, exclusive of table, maps, bibliographies and appendices.

Signature ______________________________

Date __________________________________

Acknowledgments

My supervisors Jeff Walker and Andrew Western have shaped both this study and my development as a hydrologist. I thank Jeff and Andrew for always being available, despite numerous other demands on their time. I also thank Rodger Grayson who started the journey as a supervisor and is now sailing the world. I sincerely thank Jeff, Andrew and Rodger for showing me the importance of field work (and soil moisture), and the necessity of hands on data collection for the advancement of science. I cannot thank Herb McQueen enough for all that he has done for me during the course of this study. Herb was almost another supervisor, invited me into his home and work, introduced me to family and colleagues and gave me the keys to the SG.

I thank Jim Cull and Monash University for providing the Scintrex CG-3M gravimeter used in this thesis. Also David Crossley, Jaako Mäkinen, and Tero Hokkanen for sharing hard to find gravity references; Herb Dragert and Lindsay Thomas for providing advice on gravity field work; and Ray Tracey for pointing out the importance of ocean tide loading in Australia.

I would like to thank the Melbourne University technical staff. Thanks to Rodger Young for everything he did; Geoff Duke for metal fabrication; and Toney Lowe for help in the soils lab. I would also like to thank everyone who contributed to field work in the Murrumbidgee River Catchment. In particular Merrick Underwood, Kevin Ellett and Matt Turner who assisted with site installation.

This study was funded by Australian Research Council Discovery Project Grant DP0343778 which is gratefully acknowledged. Access to the soil moisture monitoring sites in the Murrumbidgee River Catchment was provided by numerous farmers, and is very much appreciated. Similarly the Australian National University is acknowledged for providing access to gravity benchmark sites around Mt Stromlo.

While at Melbourne University I had the pleasure of sharing an office with Matt Turner, Chris Ruediger and Steve Wealands. I learnt, and continue to learn a lot off every one of you guys, thankyou for everything. Thanks also to Rob Pipunic for sharing data and knowledge, and more importantly keeping me company, engaged and motivated through to the end. I would also like to personally thank Andrew Frost, for all the support over the years, particularly while working together the last couple of years. Thankyou to my dad Ken for being there when I needed him the most, and lending a hand. Also my mum El for knowing not to ask how the thesis was going. Thanks also to the Griffith side of the family, Fig, Garry and Madeleine for doing fun stuff with my girls and helping in all sorts of ways.

I would like to thank everyone from the Bureau of Meteorology for their understanding and patience, particularly my colleagues in water resources assessment and flood forecasting and warning. I would like to sincerely thank my current and past supervisors Carl Daamen and Soori Sooriyakumaran who not only gave me time and space to complete my PhD while working, but also provided endless encouragement to complete this study.

I could not have done this without the love and support of my family Marnie, Esther and Audrey. Everything I have accomplished I owe to the support of Marnie Griffith. This thesis is yours.

Contents

List of Figures

List of Tables

Acronyms

1D	One Dimensional
2D	Two Dimensional
3D	Three Dimensional
ABIC	Akaike Bayesian Information Criteria
AC	Alternating Current
ACCESS	Australian Community Climate and Earth System Simulator
AET	Actual EvapoTranspiration
AIC	Akaike Information Criteria
AMSR-E	Advanced Microwave Scanning Radiometer - EOS
AMSR2	Advanced Microwave Scanning Radiometer 2
ANU	Australian National University
ASCAT	Advanced Scatterometer
ASCII	American Standard Code for Information Interchange
AVHRR	Advanced Very High Resolution Radiometer
AWS	Automatic Weather Station
BAYTAP-G	BAYesian Tidal Analysis Program - Grouping model
BIC	Bayesian Information Criteria
CABLE	CSIRO Atmosphere Biosphere Land Exchange
CGS	Centimetre Gram Second system of units
CSIRO	Commonwealth Scientific and Industrial Research Organisation
CTE	Cartwright, Tayler, Edden tidal potential catalogue
DEM	Digital Elevation Model
DVZ	Deeper Vadose Zone
EC	Electrical Conductivity
ECMWF	European Centre for Medium Range Weather Forecasting
EOP C04	Earth Orientation Parameters (series C04) from IERS
EOS	Earth Observing System
ET	EvapoTranspiration
FAO	Food and Agriculture Organization of the United Nations
GCM	Global Climate Model
GGP	Global Geodynamics Project

GLDAS	Global Land Data Assimilation System
GPR	Ground Penetrating Radar
GPS	Global Positioning System
GRACE	Gravity Recovery And Climate Experiment
GW	Ground Water (saturated zone)
IERS	International Earth Rotation Service
IVZ	Intermediate Vadose Zone
LaD	Land Dynamics model
LAGEOS	LAser GEOdynamics Satellite
LCR	LaCoste and Romberg
LSM	Land Surface Model
MSE	Mean Square Error
MSMMN	Murrumbidgee Soil Moisture Monitoring Network
NetCDF	Network Common Data Form
NMM	Neutron Moisture Meter
NWP	Numerical Weather Prediction
PET	Potential EvapoTranspiration
PVC	PolyVinyl Chloride
RMS	Root Mean Squared
RMSE	RMS Error
RSES	Research School of Earth Sciences
RZ	Root Zone
SG	Superconducting Gravimeter
SI	International System of units
SMAP	Soil Moisture Active Passive
SMOS	Soil Moisture and Ocean Salinity
TDR	Time Domain Reflectometry
TWS	Terrestrial Water Storage
UNESCO	United Nations Educational, Scientific and Cultural Organization
WGHM	WaterGAP Global Hydrological Model
WT	Water Table

Chapter 1

Introduction

Temporal variations in terrestrial water storage impact the mass of the Earth, which in turn changes the Earth's gravity field. This research hypothesises that temporal variations in soil moisture and groundwater can be monitored using ground-based gravity data. However, because these gravity changes are small, all external influences must be eliminated. Moreover, the soil moisture and groundwater evolution must be extracted from the total terrestrial water storage change. This thesis develops and tests such methods using experiment data.

It is first established what other signals are larger than the soil moisture signal in ground-based gravity data. Methods to correct these signals are identified, developed, and tested using a precise gravity data set from the superconducting gravimeter (SG) in Canberra, and gravity data collected from a field portable Scintrex CG-3M relative gravimeter. The methods to achieve high precision gravity measurements at multiple sites are tested, both around the SG at Mt Stromlo (at geodetic benchmarks) and in the field at soil moisture monitoring sites. They are then used at a number of soil moisture monitoring sites for two field campaigns, during dry and wet conditions. At each site soil moisture, groundwater level, and precipitation are measured, together with gravity observations using a Scintrex CG-3M relative gravimeter. The gravity changes at each soil moisture monitoring site (relative to a hydrologically stable bedrock reference site) are compared to the observed terrestrial water storage variations. Finally, a method is developed to assimilate gravity into a land surface model and retrieve the soil moisture signal at multiple depths in the soil profile. This variational data assimilation method is used to disaggregate gravity observations that are both a temporal average and a vertically integrated aggregate of water in the soil profile, including soil moisture and groundwater level variations.

1.1 Motivation and Problem Statement

Knowledge of the spatial and temporal distribution of soil moisture is critical for a number of applications. For flood forecasting it determines the partitioning of rainfall into infiltration and runoff (Bronstert and Bárdossy, 1999; Nied et al., 2013). In groundwater studies it determines the amount of recharge to the aquifer (Wang et al., 2009; Carrera-Hernández et al., 2012). Soil moisture is a dominant driver for numerical weather prediction, and global climate modelling (Milly and Dunne, 1994; Ducharne and Laval, 2000) where it is modelled using a land surface model (Pitman, 2003). However the distribution of soil moisture is not well understood as it is highly variable in both space and time (Western et al., 1999; Cosh et al., 2004; Brocca et al., 2012). Therefore there is a need for improved simulation of soil moisture and validation of these predictions with field observations.

Traditional methods to measure soil moisture have been in-situ, using probes or oven dried soil samples. These traditional techniques are destructive, labour intensive, and measure a limited spatial extent of soil moisture (Walker et al., 2004). Newer cosmic ray probes can non-invasively measure soil moisture but are limited in the depth that can be observed (maximum of 70 cm), with the measurement depth varying according to soil water content, to a maximum depth of only 12 cm for saturated soils (Zreda et al., 2008; Desilets et al., 2010; Franz et al., 2012). Therefore there is a need to be able to non-invasively measure the total depth integrated soil moisture.

Ground-based gravity observations have the potential to be used as a non-invasive method to measure depth integrated soil moisture. However before ground-based gravity data can be used to routinely monitor soil moisture, techniques must be developed to achieve the precision required. As shown in Chapter 2, a precision of 4.2 μGal (42 nm/s^2) is required from the gravity observation to detect a soil moisture change of 5 % vol/vol over the top 2 m of the soil profile (Bonatz, 1967). It is with this in mind that a methodology is developed to achieve that precision, and in doing so determine what signals in gravity data are most important for correction (i.e. the signals larger than the soil moisture signal magnitude of 4.2 μGal) and what additional software and data is required to remove these unwanted signals.

A limited number of studies have measured individual components of terrestrial water storage, such as snow (Breili and Pettersen, 2009), soil moisture (Krause et al., 2009), or groundwater (Wilson et al., 2012), and compared that component (or a number of components) to gravity data from a single site (Creutzfeldt et al., 2010a), or a network of sites (Lambert and Beaumont, 1977). However, no study has observed the total terrestrial water storage (TWS), being the depth integrated soil moisture and groundwater, and compared this to co-located gravity data, with soil moisture measured directly below the gravimeter. Furthermore, very few studies have investigated the soil moisture component of TWS and it has not been conclusively shown that a soil moisture signal can be detected in ground-based gravity at a network of soil moisture monitoring sites.

Gravity at field sites is averaged to increase precision, consequently methods are required to retrieve the temporal TWS signal from temporally averaged gravity data. Moreover, to monitor soil moisture, techniques are required to vertically disaggregate the depth integrated TWS signal into its soil moisture and groundwater components.

This thesis develops a general method that can be applied anywhere, to non-invasively observe depth integrated soil moisture with ground-based gravity data, and also retrieve the temporal soil moisture signal at multiple depths throughout the soil profile. The soil moisture profile retrieval method developed in this thesis is quite general and could also be applied to remotely sensed gravity (e.g. GRACE), and used with or without complementary near-surface soil moisture data, either in-situ or remotely sensed (e.g. AMSR-E).

1.2 Objectives and Scope of Thesis

This thesis seeks to address three key research questions: how to monitor soil moisture changes with ground-based gravity data, whether these changes are detectable with current technology, and how useful would this information be if it were accessible? More specifically:

1. What gravity precision is achievable in the field? i.e. What factors are important for monitoring soil moisture with ground-based gravity data, and what is required to obtain a sufficiently precise measurement to detect TWS changes (soil moisture in particular)?

2. Is there a detectable TWS signal (particularly soil moisture) in ground-based gravity data? i.e. Can ground-based gravity data be used to monitor soil moisture with current technology?

3. Can the TWS signal (particularly soil moisture) be retrieved from ground-based gravity data? i.e. Can the TWS signal be extracted from gravity changes and can TWS be disaggregated into profile soil moisture and groundwater components?

The three objectives related directly to the three key research questions are:

1. **Achieving** high precision ground-based gravity data (to enable the detection of a soil moisture signal).

2. **Detecting** a soil moisture signal in ground-based gravity data.

3. **Retrieving** a soil moisture signal from ground-based gravity data (using data assimilation and a land surface model).

The scope of this thesis is limited to:

- Ground-based gravity (no GRACE or any other satellite data is considered).

- Relative gravity (no absolute ground-based gravity data is used).

- Field point gravity (no laboratory/continuous studies of gravity and hydrology are conducted).

- Scintrex field gravity data (no other gravity meter is used in the field, for example LaCoste and Romberg).

- Temporal one dimensional investigation (no consideration is given to spatial fields of gravity, soil moisture or groundwater).

- Temperate climate (snow is not considered).

- Existing models and algorithms (no model development is attempted).

1.3 Thesis Outline

This thesis develops a general method that can be applied anywhere, to non-invasively observe depth integrated soil moisture with ground-based gravity data, and also develops a technique to retrieve the temporal soil moisture signal at multiple depths throughout the soil profile by ground-based gravity data assimilation into a land surface model. The organisation of the thesis is as follows. Chapter 2 is a review of literature on variations in ground-based gravity (what gravity is, why it changes and how to measure it), hydrological signals in ground-based gravity (with a focus on soil moisture), and retrieval of a hydrological signal from ground-based gravity. Chapter 3 describes the methodology used in the thesis to address the research questions and achieve the three objectives of the thesis (achieving high precision ground-based gravity, detecting a soil moisture signal in ground-based gravity, and retrieving a soil moisture signal from ground-based gravity). Chapter 4 investigates the various factors affecting the precision of ground-based gravity data (at a field site), while Chapter 5 uses this information to detect a soil moisture signal in ground-based gravity data. Chapter 6 retrieves a soil moisture signal from ground-based gravity data using variational data assimilation and a land surface model. Finally Chapter 7 summarises what has been discovered and proposes directions for future research. Consequently this thesis can be considered to consist of 5 main parts:

1. Background (Chapters 1-3)

2. Achieving high precision gravity data (Chapter 4)

3. Detecting a soil moisture signal in gravity data (Chapter 5)

4. Retrieving the soil moisture profile from gravity data (Chapter 6)

5. Conclusions (Chapter 7).

Some parts of this thesis are already published in peer-reviewed journal or conference papers. The Murrumbidgee Soil Moisture Monitoring Network (MSMMN) data set is described in Smith et al. (2012), and available at both `http://www.oznet.org.au` and the International Soil Moisture Network data hosting facility `http://ismn.geo.tuwien.ac.at`. The research approach to detect a terrestrial water storage signal in gravity data is published in Smith et al. (2005), and preliminary results in Smith et al. (2006). The method and some results from retrieving a soil moisture profile from ground-based gravity data (assimilation into a land surface model) are published in Smith et al. (2011). Finally the soil samples and particle size analysis from some MSMMN sites contributed to the validation of the general soil moisture sensor calibration method published in Rüdiger et al. (2010).

Chapter 2

Literature Review

The previous chapter highlighted the importance of soil moisture and the benefits of monitoring terrestrial water storage (groundwater, soil moisture and snow) with ground-based gravity data.

This chapter describes the Earth's gravity and why it changes, both spatially and temporally (section 2.1). Methods to measure ground-based gravity are presented (section 2.2). Gravity signals larger than soil moisture are identified (section 2.3 and 2.4) together with correction methods. Previous studies that have analysed hydrological signals (particularly soil moisture) in gravity data are reviewed (section 2.5). The findings from this literature review will be used to guide the research approach for this thesis, described in the following chapter.

2.1 Gravity of the Earth

This section introduces theoretical aspects of gravity, including important mathematical representations and approximations that are relied on later in the thesis. The elementary theory of the gravity of the Earth is presented first in Cartesian (rectangular) coordinates for the simple case of a flat Earth and developed from the attraction of point masses. A summary of the theory is then given for the more realistic (but still simplified) case of a spherical, rotating Earth.

While simple gravity theory is preferred for ground-based gravity investigations at local scales (less than 50 km) a knowledge of the more complex global gravity theory (in spherical coordinates) is required to understand the nature of the geophysical signals in ground-based gravity (such as Earth tides) that must be removed from the data (to create a gravity residual) before the gravitational effect of terrestrial water storage can be modelled in Cartesian coordinates and compared to the gravity residual.

2.1.1 Cartesian Coordinates

This subsection describes the approximations typically used in ground-based gravity, particularly to describe the gravitational attraction of terrestrial water storage within 10 km (generally within 1km or less) of a gravimeter.

Consider two point masses m_1 and m_2 separated by a distance r. Newton's Law of Gravitation describes an attractive force $\mathbf{F}$ on the point mass m_2

$$\mathbf{F} = G\left(\frac{m_1 m_2}{r^2}\right)\mathbf{r_1} \tag{2.1}$$

where $\mathbf{r_1}$ is a unit vector pointing from m_2 to m_1 and the experimentally determined universal gravitational constant $G = 6.672 \times 10^{-11}$ m^{3}kg^{-1}s^{-2} (Telford et al., 1990).

Newton's Second Law of Motion states the force applied to an object is the product of its mass and the acceleration applied,

$$\mathbf{F} = m\mathbf{a} \tag{2.2}$$

where $\mathbf{a}$ is acceleration in the direction of the force $\mathbf{F}$. Substituting Eq. (2.2) into Eq. (2.1) gives the gravitational acceleration caused by the point mass m_1

$$\mathbf{g} = G\left(\frac{m_1}{r^2}\right)\mathbf{r_1} \tag{2.3}$$

Taking m_1 and r to be the average mass and radius of the Earth, and $\mathbf{r_1}$ as pointing towards the centre of the Earth gives the average ground-based gravity

$$g_{\text{Average}} \approx 9.8 \text{ m/s}^2 = 980 \text{ Gal}. \tag{2.4}$$

Deviations from the average ground-based gravity (typically referred to as anomalies and changes for spatial and temporal deviations, respectively) can be represented as Δg (μGal).

The CGS unit Gal was named after Galileo Galilee (Jeffreys, 1962) and is used exclusively in gravimetry, usually expressed as mGal or for more precise ground-based gravity measurements (such as in this thesis) as μGal.

$$1\ \mu\text{Gal} = 10^{-8}\ \text{m/s}^2 = 10\ \text{nm/s}^2 \tag{2.5}$$

By differentiating Eq. (2.3) with respect to r and inserting the average mass and radius of the Earth the "free air correction" is derived,

$$\Delta g_{\text{Free Air}} = -2G\left(\frac{m_{\text{Earth}}}{r^3_{\text{Earth}}}\right) \approx 308.6\ \mu\text{Gal/m} \approx \frac{\partial g}{\partial z} \tag{2.6}$$

The free air correction gives an approximate change in gravity over a vertical distance, with gravity decreasing with distance from the centre of the Earth. Note that the derivative of Eq. (2.3) with respect to r (free air correction) is only approximately equal to the change in gravity at the surface with respect to vertical height (z) due to local subsurface density anomalies and the flattening of the Earth at the poles (i.e. the Earth is not a homogeneous sphere).

The free air correction indicates that a change in elevation of approximately 3 mm results in a change of ground-based gravity of 1 μGal (Eq. 2.6). Consequently changes in gravimeter elevation due to (periodic) flexure of the Earth's crust caused by the gravitational attraction of celestial bodies (e.g. the Moon and Sun), and loading of atmospheric pressure and ocean tides cause gravity changes, and must be removed from the ground-based gravity data (as in this thesis) to detect a terrestrial water storage signal. Furthermore, the free air correction suggests a portable gravimeter must be repositioned within 3 mm of the original elevation for a 1 μGal precision. This is achieved for portable gravimeters (and in this thesis) by establishing rigid platforms with marked or indented positions for the gravimeter legs, and fixing one of the gravimeter levelling legs to maintain a constant gravimeter height above the platform.

The gravitational effect of a density anomaly in the Earth's subsurface (e.g. mineral deposit, or terrestrial water storage) can be estimated by calculating the gravitational attraction of a right vertical prism (Nagy, 1966)

$$\Delta g_{\text{Nagy}} = \mathrm{G}\rho \left|\left|\left| \mathrm{x}\ln(\mathrm{y}+\mathrm{r}) + \mathrm{y}\ln(\mathrm{x}+\mathrm{r}) - \mathrm{z}\arcsin\frac{\mathrm{z}^2+\mathrm{y}^2+\mathrm{yr}}{(\mathrm{y}+\mathrm{r})\sqrt{(\mathrm{y}^2+\mathrm{z}^2)}} \right|_{\mathrm{z}_1}^{\mathrm{z}_2}\right|_{\mathrm{y}_1}^{\mathrm{y}_2}\right|_{\mathrm{x}_1}^{\mathrm{x}_2} \mu\mathrm{Gal} \tag{2.7}$$

where ρ is density (kg/m^3) and $r = \sqrt{x^2+y^2+z^2}$ is the distance to the prism vertices. The gravitational anomaly due to a rectangular prism is dependent on all three dimensions of the prism as well as depth (and lateral distance) to the (density) anomaly. In practice a (density) anomaly would be subdivided into a grid and the gravitational attraction of each pixel calculated (using Eq. (2.7)) and summed. The height and depth of the pixels may be challenging to determine, particularly for terrestrial water storage, where a digital elevation model (DEM) is typically used as the grid. For this reason the prism formula of (Nagy, 1966) is not used in this thesis.

The necessity of knowing the spatial coordinates of multiple rectangular pixels is removed by using the Bouguer slab approximation. The Bouguer slab approximation is used in this thesis to calculate the gravity change due to terrestrial water storage (in particular soil moisture and groundwater). The Bouguer slab approximation is derived by calculating the gravitational attraction of a subsurface (vertical) cylinder, and extending the radius of the cylinder to infinity (Telford et al., 1990)

$$\Delta g_{\text{Bouguer}} = 2\pi\mathrm{G}\rho\mathrm{h}\ \mu\mathrm{Gal} \tag{2.8}$$

where ρ is density (kg/m^3) and h is the thickness (or height) of the slab (m). The Bouguer slab approximation is not only independent of lateral extent, but also depth to the anomaly. This approximation can be used to represent areally extensive time varying gravity anomalies, for example terrestrial water storage (groundwater, soil moisture and snow) resulting from precipitation. Note the sign of the Bouguer slab approximation is reversed (i.e. the ground-based gravity is reduced) if the anomaly is above the surface, or more precisely above the gravimeter measuring point. Consequently the hydrological cycle (precipitation, snow melt, runoff and infiltration, evaporation and evapotranspiration, groundwater recharge and discharge, and streamflow) in complex terrain and particularly cool climates (with snow cover) can lead to complex hydrological signals in ground-based gravity, more so if the gravimeter is located underground (e.g. in a tunnel deep into the side of a mountain). For this reason the experimental sites used in this thesis are located in a temperate climate at grass covered valley and gentle hillslope sites, on non-reactive (silt loam) soils, overlying an unconfined (alluvial) aquifer. Furthermore the gravimeter is located at the ground surface on a rigid platform (that allows precipitation and evapotranspiration to pass). Lastly, precipitation, soil moisture (throughout the profile to the water table), and groundwater are all monitored within 2 m of the gravimeter.

Inserting the currently accepted value of G (6.672×10^{-11} m^{3}kg^{-1}s^{-2}) and the density of water (1000 kg/m^3) into Eq. (2.8) gives the Bouguer slab approximation of the local gravity effect due to precipitation,

$$\Delta g_{\text{Precipitation}} = 0.04192\text{P } \mu\text{Gal} \tag{2.9}$$

where P is precipitation (mm). Assuming a gravimeter below the surface (or snow line), and no snow melt, a 24 mm (snow water equivalent) snowfall event corresponds roughly to a 1 µGal decrease in gravity. Conversely, assuming a gravimeter above the surface, and perfect infiltration (i.e. negligible runoff, evaporation and evapotranspiration) a 24 mm rainfall event leads to an approximately 1 µGal increase in ground-based gravity.

Similarly the Bouguer slab approximation can be used to estimate the effect of a change in groundwater or soil moisture below the gravity meter (following the same approach as for rainfall). For groundwater in an unconfined aquifer,

$$\Delta g_{\text{Groundwater}} = 41.92\text{S}_\text{y}\Delta\text{H } \mu\text{Gal} \tag{2.10}$$

where S_y is specific yield and ΔH is the change in height of the water table (m). Whereas for soil moisture (in a non-swelling and incompressible soil),

$$\Delta g_{\text{Soil Moisture}} = 41.92\Delta\theta\text{H } \mu\text{Gal} \tag{2.11}$$

where $\Delta\theta$ is change in volumetric water content and H is the thickness of the soil profile the water content is measured over (m). Consequently a change in water table height of around 48 cm corresponds to a 1 μGal change in gravity (when specific yield is 5 %), and a change in soil moisture of 2.4 % vol/vol over a 1 m soil profile also results in a 1 μGal gravity change.

By calculating the gravitational attraction of a subsurface vertical cylinder (of thickness equal to the variation in groundwater level) and comparing it to the attraction of a cylinder with infinite radius (i.e. the Bouguer slab approximation) it is possible to show that 90 % of the gravity effect of a groundwater level variation is given by a cylinder of (average water table) depth d and radius $10d$ (Leirião et al., 2009). This can be used as an estimate for the gravimeter "footprint" when using ground-based gravity to monitor groundwater level (e.g. for a depth to groundwater level of 5 m, 90 % of the gravity signal due to groundwater level variation comes from within 50 m of the gravimeter).

Other studies (Hokkanen et al., 2006; Creutzfeldt et al., 2008; Hasan et al., 2008; Longuevergne et al., 2009) have used a DEM with uniform soil moisture, generally represented as a layer of water at the surface, together with the prism formula of Nagy (1966) to calculate a "footprint" when using ground-based gravity to monitor soil moisture. For example, Longuevergne et al. (2009) found 90 % of the gravity signal due to soil moisture (for a soil water content of 1 mm), comes from within 30 m of the gravimeter at Strasbourg, France, and 100 % of the signal is from a radius of 100 m (actually a square of 100 m half length centred on the gravimeter).

While the concept of a gravimeter "footprint" for monitoring groundwater level variations is useful, the assumption of constant soil moisture content over large areas (up to 400 km^2 in Creutzfeldt et al. (2008)) with differing elevations, land cover and soil type is a gross approximation that renders the concept of a gravimeter "footprint" for monitoring soil moisture variations indicative at best. Furthermore the "footprint" is heavily dependant on the local topography around the gravimeter (Longuevergne et al., 2009) and is calculated as only 100 m at Strasbourg, France, but up to 1 km at Moxa, Germany (Hasan et al., 2008).

In this thesis the "footprint" concept is not explored as the focus is on 1D (vertical) terrestrial water storage and the soil moisture and groundwater level observations are within 2 m of the gravimeter (and gravity observations) at all field sites. The Bouguer slab approximation is used to convert observed soil moisture and groundwater level variations to a gravity change that is compared to the change in gravity observed at the field sites with a portable relative gravimeter.

2.1.2 Spherical Coordinates

This subsection describes the gravitational attraction of the Earth in spherical coordinates, setting out the temporal variations in ground-based gravity (Earth tides, ocean tide loading, and polar motion) due to the Earth's rotation and interaction with other celestial bodies. These temporal (and spatial) variations must be removed before the smaller signal of terrestrial water storage can be detected in ground-based gravity.

For a rotating system (such as the Earth) the gravity acceleration (or simply gravity) $\boldsymbol{g}$ consists of gravitation $\boldsymbol{b}$ and centrifugal acceleration $\boldsymbol{z}$ (Fig. 2.1)

$$\boldsymbol{g} = \boldsymbol{b} + \boldsymbol{z} \tag{2.12}$$

The centrifugal acceleration $\boldsymbol{z}$ depends on the perpendicular distance $\boldsymbol{d}$ to the axis of rotation and the vector of rotation $\boldsymbol{\omega}$ (Fig. 2.1)

$$\boldsymbol{z} = (\boldsymbol{\omega} \times \boldsymbol{r}) \times \boldsymbol{\omega} = \omega^2 \boldsymbol{d} \tag{2.13}$$

where the angular velocity of the Earth ω is measured by the International Earth Rotation Service (subsection 2.3.4).

Using the point mass formula (Eq. (2.3)) for gravitational attraction, the Earth's

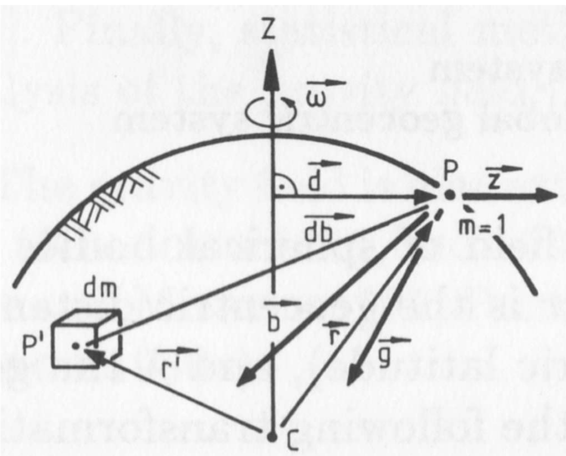

Fig. 2.1 Gravity acceleration (from Torge (1989)). Gravity $\boldsymbol{g}$ at a point P on the surface of the rotating Earth is the sum of (the Earth's) gravitation $\boldsymbol{b}$ and centrifugal acceleration $\boldsymbol{z}$.

gravitation $\boldsymbol{b}$ is given by

$$\boldsymbol{b} = G \iiint\limits_{Earth} \left(\frac{\boldsymbol{r}' - \boldsymbol{r}}{|\boldsymbol{r}' - \boldsymbol{r}|^3} \right) dm \tag{2.14}$$

where $\boldsymbol{r}'$ and $\boldsymbol{r}$ are the geocentric (originating from the centre of the Earth) position vectors of the point (source) mass P' and the position on the surface (of the attracted point mass) P (Fig. 2.1).

Computations involving vector operations are simplified by considering a scalar gravitational potential V rather than the vector gravity tidal acceleration $\boldsymbol{b}$, where

$$\boldsymbol{b} = \nabla V = \frac{\partial V}{\partial \boldsymbol{r}} \tag{2.15}$$

and the gravitational potential of the Earth V is

$$V = G \iiint\limits_{v} \left(\frac{\rho(\boldsymbol{r}')}{|\boldsymbol{r}' - \boldsymbol{r}|} \right) dv \tag{2.16}$$

with v the volume of the Earth and the mass element dm now expressed by the volume density $\rho(\boldsymbol{r}')$ and volume element dv, with

$$dm = \rho dv. \tag{2.17}$$

In practice the subsurface density of the Earth $\rho(\boldsymbol{r}')$ is not well known, and Eq. (2.16) can not be used to predict gravitational potential. Rather the potential is derived from ground-based gravity observations taken at a point P on the surface (with a gravimeter) or in the exterior space of the Earth (Fig. 2.2) with a satellite.

Above the surface of the Earth the gravitational potential V can be represented as a spherical harmonic solution to Laplace's equation. When the atmospheric and ocean mass is neglected, and the exterior space of the Earth is considered mass free ($\rho = 0$), Laplace's differential equation is satisfied

$$\nabla^2 V = 0 \tag{2.18}$$

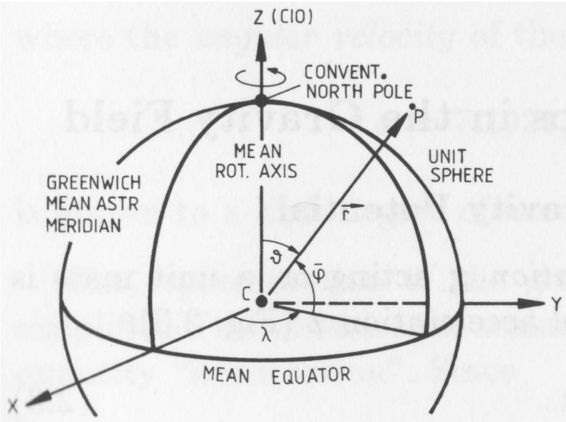

Fig. 2.2 Geocentric coordinate system (from Torge (1989)).

where $\nabla^2 = \nabla \cdot \nabla$ is the Laplacian differential operator. A solution of Eq. (2.18) is given by the spherical harmonic expansion of the gravitational potential V into associated Legendre functions $P_{l,m}(t)$

$$V = \frac{GM}{r}\left[1 + \sum_{l=2}^{\infty}\left(\frac{a}{r}\right)^l \sum_{m=0}^{l} P_{l,m}(\cos\theta)(C_{l,m}\cos m\lambda + S_{l,m}\sin m\lambda)\right] \tag{2.19}$$

where GM is the geocentric gravitational constant with M the total mass of the Earth (including the atmosphere), a the semimajor axis (or equatorial radius) of the ellipsoidal Earth model, r and θ the geocentric and polar distance (equal to 90 ° - geocentric latitude), and λ geographical longitude (Fig. 2.2). The geodetic constants GM, a, and ω are given by the Geodetic Reference System 1980 (GRS80) proposed by the International Association of Geodesy (Moritz, 1980). The associated Legendre functions $P_{l,m}(t)$ are composed of Legendre polynomials $P_l(t)$

$$P_{l,m}(t) = (1-t^2)^{m/2}\frac{d^m}{dt^m}P_{l,0}(t) \tag{2.20}$$

and the Legendre polynomials $P_l(t)$ are given by

$$P_{l,0}(t) = P_l(t) = \frac{1}{2^l l!}\frac{d^l}{dt^l}(t^2-1)^l \tag{2.21}$$

Similar to Eq. (2.14) the spherical harmonic coefficients $C_{l,m}$ and $S_{l,m}$ are mass integrals of the gravitational field

$$\left\{ \begin{array}{c} C_{l,m} \\ S_{l,m} \end{array} \right\} = \frac{k}{M} \frac{(l-m)!}{(l+m)!} \iiint\limits_{Earth} \left(\frac{r'}{a} \right)^l P_{l,m}(\cos\theta') \left\{ \begin{array}{c} \cos m\lambda' \\ \sin m\lambda' \end{array} \right\} dm \tag{2.22}$$

The Earth's gravity field can be described by levels of constant gravity potential W

$$W = V + Z \tag{2.23}$$

where the centrifugal potential Z is given by

$$Z = \frac{\omega^2}{2} d^2 = \frac{\omega^2}{2} r^2 \sin^2\theta = \frac{\omega^2}{3} r^2 \left(1 - P_{2,0}(\cos\theta)\right) \tag{2.24}$$

for Cartesian coordinates, polar coordinates, and spherical harmonics respectively.

The equipotential surface W corresponding to the Earth's mean sea level is called the geoid. The primary means to infer the Earth's gravity field at global to regional spatial scales is satellite tracking. By measuring the geocentric position of satellites (e.g. the twin Gravity Recovery And Climate Experiment (GRACE) satellites, or the older LAGEOS (LAser GEOdynamics Satellite)) with high precision, their orbit can be inverted to calculate the Earth's gravity field. A satellite geoid model typically consists of numerical values for $C_{l,m}$ and $S_{l,m}$ (Wahr et al., 1998).

2.2 Gravity Measurement

This section overviews the various gravimeters available and discusses comparative advantages with a focus on the applications in this thesis: detecting and retrieving a soil moisture signal in ground-based gravity data; and achieving highly precise gravity data via accurate gravity corrections (to enable the detection and retrieval of a soil moisture signal). It is established that a portable relative gravimeter is most suitable to detect a soil moisture signal at multiple sites, and the highly precise (relative) superconducting gravimeter (SG) is most suitable to test accurate gravity corrections. This section also discusses gravimeter calibration (not necessary for absolute gravimeters) and gravity networks with a focus on the network needed to detect and retrieve a soil moisture signal at multiple sites.

The primary means to infer the Earth's gravity field at local to regional spatial scales is ground-based gravity measurement. Gravity meters measure the vertical component of the Earth's gravity field at a point in space and time. Depending on the type of meter these measurements can be either absolute or relative (to another point in time and also space if the gravimeter is portable). Absolute meters typically measure the time taken for a proof mass to fall a fixed distance (using laser interferometry) (Niebauer, 1989; Niebauer et al., 1995; Niebauer, 2007), whereas portable relative meters typically measure the extension of a spring using capacitance (Timmen, 2010). Portable relative gravimeters suffer a drift in the apparent gravity value due to yielding of the spring that is under constant tension. The highly precise superconducting gravimeter is a stationary relative gravimeter that measures the change in voltage required to keep a superconducting sphere levitating in the centre of a magnetic field (Prothero and Goodkind, 1968; Neumeyer, 2010).

2.2.1 Absolute Gravimeters

Absolute gravimeters are not "absolute" in the sense that they suffer from negligible drift in the gravity measurement, but rather absolute in the sense that the gravity measurement technique uses SI standards of length and time to determine the gravity value. The most accurate (Table 2.1) commercially available absolute gravimeter is the Micro-g Solutions FG5 (Robertsson et al., 2001). However it is bulky, with all necessary equipment weighing around 350 kg (Francis et al., 2005). Furthermore the FG5 has a considerable power requirement (Table 2.2), and a narrow operating temperature range that severely inhibits its ability in the field. The Micro-g Solutions A-10 can be transported in the back of a dedicated van and operates in field conditions (e.g. sub-zero temperatures (Ferguson et al., 2008)) but is much less accurate (Vitushkin et al., 2002; Liard and Gagnon, 2002; Schmerge and Francis, 2006). A small, field portable, accurate prototype (cam-driven) absolute gravimeter has been built (Vitouchkine and Faller, 2002; Faller and Vitouchkine, 2003, 2005). While this instrument would seem to have great potential for hydrological application, and the developers have stated their desire to compete with relative gravimeters in field applications (Faller, 2002), it is not available commercially. More recent work (Peters et al., 1999, 2001; de Angelis et al., 2009; Schmidt et al., 2011) has focused on the development of absolute gravimeters that drop atoms, thereby reducing the size of the gravimeter and increasing accuracy by avoiding the recoil effect of a traditional proof mass.

While absolute meters are not subject to drift, they have other problems such as systematic errors due to rotation of the proof mass as it falls (Hanada et al., 1996; Rothleitner et al., 2007; Rothleitner and Francis, 2010) and other systematic errors (Marson et al., 1995; Liard et al., 1995; Robertsson, 2007; Bich et al., 2011). Furthermore the FG5 requires the vertical gravity gradient to be determined at each site with a portable relative gravimeter as it uses this in the equation of motion that is solved to give the absolute gravity (acceleration) (Marson et al., 1995). Additionally in-situ calibration of the FG5 laser at each observation site should be conducted during setup as the frequency characteristics of the laser beam can be affected by magnetic fields (Marson et al., 1995).

There have been a number of international comparisons of absolute gravimeters (Marson et al., 1995; Robertsson et al., 2001; Vitushkin et al., 2002; Francis et al., 2005; Jiang et al., 2012a) that have shown biases in the absolute values reported (Marson et al., 1995; Robertsson et al., 2001; Vitushkin et al., 2002) and previously undetected systematic errors (Marson et al., 1995; Robertsson et al., 2001; Jiang et al., 2012a). However agreement between instruments in the most recent comparisons have been encouraging (Marson, 2012).

Despite this the FG5 has been used in some field studies, such as:

- evaluating crustal motion in Europe along a 120 km eight station profile (Van Camp et al., 2002),
- monitoring post glacial rebound in North America (Lambert et al., 2006),
- ice mass changes in Greenland (van Dam et al., 2000),
- water storage variations in a karst aquifer in France (Van Camp et al., 2006a; Jacob et al., 2008, 2009, 2010), and
- hydrology and gravity in Africa (Hinderer et al., 2009; Pfeffer et al., 2011).

The smaller field portable A-10 absolute gravimeter has also been used in a field study (Ferguson et al., 2008).

In this thesis an absolute gravimeter is not used in the field because the operating temperature range is too restrictive, a dedicated power source is required at each site, the accuracy of the more portable A-10 is not high enough to detect a terrestrial

Table 2.1 Gravimeter performance specifications. Accuracy is agreement between instruments (limited to the same model of gravimeter, typically absolute). Repeatability is agreement between the same instrument (typically a field relative gravimeter) revisiting the same site after transportation, and is generally the error (standard deviation) for the gravity estimate at that site after network adjustment (Niebauer, 2007). Precision is given for a quiet site, and is therefore dominated by system noise (environmental noise is assumed negligible). Time to 1 µGal precision assumes white (system) noise only (i.e. mechanical, environmental, and geophysical signals are assumed negligible). Note PET and gPhone drift usually goes to 17 µGal/day with age, Burris meter drift goes to 10 µGal/day with age, also CG-3M and CG5 drift is residual after a linear drift of approximately 400 µGal/day is automatically removed. Note 1 µGal is approximately equivalent to 24 mm terrestrial water storage (TWS) by the Bouguer slab approximation.

Manufacturer	Gravimeter	Type	Usage	Accuracy (µGal)	Repeatability (µGal)	Precision (µGal/sqrt(Hz))	Time to 1 µGal Precision (min)	Drift (µGal/day)
Micro-g	FG5	Abs	lab	2	1	15-50	3.75-60	N/A
Micro-g	A-10	Abs	field	10	10	100	166.67	N/A
GWR	OSG	Rel	lab			0.1	0.00017	0.005
GWR	iGrav	Rel	field?			0.3	0.0015	0.015
LCR	PET	Rel	lab	1		6	0.6	50
LCR	gPhone	Rel	lab	1		3	0.15	50
LCR	Model-G	Rel	field	40	10-20			33
LCR	Model-D	Rel	field	10	5			17
LCR	Graviton EG	Rel	field		3-20			33
ZLS	Burris	Rel	field		5-7			33
Scintrex	CG-3M	Rel	field		5			20
Scintrex	CG5	Rel	field		5			20

Table 2.2 Gravimeter operating constraints. PET weight is exclusive of laptop and accessories. OSG weight is 70 kg plus 75 kg compressor, power budget is 124-151 W for the compressor and 0.1-5 W for the coldhead, temperature range is based on specifications of the coldhead.

Manufacturer	Gravimeter	Type	Usage	Weight (kg)	Power consumption (W)	Temperature range (°C)	Availability
Micro-g	FG5	Abs	lab	150	500	20-30	
Micro-g	A-10	Abs	field	105	200-300	-18-38	
GWR	OSG	Rel	lab	145	124.1-156	5-28	not available (during study)
GWR	iGrav	Rel	field?	39	1300	4-38	not available (during study)
LCR	PET	Rel	lab	13.8	24		discontinued
LCR	gPhone	Rel	lab	58	100-330		not available (during study)
LCR	Model-G	Rel	field	10	3	0-45	discontinued
LCR	Model-D	Rel	field	15	3	0-45	discontinued
LCR	Graviton EG	Rel	field	9	6	-10-45	discontinued
ZLS	Burris	Rel	field	6	4	-15-50	not available (during study)
Scintrex	CG-3M	Rel	field	11	5	-40-45	discontinued
Scintrex	CG5	Rel	field	8	4.5	-40-45	

water storage variation, and the cost of absolute gravimeters is high. In addition, an absolute gravimeter was not available at the time of the study. However data from an FG5 (collected from studies independent of this thesis) is used in two laboratories (at Mt Stromlo, Canberra) to calibrate the superconducting gravimeter (SG), and determine two absolute gravity benchmarks around Mt Stromlo.

2.2.2 Relative Gravimeters

Relative gravimeters, measure gravity (changes) relative to another point in time. Relative gravimeters do not measure gravity directly but rather infer gravity changes (by monitoring the position of a proof mass in the gravimeter) through measurement of another quantity, typically voltage (required to stabilise the proof mass) that is converted to gravity units using a calibration. Relative gravimeters include the high precision, low drift SG and the less precise, high drift, portable spring gravimeters (Table 2.1 and 2.2).

The superconducting gravimeter uses powerful magnets to levitate a superconducting niobium sphere within a vacuum chamber that is supercooled (close to absolute zero) with liquid helium (Richter and Warburton, 1998; Goodkind, 1999). A change in the voltage used to centre the sphere in the chamber indicates a change in gravity. An absolute gravimeter (FG5) is typically used to periodically calibrate the SG relative gravimeter and generate a gravity transfer function for the voltage reading (Hinderer et al., 1991, 1998; Almalvict et al., 2001). SGs suffer from a small level of drift four orders of magnitude smaller than portable relative gravimeters (Table 2.1). Furthermore since SGs frequently record a step in the gravity data following a helium refill (Van Camp and Francis, 2007), they require regular calibration (yearly is recommended) (Neumeyer, 2010). Once calibrated and corrected for drift (if necessary), SGs give highly precise (Table 2.1) measurements of gravity (Van Camp and Francis, 2007). Due to their high precision, bulk, power consumption (Table 2.2) and setup requirements, GWR superconducting gravimeters (SG) are primarily used for gravity observations in a laboratory (Meurers, 2001a; Neumeyer, 2010). The current standard model is the Observatory SG (OSG). Older models include: the Compact Tidal Gravimeter, such as the SG (CT031) used at Mt Stromlo, Canberra; and the dual sphere SG used at Wetzell and Moxa in Germany.

A list of the 25 current (as of 2010), eight new (or planned) and six former laboratory SGs operating worldwide as part of the Global Geodynamics Project (GGP) is available at `http://www.eas.slu.edu/GGP/ggpstations.html`.

Recently, a smaller field based version of the OSG, the iGrav (formerly known as FSG) became available (Wilson et al., 2012), however power consumption (1.3 kW) remains a severe limitation and requires the iGrav to be connected to mains (AC) power. While the iGrav is claimed to have the same desirable properties as the larger OSG (i.e. high precision and negligible drift), with the advantage that it can be transported to multiple sites, its performance (in the field or otherwise) has not yet been documented in any scientific literature. Furthermore the only study using an SG in the field (a modified OSG) has so far been disappointing (Wilson et al., 2012), with unexpectedly high drift of the relative gravity, large spurious unexplained short term variations in the gravity data, and large data gaps due to sagging enclosure floors and the gravimeter tilting following a rainfall event. In the field an enclosure and permanent (concrete) monument is required for an SG, which shields the soil below the gravimeter from precipitation and is not ideal to detect a terrestrial water storage signal (particularly soil moisture) in ground-based gravity data, such as in this thesis. Lastly with an instrument as sensitive and expensive as the SG, site security would be a serious issue.

In this thesis the highly precise SG in Canberra (the only SG in Australia) was used to test the corrections required to remove signals in gravity data larger than the terrestrial water storage (TWS) signal. The SG in Canberra is well suited for this purpose as the noise level and drift are low (Xu et al., 2004a; Harnisch and Harnisch, 2006b). Furthermore the TWS signal is negligible (Van Camp et al., 2010) as the SG is on a concrete pier attached to bedrock on top of a mountain (Mt Stromlo) in a temperate climate (mean annual precipitation and actual ET of around 620 and 600 mm respectively), with all soil above the gravimeter removed and the nearby surroundings consisting of occasionally used roads, carparks and buildings.

Portable relative gravimeters are field capable (unlike SG), but suffer from significant drift (Table 2.1) due to elastic relaxation of the gravimeter sensor (a spring under tension). Consequently, repeat measurements are required at the same location to remove the effect (Rymer, 1989). Once corrected for drift (and calibrated), portable relative meters give precise measurements of gravity (Jiang et al., 2012b).

LaCoste and Romberg and Scintrex are the largest manufacturers of portable relative gravimeters. The LaCoste and Romberg meters operate using a mechanical zero length spring, whereas the Scintrex gravity meters use a fused quartz sensor (Torge, 1989; Timmen, 2010). Both companies provide a variety of gravimeters, but the most precise field gravimeters are the CG-3M (or newer CG5 with improved interface, 6 Hz sampling and raw data logging mode) from Scintrex, and the Model-D meter (or older Model-G meter) from LaCoste and Romberg. Due to the low power consumption (Table 2.2), mostly required to maintain the vacuum the gravimeter sensor is in at a constant high temperature (so that ambient temperature fluctuations do not affect the spring tension), in the field both gravimeters are powered by a 12 V sealed lead acid battery that needs recharging after 12 hours. A Scintrex CG-3M was used for this thesis.

More recently LaCoste and Romberg released two relative gravimeters that are derived from the Model-G meter, the Graviton EG and the PET meter. The Graviton EG is an electronic version of the G meter with automatic levelling and data recording (Hwang et al., 2010). Production of the Model-D meter was discontinued in the year 1999 and the Model-G meter in 2004 (Nabighian et al., 2005). It appears the Graviton EG also is no longer commercially available. The PET meter comes bundled with a laptop and is intended for continuous operation at one site (Riccardi et al., 2011). The gPhone (formerly known as the PET meter) is based on the same principles as the Model-G meter but improved in a number of areas. Likewise the Burris meter is based on the LaCoste and Romberg Model-G meter but improved in various areas and manufactured by ZLS Corporation.

There are few applications in which the superconducting gravimeter has been transported or used in the field (Flach et al., 1993; Wilson et al., 2012). Generally portable relative gravimeters are used in field applications such as:

- LaCoste and Romberg G and D meters (Montgomery, 1971; Lambert and Beaumont, 1977; Dragert et al., 1981; Becker et al., 1986, 1987; Mäkinen and Tattari, 1988, 1991a,b; Pool and Eychaner, 1995; Pool and Schmidt, 1997; Pool, 2008; Naujoks et al., 2008),
- LaCoste and Romberg Graviton EG (Hwang et al., 2010),
- LaCoste and Romberg gPhone (Kang et al., 2011),
- Scintrex CG-3M (Bonvalot et al., 1998; Hare et al., 1999; Debeglia and Dupont,

2002; Gabalda et al., 2003; Smith et al., 2005, 2006; Ferguson et al., 2007; Chapman et al., 2008), and
- Scintrex CG5 (Davis et al., 2008; Gehman et al., 2009; Hwang et al., 2010; Jacob et al., 2009, 2010; Christiansen et al., 2011c,b,a; McClymont et al., 2012).

In this thesis the Scintrex CG-3M is used in the field to observe gravity because it is one of the most reliable, and light, field portable gravimeters in the world (Table 2.1 and 2.2), with low power consumption, wide operating temperature range, and repeatability comparable to LaCoste and Romberg gravimeters. Unlike the LaCoste and Romberg gravimeters, the Scintrex is not susceptible to magnetic fields (as the sensor is fused quartz rather than a metal spring) and the Scintrex CG-3M stores the gravity data (and associated gravimeter parameters) internally in the gravimeter memory, which can be later downloaded in a digital format. Furthermore a Scintrex CG-3M was available at the time of this study.

An international comparison of absolute gravimeters allows a comparison of portable relative gravimeters (used for the absolute gravimeter gravity gradients). Fifteen LaCoste and Romberg (both D and G Meters), four Scintrex CG-3M and one Sodin gravimeter were compared at the fourth international comparison of absolute gravimeters in 1994 with Becker et al. (1995) finding that the Scintrex CG-3M precision was comparable to that of the LaCoste and Romberg gravimeters. At the seventh international comparison of absolute gravimeters in 2005 the Scintrex gravimeters made up the bulk of the data with six LaCoste and Romberg meters (D, G and one EG), eight Scintrex meters (CG-3M and CG5) and one ZLS Burris meter compared. Furthermore results from the Scintrex gravimeters were considered to be slightly less uncertain than those of the LaCoste and Romberg gravimeters (Jiang et al., 2009). At the most recent comparison, for the first time, no LaCoste and Romberg gravimeters participated (Jiang et al., 2012b). There were however, two ZLS Burris meters and seven Scintrex CG5 (and no other relative gravimeter). Jiang et al. (2012b) found that the ZLS Burris meter and Scintrex CG5 both performed well and were in good agreement with each other, and in earlier studies they had not found any significant differences in the uncertainties of the CG5 and CG-3M.

In an earlier relative gravimeter intercomparison Becker et al. (1987) compared thirteen LaCoste and Romberg Model-D gravimeters and recommended the use of a spring suspension device to transport the gravimeters (to minimise vibrations) and using more than one gravimeter in a network to improve accuracy. A spring suspension device is used in this thesis to transport the relative gravimeter. Becker et al. (1987) also stated

> "In classifying the performance of a gravimeter, precision must be distinguished from accuracy. The precision is a measure of the consistency of the observations of an instrument and can be determined by the free or unconstrained adjustment of the data. The accuracy is determined by comparing the results from one instrument with a set of reference values."

They found that some gravimeters had high precision but low accuracy (compared to gravity values on a calibration line) whereas others had poor precision and average accuracy. Free (or unconstrained) network adjustment is used in this thesis (with relative gravity observations from a Scintrex CG-3M) and is discussed further below (subsection 2.2.4).

Jousset et al. (1995) compared two Scintrex CG-3M gravimeters to fourteen LaCoste and Romberg meters and found the results were similar except for one point on a calibration line where the values of the two Scintrex gravimeters were systematically different to the LaCoste and Romberg meters. They suggested this may be due to local magnetic conditions that affect the LaCoste and Romberg meters but not the Scintrex. Jousset et al. (1995) also found a systematic variation in the internal Scintrex CG-3M temperature after removing AC power (and using the 12 V battery) and stated that the influence of battery voltage variations may be a source of error through the gravimeter temperature correction. The influence of battery voltage variations on both the gravimeter internal temperature and relative gravity is assessed in this thesis.

Jousset et al. (1995) recommended recording gravity over several minutes (rather than a single observation) to improve the result. Relative gravity is observed over twenty minutes (eight measurements of approximately 2 minute duration) at each field site in this thesis. Niebauer (2007) state that most gravity surveys use an integration time of 3 to 15 minutes for the relative gravity observation as this is the crossover point where the gravimeter drift is greater than the system noise and averaging no longer reduces noise. This result is derived using the equation $T_{obs} = (\eta/d)^{2/3}$ where T_{obs} is the integration time (seconds), d is the drift (µGal/s) and η is the spectral noise amplitude for the gravimeter (see Table 2.1), in µGal/$\sqrt{\text{Hz}}$. This assumes uncorrelated (white) system noise, and linear drift (i.e. no post transport stabilisation). Post transport stabilisation of the relative gravity measurements is assessed at each field site in this thesis by comparing the gravity change of the first eight measurements for all field observations at each site.

2.2.3 Gravimeter Calibration

In order to accurately measure a change in gravity with a relative gravity meter the meter must be well calibrated. Calibration can be performed on a calibration line (typically a mountain range) (Valliant, 1969b) where changes in elevation result in large gravity changes over small distances. With this method the gravimeter is calibrated against previous gravity values for points along the line, with these values typically determined from previous measurement with another (calibrated) relative gravity meter.

Other methods of calibration include positioning a known mass of uniform size and density a known distance from the gravimeter (Gilbert, 1958; Achilli et al., 1995; Varga, 1995; Varga et al., 1995; Csapó and Szatmári, 1995; Baldi and Casula, 1997), or using a moving platform to generate a known acceleration (Valliant, 1973; Richter et al., 1995b; Van Ruymbeke et al., 1995), or tilt (Moore and Farrell, 1970). Alternatively an absolute gravity meter (Hinderer et al., 1991; Francis et al., 1998; Almalvict et al., 2001; Imanishi et al., 2002; Fukuda et al., 2004; Tamura et al., 2005) or another calibrated relative meter such as the low drift, high precision superconducting gravimeter (Francis and Hendrickx, 2001) can be used by operating the two gravimeters side by side for a period of time exceeding one day (Hinderer et al., 1998; Francis and Hendrickx, 2001; Meurers, 2002).

2.2.4 Gravity Networks

Due to the short set up time and ease of transportability, spring based portable relative gravimeters such as the LaCoste and Romberg (or ZLS) and Scintrex meters (CG-3M and CG5) are best suited to small gravity networks with limited spatial scale that do not take long to survey and have minimal transportation requirements (Lambert and Beaumont, 1977; Hipkin, 1978; Dragert et al., 1981; Lyness and Lagios, 1984; Mäkinen and Tattari, 1988, 1991a,b; Naujoks et al., 2008; Christiansen et al., 2011a,b,c), whereas absolute gravimeters are best suited to large gravity networks requiring long transportation times (Hinderer et al., 2009). Similarly absolute gravimeters are useful for networks where gravity changes are observed over long periods of time (Lambert et al., 2001; Van Camp et al., 2002; Lambert et al., 2006; Van Camp et al., 2011). Absolute gravimeters can also be used to establish base stations for relative gravity networks (Niebauer, 2007; Jacob et al., 2010; Hwang et al., 2010), see Fig. 2.3.

The shape of gravity networks varies depending on the nature of the study. For investigations of linear features for maximal distance covered a linear profile is used, sometimes with a stepping site (observation) sequence (e.g. A-B-C-B-C-D-C-D-E) or a ladder sequence (e.g. A-B-C-D-E-D-C-B-A) to control drift. For more precise estimation of gravity at each site a network of closed loops is used (e.g. A-B-C-A-D-E-A), preferably with each site tied to every other site (e.g. A-B-C-A-D-E-A-D-C-E-B-D). Note that in this case the number of ties (gravity difference between successive sites) is approximately doubled. The gravity differences between the sites forming a closed loop (e.g. A-B-C-A) should sum to zero, network adjustment is used to enforce this condition and distribute observational errors evenly around the network. To investigate gravity changes through time a complete homogeneous network of sites with the most precise estimate of gravity possible at each site at each

Fig. 2.3 Hybrid gravity survey offered by Micro-g LaCoste (from `www.microglacoste.com`). Red crosses are stations occupied by an absolute gravimeter (A-10) while all crosses (red and grey) are occupied by a relative gravimeter (CG-5).

time is desirable. If possible this network should be tied into an absolute benchmark, or alternatively a continuously operating (low drift) superconducting gravimeter. In this thesis a complete homogeneous network of 4 or 5 sites was used with one of the sites a stable bedrock reference site. An attempt was made to tie the bedrock site to an SG, but travel time of approximately 3 hours resulted in uncertain ties.

Gravity Network Adjustment

Network adjustment is used to ensure consistency of relative (and possibly absolute) ground-based gravity observations in a network. It also increases (on average) the precision of any given relative (to another site) gravity observation and consequently the precision of ground-based gravity observations at a site. Network adjustment can adjust the difference between sites (Cook, 1953; Lambert and Beaumont, 1977; Becker et al., 1987; Hwang et al., 2002) or the gravity at an individual site (Garland and Cook, 1955; Hipkin, 1978; Lagios, 1984; Becker et al., 1987; Gabalda et al., 2003). Minimising the difference is the most common (as it allows removal of the relative gravimeter bias by simple differencing of gravity observations at successive sites) and can use free or fixed constraints (Hwang et al., 2002). A fixed constraint is used when a reliable absolute gravity observation and error estimate is available to fix the gravity at one site; otherwise free adjustment allows the gravity to be adjusted at all sites. The network adjustment method of Hwang et al. (2002) has been used in a number of recent studies (Smith et al., 2006; Jacob et al., 2010) and is used in this thesis.

2.3 Geophysical Signals in Gravity Data

This section describes geophysical signals in ground-based gravity that range in frequency from the unpredictable short duration of earthquakes, to predictable ter-diurnal to semi-annual Earth tides, less predictable ocean tide loading at the same period as the principle Earth tides (semi-diurnal and diurnal), extremely predictable annual polar motion, and unpredictable but slow long period post glacial rebound that is a response to a forcing 7000 years ago. These geophysical signals cause temporal gravity changes that must be removed from ground-based gravity observations before the terrestrial water storage signal can be detected, or a soil moisture signal retrieved. Where appropriate the strength of the signals in Australia and methods to correct the ground-based gravity are indicated.

2.3.1 Earthquakes

While earthquakes are impossible to predict (Geller, 1997), earthquake monitoring services are available. Earthquakes have a significant impact on the Earth's gravity through redistribution of the Earth's mass, as well as shifting and acceleration of the Earth's surface. Unless a global mode is excited (such as happened after the 2004 9.3 Sumatran earthquake) the temporal duration of an earthquake is generally limited to less than 10 minutes (Park et al., 2005).

Earthquakes are monitored continuously by both the United States Geological Survey, USGS (`http://earthquake.usgs.gov`) and Geoscience Australia, GA (`http://www.ga.gov.au/earthquakes`), among others. After an earthquake gravity typically reverts to the prior value, although some studies (Imanishi et al., 2004; Kim et al., 2009; Neumeyer, 2010) have possibly indicated a small offset in gravity (0.05-0.1 μGal) at sites within 500 km of the epicentre, due to a redistribution of the crust and shift in crustal loading.

2.3.2 Earth Tides

Earth tides are the largest signal present in ground-based gravity data, and must be removed before a hydrological signal can be detected. Earth tides range in frequency from ter-diurnal to semi-annual (or even infinite period constant Earth tides) and in amplitude up to 150 μGal for a combined Earth tide signal. While Earth tides are extremely predictable (as they are based on the motion of the planets), the Earth's response to the tides is less predictable, and is described by seismic models of the Earth.

This subsection begins by describing the concept of vectorial tidal acceleration due to the Earth's rotation and the gravitational attraction of the celestial bodies (principally the Moon and Sun). A scalar tidal potential is then developed that avoids the need for vector operations and allows the summation of Earth tides (so that tides with negligible amplitude can be ignored). Next the concept of a

Table 2.3 Maximum tidal acceleration on the surface of the Earth due to the Moon, Sun and other celestial bodies in the Solar System (after Wenzel (1997)).

Celestial body	Maximum tidal acceleration (μGal)
the Moon	137
the Sun	50
Venus	0.00588
Jupiter	0.000654
Mars	0.000118
Mercury	0.0000364
Saturn	0.0000236
Uranus	0.000000367
Neptune	0.000000106
Pluto	0.00000000000761

tidal potential catalogue of the most significant Earth tides is discussed. The last two subsections present the Earth's elastic response to Earth tides, and Earth tide programs available to both analyse ground-based gravity data (to determine the parameters for the elastic response) and predict Earth tides at an arbitrary location (including the elastic response).

Tidal Acceleration

Tidal acceleration on the Earth is illustrated in Fig. 2.4 for the simplified case of an Earth-Moon system, with an irrotational and vertically inclined Earth and the Moon considered a point mass. The tidal acceleration $\boldsymbol{b_t}$ at a point P on the Earth's surface is the sum of the lunar gravitation $\boldsymbol{b}$ and gravitation due to other celestial bodies in the Solar System, principally the Sun (see Table 2.3) and the centrifugal (or orbit) acceleration $\boldsymbol{b_0}$.

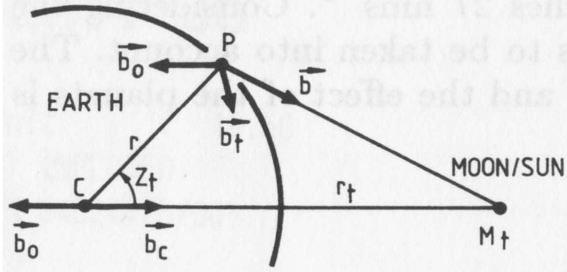

Fig. 2.4 Tidal acceleration (from Torge (1989)). The tidal acceleration $\boldsymbol{b_t}$ at a point P on the Earth's surface is the sum of the lunar gravitation $\boldsymbol{b}$ and the centrifugal (or orbit) acceleration $\boldsymbol{b_0}$. See also Fig. 2.1 for gravity acceleration due to the Earth.

The centrifugal acceleration is a resultant force of the Earth-Moon orbit around the barycentre of the system (located inside the surface of the Earth) (Wenzel, 1997). The centrifugal acceleration $\boldsymbol{b_0}$ is constant everywhere within and on the surface of the Earth (Fig. 2.4), whereas the lunar acceleration $\boldsymbol{b}$ varies with latitude due to the spatial extent of the Earth. Consequently tidal acceleration (or Earth tide) $\boldsymbol{b_t}$ varies with latitude (Fig. 2.5).

Furthermore due to the inclination of the Earth's rotational axis the Earth tides vary in time with the principal diurnal and semi-diurnal tides (Table 2.4) corresponding to the Earth's rotation period (or solar day).

Tidal Potential

As for the simplified case of a non-orbiting, but rotating spherical Earth (subsection 2.1.2), gravitational computations are again simplified by considering a scalar gravity tidal potential V_t rather than the vector gravity tidal acceleration $\boldsymbol{b_t}$.

$$\boldsymbol{b_t} = \boldsymbol{b} + \boldsymbol{b_0} = \operatorname{grad} V_t = \frac{\partial V_t}{\partial \boldsymbol{r}} \tag{2.25}$$

Gravity tidal acceleration (Eq. 2.25) is analogous to gravity acceleration (Eq. 2.12)) and correspondingly the gravity tidal acceleration potential (Eq. 2.25) is analogous to the gravitational potential (Eq. 2.15, compare also Fig. 2.4 and Fig. 2.1). Similar to the gravitational potential (Eq. 2.19), the tidal potential can also be expanded into a series of Legendre polynomials $P_l(t)$ (see Eq. 2.21 for a definition of Legendre polynomials)

$$V_t = \frac{GM_t}{r_t} \sum_{l=2}^{\infty} \left(\frac{r}{r_t}\right)^l P_l(\cos Z_t) \tag{2.26}$$

where G is the gravitational constant, M_t the mass of the Moon/Sun, Z_t the geocentric zenith angle, r the geocentric radial distance to the attracting point on the surface of the Earth, and r_t the geocentric radial distance to the Moon/Sun (Fig. 2.4). The tidal potential can then be expanded into a series of spherical harmonics

$$V_t = \frac{GM_t}{r_t} \sum_{l=2}^{\infty} \left(\frac{r}{r_t}\right)^l \frac{1}{(2l+1)} \sum_{m=0}^{l} \bar{P}_{l,m}(\cos\theta)\bar{P}_{l,m}(\cos\Theta_t)\cos(m\lambda - m\Lambda_t) \tag{2.27}$$

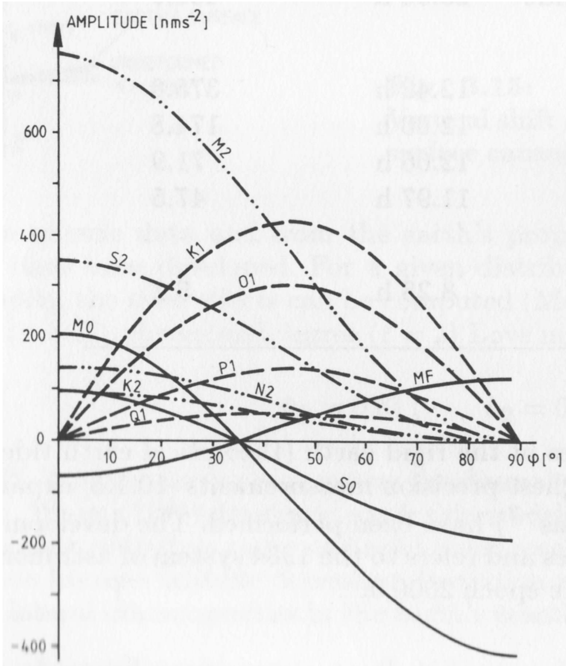

Fig. 2.5 Amplitude of the principal Earth tides as a function of latitude (from Torge (1989)). Long period tides have a suffix of 0 (or F) and are shown as a solid line, diurnal tides have a suffix of 1 and are dashed, semi-diurnal tides have a suffix of 2 and are shown as a dash with two dots. Canberra in Australia, and the field sites in this thesis, are around 35 ° S where the long period tides are zero but both the diurnal and semi-diurnal tides are large.

Table 2.4 Principal Earth tides due to the Moon and Sun (after Torge (1989)). Amplitude is given for 45 ° latitude (see Fig. 2.5).

Wave group	Darwin symbol	Earth tide	Period	Amplitude (μGal)
Long period	M0	Constant lunar tide	∞	10.29
	S0	Constant solar tide	∞	4.77
	Ssa	Declination tide to S0	182.62 d	1.48
	Mm	Elliptic tide to M0	27.55 d	1.68
	Mf	Declination tide to M0	13.66 d	3.19
Diurnal	O1	Main diurnal lunar tide	25.82 h	31.06
	P1	Main diurnal solar tide	24.07 h	14.46
	Q1	Elliptic tide to O1	26.87 h	5.95
	K1	Declination tide to O1, P1	23.93 h	43.69
Semi-diurnal	M2	Main lunar tide	12.42 h	37.56
	S2	Main solar tide	12.00 h	17.48
	N2	Elliptic tide to M2	12.66 h	7.19
	K2	Declination tide to M2, S2	11.97 h	4.75
Ter-diurnal	M3	ter-diurnal lunar tide	8.28 h	0.52

where $\bar{P}_{l,m}(t)$ are the fully normalised Legendre polynomials, θ, Θ, λ, Λ are the polar distance and geographical longitude of the attracting point on the surface of the Earth P and the Moon/Sun respectively (Fig. 2.2 and Eq. 2.19).

The gravity tidal potential is derived from the ephemerides (position of the Sun, Moon, Earth and other planets in the solar system). The ephemerides can be calculated analytically (Brown, 1905; Bretagnon, 1982; Chapront-Touzé and Chapront, 1983) or numerically (with more accuracy) by using astronomical observations to fit parameters to numerically integrated equations of motion (Standish, 1982; Krasinsky et al., 1993). The analytical ephemerides can be used to calculate tidal gravity acceleration directly (Petit, 1954; Longman, 1959, 1961; Harrison, 1971; Merriam, 1992b) or to develop a gravity tidal potential (Munk and Cartwright, 1966). However this time domain application (or response method) is limited to the case of a rigid oceanless Earth (i.e. the tidal response is constant for all frequencies) and is typically only used to create an independent 'benchmark' series to assess the accuracy of tidal potential catalogues (see Table 2.5). The automatic Earth tide correction computed in real time within the Scintrex CG-3M gravimeter used in this thesis is the Longman (1959, 1961) tidal gravity acceleration (based on analytical ephemerides).

Tidal Potential Catalogue

The gravity tidal potential is typically expanded into spherical harmonics and Fourier transformed into a tidal potential catalogue. Depending on the ephemeride derivation (analytical or numerical) the spectral analysis can also be either analytical (Doodson, 1921; Xi, 1989; Roosbeek, 1996) or numerical (Cartwright and Tayler, 1971; Cartwright and Edden, 1973; Büllesfeld, 1985; Tamura, 1987, 1994; Hartmann and Wenzel, 1995a,b). A selection of tidal catalogues is shown in Table 2.5. A tidal potential catalogue is a table of amplitudes, phases and frequencies for a selection of tides and easily allows the use of additional information from seismology models of the Earth's elasticity (and possibly ocean tide loading models). The tides are summed to give the gravity tidal acceleration. The number of tides and corresponding accuracy of the catalogue is primarily dependant on the choice of degree to truncate the infinite series in Eq. 2.26.

The Hartmann and Wenzel (1995a,b) tidal potential catalogue uses a maximum

Table 2.5 Tidal potential catalogues (after Wenzel (1997)). Accuracy is root mean square difference of gravity between a benchmark series and the tides calculated with the potential catalogue (Wenzel, 1997).

Author(s)	Number of waves	Maximum degree	Accuracy (μGal)
Doodson (1921)	377	3	0.10408
Cartwright and Tayler (1971), Cartwright and Edden (1973)	505	3	0.03844
Büllesfeld (1985)	656	4	0.02402
Tamura (1987)	1200	4	0.0834
Xi (1989)	3070	4	0.0642
Tamura (1994)	2060	4	0.0308
Roosbeek (1996)	6499	5	0.0200
Hartmann and Wenzel (1995a,b)	12935	6	0.0014

degree (l) of six for the Moon, three for the Sun and two for the planets in the Solar System (Table 2.5). However around 98 % of the tidal potential (V_t) is due to terms of degree two (Wenzel, 1997), with smaller degree terms (i.e. degree one) not contributing due to system equilibrium (Eq. 2.26 and 2.27). While the eight main (diurnal and semi-diurnal) Earth tides are given in Table 2.4 together with the three main (time varying) long period tides and the principal ter-diurnal tide, the tidal potential catalogue of Hartmann and Wenzel (1995a,b) includes 12935 Earth tides (Table 2.5). The spectrum of the Hartmann and Wenzel (1995a,b) tidal potential shows the richness of the Earth tides particularly in the diurnal and semi-diurnal frequency bands (Fig. 2.6).

A wave group is a collection of Earth tides with a similar frequency. Multiple wave groups are clearly visible in Fig. 2.6. The frequency width of a wave group, and the ability to separate individual Earth tides, depends on the precision of the gravimeter, background noise (that may include environmental signals including soil moisture), length of record, amplitude of the Earth tide (signal to noise ratio) and amplitude of Earth tides with a similar frequency. For example, even though the amplitude of both K1 and P1 are quite large (Table 2.4 and Fig. 2.6), they are commonly represented as one wave group (as in the top panel of Fig. 2.6) due to their proximity in frequency (Table 2.4 and Fig. 2.6).

In this thesis the tidal potential catalogues of Cartwright and Tayler (1971);

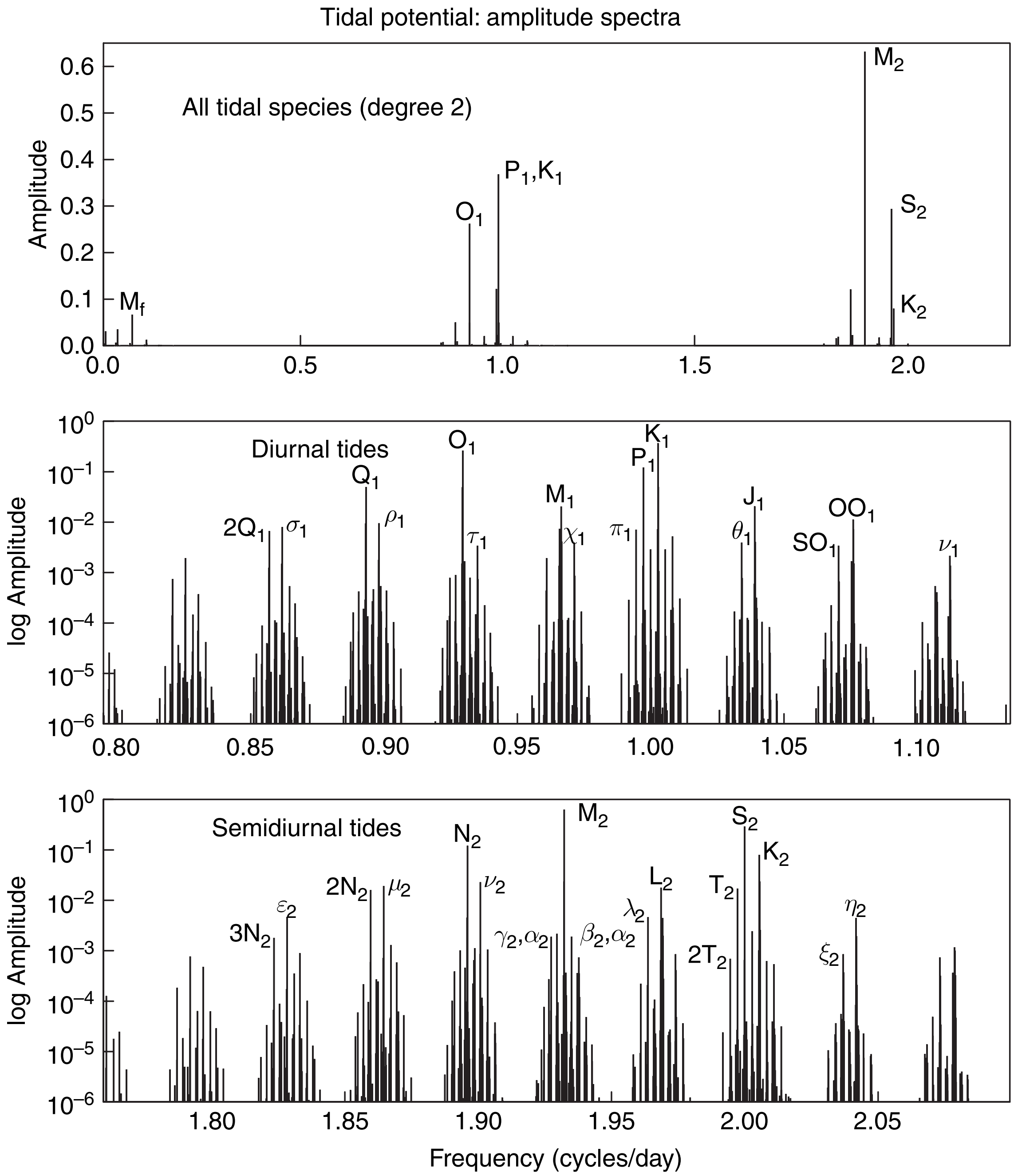

Fig. 2.6 Hartmann and Wenzel (1995a,b) tidal potential spectrum (from (Agnew, 2007)).

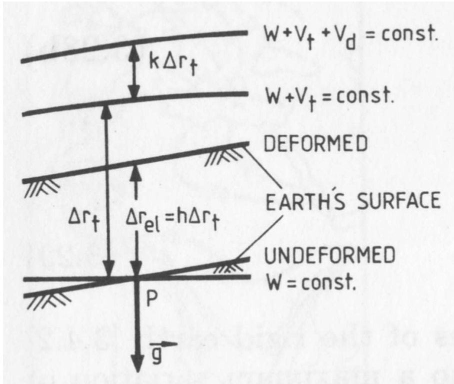

Fig. 2.7 Displacement of the Earth's surface in the radial (vertical) direction due to the tidal potential (V_t). Displacement of the equipotential surface (Δr_t) is also shown, as is the additional displacement of the equipotential surface ($k\Delta r_t$) due to the deformation potential (V_d) caused by the mass displacement (from Torge (1989)).

Cartwright and Edden (1973); Tamura (1987); and Hartmann and Wenzel (1995a,b) are assessed with high precision SG gravity data at Canberra, and less precise Scintrex CG-3M data at both Canberra and Melbourne. The Tamura (1987) tidal potential catalogue is used to correct ground-based gravity data (from a Scintrex CG-3M) at the field sites (100 km west of Canberra) to enable the detection of a terrestrial water storage signal (and retrieval of a soil moisture signal).

Elastic Earth Response

The tidal potential V_t (Eq. 2.26) causes a shift of the equipotential surface W (Eq. (2.23)) in the radial direction Δr_t (Fig. 2.7), where

$$\Delta r_t = \frac{V_t}{g} \tag{2.28}$$

This shift of equipotential surface causes a deformation of the elastic Earth that is described by Love (1909) for the case of a spherical, irrotational, elastic Earth model. Wahr (1981) gives the theory for an elliptic, rotating, elastic and oceanless Earth model. The deformation of the surface of the Earth in the radial direction Δr_{el} is proportional to the shift of the equipotential surface Δr_t (Fig. 2.7). Similarly the deformation potential V_d caused by the mass displacement is proportional to the tidal potential V_t.

The two proportionality constants (h and k) for the surface of the Earth and equipotential surface respectively are known as Love numbers (Torge, 1989). Love numbers depend on the degree of the spherical harmonic expansion of the tidal potential (Eq. 2.27). Spherical density models of the Earth such as 1066A (Gilbert and Dziewonski, 1975) or the preliminary Earth model (PREM) of Dziewonski and Anderson (1981) are used to calculate Love numbers (Wahr, 1981; Dehant, 1987). Wahr (1981) derived Love numbers for an elliptic, rotating, elastic and oceanless Earth model, whereas Dehant (1987) include the effects of an inelastic Earth mantle. Dehant et al. (1999) present Love numbers for an elliptic, rotating, elastic and oceanless Earth model with an inelastic mantle and the effects of mantle convection included, the parameters of the mantle convection model are set to reproduce the observed geoid (amongst other constraints). Mathews (2001) derived newer parameters from PREM with the dynamic flattening of the Earth model modified to fit geodetic observations, while Xu et al. (2004a) derived Love numbers from stacked gravity observations of the GGP network of SGs, in particular observed O1 and M2 tides. At Wuhan, China all three recent parameter sets give similar results (Zhou et al., 2009b), with gravity derived from the Xu et al. (2004a) and (Dehant et al., 1999) parameters particularly close (discrepancy less than 0.03 μGal), however the pairwise difference from any two of the three parameter sets is less than 0.15 μGal. Indeed Xu et al. (2004a) state their Love numbers are similar to those of Dehant et al. (1999) for semi-diurnal and Mathews (2001) for diurnal tides.

Recent studies have considered the effect of lateral inhomogeneity on Earth tides (Fu and Sun, 2007) and presented Love numbers for a convecting, laterally heterogeneous, and aspherical Earth (Métivier and Conrad, 2008). In this thesis the Love numbers of Dehant (1987) and Dehant et al. (1999) are assessed, with the Dehant et al. (1999) parameters used (together with the Tamura (1987) tidal potential catalogue) to correct gravity (from a Scintrex CG-3M gravimeter after re-applying the real time Earth tide correction of Longman (1959, 1961)) to enable the detection of a terrestrial water storage signal at field sites.

Degree two ($l = 2$) Love numbers for the surface of the Earth are $h_2 = 0.61$ and $k_2 = 0.30$ (Torge, 1989) so that the radial deformation of the Earth's surface is less than the radial shift of the equipotential surface induced by the tidal potential (Fig. 2.7) (i.e. $h_2 < 1$) and the consequent radial displacement of the equipotential surface due to the deformation potential (V_d) is about half the radial deformation of the Earth's surface (i.e. $k_2 \approx 0.5h_2$).

The Love numbers can be used to calculate a theoretical amplitude factor for the Earth tides with

$$\delta_l = 1 + \frac{2}{l}h_l - \frac{l+1}{l}k_l = 1.16 \tag{2.29}$$

a global average. Consequently the amplitude of the Earth tides on an elastic Earth are approximately 16% greater than that of a rigid (unyielding) Earth. The phase change of the Earth tides is zero for an elastic Earth (Hinderer et al., 2007), but the inelastic mantle causes shifts in the phases of the Earth tides (Agnew, 2007).

Earth Tide Programs

The three Earth tide programs most commonly used to analyse superconducting gravimeter (SG) gravity data are ETERNA, VAV, and BAYTAP-G (Dierks and Neumeyer, 2002; Ducarme et al., 2006; Ducarme, 2009). By analysing a gravity time series (at a single location) an Earth tide program can be used to determine the amplitude and phase parameters for a wave group of Earth tides (from a tidal potential catalogue) at that specific location (e.g. Mt Stromlo, Canberra). More usefully for this thesis an Earth tide program can also be used to separate the gravimeter drift component and other signals in the gravity data set (i.e. the gravity response to meteorological data sets) that may be physically based signals (i.e. a gravity response to external forcing) or instrumental artefacts (i.e. the gravimeters response to external forcing). For an Earth tide program to be able to analyse portable relative gravimeter data (e.g. Scintrex CG-3M as used in this thesis) it must be able to handle data gaps (due to manual downloading the gravimeter) and drift in the gravity time series.

The Earth tide program ETERNA (Wenzel, 1996) analyses a stationary gravity time series and fits an amplitude factor and phase shift to up to 85 wave groups including the option of fitting a scalar factor to up to eight associated data sets (e.g. air pressure or temperature) and a (Tschebyscheff) polynomial drift to the gravity data (e.g. for a spring based relative gravimeter). Seven different tidal potential catalogues can be used (all in Table 2.5 except Tamura (1994)) including the Hartmann and Wenzel (1995a,b) catalogue. ETERNA can also be used in a predictive mode to calculate Earth tides at a location but is limited to using the Love numbers of Dehant (1987). Data gaps are a problem with ETERNA as the analysis method uses long antialiasing filters (167 hours for recommended filters) that inflate the gaps.

The Earth tide program VAV (Venedikov et al., 2003, 2005) has similar functionality to ETERNA but operates on blocks of data that are multiples of the diurnal signal (i.e. 24 or 48 hour blocks). This gives the program the ability to deal with irregular data (including gaps). For each block of data a polynomial drift can be fitted. VAV uses the tidal potential catalogue of Tamura (1987). VAV can have up to twelve wave groups (when analysing data in 48 hour blocks) but six wave groups (and 24 hour blocks) is the standard. The program can automatically select the number of wave groups based on the length of the data or alternatively the user can specify. The model selection Akaike Information Criteria (AIC) of Akaike (1974) is used to choose between different numbers of wave groups or drift models, with the lowest AIC preferred.

Similar to VAV, the Earth tide program BAYTAP-G (Bayesian Tidal Analysis Program - Grouping model) also determines wave groups automatically depending on the length of the observation record (Tamura et al., 1991; Tamura, 1999). A novel feature of BAYTAP-G is the ability to automatically fit a nonlinear (and non-polynomial) drift to the observations, indeed a separate drift parameter is estimated for each time step. Furthermore BAYTAP-G can also deal with gaps by interpolation of the data using the estimated drift. Given a time series of observations BAYTAP-G calculates tidal parameters (phase and amplitude), linear response to external datasets (at any lag), and trend under the assumption of smoothly varying drift. Additionally BAYTAP-G can interpolate missing data, detect outliers and estimate step changes (Tamura, 1999). Similar to VAV the Akaike Bayesian Information Criteria (ABIC) is used to select amongst different numbers of wave groups, drift models and response weights (at different lags) for associated datasets. ABIC can be considered an extension of AIC (Akaike Information Criteria) to Bayesian models (Tamura et al., 1991), which is necessary when considering the goodness of fit of a stochastic drift (as opposed to a deterministic drift, for example, polynomial drift).

Unlike ETERNA, VAV, and BAYTAP-G, the Earth tide program Tsoft is used more for visualisation and data inspection than automatic analysis (Van Camp and Vauterin, 2005). However Tsoft is equipped with the newer Dehant et al. (1999) Love numbers and can be run in predictive mode (using the Tamura (1987) tidal potential catalogue).

The BAYTAP-G Earth tide program is used in this thesis to analyse the Scintrex CG-3M gravity response to three meteorological variables (atmospheric pressure, air temperature, and relative humidity). The Earth tide programs BAYTAP-G and ETERNA are used in this thesis to analyse the SG (and atmospheric pressure) data at Canberra. The Tsoft Earth tide program is used in this thesis to predict (using a tidal potential catalogue with wave group amplitude and phase parameters from a seismic model) an Earth tide (and polar motion) signal for a specific location and time (e.g. field sites) to be removed from the Scintrex CG-3M gravity data. It is also used to remove predicted signals from the SG data at Canberra (for comparison to the analysis of ETERNA and BAYTAP-G, and verification of the gravity correction methods used at the field sites 100 km west of Canberra). While it is believed that VAV would lead to similar results as ETERNA or BAYTAP-G (Dierks and Neumeyer, 2002), the Earth tide program VAV was not used in this thesis.

2.3.3 Ocean Tide Loading

In addition to the elastic Earth response to Earth tides, further shifts in the equipotential surface (together with the observed amplitude and phase of Earth tides) are caused by ocean tide loading. The ocean tides exert a variable pressure or load on the Earth's crust. This causes a temporal change in ground-based gravity (at a point on land) in three ways:

1. Newtonian gravitational attraction of the additional oceanic tidal mass (insignificant except for coastal areas);
2. change in elevation (vertical displacement) of the gravity site due to flexure of the crust; and
3. change of gravity (a vertical acceleration) due to horizontal and vertical accelerations of the crust known as rippling (Farrell, 1972).

Ocean tides and Earth tides share the same principal tidal frequencies (Table 2.4) as they are forced by the same astronomical ephemerides. While the spatial distribution of Earth tides varies smoothly (Fig. 2.5), the spatial distribution of ocean tides (and consequent loading) is much less predictable (Fig. 2.8) due to the discontinuity at coastlines, complex spatial structure of ocean basins and areas of zero tidal amplitude (amphidromes). The (eleven) main ocean tide constituents in order

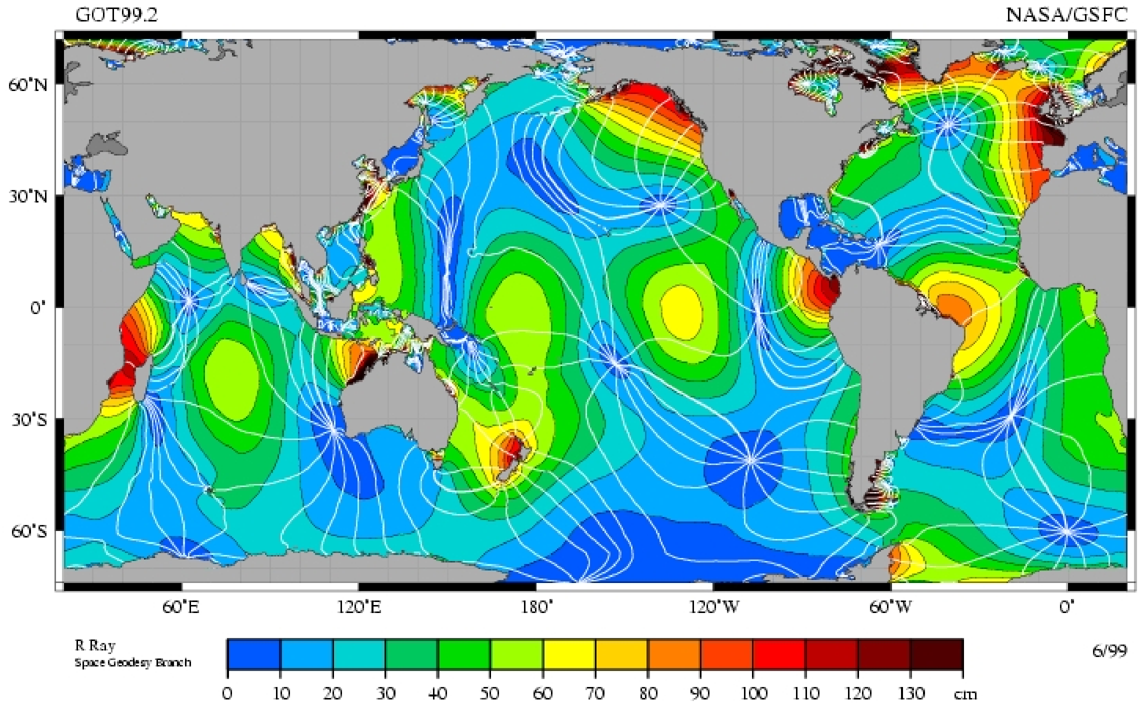

Fig. 2.8 The semi-diurnal main lunar tide M2 for the ocean tide model GOT99.2 (Ray, 1999). Cotidal lines (spaced at phase intervals of 30 degrees) are shown in white. Amphidromes are located at the intersection of cotidal lines where the M2 amplitude is zero (dark blue). From `http://svs.gsfc.nasa.gov`.

of decreasing significance are the four semi-diurnal (M2, S2, N2, K2), four diurnal (K1, O1, P1, Q1) and three long period tides (Mf, Mm, Ssa), shown in Table 2.4 and Fig. 2.5 and 2.6 (Schwiderski, 1980b). Consequently a tidal analysis of a gravity time series using an Earth tide program (such as ETERNA or BAYTAP-G) gives an amplitude factor and phase shift for a wave group that is a combined response of the elastic Earth to both Earth tides and ocean tide loading. Therefore Earth tide programs can not be used to determine the ocean tide loading effect at a given site.

There are two main methods to compute the tidal loading (Agnew, 2007): summing spherical harmonics after developing a loading potential (using a spherical harmonic expansion of the tidal elevation); and convolution of the tidal height with a Green function that gives the response to a point load. Summing spherical harmonics is more computationally efficient (for global loading), however convolution with a Green function is typically used as it is easier to compute tilt, strain and non-tidal (e.g. atmospheric pressure) loading. It is also easier to use a Green function with a mask for the area of interest. Available programs to convolve the Green function with a ocean tidal height include GOTIC2 (Matsumoto et al., 2001), NLOADF (Agnew, 1997), and the ocean tide loading provider `http://www.oso.chalmers.se/~loading`, a web based service that uses the OLFG/OLMPP loading program (Scherneck, 1991).

The ocean tide model inputs for the loading programs consist of amplitude and phase for each ocean tide (relative to the gravitational tidal potential at the Greenwich meridian) on a regular grid. The ocean tides represented for each ocean tide model in the three different loading programs (OLFG/OLMPP, NLOADF, and GOTIC2) are shown in Table 2.6-2.8. The OLFG/OLMPP ocean tide loading program has the greatest selection of ocean tide models, with all of the models used in the NLOADF or GOTIC2 programs included at the ocean tide loading provider website. However OLFG/OLMPP calculates the ocean tide loading with a maximum of 11 ocean tides, while GOTIC2 uses up to 21 ocean tides for a single model. Furthermore the resolution of the ocean tide grids and coastline affect the accuracy of the loading computation and may differ between ocean tide loading programs. All three loading programs are tested in this thesis on SG gravity data at Canberra (100 km from the Pacific coast of Australia), and Scintrex CG-3M data at Melbourne (adjacent to Port Phillip Bay). The field sites in this thesis (where the gravitational effect of ocean tide loading is removed from Scintrex CG-3M gravity data) are located 100 km west of Canberra, and 200 km from the east coast of Australia.

The magnitude of ocean tide loading is generally 0.3 to 3 μGal (Baker and Bos, 2003). Three FG5 absolute gravimeters were deployed simultaneously at Mt Stromlo, Canberra in the year 1997, prior to commencement of continuous measurements of ground-based gravity with the SG (Gladwin et al., 1997). The three absolute gravimeters detected semi-diurnal and diurnal ocean tide loading signals of 2-6 μGal amplitude. Later Sato et al. (1998) compared the output of four different ocean tide models to 130 days of gravity data from the SG at Canberra and found loading amplitudes of 0.5-2.8 μGal additional to (and out of phase of) the four main solar and lunar tides. Merriam (1981) even found ocean tide loading amplitudes

Table 2.6 Ocean tide models that are available at the ocean tide loading provider website `http://www.oso.chalmers.se/~loading`. The 8 major short period (M2, S2, K1, O1, N2, P1, K2, Q1) and 3 main long period (Mf, Mm, Ssa) ocean tides are provided for each model.

Ocean Tide Model	Ocean Tides from FES99	Reference
AG06		Andersen (1995a,b); Andersen et al. (1995, 2006)
CSR3.0	Mf, Mm, Ssa	Eanes and Bettadpur (1994a,b, 1995)
CSR4.0	Mf, Mm, Ssa	Watkins and Eanes (1997)
EOT08a		Savcenko and Bosch (2008)
FES94.1		Le Provost et al. (1994)
FES95.2	Mf, Mm, Ssa	Le Provost et al. (1998)
FES98		Lefèvre et al. (2000)
FES99		Lefèvre et al. (2002)
FES2004		Letellier (2004); Lyard et al. (2006)
GOT00.2	Mf, Mm, Ssa	Ray (1999)
GOT4.7		Schrama and Ray (1994)
GOT99.2b	Mf, Mm, Ssa	Ray (1999)
NAO.99b		Matsumoto et al. (2000)
Schwiderski		Schwiderski (1980a,b)
TPXO.5	Ssa	Egbert et al. (1994); Egbert and Erofeeva (2002)
TPXO.6.2	Ssa	Egbert et al. (1994); Egbert and Erofeeva (2002)
TPXO.7.0		Egbert et al. (1994); Egbert and Erofeeva (2002)
TPXO.7.1		Egbert et al. (1994); Egbert and Erofeeva (2002)

of 0.1-0.9 μGal for the six strongest solar and lunar partial tides at Alice Springs (approximately 1000 km from the nearest coast).

Schwiderski (1980a,b), the original ocean tide model used for ocean tide loading, is still considered a benchmark when presenting results from other ocean tide models. The Schwiderski (1980a,b) solution (like previous ocean tide models) is on a 1° resolution global grid but is far more accurate in shallow seas as it assimilates tide gauge observations (mostly coastal and island, and some seafloor). The ocean tide models after Schwiderski (1980a,b) all use the TOPEX/Poseidon altimeter data (representing sea surface height).

Timofeev et al. (2006) found that CSR3.0, CSR4.0 and FES02 gave the best results for the Atlantic coast of France. For the Canary Islands, Arnoso et al. (2006) found that all nine ocean tide models they assessed (Schwiderski, FES95.2,

Table 2.7 Ocean tide models and ocean tides that are available with the ocean tide loading software NLOADF (Agnew, 1997).

Ocean Tide Model	Short Period Ocean Tides	Long Period Ocean Tides
CSR3.0	M2, S2, K1, O1, N2, P1, K2, Q1	
FES95.2	M2, S2, K1, O1, N2, K2, Q1	
GOT00.2	M2, S2, K1, O1, N2, P1, K2, Q1	
Schwiderski	M2, S2, K1, O1, N2, P1, K2, Q1	Mf
TPXO.6.2	M2, S2, K1, O1, N2, P1, K2, Q1	Mf, Mm

Table 2.8 Ocean tide models and partial tides that are available with the ocean tide loading software GOTIC2 (Matsumoto et al., 2001).

Ocean Tide Model	Short Period Ocean Tides	Long Period Ocean Tides
CSR4.0	M2, S2, K1, O1, N2, P1, K2, Q1, M1, J1, OO1, 2N2, μ2, ν2, L2, T2	
GOT99.2b	M2, S2, K1, O1, N2, P1, K2, Q1	
NAO.99b	M2, S2, K1, O1, N2, P1, K2, Q1, M1, J1, OO1, 2N2, μ2, ν2, L2, T2	Mtm, Mf, Mm, Ssa, Sa

TPXO.2, TPXO.6, CSR3.0, CSR4.0, NAO.99b, GOT99.2b, GOT00.2) were in close agreement, with TPXO.2 and Schwiderski the most deviant. Francis and Melchior (1996) found no significant difference between Schwiderski, FES95.2 and CSR3.0 models for south Western Europe. Similarly Van Camp (2003) found the differences in calculated gravity with Schwiderski, FES95.2 and CSR3.0 to be less than 0.1 μGal at Membach, Germany. Almalvict et al. (2001) assessed Schwiderski, CSR3.0 and FES95.2 at Mt Stromlo, Canberra and found that all models halved the set standard deviation of an FG5 absolute gravity determination (from 3 μGal to 1.4-1.7 μGal), with CSR3.0 giving the best result and FES95.2 the worst. Similarly Xu et al. (2004a) show FES95.2 performs badly at Canberra for the M2 tide. In this thesis all 18 ocean tide models provided with the loading models (Table 2.6-2.8) are assessed at Mt Stromlo, Canberra.

2.3.4 Polar Motion

Polar motion is the movement of the Earth's axis of rotation relative to its mean location (for 1900 to 1906) (Torge, 1989). Polar motion (Fig. 2.9) can be decomposed into three clear signals:

1. A misalignment of the Earth's instantaneous rotation axis and principal axis of inertia that results in a prograde (counter-clockwise when viewed from the North Pole) polar motion (Fig. 2.10). This Chandler oscillation (Chandler, 1891, 1892) has a period of around 432 days (Fig. 2.10). Although the Chandler wobble is a free oscillation it is damped by friction in the anelastic mantle (Seitz and Schuh, 2010). Therefore it must be excited by another signal with a resonant frequency such as,
2. an annual oscillation thought to be caused by seasonal mass redistribution in the ocean and atmosphere (Gross, 2000; Brzezinski and Nastula, 2000; Gross et al., 2003; Seitz and Schmidt, 2005; Seitz and Schuh, 2010). The annual oscillation and Chandler oscillation can be clearly seen to combine with a beat frequency of 6 years (Fig. 2.9).
3. An irregular drift (Fig. 2.10) thought to be due to post glacial rebound in Canada (Fig. 2.11) and Europe (Milne and Mitrovica, 1998).

Polar motion is calculated by a first-order perturbation of the centrifugal potential (Eq. 2.24) (Wahr, 1985; Torge, 1989)

$$\Delta g_{\text{Polar Motion}} = -\delta\omega^2 R \sin 2\theta \left(x \cos\lambda + y \sin\lambda\right) \tag{2.30}$$

where δ is the gravimetric factor, ω is the mean angular velocity of the Earth, R is the radius of the Earth, θ is latitude, λ is longitude, x and y are the instantaneous pole coordinates. The gravimetric factor of long period tides 1.16 (Eq. 2.29) is used (Wahr, 1985; Xu et al., 2004b; Neumeyer, 2010) due to a lack of knowledge (Timmen, 2010). The mean angular velocity of the Earth (ω) is from the International Earth Rotation Service (IERS) Conventions 2003 (McCarthy and Petit, 2004; Neumeyer, 2010) while the daily instantaneous pole coordinates (x and y) are sourced from the EOP C04 series of Earth orientation parameters available at the IERS website `http://www.iers.org`. The IERS polar motion data is a combination of geodetic observations including: Very Long Baseline Interferometry (VLBI), Lunar and

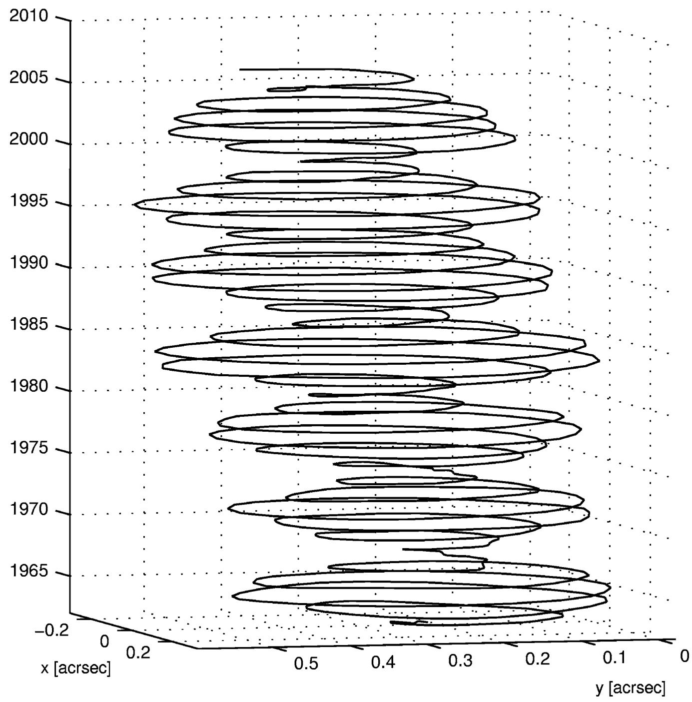

Fig. 2.9 Polar motion (from Timmen (2010)).

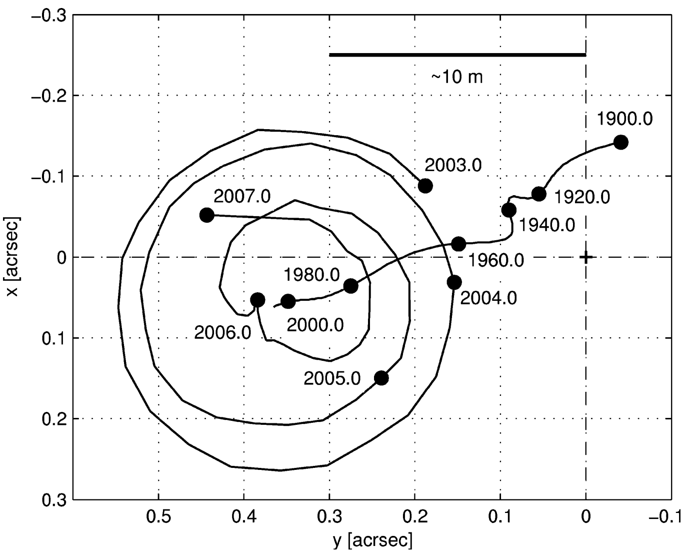

Fig. 2.10 Polar motion viewed from the North Pole (from Timmen (2010)).

Satellite Laser Ranging (LLR and SLR respectively), and Global Positioning System (GPS) measurements (Dick and Richter, 2008; Neumeyer, 2010).

The gravitational effect of polar motion attains a maximum at mid-latitudes $\theta = 45\,^\circ$ (Eq. 2.30). The field sites in this thesis and the SG at Canberra used to test the gravity corrections are located at approximately 35 ° S. Consequently while the long term Earth tides at the field sites in this thesis are expected to be negligible (Fig. 2.5), the gravitational effect of polar motion (a semi-annual tide) is expected to be significant. Wahr (1985) modelled polar motion using LAGEOS laser ranging data and Love numbers to represent the additional gravity effect of crustal deformation and concluded that a change in gravity of as much as 10 to 13 µGal in one year is possible at mid latitudes. Polar motion can now be measured with an accuracy better than 0.1 ″ (or 0.1 mas) (Dick and Richter, 2008; Seitz and Schuh, 2010), resulting in a residual error for the polar motion correction of less than 0.1 µGal at 52.44 ° N (Timmen and Wenzel, 1994; Timmen, 2010). For this thesis polar motion is calculated by the Tsoft Earth tide program (Van Camp and Vauterin, 2005) using the IERS polar motion data (EOP C04) from `http://www.iers.org`.

2.3.5 Post Glacial Rebound

Post glacial rebound (or glacial isostatic adjustment) is a continuing displacement of the Earth's crust due to the melting of glacial ice sheets at the end of the last ice age. The melting took about 14,000 years to complete and ended at approximately 5,000 B.C. (Peltier, 1994).

Post glacial rebound causes a theoretical vertical displacement of approximately 1 cm/year near Hudson Bay in Canada, which amounts to about a 2 µGal/year decrease in gravity (Pagiatakis and Salib, 2003). A series of measurements were taken around Canada with LaCoste and Romberg Model-G meters and corrected for Earth tides and ocean tide loading effects (via global and regional ocean tide models). The corrected measurements were then subjected to a least squares adjustment. The outcome was an average Canadian post glacial rebound rate of about -1 µGal/year with an uncertainty of about 0.25 µGal/year.

While significant in Canada, particularly around the Hudson Bay area (Fig. 2.11) post glacial rebound is not significant in Australia, or indeed most of the southern

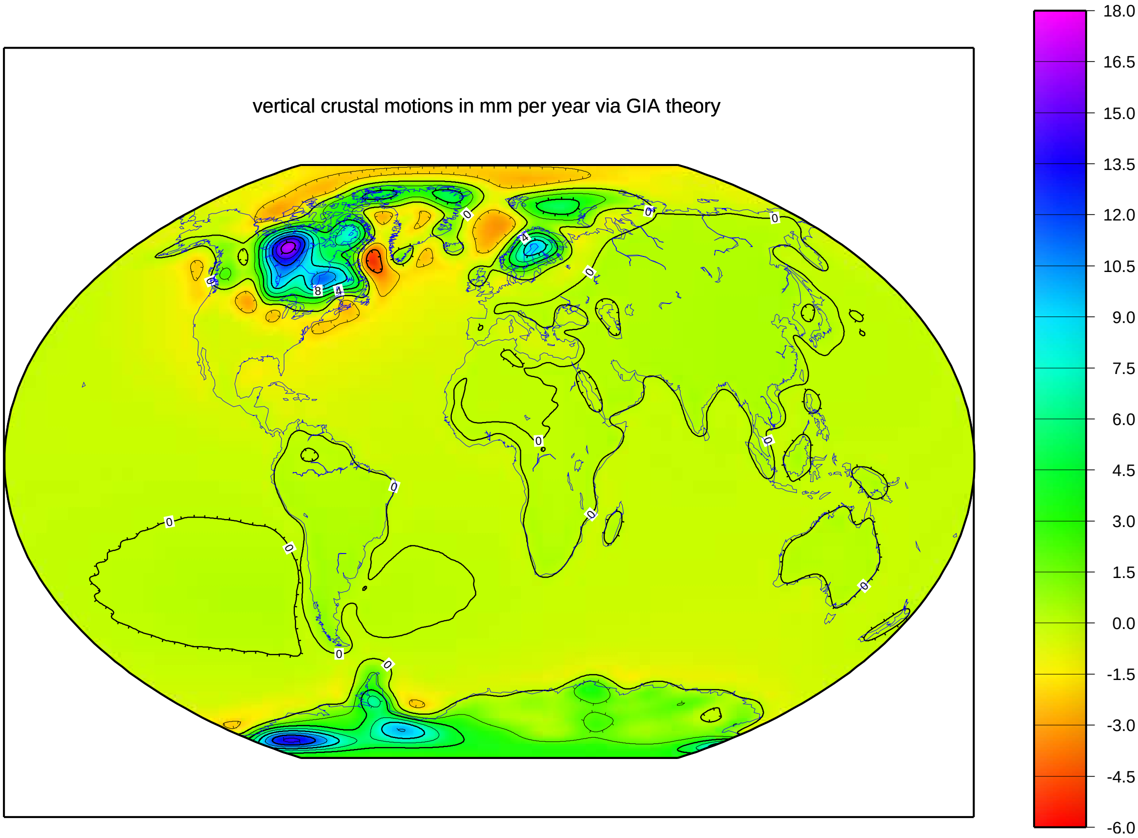

Fig. 2.11 Post glacial rebound (from Paulson et al. (2007)).

hemisphere except Antarctica (Paulson et al., 2007). Consequently post glacial rebound is neglected in this thesis.

2.4 Meteorological Signals and Instrumental Artefacts in Gravity Data

Meteorological signals in ground-based gravity and gravimeter instrumental artefacts are considered together due to the lack of compelling evidence for the detection of meteorological signals in ground-based gravity (other than atmospheric pressure) and the difficulty in determining what is solely an instrumental artefact and what is a causal meteorological signal in ground-based gravity data (Niebauer, 2007).

2.4.1 Atmospheric Pressure

The atmospheric pressure signal in ground-based gravity is significant for all places on the Earth, and must be removed from gravity data to detect a terrestrial water storage signal or retrieve a soil moisture signal. While the highly predictable ephemerides result in predictable Earth and ocean tides, the atmospheric pressure is not as predictable, and is generally observed rather than modelled.

Like ocean tides the atmospheric pressure contribution to ground-based gravity is compromised of the direct Newtonian attraction of the atmospheric mass (generally causing a reduction in gravity as the most significant mass is above the site of interest), and also a loading effect due to the downward pressure of the atmosphere on the Earth's surface. The atmospheric loading causes a deformation of the Earth and reduction in the surface elevation that results in an increase in gravity (Eq. 2.6).

Warburton and Goodkind (1977) found that the Newtonian attraction of the air mass was by far the dominant process, and the net result of an increase in atmospheric pressure was a decrease in gravity. Müller and Zürn (1983) claim the Newtonian attraction is 5 to 10 times greater than the loading effect, while van Dam and Wahr (1987) studied the effect of atmospheric loading and concluded that the direct Newtonian attraction is usually three orders of magnitude larger than the loading effect, but the loading could still make changes of 2-4 μGal at Boulder, Colorado. Neumeyer (2010) give a rough estimate for the gravity changes due to the attraction and loading terms of -0.43 μGal/mbar and 0.13 μGal/mbar respectively.

Melchior et al. (1982) used an earlier version of the Earth tide program VAV (Venedikov et al., 2003) with 1 year of hourly gravity and atmospheric pressure data (for 1975) at Alice Springs, Australia and found an atmospheric pressure admittance (combined effect on gravity of both attraction and loading) of -0.29 μGal/mbar. Zhou et al. (2009a) used the Earth tide program ETERNA (Wenzel, 1996) on 7 years of hourly data (1998-2004 inclusive) from the SG and adjacent barometer at Canberra, Australia and determined an atmospheric pressure admittance of -0.31 μGal/mbar.

The admittance between local pressure and ground-based gravity integrates the atmospheric pressure Newtonian attraction and loading effects (around -0.43 and 0.13 μGal/mbar respectively (Neumeyer, 2010)) into a single scalar factor that has been found by both theoretical models (Merriam, 1981, 1992a; Sun et al., 1995; Kroner and Jentzsch, 1997; Boy et al., 1998b) and correlations between observations (Warburton and Goodkind, 1977; Merriam, 1981; Spratt, 1982; Levine et al., 1986; Crossley et al., 1995; Neumeyer, 1995; Kroner and Jentzsch, 1999; Arnoso et al., 2002; Crossley et al., 2002; Simon, 2002; Meurers, 2004; Hu et al., 2005, 2006; Abd El-Gelil et al., 2008) to be between approximately -0.3 and -0.4 μGal/mbar. Furthermore, Arnoso et al. (2002) found a seasonal trend (monthly varying admittance) at the Boulder SG, while Simon (2002) found a seasonal variation in the Newtonian attraction component due to seasonal air mass warming.

An accurate and currently accepted theoretical determination of the pressure admittance is that of Merriam (1992a),

$$\Delta g_{\text{Local Atmospheric Pressure}} = -0.356\,(p - p_n) \tag{2.31}$$

where p is measured barometric pressure (mbar) and p_n is normal atmospheric pressure modelled by

$$p_n = 1013.25\left(1 - \frac{0.0065H}{288.15}\right)^{5.2559} \tag{2.32}$$

where H (m) is station elevation (Torge, 1989). Merriam (1992a) found approximately 99 % of the pressure admittance within a 25 km radius of the gravimeter is caused by Newtonian attraction. Furthermore, primarily due to the curvature of the Earth, Merriam (1992a) found an annulus within approximately 50-250 km of the gravimeter does not contribute to the admittance (Table 2.9), whereas the pressure outside this zone contributes approximately 10 % (opposite in sign to the local pressure).

Due to the fact that a pressure cell rises in warmer air, causing a shift in the cell's centre of gravity, Merriam (1992a) claims there is also a minor temperature admittance,

$$\Delta g_{\text{Local Temperature}} = 0.013\,(T_a - 15) \tag{2.33}$$

where T_a is the observed atmospheric temperature and 15 °C is a reference temperature. However this claim is not rigorously defended by Merriam (1992a) and is not bourne out in other studies (Dittfeld, 2001; El Wahabi et al., 2001). Abe et al. (2010) found the difference between using the temperature admittance or not

Table 2.9 Contribution of regional atmospheric pressure to observed gravity signal via pressure admittance. Results from Merriam (1992a). Note that the switch in sign of the correlation means that an increase of pressure within 50 km of the gravimeter results in a decrease of observed gravity, whereas an increase in pressure in the zone within 250 and 500 km of the gravimeter results in a increase in gravity.

Distance from gravimeter	Contribution to admittance	Correlation
0-50 km	90 %	Strongly Positive
50-250 km	0 %	Zero
250-500 km	10 %	Weakly Negative

when calculating an atmospheric pressure signal in gravity based on the approach of Merriam (1992a) was only 0.04 μGal at the Moxa SG (RMS over a 4 year period). In general any atmospheric temperature signal in ground-based gravity will be masked by the temperature of the enclosure the gravimeter is operating in and also any temperature shielding that is part of the gravimeter construction.

Recent literature (Neumeyer et al., 2004, 2006, 2007, 2008; Boy and Chao, 2005; Gitlein and Timmen, 2007; Abd El-Gelil et al., 2008; Klügel and Wziontek, 2009; Abe et al., 2010) has investigated the use of global three dimensional (3D) grids of atmospheric pressure (together with air temperature and specific humidity) from Numerical Weather Prediction (NWP) models of the atmosphere (such as from the European Centre for Medium Range Weather Forecasting, ECMWF) to calculate both the Newtonian attraction of the atmospheric mass (using the hydrostatic equations of dry air and water vapour to calculate air density) as well as the atmospheric pressure loading with a Green's function (Farrell, 1972; Merriam, 1992a; Sun et al., 1995).

Previous studies used global two dimensional (2D) grids of surface pressure (and air temperature) together with an assumption of hydrostatic equilibrium (to give a standard altitude dependant air density distribution) to approximate the attraction component (Niebauer, 1988) and a Green's function (Farrell, 1972) to calculate the atmospheric pressure loading (Spratt, 1982; van Dam and Wahr, 1987; Merriam, 1992a; Sun et al., 1993, 1995; Mukai et al., 1995; Kroner and Jentzsch, 1997, 1998, 1999; Neumeyer et al., 1998; Vauterin, 1998; Boy et al., 1998a,b, 2001, 2002, 2009; Boy and Lyard, 2008; Abd El-Gelil et al., 2008; Abe et al., 2010; Crossley et al., 2012). However this data intensive approach is dependant on the accuracy of the atmospheric model (Boy et al., 2002; Boy and Chao, 2005; Wünsch et al., 2011) and the Green's function, furthermore it is generally limited by the coarse resolution of the atmospheric (NWP) model output (typically 6 hour and 0.5 °).

The standard approach (Warburton and Goodkind, 1977; Crossley et al., 2012) to remove an atmospheric pressure signal from ground-based gravity data is through the use of an atmospheric pressure admittance (generally -0.3 μGal/mbar) that is used with observed barometric pressure recorded at the station level, typically adjacent to the gravimeter. This is the approach used in this thesis. Abe et al. (2010) found the classical admittance approach only differed with that of the 2D and 3D approaches (using ECMWF data) at the Moxa SG by 0.4 or 0.5 μGal respectively (RMS over a 4 year period). Abd El-Gelil et al. (2008) calculated a frequency dependant admittance for the Cantley SG and found improved results (reduction of the residuals of 95.4 %) compared with using global atmospheric data (which reduced residuals by 92.2 %), however the frequency dependant admittance only ranged from -0.29 to -0.44 μGal/mbar (for low and high frequency admittance respectively).

In this thesis the SG data at Canberra is assessed for a seasonally varying atmospheric pressure admittance using data recorded by an adjacent barometer. The seasonal variation of the atmospheric pressure admittance at Canberra is considered representative of the field sites used in this thesis (100 km west of Canberra) where ground-based gravity is observed with a Scintrex CG-3M and atmospheric pressure, air temperature, relative humidity, and wind speed are measured adjacent to the gravimeter with a portable weather tracker. The response of the Scintrex CG-3M gravimeter to the meteorological variables measured by the portable weather tracker (excluding wind speed) is also assessed in this thesis (indoors) at both Melbourne and Canberra.

2.4.2 Instrumental Artefacts

Instrumental artefacts are apparent changes in gravity that are present after removing known signals and may be due to the construction or response (to some sort of external forcing) of a particular gravimeter. Instrumental effects are speculative, partly because gravimeters are high precision instruments, and also because typically only one gravimeter is measuring ground-based gravity at a particular location. The discussion is limited in scope to relative gravimeters, such as used in this thesis.

Humidity

Humidity has been known to affect relative gravimeters. In older pendulum type meters it was known to affect the apparent pendulum length (Valliant, 1969a), whereas for the Askania (El Wahabi et al., 2000) and LaCoste and Romberg ET and Model-G meters it has been shown to affect the drift rate (Bastien and Goodacre, 1989; El Wahabi et al., 2000, 2001; Pálinkáš, 2006).

However it is difficult to separate the influence of air temperature and relativity humidity due to the high correlation between the two meteorological signals (with humidity dependant on temperature) (El Wahabi et al., 2000, 2001). While it is not clear if humidity has any impact on the gravity data from a Scintrex CG-3M, the relationship between humidity and gravity is investigated in this thesis at both Melbourne and Canberra.

Temperature

Air temperature has been shown to affect relative gravimeter drift (Gilbert, 1958; Badell et al., 1982; Bonatz, 1987; Ducarme and Somerhausen, 1997; Arnoso et al., 2000), gravity (Torge and Wenzel, 1974; Jentzsch and Melzer, 1989), vertical gravity gradient (Kroner et al., 2002), gravimeter electronics and reference voltage (Ducarme, 1979; Richter and Warburton, 1998), gravimeter tilt (Jentzsch and Melzer, 1989), and post transport stabilisation (Hipkin, 1978).

Similar to humidity, changes in temperature have shown a very strong correlation with gravimeter drift for the older Worden gravimeter (Gilbert, 1958). Note that the Worden design is very similar to the Scintrex CG-3M (Torge, 1989) and this meter also uses a fused quartz sensor that is very sensitive to temperature variations (Weiss and Block, 1970). A noticeable temperature effect was found in the long term drift of a LaCoste and Romberg Model-G gravimeter (Arnoso et al., 2000), with a linear regression coefficient of -32 μGal/°C derived for periods of 15 days. While Ducarme and Somerhausen (1997) found a room temperature increase of 5 °C reduced the drift of a Scintrex CG-3M by increasing the temperature compensation of the gravimeter.

Similarly Badell et al. (1982) found a correlation between LaCoste and Romberg Model-G drift irregularities and room air conditioning defects, specifically the fairly consistent drift of around -5 μGal/day switched sign to a positive drift of around the same magnitude shortly after an air conditioning defect at the Western Venezuelan site. Bonatz (1987) stated that the main source of drift for Askania gravimeters was the response of the sensor to temperature variations, and recommended stabilising the temperature to within 0.1 °C for both the room (the gravimeter is operating in) and the gas volume (internal to the gravimeter) enclosing the gravimeter sensor.

Torge and Wenzel (1974) found a large temperature admittance (-100 μGal/°C) between room temperature and an Askania gravimeter, however the admittance for a LaCoste and Romberg Model-G gravimeter was only 1.9 μGal/°C (with a MSE of 1.2 μGal/°C). Kroner et al. (2002) observed a very strong correlation between temperature and the difference of the gravity from two sensors vertically separated by 20 cm in a dual sensor SG in Moxa, Germany which they attributed to changes in soil moisture (also strongly correlated to air temperature).

Richter and Warburton (1998) found a strong correlation between temperature (of the SG control electronics) and gravity and further hypothesised that temperature would affect the reference voltage of the gravimeter and therefore cause spurious changes in gravity. Ducarme (1979) stated the greatest problem with calibration of a Geodynamics TRG 1 Earth Tides Gravity Meter was the temperature dependence of the (reference) calibration voltage and recommended checking the calibration voltage regularly.

Jentzsch and Melzer (1989) mention observing a strong correlation between air temperature changes and gravity from a LaCoste and Romberg ET Meter, together with correlations between the gravimeter levels, inner and outer (gravimeter) heater temperatures. From this they hypothesised that thermal gradients were deforming the geometry of the gravimeter but admitted further work was required. Hipkin (1978) also hypothesised that thermal gradients inside a LaCoste and Romberg G meter were causing nonlinear (logarithmic) drift after unclamping the gravimeter sensor.

In this thesis the relationship between air temperature, internal gravimeter temperature, gravimeter battery voltage and gravity is assessed for the Scintrex CG-3M gravimeter.

Post Transport Stabilisation

Relative gravimeters exhibit a drift in the reported gravity value due to elastic extension of the spring sensor (spring ageing) that is mostly linear and also a drift due to transportation that combines effects from temperature changes, spring hysteresis (from the meter being off level), battery voltage discharge, and any transportation shocks or vibrations (Timmen, 2010).

Hipkin (1978) found a post transport stabilisation effect of 30 μGal (over 1 hour) for a LaCoste and Romberg G Meter that they attributed to thermal gradients in the gravimeter oven (that houses the gravimeter sensor). Lyness and Lagios (1984) also found a post transport stabilisation effect of 30 μGal (over 1 hour) for a LaCoste and Romberg G Meter. Hamilton and Brulé (1967) stated that the drift of LaCoste and Romberg meters is dependant on the vibrations induced by transport with the meter particularly susceptible to the (resonant) frequency 48 Hz and recommended using a special carrying case to limit vibrations in the range 30-70 Hz. Dragert et al. (1981) used a suspension case for transportation of a LaCoste and Romberg D Meter (designed to minimise vibration), while a spring suspension case (Fig. 2.12) was also used for the international comparison of D Meters (Becker et al., 1987).

Haynes (1999) reported a post transport stabilisation effect for the Scintrex CG-3M of 40 μGal over 20 minutes. Hackney (2001) reported a post transport stabilisation effect for a Scintrex CG-3M of 60 μGal over 20 minutes. Ferguson et al. (2007) report a post transport stabilisation of 10 μGal over 2 minutes for a Scintrex CG-3M. Gettings et al. (2008) fit a (weighted) linear trend to Scintrex CG-3M data 3 to 15 minutes after a reading begins if the post transport stabilisation trend line is greater than 97.2 μGal/hour. McClymont et al. (2012) reported a post transport stabilisation effect for the Scintrex CG-5 of 35 μGal over 7 minutes.

Flach et al. (1993) found that a movable SG had a much larger drift (3 μGal/day) than when it was stationary and that several hours were required post transport for the niobium sphere to stabilise. Consequently this SG, originally conceived as a portable SG, had to be used as a stationary instrument (Jentzsch et al., 1995). Wilson et al. (2012) also observed a large drift rate for an SG deployed in the field (to monitor groundwater) of 0.9 μGal/day, almost 30 times larger than the manufacturers specifications. Van Camp and Francis (2007) also report a strong

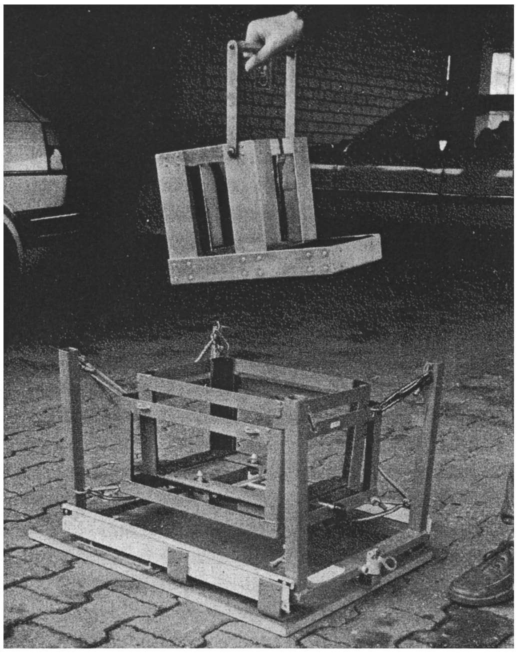

Fig. 2.12 Suspension based transportation device for LaCoste and Romberg D Meter (from Becker et al. (1987)).

transient drift in SGs following installation that may be due to magnetic field or thermal leveller stabilisation.

The post transport stabilisation effect is investigated in this thesis for the Scintrex CG-3M by taking eight measurements of gravity (of approximately 2 minute duration) over a 20 minute period for each gravity observation at a field site. A custom designed suspension case is also constructed and used for vehicular transportation.

2.5 Hydrological Signals in Gravity Data

This section describes studies that have investigated a hydrological signal (in particular soil moisture) in ground-based gravity. The focus of the discussion is on hydrological observations that were compared to gravity observations.

Hydrological signals in ground-based gravity have mostly been investigated at the 25 superconducting gravimeter (SG) sites that form the Global Geodynamics Project (GGP) (Crossley et al., 1999; Meurers, 2001a; Crossley and Hinderer, 2009) (Fig. 2.13), where the hydrological signal must be removed from the ground-based gravity data to investigate small geophysical signals in the gravity residual. The

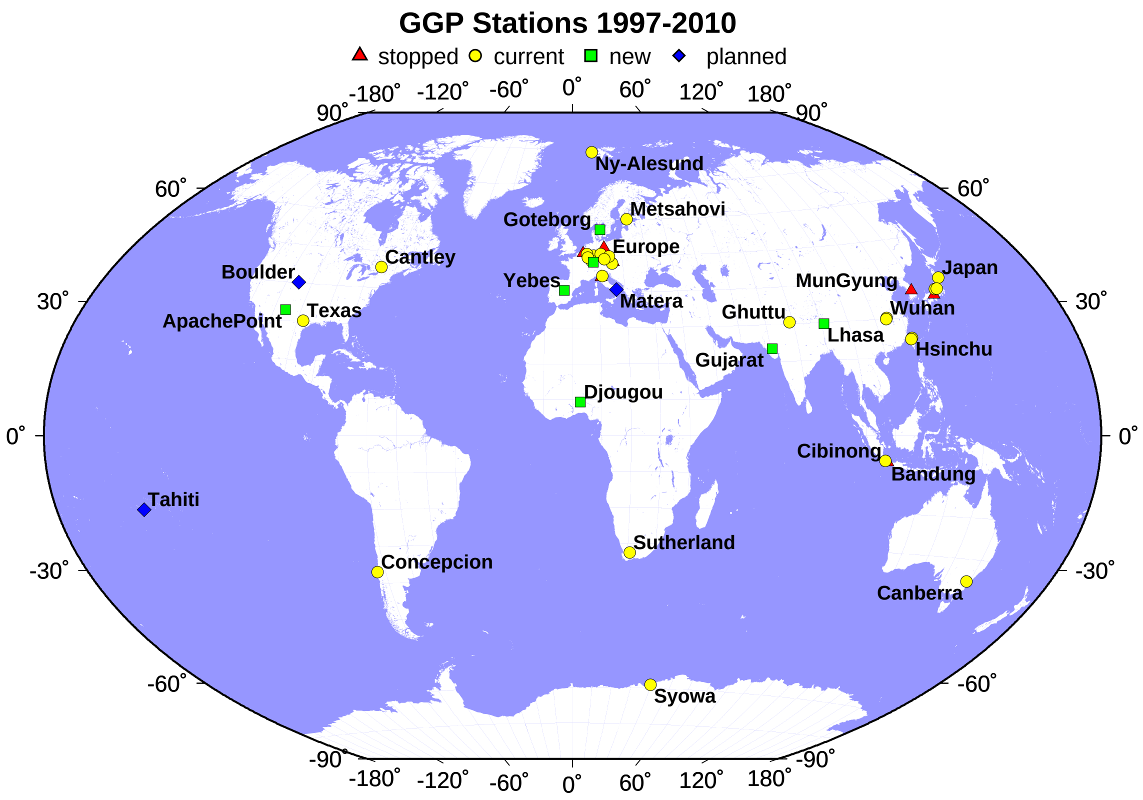

Fig. 2.13 Global Geodynamics Project (GGP) network of superconducting gravimeters (for 1997–2010). Blue, green, yellow and red are planned, new, continuing and discontinued sites respectively (from `http://www.eas.slu.edu/GGP/ggpmaps.html`).

gravity data from an SG is initially corrected for earthquakes (using a program such as Tsoft), then the combined effects of Earth tides, elastic Earth response, and ocean tide loading using an Earth tide program such as ETERNA. Polar motion is also considered a long period tide and removed. Finally the atmospheric pressure effect (combined attraction and loading) is removed using atmospheric pressure data. The gravity data after the:

- Earth tide
- elastic Earth response
- ocean tide loading
- atmospheric pressure attraction and loading, and
- polar motion

effects are removed is referred to as a gravity residual. It is the gravity residual that is compared to hydrological data to determine whether a hydrological signal is detectable in the ground-based gravity data.

Most often the SG gravity residual is compared to precipitation or groundwater level data. Only a handful of studies have observed both soil moisture and ground-based gravity and none have observed the total terrestrial water storage from the surface to groundwater.

The studies that have observed both soil moisture and gravity have mostly been at SG observatories:

- Potsdam, Germany (Kroner and Jentzsch, 1998)
- Richmond, Florida (Peter et al., 1994)
- Bandung, Indonesia (Abe et al., 2006)
- Matsuhiro, Japan (Imanishi et al., 2013)
- Strasbourg, France (Longuevergne et al., 2009)
- Membach, Belgium (Van Camp et al., 2006b)
- Wetzell, Germany (Harnisch and Harnisch, 2002; Klügel et al., 2006; Creutzfeldt et al., 2010a,c,b, 2012)
- Moxa, Germany (Kroner, 2006; Kroner et al., 2007; Krause et al., 2006, 2009).

A limited number of field studies (generally using portable relative gravimeters) have investigated soil moisture signals in ground-based gravity. In a single study an absolute gravimeter was used at an observatory on Asama Volcano, Japan (Kazama and Okubo, 2009). While in two investigations a portable relative gravimeter was used at flat, grass covered, experimental hydrological field sites in Finland and Norway. The experimental field sites had sandy soils and a shallow (monitored) groundwater level (Mäkinen and Tattari, 1988, 1991a,b) or deeper unobserved groundwater (Christiansen et al., 2011b).

All previous studies have investigated soil moisture and ground-based gravity changes at a single site, except Mäkinen and Tattari (1991a,b) who investigated changes at two sites. In this thesis terrestrial water storage (TWS), including soil moisture (from the surface to the groundwater level), and groundwater level is compared to ground-based gravity observations at 4 sites in a temperate climate (without a TWS component of snow). Moreover, all gravity and hydrology observations at a site are made at the same time and location (within 2 m).

2.5.1 SG Sites

Goodkind (1979) stated the importance of monitoring groundwater when observing gravity. Earlier studies of the effects of hydrological changes on gravity were almost all exclusively in the form of groundwater (or rainfall) correlated with continuous SG measurements (Goodkind, 1986; Richter et al., 1995a; Mukai, 1997; Takemoto et al., 2002). Initial studies focused on finding a groundwater admittance (similar to an atmospheric pressure admittance), using an additional time series (observed at the site) of groundwater level (or simply precipitation) to remove the hydrological signal in SG gravity data (Bower and Courtier, 1998; van Dam and Francis, 1998; Harnisch and Harnisch, 1999).

Goodkind (1986) found 1 hour cumulative rainfall gave an increase in gravity at a SG in California of 0.54 μGal/cm. The authors claimed that there was negligible runoff at the site and that groundwater flow from the upslope contributing area of the catchment caused the greater value of 0.54 compared to the theoretical Bouguer slab approximation of 0.42 μGal/cm (Eq. 2.10). While this is certainly possible, there was no hydrological supporting data.

Crossley et al. (1998) developed a groundwater model with rainfall input. The model had recharge and discharge parameters that were calibrated to the continuous SG gravity data via a Bouguer slab approximation. The model was calibrated on the first 200 days of SG gravity residual data and validated over 2 years (including the calibration period). The prediction was good for the calibration period (as would be expected) but very poor for the validation data. There were no piezometers available to validate the groundwater level prediction, so it may have been that the Bouguer slab approximation was sufficient but the groundwater model required improvement.

Other models (with rainfall input) have been used to estimate groundwater (Bower and Courtier, 1998; Imanishi et al., 2006; Lampitelli and Francis, 2010) or soil moisture (Peter et al., 1994; Crossley et al., 2006; Meurers et al., 2007) storage, and convert this to gravity with a Bouguer slab approximation or layer of constant thickness for each cell of a digital elevation model (Meurers et al., 2007). These conceptual models used to correct the SG residuals for hydrological signals were calibrated to the SG residual.

Sutherland, South Africa

The SG at Sutherland, South Africa is 200 km from the Atlantic Ocean at an elevation of 1800 m (Neumeyer et al., 2001). Groundwater level was measured 2 km from the SG together with observations from a weather station at the SG (rainfall, air temperature, pressure, humidity, wind speed and direction). When using the model of Crossley et al. (1998) (and observed rainfall), gravity residuals were not correlated (coefficient 0.04) with the modelled gravitational effect of groundwater (Harnisch and Harnisch, 2006a). Furthermore (observed) groundwater level was only weakly correlated (coefficient -0.22) with the gravity residuals (Harnisch and Harnisch, 2006a).

The poor correlation between observed gravity and groundwater level may be due to the distance from the SG to the piezometer (2 km). In this thesis the piezometer at each of the field sites is located within 2 m of the (Scintrex CG-3M) gravimeter.

MunGyung, Korea

At MunGyung, Korea a borehole was drilled only 3 m from the SG to monitor groundwater level (Kim et al., 2009). The SG is located 108 m above sea level on limestone bedrock. Kim et al. (2009) calculated a groundwater admittance of 0.29 μGal/m with a maximum groundwater level variation of 2.7 m, corresponding to a maximum gravity variation of 0.7 μGal. The groundwater level mostly ranged from 1-3.5 m below the surface but the correlation with the gravity residuals was poor. Kim et al. (2009) concluded a local hydrology model was required around the SG site together with further observations of precipitation, groundwater level and soil moisture at representative locations. In this thesis, precipitation, soil moisture and groundwater level are all monitored at each of the field sites, together with ground-based gravity (from a Scintrex CG-3M).

Potsdam, Germany

Neumeyer (1994) determined a groundwater admittance of 7.1 μGal/m based on 468 days of groundwater level and gravity data at Potsdam, Germany. The admittance (linear regression coefficient) was calculated using a gravity residual after correction of the gravity for Earth tides, polar motion and atmospheric pressure effects.

Neumeyer and Dittfeld (1997) determined a much larger admittance of 15.2 μGal/m (±8.0 μGal/m with a correlation coefficient of only 0.57) using multiple regression of Earth tide corrected gravity, predicted polar motion, atmospheric pressure and groundwater level (over three years), but stated the value should be interpreted cautiously (due to the low correlation) and did not use the groundwater admittance for further analysis. They concluded a network of groundwater measurement points was required around the gravimeter for a hydrologically representative result. Indeed, water level variations occurred 50 m below the gravimeter (Dittfeld, 2000) and were only measured once a month (Dittfeld, 2001).

Kroner and Jentzsch (1998) found a high correlation between gravity (after correction for air pressure) and soil moisture of 0.67 over only 60 days. It is not clear how the soil moisture was measured. Using only 660 days of data but the same groundwater level observations 200 m from the Potsdam SG, Neumeyer et al. (1999) calculated a groundwater level admittance of 2.5 μGal/m, corresponding to a maximum effect of 1.4 μGal (or 0.56 m of groundwater level variation) and had a correlation coefficient with gravity of only 0.4. Neumeyer et al. (1999) state that the aquifer was not well known and the modelling assumption (linear response of gravity to groundwater level variations 200 m from the SG) may be incorrect. Further investigations are not available as the Potsdam SG was decommissioned in 1998 (Dittfeld, 2000).

In this thesis a groundwater admittance is not calculated, rather groundwater level increases are converted to mass changes, using maximum observed soil moisture as an estimate of saturation. Soil moisture from the groundwater level to the surface is also observed and converted to a terrestrial water storage mass. The gravitational effect of the (terrestrial water storage) mass changes are modelled with a Bouguer slab approximation (e.g. Eq. 2.9).

Bad Homburg, Germany

Harnisch et al. (2006) found annual variations in the residual gravity from the SG at Bad Homburg, Germany. These annual variations correlated well with groundwater level variations in three locations, particularly the shallow groundwater level only 2.5 m below the surface measured weekly 3.5 km from the gravimeter as well as hourly 200 m from the SG. The correlation with the deeper groundwater level (12.5 m below the surface) only 110 m from the gravimeter (at hourly resolution) was not as good, with a suggestion this may have been a confined aquifer. Furthermore the annual range of the shallow groundwater levels were around 0.7 m whereas the annual range of the deeper groundwater level was 1.4 m. A groundwater admittance of 2.8 μGal/m was determined for the deeper groundwater level 110 m from the SG and 5.0 μGal/m for the shallow groundwater level 200 m from the SG. Both groundwater admittances reduced the variation of the SG residual after correcting for groundwater levels, however using the shallow groundwater level gave more reduction of both the long term (annual) and short term (monthly) variation. In this thesis the piezometers are only 10 m deep (and represent an unconfined aquifer), with observed groundwater level within 4 m of the surface.

Medicina, Italy

The SG at Medicina, Italy is located on the Po River Plain, with groundwater level monitored 700 m from the gravimeter (Schwahn et al., 2000). After correcting for Earth tides, atmospheric pressure and polar motion, unexplained annual oscillations were present in the residual gravity (Schwahn et al., 2000; Zerbini et al., 2001, 2002). A clear response to rainfall is seen in the gravity residual for some events but not others. Schwahn et al. (2000) conclude further investigations are needed.

The groundwater level was measured every 30 minutes with the water level ranging from about 20 cm to 2 m below the surface with a clear annual variation (Zerbini et al., 2001). A groundwater level admittance of 2.2 μGal/m was calculated using only the groundwater level data to 1 m depth below the surface, when the groundwater level was below 1 m depth no groundwater correction was used (effectively a groundwater admittance of 0 μGal/m). Zerbini et al. (2002) conclude that in-situ environmental observations are needed to model the seasonal effects properly. Using more groundwater level data the groundwater level admittance was calculated to be 4.3 μGal/m (Romagnoli et al., 2003). An attempt to model the annual oscillations in the gravity residual was made by considering thermal expansion of the GPS antenna and concrete pillar, and soil consolidation due to a falling water table, however the maximum water table depth was only 2.3 m (Romagnoli et al., 2003).

The annual oscillations in gravity at Medicina, Italy correlate quite well with the annual oscillations at Bad Homburg, Germany with both SGs located above the ground surface (Crossley et al., 2006; Longuevergne et al., 2009).

The unexplained annual oscillations at both Bad Homburg and Medicina may be due to (unobserved) soil moisture changes. In this thesis, gravity data (from a Scintrex CG-3M) corrected for Earth tides, atmospheric pressure, polar motion, and ocean tide loading is compared to observed soil moisture (and groundwater level) variations at field sites, with the gravimeter above the surface and within 2 m of the groundwater level and soil moisture monitoring.

Richmond, Florida

Peter et al. (1994) measured rainfall, groundwater and soil moisture adjacent to an SG near Miami, Florida for 1.5 years. The Richmond site, 10 km south of Miami, consists of very porous, coralline limestone in the upper 10 m of the profile with a thin cover of sandy soil. There were frequent storms in the summer with rainfall rates in excess of 5 cm/hour and minimal runoff (due to negligible slope), resulting in ponded rainfall that quickly infiltrated the subsurface.

Rainfall was measured (at 2 minute resolution) together with (hourly) groundwater level at four 10 m deep wells within 10-100 m of the SG (Peter et al., 1994; Harnisch and Harnisch, 1995). The groundwater level ranged from 2.7-3.8 m (Peter et al., 1994) with a difference of groundwater level between the four wells of only 1 cm (Harnisch and Harnisch, 1995). Soil moisture was measured (weekly) with a neutron moisture meter (NMM) at an access tube adjacent to the SG building, about 3 m from a groundwater well. Soil moisture was measured from 0.25-2.75 m depth at 25 cm intervals with an observation time of 1 minute (with both descending and ascending measurements taken). Soil moisture ranged from 10-35 % vol/vol and generally increased with depth. The internal calibration of the NMM was used to convert neutron counts to soil moisture. An attempt was made to calibrate the NMM with gravimetric soil moisture samples taken at 50 cm depth each time the NMM was used, but the brittle limestone crumbled with sampling.

In this thesis rainfall is measured at each site at 1 s resolution, groundwater level is also observed at each site (20 minute resolution) with a single well to approximately 10 m depth. The piezometer is also used as an access tube to measure profile soil moisture (every 30 cm) with an NMM, from 12 cm depth to the groundwater level, with descending and ascending measurements. In this thesis the NMM count ratio is calibrated to three soil moisture sensors in the top 90 cm of the profile (calibrated in a laboratory using the site soil). The soil moisture sensors are also verified in the field using 30, 60 and 90 cm time domain reflectometry (TDR) measurements of soil moisture at the time of the NMM (and gravity) observations.

Peter et al. (1994) found a seasonal change in groundwater level of 0.5 m (3.1-3.6 m) corresponded to a gravity variation of 9 μGal, whereas a seasonal change in soil moisture of only 3 % vol/vol (24-27 % vol/vol) corresponded to a gravity change of 1 μGal. A short term increase in groundwater level of 1.1 m resulted in the largest observed gravity change of 20 μGal. Specific yield of the aquifer was calculated using the observed groundwater level and a Bouguer slab approximation (Eq. 2.10) for the gravity effect of the groundwater level change (i.e. a 42 μGal/m groundwater level admittance). This corresponded to an estimate of specific yield of 43 %, which is in agreement with both the maximum and seasonal effect of groundwater level on gravity. The specific yield of the Biscayne Aquifer at this location was determined independently via a canal drawdown test (Bolster et al., 2001) and found to be between 0.050 and 0.57 (dependant on the piezometer tested), so the calibrated value of 0.43 using gravity and groundwater level is not unreasonable.

The response of gravity to rainfall was almost instantaneous, with a typical increase after a storm of up to 7 μGal (Peter et al., 1994), but the groundwater level response was delayed by several hours (Harnisch and Harnisch, 1995). Harnisch and Harnisch (1995) claim the instantaneous gravity response to rainfall is due to the gravitational effect of soil moisture. Peter et al. (1994) found that rainfall events less than 5 mm produced no gravity change, whereas rainfall events of 5-50 mm had an admittance similar to a Bouguer slab approximation for soil moisture based on all rain infiltrating (i.e. 0.42 μGal/cm rainfall admittance, Eq. 2.9). Peter et al. (1994) also found larger rainfall events (from 50-180 mm) had a much lower admittance and resulted in gravity changes of only 2-4 μGal, which they interpreted as the soil moisture being saturated (and rainfall ponding on the surface).

Peter et al. (1994) developed an event based empirical model of soil moisture using observed rainfall that consisted of two exponential functions representing small and large rainfall events, and a decay function that drained the soil moisture completely after around 15 days. The three parameters in the model were fit to gravity residuals (using a Bouguer slab approximation for the gravity effect of soil moisture) for several rainfall events. The modelled soil moisture was reinitialised to the soil moisture observed by NMM every week. The model (incorporating soil moisture observations) was used to correct the SG gravity for a hydrological (terrestrial water storage) signal. Peter et al. (1994) conclude more frequent soil moisture observations would have improved the soil moisture model and understanding of the local hydrology and its effect on gravity. In this thesis (0-90 cm) soil moisture is observed at each of the (gravity) field sites every 20 minutes. Groundwater level is also observed every 20 minutes, and rainfall every second.

Bandung, Indonesia

Takemoto et al. (2002) installed piezometers near the SG at Bandung, Indonesia to determine the effect of groundwater changes on gravity. The groundwater level variations were measured (with a pressure transducer) at subdaily resolution in a well approximately 200 m from the SG. Groundwater level increases of 1 m were shown to correlate well to a 4.2-4.4 μGal increase in the gravity residual 13-20 days later. This magnitude of gravity change is well explained by the Bouguer slab approximation with a porosity of 10 % (Eq. 2.10). However why there should be a lag between the change in groundwater level and the gravity residual was not readily apparent.

Soil moisture monitoring equipment and also a rain gauge were installed at the site in order to further assess hydrological influences on gravity. Abe et al. (2006) found that gravity changes immediately after rainfall due to soil moisture storage above the SG are opposite in sign to later groundwater changes below the SG. Specifically short term (6 hour) decreases in gravity were associated with rainfall events, with a gravity decrease of 0.4 μGal predicted from (modelled) soil moisture changes above the gravimeter (that is 2.7 m below the soil surface). The modelled soil moisture was verified with observed soil moisture at 30, 60 and 90 cm depths. In this thesis soil moisture is observed (every 20 minutes) at each of the field sites at 0-30, 30-60 and 60-90 cm depth, with the gravimeter above the soil surface.

Vienna, Austria

Similar to the SG at Bandung, Indonesia, the SG at Vienna, Austria is located 8 m below the surface (Meurers, 2006; Longuevergne et al., 2009), and rainfall events correspond to decreases in the gravity residual (Meurers, 2000, 2001b, 2004; Meurers et al., 2007). The gravity actually begins decreasing 10 to 20 minutes before the rainfall event (Meurers, 2000, 2001b, 2004; Meurers et al., 2007), with an identical effect observed by a LaCoste and Romberg D Meter that was observing synchronously to the SG (Meurers, 2004). While Meurers (2000, 2001b, 2004) and Meurers et al. (2007) attribute this to either vertical air mass redistribution or vertical water mass redistribution (both due to convective rainfall events), it could be due to the precipitation gauge (used for the SG) inadequately representing the local areal rainfall (and consequent soil moisture and ponding). Furthermore the decrease in gravity prior to precipitation could be due to local meteorological effects during the rainfall events such as convection (Meurers, 2000, 2001b; Meurers et al., 2007) or the passage of a cold front (Müller and Zürn, 1983). Indeed the rapid decreases in gravity prior to rainfall events are shown to correlate well with sudden drops in air temperature, together with air pressure (Meurers et al., 2007).

A fairly robust rainfall admittance of 0.025 μGal/mm was calculated for rainfall events greater than 5 mm (Meurers et al., 2007), that corresponded to about a 0.8 μGal reduction in gravity following a 30 mm rainfall event. Hydrological monitoring equipment was not installed at the Vienna SG (Harnisch and Harnisch, 2006b), however the gravity residual correlated well on an annual scale with groundwater level observations in the valley below the gravimeter and also Global Land Data Assimilation System (GLDAS) modelled soil moisture (Crossley et al., 2006).

Matsuhiro, Japan

The SG at Matsuhiro, Japan is also situated below the surface (30 m) in a tunnel dug into the side of a mountain (Imanishi et al., 2006). A 1.4 μGal decrease in gravity over one hour was shown to coincide with a 38.5 mm rainfall event (Imanishi et al., 2006). Similarly, Nawa et al. (2009) show a 1.5 μGal decrease in gravity following about 30 mm of rainfall at the SG at Inuyama, Japan that is also installed in a tunnel, 40 m below the surface. Imanishi et al. (2013) installed a weather station at the top of the mountain to complement the weather station near the entrance to the tunnel, a soil moisture sensor at 15 cm depth at the top of the mountain, and a rain gauge in the tunnel to measure drips from the roof of the tunnel (40 m below the surface) roughly 3 hours after a rainfall event. They analysed the water budget of the mountain the Matsuhiro SG is installed in (Mt. Maizuru) and concluded that soil moisture storage at the surface of the mountain was causing the gravity changes.

Concepción, Chile

The SG at Concepción, Chile is located on a hill in one of the most seismically active areas of the world, with the largest ever recorded earthquake (9.5 in 1960) occurring only 150 km south of the SG (Wilmes et al., 2006). The BioBio River is located only 2 km west of the SG and joins the Pacific Ocean after only 10 km. To control erosion the SG is surrounded by small Eucalyptus trees and boulders embedded in clay soil.

After removing Earth tides, atmospheric pressure, polar motion and an additional annual sinusoidal signal (with an amplitude of 6 μGal) the gravity residuals correspond well with the modelled effect of hourly rainfall (measured 100 m from the SG) using the two parameter conceptual model of Crossley et al. (1998). The cause of 6 μGal annual component in the gravity residual is not known, with groundwater data not available around the SG, but the nearby BioBio river varies annually by 2 m in height and 1.5-2 km in width (Wilmes et al., 2006).

Walferdange, Luxembourg

Similar to the SG at Concepción, Chile, the SG at Walferdange, Luxembourg is located approximately 2 km to the east of a river (Lampitelli and Francis, 2010). Like many other SG sites in the GGP network (Fig. 2.13) the gravimeter is at the end of a 800 m tunnel cut in the side of a hill and is located 80 m below the surface. The gravimeter is 295 m above sea level and approximately 50 m above the Alzette River. Lampitelli and Francis (2010) use a tank model similar to Imanishi et al. (2006) to estimate groundwater storage based on precipitation input. Similar to Meurers et al. (2007), the groundwater storage is converted to gravity for each cell of a DEM. Using a 20 m resolution DEM Lampitelli and Francis (2010) determined an admittance of 36 μGal/m for the 2 x 2 km area above the SG. This compares to an admittance of 42 μGal/m from the Bouguer slab approximation. Rainfall (1 minute resolution) from a site 1.5 km from the SG was used to drive the tank model of Imanishi et al. (2006), with an additional annual sinusoid fit as part of the gravity recovery after rainfall. The RMS of the gravity residual over 5 years is 1.9 μGal, using the tank model with the annual sinusoid reduced this to 0.9 μGal or 77 % less. However when the tank model was used without an annual sinusoid (as in Imanishi et al. (2006)) the gravity residual was only reduced by 25 %. Lampitelli and Francis (2010) attempt to defend the use of an annual sinusoid on the basis of variability in hydraulic conductivity due to groundwater temperature (and viscosity), infiltration variability due to root zone saturation, evapotranspiration variability due to air and soil temperature, or spatial variability of rainfall. However, similar to the SG at Concepción, which is also located 2 km to the east of a river, the cause of the annual component in the gravity residual is not known. Soil moisture, groundwater and rainfall are not monitored near the Walferdange SG. The annual signal in the Walferdange SG gravity may be due to unobserved soil moisture changes.

River height level from a site 1.6 km from the SG was contrasted with rainfall and gravity changes (for 45 rainfall events ranging from 2-43 mm). It was found that the gravity residual decreased in response to rainfall almost immediately, with an average delay between maximum precipitation intensity and gravity (time derivative) of only 4 minutes. However, the response of the river height level to rainfall was delayed. Consequently the Walferdange SG gravity residuals decreased before the river height levels increased, making correction of gravity residuals by river height level problematic. Although it did indicate a possible novel use of the SG gravity residuals for river level forecasts in this area. However, Lampitelli and Francis (2010) still found that the correlation of the event rainfall and river height level was stronger (0.68 with an admittance of 2.2 cm/mm) than the correlation of gravity changes and river height level (0.59 with corresponding admittance of 45 cm/μGal).

Metsähovi, Finland

The SG at Metsähovi, Finland is located on a small hill on crystalline (granite) bedrock (Virtanen, 2000, 2001; Hokkanen et al., 2006, 2007a), with a thin layer of soil

(Hokkanen et al., 2006, 2007b). The soil is mainly till with a maximum depth of 5 m (average 0.8 m) that increases with distance from the SG, the porosity of the till is 20 % (Hokkanen et al., 2006, 2007a). Groundwater level was observed (every minute) at a 33 m deep borehole 3 m from the SG (Virtanen, 2000; Virtanen et al., 2006). The groundwater level ranged from 5-7 m below the surface and is well correlated (coefficient of 0.83) with the gravity residuals over 11 years (Virtanen, 2000, 2001, 2002; Virtanen et al., 2006). An admittance of 2.0 μGal/m was calculated over almost 2 years (Virtanen and Kääriäinen, 1998) and also 5 years (Virtanen, 2000), and 2.8 μGal/m over 5.75 years (Virtanen, 2001). Correcting the gravity residual for hydrological effects using the groundwater level admittance reduced the RMS of the gravity residuals from 2.1 μGal over 5.75 years to 1.4 μGal. Rainfall was shown to have an immediate influence on the gravity residual (through soil moisture), with a 20 mm rainfall event corresponding to a gravity increase of 1 μGal, whereas the groundwater level response to rainfall was delayed by some hours (Virtanen, 2001). Similarly Virtanen and Kääriäinen (1998) observed a response to rainfall of 2 μGal for a 50 mm event.

A second access tube for soil moisture and groundwater was located 70 m from the SG in a swamp, with a depth of only 1.7 m to bedrock (Hokkanen et al., 2006, 2007b). The surface level of the access tube was around 5.5 m below the SG. The highest groundwater level reached the soil surface, while the deepest groundwater level was below the 1.7 m depth of the access tube. The groundwater level in the deeper piezometer (adjacent to the SG) was correlated to the level in the access tube, with a range of around 6-8.5 m depth. The groundwater level of the two piezometers followed the same annual pattern, and the maximum groundwater level for both was the same (relative to the SG), but the groundwater level in the swamp responded to rain faster, and was generally 50 cm higher than the groundwater level recorded in the well 3 m from the SG (Hokkanen et al., 2006, 2007b). Hokkanen et al. (2007b) attributed the slower rise of the groundwater level in the well near the SG to small bedrock fractures slowing the recharge rate (compared to infiltration of rainfall into the soil around the piezometer in the swamp), however it was also acknowledged that the groundwater level in the swamp represented runoff from a larger area. Only 1.5 years of groundwater level data was available from the second well (Hokkanen et al., 2006) as the swamp dryed up after storms destroyed the forest around the

SG (Virtanen et al., 2006). Subsequently the groundwater level at the borehole next to the SG has risen, and the seasonal variations reduced (groundwater level ranges from 4.5-5.5 m). This also corresponded to much less annual variation in the SG gravity residual. However, the groundwater level was still well correlated with the gravity residual (Virtanen et al., 2006). Virtanen (2000) consider soil moisture changes could be as significant a hydrological signal as groundwater level variations, with an anticipated annual soil moisture signal of up to 10 μGal in Finland, and recommended mapping both terrain and soil moisture to a distance of 100-200 m from the SG.

The height was measured at 2100 points within 100-150 m of the SG and used to create a detailed DEM (Virtanen, 2001). The DEM was then used to calculate the effects of soil moisture or snow around the SG, with a calculated effect of 1.1 μGal for 100 mm water equivalent. Virtanen (2001) concluded snow depth and density should be monitored on the roof of the SG observatory and to a distance of 100 m around the SG, with additional access tubes installed to monitor soil moisture. Virtanen (2001) planned to map the soil depth (to bedrock) for 100 m around the SG with drilling; install additional groundwater access tubes; and study soil moisture with TDR and gravimetric soil samples.

Hokkanen et al. (2006) used both a 100 x 100 m and 200 x 200 m grid around the SG to determine the horizontal zone of influence, but excluded the 10 x 10 m area in the centre of the grid for the SG observatory. A three dimensional polygon model of surface water mass and groundwater mass (on top of bedrock) was created (with a 10 m resolution). It was not clear how the bedrock elevation was mapped. The gravity effect was highest when considering the 200 m area, this is understandable as the SG location is close to the highest elevation in the local area. For the same amount of water, the groundwater effect was stronger than a layer of water on the surface (a proxy for soil moisture) due to the geometry of the local area. For the groundwater mass variations, Hokkanen et al. (2006) found that the Bouguer slab approximation underestimated the gravity effect, by about 50 or 66 % compared to the gravity effect predicted when using a maximum grid extent of 200 or 100 m respectively. While for the surface water mass variations the Bouguer slab approximation was more accurate, and only about 75 or 83 % of the gravity effect of soil moisture (or snow) predicted using a maximum grid extent of 200 or 100 m (respectively). Hence the Bouguer slab approximation is a good approximation for the gravitational effect of soil moisture in the near vicinity (100 m) of the gravimeter. In this thesis the Bouguer slab approximation is used to model the gravitational effect of soil moisture (and groundwater) observed within 2 m of the (Scintrex CG-3M) gravimeter.

A ground penetrating radar (GPR) survey of a 22 x 22 m area around the SG observatory found 6 large fractures in the bedrock below the SG (Hokkanen et al., 2006). The GPR survey observed to a depth of 6 m (Hokkanen et al., 2007a), however the bedrock immediately below the SG could not be observed as reflections in the SG building were poor (Hokkanen et al., 2006, 2007a). An additional structural geology investigation found some vertical fractures (not visible in the GPR data) that were mostly filled (presumably with soil). The fractures were in the order of 2-3 cm (Hokkanen et al., 2006), and mostly open (Hokkanen et al., 2007a). The six fractures detected were extrapolated below the SG building and digitised to six triangulated irregular networks (TIN). Each TIN was offset vertically by 1, 2.5 or 5 mm and the modelled gap assumed to be filled by groundwater. The gravity effect of the groundwater was calculated for different fracture thickness and soil porosity (filling the gap) and found to vary from around 0.03-0.15 μGal for a gap thickness of 1-5 mm (respectively) and a porosity of 30 %.

One of the first investigations into the effect of snow on ground-based gravity was conducted at the Metsähovi SG in Finland. A clear 2.3 μGal increase in the gravity residual was evident when 23 ton of snow was removed from the roof of the SG observatory. The thickness of the snow was 50-70 cm, with a mean water equivalent of 107 mm. The snow effect was verified with a model of the peaked roof using a grid mesh of 50 x 50 x 10.7 cm to cover the 12 x 16 m roof that varied from 2.5-6.5 m above the ground. The snow removed from the roof was also modelled around the SG building at 1 m distance (and 36 cm below the floor). The modelled snow effect around the building after removal from the roof was 0.35 μGal, the modelled effect of the snow when it was still on the roof was 1.95 μGal. The snow on the roof above the SG caused a decrease in gravity, but an increase once it was removed and located around the SG building, so the combined effect was modelled as 2.3 μGal, as observed (Virtanen, 2000). Observed snow depth (40-80 cm, corresponding to a water equivalent of 60-120 mm) at 30 points within 25 m of the gravimeter was extrapolated to 50 m around the SG and used together with a DEM to calculate a gravitational effect of only 0.4 μGal, however the terrain height only varied by 1.5 m (all below the SG). In this thesis snow is not considered as the field sites are located in a temperate climate.

Virtanen (2000) conclude that the performance of SGs make hydrological models necessary and a well equipped gravity station needs mapping of the local terrain and knowledge of local hydrological conditions. Furthermore weather conditions, groundwater level and soil moisture should all be monitored regularly, with the local recharge and discharge mechanism for rainfall and snowfall modelled. Conversely Virtanen et al. (2006) state that gravity data can be used to improve hydrological models of different spatial extent (local, regional and global). In this thesis gravity data is assimilated into a land surface model (that can be run locally, regionally or globally) to improve soil moisture modelling by providing a constraint on the (terrestrial water storage) water balance.

Strasbourg, France

The SG at Strasbourg, France is located in a bunker on a hill, about 10 m underground (Llubes et al., 2004). The elevation of the SG is around 180 m (Amalvict et al., 2006) and groundwater level was monitored every minute (Amalvict et al., 2004) at a well in the bunker (Llubes et al., 2004), with the water level approximately 50 m below the SG (Amalvict et al., 2004), or 60 m below the surface. The groundwater level varied from about 133.7 to 134.2 m elevation over four years with an annual variation of 20-30 cm (Amalvict et al., 2004).

Amalvict et al. (2004) calculated the gravitational effect of the groundwater level using a Bouguer slab model and porosity of 15 % (based on geology) that corresponded to a 1.9 μGal change of gravity for the typical annual change in groundwater level of 30 cm. The predicted change in gravity based on groundwater level variation showed a rough correlation with the SG residuals. Amalvict et al. (2004) concluded the hydrological modelling needed to be improved by considering soil moisture, snow and observed precipitation. In this thesis the hydrological modelling used to retrieve a soil moisture signal from ground-based gravity considers soil moisture, snow and observed precipitation (together with other atmospheric forcing variables such as air temperature, humidity, atmospheric pressure, wind speed and downward short and longwave radiation).

Llubes et al. (2004) stated the difficulty of estimating the soil moisture effect on gravity without any data, and developed a physical model of the gravitational effect of soil moisture based on two half cylinders (extending to infinity), at height 190 m to the east of the SG and 185 m to the west, with an internal radius of 30 m (corresponding to the bunker with an assumption of no soil moisture above or below it). It appears the temporal variation of soil moisture was modelled using the difference of climatological monthly averages of rainfall and evapotranspiration estimated at the airport 10 km from the SG site, together with hydrological knowledge of the soil moisture water holding capacity and annual groundwater recharge. The soil moisture water holding capacity was estimated to be around 17-20 % vol/vol over the top 1 m of soil profile (or 170-200 mm), and recharge to the aquifer around 200 mm/year from a 25 m deep loess layer on top of the local sand aquifer.

Llubes et al. (2004) claimed a good correlation of groundwater level with gravity and determined an admittance of 20 µGal/m and porosity of 40 %, which they admit is probably an overestimate. Harnisch and Harnisch (2006a,b) determined a groundwater admittance of 15.2 µGal/m using 6 years of data. Llubes et al. (2004) modelled an annual signal of amplitude 3 µGal and 1 µGal for groundwater level and soil moisture respectively. The magnitude of the combined gravity effect of the modelled groundwater level and soil moisture (8 µGal) corresponded well to the magnitude of the observed gravity residuals over 3 years (also around 8 µGal) but underestimated an annual peak in the gravity residuals in the last 0.5 year of the record by 4 µGal. Llubes et al. (2004) concluded that there was a lack of adequate environmental data at the local scale and detailed hydrogeological studies needed to be undertaken around the Strasbourg SG, together with monitoring of environmental parameters at a suitable resolution in time and space. They further stated that special attention must be paid to monitoring the unsaturated zone. In this thesis the unsaturated zone is monitored from the surface to the groundwater level. Precipitation and groundwater level are also monitored.

Longuevergne et al. (2009) installed two Sentek EnviroSMART configurable soil water content profile probes around the Strasbourg SG to measure soil moisture at 5 minute resolution. They stated that most of the variation in soil moisture occurred in the top 20 cm of the profile. One soil moisture profile probe was installed in the 1 m thick soil above the gravimeter to measure soil moisture at 10, 20, 30, 50 and 80 cm depths in a single access tube. A second 2 m probe was installed in front of the bunker (the SG is located in) to assess spatial variability of soil moisture and deep infiltration, data from this probe is not discussed by Longuevergne et al. (2009). The soil moisture sensors were calibrated using three gravimetric soil samples taken at the depth of each sensor. The approach of Schwank et al. (2006) was used to convert the raw measurement to a relative permittivity that was then calibrated to volumetric soil moisture (from the gravimetric samples) with a quadratic equation. While not attempted, Longuevergne et al. (2009) mentioned the possibility of calibrating the soil moisture sensors to the gravity data. Longuevergne et al. (2009) stated that in-situ calibration of the soil moisture sensors was necessary for both short term and seasonal soil moisture changes, with the amplitude of the annual variation in some sensors reduced by a factor of three after calibration. However they also stated the calibration of the soil moisture probes was not perfect, and more gravimetric samples should be used to refine the calibration. Moreover the mismatch between the footprint of the soil moisture probes and the gravimeter when measuring soil moisture (approximately 5 cm and 100 m respectively) remained the greatest source of uncertainty (Longuevergne et al., 2009). In this thesis soil moisture is observed within 2 m of the (Scintrex CG-3M) gravimeter with three 30 cm water content reflectometers (Campbell Scientific CS616) vertically installed to measure the 0-90 cm soil moisture and a NMM used to measure the profile soil moisture from the surface to the groundwater level. The NMM is calibrated to the three 0-90 cm CS616 probes, and these probes calibrated in a laboratory with site soil. This work used and contributed to Rüdiger et al. (2010). The 0-90 cm CS616 probe laboratory calibrations are verified in the field with independent observations of soil moisture using 30, 60 and 90 cm long time domain reflectometry (TDR) probes within 2 m of the 0-90 cm CS616 probes.

The soil thickness above the Strasbourg SG (bunker) was determined using applied geophysics prospecting and a dynamic penetrometer (Longuevergne et al., 2009). The SG is located under 1 m of soil followed by 3 m of concrete (the bunker roof). An 80 x 90 m DEM with 25 cm vertical precision was created above the SG through a real time kinematic GPS survey and embedded in a regional DEM to cover the 2 km area around the SG. The gravitational effect of a 1 mm water layer on the DEM was calculated, and an admittance of 30.5 μGal/m determined. From this it was found that the soil moisture integration radius (or footprint) of the gravimeter was around 100 m.

The soil moisture measurements above the SG in the top 1 m of the profile were converted to a terrestrial water storage and multiplied by the soil moisture admittance to create a gravitational soil moisture effect. It was assumed the soil moisture in the top 1 m of the profile at one location was representative of the soil moisture to the SG depth (around 6 m to the gravimeter sensor) and within a 100 m radius of the SG. The groundwater level admittance of Llubes et al. (2004) (20 μGal/m) was used together with a realistic porosity (not stated by Longuevergne et al. (2009)) and observed groundwater level (50 m below the SG) to model both the groundwater and all soil moisture in the 50 m vadose zone below the gravimeter. The magnitude of the gravity effect of the modelled groundwater level (7 μGal) corresponded well with the magnitude of the observed gravity residuals over 6.25 years (around 9 μGal) but again (similar to Llubes et al. (2004)) for the year 2007 an annual peak in the gravity residuals in the last 0.5 year of the record was underestimated by 4 μGal. Furthermore, the annual peaks in groundwater level only clearly corresponded to the annual peaks in gravity for the two wettest years where both groundwater level and gravity were highest, and for these years the gravity peak was maintained for months (with weekly variations of 1 μGal) whereas the groundwater level peak was in the order of days. Furthermore the groundwater peak preceded the gravity peak for these wettest years. This could be explained by a drying of the soil moisture after the groundwater level has peaked that continues to increase the gravity.

Amalvict et al. (2006) presented a reasonable agreement between gravity residuals and the gravitational effect of modelled soil moisture (they stated snow was negligible) from the LaD model and GLDAS, with LaD capturing the linear trend and increase in gravity residuals of 10 μGal over 6 years (GLDAS only modelled the last 2 years of data). Crossley et al. (2006) also demonstrated a good agreement between GLDAS and gravity residuals over 3.5 years, and stated the correlation coefficient of groundwater level with gravity at Strasbourg (over the same period) was only 0.05 and the groundwater level appeared to have little relation with either the modelled hydrology or the observed gravity. The GLDAS gravity effect was well anti-correlated with the SG residuals over 6 years (Longuevergne et al., 2009). There was some correspondence of the SG residual with the gravity effect calculated from the soil moisture observations (above the SG), particularly when gravity was decreasing from an annual peak (i.e. the surface soil moisture probes were showing increasing soil moisture above the gravimeter), however the observed soil moisture covered less than 2 years (Longuevergne et al., 2009). There appears to be a complex interaction between soil moisture above (and adjacent to) the gravimeter, soil moisture in the 50 m vadose zone below the gravimeter and the groundwater level below that. Longuevergne et al. (2009) conclude that further work should focus on the estimation of the soil moisture below the gravimeter. In this thesis soil moisture is observed from the surface to groundwater level, with groundwater level (and precipitation) also observed, and the (Scintrex CG-3M) gravimeter measuring gravity above the soil surface.

Membach, Belgium

The SG at Membach, Belgium is also located underground, 48 m below the surface (Meurers et al., 2007), at the end of a 140 m tunnel cut into a hill (Francis et al., 2004). Similar to other SG sites, a large annual oscillation is observed in the gravity residual of the Membach SG, but the amplitude varies each year. When an annual sinusoid was fit to the residuals the amplitude was 3 μGal. The annual amplitude of the gravity signal computed from the LaD model was also 3 μGal (Francis et al., 2004), and the Membach SG gravity residuals were correlated with GLDAS modelled soil moisture at the annual scale (Crossley et al., 2006). Similar to the Vienna SG, Meurers et al. (2007) determined a strong rainfall admittance of 0.039 μGal/mm for rainfall events greater than 10 mm that corresponded to a 1.2 μGal reduction in gravity following a 30 mm rainfall event.

The gravity residuals were anti-correlated (over almost 5.5 year) with two water storage reservoirs (capacities ranging from 10-25 Gl) located 3 and 6 km from the SG. The loading and Newtonian mass effect of the reservoir 3 km from the SG was calculated for a storage change of 10 Gl assuming a point mass reservoir and found to be only 0.02 μGal and 0.2 μGal respectively, much less than the 3 μGal annual signal present in the gravity residual. Furthermore, the gravity residuals decreased hours after significant rainfall (with the maximum decrease of 4 μGal corresponding to 150 mm precipitation over 3 days), and then slowly (days later) returned to levels prior to the rainfall, whereas the reservoir storage increased and remained at the higher level. Consequently the correlation of the reservoir storage level with the gravity residual may in fact be due to a correlation of the gravity with soil moisture and possibly groundwater. Francis et al. (2004) recommended the installation of a shallow monitoring well above the gravimeter.

Geological investigations have indicated there is no aquifer near the Membach SG, with the effective porosity of the argillaceous sandstone 1 %, and the saturated hydraulic conductivity only 10^{-11}-10^{-8} m/s (Van Camp et al., 2006b). Furthermore a NMM access tube could not be installed in the silty soil 48 m above the gravimeter, and gravimetric soil moisture measurements could not be made below 60 cm as the gravel (sandstone block) content increased with depth, making hand digging or coring impossible below 1 m (Van Camp et al., 2006b). Indeed two soil samples contained gravel contents (particle diameter greater than 3.1 cm) of 27 and 53 %. Consequently Campbell Scientific CS616 water content reflectometers were (horizontally) installed above the gravimeter at depths of 30, 35, 50 and 60 cm below the soil surface to measure soil moisture every hour. The water content reflectometers were calibrated to 5 gravimetric soil samples (covering the range 10-25 % g/g) taken from depths 20-30, 40-50 and 60-70 cm, at a distance 10 m from the CS616 probes. A linear calibration was derived as insufficient samples were available for a quadratic calibration. Gravel content was removed from the gravimetric samples prior to oven drying, with the assumption that water content of the gravel (and sandstone blocks) did not vary. Consequently bulk density of the gravimetric samples was not used and the water content reflectometers were simply calibrated to gravimetric water content and used to measure gravimetric water content, not volumetric water content. In this thesis soil samples from the (gravity) field sites are used in the laboratory to calibrate the CS616 soil moisture sensors to multiple water contents (and soil temperatures). The calibration procedure is described in Rüdiger et al. (2010) and in Appendix C.

Electrical tomography and seismic refraction profiles were used to determine a weathered zone above the bedrock that varied in thickness from 1-8 m within a 100 m radius of the SG, with an average thickness of 3.4 m (Van Camp et al., 2006b). The weathered zone consisted of silty soil with a gravel content increasing with depth. The 13 seismic refraction profiles around the SG were used together with a DEM to calculate a 200 x 200 m grid above the SG with variable depth (and height) of 5 m (lateral) resolution cells. The gravitational attraction of each cell was calculated assuming a uniform vertical soil moisture content in the cell based on the average soil moisture from the four water content reflectometers installed above the Membach SG. It is doubtful the 30-60 cm average soil moisture would accurately reflect the 0-8 m average soil moisture, and indeed 65 % (or 1040) of the cells have a depth greater than 1 m. Further, a single bulk density of 1470 kg/m^3 was calculated from a soil sample taken 30-60 cm below the soil surface, 10 m from the soil moisture probes. This was used together with a (gravimetric) estimate of the percentage of particles smaller than 3.1 cm to convert the gravimetric soil moisture (from the 4 water content reflectometers) to a volumetric soil moisture for each cell. Despite using observed soil moisture and bulk density in the top 1 m of the soil profile at one location to estimate soil moisture to a depth of 8 m over a 40000 m^2 area at a 5 m resolution, the soil moisture correction significantly reduced the seasonal variation of the Membach SG gravity residuals (over 14.5 months) from 1.5 μGal to 0.03 μGal (Van Camp et al., 2006b).

Wetzell, Germany

The SG at Wetzell, Germany is a dual sphere SG, with the spheres vertically separated by 20 cm (Richter and Warburton, 1998; Harnisch et al., 2000). The SG is located on a flat mountain top in the Bavarian Forest, surrounded by grassland and bushes (Klügel, 2002; Creutzfeldt et al., 2010b, 2012), with weathered gneiss (metamorphic crystalline bedrock) below the station (Harnisch and Harnisch, 1999). The upper 2 m of the profile is sandy loam (caused by total decomposition of the bedrock), followed by boulders up to 1-2 m in size, then a smooth transition from weathered bedrock to solid rock below 7-14 m (Klügel, 2002). The solid rock has faults (Harnisch and Harnisch, 1999) and fractures (Klügel, 2002). The sandy loam has low permeability, the weathered and partly weathered bedrock medium permeability (except the boulders were permeability is negligible), while the fractured bedrock has a highly variable permeability (Klügel, 2002).

Harnisch and Harnisch (1999) presented a rise in the gravity residual of around 0.5 μGal after a rainfall event of 24 mm over 15 minutes. This rise was predicted well with the model of Crossley et al. (1998). A positive correlation was found between absolute gravity measurements (from an FG5) and groundwater level (over 2 years), with a groundwater level admittance of 6.9 μGal/m calculated for the FG5 (Harnisch and Harnisch, 2002).

Groundwater level was measured at four bores 150-250 m from the SG, with the groundwater level height and temporal variation at each location reasonably different (Harnisch and Harnisch, 2002). At the closest bore to the SG, groundwater level varied from around 3.5-7.5 m depth with an annual signal evident and a peak around early spring. Soil moisture was measured about 20 m from the SG at 50 cm depth with a TRIME-EZ probe. There was not a clear correlation of groundwater level (over 3.25 years) or soil moisture variations (over 1.25 years) with the SG gravity residual (Harnisch and Harnisch, 2002), regardless Harnisch and Harnisch (2006a) determined a groundwater level admittance of 5.2 μGal/m (for the SG) after first applying a 30 day moving average to the groundwater level data (to remove spikes in the groundwater corrected gravity residual). When the correction was applied the range of the SG residual was halved, from about 20 μGal to 10 μGal over 5 years (Harnisch and Harnisch, 2006a), or 30 μGal to 15 μGal over 6 years (Klügel et al., 2006).

Klügel et al. (2006) attempted to measure integral soil moisture variations on a 50 m profile adjacent to the piezometer 150 m from the SG. There was a loose correlation with groundwater level and soil moisture observed by TDR (over 35 days), but not a good correlation with the gravity residuals. Klügel et al. (2006) conclude the method may be inadequate, but regardless the integral soil moisture monitoring should be closer to the SG and soil temperature should also be observed to correct diurnal oscillations in the soil moisture measurement. In this thesis, soil moisture is monitored from the surface to the groundwater level (together with groundwater level and rainfall), within 2 m of the (Scintrex CG-3M) gravimeter. Additionally soil temperature is monitored (every 20 minutes) to correct the diurnal oscillations in the 0-90 cm soil moisture measurement from three Campbell Scientific CS616 water content reflectometers (Rüdiger et al., 2010; Smith et al., 2012).

Creutzfeldt et al. (2008) investigated the gravity effect of terrestrial water storage changes using a DEM and assuming the TWS changes are distributed uniformly across every grid cell, and also uniformly to the same depth (1 m) within every grid cell. They used the MacMillan equation from Leirião et al. (2009), with nested (square) domains around the SG with a radius (half length of square) of 50 m, 0.5 km, 2 km, 5 km and 10 km, and corresponding DEM grid cell resolutions of 25 cm, 2.5 m, 10 m, 25 m and 50 m. The 25 cm resolution DEM was derived from a differential GPS survey of 14000 points within 300 m of the SG. Creutzfeldt et al. (2008) found that for a domain of 20 x 20 km with the SG at the centre, 1 m of water under the surface (in the top 1 m of soil) caused a gravity change of 41.9 μGal (exactly the same as the Bouguer slab approximation) when the topography is flat, and 52.49 μGal when the nested DEM was used. However when the 1 m of water was removed from the (1.4 x 1.4 m, and 1.2 m deep) area covered by the SG concrete foundation, the gravity change using the DEM dropped by 8.47 μGal (down to 44.02 μGal and again close to the Bouguer slab approximation). Clearly the soil moisture directly below the SG (and within 1.5 m of the SG) is a very significant portion of the total hydrological signal in gravity. Indeed Creutzfeldt (2010) conclude that the hydrological signal from directly under the gravimeter (and within a 2 m radius) is one of the most important areas of future research need, and suggest it could be studied by minimising the impact of the gravimeter surrounding on the hydrological system, measuring the terrestrial water storage within 2 m of the gravimeter, and ensuring all terrestrial water storage variations occur below the gravimeter. That is the approach followed by Smith et al. (2005, 2006) and in this thesis.

At Wetzell, Creutzfeldt et al. (2008) found that 84-91 % of the hydrological signal came from within 500 m of the SG, while 52-80 % was from within 50 m of the SG (for a depth to terrestrial water storage of 1-20 m, with the deeper mass corresponding to a weaker gravity signal). Similarly (using a comparison of a cylinder to a Bouguer slab approximation) Leirião et al. (2009) concluded that for a flat area 90 % of the gravity signal came from a radius of within 200 m of the gravimeter (when the depth to the mass was 20 m), while Creutzfeldt et al. (2008) found 95 % came from within 500 m and 66 % from 50 m (also for a depth to mass of 20 m). Creutzfeldt et al. (2008) concluded that detailed hydrological measurements were required within 100 m of the SG.

Creutzfeldt et al. (2010a) installed 18 TDR 0-30 cm soil moisture sensors on a 20 m transect (with the most distant probe about 30 m north of the Wetzell SG). Two tensiometers were installed near the soil moisture transect measuring soil suction at 1 and 1.4 m depth (17 m from the SG). Four (vertical) soil moisture profiles were installed using (horizontal) 7.5 cm long TDR probes. Soil moisture was measured at 0.3, 0.4, 0.6, 1, 1.5 and 2 m depths. Two profiles (missing the deep 2 m soil moisture sensors) were located 17 m south of the SG and 1 m apart. The other two of the four profiles were located 6 m south and 17 m north of the SG, with the profile 17 m north at the same location as the two tensiometers (and soil moisture transect). The general calibration of Topp et al. (1980) was used with the TDR probes and all soil moisture measurements were at 15 minute resolution. The soil was classified as gravelly sandy loam (Cambisol) with an average depth of 1.25 m, with saprolite (weathered bedrock) below 1.25 m containing 14 % gravel and 80 % sand. The saprolite saprolite depth was estimated as 11 m, with groundwater in a fractured bedrock zone from 11-19 m depth.

Creutzfeldt et al. (2010a) installed two groundwater bores less than 10 m from the SG with a groundwater level range of 11.5-14.5 m depth, and a correlation of 0.999 over 1.75 years. Using the average groundwater level from the two bores Creutzfeldt et al. (2010a) determined a groundwater level admittance of 2.7 μGal/m, however the correlation with the Wetzell SG gravity residuals was only 0.51. Creutzfeldt et al. (2010a) also installed a snow pillow and ultrasonic distance sensor to measure snow mass and depth. A 2.5 m rise of the groundwater level (over 2 weeks in early spring) occurred after snowmelt of 65 cm of snow (75 mm snow water equivalent), and corresponded to a 6 μGal increase in gravity.

Creutzfeldt et al. (2010a) stated that they were not aware of any studies that have measured all the possible water storages and compared them to a gravity signal. However this was discussed in Smith et al. (2005) and studied by Smith et al. (2006) and this thesis. Creutzfeldt et al. (2010a) proposed a 1D vertical approach (like Smith et al. (2006) and this thesis) on the assumption that hydrological variation is more significant with depth than laterally. Again, like Smith et al. (2006) and this thesis, Creutzfeldt et al. (2010a) estimated the gravity effect of each terrestrial water storage component including: root zone soil moisture, deeper vadose zone soil moisture, groundwater in the saturated zone, and snow (not studied by Smith et al.

(2006) or in this thesis due to the climate of the location). However, unlike Smith et al. (2006) and this thesis, Creutzfeldt et al. (2010a) did not measure the water storage changes in the deeper vadose zone (1.25-11.0 m depth in the profile) between the root zone soil moisture and the groundwater level.

Water storage for the deeper vadose zone was estimated by Creutzfeldt et al. (2010a) by calculating the difference of infiltration from the root zone soil moisture and recharge to the groundwater (in the saturated zone). Infiltration was estimated from Darcy's law with the tensiometers at 1.0 and 1.4 m depth used to estimate the pressure head gradient (deemed applicable for the gradient at 1.25 m depth), and the Van Genuchten (1980) unsaturated hydraulic conductivity (with the Mualem (1976) soil water retention curve). Saturated hydraulic conductivity was calculated as the median of 28 field samples (that varied over four orders of magnitude) using soil cores from 0.6-6.35 m depth (taken from the profile with the tensiometers and drilling from one of the piezometers), together with estimates from a permeameter used at different depths.

Groundwater recharge was estimated using a combination of the master recession curve (to estimate discharge) and water table fluctuation method (to estimate groundwater storage). The master recession curve is calculated by linear regression to give an estimate of the change in groundwater level with time for any given groundwater level. The water table fluctuation method simply estimates groundwater storage as the product of specific yield and change in groundwater level. The specific yield was estimated by a pumping test and two different methods (Jacob straight line and Theis), with the specific yield value an average of four estimates calculated using the two methods on both the groundwater level drawdown and recovery. The calculated groundwater recharge estimates were significantly lower than recharge estimates from other studies calculated for a nearby region. The recharge estimates were also much lower than the estimated percolation into the vadose zone storage from the root zone soil moisture.

The deeper vadose zone (1.25-11.0 m) storage was assumed to be zero at an arbitrary date 5 months before the end of the study period, and also zero at the start of the study (15 months earlier). Moreover, the recharge estimate to the saturated zone (below 11.0 m) was adjusted to match the infiltration estimate from the root zone (at 1.25 m depth) by using a specific yield much larger (three times) than obtained with the pump test (that obtained five specific yield estimates for the saturated zone). It is not clear why these assumptions were made.

Groundwater storage was calculated using the specific yield estimate from the pumping test (not the specific yield used for the groundwater level recharge from the deeper vadose zone) and the mean groundwater level from the two piezometers together with a bedrock depth estimate of 19 m based on observation from diamond core drilling. Soil storage from 0.3-1.25 m depth was calculated as the average of all available soil moisture sensors. It appears that the soil moisture data from the deeper TDR probes at 1.5 and 2 m depth were not used in the study. Top soil storage was calculated using all 0-30 cm TDR probes, and snow storage was simply snow water equivalent from observations using the snow pillow.

Each storage estimate (snow, surface soil moisture, soil moisture, deeper vadose zone, and groundwater) was distributed with a uniform thickness over the 4 x 4 km DEM from Creutzfeldt et al. (2008). A gravity estimate was calculated using the method of Creutzfeldt et al. (2008) (the Macmillan formula from Leirião et al. (2009)) and compared to the Wetzell SG gravity residual. The correlation of the SG residual with the estimated gravity effect of snow, surface soil moisture (0-30 cm) and deeper vadose zone soil moisture (1.25-11 m) was weak (-0.09, 0.09 and 0.49 respectively over 21.5 months). Creutzfeldt et al. (2010a) claimed the correlation with snow was weakly negative due to the snow mass on the roof of the SG building and the gravitational effect of surrounding snow below the SG mostly cancelling. The correlation of gravity with soil moisture (0.3-1.25 m) and groundwater level was good (0.64 and 0.71 respectively), with the SG residual range of around 11 μGal corresponding to an estimated (peak to peak) soil moisture and groundwater level component of 4.5 and 1 μGal (respectively).

Creutzfeldt et al. (2010c) installed a weighing lysimeter (with a 1.5 m deep soil monolith and 1 m^2 surface area) about 40 m north of the SG (adjacent to the TDR based 0-30 cm soil moisture transect). The bottom boundary of the lysimeter was maintained consistent with the surrounding soil using a tensiometer installed in the monolith, and another in the adjacent soil. A suction cup rake and bidirectional pump maintained the lysimeter soil suction at the same level as in the adjacent natural soil. However, it is not clear if the soil type (and profile) in the lysimeter was identical to the adjacent soil.

Both the soil monolith and drainage tank (used with the pump) were weighed. Precipitation, actual evapotranspiration and deep drainage (at 1.5 m depth) was estimated from the lysimeter at 1 minute resolution (with an accuracy of 0.01 mm). Measured snow water equivalent was removed from the lysimeter weight.

The terrestrial water storage below the lysimeter was estimated as the difference between drainage from the lysimeter and groundwater discharge. Both the groundwater discharge and vertical soil moisture distribution between the lysimeter and groundwater level were estimated using the HYDRUS 1D (Richard's equation based) model. The model HYDRUS 1D was used together with: the Van Genuchten (1980) unsaturated hydraulic conductivity, Mualem (1976) soil water retention curve, soil hydraulic parameters from Creutzfeldt et al. (2010a), and the mean observed groundwater level (from the two piezometers) as a bottom boundary condition. The model domain was split into two zones: the deeper vadose zone (saprolite), from 1.5-11 m; and the saturated zone (fractured bedrock), from 11-19 m. The same parameters were used for both (with residual soil moisture only 0 % vol/vol), except the saturated soil moisture (only 2 % vol/vol in the saturated zone, compared to 38 % vol/vol in the vadose zone), and saturated hydraulic conductivity (significantly higher in the fractured bedrock at 1.1 cm/h, compared to 0.2 cm/h in the saprolite). The saturated soil moisture and hydraulic conductivity is linearly interpolated between 8-11 m for a smooth transition between the two zones. Initial conditions were based on a spin up using drainage (infiltration from the soil moisture) estimated by Creutzfeldt et al. (2010a) using two tensiometers and Darcy's law.

Again (as in Creutzfeldt et al. (2010a)) the gravity effect of the observed snow, soil moisture from the lysimeter, groundwater level and modelled saprolite soil moisture was calculated using the method of Creutzfeldt et al. (2008) (the Macmillan formula from Leirião et al. (2009)) by assuming a uniform (spatial) water storage over a 4 x 4 km DEM (from Creutzfeldt et al. (2008)), with the storage underneath the 50 m^2 SG building excluded. The TDR soil moisture probes were not used in the gravity calculation. The estimated gravity effect of the hydrological changes (based on the snow pillow, lysimeter, soil moisture model and observed groundwater level) is in excellent correspondence with the observed SG gravity with a correlation of 0.987 (over 1 year) and an RMSE of 0.6 μGal (over a range of 10 μGal). However the model domain and parameters were no doubt adjusted to minimise the SG residual (i.e. the model would be calibrated to the SG residual gravity even if it is not explicitly stated in Creutzfeldt et al. (2010c)) When the SG gravity is corrected for the effect of hydrology the standard deviation of the SG residual is only 0.44 μGal (with a range of around 3 μGal). Creutzfeldt et al. (2010c) recommend installing lysimeters for SG sites (as the cost is justified because they are only one tenth of the cost of an SG), together with a local hydrological monitoring program.

Creutzfeldt (2010) also recommend installing lysimeters for SG sites, but acknowledge that for sites with lower resolution temporal gravity sampling such as field sites, this may be cost prohibitive and recommend using a NMM instead (to measure profile soil moisture). For field sites, they suggest using an NMM during field campaigns in conjunction with continuously operating soil moisture probes, ground water level probes and rain gauges. This is the approach followed by Smith et al. (2005, 2006) and in this thesis.

Creutzfeldt et al. (2010b) calibrate the conceptual rainfall-runoff model HBV to the SG residual gravity, groundwater level and soil moisture (over 1.5 years), and validate over another 1.5 years. The correlation for the SG calibration was very good, ranging from 0.98-0.99 for the calibration period and 0.84-0.99 for the validation period. The groundwater level correlation was not as good (0.67-0.94 for calibration depending on bore and period used, and 0.31-0.89 for validation), whereas the soil moisture calibration was reasonable for one sensor (ECHO, 0.80-0.89 for calibration and 0.76-0.81 for validation), but bad for another (TRIME-EZ, correlations of 0.51-0.52 for both calibration and validation). Creutzfeldt et al. (2010b) claim that the conceptual model calibrates (and validates) well to the SG gravity residual due to the gravity and conceptual model both being (spatially) lumped representations of the terrestrial water storage. Creutzfeldt et al. (2010b) state that future investigations of the hydrological signal in gravity should consider the lateral variability of terrestrial water storage, and in future a physically based model will be used around the Wetzell SG to investigate the spatial variability of soil moisture along the hillslope.

However Creutzfeldt et al. (2012) again use the conceptual rainfall runoff model HBV and calibrate the model to 10 years of SG gravity data. The modelled water storage from the calibrated model was then regressed against the SG gravity to give a (linear) conversion of SG gravity to terrestrial water storage (25.7 mm/μGal) that is equivalent to a terrestrial water storage admittance of 39 μGal/m, close to the Bouguer slab approximation. Creutzfeldt et al. (2012) also installed three clusters of 0-30 cm soil moisture (TDR) probes, consisting of 45 probes within 20 m of the SG, 21 probes about 80 m north east of the SG, and 26 probes 220 m to the east (and about 20 m downslope). Creutzfeldt et al. (2012) find that for the 5.5 km^2 gauged headwater catchment that the SG is in (the V-notch weir is approximately 500 m south east of the SG) the terrestrial water storage (that is just the scaled SG gravity) is better correlated to the runoff coefficient (0.46) than the average 0-30 cm soil moisture from each of the three TDR clusters (correlation of 0.31-0.36).

Moxa, Germany

Similar to the SG in Indonesia, Kroner (2001) found a lag when correlating groundwater level and SG (residual) gravity at Moxa, Germany. They also attributed the lag to soil moisture storage in the hillslopes above the SG and concluded longer (groundwater level) data sets and more information on the local hydrology, including a hydrogeological model of the local area were required. This model (and further data sets) are described in Krause et al. (2009); Naujoks (2009) and Naujoks et al. (2010).

The SG at Moxa (like the SG at Wetzell) is a dual sphere SG (Richter and Warburton, 1998) located in a small valley with the observatory built into the side of a hill. The roof above the SG is covered by a 2-3 m layer of gravel and clay soil (Kroner, 2001; Kroner et al., 2004; Llubes et al., 2004).

The gravitational effect of soil moisture within 1 km of the SG was estimated using a DEM and the Bouguer slab approximation for each grid cell (Kroner, 2001; Llubes et al., 2004). Assuming a soil depth of 1 m and a soil moisture change of 10 % vol/vol, a gravity reduction of 1.92 μGal was estimated, while the contribution of just the rooftop area was a reduction of 1.18 μGal. An experiment was conducted where firemen sprayed 17 m^3 of water on the roof over 30 minutes, this corresponded to a 1.15 μGal reduction in gravity (Kroner, 2001). The volume of water sprayed on the roof corresponded to 4 cm over the roof area, or an admittance of 30 μGal/m (Llubes et al., 2004), lower than the Bouguer slab admittance of 42 μGal/m. A gravity difference between the two (20 cm) vertically separated spheres in the dual sphere SG of up to 0.05 μGal was observed, corresponding to the gravitational effect from a cylindrical approximation of the water mass in the roof (Llubes et al., 2004).

Due to the location of the SG there is an anti-correlation between the gravity residuals and precipitation (Kroner et al., 2004). For one event 8 mm of rainfall (over 1 hour) corresponded to a drop in gravity of 0.6 μGal, interestingly there was a 0.05 μGal rise immediately before the 0.6 μGal drop. This 8 mm rainfall event also corresponded to a 35 mm rise in groundwater level (Kroner et al., 2004). Hasan et al. (2006) noted precipitation of 5 mm or more caused a drop in gravity, and corresponding peak in the deeper groundwater level after a peak in streamflow. Hasan et al. (2006) used time series analysis on rainfall events greater than 8 mm (over 4 hours), where events were separated by at least an 8 hour period with a maximum precipitation rate of 1 mm/hour. Impulse Response Functions (IRF) were computed using the z transform (backwards shift operator) and BIC (to choose a parsimonious model structure). The selected IRF used 1 autoregressive and 3 moving average parameters (i.e. rainfall over 3 hours previous) and explained around 60 % of the gravity variation. Hasan et al. (2006) state that the IRF is only applicable for rainfall events (i.e. it models an impulse response) and does not account for redistribution of water in the catchment over longer periods (days). Kroner and Jahr (2006) state that unlike the Vienna SG, the gravity at Moxa does not steadily increase to its previous level after a sudden decrease due to a rainfall event. In fact Kroner and Jahr (2006) identify periods of oscillation in the gravity residual 3-8 days after a rainfall event that are not present in the groundwater level (or atmospheric pressure) and hypothesise that these oscillations may be related to hydrological flow processes in the catchment, specifically soil moisture infiltrating the 35 m hill (covered with Spruce forest) behind the SG. However soil moisture was not observed.

There are three piezometers about 50 m from the SG, one is 100 m deep and the other two 50 m deep (Jahr et al., 2001). The groundwater level at the 50 m deep piezometer is around 2-3 m below the surface (Kroner et al., 2004), and well anti-correlated (over 1.5 years) with short term gravity residuals (periods less than 3 months), and positively correlated over the long term but with groundwater level lagging gravity variations (Kroner, 2001; Kroner et al., 2001). Kroner (2001) conclude that the hydrological variations must be predominantly from an area above the SG for periods of hours to weeks, and over the long term shift to an area below the SG. Kroner et al. (2004) suggest that the hydrological changes in the area of the SG are largely reflected in the groundwater level variations and determine a frequency dependant groundwater admittance of 6 μGal/m for long tides (e.g. annual), and 5.5 μGal/m for diurnal and shorter. Llubes et al. (2004) found that the groundwater level and gravity residuals were anti-correlated (over 1 year), but that the admittance changed from one rainfall event to the next (varying from 5-15 μGal/m). Harnisch and Harnisch (2006b) state they were not successful at a first attempt to use the groundwater level variations for correction of the gravity residuals. Hasan et al. (2006) found the relation between groundwater level and gravity residuals varied according to the season, with the monthly correlation generally negative (and most strongly when annual temperature is at its maximum, in summer), and positive when monthly temperature drops below 0 °C (when the soil moisture is frozen). Kroner et al. (2002) found that the difference in the two gravity signals from the dual sphere SG was extremely well anti-correlated with air temperature over 2.25 years. They attribute this to soil moisture changes that are strongly correlated with air temperature. Note that the difference of gravity signals from two gravity sensors vertically separated, when divided by the separation distance, is a first order approximation of a vertical gravity gradient, and the vertical gravity gradient decreases with the distance to a point mass cubed (rather than squared for gravity). Therefore a vertical gravity gradient will have a stronger soil moisture signal, relative to other signals further from the gradiometer (e.g. groundwater level variations). Kroner et al. (2004) show the gravity signal from one sphere correlates reasonably with groundwater level, but not the difference of the two spheres (over 3.75 years). The two sensors have a slightly different response to the hydrological effect, due to the marginally different distance (20 cm) the two sensors have to the water masses. Kroner et al. (2004) conclude the hydrogeological situation of the Moxa observatory must be better understood and longer datasets are needed.

Below the Moxa SG is a 2 m thick weathering layer, followed by steeply dipping layers of clefted metapelite to a depth of more than 100 m (Kroner and Jahr, 2006). Water was visible in the gap between the SG pier and the observatory floor during times of heavy rainfall (such as spring). As an experiment Kroner and Jahr (2006) injected 47 m^3 of water into the gap (over 9 hours). The groundwater level rose by

60 cm at the shallow piezometers 0 and 4 m from the SG, but by more than 80 cm at the piezometer 8 m from the SG. The resulting rise in gravity was almost 2 μGal and extremely well correlated with the groundwater level at the piezometer 8 m from the SG (it returned to its original level 40 hours after the experiment). In another experiment, the 35 m eastern hill adjacent to the SG was irrigated on a gently sloping area 50-80 m from the SG with 20 m^3 of water over 1 hour. The irrigation rate was chosen to mimic the thawing of snow in early spring. A 1.2 m deep observation pit was dug 20 m downslope of the edge of the irrigation area (about 30 m from the SG). While the pit was dry when first dug, water was observed first seeping, then flowing into the pit 50 minutes after the end of the irrigation. After 30 minutes the irrigation water stopped flowing into the pit and rapidly infiltrated (into the hill behind the SG). The irrigation experiment caused a decrease in gravity of 0.2 μGal over 4-5 hours, followed by a stable gravity residual for about an hour which Kroner and Jahr (2006) attribute to an equivalent inflow and outflow of water with regards to the SG location. Lastly an increase in gravity of 0.6 μGal commenced 6.4 hours after the irrigation on the hillslope, 1 hour before an almost 1 m rise in groundwater level at the SG, and 4 hours before a 80 cm rise in groundwater level 8 m from the SG. The maximum gravity change was reached 1 day after the irrigation experiment, which Kroner and Jahr (2006) attribute to most of the water having infiltrated below the SG. They also state the increase in gravity is much larger than the decrease (for the same volume of water) as the water mass is closer to the SG (after infiltration and lateral flow). Kroner and Jahr (2006) modelled three different flow paths and concluded the irrigation water moved parallel to the ground surface at a depth of about 2 m (following the weathering layer) for the gentle and medium slope, and a depth of about 5 m (through metapelite clefts) for the steep slope 20 m behind the SG. The modelled gravity variation from this flow path matches the observed gravity residual extremely well over 8 hours, with a maximum difference of only 0.02 μGal.

Kroner and Jahr (2006) conclude gravity observations can be used to validate hydrological modelling. Furthermore the experiments indicate which hydrological fluctuations around the SG need to be considered, how large the effect is, and appropriate modelling techniques. Kroner and Jahr (2006) state that soil moisture sensors have been installed and future work will use those and streamflow measurements to model the hydrological effect, especially in the hillslope above the SG, rather than just using the deep groundwater level admittance.

Kroner (2006) found that the rainfall effect can vary widely, with a 3 mm event reducing gravity by 0.6 μGal but a 14 mm event only reducing gravity by 0.7 μGal. Consequently they removed all vegetation on the roof above the SG, levelled the surface (with a slope), and covered it with a plastic sheet and 4 cm of gravel. The additional mass of 40 tons on the roof caused a decrease of 1.97 μGal in the top sphere and 1.9 μGal in the bottom sphere, consistent with the geometry, thickness and density of gravel. Soil moisture probes (TRIME-EZ) at 30 cm and 1 m depth on the roof show the insulation from rain is effective. However even after covering, rainfall events of 12, 15 and 5 mm still caused gravity decreases of 0.5, 0.5 and 0.25 μGal due to the surrounding soil moisture. Furthermore the roof lining is not effective for winter when the roof is covered with snow (Kroner, 2006).

At Moxa the peak to peak amplitude of different hydrological influences (including snow) is 3.5 μGal (Kroner et al., 2007). Snowmelt was observed via the groundwater level, monitored in a gap between the SG pier and observatory floor, with a 900 mm rise in 1 day corresponding to a 3.5 μGal rise in gravity over the same period. Snow was modelled by accumulating precipitation during periods with air temperature less than 0 °C (Kroner et al., 2007). When air temperature is above 0 °C, a simple snow melt model that uses degree-days above a reference temperature is used, similar to Bower and Courtier (1998). The snow model corrects well three monthly events during winter of 1, 1.5 and 2 μGal, and reduces the range of gravity residual over winter from 4.5 μGal to 2.5 μGal. Kroner et al. (2007) modelled the gravitational effects of observed groundwater level and soil moisture, using a 5 m resolution DEM for the area within 700 m of the SG. The gravitational attraction of soil moisture over the top 1 m and groundwater level in the valley (to a depth of 2 m) was calculated via Nagy (1966). The groundwater level observations at one well were used with the lower boundary of 2 m for the saturated zone determined by resistivity measurements, and a porosity of 25 % assumed to represent a gravel and loam mix. Soil moisture observations (from three sites) at 30 and 100 cm depth were linearly interpolated to give soil moisture every 10 cm (over the top 1 m). It is not clear how this estimated soil moisture at three sites (valley bottom, hill side, and top of hill) was distributed over the area covered by the DEM. The soil moisture and groundwater level based corrections were not as successful as the snow correction, with the (peak to peak) gravity residual (over 4 months following snowmelt in early spring) actually increasing from around 2.75 μGal to 3.25 μGal. Kroner et al. (2007) note that future work will attempt to improve snow and soil moisture corrections by incorporating detailed topographic information around the SG into the modelling, and improve groundwater level corrections by analysing and comparing various groundwater level measurements in the valley as well as determining the aquifer depth along the valley by resistivity measurements.

The valley floor between the SG observatory and the Silberleite Creek is filled with debris from the construction of the observatory, and this can be considered as a very permeable groundwater aquifer that drains water to (and from) the stream (Krause et al., 2006, 2009). Hasan et al. (2006) show that the streamflow, deep, and shallow groundwater levels are all very well correlated (over 1.5 months), and conclude that the groundwater level observations are from a shallow aquifer that is well connected to the creek. Hasan et al. (2006) claim more research is needed to include groundwater dynamics into a hydrological model of the catchment. Hasan et al. (2008) used a hillslope groundwater model recharged by the drainage from a lumped catchment water balance model. Soil moisture, recharge, evapotranspiration and runoff were modelled with the lumped model at hourly resolution using the 3 km^2 catchment as a single modelling unit. The results of the lumped model were distributed within the catchment using a 20 m resolution DEM within a 4 km radius of the SG. The hillslope groundwater model was applied to 16 hillslopes in the catchment and run at daily resolution. Snow was modelled following Kroner et al. (2007), and like Kroner et al. (2007) the gravitational effect of soil moisture, snow and groundwater was calculated for each grid cell using Nagy (1966). Hasan et al. (2008) assessed the gravitational effect of the cells within the 4 km radius of the SG and found that most of the gravity variation due to soil moisture and snow comes from a region within 1 km of the SG, with an admittance of 40 μGal/m (for both snow and soil depths of 0.1-2 m). The soil depth and field capacity (used to determine when recharge occurs to the groundwater model) of the hourly lumped catchment water balance model was calibrated to the hourly gravity residuals with a resultant Nash Sutcliffe Efficiency (NSE) of 0.7. Conversely the specific yield and hydraulic conductivity of the daily hillslope groundwater model was calibrated to the daily streamflow with a NSE of 0.6. Subsequently the combined water balance and groundwater hillslope models were able to reduce the (peak to peak) gravity residual from 4.5 μGal to about 2.75 μGal over almost 2 years. This is comparable to the result of Kroner et al. (2007), obtained just using a simple snow model for winter (residual reduction from 4.5 μGal to 2.5 μGal).

Krause et al. (2006) installed five soil moisture probes (Adcon C-Probe) around the SG and conducted a soil mapping campaign for the entire catchment to provide better information for hydrological modelling. The soil map of 15 soil types was created with 30 soil profiles, soils are mostly silty to loamy with a considerable rock fraction (cambisol, like at the Wetzell SG), and groundwater influenced soils (gleysol) in the valley (Krause et al., 2006, 2009). The soil at the five soil moisture sites (all within 400 m of the SG and 200 m of the creek) is cambisol, except the most distant site (located in the valley) which is gleysol. The soil depth is 40-70 cm with a corresponding rock fraction of less than 10 to 70 % (for the 6 cm deep A horizon and 10 cm deep C horizon respectively). Although it has the major influence on gravity Krause et al. (2006, 2009) were unfortunately not able to drill and install a soil moisture probe on the slope to the east of the SG, and a site 300 m north of the SG is the only representation of the eastern portion of the 3 km^2 catchment. The C-Probes, like the Sentek probe used at Strasbourg (Longuevergne et al., 2009) allow the installation of up to six sensors at different depths in a single probe. Each probe is installed in a plastic tube and has a measurement radius of 10 cm. A 0.2 mm resolution raingauge was also installed together with each soil moisture probe, with both precipitation and soil moisture recorded every 15 minutes. Each site measured soil moisture at four or five depths (multiples of 10 cm) in the top 70 cm. It is not clear if the soil moisture probes were calibrated (to the site soil).

A distributed conceptual water balance model (used to determine the soil water balance using two stores for each hydrological response unit (HRU)) was run for almost 8 months, using an hourly timestep and 337 HRU (Krause et al., 2006, 2009). The model was not calibrated due to the short time period covered, and consequently overestimated catchment streamflow (Krause et al., 2006). When calibrated to daily or hourly streamflow an NSE of 0.77 and 0.68 (respectively) was obtained (Krause et al., 2009), but the model still overestimated catchment streamflow.

The modelled soil moisture is generally in the range of the observed soil moisture at each location (noting the range is 25 % vol/vol between the four or five sensors at different depths (within 70 cm of the surface) at a single site), however the modelled soil moisture shows much more dynamic behaviour than the observations (Krause et al., 2006, 2009). Furthermore, the model is most correlated with the observed soil moisture at 10 cm depth at each site (that corresponds to the measurement in the topsoil), but generally overpredicts this soil moisture by 10 % vol/vol at each site (Krause et al., 2006). When the model was uncalibrated (Krause et al., 2006) the soil water balance was determined using two stores for each HRU, but when the model was calibrated (Krause et al., 2009) the soil water balance was modelled for three soil horizons in each HRU using two stores for each horizon. The calibrated model showed the same positive bias of modelled soil moisture to observed 10 cm depth soil moisture, but the bias was larger for the A horizon, and close to zero or negative for the deeper horizons, corroborating the results from Krause et al. (2006) when a depth integrated soil moisture was modelled for each HRU.

A depth weighted average soil moisture observation was calculated for each site and compared to the gravity residuals for 3 months (over summer and into autumn) (Krause et al., 2006, 2009). The site 300 m north of the observatory that best represents the eastern hill previously deemed significant, showed the best anti-correlation with the gravity residual, while some of the largest peaks in the gravity residual are evident in the highest elevation (and most distant) soil moisture sites. This shows the ability of the SG to integrate catchment soil moisture instantaneously, which is further supported by modelled catchment average soil moisture that is reasonably well anti-correlated with the gravity residual. Krause et al. (2006, 2009) conclude that further analysis of the gravity residuals and in-situ (soil moisture, groundwater level, runoff and precipitation) measurements will further improve the model simulation capabilities.

A number of field campaigns were conducted to measure the gravity differences in a network local to the SG with LaCoste and Romberg G and D gravimeters (Naujoks et al., 2006; Kroner et al., 2007; Naujoks et al., 2008; Naujoks, 2009; Naujoks et al., 2010). However, unlike in this thesis, the hydrological variations (terrestrial water storage) were not measured. The network originally consisted of 12 points within 300 m of the SG (Kroner et al., 2007; Naujoks et al., 2008; Naujoks, 2009) but was reduced to only six points on an east west profile (within 40 m of the SG) following consideration of the time taken to observe the network (Naujoks et al., 2008; Naujoks, 2009), together with an anomalous magnetic field influencing the gravity measurements with the LaCoste and Romberg gravimeters at two sites, and slippery conditions at a third site (Naujoks, 2009). This meant that the planned north south profile along the Silberleite valley could not be studied (Naujoks, 2009).

Nine site differences (or ties) were observed between the six sites on the 65 m profile (Kroner et al., 2007), with a maximum height difference between sites of only 25 m (Naujoks et al., 2008). To avoid shocks during transportation and shorten travel time, a cable car style lift was used to transport the gravimeter from the SG observatory to the point 40 m distant on the steep hillslope (Naujoks, 2009), all other points are within 25 m of the SG (Naujoks et al., 2008; Naujoks, 2009; Naujoks et al., 2010). Each tie was measured at least five times (per gravimeter) using 3-5 gravimeters (four Model-G and one Model-D) at each site. Each observation at a site was the average of three readings with the same gravimeter, with the measurements made at the same point on concrete pillars of 30 cm diameter and 1 m depth (with a mark made so the gravimeter was always repositioned in the same location). All the gravity ties (with all gravimeters) were combined in a network adjustment for each field campaign. After network adjustment tie (or site gravity difference) standard deviations range from 0.9-1.4 µGal for a campaign, and consequently a standard deviation of 1.3-2.0 µGal for a change in gravity difference (between any two sites) between two campaigns (Naujoks et al., 2008). There were approximately 200 gravity ties in the network adjustment, with the stepping method used to measure the six sites in the east-west profile. There were a total of 17 campaigns over almost 2.5 years, although the results of six of the campaigns were discarded in subsequent analysis (Naujoks et al., 2010). The gravimeters were calibrated on the Hannover calibration line during the period of the field campaigns. Standard deviation for a gravity tie ranged from 4.3-9.7 µGal for the D Meter (dependant on campaign) and 2.2-14.1 µGal for the four G Meters (Naujoks et al., 2008). When the data from all gravimeters was pooled the standard deviation for a tie (site difference) ranged from 5.4-8.8 µGal, and after network adjustment was 0.9-3.1 µGal (dependant on campaign), while the standard deviation for a single site (after network adjustment) ranged from 0.6-2.2 µGal (Naujoks et al., 2008).

Changes in gravity ties were detected between points in the valley and on the steep slope east of the SG. The difference was bigger during dry conditions (by

13 μGal between the SG and hill top site, or 6.5 μGal for a valley site and the hill top site, or -6 μGal for a valley and the SG site) and smaller when wet (around 0 μGal for all three ties) indicating significant water storage in the hill (Naujoks et al., 2006; Kroner et al., 2007; Naujoks et al., 2008; Naujoks, 2009; Naujoks et al., 2010). Soil moisture was monitored at 1 m depth on the roof above the SG, but covered 10 months into the study (after 7 field campaigns), and at 1 m depth in the valley 20 m from the SG. Groundwater level was also monitored at the point in the valley and at the SG. However no comparison between the soil moisture, groundwater level and site gravity differences was done. Subsequently a 3D gravity model of the SG surroundings was created (Naujoks et al., 2010) and combined with the hydrological model (and calibration) of Krause et al. (2009) to give predicted gravity changes (due to hydrological effects) at the gravity network sites. The modelled gravity for the site differences very loosely corresponded to the observed site gravity differences after network adjustment.

In this thesis gravity is observed with a Scintrex CG-3M relative gravimeter at a hydrologically stable bedrock reference site and 3 or 4 soil moisture monitoring sites where terrestrial water storage (TWS) is observed (profile soil moisture from the surface to groundwater level, and groundwater level). After network adjustment the gravity changes at each site (relative to the hydrologically stable bedrock reference site) between field campaigns 6 months apart that captured the peak to peak seasonal variation of TWS are compared to observed TWS change.

A 2.75 μGal annual variation of gravity (due to hydrology) is expected at Moxa based on land surface model data from Global Soil Wetness Project (GSWP) (Kroner et al., 2004). Crossley et al. (2006) show there is very little correspondence between GLDAS modelled soil moisture and the SG gravity residual (which they hypothesise may be due to the SG location being half above the soil horizon and half below), however Naujoks et al. (2010) found that after correcting for local hydrological effects (with a combination of observations and modelling) there is a strong correlation of the gravity residuals (annual amplitude 3.5 μGal) with both modelled (WGHM), and observed (GRACE) large scale hydrological changes (with annual amplitudes of around 3.5 μGal and 5.5 μGal respectively). Naujoks et al. (2010) conclude that future research should focus on deriving constraints from ground-based and satellite gravity observations to improve regional and global hydrological models. In this thesis ground-based gravity observations are assimilated into a land surface model (that can be run locally, regionally, or globally) to improve soil moisture simulation.

2.5.2 Absolute Gravimeter Sites

In addition to studies at the GGP SG sites, hydrological investigations have been conducted at two observatories where absolute gravity is monitored with an FG5. Breili and Pettersen (2009) studied the gravitational effect of snow in Norway, while Kazama and Okubo (2009) investigated the gravitational effect of groundwater on a volcano in Japan. Due to the mechanical nature of the current standard absolute gravimeter (FG5) and operational wear and tear, the absolute gravimeter observations are either sparse over a long period of time, or frequent over a short time window.

Breili and Pettersen (2009) observed absolute gravity in Norway for 3 years (26 observations of 30-60 minute duration) and found seasonal variations of up to 10 μGal in spring. The groundwater level correlation with gravity was only -0.16 but increased to 0.63 when snow periods were excluded. Groundwater level was measured at a 30 m deep well adjacent to the gravimeter, soil moisture was not observed. Mean groundwater level depth was 20 m and the range of variation during the 3 years was 3.36 m. Rainfall and snow depth were measured at a weather station less than 1 km from the gravimeter, with rainfall used as a proxy for soil moisture during periods without snow cover. A Bouguer slab model was used for groundwater and soil moisture (with soil moisture represented by rainfall with an admittance), with a porosity of 0.05 and rainfall admittance of 0.59 μGal/mm determined from periods without snow cover. The gravitational effect of groundwater reached 5 μGal during snowmelt periods, while the soil moisture effect (calculated from rainfall) was up to 3 μGal.

A 1 m resolution DEM was calculated for 200 m around the gravimeter using interpolated kinematic precise point positioning GPS measurements. The gravitational effect of snow depth uniformly distributed across the DEM (excluding the 5 x 5 m area of the observatory in the centre) was calculated using a point mass formula and snow mass, with snow mass calculated from snow depth (observed 1 km from the site) and density (calculated from a daily 1 km resolution snow water equivalent and snow depth map of Norway). Snow on the roof of the observatory was ignored.

The gravity effect of the snow within 200 m of the FG5 was up to 13.4 μGal. Snow loading (from a circle of radius 200 km that was not centred on the gravimeter but offset by at least 50 km) was calculated using the previously determined daily snow density and snow depth observations from the nearest weather station to the grid cell, together with a Green's function. The regional (within 250 km of the FG5) snow loading only reached 1.2 μGal and was only 10 % of the local (within 200 m of the gravimeter) Newtonian snow attraction. Consequently 90 % of the snow signal is from within 200 m of the gravimeter (with 90 % of the Newtonian snow signal from within only 80 m of the gravimeter). When a linear trend (-1.9 μGal/year) is removed from the gravity observations (to account for a post glacial rebound signal) the calculated hydrological effects of snow, groundwater level and rainfall correspond well with the gravity observations with a correlation of 0.92 and range of the residual (after correcting for hydrological effects) of around 9 μGal.

Kazama and Okubo (2009) observed absolute gravity every two hours on a volcano in Japan for 3 months (with a data gap of 5 days), and observe an 18 μGal rise after a 250 mm rainfall event (over 10 days) that is somewhat correlated to an observed increase in groundwater level of 0.6 and 0.5 m at two piezometers 1.5 and 4 km (respectively) from the FG5, but does not correspond to average soil moisture observed at the gravimeter with six soil moisture sensors at 10, 20, 30, 40, 60 and 100 cm depth (using a single Profile Probe PR2).

Kazama and Okubo (2009) model groundwater level with a 2D diffusion equation for an unconfined aquifer and soil moisture with Richard's equation. Soil depth is 200 m and consists of pumice and volcanic ash. An impermeable layer (bedrock) is set at a depth 506 m below the gravimeter, based on electromagnetic resistivity observations. The modelled groundwater does not correspond well with the observed groundwater level, particularly at the piezometer closest to the gravimeter. The modelled soil moisture is roughly similar to the average of the six soil moisture sensors but at times deviates by 5 % vol/vol when the observed range is only around 9 % vol/vol. The calculated gravity effect of the modelled soil moisture and groundwater corresponds well with the observed gravity for the first 20 days and last 40 days of FG5 absolute gravity observations (when the gravity does not vary) and tracks the rise of the gravity observations following the observed rainfall event well for the first half of the rise, but then underestimates the peak gravity by about 6 μGal. The underestimation of the peak gravity is a result of the hydrological model not maintaining enough water mass, and may be due to the effective rainfall being calculated as the difference of observed rainfall and climatological PET (used as AET), or as claimed by Kazama and Okubo (2009) the large 50 m resolution DEM based grid cells used for the finite difference solution of the soil moisture and groundwater models. Kazama and Okubo (2009) also state the importance of suitable soil parameters for accurate hydrological and gravity modelling. In this thesis soil parameters for the hydrological and gravity modelling are tuned to the site based on soil samples and particle size analysis, together with a high resolution soil survey map.

2.5.3 Field Sites

Traditionally relative gravimeters have been used in the field (and consequently in studies of hydrology and gravity) due to the gravimeters low cost, portability, and high precision. Furthermore, unlike superconducting or absolute gravimeters (housed in a building), relative gravimeters can be used to monitor hydrological variations (that are minimally impacted by the gravimeter plinth and enclosure) directly below the gravimeter. Lastly relative gravimeters operate using batteries whereas absolute and superconducting gravimeters require a dedicated AC power source (ranging from 120-1300 W).

Superconducting Gravimeters

In the only example of a field deployment of an SG Wilson et al. (2012) observed gravity for 6 months adjacent to a piezometer on a karst aquifer in Texas. The well depth was almost 100 m with an average water table depth of around 55 m (approximately 40 m below the geological formation containing limestone caves). Due to the depth to the groundwater level it was estimated that 90 % of the groundwater signal in the observed gravity was from within 1 km of the SG. The groundwater level only varied by around 30 cm during the field experiment. The SG and rack mount electronics (and a barometer) are housed in a shed with a permanent 2 kW power supply connected (a power requirement that cannot be accommodated by solar panels). Holes were drilled to 70 cm depth in outcropping limestone and 25 mm diameter steel rods cemented into the holes. The plywood shed floor and a separate concrete monument for the SG were attached to the steel rods. Problems with both the shed floor (sagging) and the gravimeter monument shifting (after a 45 mm rainfall event) led to gaps in the SG gravity data (of 15 and 18 days respectively). The SG and atmospheric pressure data was sampled at 1 Hz and decimated to 15 minute observations, groundwater level was also observed every 15 minutes. A weather station with soil moisture probes was installed but the data is not discussed in detail. Wilson et al. (2012) state soil moisture was generally close to zero (due to drought conditions) except for a couple of days after rainfall events.

While the drift of a laboratory SG is generally low, the drift of this SG was determined as 0.9 μGal/day in laboratory testing prior to deployment in the field. In the field Earth tides and drift were removed through a complicated procedure of fitting to the SG data three times, where first both a linear and exponential drift were separately estimated and removed from the SG data. The linear drift and theoretical tides were both fit to the SG data, where the theoretical Earth tides were predicted using Tsoft (Van Camp and Vauterin, 2005) and the Dehant et al. (1999) Love numbers (and presumably the Tamura (1987) tidal potential catalogue used in Tsoft). The linear drift was then removed from the SG data and the theoretical Earth tides fit a second time to yield an SG calibration factor (to convert the raw volt measurement to gravity units). The predicted Earth tides were then removed and an exponential drift fit and removed from the SG gravity data. The pressure admittance was calculated as -0.338 μGal/mbar based on regression of the atmospheric pressure data and SG gravity over a 30 day period. The final SG residual has significant short period variations of up to 10 μGal, and negative spikes of 7 μGal. An explanation is not given for these significant artefacts in the data.

A quadratic trend of the SG residual correlates well with the residual groundwater level (after atmospheric pressure effects are removed from the groundwater level) over the 180 day field experiment, with the gravity increase of approximately 4 μGal corresponding to an increase in groundwater level of around 30 cm. Wilson et al. (2012) acknowledge that the clear presence of an atmospheric pressure signal in the groundwater level data indicates the piezometer is sampling a confined aquifer (which is also indicated by the stratigraphy of the bore log and the groundwater level), as the groundwater level of an unconfined aquifer is not affected by atmospheric pressure variations. Wilson et al. (2012) conclude that for hydrological studies the SG will be most useful when combined with other gravimeter types (such as absolute and relative).

Absolute Gravimeters

A small number of studies have investigated the effect of terrestrial water storage variations on absolute gravity obtained with an FG5 (Van Camp et al., 2006a; Jacob et al., 2008, 2009, 2010; Hinderer et al., 2009; Pfeffer et al., 2011) or in one case an A-10 (Ferguson et al., 2008). Most of these studies investigated groundwater storage deep below the soil profile, ranging from 47-60 m in Van Camp et al. (2006a) to more than 160 m in Jacob et al. (2008, 2009, 2010) to 2.5 km in Ferguson et al. (2008). In no studies with an absolute gravimeter was soil moisture observed and compared to the absolute gravity observations. Indeed, except the study of Van Camp et al. (2006a) where groundwater level was observed in a cave, and Pfeffer et al. (2011) where a relatively shallow water table of 12 m was observed due to long term rising groundwater levels, the groundwater level was not observed.

Ferguson et al. (2008) monitored deep groundwater injected via wells to increase oil production in Prudhoe Bay, Alaska. An A-10 was used to observe gravity during winter at over 300 sites in a 150 km^2 area (12 x 12 km) that covered both land and the frozen bay (the seven injection locations are in the bay). Gravity was observed along 6 transects with a station spacing of 380 m, as well as a grid with sites typically separated by 760 m. At each site absolute gravity was observed (with an A-10), and a GPS antenna mounted directly on the gravimeter was used (together with GPS base stations) to determine the location (with real time kinematic GPS) and elevation (with fast static GPS). Four field campaigns were conducted over four years, with the last three campaigns using two groups of operators, two (snow cat) tracked vehicles and two gravimeters to monitor different parts of the network simultaneously. For each observation the snow was cleared to solid ice or frozen soil before placing the gravimeter on a metal plate. A tent was used to shield the gravimeter during measurements. Gravity observations take 20-30 minutes and consist of 6 measurements of 120-200 drops at 1 Hz sample rate. The absolute gravity is corrected for Earth tides, ocean tide loading, atmospheric pressure, and polar motion. It is not clear how these corrections are made, but they are probably standard (manufacturer) A-10 corrections. Despite the A-10 being an absolute gravimeter, Ferguson et al. (2008) report a drift in the gravimeter laser of 2 μGal/year and a much smaller drift in the atomic clock of 0.08 μGal/year. When snow was removed prior to an absolute gravity observation, the depth of snow was recorded and used to correct for the effect of the 1 m diameter hole in the snow created (assuming a snow density based on a number of snow samples). The average correction for snow within 50 cm of the gravimeter was 1.5 μGal but can be up to 7.5 μGal (depending on snow cover). Groundwater level was not observed and soil moisture was frozen.

In Van Camp et al. (2006a) the groundwater level of a karst aquifer in Belgium was observed (in a cave) and varied from 47-60 m below the surface. The groundwater level increased after flood events breached the canalised river and recharged the aquifer via a swallow hole adjacent to the river. Absolute gravity was observed (with an FG5) on the surface every 4 hours during two flood events. The observed gravity during the second larger flood event reached 9 μGal and correlated very well with the groundwater level in the cave that increased by 13 m. However the observed gravity change was much less than the 25 μGal change expected based on the observed groundwater level and an assumed specific yield of 5 %. For the first flood event the gravity was not as well correlated to the groundwater level, with a 6 μGal increase in gravity lagging a 10 m increase in groundwater level by around 2 days, this may have been due to the first flood event being a superposition of four rainfall events. Indeed Van Camp et al. (2006a) conclude that future work should investigate the gravitational effect of soil moisture.

In a sequence of studies on the Larzac plateau in France (Jacob et al., 2008, 2009, 2010) monthly absolute gravity measurements over 16, 26 or 33 months (respectively) at three sites on a 6 km profile were used to assess water storage in a karst aquifer and test the hypothesis that there was significant storage in the vadose zone and epikarst above the aquifer (particularly around the recharge area). Increases in absolute gravity of up to 15 μGal were observed after significant rainfall events (greater than 100 mm/day) that led to observed spring discharge from the karst aquifer (Jacob et al., 2008). To understand the hydrology a simple water balance model was used in Jacob et al. (2008), while in Jacob et al. (2009) and Jacob et al.

(2010) additional relative gravity measurements were made with a Scintrex CG5. In Jacob et al. (2009) the relative gravity observations were at the surface and 60 m below the surface down a pot hole, while in Jacob et al. (2010) a traditional relative gravity network of 40 sites was made (on the surface) around one of the absolute gravity monitoring sites (while integrating the other two absolute gravity sites into the network). Groundwater level or soil moisture was not observed in Jacob et al. (2008, 2009, 2010).

The scale of the gravity network in Hinderer et al. (2009) (four sites with station separations of around 500-1100 km) covering three countries (Algeria, Niger and Benin) in Africa precludes usage of relative gravimeters (due to unknown drift over multiple hours of transport) and can only be realised with absolute (or permanently installed superconducting) gravimeters. Indeed the network consists of four absolute gravity sites (that are observed every 3 months) with one site (in Djougou, Benin) hosting a (continuously operating) SG. Finally (every 6 months) Hinderer et al. (2009) plan to make absolute gravity measurements from 10 m to 10 km around one of the (FG5) sites with an A-10. The project is intended to continue for 3 years (Hinderer et al., 2009).

Initial results (for one year) from one of the four absolute gravity sites in Hinderer et al. (2009) are shown in Pfeffer et al. (2011) for the site in Niger. Four absolute gravity observations are compared to water level variations in four wells (depth 20-30 m and water table depth of 12-18 m) and a natural recharge pond. The four wells and pond are on a transect (with one well in the pond), with the pond (and most distant piezometer) 190 m from the gravimeter. The absolute gravity observations were made at night time (to avoid heating effects) on a 1 m^3 concrete pad in a traditional hut. A power source for the FG5 is not discussed. A gravity increase of 8.7 μGal is observed over almost 7 weeks after monsoonal rain that corresponds with an increase in the groundwater level at the four wells of 2.5-4.5 m with the largest increase directly under the recharge pond (and the magnitude of variation decreasing with distance from the pond). When considering the absolute gravity observation standard deviation of 1.4-2.0 μGal, the four gravity observations correspond roughly with the groundwater level variations using a specific yield of 7-11 %. Pfeffer et al. (2011) estimate 80 % of the gravitational effect of groundwater level variation comes from within 70 m of the FG5 and consequently only covers two of the four wells (with the smallest observed groundwater level change) and not the pond. When soil moisture estimates (based on maximum observed soil moisture at a site 2 km away) were included in the calculated gravity changes (together with observed groundwater level variations) the specific yield estimate was significantly lower than when specific yield was estimated using groundwater level changes alone. Pfeffer et al. (2011) estimate 96 % of the gravity signal from soil moisture is from within 50 m of the FG5. Soil moisture was not observed within 2 km of the absolute gravity site.

Relative Gravimeters

For the first time Montgomery (1971) presented ground-based gravity observations as a method to determine (unconfined) aquifer specific yield, when used in conjunction with observed groundwater level variations (in a piezometer), and a Bouguer slab model for the gravitational effect of the groundwater level change. The gravity observations were made adjacent to piezometers (in Arizona) on 30 cm deep concrete monuments (35 cm diameter) and tied to a bedrock reference site where groundwater variations were assumed negligible. Montgomery (1971) recommended marking or grinding points on the concrete monument to put the gravimeter legs each time, and fixing one leg of the gravimeter to reduce elevation errors (that were 5 μGal) to 1 μGal. Montgomery (1971) also recommended screening the gravimeter (with a tent or umbrella) to reduce errors in observed gravity due to temperature induced tilt of the gravimeter (that was estimated to be 10 μGal). Montgomery (1971) modelled the gravitational effect of soil moisture based on observed monthly rainfall using a Bouguer slab model and found it to be up to 4 μGal, which was well under the 26 μGal error computed for the field campaign (using a LaCoste and Romberg G meter). Montgomery (1971) claimed modifications to the gravimeter and more accurate tidal corrections could reduce the computed error to 10 μGal, and recommended observing soil moisture (with a NMM) if large changes are expected.

The method of Montgomery (1971) was applied in subsequent studies using a LaCoste and Romberg D meter (Pool and Eychaner, 1995; Pool and Schmidt, 1997; Pool, 2008) or Scintrex CG5 (Gehman et al., 2009) and observed groundwater levels together with a Bouguer slab model to determine aquifer specific yield in Arizona

Pool and Eychaner (1995); Pool and Schmidt (1997); Pool (2008), California Metzger et al. (2002); Howle et al. (2003), and Colorado Gehman et al. (2009), in none of these studies was soil moisture measured, although Pool (2008) again highlights the importance of soil moisture to the observed gravity change. In this thesis an NMM is used during gravity field campaigns to observe profile soil moisture from the surface to groundwater level, while 0-90 cm soil moisture and groundwater level are also continuously measured (together with precipitation). The soil moisture and groundwater level (and precipitation) measurements are taken within 2 m of a rigid triangular platform with a hollow centre that allows precipitation and evapotranspiration to pass. The solid platform used to take gravity measurements with a Scintrex CG-3M relative gravimeter is located less than 10 cm from the grass covered soil surface and attached to 3 approximately 2 m long star pickets (inserted fully in the soil).

In one of the first studies conducted in the field, Lambert and Beaumont (1977) investigated the effect of coastal groundwater level changes on observed relative gravity by attaching mounts to piezometers near the east coast of Canada and conducting four field campaigns over 2 years using a LaCoste and Romberg D meter. Each campaign was in spring and autumn and designed to capture the maximum and minimum groundwater levels, which were expected to vary by up to 5 m. They used two small study areas in their investigation, 0.6 and 3 km profiles each running perpendicular from the coast inland, covering 6 bores, with a surface elevation change of less than 15 and 30 m respectively. With each area containing only a handful of sites (four and five respectively). Because of this they were able to construct complete homogeneous gravity networks so that every pair of sites in each area was connected, and by the same number of ties (ten, or nine for one campaign). Lambert and Beaumont (1977) point out that for a gravimeter standard deviation of 5 µGal at least ten repeated observations are required to achieve a precision of 1-2 µGal on the gravity difference. The sites were observed in a manner that covered the whole network (with at least one tie between each pair of sites) and then repeated the coverage (ten times), rather than repeating all the ties between a pair of sites before moving on to the next pair. The gravimeter was transported by car (resting on a horsehair cushion) and shielded at each site from wind and sunshine by a tent. The gravimeter was placed on a mount attached to the top of the steel cased piezometers at each site (except one site in the larger network without a piezometer where a 2 m deep concrete pier was used). While not discussed it appears the entire field campaign was observed without a break with a plot showing 100 ties over the five site network in a consecutive period of 26 hours. Network adjustment was performed on the gravity ties with a linear drift for the whole campaign estimated as part of the network adjustment. After network adjustment the standard deviation of the ties ranged from 4.9-5.1 μGal at the four site network and 4.9-7.2 μGal at the five site network (average of 65 and 112 ties respectively), with a precision on the gravity estimate at a single site ranging from 0.9-1.4 μGal (gravity was assumed constant at one site in each network with no error attributed to this value). Over 6 months (spring to autumn) a statistically significant decrease of gravity at three of the sites in the smaller four station network was observed relative to the reference site closest to the coast (chosen as the reference as the smallest groundwater level variations were observed at this location). The gravity decreases ranged from 10 μGal to 8.5 μGal closer to the coast and corresponded to an observed groundwater level decrease of 2.5 m at the site furthest from the coast. Lambert and Beaumont (1977) mention the groundwater level at the reference site (within 50 m of the coast) and adjacent gravity site (where an 8.5 μGal decrease was observed) was corrected to remove tidal fluctuations in groundwater level of up to 0.5 m. Solid Earth tides were computed with the Longman (1959, 1961) method, the gravitational effect of air pressure and ocean tide loading was not considered.

At the larger five station network (on a 3 km profile) groundwater level changes of up to 7 m were observed at the reference site (1.5 km from the coast), however (like the smaller network) the gravity was assumed to remain constant at this site. The (6 month) gravity changes at the other four sites relative to this site range from less than 1 to 8.9 μGal but were generally of the opposite sign to the observed groundwater level change (at three of the four sites where groundwater level is observed). Indeed Lambert and Beaumont (1977) point out that the piezometer at the reference site and site 3 km inland (where gravity increases of up to up to 4 μGal from autumn to spring are observed relative to the reference site) were cased to 30 m depth with a thin 2.5 m cover of unconsolidated material covering claystone (so the observed groundwater level may have been from a confined aquifer). Lambert and Beaumont (1977) claim that unobserved soil moisture is having a significant effect on the observed gravity changes with an expected 20 % vol/vol increase from autumn to spring of the loam till (8-28 % vol/vol) resulting in a gravity change of 4.3 μGal (over the 2.5 m soil depth at the two sites). Soil moisture (and rainfall) were not observed.

Pool (2008) also found significant gravity increases at piezometers (in Arizona) cased to a significant depth with the deep groundwater level not corresponding to observed gravity changes. Pool (2008) also claim unobserved soil moisture changes in the unsaturated zone are causing the observed gravity changes, and point out that observed soil moisture (about 100 km from the piezometers) is equivalent to a gravity signal of 4 μGal.

Lambert and Beaumont (1977) coin the term microgravimetry (but dismiss it in favour of the SI compliant term nanogravimetry) and forsee the usage of gravity observations together with well pumping (to force a change in the groundwater level). Such usage is described theoretically in Damiata and Lee (2006) and Leirião et al. (2009) and investigated via synthetic studies (Blainey et al., 2007; Herckenrath et al., 2012) and a real field study (Christiansen et al., 2011a) to determine the aquifer specific yield and hydraulic conductivity from relative gravity observations and well drawn down data. Other studies have used gravity observations to track injected water via a well (Hare et al., 1999; Ferguson et al., 2007, 2008; Hare et al., 2008; Davis et al., 2008) or recharge ponds (Chapman et al., 2008).

Dragert et al. (1981) used two LaCoste and Romberg D Meters (simultaneously) to observe gravity changes at up to 27 sites along three profiles of 40-90 km on Vancouver Island, Canada, twice a year (separated by 4 months) for 3 years. Due to the large area covered the profile method was used for the survey (rather than the complete network recommended by Lambert and Beaumont (1977)), however the two northern profiles (one of which was along the edge of a 40 km long lake) used interlocking triangles (i.e. each site was connected to at least three neighbouring sites on the profile). At each site gravity was repeatedly observed at exactly the same location (and orientation) by using brass plates attached to bedrock with indentations in the brass plates to exactly position the gravimeter legs, and the same height by fixing one of the levelling legs of the gravimeter (and levelling with the other two legs). The gravity measurements were taken in a tent to shield the gravimeter from the wind and sun, and a suspension case was used for transportation between the sites to minimise the vibration of the gravimeter (after the findings in Hamilton and Brulé (1967)). The survey method consisted of at least 8 consecutive ties between any two sites (contrary to the recommendation of Lambert and Beaumont (1977)) to minimise the gravitational effect of atmospheric pressure and ocean tide loading. The standard deviation of a tie (gravity difference between two adjacent sites) averaged 1.8 μGal over the 6 field campaigns, with each campaign taking 18 days to complete. The error in the estimated gravity values at each site after network adjustment increased with distance from the arbitrary reference sites (where gravity was assumed zero with a zero error), Dragert et al. (1981) attributed this to the loose network control of the profile method. A separate network adjustment was performed for each gravimeter with the gravimeter readings at the same site and time (relative to the reference site) disagreeing significantly both before and after network adjustment, with gravity differences between the two LaCoste and Romberg D Meters (after network adjustment) reaching up to 40 μGal (at the same site at the same time) and the standard deviation of the variation from the average of the two gravimeters 4.2 μGal, even though the gravimeters were calibrated before and after each field campaign on a calibration range.

Dragert et al. (1981) highlight the issue of a large hydrological (lake level) change during a long (18 day) field campaign and the bias this creates on the gravity estimates after network adjustment, which they estimate at 5 μGal at one site adjacent to the lake (and all subsequent sites observed after this event and tied back to the site adjacent to the lake), due to an 84 cm lake level increase caused by an upstream dam release. The calculated gravitational effect of lake level variations (maximum of 3 m) correlated well with observed gravity variations at two sites (although the observed gravity at one of these sites was adjusted to account for the lake effect) but not at the other 4 sites that were expected to be affected by lake level variations. Groundwater level and soil moisture was not observed on Vancouver Island, the method of Lambert and Beaumont (1977) was used for network adjustment that used the Earth tide correction of Longman (1959, 1961), the gravitational effects of atmospheric pressure and ocean tide loading were not calculated.

Christiansen et al. (2011a) used a Scintrex CG-5 to observe gravity changes over 4 months at 5 sites on a 150 m profile perpendicular to the Matsibe River in Botswana, the elevation of the sites varied by less than 1 m. Gravity pads were constructed by pouring approximately 10 l of concrete into a hole dug in the ground (compacted sand), piezometers were installed to a depth of 3.5-5 m adjacent to the gravity pads with a groundwater level of 2-3 m below the surface. Soil moisture was not observed. A flood event of 38 days was used to calibrate a groundwater model with both gravity changes and observed groundwater level, during this period the river height increased to 62 cm (from a dry river bed), with a width of almost 70 m (the first gravity site was located on the edge of the flooded river 35 m into the profile). Before the flood event the depth to groundwater level was observed in the middle of the river bed to be approximately 2 m. All gravity sites were tied to a reference site 450 m from the river by 6 ties in succession (like Dragert et al. (1981)) over an hour, the gravimeter was transported by hand (and foot). During measurement the gravimeter was shaded from sun and wind, and the gravimeter height maintained by marking the tripod position on the concrete pad and fixing one levelling leg. The gravity data was corrected for Earth tides using the tidal potential catalogue of Cartwright and Tayler (1971); Cartwright and Edden (1973), it is not clear what Love numbers are used. The accuracy of the gravity changes (difference of a gravity tie through time) were estimated to be 4 μGal. Using the prism formula of Leirião et al. (2009) the (Newtonian) gravity effect of the river water was estimated to be less than 0.2 μGal at the site 35 m into the profile on the flooded rivers edge.

River recharge and evapotranspiration were assumed to be temporally and spatially constant, with soil moisture change assumed negligible. Both an analytical and numerical (MODFLOW) groundwater model were calibrated (using PEST) to synthetic and real gravity and groundwater level data to determine the specific yield, (lateral) hydraulic conductivity, river recharge, and evapotranspiration. Christiansen et al. (2011a) conclude (on the basis of parameter cross correlation and individual parameter uncertainty and identifiability) that an even weighting of gravity and groundwater level data in the calibration is optimal and while the gravity data is particularly sensitive to specific yield it can also be used to retrieve the other parameters including evapotranspiration (assumed spatially and temporally constant). Soil moisture was not retrieved.

In the study of Jacob et al. (2009) gravity was observed with a Scintrex CG5 at the surface of a plateau in France and 60 m down a pothole (in the karst aquifer).

Four observations were made at the surface and three down the pothole (over one day), with one of the gravimeter levelling legs fixed to maintain a constant height. Markings were made on the rock at the surface and down the pothole to reposition the gravimeter legs in exactly the same location each time. Each observation (at the surface or down the pothole) consisted of five gravity measurements, each averaged over 90 s (with a 6 Hz sampling rate). The gravity observations were corrected for Earth tides using the tidal potential catalogue of Tamura (1987) it is not clear what Love numbers were used, ocean tide loading with the ocean tide model FES2004 (the loading method or model is unclear), and atmospheric pressure using a standard admittance of -0.3 μGal/mbar and observed pressure data (with a 15 minute resolution). A polar motion correction was not calculated. The observations at the surface and down the pothole were adjusted via least squares to give an estimate of the gravity difference (from surface to bottom of pothole) and linear drift for the (day long) campaign. Six campaigns were conducted over 17 months and the resultant gravity changes compared to observed absolute gravity at three sites during the campaigns. A good correlation was found (for the 6 data points) for two of the sites closest to the pothole (correlations of 0.95 and 0.89) but the correlation at the third site (0.49) was not as convincing. Soil moisture and groundwater level were not observed.

For the study of Jacob et al. (2010) the Scintrex CG5 was used to observe gravity at 40 sites over a 10 x 10 km area on the surface of the plateau in France, with a typical site separation of 1.5 km. As in Jacob et al. (2009) gravity sites were marked on rock and the gravimeter leg held fixed. Similarly, following Jacob et al. (2009), Earth tides were corrected using the tidal potential catalogue of Tamura (1987) with Love numbers not mentioned, ocean tide loading with the ocean tide model FES2004 (with the loading model not described), atmospheric pressure with a standard admittance of -0.3 μGal/mbar and observed pressure (15 minute resolution) at a single site, and polar motion not calculated. Four field campaigns were conducted over 22 months, with each campaign consisting of 12 loops of 5-10 sites beginning and ending at the same absolute gravity site (for all loops and campaigns). The campaign durations were 8-11 days with gravity observed at 40 sites and 101-114 ties (gravity difference between consecutively observed sites) created, resulting in approximately 10 ties observed per day. The gravity network sampling was designed to observe gravity at most sites twice (in different loops), however most of the gravity ties between sites were only repeated once, with only four ties repeated three times (and none repeated more than three times). Furthermore while the three absolute gravity sites were part of the network, there were no ties (directly) between the absolute gravity sites. Again like Jacob et al. (2009) gravity observations at each site consisted of five 90 s duration measurements sampled at 6 Hz. During measurements a tent was used to shield the gravimeter from the wind and sun, as in Montgomery (1971); Lambert and Beaumont (1977); Dragert et al. (1981); Christiansen et al. (2011a). The gravity ties were adjusted using the method of Hwang et al. (2002) to estimate gravity at each site (relative to the absolute gravity site each loop began and ended at) and linear drift (for each loop). Standard deviation of the gravity tie residuals (difference of observed gravity tie and estimated gravity tie after network adjustment) was 2.9-5.8 μGal (for the four field campaigns). While the average error (over all 40 sites) of site gravity (estimated from the network adjustment) ranged from 2.4 μGal to 5.0 μGal for the four field campaigns. This corresponded to an estimated error of 4.0-5.5 μGal on the average (over 40 sites) gravity change (from one field campaign to the next), that ranged from -12.3 μGal to 13.2 μGal for the four campaigns. The 12.2 μGal decrease of average gravity (over 40 sites) between the first and second campaign contrasted with observed absolute gravity decreases at the three absolute gravity sites of 2-18 μGal, while the subsequent 13.2 μGal increase of average gravity (over 40 sites) between the second and third campaign corresponded well with absolute gravity increases of 11-15 μGal. The last 12.3 μGal decrease in average gravity (over 40 sites) between the third and fourth campaign contrasted to a 1 μGal increase in absolute gravity at one site, and decreases in absolute gravity of 7 and 10 μGal at the other two sites. Jacob et al. (2010) hypothesise that variations in observed gravity between the 40 sites may be due to spatially variable evapotranspiration and state that the soil depth and vegetation type is highly variable between the sites. Soil moisture and groundwater level were not observed.

Christiansen et al. (2011c) used a Scintrex CG5 over four days at three sites around a 20 x 30 m reservoir (usually used to test model ships) in a laboratory in Denmark to measure the gravity changes associated with lowering the water level by 68.4 cm. During the four day experiment (water drainage took only 1.15 hours) there was less than 5 mm of rainfall. Gravity was measured with a network of 3 sites around the reservoir, two at the midpoint of the short and long edges, and one in the centre of the reservoir. All three sites consisted of platforms with the location for the gravimeter marked. The site in the centre consists of a platform attached to a 2.8 m pole, with the platform only 30 cm above the initial water level. The two other sites were 10 and 15 m from the central site and consisted of platforms attached to the edge of the reservoir. It is not clear how thick the central pole in the reservoir was or generally how stable the three platforms were, indeed observed tilts of up to 200 arc seconds over 67.3 hours at the central site (and 100 arc seconds over the initial 5 hours) indicate the central platform on a pole was clearly not stable. A fourth hydrologically stable reference site was used 72 m from the central site. The gravitational effect of the water level change was calculated at the reference site using the prism formula of Nagy (1966) and deemed negligible. Conversely a 1 m change in water level at the central site was calculated as 41.9 μGal using the Bouguer slab approximation and only 37 μGal using the formula of Nagy (1966) (due to the finite dimensions of the reservoir). The gravimeter was transported by hand to the two sites on the edge of the reservoir and by rowboat to the central site, it is not clear how the gravimeter was transported to the reference site but based on the distance involved it was probably by hand. The gravimeter was shaded by an umbrella when taking measurements at the reference site. The depth of water was initially 2.5 m with the central platform approximately 32.5 cm above the water level and the other two sites 85.5 and 94.3 cm above the initial water level (i.e. the elevation of the three sites on the reservoir differed by a maximum of 62 cm), it is not clear what the elevation of the reference site was. It appears one of the gravimeter levelling legs was not held fixed but rather the height of the gravimeter above the platform was measured (at one of the levelling legs) with a ruler and the gravimeter adjusted to the same height for each measurement, the levelling of the gravimeter was then done using the other two levelling legs (as would be done if one of the legs were held fixed).

The network was observed at the start and end of the four day experiment, with 6 consecutive ties between the reference site and each of the sites on the reservoir (as in Christiansen et al. (2011a); Dragert et al. (1981)), giving a total of 18 ties for each of the two campaigns. Each observation at a site consisted of 3 measurements of 55 s duration with a 6 Hz sampling rate. The gravity observations were corrected (using the same method as Christiansen et al. (2011a)) for Earth tides using the Cartwright and Tayler (1971); Cartwright and Edden (1973) tidal potential catalogue (the Love numbers used are not mentioned), ocean tide loading using the FES2004 ocean tide model (the method of loading is not clear), and atmospheric pressure using a standard admittance of -0.3 μGal/mbar and air pressure data from a weather station 5 km from the study site. A polar motion correction was not calculated. The gravity difference between the reference site and each of the three sites on the reservoir was calculated by network adjustment of just the 6 ties between the reference site and the site of interest, as well as a standard network adjustment of all 18 ties from all four sites in the network. A linear drift was also estimated as part of the network adjustment. After network adjustment the gravity estimate error at each site was 2 μGal (for both the estimates using a 4 site network, and those adjusting the gravity difference between only 2 sites), except for one case of a 3 μGal error when the network adjustment used only the 6 ties between that site and the reference site. Consequently the error on the gravity change at each of the three sites on the reservoir is 3 μGal, with a reduction in observed gravity (after network adjustment) of 27 μGal at the central site and 16 and 21 μGal at the other two sites. This corresponded well with the calculated gravity reduction using the Nagy (1966) formula of 27 μGal for the central site and 16 μGal for both of sites on the edge. Christiansen et al. (2011c) can not explain the 5 μGal discrepancy between the observation and prediction at one of the sites on the edge of the reservoir, but point out it is not statistically significant given the 3 μGal standard error on the gravity change at that site.

Between the two network campaigns gravity was observed continuously (55 s duration measurements with a 6 Hz sample rate) at the central site to determine the gravimeter drift (over two days) and observe gravity during the water release (about 56 min of gravitational drainage followed by 13 min of pumping). Despite arguing that the gravimeter tilt should be kept less than 20 arc seconds to reduce tilt error to less than 1 μGal, Christiansen et al. (2011c) show results from the time series observation used to determine gravimeter drift and monitor the removal of water storage where the gravimeter tilt reaches 200 arc seconds. Using the time series from 14-66 hours into the experiment (ignoring the large tilt period of the initial 14 hours) the drift was calculated as 17.2 μGal/hour (or 413 μGal/day). Over the 1.15 hour period of water storage removal the change in gravity due to drift (20 μGal) is comparable to the observed change in gravity due to the water storage decrease (27 μGal). Similarly, drift calculated during network adjustment of the reference site and 3 reservoir sites was calculated as 17 μGal/hour before the water storage removal, and 23 μGal/hour after (with standard deviations of 5 and 9 μGal respectively). For the central site, the observed gravity decrease of 27 μGal (from the time series of gravity measurements every 55 s) corresponds well with the observed gravity change of 27 μGal after network adjustment (of the network observations before and after the water was removed) and the calculated gravity change of 27 μGal from the prism formula of Nagy (1966). However the RMSE of the observed gravity time series (with 55 s duration measurements averaged to approximately 5 minute observations) and the calculated gravity series using the observed water level and Nagy (1966) formula was 6.5 μGal. The RMSE would probably have been higher if the original gravity measurement resolution of 55 s was used (water level was measured every 5 s). Christiansen et al. (2011c) acknowledge the RMSE between observed water level and gravity at the central site is high and most probably due to vibrations (of the moving water) and the instability of the platform on a 2.8 m pole of unknown diameter. Christiansen et al. (2011c) do not mention what happens to the boat after transporting the gravimeter to the central site, but presumably it contributes to the noise. In discussing the applicability of ground-based gravity to monitor terrestrial water storage, Christiansen et al. (2011c) conclude that gravity changes will always integrate the terrestrial water storage over groundwater and soil moisture changes and that additional information is required to disaggregate the terrestrial water storage and retrieve soil moisture changes. In this thesis a land surface model (vertical 1D Richard's equation based soil moisture model) is used to disaggregate TWS from ground-based gravity observations and retrieve profile soil moisture.

In one of the first field studies of the effect of soil moisture on gravity variations Mäkinen and Tattari (1988) used two LaCoste and Romberg Model-G meters to monitor gravity at a hydrological experimental field site in Finland for three years. The gravity field campaigns were conducted at 2 week to 2 month intervals. Each campaign consisted of 2 consecutive survey days (one with each gravimeter). For each day gravity was measured first at the hydrological experimental site, then at a bedrock reference station (a granite outcrop 2 km from the site) where the variation in water storage was considered negligible. This was repeated another five times, giving a total of six observations each at the hydrological field site and the bedrock reference station or 11 gravity ties between the two sites, which took one person (with car transport) 6 hours to complete. Apparently the gravity difference between the two sites was only 60 μGal (which corresponds to an elevation difference of 19.4 cm by the free air equation (Eq. 2.6)).

Groundwater and soil moisture were monitored in two separate access tubes approximately 6 m apart. The aquifer is unconfined with a specific yield of 0.265 and average groundwater level of 7 m below the surface. The groundwater level was measured once a week with a tape measure. The maximum variation was 1.37 m in the 17 years from 1968 to 1985. For this same period the mean annual precipitation was 613 mm and the maximum soil moisture variation (in the top 3 m) was 185 mm (or 6.2 % vol/vol). Soil moisture was measured every month or two with an NMM, with the interval shortened to two or three weeks during snow melt. The access tube for the NMM was 3 m deep and neutron counts were observed every 10 cm (for 15 seconds) descending and then ascending (the counts above 20 cm were discarded due to neutrons escaping to the atmosphere). The gravity observations were made on a cylindrical concrete pier (115 cm diameter and 55 cm high) about 8 m from the NMM access tube and 2 m from the piezometer.

The gravity change predicted from the observed soil moisture (from 20 to 300 cm) using a Bouguer slab model was 8 μGal and from the groundwater level 6 μGal (with a total predicted effect of 13 μGal). The maximum observed range of gravity was 13 μGal (averaging the surveys from the two gravimeters for 29 field campaigns) and the range of the residual was 8 μGal (after subtracting predicted from observed gravity) with a standard deviation of 2.0 μGal. A correlation of 0.77 was found between predicted and observed gravity.

The investigations of Mäkinen and Tattari (1988) were extended in Mäkinen and Tattari (1991a) to cover an extra 19 months of data at the original site and to monitor a second hydrological experimental field site in Finland selected to have more clay (and silt) in the soil. As in the study of Mäkinen and Tattari (1988) gravity observations were made at the second site on a concrete pier (height 55 cm and diameter 95 cm). Groundwater and soil moisture were monitored with a tape measure and NMM respectively (the access tube for soil moisture at the second site was deeper at 4 m) at two week and one to two month intervals respectively (with the soil moisture observations occurring every two to three weeks during snow melt and groundwater always measured at the same time as soil moisture). The second site had a different bedrock reference site 5 km from the site with a gravity difference of 30 μGal (that only corresponds to an elevation difference of 9.7 cm by the free air equation (Eq. 2.6)). The soil type at the second site contained more silt and clay than the first site (that is predominantly sand), the water table (again in an unconfined aquifer) was much closer to the surface (average groundwater level depth of around 1.5 m) and the specific yield of the aquifer was much lower at 0.05 (compared to 7 m and 0.265 respectively at the first site) so that the groundwater change of 1.6 m corresponded to a terrestrial water storage (TWS) change of only 80 mm and a predicted gravity change of 3 μGal (Mäkinen and Tattari, 1991b). The change in soil moisture at the second site was negligible (compared to a 185 mm TWS change at the first site). In total 45 gravity observations were made at the first site and 25 at the second, with the standard deviation of the mean of the two gravimeters higher at the second site (2.1 μGal) than the first (1.5 μGal). The range of observed gravity at the second site was 12 μGal (similar to the 13 μGal range observed at the first site), however the predicted gravity (from soil moisture and groundwater observations) was only 3 μGal peak to peak (compared to 13 μGal at the first site). The reason for the discrepancy between the predicted and observed gravity at the second site is unknown (Mäkinen and Tattari, 1991a,b) however the gravity changes observed at both sites are similar and there was a drainage ditch and (possibly cropped) field within 4 and 200 m (respectively) of the second site that may have affected the representativeness of both the groundwater level and soil moisture observations at that site. Mäkinen and Tattari (1991b) conclude that large seasonal changes in evapotranspiration cause too much uncertainty in terrestrial water storage for rainfall data to be used as a sole estimator of hydrologically induced changes of gravity. Furthermore, only groundwater level data is not enough for a successful determination of the total water storage change in the profile, soil moisture measurements down to the groundwater level are necessary, particularly for sandy soils. In this thesis gravity is observed (with a Scintrex CG-3M) at 4 sites (with silt loam soil) where profile soil moisture is measured down to the groundwater level (with an NMM and permanently installed soil moisture sensors), together with groundwater level and precipitation. The observed TWS is converted with a Bouguer slab approximation to a predicted gravity change and compared to observed gravity changes.

Similar to Christiansen et al. (2011a) who calibrated a groundwater model (MODFLOW) to gravity changes observed with a Scintrex CG5 at a small field area (150 m profile), Christiansen et al. (2011b) calibrate a soil moisture model (MIKE SHE) to gravity changes (observed with a Scintrex CG5) in a small field site (107 m^2). Christiansen et al. (2011b) conducted an irrigation experiment over 3 weeks in Norway on a grass field with a 6 % slope. The rooting depth of the grass, precipitation and evapotranspiration during the irrigation experiment is unclear. However the entire 10.33 x 10.33 m irrigation area was covered by a large tent to minimise the effects of precipitation and evapotranspiration. Groundwater level was not observed, with the site 30 m above a nearby lake level (lateral distance to the lake is unclear). The vadose zone is 25-30 m deep and consists of glacial deposits that are mainly sand and gravel with clay lenses. While groundwater level was not monitored, four access tubes to a depth of 11 m were installed in the centre 3.5 x 3.5 m of the irrigation area. The access tubes were used to measure soil moisture via ground penetrating radar (GPR) with a transmitter and receiver inserted in two tubes and the ratio of the wave velocity from GPR in the soil and air used to calculate a relative permittivity that was converted to soil moisture using the calibration of Topp et al. (1980). Soil moisture was measured (daily, with three data gaps in the 21 days) every 25 cm from the surface to 10 m depth, but the 0-1 m soil moisture from GPR was deemed unreliable and the observation at 1.25 m was somehow extrapolated to the surface. How the 1.25 m soil moisture was extrapolated to the surface is unclear. Gravity was observed at 3 sites (each separated by about 5 m) and tied to a reference site 30 m away. Transportation was not discussed but with the distances involved it is reasonable to assume the gravimeter was transported by hand (as in Christiansen et al. (2011a,c)). Gravity observations were made with the same method as Christiansen et al. (2011a,c)) with 10 ties in succession between a single site and the reference site. This follows the approach of Dragert et al. (1981) who observed a much larger network of 27 sites on 3 profiles of 40-90 km length, but is contrary to the recommendations of Lambert and Beaumont (1977) who observed two networks of 4 and 5 sites over profiles of only 0.6-3 km that are much more compatible with the scale of the network used by Christiansen et al. (2011b). Each gravity observation at a site consisted of three or four 55 s gravity observations that were corrected for Earth tides using the Cartwright and Tayler (1971); Cartwright and Edden (1973) tidal potential catalogue (as done for Christiansen et al. (2011a,c)), Love numbers were not discussed. Ocean tide loading, polar motion and post glacial rebound were not calculated. Similarly the gravitational effect of atmospheric pressure was not calculated. Forty gravity ties were made to the central site in the irrigation area, with only 16 and 4 ties made to the other two gravity sites 30 cm outside the irrigation area. The average standard deviation of the gravity changes (of a gravity tie through time) was 1.7 μGal. The platform for the gravimeter at the two sites outside the irrigation area was created by pouring concrete directly into a hole dug in the soil (similar to Christiansen et al. (2011a)) to create concrete cubes with a 40 cm side length. The platform for the central gravity site was somehow created above the irrigation system. Similar to Christiansen et al. (2011c), the stability of the central gravimeter platform that was the main focus site of the study is unclear. In this thesis the stable stainless steel gravimeter platform is attached to three approximately 2 m star pickets inserted in the soil to depth of refusal (and ground to surface level).

Below 6 m, the maximum observed soil moisture was 10 % vol/vol, while from 1-5 m the soil moisture only varied from 8-18 % vol/vol, the range of soil moisture in the top 1 m of the soil profile is unknown. The soil moisture from 1.25 m was extrapolated to the surface, how this was done is unclear. The terrestrial water storage (TWS) from 0-10 m observed via the (GPR) soil moisture was compared to the known volume of irrigation water and found to agree for the first 7 days of the irrigation experiment but after this point the observed TWS from 0-10 m did not increase (as soil moisture did not increase at any depth). At the end of the irrigation experiment the discrepancy between the TWS and irrigation volume reached around 70 % (about a 90 m^3 water loss). The observed gravity changes reflected the TWS with a clear correlation with both the irrigation volume and TWS for the first 5 days of the experiment that corresponded to a 5 μGal increase in gravity. Observed gravity changes reached 15 μGal with a mean maximum of around 9 μGal that correspond to a mean maximum of TWS of around 50 m^3 (despite 130 m^3 being applied via drip irrigation). However scatter of up to 20 μGal and a sinusoidal variation with a weekly period and 5 μGal amplitude was observed. Christiansen et al. (2011b) could not explain the observed sinusoidal gravity changes despite the gravity observations at both the site in the centre and edge of the irrigation area showing the same behaviour. Furthermore the magnitude of gravity changes at both sites was equivalent despite initial modelling using a Richard's equation model of soil moisture (MIKE SHE) indicating the magnitude of gravity change at the central site (modelled change of 20 μGal) should be double that of the site on the edge of the irrigation area.

A sensitivity analysis of the gravity data to the soil moisture hydraulic parameters was conducted by generating synthetic gravity with the method of Leirião et al. (2009) from modelled soil moisture using a constant infiltration rate (of 86.2 mm/day). The soil properties were spatially homogeneous to a depth of 25 m (with the model using 4 cm layers), and based on laboratory analysis of field samples from a site nearby (30 m distant). Saturated hydraulic conductivity was 93.7 mm/h (or 2.25 m/day), residual and saturated soil moisture 0.4 and 42 % vol/vol respectively, and two water retention curve shape parameters were also set. The five parameters were varied by 5 % from the initial values and the model run for 3 weeks using the constant infiltration forcing and an initial soil moisture of 10 % based on (GPR) soil moisture observations. The model was not sensitive to the residual soil moisture content as the initial and subsequent soil moisture was higher than the residual soil moisture, the model was also not sensitive to one of the water retention curve shape parameters. The model was most sensitive to the saturated soil moisture parameter with a change of up to 1.5 μGal (corresponding to a change in saturated soil moisture from 42 to 44.1 % vol/vol), and to a lesser extent the saturated hydraulic conductivity (0.5 μGal change). The magnitude of the (gravity effect of the) soil moisture signal is calculated to be 20 μGal at the central gravity site and up to 10 μGal at the two sites on the edge of the irrigation area using the (parameters based on lab analysis of field samples). Christiansen et al. (2011b) also make the point that the gravimeter is most sensitive to soil moisture near the surface of the soil profile and in the synthetic example 5 μGal of the 20 μGal gravity change at the central site is due to soil moisture from 0-1 m depth, while 10 μGal is from soil moisture from 0-2.5 m depth, 15 μGal from soil moisture at 0-5 m depth and 20 μGal due to soil moisture from the surface to 10 m depth.

A Richard's equation model of soil moisture (MIKE SHE) was calibrated (using PEST) to both synthetic and real gravity (observed with a Scintrex CG5) to determine saturated soil moisture, hydraulic conductivity and a water retention curve shape parameter (previously identified as retrievable). For the synthetic gravity data (with a 1.7 μGal error applied) calibrating one parameter at a time (while fixing the other two to the true values) was successful in retrieving each of the parameters and with very narrow error bounds. When two parameters were retrieved simultaneously (while holding one fixed to the true value) the error bounds were much larger and the parameters were underestimated from the true value, although in all cases (except one) the error bounds covered the true value (as the error bounds were so large). Christiansen et al. (2011b) were not successful in calibrating all three parameters at once or the combination of saturated hydraulic conductivity and the shape parameter and mention a strong dependency on the initial parameters. While an initial estimate of soil moisture was required for the calibration (assumed as 10 % vol/vol), the initial soil moisture was not calculated as part of the calibration. For the calibration to the real gravity data only the gravity changes at the centre site for the first 15 days of the 21 day irrigation experiment were used. Furthermore the calculated gravity was based on modelled soil moisture from 0-5 m depth only (even though soil moisture was modelled to 25 m depth). Again the calibration was unable to retrieve all three parameters simultaneously, or the combination of saturated hydraulic and the shape parameter, or indeed the shape parameter alone. Again as in the synthetic case, when two parameters were calibrated simultaneously the error bounds were large but when a single parameter was calibrated it was precisely retrieved. The estimated saturated hydraulic conductivity based on the field data was higher than the default parameter used. Again while an initial estimate of soil moisture was required for the calibration, the initial soil moisture was not calculated as part of the calibration. Furthermore the temporal or spatial distribution of the soil moisture was not retrieved. Soil moisture was not retrieved from ground-based gravity. In this thesis (profile) soil moisture is retrieved from ground-based gravity using a Richard's equation based land surface model and PEST to calibrate the initial soil moisture conditions (for a moving window) to the gravity observations.

Section Summary

From the studies of hydrology and gravity some common threads emerge, most studies have focused on a time series at a single site (SG) with complex topography, and hydrological observations varying distances from the SG. Quite often the SG is not on the soil surface which complicates the interpretation of the hydrological signal (in the observed ground-based gravity data) as anomalous mass above the gravimeter cause a reduction in observed gravity, whereas terrestrial water storage (TWS) below the gravimeter causes an increase in ground-based gravity. The most common TWS observations are groundwater level, although it is not always clear the groundwater level observation is from an unconfined aquifer, with some deep piezometers used in a number of studies. Snow is only considered in a handful of studies, but only affects some sites (depending on climate) and for only a portion of the (time period covered by the) ground-based gravity data set (snow cover and snow melt). Likewise soil moisture is generally not observed. No studies except Smith et al. (2006) and this thesis have observed the entire TWS (profile soil moisture from the surface to groundwater level, and groundwater level) and ground-based gravity at the same time and location (within 2 m). No studies have used a gravimeter platform that allows soil moisture to be observed directly below the gravimeter, as is done in Smith et al. (2005, 2006) and this thesis. No studies have retrieved soil moisture from ground-based gravity, as done in Smith et al. (2011) and this thesis. No studies have assessed the precision (or accuracy) of corrections to the field gravity at a nearby high precision SG, such as is done in this thesis. No studies have considered the robustness of the field gravity network sampling, network adjustment, and gravity change detection, such as is done in this thesis. No studies have systematically corrected field ground-based gravity observations for Earth tides, elastic Earth response, ocean tide loading, atmospheric pressure (attraction and loading), and polar motion as done in this thesis, and directly transferable to gravity observations using an absolute gravimeter or SG. No studies have assessed the impact of internal gravimeter temperature and battery voltage on gravity and explicitly corrected for both.

When observing ground-based gravity in the field with a relative gravimeter, such as in this thesis, high precision observations have been made by:

- Indenting (or marking) the location of the gravimeter feet on a rigid unmovable platform.
- Fixing one levelling leg of the gravimeter.
- Shading the gravimeter from the sun and wind during a measurement.
- Transporting the gravimeter by hand or using a suspension carry case for vehicular transport.
- Tieing gravity field sites to a hydrologically stable (preferably bedrock) reference site.
- Tieing all sites to every other site in the network (a complete network).
- Tieing each pair of sites by at least 8 ties.
- Tieing all pairs of sites in the network by the same number of ties (a homogeneous network).
- Taking multiple measurements of gravity at each site and averaging for each observation (half a tie).
- Integrating a measurement over 1-3 minutes.
- Taking an observation at each site as an average of measurements over approximately 10-20 minutes.
- Using a recent Earth tide potential catalogue for Earth tide corrections instead of using the Longman (1959, 1961) correction.
- Correcting ocean tide loading using a recent ocean tide model.
- Correcting for an atmospheric pressure effect using atmospheric pressure data.
- Using network adjustment on the gravity differences.
- Calibrating the relative gravimeter.

The gravimeter footprint is around:

- 80 m to 1 km for snow;
- 50 m to 1 km for soil moisture;
- 70 m to 2 km for groundwater level,

with the footprint for groundwater approximately 10 times the groundwater level depth (Leirião et al., 2009). Consequently the Bouguer slab approximation is a good approximation of the gravity effect of TWS (snow, soil moisture, and groundwater) within 100 m to 1 km of the gravimeter (Mäkinen and Tattari, 1988, 1991a,b; Peter et al., 1994; Kroner, 2001; Llubes et al., 2004; Hokkanen et al., 2006; Creutzfeldt et al., 2008; Hasan et al., 2008; Longuevergne et al., 2009; Lampitelli and Francis, 2010; Christiansen et al., 2011c).

2.6 Chapter Summary

This chapter described the relationship between ground-based gravity and terrestrial water storage (TWS). The gravity signals larger than TWS were discussed together with methods for their correction. The gravity meters currently available were discussed together with the gravimeters relative pros and cons for detecting terrestrial water storage. This was followed by examples where a terrestrial water storage has been detected in ground-based gravity data with superconducting (SG), absolute, and relative gravimeters. There was a particular focus on studies that had detected a soil moisture signal in ground-based gravity data. No studies have retrieved a soil moisture signal from ground-based gravity data.

For local studies of TWS the gravity of the Earth can be represented in Cartesian coordinates, with the average gravity at the surface 9.8 m/s^2 or 980000000 μGal. Variations in elevation result in a change of gravity of approximately 1 μGal/3mm. The effect of TWS on ground-based gravity can be approximated by a rectangular prism of infinite extent (the Bouguer slab approximation) with approximately 24 mm of TWS corresponding to a 1 μGal gravity change. Larger changes in gravity from Earth tides are due to the Earth's rotation and the gravitational attraction of celestial bodies, principally the Moon and Sun. The theoretical Earth tides are tabulated in tidal potential catalogues, however due to unknown subsurface density variations the actual Earth tides at any location are scaled and offset by parameters (Love numbers). The Love numbers are approximated globally by seismic models of the Earth or determined at a specific location through analysis of a tidal dataset (such as gravity data). Earth tide programs can be used to analyse gravity datasets, or predict Earth tides at a location. Ocean tide loading also causes significant changes in gravity due to redistribution of the ocean mass and flexure of the Earth's crust (that causes both a redistribution of subsurface density, and a change in elevation). Ocean tide loading can be predicted through a combination of an ocean tide model and a loading model (based on a Green function). Ocean tide loading has been found to be significant at Canberra, and even detectable in gravity data from Alice Springs in the centre of Australia. Polar motion is the movement of the Earth's axis of rotation and it results in a significant effect on gravity over 6 months, with a maximum effect at mid-latitudes. The polar motion effect can be predicted extremely precisely using an Earth tide program and data from the International Earth Rotation Service. Post glacial rebound (or glacial isostatic adjustment) is the prolonged response of the Earth's crust to glacial loading during the last ice age (that ended in 5000 B.C.). Post glacial rebound causes a change in gravity due to the change in elevation but is not significant in the Australian region. Atmospheric pressure variations result in a change in gravity due to air mass and density variation, and loading of the Earth's crust (similar to ocean tide loading). Some studies are using global grids of atmospheric pressure from numerical weather prediction (NWP) models, but the standard approach is to correct for observed atmospheric pressure at the site using a pressure admittance of around -0.3 μGal/mbar. Other meteorological signals such as air temperature and relative humidity have not conclusively been shown to affect gravity data.

Ground-based gravity can be measured by absolute or relative gravimeters, with the stationary superconducting gravimeter (SG), the most precise gravimeter currently available. Based on the power and enclosure requirements, transportability, operating range, and cost a portable relative gravimeter is most suited to detect a TWS signal in ground-based gravity data. The Scintrex CG-3M relative gravimeter is one of the most precise portable relative gravimeters with a repeatability of around 5 μGal, however the gravimeter (like all relative gravimeters) suffers from a linear drift of around 420 μGal/day. Additionally a post transport stabilisation effect has been reported for many portable relative gravimeters, including the Scintrex CG-3M.

Hydrological signals in ground-based gravity data have predominantly been investigated at the 25 SG sites distributed worldwide that contribute to the Global Geodynamics Project (GGP). The superconducting gravimeter at Canberra is the only SG in Australia and has been shown to contain no TWS signal in the gravity data. Only a handful of studies have investigated the soil moisture signal in gravity data, and all studies have analysed a single site, except one study that investigated two sites. Most studies of TWS and gravity data have involved groundwater level variations or precipitation data, with some studies also analysing snow cover. No studies have observed total TWS (profile soil moisture from the surface to groundwater level, and groundwater level) and ground-based gravity at the same time and location (within 2 m). No studies have used a gravimeter platform that allows soil moisture to be observed directly below the gravimeter. No studies have retrieved the soil moisture (or TWS) signal from ground-based gravity data.

Chapter 3

Research Approach

The previous chapter presented a literature review of soil moisture monitoring with ground-based gravity data. Informed by the literature review this chapter presents a research approach for the thesis.[1] The approach addresses the following objectives that will be the focus of the chapters as shown:

1. Achieving high precision gravity data.

   (Chapter 4)

2. Detecting a soil moisture signal in gravity data.

   (Chapter 5)

3. Retrieving a soil moisture signal from gravity data.

   (Chapter 6)

The method to detect a soil moisture signal in gravity data is first described in section 3.1, as this determines the gravimeter selection and research approach to achieve high precision gravity data (section 3.2). Lastly the approach developed in this thesis to retrieve a soil moisture signal from gravity data is presented in section 3.3.

[1] Parts of this chapter have been published in the peer-reviewed journal paper Smith et al. (2012), and peer-reviewed conference papers Smith et al. (2005, 2006).

3.1 Detecting a Soil Moisture Signal in Gravity Data

This section describes the research approach used in Chapter 5 to detect a soil moisture signal in ground-based gravity data. The soil moisture monitoring network and data is described in subsection 3.1.1, while the gravity network and data is described subsection 3.1.2. Preliminary results are shown where gravity differences are compared to soil moisture observations at two sites (subsection 3.1.3).

While decades of research has been conducted into the exact hydrological behaviour around particular SGs such as:

- Wetzell, Germany Harnisch and Harnisch (1999, 2002, 2006a,b); Harnisch et al. (2000); Klügel (2002); Klügel et al. (2006); Creutzfeldt et al. (2008, 2010a,b,c, 2012), or

- Moxa, Germany Kroner (2001, 2006); Kroner et al. (2001, 2002, 2004, 2007); Kroner and Jahr (2006); Llubes et al. (2004); Harnisch and Harnisch (2006a,b); Hasan et al. (2006, 2008); Krause et al. (2006, 2009); Naujoks et al. (2006, 2008, 2010),

little research has been done into how best to monitor terrestrial water storage (particularly soil moisture) in a general field setting with ground-based gravity. Furthermore, as highlighted by Creutzfeldt et al. (2010a), the most dominant terrestrial water storage signal in ground-based gravity is soil moisture directly under the gravimeter, and this is a minimal factor at any SG. Moreover, no hydrological signal has been detected at Canberra (Harnisch and Harnisch, 2006b; Van Camp et al., 2010), the only SG located in Australia.

While some indication of a soil moisture signal from directly above the SG was observed in the gravity residual at:

- Moxa, Germany (Kroner, 2001, 2006; Llubes et al., 2004),

- Membach, Germany (Van Camp et al., 2006b),

- Strasbourg, France (Longuevergne et al., 2009),

- Bandung, Indonesia (Abe et al., 2006), or
- Matsuhiro, Japan (Imanishi et al., 2006, 2013),

the analysis of terrestrial water storage effects on ground-based gravity is complicated when there is a mixture of soil moisture and groundwater both above and below the gravimeter (Kroner, 2001, 2006; Kroner et al., 2001, 2004; Kroner and Jahr, 2006; Llubes et al., 2004; Hasan et al., 2008; Naujoks et al., 2008, 2010; Krause et al., 2009; Longuevergne et al., 2009; Takemoto et al., 2002; Abe et al., 2006; Imanishi et al., 2006, 2013), as ground-based gravity is reduced when mass is above the gravimeter but increased when it is below, and gravitational drainage of soil moisture and groundwater together with an upward flux of soil moisture due to evapotranspiration ensures a temporal variation of the signal. Lastly, SGs are typically located in complex mountainous topography and humid climates. Little work has been done into investigating ground-based gravity variations and hydrology in alluvial grassland locations in a temperate climate where the soil moisture signal will dominate. In this thesis a network of soil moisture monitoring sites (Smith et al., 2012) is installed and observed with a portable (Scintrex CG-3M) gravimeter (Smith et al., 2005). The soil moisture probes are well calibrated (Rüdiger et al., 2010) and compared to the network adjusted gravity observations (Smith et al., 2006).

3.1.1 Murrumbidgee Soil Moisture Monitoring Network

The description here is primarily from the journal paper Smith et al. (2012), and describes the 10 year and ongoing Murrumbidgee Soil Moisture Monitoring Network (MSMMN) data set from the semi-arid to humid 82000 km^2 Murrumbidgee River Catchment. The MSMMN data set is available at `http://www.oznet.org.au` and is also part of the International Soil Moisture Network (Dorigo et al., 2011a,b) at `http://ismn.geo.tuwien.ac.at`.

Overview

The MSMMN data set primarily constitutes root zone soil moisture (top 90 cm depth) measured continuously at 38 sites within the 82000 km^2 Murrumbidgee River Catchment. Additionally, soil temperature is measured continuously for various depths at each site, together with precipitation. Land surface model (LSM) forcing data are also available for a large number of sites due to their co-location with Bureau of Meteorology automatic weather stations (AWS). Other data available for a limited number of sites includes soil suction (at 18 sites); soil texture analysis (at 13 sites); and surface fluxes from eddy correlation (at one site for 16 months).

The first 18 sites of the MSMMN were installed during September to November 2001. Eight of the sites are co-located with AWS, while the remaining ten sites are grouped in two clusters of 150 km^2 (the headwaters of Kyeamba and Adelong Creek catchments). The MSMMN was augmented two years later (as part of this thesis) with 20 more (second generation) soil moisture monitoring sites that also record soil moisture over the root zone, soil temperature at a single depth, and precipitation. The second generation sites were upgraded in 2006 to include 0-5 cm soil moisture sensors and soil temperature sensors at 2.5 cm. All MSMMN sites are installed as catchment average soil moisture monitoring (CASMM) sites, in accordance with the recommendations of Grayson and Western (1998) (i.e. mid-slope, in neutrally convergent areas with an aspect close to the catchment average). The second generation sites were installed in two focus areas that complement the first generation sites. The first focus area completes instrumentation of the Kyeamba Creek catchment (extending to the confluence with the Murrumbidgee River) while the second group of sites in the Yanco region is in a (staggered) grid formation to support the usage of remotely sensed soil moisture data (Fig. 3.1).

Recently (August 2009) an additional 24 sites have been installed in two 100 km^2 focus areas near two second generations sites in the Yanco Region. These newer sites measure surface soil moisture (0-5 cm) and soil temperature at three depths (1, 2.5 and 5 cm). These sites have been installed in such a way that they provide validation data at the approximately 36, 9 and 3 km scales of the SMAP satellite (Entekhabi et al., 2010).

Scientific Importance and Use of Data

The MSMMN data can be used for various purposes. For example, the forcing and soil moisture data have been used for land surface model validation and development (Richter et al., 2004).

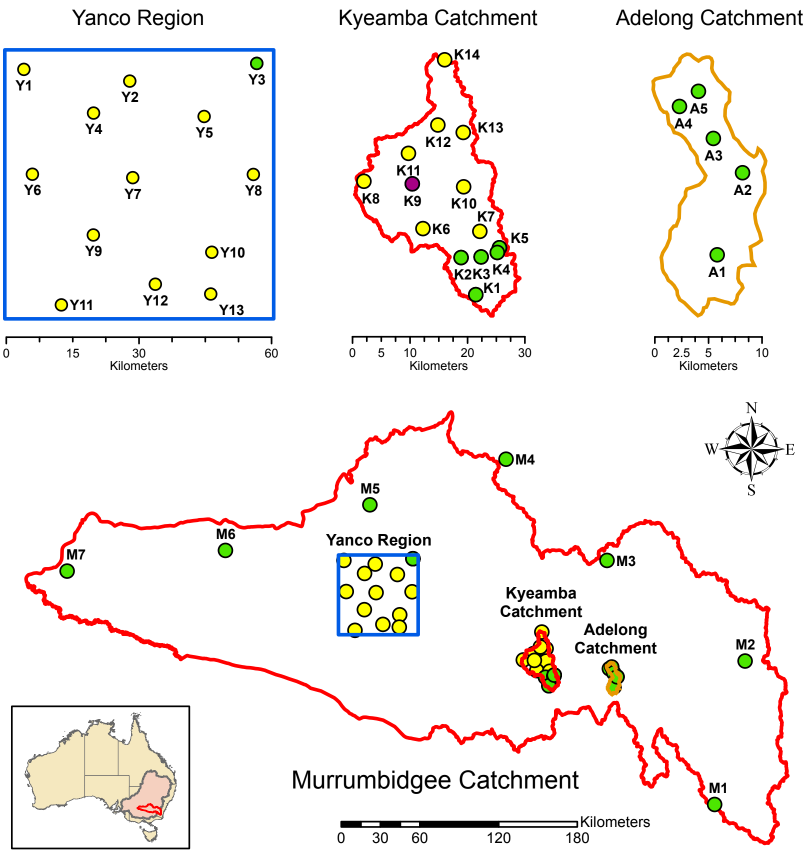

Fig. 3.1 The Murrumbidgee Soil Moisture Monitoring Network (MSMMN) with the Murrumbidgee Catchment and three focus areas shown (modified from Smith et al. (2012)). First and second generation sites are indicated by green and yellow dots respectively, with the purple dot (K9) representing an externally maintained site (with different equipment). Regional Murrumbidgee sites are prefixed with M, likewise Yanco, Kyeamba and Adelong sites are prefixed with Y, K and A. The site M2 is at the Canberra airport. The location of the Murrumbidgee Catchment within the Murray Darling Basin and Australia is shown in the inset.

The MSMMN data is also well suited to studies involving remotely sensed data sets. Using the MSMMN, Ellett et al. (2006) presented a framework to assess the potential of remotely sensed gravity to provide new insight on the hydrology of the Murray Darling Basin. Draper et al. (2009) conducted an evaluation of the AMSR-E satellite soil moisture product and found that the MSMMN in-situ (point) data captured the temporal behaviour of the AMSR-E (areal average) soil moisture measurements and recommended the use of MSMMN data for temporal verification of remotely sensed soil moisture. Latent heat flux data from the MSMMN has been used for validation of MODIS derived evapotranspiration (Guerschman et al., 2009).

The MSMMN sites and data have also been used as the basis of a number of successful field campaigns aimed at developing soil moisture satellite missions using airborne simulators, including the National Airborne Field Experiment in 2006 (Merlin et al., 2008), and more recently the Australian Airborne Cal/val Experiments for SMOS (Peischl et al., 2012), and the Soil Moisture Active Passive Experiments.

The MSMMN has been included as part of the International Soil Moisture Network (ISMN) dataset (Dorigo et al., 2011a,b) and is available at `http://ismn.geo.tuwien.ac.at` as well as `http://www.oznet.org.au`.

Catchment Description

The 82000 km^2 Murrumbidgee River Catchment is located in southern New South Wales (34 ° to 37 ° S, 143 ° to 150 ° E). The Murrumbidgee Catchment is part of the Murray Darling Basin (MDB), located in eastern Australia (Fig. 3.1 inset) that provides 35 % of Australia's gross value of agricultural production (Australian Bureau of Statistics, 2010). This makes the MDB a critical study area for understanding the effect of climate change; drought recurrence; land surface and atmosphere interactions, and feedbacks. It is clearly also an important place to assess the skill of satellites to remotely sense soil moisture. Finally, the diverse climatic, topographic and land cover characteristics of the Murrumbidgee Catchment, typical of much of Australia, make it an excellent demonstration test-bed for land surface model development.

The Murrumbidgee Catchment shows significant spatial variability in climate, soil, vegetation and land use (Fig. 3.2). Elevation varies from 50 m in the west of the catchment to more than 2000 m in the east. Climate variations are primarily associated with elevation, varying from semi-arid in the west, where the average annual precipitation is 300 mm, to humid in the east, where average annual precipitation reaches 1900 mm in the Snowy Mountains. Mean annual areal potential evapotranspiration is fairly uniform across the catchment with a minimum of 1000

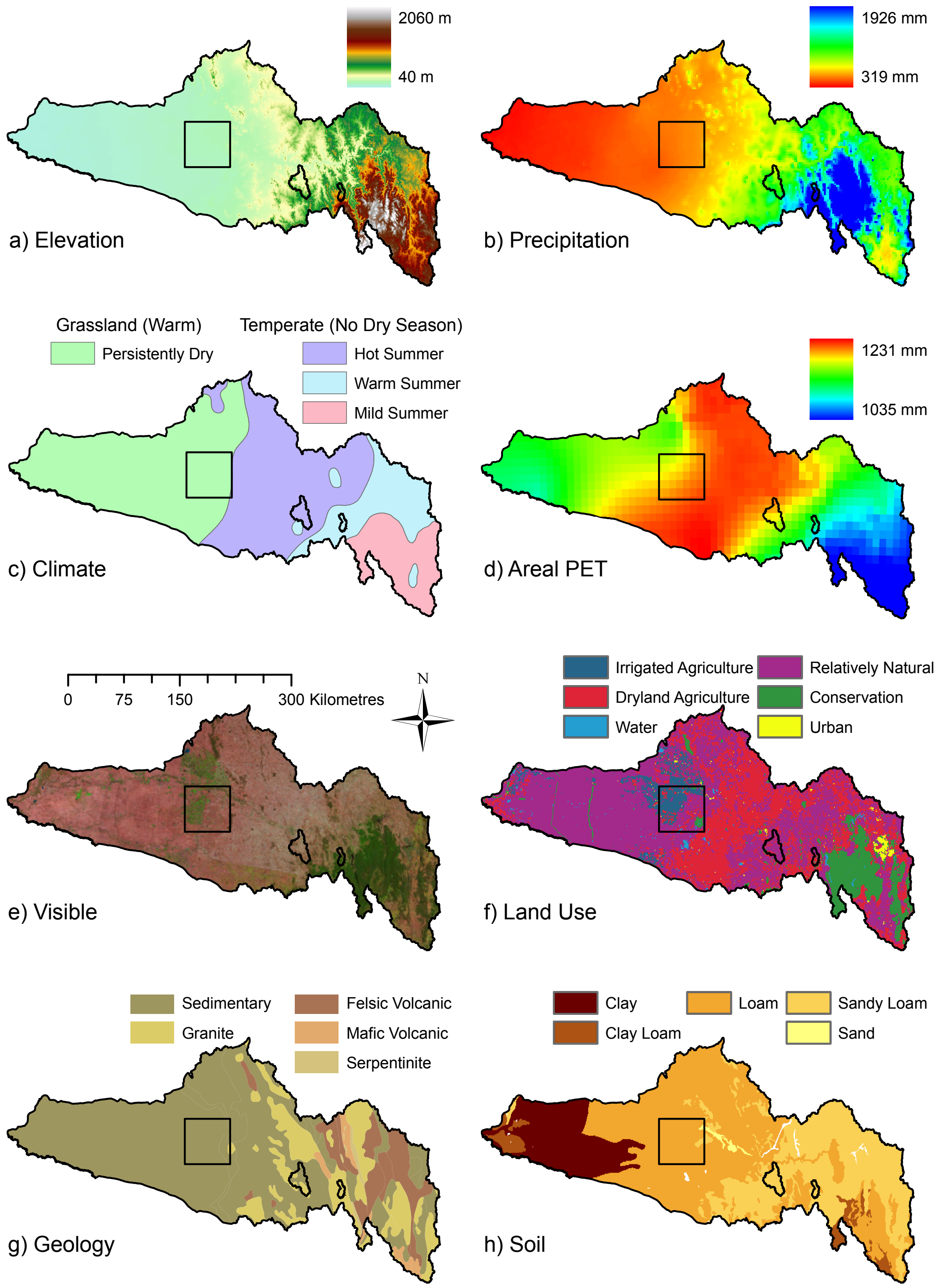

Fig. 3.2 Publicly available Murrumbidgee Catchment spatial datasets.

mm in the south east and a maximum of 1200 mm in the centre of the catchment. The mean annual areal actual evapotranspiration in the Murrumbidgee is roughly equivalent to precipitation in the west but (is water limited and) represents only half of the precipitation in the east; maximum mean monthly precipitation occur in winter and spring.

Soils range from sandy to clayey, with the western plains dominated by finer textured soils and the eastern half of the catchment predominantly medium to coarse textured soils. The geology is primarily meta-sediments with granite intrusions in the more elevated eastern part of the catchment, and aeolian sediments in the western riverine plains. Land use in the catchment is predominantly agricultural with the exception of steeper parts of the catchment, which are a mixture of native eucalypt forests and exotic forest plantations. Agricultural land use varies greatly in intensity and includes pastoral, more intensive grazing, broad-acre cropping, and intensive agriculture in irrigation areas along the mid-lower Murrumbidgee.

Within the Murrumbidgee River Catchment 31 sites are contained in three focus areas of increasing scale; Adelong Creek catchment with 5 sites, Kyeamba Creek Catchment located further west with 13 sites, and the Yanco Region in the western plains with 13 sites (Fig. 3.1). Adelong Creek catchment is a small catchment (approximately 145 km^2) with steep slopes; land use is sheep and beef grazing. Kyeamba Creek Catchment is a medium to small catchment (approximately 600 km^2) where topography is dominated by gentle slopes; land use is predominantly sheep and beef grazing with some dairy. The Yanco Region is a large flat area (approximately 2,500 km^2) with minimal woody vegetation; land use in the west of the region comprises irrigation (the Coleambally Irrigation Area) with rice and barley as the main rotations, while elsewhere land use is dryland cropping (predominantly north) and native pasture (south east). The final 7 MSMMN sites are located near regional centres throughout the catchment. See `http://www.oznet.org.au` for further information.

Data Summary

Common to all sites is a tipping bucket raingauge (Fig. 3.3); three vertically installed Campbell Scientific water content reflectometers that measure soil moisture in the upper 90 cm of the profile (0-30, 30-60 and 60-90 cm); a surface soil moisture probe

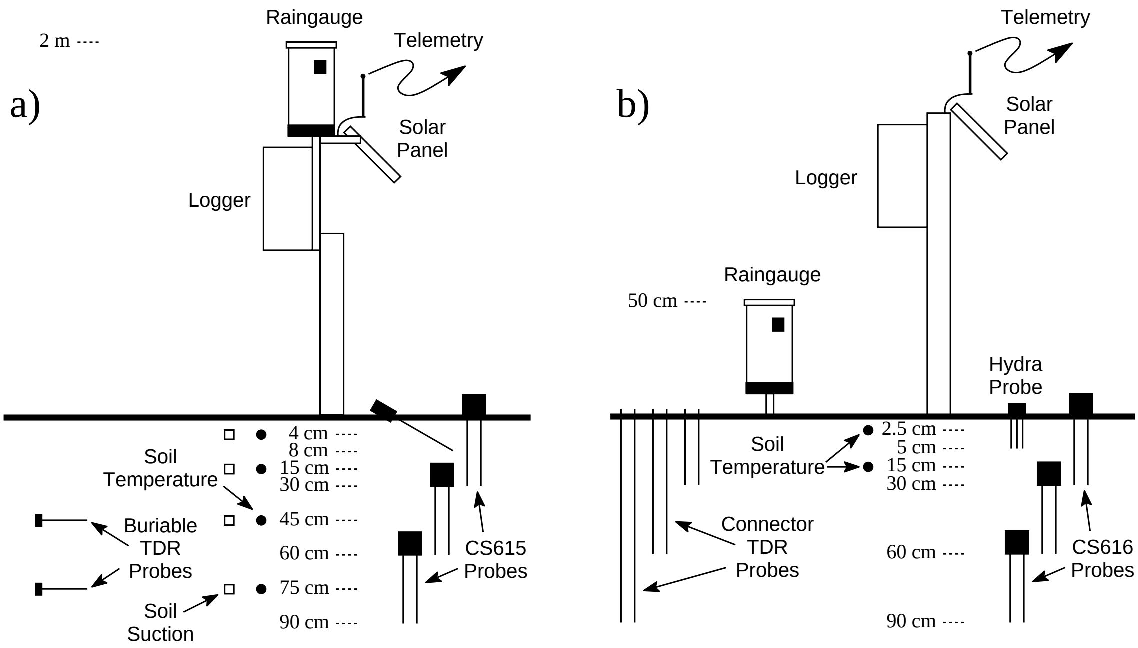

Fig. 3.3 Schematic of the soil moisture monitoring sites: a) first generation, b) second generation.

(0-5 or 0-8 cm); a soil temperature probe at 15 cm depth; and a surface temperature probe (2.5 or 4 cm). Data availability timelines allow a simple visual inspection of data coverage (and gaps) and can be found for each sensor on a site by site basis at `http://www.oznet.org.au`.

Sample data for the year 2005 are shown in Fig. 3.4, where land surface model (CABLE) predictions are also shown for comparison as an example of one use of the MSMMN data (e.g. Smith and Zhang (2007)). This land surface model (Kowalczyk et al., 2006) is to be used in both numerical weather prediction (NWP) and global climate modelling (GCM) in Australia as the land surface scheme of the Australian Community Climate and Earth System Simulator (ACCESS). The good agreement in major seasonal signals confirms the integrity of the field data, despite some systematic differences. The LSM wilting point parameter defines the minimum bound of predicted soil moisture (clearly visible in Fig. 3.4). Furthermore, the model uses a single set of soil parameters for the profile whereas field data supports two distinctly different soil types. This can be attributed to the systematic bias in deeper

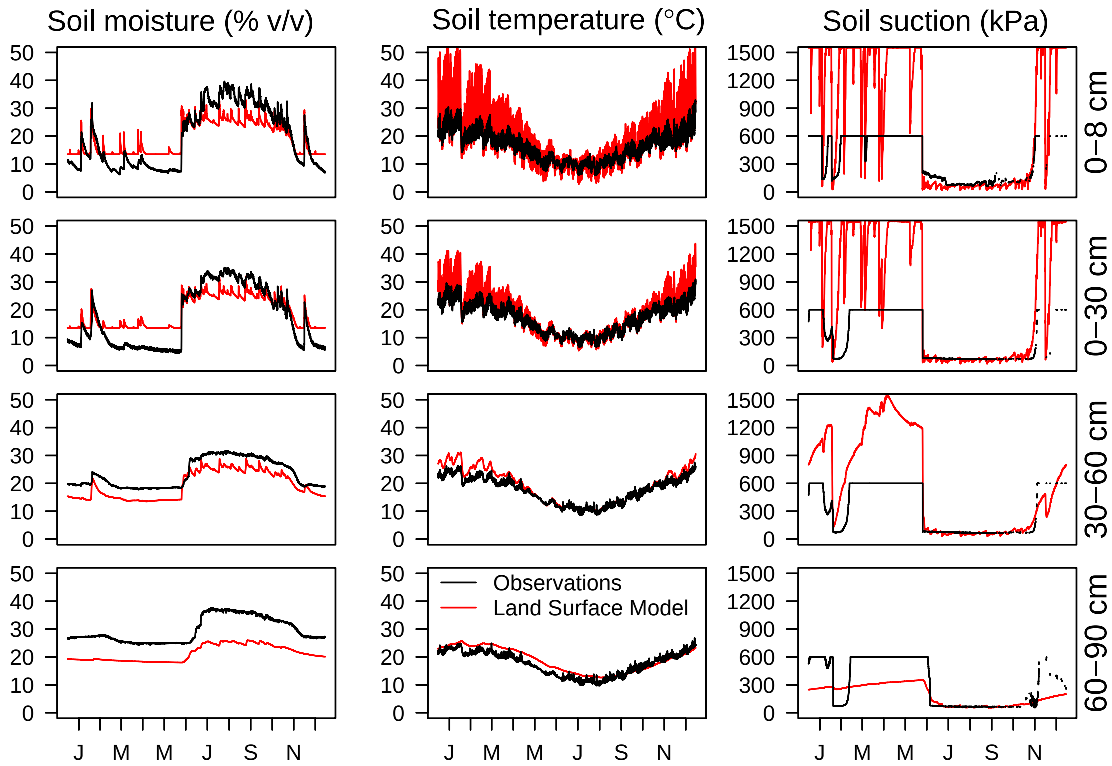

Fig. 3.4 Sample data from a first generation site (K5) for the year 2005. Soil moisture, temperature and suction are shown in black for four depths (0-8 cm, top row; 0-30 cm, second row; 30-60 cm, third row; 60-90 cm, bottom row). Land surface model (CABLE) predictions are shown in red for comparison. The top two layers of the LSM are aggregated to 0-8 cm (top row), similarly the top three LSM layers are aggregated to give 0-23.4 cm predictions (second row), the fourth and fifth LSM layers (23.4-64.3 cm and 64.3-172.8 cm respectively) are shown with observations from 30-60 cm and 60-90 cm depth (third and bottom row).

soil moisture estimates. The specific heat capacity is an estimated parameter that can possibly explain some differences in soil temperature, particularly the much greater diurnal range in near-surface and the slight phase difference for the deeper soil temperature. Moreover, the phase difference is likely to also be attributable to the single point measurement while the LSM approximates a layer of soil. The soil suction observations have a clear upper limit which is an artefact of the field instrument limitations. However, agreement is good when suction is low during wet periods (June to November). To the author's knowledge this is the first time CABLE soil suction has been compared to in-situ field data.

Soil moisture is sampled every 5 or 60 seconds then averaged to 30 or 20 minute measurements for first and second generations sites respectively, using three vertically installed 30 cm Campbell Scientific water content reflectometers. The 18 first generation sites use CS615 probes, with an additional CS615 inserted at an angle of approximately 15 ° below the surface to give 0-8 cm soil moisture (Fig. 3.3 a). As the CS615 model was discontinued in 2002, the newer CS616 (with a higher observing frequency) is installed at the 20 second generation sites, with a 5 cm long Stevens Hydra Probe vertically inserted at the surface (Fig. 3.3 b).

Permanently installed field TDR probes have been used (with a portable Trase TDR unit) to verify and refine laboratory based CS615 (Western et al., 2005) and CS616 calibrations (Yeoh et al., 2008). The CS615 period is temperature corrected to 25 °C (Western and Seyfried, 2005) using temperature sensors installed at the midpoint of each CS615 probe. The calibration approach of Rüdiger et al. (2010) is used for temperature correction and calibration of the CS616 water content reflectometers. The CS616 temperature correction uses temperature probes at 15 cm and parameters based on soil texture. The 0-5 cm Hydra Probe at the second generation sites is calibrated with both laboratory and field gravimetric soil moisture measurements according to the approach of Seyfried et al. (2005) for calibration and that of Merlin et al. (2007) for temperature correction using the temperature probes at 2.5 cm.

The calibration accuracy of the soil moisture probes ranges from an RMSE of 2.5 % vol/vol for the CS615 to 3.3 % vol/vol for the Hydra Probe (the CS616 accuracy is 3.0 % vol/vol). For comparison, the "universal" TDR calibration used for the field TDR measurements has an RMSE of 1.3 % vol/vol (Topp et al., 1980). Calibration reports for the CS615 (Western et al., 2005), CS616 (Yeoh et al., 2008), and Hydra Probe (Merlin et al., 2007) that include parameters for each CS615 and CS616 in the MSMMN are available at `http://www.oznet.org.au`.

All soil moisture data is 0.1 % vol/vol resolution with a range of 0-50 % vol/vol at all sites (with the exception of 11 probes). The median root zone (0-90 cm) soil moisture for 2002 or 2004 (first or second generation sites) to 2010 is in the range 11.8-25.5 % vol/vol for the regional Murrumbidgee sites (M1 to M7), 18.6-

33.0 % vol/vol for the Yanco Region sites (Y1 to Y13), 10.3-38.6 % vol/vol for the Kyeamba Creek Catchment sites (K1 to K14) and 23.5-33.6 % vol/vol for the Adelong Creek catchment sites (A1 to A5).

Annual median root zone (0-90 cm) soil moisture is lowest for all sites in the period 2006-2009. The highest annual median root zone soil moisture is in 2010 (except for 12 sites). Of note is the anomalously high annual median soil moisture at Y4 during 2004 (43.1 % vol/vol compared to a 2005-2010 median of 23.6 % vol/vol) when the site (located in a rice bay) was flood irrigated.

The median soil moisture (over 7 years) is spatially consistent amongst the Yanco Region sites (22.3-24.9 % vol/vol excluding 4 sites). Whereas for the Adelong Creek catchment sites the annual median soil moisture is temporally consistent over 9 years (e.g. 24.7-26.2 % vol/vol at A3 excluding the years 2006 and 2007). For the Kyeamba Creek Catchment sites median soil moisture (over 7-9 years) increases from the hillslope to the valley sites (e.g. 11.6-25.8 % vol/vol for K1 to K7).

Cumulative rainfall is recorded every 6 minutes at the first generation sites at a height of 2 m, with a precision of 0.2 mm (Fig. 3.3 a). At the second generation sites precipitation at 50 cm height is logged each tip, or each second in periods of high intensity rainfall (Fig. 3.3 b). Hydrological Services TB4 0.2 mm tipping bucket raingauges are used at all sites (accurate to 3 % at intensities of 25 to 500 mm/hour). All tipping bucket raingauge calibrations have been verified with a field calibration device that releases 20 mm of water uniformly over about 13 minutes.

Land surface model forcing data (precipitation, air temperature and pressure, relative humidity, wind speed, downward short and long wave radiation) are available for all sites at 30 minute resolution and are derived primarily from nearby AWS data; details can be found in Siriwardena et al. (2003) at `http://www.oznet.org.au`. The AWS sites are typically only located near regional centres consequently one (regional) forcing data set is available for each of the Yanco, Kyeamba and Adelong regions with local rainfall provided from the MSMMN site data. Individual forcing data sets are also available for each of M1 to M7. The forcing data begins at the start of 2000 (AWS rainfall is used prior to installation of raingauges at the MSMMN sites) which allows this year to be used for LSM spin up, and any initialisation effects to dissipate before commencement of soil moisture data in late 2001 or early 2004, for first or second generation sites respectively.

Soil temperature is logged every 6 minutes (0.1 °C resolution) at 4, 15, 45 and 75 cm depth at the first generation sites (Fig. 3.3 a) with a Unidata 6507A thermistor (0.35 °C accuracy) and every 20 minutes at 2.5 and 15 cm depth at the second generation sites (Fig. 3.3 b) with a modified Stevens Hydra Probe thermistor (0.6 °C accuracy) and Campbell Scientific T107 thermistor (0.4 °C accuracy), respectively. Soil temperature data are required for temperature correcting the soil moisture sensors (Campbell Scientific CS615, CS616, and Stevens Hydra Probe). Where soil temperature data is missing it has been estimated from nearby sites for the soil moisture calibration. Thus, all soil moisture estimates in the MSMMN data set have been temperature corrected, but only the observed temperature data has been included in the data set with the missing data flagged accordingly. The soil temperature measurements at the first generation sites are instantaneous, whereas at the second generation sites they are an average over 20 minutes (of instantaneous values sampled every 60 seconds).

Soil suction is measured instantaneously every 30 minutes at the first generation sites at the same depths as temperature (Fig. 3.3 a) with a MEA GBHeavy gypsum block (range 60-600 kPa, resolution 1.5-4 %).

Soil samples from near the MSMMN sites have been sieved and the material passing 2 mm analysed with laser diffraction by CSIRO Minerals using a Malvern Mastersizer 2000 (range 0.02 µm - 2 mm). The particle size distribution results are aggregated to classes to give soil texture for most second generation sites (generally at multiple depths).

Surface flux data are available at one site (K10) centrally located in the valley of the Kyeamba Catchment. The flux data are logged every 30 minutes from 1 January 2005 to 2 May 2006 and consist of latent and sensible heat flux measured using a CSAT 3D sonic anemometer and a Licor 7500 gas analyser (10 Hz measurements at 3 m); incoming and outgoing long and short wave radiation, measured with a CNR1 Kipp & Zonen instrument located at 1 m above the ground (sensitivity 8.58 $\mu V/W/m^2$); soil heat flux measured with two HFT3 plates and TCAV thermocouple temperature probes 8 cm below the surface; and air temperature and relative humidity measured with a HMP45C probe at 2 m. Ancillary data measured at the flux site include barometric pressure at 2 m (accuracy 0.5 mbar at 20 °C, range 600 to 1060 mbar); and wind speed and direction at 3 m measured with a 03001-5 R.M.

Young Wind Sentry (anemometer and vane ranges of 0 to 50 m/s and 0 to 355 ° respectively).

Data Quality

All data from the soil moisture monitoring sites has been visually inspected to identify errors. This checking includes comparisons between soil layers and with rainfall. In addition tipping bucket raingauge data has been checked using double mass plots of daily accumulations to identify periods of faulty gauge operation. Raingauge catch rates generally agree within 5 %. All detected erroneous data has been removed from the data base and flagged as missing. No gap filling of data has been undertaken, with all missing or poor quality data being flagged.

Data Availability

All data described here are available (in ascii, NetCDF, and spreadsheet formats) via the World Wide Web at `http://www.oznet.org.au`. The website provides all the information required for interpretation of these data, along with site photographs, maps and descriptions. Due acknowledgment in any publication or presentation arising from use of these data is required. Data collection is ongoing as at July 2013 for all sites.

3.1.2 Gravity network

Parts of the method presented here appear in the peer reviewed conference papers Smith et al. (2005, 2006).

A gravity network was developed in the Murrumbidgee Catchment to augment the Murrumbidgee soil moisture monitoring network (MSMMN). The gravity network was developed in two steps, initially a large network including 27 soil moisture monitoring sites (and two hydrologically stable reference sites) in both the Yanco Region and Kyeamba Catchment was conceived. However, following a preliminary field trial, a final network of 4 sites in the Kyeamba Creek catchment (that recognised logistical constraints identified in the preliminary trial) was used for this thesis.

At each of the sites in the Yanco Region and Kyeamba Catchment a shallow piezometer was installed with a 2 m capacitance probe to monitor groundwater level

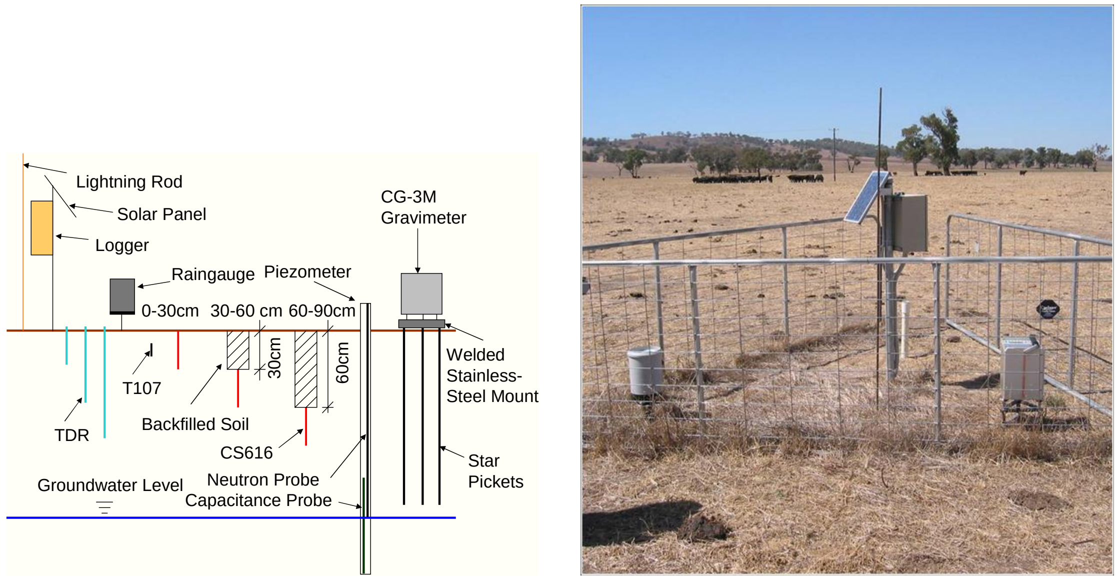

Fig. 3.5 Schematic (left) and photograph (right) of a typical field site. Time domain reflectometry (TDR) probes are 30, 60 and 90 cm long, capacitance probe is removed when using NMM, groundwater was not reached at all sites. Tipping bucket raingauge is visible in left of photograph, logger and piezometer in centre, and gravimeter to the right. Soil moisture monitoring sites are enclosed by three 4.25 m long gates. Soil moisture monitoring site shown here in photograph is K10.

(Fig. 3.5). This PVC tube was also used as an access tube for periodic neutron moisture meter (NMM) measurements taken to the depth of the water table or bottom of the bore. Steel platforms for the gravimeter were installed close to the soil surface on stable 2 m star pickets inserted to depth of refusal. The gravimeter platform was designed as a cut out triangle to allow precipitation and evapotranspiration to pass while maintaining maximal rigidity (Fig. 3.6). The platform was custom designed to the dimensions of the Scintrex CG-3M gravimeter stand (Fig. 3.12).

The initial gravity network consisted of 29 sites in two groups (Yanco Region and Kyeamba Catchment) spaced 100 km apart (Fig. 3.1) and tied into the SG in Canberra a further 100 km east of the Kyeamba Catchment. However initial results indicated a strong post-transport stabilisation effect on the gravity readings that may have been due to the long transportation times. Furthermore the need to take gravity readings at sites a number of times to increase precision of the

Fig. 3.6 Platform for Scintrex CG-3M gravimeter at soil moisture monitoring sites. The platform allows precipitation and evapotranspiration to pass and soil moisture to vary below the gravimeter.

observations (and control the relative gravimeter drift) meant the initial network was unreasonably large for one gravimeter. Without air transport (or the use of an absolute gravimeter), it was impossible to tie the network to the SG in Canberra as the closest site in the network (the bedrock reference site in Kyeamba Catchment) still required a minimum of 3 hours vehicular transport for the gravimeter from the SG.

Subsequently the network was pared down to a number of sites in Kyeamba Catchment as this region contained a granite outcrop that could be used as a local control or hydrologically stable reference site. The geology of the western plains of the Murrumbidgee Catchment that the Yanco Region is located in does not contain any bedrock outcrops (Fig. 3.2). A large shed structure with no walls but a roof and concrete slab was identified as a possible surrogate bedrock reference site. However the depth and stability of the concrete slab was uncertain, as were the effects of swelling and cracking clay soils and the heating and cooling of the metal shed structure. Furthermore the sites in the Yanco Region are further spaced than in

Fig. 3.7 Kyeamba Creek Catchment with hydrologically stable bedrock reference site (BED) and four soil moisture monitoring sites selected for gravity and terrestrial water storage analysis.

the Kyeamba Catchment, and the roads in the Yanco Region are generally unsealed while the main road in the Kyeamba Catchment is bitumen. For these reasons the Kyeamba Catchment was selected as the area for the refined gravity network.

Four sites were selected (two valley and two hillslope) to assess if hydrological changes in valleys or on hillslopes are detectable using gravity measurements both in the presence and absence of (observed) groundwater. Additionally a bedrock reference site was chosen as a hydrologically stable benchmark (Fig. 3.7). All sites were sampled in both dry and wet conditions.

Gravity Data and Sampling Strategy

Gravity may be measured by a variety of gravimeters manufactured by a small number of companies. These gravity meters can be distinctly classified as giving either a relative or absolute measurement of gravity. Absolute measurements are desirable, but the gravimeters have low precision and are not field portable. Relative (spring) gravimeters are field portable and precise but the sensor suffers from a large drift in apparent gravity value. Therefore when relative gravity meters are used for high precision microgravimetry, the drift needs to be accurately accounted for and the calibration of the gravimeter is crucial. The Scintrex CG-3M was chosen because it was the most accurate field portable, rugged gravimeter at the time (Smith et al., 2005).

The gravity observation at a site is a function of both gravity meter behaviour and gravity. The gravity values reported by the gravity meter vary linearly with time due to drift (extension) of the spring sensor. Additionally there is a short term post transport stabilisation period where the gravity changes nonlinearly with time. Both of these effects are corrected by differencing gravity observations between sites. In addition to changes in water storage, temporal changes of gravity occur due to variations in Earth tides, ocean tides, atmospheric pressure and earthquakes. Tide and pressure effects can be corrected however earthquakes must be screened for by keeping a log of all earthquakes during the gravity survey that can be obtained from `http://www.ga.gov.au/earthquakes`. Gravity observations made at each site (over 20 minutes) consist of eight consecutive measurements (every 2.5 minute) which are averaged to improve precision. The individual gravity measurements are an average of 120 one second samples but also include time taken for one second reference voltage (calibration) samples that are made every 6 seconds.

A sampling strategy was developed to construct a complete homogeneous network (Lambert and Beaumont, 1977; Vitushkin et al., 2002). A network is complete if each site is connected to every other site, if it is connected by the same number of ties then it is also homogeneous (Lambert and Beaumont, 1977). This is shown in Fig. 3.8 where a line connecting one site to another typically represents one day of measurements (that is 8 ties). A tie is formed by measuring gravity at one site then another in quick succession and taking a gravity difference. The ties with the

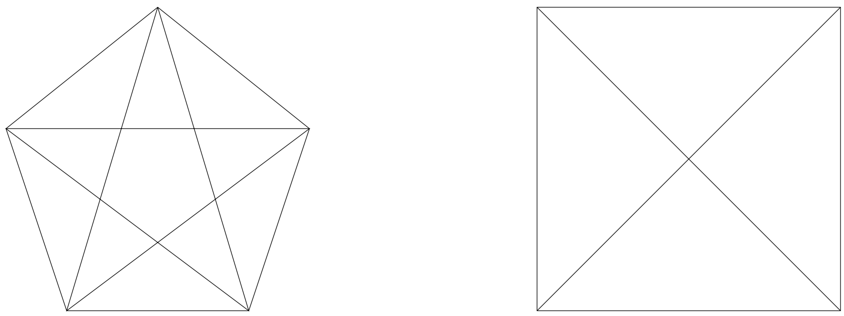

Fig. 3.8 Four and five site complete gravity networks (each vertex represents a site). The 4 site network consists of 4 closed loops (triangles), whereas the 5 site network contains 10 closed loops.

bedrock site (BED) can be used directly to determine the gravity at a soil moisture monitoring site relative to the hydrologically stable reference site, but the other ties (e.g. K5–K7) can also be used in conjunction with the BED ties to form closed loops (BED–K5–K7). The differences in these closed loops should sum to zero. By enforcing this zero sum condition outliers can be detected and the network can be strengthened by distributing the standard error at weak ties (e.g. BED–K5, where neither site has good wind protection) throughout the network. This procedure is referred to as network adjustment (Hwang et al., 2002). An initial analysis was conducted (Smith et al., 2006), and a statistically significant increase of gravity at K7 found to correspond very well with observed soil moisture and groundwater level changes (when using a Bouguer slab approximation).

3.1.3 Preliminary Results

Preliminary results of detecting a soil moisture signal in gravity data are given here and developed further in Chapter 5, after incorporating the findings of Chapter 4 to improve the precision of the gravity data. The preliminary results presented here are from the peer reviewed conference paper Smith et al. (2006). Network adjustment was performed on four and five sites at two epochs (Fig. 5.3); the results are summarised in Table 3.1. Note that the gravity differences between any three sites in Table 3.1 necessarily sum to zero after network adjustment compared to an average three station loop misclosure of 4 μGal and 10 μGal for the two epochs

Table 3.1 Gravity (relative to the hydrologically stable bedrock) and standard error for the March and September/October 2005 field campaigns after network adjustment.

	March 2005		September/October 2005	
	Gravity	Error	Gravity	Error
Site	(μGal)	(μGal)	(μGal)	(μGal)
BED	0	1.36	0	2.03
K5	8351.10	1.41	8347.91	2.03
K7	11264.34	1.39	11272.88	2.00
K10	16545.32	1.38	16546.50	1.99
K13	N/A	N/A	12413.94	2.00

prior to adjustment. The network adjustment was performed with a free network constraint (i.e. relative to a site), with BED as the constraining site. Details on the network adjustment procedure can be found in Hwang et al. (2002). A base case approach was followed where drift was modelled as linear, the pressure effect on gravity was ignored, and Earth tides were simply removed by an old model within the gravity meter (Longman, 1959, 1961). Better results are expected by modelling the drift as linear but separately for each day (rather than an average over the whole survey campaign of approximately 2 weeks), removing the pressure effect with field pressure data, and removing the Earth tides by using the nearby (100 km east) Mt Stromlo superconducting gravimeter data or using a newer Earth tide model (Cartwright and Tayler, 1971; Cartwright and Edden, 1973). Despite this, a base case approach is essential to assess the most significant corrections needed to achieve highly accurate results. The base case model passed the global model test and no outliers were detected.

A t-test (unequal variance) was performed on the site gravity estimates for each epoch. The results are shown in Table 3.2, where a significance level of 0.05 was chosen and the degrees of freedom are the sum of those for March (45) and September (74). It is assumed that no change in the gravity occurs at BED (the bedrock benchmark site). There is a significant positive change in gravity at K7 of 8.54 μGal, a reasonable, but insignificant positive change at K10, a large but insignificant negative change at K5 of 3.19 μGal, and no result for K13 as it was not measured in March. A positive change (due to increased terrestrial water storage) was expected

Table 3.2 Gravity changes between the March and September 2005 field campaigns after network adjustment. Test statistic and critical t value for a significance level of 0.05 and 119 degrees of freedom are shown.

Site	Gravity Change (μGal)	Test Statistic	Critical t Value
BED	0	0	1.98
K5	-3.19	1.29	1.98
K7	8.54	3.52	1.98
K10	1.18	0.48	1.98
K13	N/A	N/A	N/A

at all sites, except perhaps K5 (the hillslope site) where the gravitational effect of upslope moisture (a reduction) could cancel the gravitational effect of moisture underneath the gravity meter (an increase).

Precipitation, soil moisture and groundwater were measured continuously at all sites. Neutron moisture meter (NMM) counts were also taken at the time of the gravity surveys to establish the variation of soil moisture in the zone below the installed soil moisture sensors (90 cm). Two sites are presented here, K5 and K7. These were selected prior to the network adjustment on the basis that the pair represents a contrast between hillslope and valley as well as deep and shallow groundwater respectively. Coincidentally they were also the two sites that had the largest gravity changes between March and September (Table 3.2).

Both sites are used for cattle grazing and are duplex soils covered with grass. K5 has an available water capacity of about 20 % vol/vol and no water table within the shallow bore of 1.7 m depth, whereas K7 has an available water capacity of about 25 % vol/vol and a water table that varies between 2.2 and 4.7 m, with a bore depth of 9.4 m. The NMM counts for K5 and K7 in March and September 2005 are shown in Fig. 3.9. Both the March and September K7 counts stop at the water table (higher in September), the K5 counts stop at the bottom of the piezometer. There is little change in the count ratio at depth (below 90 cm) for K5, so the soil moisture change can be considered to be predominantly in the monitored zone (0-90 cm). There is more change at depth for K7 but it is assumed the bulk of the soil moisture change is captured by the CS616 sensors.

Hydrological changes can be converted to a predicted change in gravity by using a simple Bouguer slab model (Telford et al., 1990). A change in mass is converted

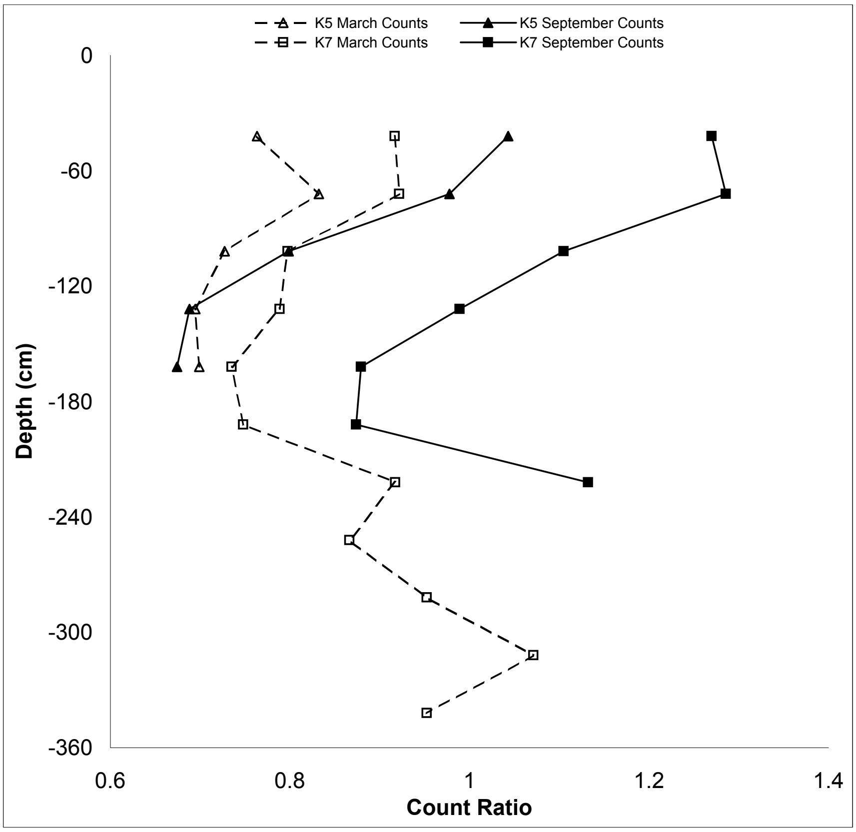

Fig. 3.9 Neutron moisture meter count ratios (relative to background radiation) at K5 and K7, March and September 2005.

to a change in gravity by assuming the mass is distributed as a horizontal sheet with infinite extent. This assumption is well suited to soil moisture and groundwater at flat sites, but the horizontal requirement is not met for hillslope sites.

Using the Bouguer slab model for soil moisture, the gravity contribution over time of each soil moisture sensor was calculated (Fig. 3.10 and 3.11). Additionally the groundwater component of the gravity at K7 was computed using an assumed specific yield of 0.05, which is considered reasonable for the alluvial sediment aquifer that this bore lies in (Cresswell et al., 2003). The water table condition below the bottom of the K5 bore (1.5 m) is unknown. However, Cresswell et al. (2003) state that the Kyeamba Creek catchment groundwater system consists of a shallow unconfined valley alluvial sediment aquifer overlying an intermediate scale fractured bedrock aquifer of specific yield around 0.01. The fractured bedrock (granite) aquifer

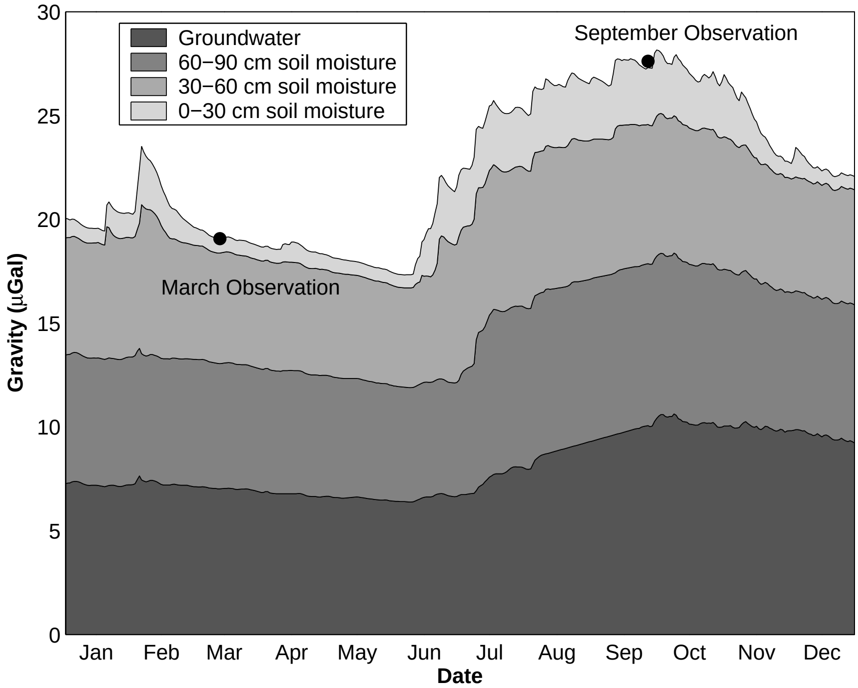

Fig. 3.10 Observed and predicted gravity at K7 using Bouguer slab model with continuous soil moisture and groundwater level observations.

is thought to cover most of the catchment.

The March gravity observation in Fig. 3.10 and 3.11 is an average of the 9 days of the gravity survey, located at the midpoint of the survey. The point is vertically shifted to equal the Bouguer slab predicted gravity at that time at each site. Similarly the September observation is an average of 15 days and is also located at the midpoint of this time period, but plotted relative to the March observation. It should be noted that it rained heavily halfway through the September survey (31 mm of precipitation was recorded in 21 hours at K7). This can be seen by the small peak in the modelled gravity to the right of the sample point in Fig. 3.10. Despite this, the agreement between the modelled and observed gravity at K7 is excellent (observation only 0.31 μGal greater than predicted). This difference of 0.31 μGal is equivalent to a 7.4 mm error in the estimate of terrestrial water storage change for the whole profile, or a 3.8 % relative error.

Unexpectedly the observed gravity at K5 has decreased markedly (but not statistically significantly at the 0.05 level). The September observation for K5 is 3.18 μGal

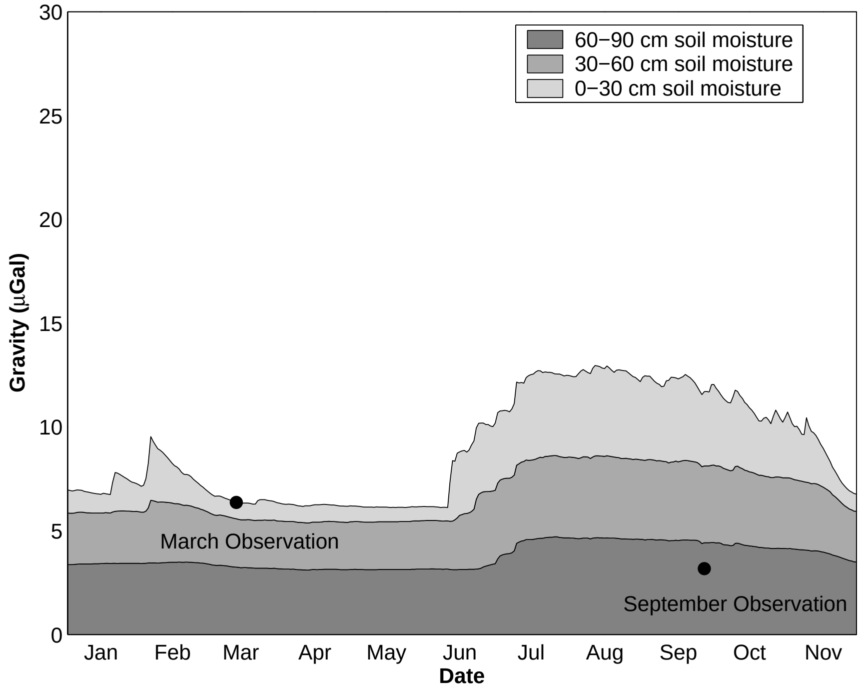

Fig. 3.11 Observed and predicted gravity at K5 using Bouguer slab model with continuous soil moisture observations.

less than the March observation, compared with a predicted increase of 5.33 µGal.

3.2 Achieving High Precision Gravity Data

This section describes the research approach followed in Chapter 4 to achieve high precision ground-based gravity data. The focus in this thesis is on the Scintrex CG-3M relative gravimeter, however the research approach in this section is directly applicable to any field portable relative gravimeter, and to a lesser extent to field capable absolute gravimeters.

While some studies have provided recommendations on particular aspects of achieving high precision ground-based gravity data with a field portable relative gravimeter, or other studies have generally highlighted aspects that should be considered for high precision microgravimetry (Rymer, 1989; Debeglia and Dupont, 2002; Gabalda et al., 2003; Smith et al., 2005, 2006; Christiansen et al., 2011c), no study has comprehensively assessed what is required to achieve high precision grav-

Fig. 3.12 GWR superconducting gravimeter (SG) at Mt Stromlo, Canberra (left) and Scintrex CG-3M at soil moisture monitoring sites in the field, approximately 100 km west of Canberra (right).

ity observations required to detect (or retrieve) a soil moisture signal. This thesis investigates gravity corrections and provides recommendations for field procedures to increase gravity data precision.

The gravimeter used for this thesis is the portable Scintrex CG-3M relative gravimeter (Fig. 3.12). Using a portable gravimeter increases the possibility of observing terrestrial water storage variations as the gravimeter does not require a permanent enclosure that may shield the soil from rainfall (or evapotranspiration), and gravity observations can be taken at multiple sites. The Scintrex CG-3M is calibrated to the high precision superconducting gravimeter (SG) at Mt Stromlo, Canberra (Fig. 3.12), with the SG in turn calibrated to FG5 absolute gravity observations. The temporal stability of the CG-3M calibration is checked by operating the CG-3M overnight adjacent to the SG before and after every field campaign, while the temporal stability of the SG calibration is checked by comparing calibration values from five FG5 absolute gravity observations over 7 years including periods both before and after the field campaigns using the Scintrex CG-3M.

3.2.1 Field Procedures to Increase Precision

This subsection describes the procedures used in Chapters 4 and 5 to increase precision of the Scintrex CG-3M gravity data at a network of soil moisture monitoring sites. These methods are guided by previous studies and aim to control external perturbations of the gravity data.

A grub screw was inserted in one levelling leg of the Scintrex CG-3M (below the red arrow in Fig. 3.12) to fix the height of the gravimeter, with the other two legs (front and back right) used to level the gravimeter. This approach of fixing one levelling leg of the gravimeter follows Montgomery (1971); Lambert and Beaumont (1977); Hipkin (1978); Dragert et al. (1981); Jacob et al. (2009, 2010) and Christiansen et al. (2011a).

A gravimeter platform at each of the soil moisture monitoring sites (Fig. 3.5, 3.6 and 3.12) was designed to exactly reposition the legs of the Scintrex CG-3M tripod for each gravity observation. For the bedrock reference site three indentations were drilled into the granite outcrop (in which the CG-3M tripod fit exactly), similarly three indentations were drilled into a rock (the geodetic benchmark AU034) near the SG in Canberra. Above the (FG5) absolute gravity benchmarks at Mt Stromlo (in the room adjacent to the SG and in a seismic vault in the valley) the locations for the Scintrex CG-3M tripod feet were traced onto the concrete floor with permanent marker. The Scintrex CG-3M was always repositioned at every site with a consistent orientation. This approach of exactly repositioning the gravimeter by creating indentations for the gravimeter tripod feet or marking the tripod position was used by Montgomery (1971); Dragert et al. (1981); Naujoks et al. (2008, 2010); Jacob et al. (2009, 2010) and Christiansen et al. (2011a,c).

Following Montgomery (1971); Lambert and Beaumont (1977); Mäkinen and Tattari (1988, 1991a,b) and Christiansen et al. (2011a,b,c) a reference site was assumed hydrologically stable and used to form gravity ties (difference of gravity observations) with the soil moisture monitoring sites. As in Montgomery (1971) and Mäkinen and Tattari (1988, 1991a,b) the reference site was located on bedrock.

By correcting for all other known signals in the gravity data, a change in the gravity ties should be due only to a change in terrestrial water storage at the soil moisture monitoring sites.

Following the approach of Bonvalot et al. (1998); Debeglia and Dupont (2002); Gabalda et al. (2003) and Tikku et al. (2006) earthquakes were monitored using the websites `http://www.ga.gov.au/earthquakes` and `http://earthquake.usgs.gov`.

Jousset et al. (1995) suggested the Scintrex CG-3M may be affected by internal temperature or battery voltage variations. Consequently, the battery voltage is manually logged before and after every gravity observation, internal temperature is logged automatically by the gravimeter.

Additional to the gravity observations at each site, atmospheric pressure (together with air temperature, relative humidity, and wind speed) is measured with a portable weather tracker (the Kestrel 4000) before and after each (20 minute) gravity observation. The air pressure, temperature, relative humidity and wind speed are accurate to 1 mbar, 0.5 °C, 3 % (relative humidity), and 0.1 m/s, respectively. Hipkin (1978) also measured pressure and temperature simultaneously with gravity. The portable barometer is calibrated to the more precise barometer used for the Canberra SG. Both the meteorological observations (from the portable weather tracker) and battery voltage measurements, each taken before and after a gravity observation, are averaged to give a single value that corresponds to the gravity observation (which is also an average over 20 minutes, but of 8 measurements).

Following the recommendations and procedure of Montgomery (1971); Lambert and Beaumont (1977); Hipkin (1978); Dragert et al. (1981); Jacob et al. (2010) and Christiansen et al. (2011a,b,c) the gravimeter is shaded at all times. At the bedrock reference site an umbrella is used, whereas at the soil moisture monitoring sites a tarpaulin or custom designed tent is hung from the gates surrounding the gravimeter platform (Fig. 3.13).

Following the findings of post transport stabilisation for LaCoste and Romberg (Hipkin, 1978; Lyness and Lagios, 1984; Hipkin et al., 1988) and Scintrex CG-3M (Haynes, 1999; Hackney, 2001; Ferguson et al., 2007; Gettings et al., 2008) or CG-5 (McClymont et al., 2012) gravimeters, a spring suspended carrying case was custom designed for the Scintrex CG-3M to transport the gravimeter in the rear of a vehicle

Fig. 3.13 Tent used for shading Scintrex CG-3M at soil moisture monitoring sites. Tent is shown here at K13. Gravimeter is visible through gap in tent.

(Fig. 3.14). This transportation device is similar to that used by Dragert et al. (1981) and Becker et al. (1987) for a LaCoste and Romberg D Meter (Fig. 2.12) and follows the recommendations of Hamilton and Brulé (1967); Dragert et al. (1981) and Herb Dragert (pers. comm., 2003, Geological Survey of Canada). The gravimeter case is suspended by firm elastic straps at eight points, with the inside of the case and also the bottom of the frame padded with thick foam.

At each site 120 (1 s) gravity samples are averaged over approximately 2.5 minutes (a reference voltage calibration sample is also taken every 6 s). The eight (2.5 minute) gravity measurements are averaged over 20 minutes to increase gravity data precision. Based on a gravity measurement error of 5 μGal (Table 2.1) this results in an uncertainty of 1.8 μGal for the 20 minute gravity observation. This approach of averaging short duration gravity measurements at each site is similar to Ferguson et al. (2008); Jacob et al. (2009, 2010); Naujoks et al. (2008, 2010) and Christiansen et al. (2011a,b,c) who averaged between three and six measurements of 1-3 minute duration (with the measurements consisting of averages of samples at 6 or 1Hz res-

Fig. 3.14 Suspension based transportation device for Scintrex CG-3M. Transportation device is shown here at K7. Gravimeter (handle) is visible at top of transportation device.

olution). Similar to Smith et al. (2006) and this thesis, Ferguson et al. (2007) also used a Scintrex CG-3M and averaged eight measurements of 2.5 minute duration over 20 minutes for a gravity observation at a site.

The (20 minute) gravity observations at each site are differenced with the gravity observation at the next site (for that survey day), to form gravity ties. Between any two sites eight ties are formed, this follows Montgomery (1971); Lambert and Beaumont (1977); Dragert et al. (1981); Mäkinen and Tattari (1988, 1991a,b); Smith et al. (2006); Jacob et al. (2009, 2010); Naujoks et al. (2008, 2010) and Christiansen et al. (2011a,b,c) who formed between one (Jacob et al., 2010) and eleven ties (Mäkinen and Tattari, 1988, 1991a,b). Using a (20 minute) gravity observation error of 1.8 μGal, eight ties between any two sites results in gravity difference uncertainty of 1.25 μGal.

Unlike Montgomery (1971); Mäkinen and Tattari (1988, 1991a,b) and Jacob et al. (2009), the gravity network in this thesis consists of more than two sites.

Furthermore, unlike Dragert et al. (1981); Jacob et al. (2010); Naujoks et al. (2008, 2010) and Christiansen et al. (2011a,b,c), in this thesis gravity ties are formed between all sites in the network, i.e. a complete gravity network is used (Lambert and Beaumont, 1977). Moreover the number of gravity ties between all sites in the network is uniform, so that the gravity network is both complete and homogenous (Lambert and Beaumont, 1977). This requires $3n$, $6n$, or $10n$ gravity ties for a three, four or five site gravity network (respectively), where n is the number of ties between any two sites in the network. In this thesis eight ties connect the sites in the four or five site gravity networks. One gravity tie takes approximately 1 hour to complete, when considering transportation and two gravity observations of 20 minute duration.

The Scintrex CG-3M can be operated in the field on battery power for approximately 10 hours. For the four and five site networks a field campaign consists of 7-15 consecutive survey days with 2-10 ties (typically eight) completed in a day. For these networks (and campaigns), each survey day begins and ends with a gravity observation at the bedrock reference site. This approach is similar to Jacob et al. (2010) and Christiansen et al. (2011a,b,c) who began and ended each survey day at the same site (closing the gravity loop). For the three site networks only three gravity ties are formed between sites so the entire field campaign (consisting of nine ties) can be conducted in a single survey day.

Due to the geography of the study area, the (four or five site) gravity network is essentially a profile network using a single road adjacent to Kyeamba Creek to access all sites, with the bedrock reference site located at the end of the profile (Fig. 3.7). Consequently the network sampling strategy is generally a profile method starting and finishing at the bedrock reference site, measuring the same ties going out and coming back to the bedrock site to finish each survey day, but with the profile for each day consisting of different sites, thereby observing much of the network at roughly the same time, as recommended by Lambert and Beaumont (1977). Furthermore, where possible successive repetitive ties between two sites are conducted to minimise temporal variations in gravity, as recommended by Dragert et al. (1981).

The gravity ties for a field campaign (approximately 9, 48, and 80 ties for three, four, and five site networks, respectively) are used in a network adjustment (Hwang et al., 2002) that consistently distributes the errors from the observed gravity ties around the network. This approach of network adjusting gravity differences follows Lambert and Beaumont (1977); Hipkin (1978); Dragert et al. (1981); Vitushkin et al. (2002); Smith et al. (2006); Jacob et al. (2009, 2010); Naujoks et al. (2008, 2010); Christiansen et al. (2011a,b,c) and Jiang et al. (2009, 2011, 2012b). Network adjustment produces a precise estimate of the gravity difference between any two sites, and an estimate of the gravity error at each site. The results are presented as estimates of (relative) gravity and error at each site in the network, with the relative gravity estimate for all sites in the network summing to zero.

Prior to network adjustment the gravity observations at each site are corrected for Earth tides, ocean tide loading, polar motion, atmospheric pressure, and battery voltage. The methods for correction are selected based on testing (subsection 3.2.2 and 3.2.3). The software Tsoft (Van Camp and Vauterin, 2005) is used to correct for Earth tides and polar motion, with polar motion data from IERS (`http://www.iers.org`). The tidal potential catalogue of Tamura (1987), and Love numbers of Dehant et al. (1999) are used for the Earth tide correction. The CSR4.0 ocean tide model (Watkins and Eanes, 1997) and GOTIC2 loading software (Matsumoto et al., 2001) is used to correct for ocean tide loading. Atmospheric pressure is corrected using an admittance (-0.394 μGal/mbar) and pressure data from the portable weather tracker. The gravity observation at each site is corrected for Scintrex CG-3M battery voltage using data manually obtained from the gravimeter at the start and end of each 20 minute gravity observation. The post transport stabilisation effect in the gravity data is corrected by removing the average post transport stabilisation for each site.

3.2.2 Laboratory Testing of Gravity Corrections

This subsection summarises the data and methods used to test gravity corrections in Chapter 4. The gravity corrections are applied (in Chapter 5) at each of the soil moisture monitoring sites (and bedrock reference site), located around 35.4 ° S, 147.6 ° E, and elevation 300 m. Testing of the gravity corrections is conducted at both Canberra (35.3 ° S, 149.0 ° E, elevation 760 m and approximately 100 km from the (east) coast of Australia) and Melbourne (37.8 ° S, 145.0 ° E, elevation around 80 m, and adjacent to Port Phillip Bay on the south coast of Australia). For the testing at Canberra, both the (GGP) SG and Scintrex CG-3M gravity data are used, together with meteorological observations from the portable weather tracker deployed adjacent to the Scintrex CG-3M, (GGP) barometric pressure adjacent to the SG, and IERS polar motion data.

The testing at Canberra includes corrections for geophysical and meteorological signals in gravity data including:

- Earth tides (using Tsoft, ETERNA, and BAYTAP-G);
- ocean tide loading (using GOTIC2, NLOADF, and OLFG/OLMPP);
- polar motion (using Tsoft); and
- atmospheric pressure (using ETERNA, and BAYTAP-G).

Additional meteorological signals are assessed for their influence on the Scintrex CG-3M data, these include:

- air pressure, air temperature and relative humidity (using correlation, and BAYTAP-G).

The testing at Melbourne uses only Scintrex CG-3M data and adjacent meteorological observations (from the portable weather tracker) and verifies the best performing corrections from the Canberra testing. These include corrections for:

- Earth tides (using Tsoft, and BAYTAP-G);
- ocean tide loading (using GOTIC2); and
- atmospheric pressure (using BAYTAP-G).

Additionally meteorological signals are assessed again for their influence on the Scintrex CG-3M data, these are the same variables and methods used in Canberra:

- air pressure, air temperature and relative humidity (using correlation, and BAYTAP-G).

The testing at Melbourne verifies that the conclusions from the Canberra testing are valid for a site more distant from the Canberra SG (450 km) than the field sites (only 100 km). Some additional assessment of instrumental artefacts in the Scintrex CG-3M data includes:

- battery voltage, internal gravimeter temperature, and air temperature (using correlation, and regression); and
- post transport stabilisation.

3.2.3 Assessment of Precision Achievable in the Field

The gravity corrections and Scintrex CG-3M relative gravimeter instrumental artefacts are assessed again in the field (Chapter 4). The field testing assesses the:

- gravity data precision achievable in the field;
- repeatability of field gravity observations; and
- robustness of methods, in particular the effect of outliers.

The instrumental artefacts in field gravity data that are investigated include:

- drift;
- post transport stabilisation, and its relationship to:
  - transportation method, and
  - time of transport.

The optimal corrections determined from the laboratory research are used at field sites together with network adjustment, and compared to:

- SG residuals (at Mt Stromlo, Canberra);
- a difference of two absolute gravity benchmarks (at Mt Stromlo); and
- observed rainfall and terrestrial water storage at Kyeamba Creek Catchment (100 km west of Canberra).

3.3 Retrieving a Soil Moisture Signal from Gravity Data

A method to detect the terrestrial water storage signal in ground-based gravity (using field data) has been discussed in Section 3.1 (and is applied in Chapter 5). This section describes an approach (used in Chapter 6) to disaggregate the terrestrial water storage signal (depth integrated soil moisture and groundwater) and retrieve profile soil moisture from ground-based gravity.

It is assumed that a terrestrial water storage signal is present in ground-based gravity data, and that the gravity data has been corrected for all other signals (such as Earth tides, ocean tide loading, polar motion, and atmospheric pressure), using corrections such as those determined in Chapter 4. It is also assumed that all hydrological processes occur in one (vertical) dimension only, with infinite lateral extent. These assumptions are satisfied for this thesis by generating synthetic gravity observations from observed 0-30, 30-60, and 60-90 cm soil moisture, together with observed groundwater level and an assumption that the 60-90 cm soil moisture is representative of the soil moisture (from 90 cm depth) to the groundwater level. The hydrological observations are converted to a gravity value using the Bouguer slab approximation, and the gravity of each of the terrestrial water storage components summed to generate a synthetic ground-based gravity observation at the surface.

A ground-based gravity observation at the Earth's surface is an integral measurement of all terrestrial water storage below the gravimeter. Consequently, retrieving the profile soil moisture is an underdetermined inverse problem (i.e. there are more unknowns than observations). This can only be solved by using additional (prior) information (effectively additional observations) thereby making the inverse problem well defined. A simple way of doing this is by using (prior) estimates of the profile soil moisture as part of the gravity inversion. The prior estimates of profile soil moisture are easily generated by a physically based hydrological model that simulates profile soil moisture.

This use of a hydrological model together with ground-based gravity (or other geophysical observations) has been termed hydrogeophysical inversion (Ferré et al., 2009; Hinnell et al., 2010). Studies to date (Damiata and Lee, 2006; Blainey et al., 2007; Christiansen et al., 2011a; Herckenrath et al., 2012) have typically used a groundwater model, forward modelled the terrestrial water storage (neglecting soil moisture and evapotranspiration) to create a ground-based gravity signal, and compared this predicted gravity to the observed gravity. By minimising the sum of square of differences of the predicted and observed gravity, the ground-based gravity observations are used to estimate groundwater model parameters (specific yield and saturated hydraulic conductivity). No study has used this process to estimate the hydrological model states (water storage) that are temporally variable (unlike the time invariate parameters). In the only study considering soil moisture Christiansen et al. (2011b) retrieved hydrological model (soil hydraulic) parameters and assumed ET was negligible, groundwater was not modelled. While Christiansen et al. (2011b) needed to assume an initial soil moisture for the hydrological modelling (i.e. it was a nuisance parameter), they did not attempt to retrieve the initial soil moisture as part of the parameter calibration. In this thesis the hydrological model parameters are fixed but the initial soil moisture is retrieved using the same calibration scheme (PEST) as used by Christiansen et al. (2011a,b).

The approach in this thesis is to use ground-based gravity data to calibrate a Richard's equation based soil moisture model contained within a land surface model (that also estimates evapotranspiration, heat flux, and snowpack). Unlike Christiansen et al. (2011b), the parameters of the Richard's equation are not calibrated but set to values based on soil maps, soil samples, and particle size analysis. In this thesis the initial soil moisture state (that was assumed in Christiansen et al. (2011b)) is "calibrated" with PEST (Doherty, 2010). Using a fixed window that is shifted through the data set (without overlapping or skipping data), the initial soil moisture is calibrated for a number of windows (Smith et al., 2011). This is brute force variational assimilation (Calvet and Noilhan, 2000; Sabater et al., 2007; Rüdiger, 2007), see Fig. 6.2 (a), with ground-based gravity observations assimilated. Additionally near-surface soil moisture observations are assimilated, to test the hypothesis that near-surface soil moisture observations will assist the gravity data inversion.

After estimating initial soil moisture content for multiple layers (six) in the profile, the (Richard's equation based) hydrological model is used to propagate the estimated soil moisture in time, evapotranspiration is also modelled (using a Penman-Monteith equation). Both soil moisture and evapotranspiration (together with soil heat, snow depth and density) are modelled with the CSIRO Atmosphere Biosphere Land Exchange (CABLE) land surface model (Kowalczyk et al., 2006). Land surface models are developed to provide important feedbacks to the atmosphere in weather or climate modelling (Pitman, 2003). In this thesis the land surface model is run in an offline mode (not coupled to an atmospheric model) and the meteorological forcing is provided by observations (Smith et al., 2012; Siriwardena et al., 2003).

The CABLE land surface model (Kowalczyk et al., 2006) was selected for this thesis as it is an Australian model that can deal with Australian (semi-arid) conditions (Smith and Zhang, 2007) and performs well at the Murrumbidgee soil moisture monitoring sites (Fig. 3.4 and 6.1). Furthermore it is a community land surface model with an open and active code base (available at `http://trac.nci.org.au/trac/cable/wiki`). Lastly CABLE is the land surface model within the Australian Community Climate and Earth System Simulator, ACCESS (Bi et al., 2013), that is used for both climate (Kowalczyk et al., 2013) and weather prediction (Puri et al., 2013).

CABLE requires various data sets to run. These include atmospheric forcing data (for offline runs where the land surface model is not coupled to an atmospheric model), leaf area index (LAI), vegetation and soil parameters. Forcing data is sourced from a dataset compiled primarily from automatic weather stations (AWS) (Smith et al., 2012; Siriwardena et al., 2003), while mean monthly LAI is derived from Advanced Very High Resolution Radiometer (AVHRR) data for the period 1981-94 (Lu et al., 2003). CABLE is bundled with global soil and vegetation parameters at 2 ° resolution (Potter et al., 1993). In this thesis, where possible, the coarse resolution soil parameters (Zobler, 1999) are replaced with site specific parameters derived from soil samples and soil texture analysis, which are sanity checked with a 1:100,000 scale regional soil map (John Gallant, pers. comm., 2002, CSIRO Land and Water), Fig. 5.4.

To model a ground-based gravity change due to a terrestrial storage variation it is desirable that the land surface model explicitly incorporates groundwater dynamics. While some land surface models attempt to model groundwater explicitly (e.g. York et al. (2002); Yeh and Eltahir (2005a,b)), CABLE implicitly models groundwater through soil saturation (using a physically based Richard's equation). For this thesis the terrestrial water storage is modelled by CABLE (as soil moisture) to a depth of 4.6 m. Terrestrial water storage observations are generated from soil moisture and groundwater level observations. The observed groundwater level is shallow and always within 4.6 m of the ground surface. Therefore both modelled and observed terrestrial water storage do not change below 4.6 m, and a deep groundwater model is unnecessary.

As twenty minute resolution soil moisture and groundwater level (terrestrial water storage) observations are used to generate synthetic gravity observations, there is a great deal of flexibility in the type of gravity observation assimilated and the temporal resolution of the observations (both gravity and near-surface soil moisture). In order for the assimilation results from the synthetic ground-based gravity to be more easily generalisable to both ground-based and remotely sensed gravity (and soil moisture) the assimilation windows and near-surface soil moisture observation times are chosen to correspond with products from the Gravity Recovery and Climate Experiment (GRACE) and Advanced Microwave Scanning Radiometer-EOS (AMSR-E) satellites for gravity and near-surface soil moisture (respectively). Furthermore the ground-based gravity observation types are generated to mimic both GRACE products (i.e. mean gravity anomalies) and ground-based gravity observation types (i.e. gravity differences and absolute gravity), while the near-surface soil moisture mimics both ASMR-E products and in-situ soil moisture observations.

The Bouguer slab approximation is used to convert terrestrial water storage (soil moisture and groundwater) to ground-based gravity. Due to GRACE observations being monthly gravity anomalies (a difference of monthly with climatological average gravity) the initial assimilation window is one month and the initial observations are average gravity over the window or near-surface soil moisture every 3 days, the worst case repeat time of AMSR-E (Njoku et al., 2003). Experiments are conducted to assess whether gravity, near-surface soil moisture, or both gravity and near-surface soil moisture assimilation is most effective in retrieving the observed profile soil moisture (0-30, 30-60, and 60-90 cm) and terrestrial water storage. Different gravity data types, and assimilation window lengths are also tested.

The techniques developed in this thesis can be used to non-invasively monitor soil moisture (or terrestrial water storage) with ground-based gravity data and retrieve profile soil moisture (or integral terrestrial water storage) at the field scale. The assimilation technique could be used on a point scale or on a regional, continental or even global (land surface) grid to assimilate either remotely sensed or ground-based gravity (or soil moisture) and improve profile soil moisture simulation (and terrestrial water storage) in a land surface model (that may improve weather or climate simulations).

3.4 Transferability of Methods

Much of the data and methods used in this thesis are publicly available and readily transferable to any site in the world. Data that was used, documentation, and where it can be publicly found includes:

- SG gravity and accompanying pressure data (Crossley and Hinderer, 2009) from `http://ggp.gfz-potsdam.de`;
- soil moisture (and precipitation) (Smith et al., 2012) from `http://www.oznet.org.au`;

- land surface model forcing data (Siriwardena et al., 2003; Smith et al., 2012) from `http://www.oznet.org.au`;
- earthquakes from `http://www.ga.gov.au/earthquakes` and `http://earthquake.usgs.gov`;
- polar motion from `http://www.iers.org`.

Methods and models used, documentation, and where they can be publicly found includes:

- Tsoft (Van Camp and Vauterin, 2005) from `http://seismologie.oma.be/TSOFT/tsoft.html` and `http://www.upf.pf/ICET/soft/index.html`;
- ETERNA (Wenzel, 1996) from `http://www.eas.slu.edu/GGP/ETERNA34` and `http://www.upf.pf/ICET/soft/index.html`;
- BAYTAP-G (Tamura et al., 1991; Tamura, 1999) from `http://www-geod.kugi.kyoto-u.ac.jp/iag-etc/etcdat/baytapg/baytapg.zip` see also `http://www-geod.kugi.kyoto-u.ac.jp/iag-etc/etcdat/aareadme.1st` and `http://igppweb.ucsd.edu/~agnew/Baytap/baytap.html`;
- NLOADF (Agnew, 1997) from `http://www.whigg.cn/yanhm/fortran.htm` and `http://igppweb.ucsd.edu/~agnew/Spotl/spotlmain.html`;
- SPOTL (Agnew, 1996) from `http://igppweb.ucsd.edu/~agnew/Spotl/spotlmain.html`;
- GOTIC2 (Matsumoto et al., 2001) from `http://www.miz.nao.ac.jp/staffs/nao99/index_En.html`;
- OLFG/OLMPP (Scherneck, 1991) from `http://www.oso.chalmers.se/~loading`;
- network adjustment (Hwang et al., 2002) from `http://space.cv.nctu.edu.tw/research/Past_reseach/moi_gravity.htm` or `http://www.iamg.org/index.php/publisher/articleview/frmArticleID/105`;

- CABLE (Kowalczyk et al., 2006)
  from `http://trac.nci.org.au/trac/cable/wiki`;

- PEST (Doherty, 2010) from `http://www.pesthomepage.org`.

3.5 Chapter Summary

This chapter presented a research approach to monitor soil moisture with ground-based gravity data and in doing so addressed the 3 objectives of this thesis:

1. **Achieving** high precision gravity data (to monitor soil moisture)

2. **Detecting** a soil moisture signal in gravity data

3. **Retrieving** a soil moisture profile from gravity data

To detect a soil moisture signal in ground-based gravity data 20 sites in the Murrumbidgee Soil Moisture Monitoring Network were installed and augmented with a piezometer (to monitor groundwater level) and stable gravity platform to measure gravity with a portable relative gravimeter (Scintrex CG-3M). However, a gravity network was established with only 4 of the soil moisture monitoring sites and an (assumed hydrologically stable) bedrock reference site in the Kyeamba Creek Catchment. The gravity network was measured in wet and dry conditions and the gravity estimate at each site (after network adjustment) compared to terrestrial water storage (profile soil moisture and groundwater level) at the soil moisture monitoring sites (Chapter 5).

To achieve high precision ground-based gravity data the relative gravimeter (Scintrex CG-3M) is calibrated with the high precision SG in Canberra, and the corrections used at the field (soil moisture monitoring and bedrock) sites tested against the SG gravity data. The network adjustment and gravity corrections are tested on a small network (3 sites) around the SG, and in the Kyeamba Catchment, with the network of two soil moisture monitoring sites (and the bedrock site) observed 8 days later (Chapter 4).

To retrieve a soil moisture signal from depth integrated ground-based gravity data a land surface model is used together with variational data assimilation. The

Bouguer slab approximation is used to generate synthetic ground-based gravity observations from soil moisture and groundwater level data. The ability of the data assimilation to retrieve the profile soil moisture is evaluated with in-situ soil moisture data (Chapter 6).

Chapter 4

Achieving High Precision Gravity Data

The previous chapter presented a research approach to investigate the measurement of soil moisture and total terrestrial water storage (TWS) with ground-based gravity data from a field portable relative gravimeter. This chapter builds on that approach by developing methods to achieve the precision necessary in ground-based gravity measurements so that a TWS signal may be detected. The methods in this chapter are focused on correcting or eliminating the largest factors that would mask the TWS signal. These include geophysical and meteorological signals, as well as instrumental effects that result from gravimeter transportation and battery power. These corrections are developed in subterranean laboratories in Melbourne, or Canberra, Australia. The Canberra gravity monitoring site is adjacent to the superconducting gravimeter (SG) at Mt Stromlo. The methods that minimise the SG gravity residual (after applying the corrections) are selected for use in the field at Kyeamba Creek Catchment, 100 km west of Canberra. Two case studies involving gravity networks of three sites are investigated to determine the gravity precision achievable in the field. At the conclusion of this chapter methods are selected to correct the relative gravity data from the Scintrex CG-3M, and the gravity precision achievable in the field is known.

This chapter begins by checking the SG and CG-3M calibrations (section 4.1). Methods to correct gravity data for the geophysical (section 4.2) and meteorological signals (section 4.3) are tested on the SG and CG-3M gravimeters in Canberra, and Melbourne. The transferability of the gravity corrections to other sites is investigated in section 4.4. Corrections for instrumental artefeacts in the Scintrex CG-3M relative gravity meter are developed in section 4.5. Finally two case studies are used to test the various corrections and determine the gravity precision achievable in the field (section 4.6).

4.1 Gravimeter Calibration

Relative gravimeters require calibration to measure a change in gravity. The Scintrex CG-3M used in this thesis was shipped with a factory calibration, and had been recently used (by Monash University) before this study. However, the calibration was checked by observing gravity with the Scintrex CG-3M adjacent to the precise superconducting gravimeter (SG) in Canberra before and after every field campaign in the Murrumbidgee River Catchment. One such check of the Scintrex CG-3M calibration against the Canberra SG is shown in this section. The SG also being a relative gravimeter, is calibrated to an absolute gravimeter. The Canberra SG calibration is checked in this section with absolute gravity (FG5) data from the time of the field campaigns in this thesis.

4.1.1 SG Calibration

The Superconducting Gravimeter (SG) at Mt Stromlo, Canberra is a GWR Instruments Compact Tidal Gravimeter (instrument number CT031) that was owned by the National Astronomical Observatory of Japan (NAOJ) and maintained by Herb McQueen of the Research School of Earth Sciences (RSES), Australian National University (ANU) but is now owned (and operated) by ANU. The SG CT031 was installed in January 1997 and has been running continuously, with a brief period of inactivity between the 18th of January and 20th of March 2003. The data gap was due to the Canberra bushfires, that completely burnt out the building used to house the gravimeter (Fig. 4.1), but miraculously did not damage the gravimeter or the room it is located in (McQueen, 2003). The Canberra SG has been calibrated to various Micro-g Solutions (now Micro-g LaCoste) FG5 absolute gravimeters with

Fig. 4.1 The observatory at Mt Stromlo in the year 2004, after the Canberra bushfires of 2003. This building houses the Canberra SG in a basement, that was fully functional and recording gravity at the time of this photograph.

Table 4.1 Canberra SG (CT031) calibrations (μGal/V), standard error is shown in brackets.

Year	FG5 Absolute Gravimeter	Transfer coefficient
1998	#110	-75.701 (0.136)
1999	#206	-75.920 (0.061)
2000	#206	-76.098 (0.169)
2004	#210	-76.225 (0.178)
2005	#111	-76.234 (0.173)

the preferred calibration from an observation in March 1999 (Almalvict et al., 2001). This resulted in a voltage to microgal transfer coefficient of -75.92±0.061 μGal/V and remains the most precise calibration (Table 4.1).

Calibration of the Canberra SG from 2004 and 2005 is considered in this thesis (Table 4.1 and Fig. 4.2 and 4.3) to assess the temporal stability of the calibration factor and check whether the loss of building material in the vicinity of the SG in 2003 (Fig. 4.1) had an impact on the SG calibration. This is because the (calibrated gravity from the) SG was used in the year 2005 to calibrate the Scintrex CG-3M relative gravimeter used in this thesis.

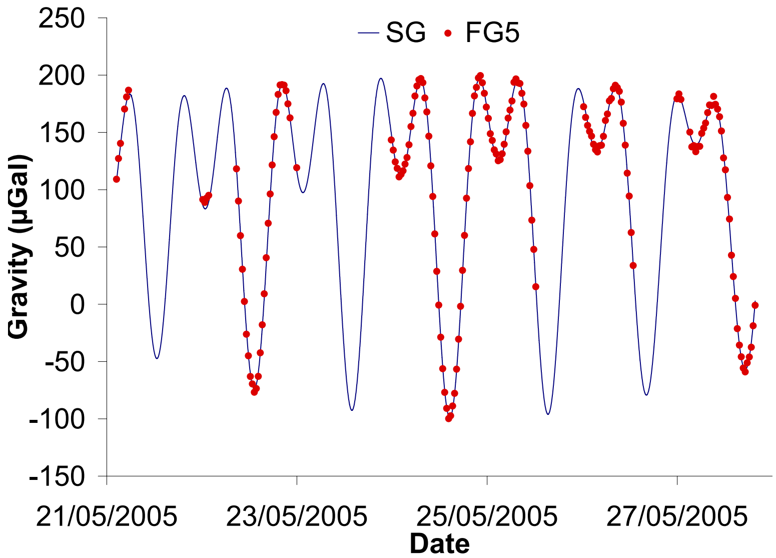

Fig. 4.2 Canberra SG and FG5 #111 gravity time series during SG calibration in 2005. The SG relative gravity is 1 minute corrected data from `http://ggp.gfz-potsdam.de`. The FG5 absolute gravity data (Herb McQueen, pers. comm., 2005, ANU RSES) has been offset by 979549588 µGal (or approximately 9.8 m/s^2). The FG5 gravity data are half-hourly sets that are an average of 120 drops, with a drop every 15 seconds.

The absolute gravimeters used for calibrations in the years 2004 and 2005 were the FG5#210 owned by Kyoto University and the FG5#111 owned by Micro-g Solutions (Table 4.1). The FG5#111 calibration from May 2005 is considered unreliable due to instrument problems (the gravimeter repeatedly lost power when left unattended overnight) that resulted in large gaps in the data set (Fig. 4.2). While the FG5#210 calibration from March–April 2004 is reasonably good (Fig. 4.3), an unusually large number of earthquakes of magnitude greater than 6.0 occurred during this period (Table 4.2). Problems have also been noted with this absolute gravimeter

Table 4.2 Number of earthquakes measured by the Canberra SG during calibrations. Data from `http://www.ga.gov.au/earthquakes`.

Year	Magnitude < 6	$6 \leq$ Magnitude < 7	Magnitude ≥ 7
2004	7	9	0
2005	8	1	0

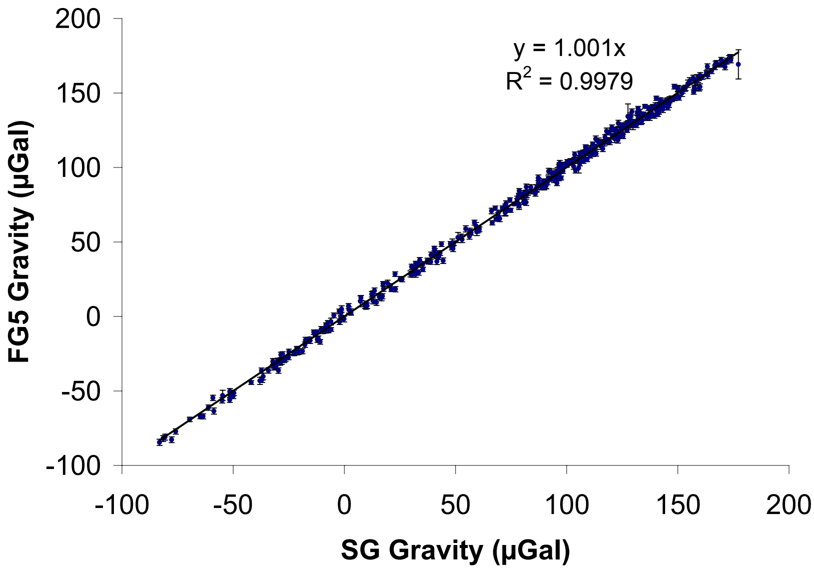

Fig. 4.3 Canberra SG calibration to FG5 #210 in 2004. The SG relative gravity is 1 minute corrected data from `http://ggp.gfz-potsdam.de`. The FG5 absolute gravity data (Herb McQueen, pers. comm., 2005, ANU RSES) has been offset by 979549515 µGal (or approximately 9.8 m/s^2) and is shown with error bars which are 95 % confidence intervals. The FG5 gravity data are hourly sets that are an average of 160 drops, with a drop every 15 seconds.

in the past (Imanishi et al., 2002; Fukuda et al., 2004; Tamura et al., 2005). Regardless, the calibrations from the years 2004 and 2005 are very similar, with transfer coefficients of -76.225±0.178 and -76.234±0.173 µGal/V respectively (Table 4.1). Both calibrations are within two standard deviations of the accepted calibration (-75.92±0.061 µGal/V). Therefore, the calibration factor of the Canberra SG may be assumed temporally stable over the years 2004 and 2005 (and indeed back to 1999), and the Canberra SG gravity data (for the year 2005) can be confidently used as a high precision reference data set.

4.1.2 CG-3M Calibration

The Scintrex CG-3M relative gravimeter used in this thesis is #507297 owned by Monash University. To check the Scintrex CG-3M factory calibration the portable gravimeter was run on AC power continuously in the room adjacent to the Canberra

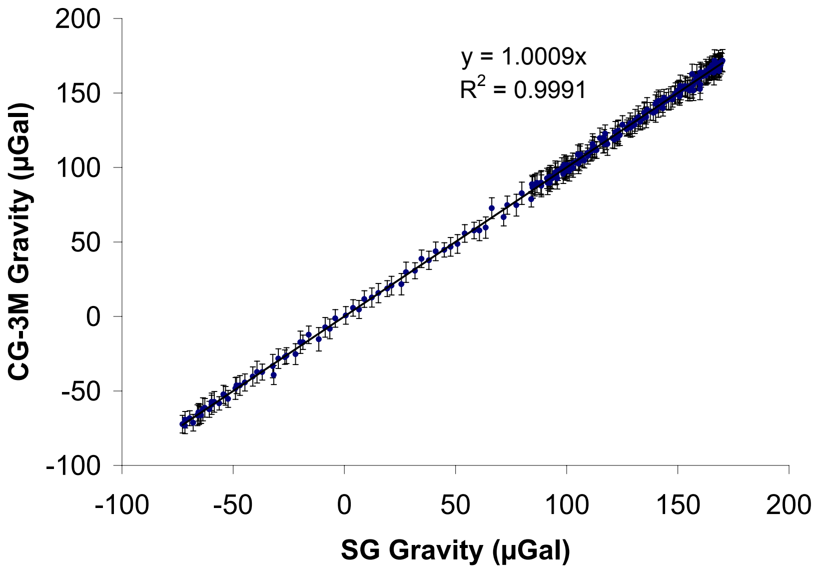

Fig. 4.4 Scintrex CG-3M calibration to Canberra SG in 2005. SG data are raw 1 second samples (Herb McQueen, pers. comm., 2005, ANU RSES). Scintrex CG-3M data are shown with error bars which are 95 % confidence intervals (an estimate of measurement precision calculated as the standard error of the 1 second samples for a 2 minute measurement). CG-3M data are 15 minute measurements that are an average of 120 samples, with a sample every 1 second.

SG at Mt Stromlo from the 24th of January to the 5th of February, 2005. Every 15 minutes an average of 120 one second samples was logged. The full data set is 13 days long, but only the initial 2.5 days are used for calibration (Fig. 4.4), due to significant earthquakes and nonlinear drift after the first 2.5 days (Fig. 4.5).

The calibration of the Scintrex CG-3M to the Canberra SG is excellent with an R^2 of 0.9991. The calibration factor of 0.998±0.002 µGal/µGal shows that the gravity data from the Scintrex CG-3M corresponds to the SG gravity data over the tidal range (300 µGal) at the µGal level (the resolution of the CG-3M output). Consequently the Scintrex CG-3M calibration provided by the manufacturers is considered reliable and temporally stable. The stability of the CG-3M calibration is further checked before and after every field campaign (as recommended by Dragert et al. (1981)) by continuously logging gravity data with the CG-3M in a room adjacent to the Canberra SG for at least 12 hours.

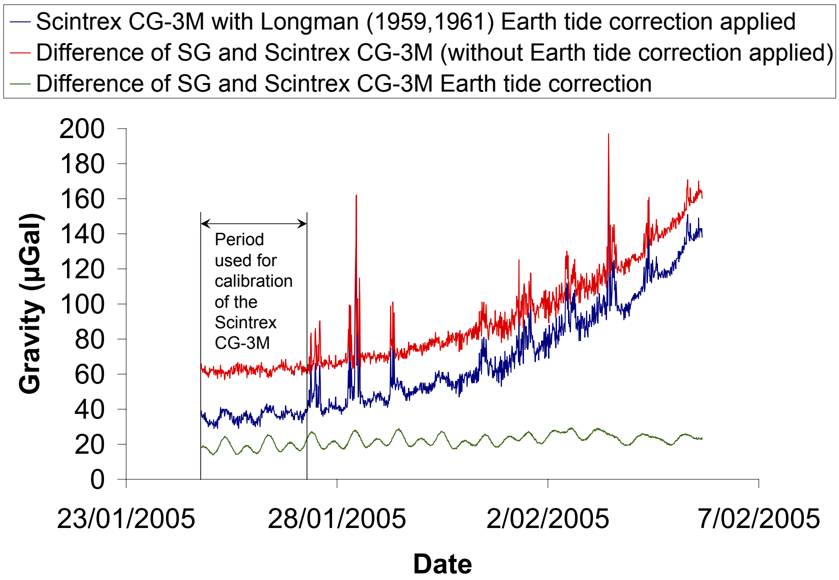

Fig. 4.5 Gravity time series during Scintrex CG-3M calibration (and subsequent 10.5 days). Scintrex CG-3M gravity is shown in blue (with in-built Longman (1959, 1961) Earth tide correction applied), difference of SG and Scintrex CG-3M gravity (without Earth tide correction applied) in red, and difference of SG and Scintrex CG-3M automatic Earth tide correction in green. Drift and earthquakes in the Scintrex CG-3M gravity data are clear after the initial 2.5 days used for calibration.

4.2 Removing Geophysical Signals

The geophysical signal is the largest temporally varying signal in ground-based gravity data and it consists of Earth tides, polar motion, ocean tide loading, post glacial rebound, and earthquakes. This section uses available predictive models for Earth tides, polar motion, and ocean tide loading, and removes the predicted geophysical signal from the (hourly) SG gravity data at Canberra for the year 2005 to create a gravity residual. The methods that minimise the standard deviation of the SG gravity residual are selected to use at the field sites in the Kyeamba Creek catchment (100 km west of the SG in Canberra). Post glacial rebound and earthquakes are not assessed as post glacial rebound is negligible in Australia (Paulson et al., 2007), and earthquakes are impossible to predict (Geller, 1997).

4.2.1 Earthquakes

The first stage of any gravity analysis must be to acknowledge the perturbing effects of earthquakes, see for example the spikes and increased noise levels (lower measurement precision) for the gravity data in Fig. 4.5. As part of the internal gravity processing the Scintrex CG-3M applies a seismic filter to remove microseismic noise, defined by Scintrex (1995) as having a period of less than 10 seconds. This microseismic noise is predominantly caused by wave action at the coast (within a few hundred kilometres of the coast), travelling storms (rapidly changing atmospheric mass distribution), and wind (blowing structures embedded in the ground such as trees and buildings). The Scintrex CG-3M seismic filter rejects one second gravity samples greater than four standard deviations from the (running) mean, however the filter is not effective at removing earthquakes. This is because during an earthquake the mean gravity value is perturbed for a period of time exceeding the duration that the gravimeter is averaging over (two minutes in this thesis). Therefore, gravity data must always be screened for earthquakes. This can be done using websites such as `http://www.ga.gov.au/earthquakes` and `http://earthquake.usgs.gov`, as well as real time email alerts. These services record the magnitude, depth and location of significant earthquakes. For the superconducting gravimeters (SG), there is publicly available Global Geodynamics Project (GGP) data at `http://ggp.gfz-potsdam.de` that includes:

- raw one minute data (created by decimating the original raw one second data),
- corrected one minute data (raw one minute data corrected for earthquakes, steps and gaps), and
- one hour data (created by decimating the corrected one minute data).

The one hour data can then be used immediately with an Earth tide program (such as ETERNA or BAYTAP-G) to analyse the Earth tides, ocean tide loading and atmospheric pressure signals in the gravity data. The one hour Canberra (Mt Stromlo) GGP data is used for all subsequent SG analysis in this thesis. However the CG-3M laboratory analysis data in this chapter does not have earthquakes removed.

Earthquake monitoring method
Geoscience Australia and United States Geological Survey websites `http://www.ga.gov.au/earthquakes` and `http://earthquake.usgs.gov`.

4.2.2 Earth Tides

To determine the most effective Earth tide prediction method at field sites (where no continuous gravity data is available for comparison), a variety of methods were trialled and compared to the Canberra SG gravity data (Fig. 4.6). The method with the smallest standard deviation (over the year 2005) of the residual (where the residual is the difference of the hourly SG gravity data and the gravity correction) was chosen for use at Kyeamba Catchment, under the assumption that the most precise prediction method at Canberra would transfer to sites 100 km west. The Tsoft Earth tide program (Van Camp and Vauterin, 2005) using the Tamura (1987) tidal potential catalogue and Love numbers of Dehant et al. (1999) gave the best results (Table 4.3 and Fig. 4.7).

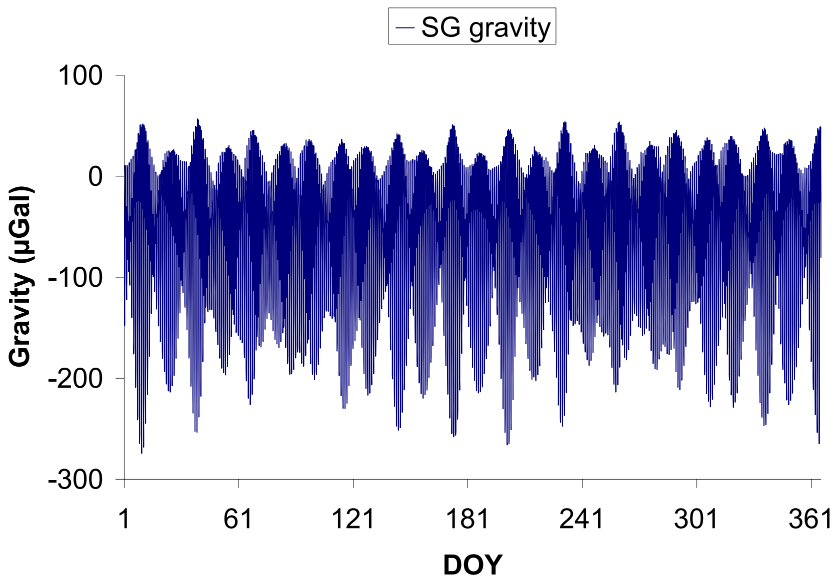

Fig. 4.6 Canberra SG gravity data for the year 2005 showing Earth tides. Hourly SG data from `http://ggp.gfz-potsdam.de`.

The Tsoft Earth tide program uses the Tamura (1987) tidal potential catalogue, whereas the ETERNA Earth tide program allows the option of using either the Tamura (1987) or Hartmann and Wenzel (1995a,b) tidal potential catalogues. However using the larger (12935 wave) tidal potential expansion of Hartmann and Wenzel (1995a,b) with ETERNA gave almost no benefit compared to the (1200 wave)

Table 4.3 Earth tide programs, Love numbers, and tidal potential catalogues used to predict gravity corrections where no continuous gravity record is available. Using Love numbers calculated from the tabulated Earth response models, the residual with respect to the Canberra SG is calculated (μGal), with the standard deviation (S.D.) reported. A time series of the residual calculated with Tsoft using the Dehant et al. (1999) Love numbers and Tamura (1987) tidal potential catalogue is shown in Fig. 4.7.

Earth Tide Program	Love Numbers	Tidal Potential Catalogue	Residual S.D.
Tsoft	Dehant et al. (1999)	Tamura (1987)	3.502
ETERNA	Dehant (1987)	Tamura (1987)	10.109
ETERNA	Dehant (1987)	Hartmann and Wenzel (1995a,b)	10.108

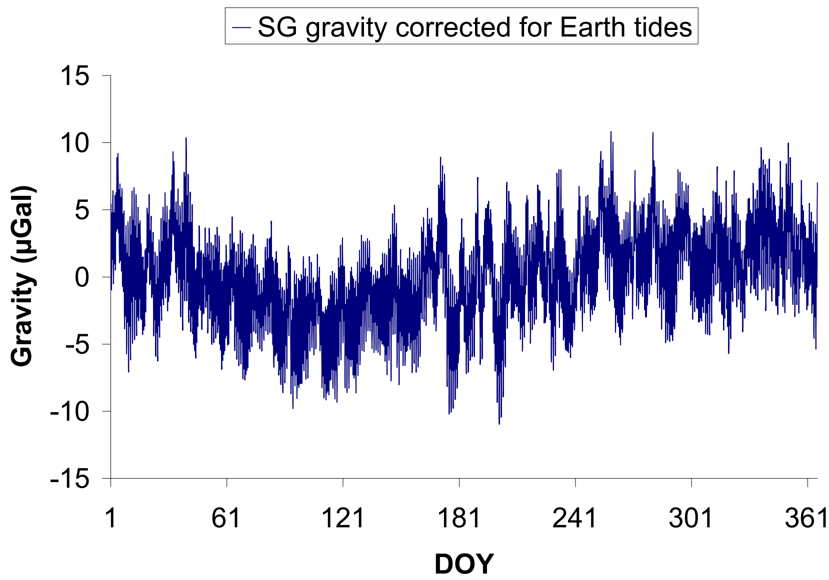

Fig. 4.7 As for Fig. 4.6 but corrected for predicted Earth tides using the Tsoft software (Van Camp and Vauterin, 2005), Dehant et al. (1999) Love numbers, and Tamura (1987) tidal potential catalogue.

Tamura (1987) potential. Moreover, when the Tamura (1987) tidal potential catalogue was used for both the ETERNA and Tsoft Earth tide programs, the standard deviation of the Canberra SG gravity residual (for the year 2005) was reduced much more using the Tsoft software (Table 4.3). This is because the ETERNA program (Wenzel, 1996) uses the older Dehant (1987) Love numbers, whereas Tsoft (Van Camp and Vauterin, 2005) utilises the newer Dehant et al. (1999) parameters (Table 4.3). Consequently the Tsoft Earth tide program was selected to remove Earth tides from gravity data.

Spatial and Temporal Variability of Earth Tide Correction

Tsoft was then used to compare the gravity predictions at Canberra and the Kyeamba Creek catchment to see if the Earth tides are similar. If the Earth tides are similar, the precisely determined Love numbers in Canberra (derived from the SG gravity data) could be used in the Kyeamba Creek catchment, or alternatively the SG could be used as a gravity base station, with the SG data used to directly remove Earth tides at the Kyeamba Creek catchment sites by differencing the gravity data for the two locations (at the same time). However it was found that the Earth tides are significantly different for the two locations (which are only 100 km apart), with the maximum (instantaneous) difference between the normalised (i.e. 0 μGal mean) predictions at each site (for 2005) reaching 6.7 μGal. Even within Kyeamba the maximum difference between each site reaches 1.0 μGal (for the BED to K13 difference, see Fig. 3.7). Consequently, the Earth tides are predicted for each Kyeamba site with Tsoft, using the Dehant et al. (1999) Love numbers for that site and the Tamura (1987) tidal potential catalogue.

Earth tide prediction method
Tsoft Earth tide program (Van Camp and Vauterin, 2005) using Tamura (1987) tidal potential catalogue and Dehant et al. (1999) Love numbers.

4.2.3 Polar Motion

Using the EOP C04 series of Earth orientation parameters available (at daily resolution) from the International Earth Rotation Service (IERS) website `http://www.iers.org`, the polar motion effect was calculated at Canberra for the year 2005 with the Tsoft Earth tide program (Van Camp and Vauterin, 2005). The predicted polar motion closely follows the Canberra SG gravity data corrected for Earth tides and atmospheric pressure (Fig. 4.8), indicating the polar motion effect is predicted well at this location with this method and implying the method may also be effective for the field sites 100 km west of the SG. Consequently the Tsoft Earth tide program was selected to predict the polar motion signal in gravity data.

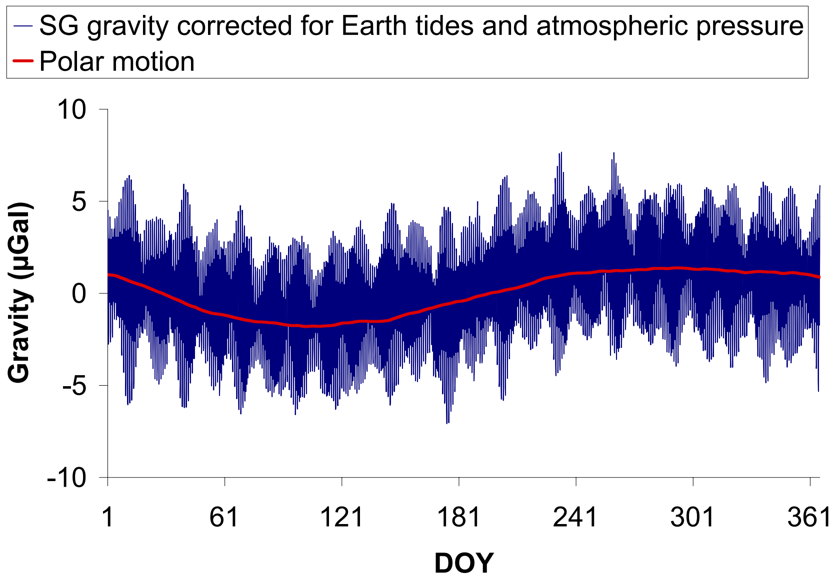

Fig. 4.8 As for Fig. 4.7 but corrected for atmospheric pressure using a standard admittance of 0.3 μGal/mbar (and hourly pressure data from `http://ggp.gfz-potsdam.de`). Also shown in red is predicted polar motion using the Tsoft software (Van Camp and Vauterin, 2005) and EOP C04 series of Earth orientation parameters from `http://www.iers.org`.

Spatial and Temporal Variability of Polar Motion Correction

The polar motion effect at the Kyeamba Creek Catchment field sites is approximately a 3 μGal increase in gravity from March to September, which is equivalent to the expected signal over this period (in both magnitude and sign) from terrestrial water storage. Therefore it is essential that polar motion is removed from the field gravity data before analysing it for a terrestrial water storage signal. The polar motion effect is almost identical at Canberra and the field site BED (a maximum difference of 0.17 μGal), therefore differencing the gravity data from the field sites with the Canberra SG gravity data for the same time would remove the polar motion effect. Alternatively, differencing the gravity data from the field sites with that from the bedrock reference site would also remove the polar motion. However, in this thesis the Tsoft Earth tide program is used, together with the IERS data to predict and remove the polar motion effect from the gravity data at each site, as this will give the most precise results. Furthermore this approach is more general and can be used with gravity data from a single site.

Polar motion prediction method
Tsoft Earth tide program (Van Camp and Vauterin, 2005) using EOP C04 series of Earth orientation parameters from the International Earth Rotation Service website `http://www.iers.org`.

4.2.4 Ocean Tide Loading

The ocean tide loading model OLFG/OLMPP (Scherneck, 1991) was used via the ocean tide loading provider at `http://www.oso.chalmers.se/~loading` to generate amplitude and phase parameters at Canberra for the eight main partial tides (M2, K1, O1, N2, S2, P1, Q1, K2) and three long period partial tides (Mf, Mm, Ssa) for 18 different ocean tide models (Table 2.6). The parameters from OLFG/OLMPP were then used with SPOTL (Some Programs for Ocean-Tide Loading, Agnew (1996) to generate gravity time series of ocean tide loading. Two other ocean tide models, NLOADF (Agnew, 1997), and GOTIC2 (Matsumoto et al., 2001), were also used to generate amplitude and phase parameters for partial ocean tides from eight ocean tide models (Table 2.7 and 2.8). Similar to OLFG/OLMPP the NLOADF parameters were also used with SPOTL to calculate time series, whereas GOTIC2 calculates both parameters and time series.

The various ocean tide loading models (OLFG/OLMPP, NLOADF and GOTIC2), and ocean tide models (Table 2.6-2.8) are assessed by calculating the standard deviation of the gravity data from the Canberra SG (for the year 2005) after also correcting for Earth tides, polar motion and atmospheric pressure signals (Table 4.4). The performance of all ocean tide models is good, reducing the standard deviation from 2.4 μGal to between 0.65 and 0.75 μGal. However, FES95.2 is significantly worse than the other models, with a standard deviation of 1.0 and 0.9 μGal when using the NLOADF and OLFG/OLMPP ocean tide loading models (respectively). These results are in agreement with Almalvict et al. (2001), who found that the greatest reduction in the residual of 12 days of absolute gravity observations from an FG5 in Canberra during March 1999 came from the CSR3.0 model (followed by Schwiderski, then FES95.2 giving the worst results). Almalvict et al. (2001) found these models reduced the standard deviation of the absolute gravity observations (after correction for Earth tides, atmospheric pressure and polar motion) to 1.4-1.7 μGal, depending on the ocean tide model used. The 0.3 μGal variation of this range is similar to the 0.7-1.0 μGal found between CSR3.0 and FES95.2 in this thesis (Table 4.4).

Most of the ocean tide models tested in this thesis have similar skill with the newer models (CSR4.0, NAO.99b, GOT99.2b, AG06, FES2004) and the oldest model (Schwiderski) all performing well at Canberra. Despite the GOTIC2 software having only three ocean tide models to choose from (Table 2.8), when using GOTIC2, the GOT99.2b and NAO.99b ocean tide models outperformed all other models used with the OLFG/OLMPP or NLOADF ocean tide loading models (except CSR4.0). While using CSR4.0 with GOTIC2 gives the best result at Canberra, CSR4.0 with OLFG/OLMPP (and SPOTL) performed only slightly worse (Table 4.4). It is clear that CSR4.0 gives the best ocean tide predictions at Canberra for 2005 and GOTIC2 produces the best ocean tide loading predictions. Consequently the CSR4.0 ocean tide model is selected to predict ocean tide loading with the GOTIC2 software.

Comparison of Ocean Tide Loading Correction to Earth Tide Programs

To further assess the selected method to predict ocean tide loading, the gravity residual at the Canberra SG (after correcting for ocean tide loading) is compared to the residuals generated by the Earth tide programs ETERNA and BAYTAP-G. The

Table 4.4 Ocean tide and loading models used to predict gravity in the Kyeamba Catchment where no continuous gravity record is available for evaluation. The residual (μGal) is with respect to the Canberra SG (the closest location to Kyeamba where the prediction methods can be assessed), with the standard deviation (S.D.) reported. The GGP 1 hour gravity and pressure data are used to calculate the residuals (with a standard admittance of 0.3 μGal/mbar), Earth tides are calculated with Tsoft and the Dehant et al. (1999) Love numbers (Table 4.3), polar motion is also removed with the IERS data and Tsoft (subsection 4.2.3). Time series of the first two rows of the table are shown in Fig. 4.7 and Fig. 4.8, while a time series of the last row is shown in Fig. 4.9 (note the change in scale of the axis for this figure).

Ocean Tide Loading Model	Ocean Tide Model	Residual S.D.
None		3.5025
None (pressure correction only)		2.6112
None (pressure and polar motion correction)		2.4123
NLOADF	FES95.2	1.0143
OLFG/OLMPP	FES95.2	0.9094
NLOADF	Schwiderski	0.7546
OLFG/OLMPP	FES94.1	0.7529
OLFG/OLMPP	Schwiderski	0.7408
OLFG/OLMPP	FES99	0.7371
OLFG/OLMPP	EOT08a	0.7193
NLOADF	TPXO.6.2	0.7190
OLFG/OLMPP	FES98	0.7178
OLFG/OLMPP	TPXO.6.2	0.7169
OLFG/OLMPP	CSR3.0	0.7114
OLFG/OLMPP	TPXO.5	0.7101
OLFG/OLMPP	TPXO.7.1	0.6977
OLFG/OLMPP	GOT00.2	0.6946
OLFG/OLMPP	TPXO.7.0	0.6935
NLOADF	CSR3.0	0.6841
OLFG/OLMPP	GOT99.2b	0.6839
OLFG/OLMPP	GOT4.7	0.6834
NLOADF	GOT00.2	0.6818
OLFG/OLMPP	NAO.99b	0.6818
OLFG/OLMPP	FES2004	0.6787
OLFG/OLMPP	AG06	0.6744
GOTIC2	GOT99.2b	0.6723
GOTIC2	NAO.99b	0.6712
OLFG/OLMPP	CSR4.0	0.6671
GOTIC2	CSR4.0	0.6525

Earth tide programs ETERNA and BAYTAP-G analyse the observed gravity (and pressure data) and calculate amplitude factors for the partial tides (and a pressure admittance), whereas the ocean tide loading model GOTIC2 predicts the loading independently of the observed gravity data, using partial tides predicted by the CSR4.0 ocean tide model (Table 2.8). The polar motion is removed from all three residuals and the pressure effect is removed from the GOTIC2 and CSR4.0 residual using a standard admittance of 0.3 μGal/mbar, whereas for ETERNA and BAYTAP-G the admittance is calculated (during analysis) as 0.35 and 0.36 μGal/mbar respectively (Table 4.5). Predictions using GOTIC2 with CSR4.0 are just as good as using ETERNA and BAYTAP-G directly on the data (Fig. 4.9), with the GOTIC2 and CSR4.0 prediction actually reducing the standard deviation of the residual by more than the BAYTAP-G analysis (Table 4.5). The 2 μGal dip clearly visible in all three residuals on 16 June is due to periodic maintenance (a liquid helium refill) of the SG (Fig. 4.9).

Table 4.5 As for Table 4.4 but showing only the (selected) ocean tide loading model (GOTIC2) and ocean tide model (CSR4.0) that minimise the standard deviation of the Canberra SG residual (μGal), together with ETERNA and BAYTAP-G Earth tide programs. A time series of the gravity residual from each row of the table is shown in Fig. 4.9.

Method	Pressure Admittance (μGal/mbar)	Residual S.D.
Tsoft, GOTIC2 and CSR4.0	0.3	0.65
ETERNA	0.35	0.40
BAYTAP-G	0.36	0.77

Spatial and Temporal Variability of Ocean Tide Loading Correction

It is assumed that the performance of the ocean tide and loading models at Canberra is indicative of the performance that can be expected at the field sites in the Kyeamba Creek Catchment, 100 km west of Canberra, and 230 km from the coast rather than 130 km. The ocean tide loading was calculated for the field site BED and Canberra for the year 2005 using the GOTIC2 ocean tide loading model and the CSR4.0 ocean tide model. The (instantaneous) difference in predicted ocean tide loading between the two locations reaches 1.3 μGal, therefore the ocean tide loading signal

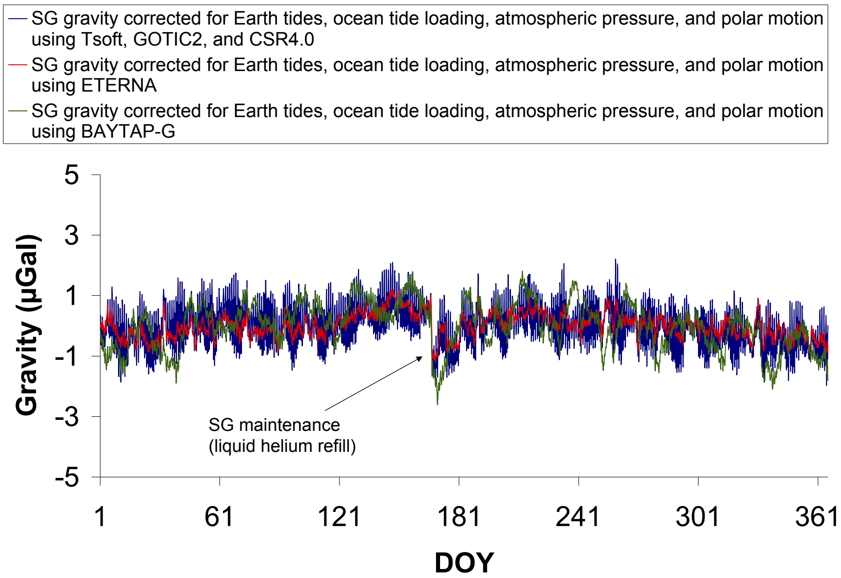

Fig. 4.9 As for Fig. 4.8 but corrected for polar motion, and predicted ocean tide loading using the CSR4.0 ocean tide model (Watkins and Eanes, 1997), and GOTIC2 loading software (Matsumoto et al., 2001). Also shown in red and green are Canberra SG gravity (as in Fig. 4.6) corrected for Earth tides, ocean tide loading, atmospheric pressure, and polar motion using the Earth tide programs ETERNA (Wenzel, 1996), and BAYTAP-G (Tamura et al., 1991; Tamura, 1999). Note the blue line uses corrections predicted independent of the SG gravity data, whereas the red and green lines use corrections fitted to the SG gravity and pressure data.

in the field gravity data (from the Scintrex CG-3M) cannot be removed by simply differencing the field gravity data with the precise gravity data from the Canberra SG, and must be removed from the gravity data at the field sites in the Kyeamba Creek Catchment by correcting for the ocean tide loading signal predicted by the GOTIC2 ocean tide loading model using the CSR4.0 ocean tide model. The ocean tide loading was calculated for the Kyeamba Creek Catchment sites (Fig. 3.7) using GOTIC2 and CSR4.0. The maximum (instantaneous) difference between field sites was found to be 0.14 μGal (at any time over the year 2005), therefore the same ocean tide loading correction could be applied to all of the Kyeamba sites, or alternatively the ocean tide loading signal in the gravity data from each site could be removed by simply differencing the gravity data from each site. However, the maximum one hour difference in ocean tide loading (both between sites and at the same site) was found to be 2.0 μGal. Due to the spacing of sites in the network (Fig. 3.7) and duration of gravity observation (20 minutes), the time between gravity observations at each site is generally no less than 1 hour. Therefore, unless multiple gravimeters are used to observe gravity at each site simultaneously, differencing gravity data from different sites (at differing times) is not a precise method to remove the ocean tide loading signal. Consequently, ocean tide loading is predicted at each site using the GOTIC2 ocean tide loading model with the CSR4.0 ocean tide model.

Ocean tide loading prediction method
GOTIC2 ocean tide loading software (Matsumoto et al., 2001) using CSR4.0 ocean tide model (Watkins and Eanes, 1997).

4.2.5 Section Summary

Earthquakes disturb gravity data but cannot be predicted and need to be monitored using services such as `http://www.ga.gov.au/earthquakes` and `http://earthquake.usgs.gov`. While the polar motion signal in gravity does not vary much over 100 km, the variation in Earth tides and ocean tide loading over this distance is significant. However ocean tide loading and Earth tide variation over approximately 20 km is negligible. Therefore a gravity base station within 20 km of field sites could be used to correct for polar motion, Earth tides and ocean tide loading by differencing the base station data with gravity data obtained from the field sites. However the significant temporal variation of ocean tide loading and Earth tides over periods as short as 1 hour, means that the travel time between sites in the network (including setting up and packing up the gravimeter) must be below 10 minutes, and the gravity observation time must also be below 10 minutes, or alternatively a dedicated base station gravimeter needs to be used in conjunction with at least one more gravimeter for the field sites (so that gravity observations from the same time can be differenced). A more pragmatic, cost effective and precise method is to correct for Earth tides, ocean tide loading and polar motion at each of the field sites using methods tested at a nearby site, or the methods selected in this thesis (tested at Canberra, Australia).

The Earth tide program Tsoft (Van Camp and Vauterin, 2005) was found to be effective for removing both Earth tides (using the Tamura (1987) tidal potential catalogue and Dehant et al. (1999) Love numbers) and polar motion (using the IERS EOP C04 data from `http://www.iers.org`), and is selected to correct these signals in gravity data at the field sites. Similarly GOTIC2 (Matsumoto et al., 2001) was found to precisely predict ocean tide loading, and is selected to be used together with the CSR4.0 ocean tide model (Watkins and Eanes, 1997), although all ocean tide models tested at Canberra gave fairly similar good results.

4.3 Removing Meteorological Signals

Atmospheric pressure loading and attraction is a clear signal in gravity data, however other meteorological signals may also be present. While geophysical signals can be predicted with software and removed from gravity data, meteorological signals must be observed adjacent to the gravimeter and compared to the gravity data to evaluate any correlation. This section uses meteorological data observed adjacent to a Scintrex CG-3M gravimeter to determine the significance of atmospheric pressure, air temperature and relative humidity signals in gravity data. A linear admittance (correction factor) is determined for atmospheric pressure, and the temporal and spatial variability of the admittance tested using the Canberra SG gravity data.

4.3.1 Atmospheric Pressure

After correcting the Canberra SG gravity data for Earth tides with the Tsoft Earth tide program (Van Camp and Vauterin, 2005), Tamura (1987) tidal potential catalogue, and Dehant et al. (1999) Love numbers, the standard deviation of the residual (corrected hourly gravity data for the year 2005) was 3.5 μGal (Table 4.4). Removing the atmospheric pressure signal using air pressure data measured adjacent to the SG and a standard admittance of 0.3 μGal/mbar further reduced the standard deviation of the gravity residual to 2.6 μGal. While removing the polar motion effect using Tsoft and IERS data reduced the standard deviation of the gravity residual further to 2.4 μGal (Table 4.4). Similarly when the ETERNA Earth tide program is used with the Hartmann and Wenzel (1995a,b) tidal potential catalogue to anal-

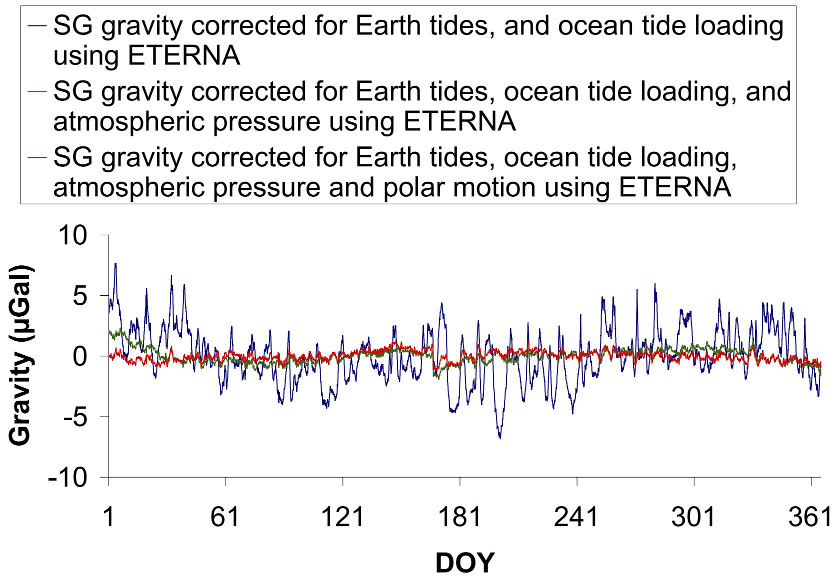

Fig. 4.10 As for Fig. 4.6 but corrected for fitted Earth tides and ocean tide loading using the ETERNA software (Wenzel, 1996), and Hartmann and Wenzel (1995a,b) tidal potential catalogue.

yse the Canberra SG gravity data (for the year 2005) the variability of the residual is significantly improved by using a pressure correction, and slightly improved further by using a polar motion correction as well (standard deviations of 2.2, 0.6 and 0.4 μGal respectively), see Fig. 4.10. Similar results were found for BAYTAP-G, with the pressure admittances determined for ETERNA and BAYTAP-G also quite similar at -0.359 μGal/mbar and -0.351 μGal/mbar respectively (Table 4.5).

Temporal Variability of Atmospheric Pressure Correction

The pressure admittance was calculated for each month (of the year 2005) using BAYTAP-G and the Canberra SG pressure and gravity data for that month only (Fig. 4.11). While there is an apparent seasonal variation of the pressure admittance, the yearly admittance value is close to the average of the twelve monthly values, with a maximum difference of 0.03 μGal/mbar (for June), which corresponds to 0.12 μGal maximum error over 12 hours for 2005 at Canberra (using a maximum observed pressure change over 12 hours of 4.0 mbar, with 3.4 mbar the maximum hourly change). Indeed, the 40 mbar maximum pressure difference at Canberra

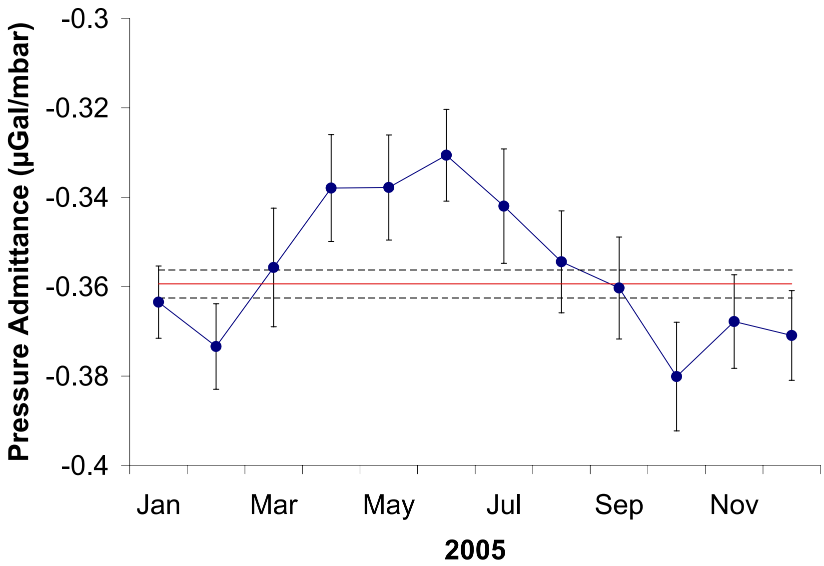

Fig. 4.11 Annual and monthly atmospheric pressure admittances for the Canberra SG for the year 2005. The pressure admittance is calculated using the BAYTAP-G Earth tide program (and hourly SG gravity and pressure data from `http://ggp.gfz-potsdam.de`). The yearly admittance is the horizontal red line with 95 % confidence intervals shown by dashed lines, the monthly admittances (calculated using gravity and pressure data for that calendar month only) are shown as blue dots with the 95% confidence limits as error bars.

over the year 2005 corresponds to 1.2 μGal maximum error from using the annual admittance rather than the monthly admittances (Fig. 4.11). Note also that the months of interest in 2005 (field campaigns) where correction of the Scintrex CG-3M gravity data is required are March and September, for which the yearly admittance is closest (Fig. 4.11). Consequently a single pressure admittance of between -0.3 and -0.4 μGal/mbar can be used at all times for all sites. However, the atmospheric pressure admittance may depend slightly on the gravimeter used due to the quality of the vacuum maintained around the gravimeter sensor (Torge, 1989), furthermore the atmospheric pressure admittance may be correcting other signals that are correlated to the atmospheric pressure but not measured (e.g. air temperature).

4.3.2 Atmospheric Pressure, Air Temperature and Relative Humidity

To assess the effect of meteorological variables on the Scintrex CG-3M the gravimeter was run in a basement in Melbourne for 3 months (8 October 2005 to 16 January 2006). The raw data, with automatic gravimeter corrections for drift and Earth tides not applied, is shown in Fig. 4.12. An average of 120 one second samples were taken, with data logged at high resolution (mostly 2.5 minutes) and then undersampled to 1 hour. Air temperature, atmospheric pressure and relative humidity were also measured with the Kestrel 4000 portable weather tracker with 0.1 °C, 0.1 mbar, and 1% resolution. The quoted accuracy of the Kestrel 4000 barometer is 3 mbar, however this pressure sensor was calibrated against the 0.2 mbar accurate (0.1 mbar precision) Yokogawa F–452 barometer used for the Canberra SG (Fig. A.1), and the resulting (linear) calibration coefficient was 1.0032 (±0.0007), with an R^2 of 0.9997 and an RMSE of 0.1 mbar. There was however a bias of 3.2 mbar between the

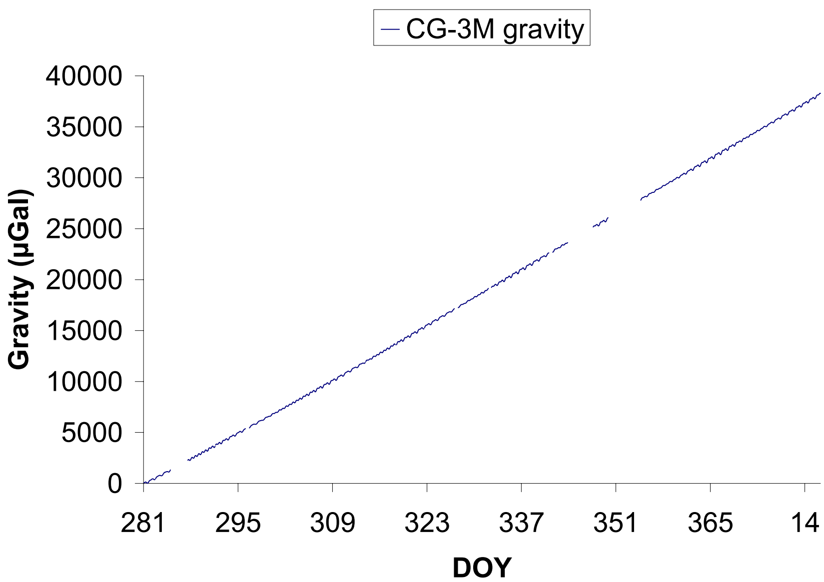

Fig. 4.12 Scintrex CG-3M gravity data for 3 months (8 October 2005 to 16 January 2006) in Melbourne. Gravity has been undersampled to hourly data. Automatic Scintrex CG-3M drift and Earth tide corrections are not applied. Strong linear drift is evident. Compare to SG gravity with negligible drift in Fig. 4.6.

Kestrel 4000 and Yokogawa F-452, as indicated by both the Kestrel 4000 and F-452 accuracy specifications. The RMSE of 0.1 mbar, is in agreement with the 0.1 mbar precision specification of the F-452 and indicates the precision of the Kestrel 4000 is also 0.1 mbar.

The raw data (Fig. 4.12) was corrected for linear drift of 344 μGal/ day (Fig. 4.13) and BAYTAP-G run on the data set to analyse the influence of meteorological variables on the CG-3M. The results for air pressure, air temperature and relative humidity are shown in Table 4.6. Both the Tamura (1987) and Cartwright and Tayler (1971); Cartwright and Edden (1973) (CTE) tidal potential catalogues were used, while the meteorological variables (air pressure, temperature and relative humidity) were analysed individually, in pairs and as a triplet. The pressure admittance calculated with BAYTAP-G is realistic and within the theoretical range (-0.3 to -0.4 μGal/mbar) as it ranges from -0.370 to -0.395 μGal/mbar depending on the

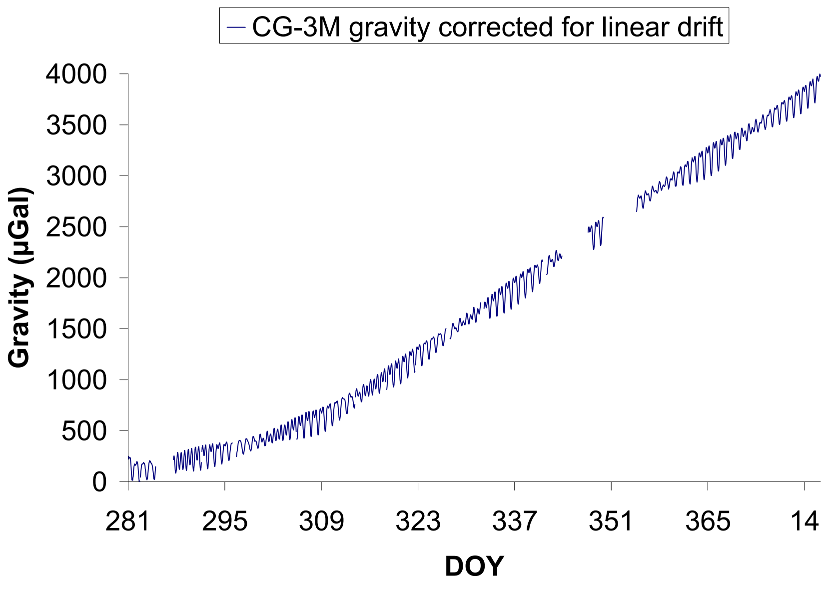

Fig. 4.13 As for Fig. 4.12 but automatically corrected for linear drift (344 μGal/day) by Scintrex CG-3M internal processing. The residual drift is non-linear but linear over periods of a week or two, with an initial lower drift rate for the first 2-3 weeks followed by a more rapid drift. The cause of the change in drift rate is unknown, but corresponds with findings of Gettings et al. (2008). Compare to SG gravity with negligible drift in Fig. 4.6.

Table 4.6 Meteorological variable and Scintrex CG-3M gravity response for 3 months in Melbourne. Response coefficients (shown with standard error in brackets) are calculated with hourly data using the Earth tide program BAYTAP-G and Cartwright and Tayler (1971); Cartwright and Edden (1973) (CTE) or Tamura (1987) tidal potential catalogues. A lower ABIC (Akaike Bayesian Information Criteria) indicates a better fit of the gravity residuals (after correcting for Earth tides and ocean tide loading) to the meteorological data sets, while a higher v indicates a trend that is closer to linear.

Tidal Potential Catalogue	Pressure Admittance (μGal/mbar)	Temperature Admittance (μGal/°C)	Humidity Admittance (μGal/%)	ABIC	v
CTE	-0.394 (0.045)			4714	45
CTE		1.620 (0.424)		4796	32
CTE			0.020 (0.020)	4799	32
Tamura	-0.392 (0.045)			4724	45
Tamura		1.617 (0.424)		4796	32
Tamura			0.020 (0.020)	4800	32
Tamura	-0.370 (0.050)	0.474 (0.411)		4739	45
Tamura	-0.395 (0.045)		0.028 (0.018)	4750	45
Tamura		1.607 (0.436)	0.002 (0.020)	4815	32
Tamura	-0.381 (0.050)	0.249 (0.425)	0.025 (0.019)	4767	45

additional meteorological variables and tidal potential catalogue used (Table 4.6). The best results came from using only pressure (shown in Fig. 4.14), judged primarily by the standard error of the admittance, but also by: range of gravity data explained by the meteorological response (13 μGal for pressure, 8 μGal for temperature, and only 0.8 μGal for humidity); minimisation of ABIC; and maximisation of the hyperparameter v. Furthermore better results (lower ABIC) were obtained with the CTE tidal potential catalogue than the Tamura due to the low resolution of the CG-3M (1 μGal) not affording additional benefit from the increased number of partial tides in the Tamura tidal potential catalogue (more than double the number contained in the CTE tidal potential catalogue and the ABIC favouring model parsimony). Consequently, an atmospheric pressure correction is calculated for the gravity data using air pressure data measured adjacent to the gravimeter and the admittance -0.394 μGal/mbar.

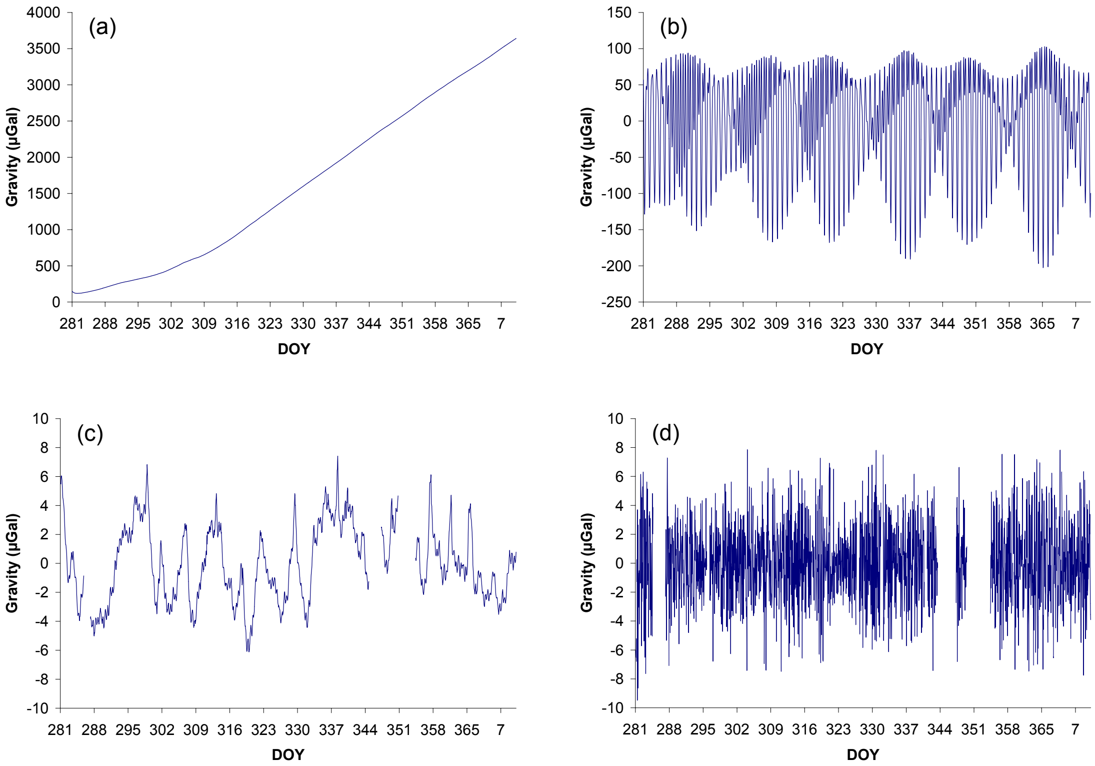

Fig. 4.14 As for Fig. 4.13 but decomposed into trend (a), Earth tide and ocean tide loading (b), atmospheric pressure (c), and irregular (d) components by the BAYTAP-G Earth tide program. Note the difference in scale between components.

Atmospheric pressure correction method

A linear pressure admittance of -0.394 μGal/mbar applied to atmospheric pressure measured with a portable barometer adjacent to the gravimeter.

It is believed the pressure response is the only real physical response (from theoretical considerations), and the temperature correction only appears reasonable (in the absence of pressure) because of the correlation of pressure with temperature (Table 4.7). Furthermore, the correlation of pressure with humidity is only -0.09 (Table 4.7) and this, coupled with the lack of any physical relationship between humidity and gravity, is why the humidity response is weak (in the sense that the admittance value is low and the standard error on the admittance is as large as the

Table 4.7 Scintrex CG-3M ancillary data and meteorological variable correlations for 3 months in Melbourne. Correlations are calculated with hourly data. Tilt X and Y (arc seconds) are measured by tilt meters internal to the gravimeter. Similarly TEMP (mK) is measured by a thermistor internal to the Scintrex CG-3M and represents the temperature of the vacuum the gravimeter sensor is located in. Air temperature (°C), atmospheric pressure (mbar) and relative humidity (%) are measured by the Kestrel 4000 portable weather tracker, adjacent to the gravimeter.

	Tilt X	Tilt Y	TEMP	Temperature	Pressure	Humidity
Tilt X	1	0.95	-0.62	-0.35	0.24	0.24
Tilt Y	0.95	1	-0.72	-0.45	0.30	0.20
TEMP	-0.62	-0.72	1	0.49	-0.17	-0.25
Temperature	-0.35	-0.45	0.49	1	-0.38	0.09
Pressure	0.24	0.30	-0.17	-0.38	1	-0.09
Humidity	0.24	0.20	-0.25	0.09	-0.09	1

admittance itself). Air pressure, temperature and humidity were also assessed for their influence on the CG-3M drift as temperature and humidity have been observed to affect the drift of other gravimeters (subsection 2.4.2). However no change of drift due to any measured variable was detected for the CG-3M. Consequently while air temperature and relative humidity were always recorded adjacent to the gravimeter (together with air pressure), no correction for air temperature or relative humidity is applied to the Scintrex CG-3M gravity data.

Air temperature and relative humidity ignored
No air temperature or humidity correction is applied (as no air temperature or humidity signal was detected in the gravity data).

4.4 Transferability of Gravity Corrections

This section tests the transferability of the corrections for geophysical and meteorological signals in gravity. The methods selected by testing on the Canberra SG gravity data for the year 2005 are applied to Scintrex CG-3M gravity data from Melbourne for the 3 month period 8 Oct 2005 to 16 Jan 2005 (Fig. 4.15).

The gravity residuals for the CG-3M data (Fig. 4.15 (b)-(d)) compare well to

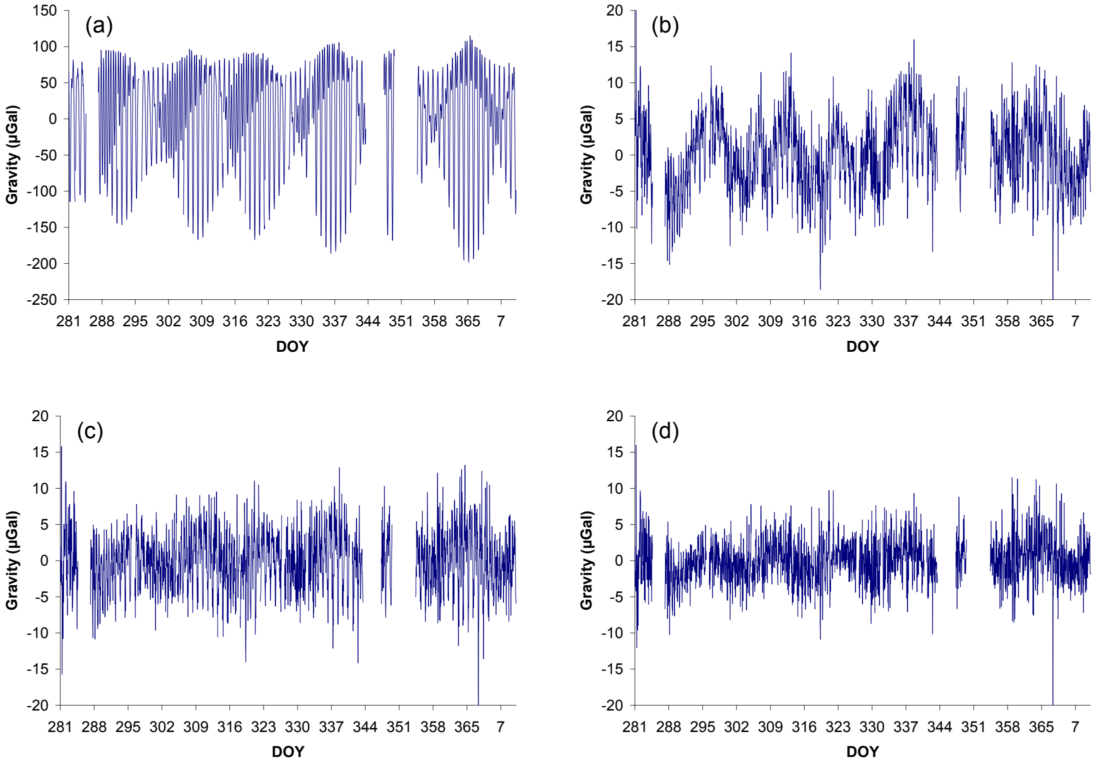

Fig. 4.15 As for Fig. 4.13 but corrected for drift (a), and Earth tides (b), and atmospheric pressure (c), and ocean tide loading and polar motion (d). Corrections are calculated using the methods in Table 4.8, except drift which uses the trend previously calculated by BAYTAP-G (Fig. 4.14 (a)).

the SG residuals (Fig. 4.7-4.9) using the same corrections (Table 4.8 and 4.9). After all corrections are applied (Fig. 4.15 (d)) a spike is visible on 2 January 2006, this is the magnitude 7.4 earthquake east of South Sandwich Islands (`http://www.ga.gov.au/earthquakes`). This earthquake affected data would typically be removed, but was left for illustration. In contrast the magnitude 7.2 earthquake off the east coast of Honshu, Japan on 14 November 2005 did not affect the gravity data in Melbourne. The ocean tide loading correction is more precise at Canberra than Melbourne (Fig. 4.9 and 4.15 (d)), as ocean tide models are uncertain close to the coast and in shallow water areas (Baker and Bos, 2003). The Melbourne site is only 5 km from Port Philip Bay and 60 km from the coast, despite this a precision of

Table 4.8 Corrections to remove geophysical and meteorological signals in gravity data.

Signal	Typical range of signal	Typical timescale of signal	Method of correction/monitoring
Earth tides	300 μGal	12 hours	Tsoft (Van Camp and Vauterin, 2005) Earth tide program using Tamura (1987) tidal potential catalogue and Dehant et al. (1999) Love numbers
Atmospheric pressure	12 μGal	36 hours	Linear admittance of -0.394 μGal/mbar applied to pressure data from barometer adjacent to gravimeter
Ocean tide loading	11 μGal	12 hours	GOTIC2 (Matsumoto et al., 2001) ocean tide loading software using CSR4.0 ocean tide model (Watkins and Eanes, 1997)
Polar motion	3 μGal	6 months	Tsoft (Van Camp and Vauterin, 2005) Earth tide program using EOP C04 series of Earth orientation parameters from the International Earth Rotation Service (IERS) website `http://www.iers.org`
Earthquakes	20 μGal	1 hour	Geoscience Australia (GA) and United States Geological Survey (USGS) websites `http://www.ga.gov.au/earthquakes` and `http://earthquake.usgs.gov`

Table 4.9 Gravity data precision achieved after applying geophysical and meteorological corrections. Standard deviation (S.D.) of gravity residual (μGal) is shown after corrections (Table 4.8) are applied to gravity data from Scintrex CG-3M in Melbourne, and SG in Canberra. Time series of the CG-3M and SG residuals are shown in Fig. 4.15 (b)-(d) and Fig. 4.7-4.9 respectively.

Correction	Scintrex CG-3M Residual S.D.	Canberra SG Residual S.D.
Earth tides	7.7	3.5
Atmospheric pressure	4.3	2.6
Ocean tide loading and polar motion	3.2	0.7

3.2 μGal was achieved using the Scintrex CG-3M (Table 4.9) that compares well to the gravity precision of 0.7 μGal achieved at Canberra (230 km from the east coast of Australia) using the SG.

The Scintrex CG-3M residuals for the Melbourne data after applying the gravity corrections to be used in the field compare well to the Canberra SG residuals after applying the same methods of correction (Table 4.9). The gravity data precision achievable with the Scintrex CG-3M at the soil moisture monitoring sites in the Kyeamba Creek Catchment (100 km west of Canberra) should be comparable to the precision achieved in Melbourne, as the ocean tide loading correction should be more precise further from the coast but field conditions could cause a degradation in data quality. Corrections necessary in the field to achieve high precision gravity data are investigated in the next section.

4.5 Removing Instrumental Artefacts

Gravity changes may also be due to mechanical changes within the gravimeter. These mechanical changes typically only manifest in field application of a gravimeter and consequently are difficult to rigorously analyse. This section investigates instrumental artefacts in Scintrex CG-3M gravity data, and recommends methods for correction when the gravimeter is used at the Kyeamba Creek Catchment soil moisture monitoring sites (Fig. 3.7). Operating procedures in the field to achieve high precision gravity data are described in section 3.2.1.

4.5.1 Drift

As shown by the trend in Fig. 4.13 and 4.14 (a) the long term CG-3M drift is nonlinear. Despite the apparent nonlinear drift of the CG-3M over the 3 month period in Melbourne a simple difference of hourly gravity values is effective in removing the long period drift (Fig. 4.16). This hourly difference roughly corresponds to the field data (from Kyeamba Creek Catchment) that is a difference of gravity observations at two sites, with the time between observations around 1 hour. Consequently, when using the Scintrex CG-3M gravimeter at the soil moisture monitoring sites, the drift can be removed simply by differencing gravity data at successive sites. The average of eight differences is also shown in Fig. 4.16 as the field data is an average of eight gravity ties between soil moisture monitoring sites. The average of the gravity differences is close to 0 μGal with a standard deviation of 0.8 μGal, showing that

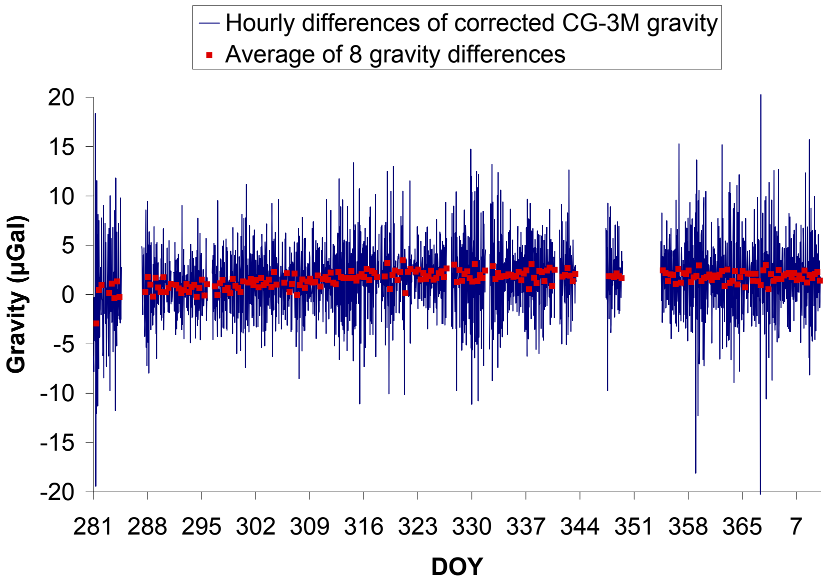

Fig. 4.16 As for Fig. 4.13 but with each hourly gravity value differenced with the preceding value (after correcting for Earth tides, atmospheric pressure, ocean tide loading and polar motion.). An average of 8 gravity differences is also shown.

differencing the gravity data and taking an average of eight ties is effective in removing the drift and achieving precise gravity data. A slight increase in the average of the gravity differences is due to the increase in drift rate after the first two weeks of the Scintrex CG-3M operating in Melbourne (Fig. 4.13).

Drift correction method

Difference gravity between sites. Repeat gravity ties (differences) between sites.

The Scintrex CG-3M manufacturers claim that drift of the thermistors used to measure the internal gravimeter temperature (TEMP) is indistinguishable from the drift of the gravimeter (Scintrex, 1995). This is assessed using the month of data from Mt Stromlo (19 January to 22 February 2005). During this period the air temperature in the subterranean room adjacent to the SG varied (slowly) from 20 to 24 °C, and the internal CG-3M temperature TEMP was well correlated with the air temperature (Table 4.10), with no drift apparent in the internal temperature of the CG-3M. Similarly, for the 3 months of data in Melbourne (8 October 2005

Table 4.10 As for Table 4.7 but for 1 month in Canberra.

	Tilt X	Tilt Y	TEMP	Temperature	Pressure	Humidity
Tilt X	1	-0.80	-0.88	-0.87	0.48	-0.63
Tilt Y	-0.80	1	0.52	0.92	-0.39	0.59
TEMP	-0.88	0.52	1	0.75	-0.29	0.78
Temperature	-0.87	0.92	0.75	1	-0.27	0.49
Pressure	0.48	-0.39	-0.29	-0.27	1	0.08
Humidity	-0.63	0.59	0.78	0.49	0.08	1

to 16 January 2006), the air temperature in the basement varied slowly from 18.5 to 23.5 °C (typical diurnal variation of 0.2 °C) and was positively correlated with the internal temperature of the CG-3M (Table 4.7 and Fig. 4.17). However, for this period a small drift in TEMP of -0.0028 mK/day (R^2 of 0.63) seems to be noticeable. This corresponds to 0.363 μGal/day using the TEMPCO temperature correction parameter of this CG-3M (-129.7 μGal/mK) and is indeed negligible compared to the residual drift of the CG-3M of 41 μGal/day for this period (Fig. 4.13). However, there is a strong negative correlation between TEMP and the tilt sensors (Table 4.7) that were also trending positive during this time (Fig. 4.17). Furthermore, all the smaller period (weekly) variations of the CG-3M internal temperature correlate well with the tilt sensors. It is believed that the CG-3M internal temperature changes are being forced by the external air temperature, and an increase in temperature (both internal CG-3M and air) causes an increase in the elasticity of the elastomer used to damp shocks to the gravity sensor in the CG-3M, thereby inducing a tilt that is detected by the sensors. Bonvalot et al. (1998) removed a linear trend from the internal temperature for three CG-3M gravimeters before analysing the relationship between the internal temperature and pressure, but unfortunately did not plot or state the magnitude or significance of the linear trend. Additionally, Bonvalot et al. (1998) found a correlation of pressure with internal temperature for one gravimeter but stated it was hardly noticeable for the other two Scintrex CG-3M gravimeters analysed. However, no significant correlation of internal temperature with pressure was found for the CG-3M and Kestrel 4000 data (from Melbourne or Canberra) used in this thesis (Table 4.7 and 4.10). Conversely, Bonvalot et al. (1998) found no correlation between internal gravimeter temperature and air temperature (although the air temperature data they used was from a station 15 km distant). While in

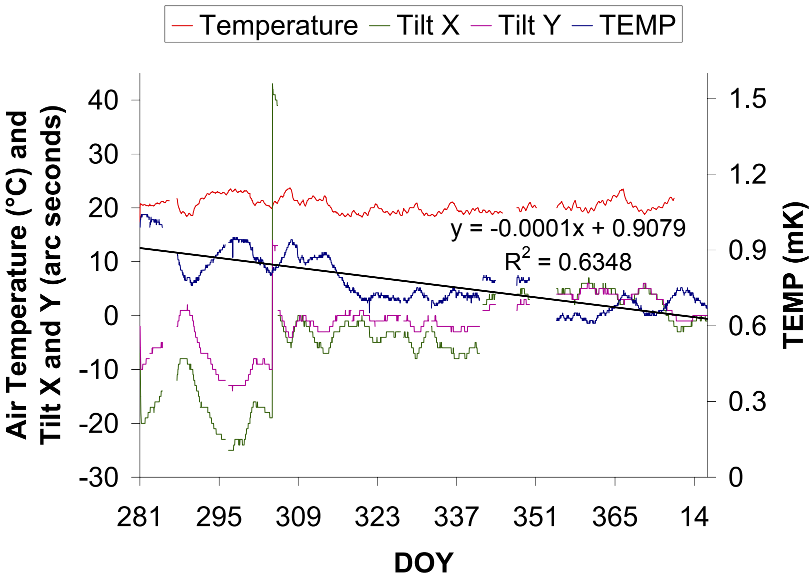

Fig. 4.17 Air temperature and CG-3M internal temperature (TEMP), together with gravimeter tilt (Tilt X and Y) for 3 months in Melbourne (see also Table 4.7 for correlations). Offset in tilt sensors on 31 October (DOY 304) and subsequent relevelling on 1 November is due to the gravimeter being disturbed in the (shared) laboratory. A small trend is noticeable in the gravimeter internal temperature (TEMP).

this thesis (using the Kestrel 4000 air temperature data for the subterranean rooms the CG-3M was located in), a correlation with the internal CG-3M temperature (TEMP) of 0.49 was found over 3 months in Melbourne and 0.75 over 1 month in Canberra (Table 4.7 and 4.10). However the air temperature was not shown to significantly affect the gravity data (Table 4.6).

4.5.2 Differential Heating

Finally, the impact of direct sunlight on the gravimeter (when taking a measurement in the field) was assessed by taking five consecutive 20 minute observations over a period of 100 minutes, with the gravimeter alternately shaded and exposed (Fig. 4.18). The sun clearly changed the X tilt through differential heating of the gravimeter (and also the Y tilt, but this is less clear due to drift in this tilt). While the actually reduced the magnitude of the X tilt, the combined effect on the X and Y axes was to increase the magnitude and variability of the gravimeter tilt. That

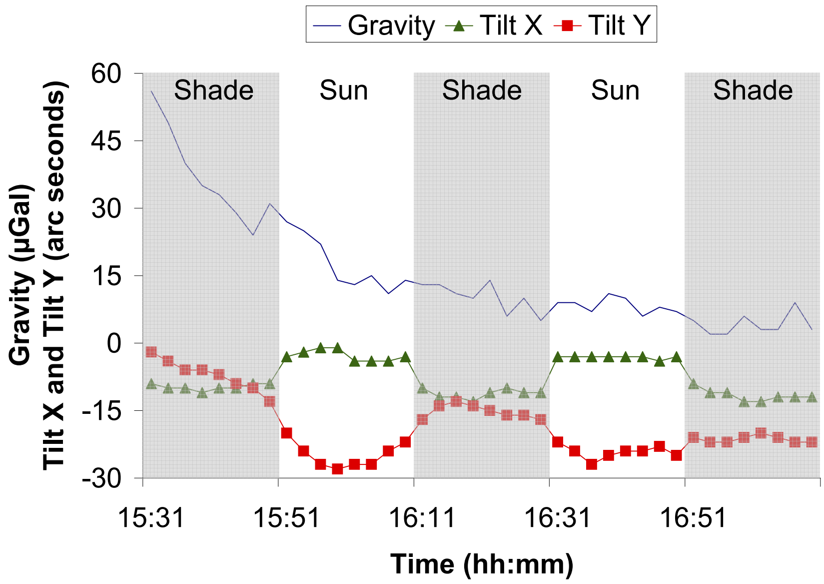

Fig. 4.18 The effect of direct sunlight on the Scintrex CG-3M. Measurements were taken every 2.5 minutes with the gravimeter shaded for the first 20 minutes, then exposed to direct sunlight for the next 20 minutes, and so on. Post transport stabilisation is evident in the first hour of gravity data.

the increased tilt does not manifest in the gravity data is testament to the accurate tilt correction being applied in real time. Nevertheless, the gravimeter was shaded at all times other than this when making an observation.

> **Differential heating correction method**
> Automatic Scintrex CG-3M tilt correction applied to gravity data.

4.5.3 Post Transport Stabilisation

It is hypothesised the (nonlinear) post transport stabilisation evident in Fig. 4.18 is due to the restabilisation of the elastomer used (between the vacuum chamber and the gravimeter housing) to protect the gravity sensor from shocks during transportation. The benefit of the elastomer is that it enables the CG-3M to be transported without clamping, as is necessary for a LaCoste and Romberg Model-G or Model-D gravimeter.

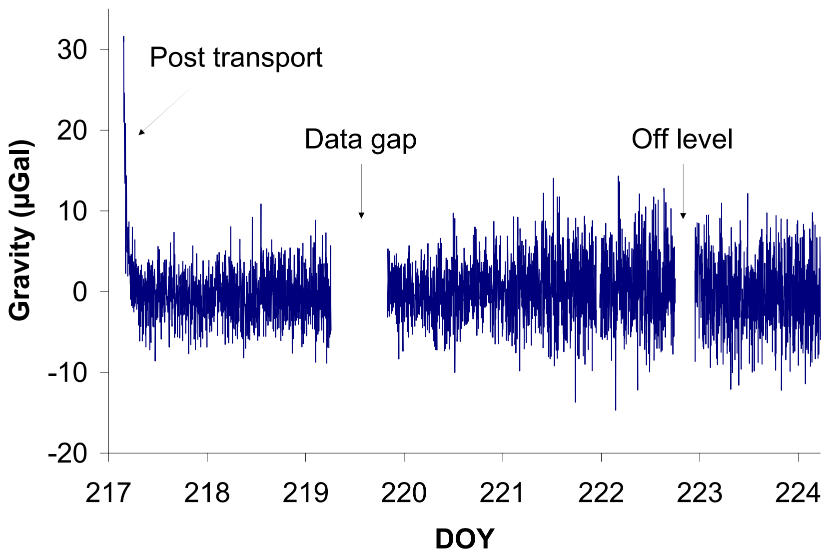

Fig. 4.19 CG-3M residual gravity after gravimeter is transported in a car for 3.6 hours and off level for 4.7 hours. Gravity data is corrected for Earth tides, atmospheric pressure, ocean tide loading and polar motion, with a quadratic drift also removed. The data gap was due to the Scintrex CG-3M internal memory being full and the data requiring downloading (and clearing). For the off level period the gravimeter was simply taken off the CG-3M (levelling) tripod and rested on the ground (with AC power attached).

A test was conducted to investigate if the post transport stabilisation effect was due to transport or simply the Scintrex CG-3M gravimeter not being levelled for an extended period of time (Fig. 4.19). While the post transport stabilisation effect is clearly linked to vehicular transport, it could be due to thermal gradients in the heated vacuum chamber housing the gravimeter sensor, as claimed by Hipkin (1978) for the LaCoste and Romberg Model-G meter. Thermal gradients in the gravimeter vacuum chamber may be caused by a change in heating between the black metal and foam transportation device (Fig. 3.14), that quite often got hot to touch, and the shaded gravity site.

Regardless of the cause of the post transport stabilisation effect, the behaviour at each of the Kyeamba Creek Catchment field sites is investigated to determine a correction. The twenty minute gravity observations at the field sites (Fig. 3.7) are an average of eight consecutive (2.5 minute) gravity measurements (subsection 3.2.1).

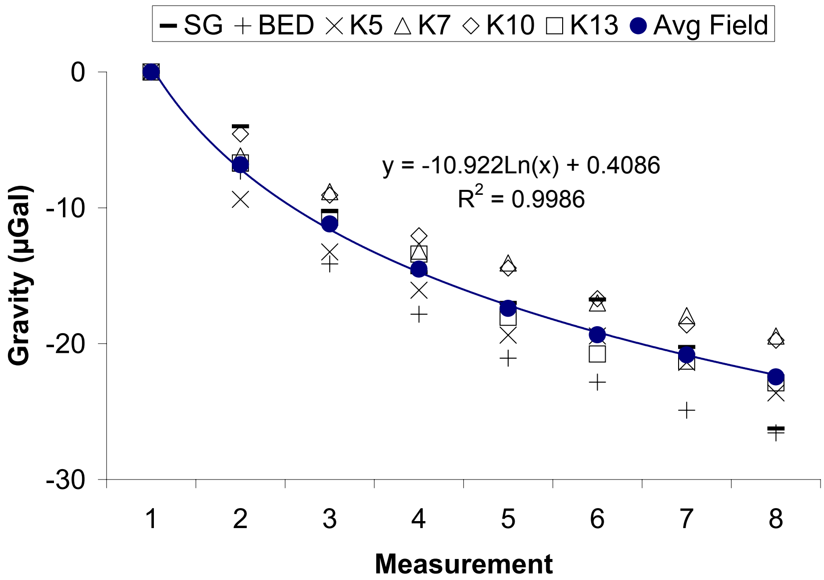

Fig. 4.20 Post transport stabilisation of Scintrex CG-3M gravity. The first gravity measurement at each site is set to 0 µGal, and the average of the subsequent measurements shown. Each gravity measurement is of 2.5 minute duration, with 8 measurements averaged (over 20 minutes) to give a gravity observation at a site. The average gravity measurements at each site are from the 16 September to 4 October field campaign, with 4 gravity observations at SG; 32 at BED; 16 at K5, K7 and K10; and 17 at K13.

Using all the gravity observations at each site during the 16 September to 4 October 2005 field campaign, the individual 2.5 minute gravity measurements at each site are averaged (Fig. 4.20), with the first measurement at each site set to 0 µGal. The average post transport stabilisation curves at each site follow the same behaviour, but the average gravity decrease over the 20 minute observation varies from 19 µGal at K7 to 27 µGal at the BED site. When the post transport stabilisation curves were averaged across all field sites (rather than each site individually) the curve was predicted extremely well (R^2 of 0.999) by a logarithmic function (Fig. 4.20).

The travel time (approximately 1 hour) and field conditions at each of the field sites in the Kyeamba Creek Catchment are similar. However, the same post transport stabilisation effect was evident at the SG site, after 3 hours of travel, when the Scintrex CG-3M was operated indoors on AC power. This indicates the post transport stabilisation effect is not related to travel time, differential heating (from sunshine), or battery voltage. While all sites display the same post transport stabilisation effect, the magnitude is slightly different at each site (Fig. 4.20). Consequently, the average post transport stabilisation effect is determined for each site and removed from the gravity data (for that site).

Post transport stabilisation correction method
Average post transport stabilisation curve for each site.

4.5.4 Battery Voltage Response

To determine the effects, of battery voltage on the Scintrex CG-3M, the gravimeter was operated in the room adjacent to the Canberra SG on 6 October 2005. Similar to the gravity data at the soil moisture monitoring sites, measurements were made every 2.5 minutes with eight measurements averaged to create a twenty minute gravity observation. Prior to the battery voltage experiment, the gravimeter had been stationary and running on AC power for 16 hours. AC power was then removed and the button on the CG-3M pressed repeatedly before and after each 20 minute gravity observation to determine the battery voltage (as this value is displayed but not logged by the gravimeter). The battery voltage measurement must be taken repeatedly as the reading can vary by as much as 0.5 V due to the gravimeter thermostat heater switching on and off (Scintrex, 1995).

A gravity residual was computed by differencing the gravity data from the SG and the Scintrex CG-3M. A time series and regression of the gravity residual and battery voltage is shown in Fig. 4.21 (a) and (b). A strong relationship was found between Scintrex CG-3M battery voltage and gravity data (R^2 of 0.842 for the linear regression). Additionally, there was an extremely strong linear relationship between battery voltage and gravimeter internal temperature (Fig. 4.21 (c) and (d)), with an R^2 of 0.982. This could be due to the heated vacuum containing the gravimeter sensor cooling as the gravimeter loses power. The strength of the relationship between battery voltage and internal temperature implies a strong correlation between internal temperature and gravity (Fig. 4.21 (e) and (f)) which is useful as internal temperature is logged by the gravimeter together with gravity data. Therefore the relationship in Fig. 4.21 (f) could be used to routinely correct the Scintrex CG-3M

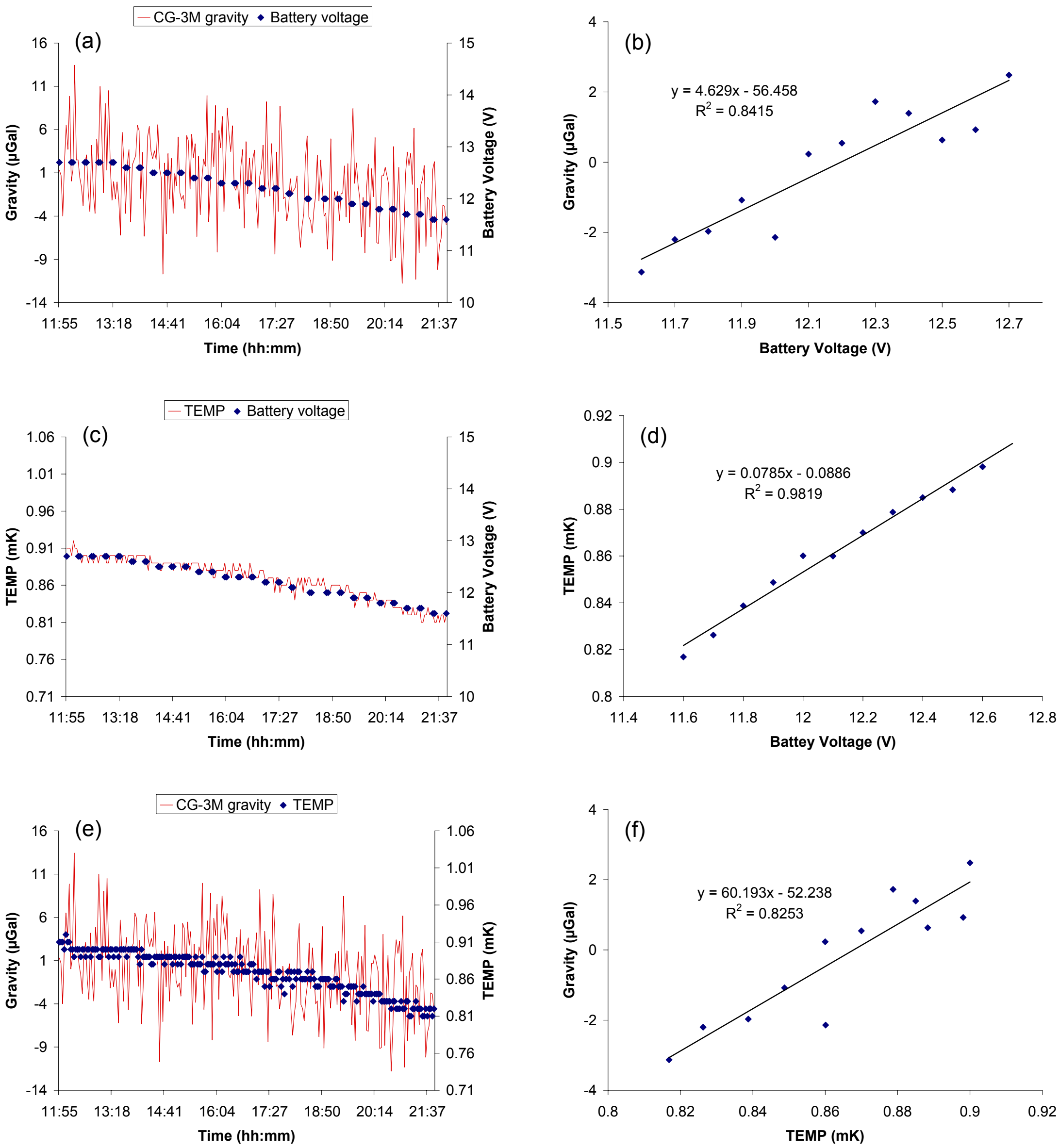

Fig. 4.21 Response of: Scintrex CG-3M gravity data to gravimeter battery voltage (a) and (b), Scintrex CG-3M internal temperature to gravimeter battery voltage (c) and (d), Scintrex CG-3M gravity data to gravimeter internal temperature (e) and (f). Gravity measurements are shown on left and averaged observations on right.

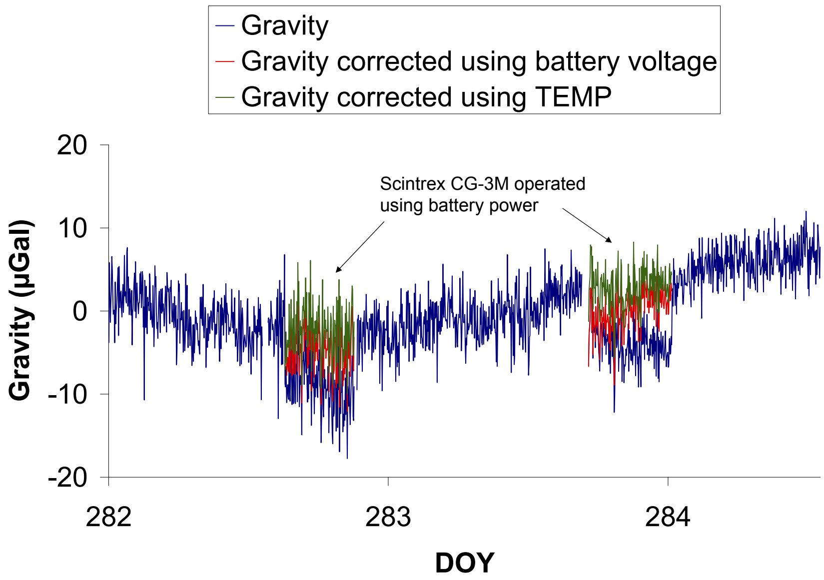

Fig. 4.22 Battery voltage and Scintrex CG-3M internal temperature (TEMP) based corrections applied to CG-3M gravity data for two periods when the gravimeter is operated on battery power. The gravity residual is calculated as a difference of the Scintrex CG-3M and Canberra SG gravity data.

gravity data for changes in battery voltage. However, the relationship of gravity and battery voltage is stronger (Fig. 4.21 (b)) and a more direct influence as the gravimeter measures changes in gravity by capacitance.

An evaluation of the battery voltage correction is shown in Fig. 4.22 where both the voltage (Fig. 4.21 (b)) and internal temperature (Fig. 4.21 (f)) approaches are used for two periods where the gravimeter was run on battery power. The battery voltage and internal temperature corrections are relative to a reference value. The voltage reference was set to 13.3 V and the sample immediately before AC power was switched off was used as the reference for TEMP (0.83 for the first period and 0.82 for the second). Both corrections work well with the TEMP based correction larger than the voltage based correction. However, it is difficult to rigorously compare the two methods as the battery voltage was only measured at the start and end of the two periods, with an additional voltage measurement made midway in the second. The battery voltage was linearly interpolated between 12.6 and 12 V for the first period and 13.3, 12.2 and 11.9 V for the second. The linear interpolation may introduce some error as battery voltage discharge is a nonlinear process. Therefore, the performance of the voltage based correction may be somewhat better in field conditions (where voltage is measured before and after every 20 minute gravity observation). Consequently, the voltage based correction (Fig. 4.21 (b)) was selected to be used with the field data at the soil moisture monitoring sites as this correction was more closely related to the gravity changes (R^2 of 0.842), and in field usage it is not clear what reference temperature should be used for the internal temperature based correction (Fig. 4.21 (f)), particularly with internal temperature correlated to air temperature (Table 4.7 and 4.10).

Battery voltage correction method
Linear correction based on Scintrex CG-3M battery voltage.

4.6 Gravity Data Precision Achievable in the Field

This section determines the gravity data precision achievable in the field using two small networks of three sites. One network is around Mt Stromlo in Canberra and consists of three geodetic benchmarks (two indoors), with one of the indoor benchmarks adjacent to the continuously operating Canberra SG. The second network is in the Kyeamba Creek Catchment, 300 km west of Canberra, and consists of two soil moisture monitoring sites, and an assumed hydrologically stable bedrock reference site. For both networks gravity observations at each site are an average over 20 minutes of eight consecutive measurements. After gravity is observed at a site the gravimeter is transported to the next site in the network. The successive gravity observations are differenced to form gravity ties. At both networks the three sites are connected by a total of 9 gravity ties (3 ties between any two sites), with the 10 gravity observations completed in a single day. Gravity network adjustment (Hwang et al., 2002) is used to estimate consistent gravity differences between all sites in the network (i.e. the gravity differences between any three sites forming a closed loop in the network sums to 0 μGal). The estimated site gravity differences at Mt Stromlo are compared to absolute gravity observations at two of the sites. Similar to the network at Mt Stromlo, the network of three sites at the Kyeamba

Creek Catchment is observed in 6.5 hours, but the bedrock reference site and soil moisture monitoring sites are observed a second time 8 days later, with the sites observed in the same order, and roughly the same time taken between observations. The repeatability of the gravity measurements, observations and site differences is assessed. Furthermore, the change in estimated site gravity differences (relative to the assumed hydrologically stable bedrock reference site) are compared to the (negligible) precipitation and terrestrial water storage change observed at the two soil moisture monitoring sites. For both networks the occurrence of earthquakes, benefit of geophysical and meteorological corrections, and presence of instrumental artefacts (drift and post transport stabilisation) in the gravity data is also assessed, together with the impact of gravity data outliers on the (network adjustment) results.

4.6.1 Mt Stromlo

The first case study involves three loops around three sites at Mt Stromlo (Fig. 4.23), with the gravimeter transported by hand to one site (AU034), and by vehicle to the other two sites (SEIS and SG). The two sites visited by vehicle are subterranean with stable temperatures and with accurate, current absolute gravity values. One of the sites also houses the continuously operating, highly precise Canberra superconducting gravimeter (SG). The AU034 site is an exposed geodetic benchmark (a rock) slightly uphill of the SG. This case study allows an assessment of the effect of vehicular transport in a network where the time between gravity observations (and distance between sites) is as small as practically possible. Furthermore the simultaneously running SG and existing absolute gravity benchmarks allow an objective evaluation of the portable gravimeter data. Finally, this case study gives an indication of the level of precision achievable for the gravity estimates using the selected methodology.

Gravity Observations

Gravity was measured with the Scintrex CG-3M relative gravity meter at the three sites around Mt Stromlo (Fig. 4.23) on 5 October 2005 (Fig. 4.24). The loop around the gravity network consisted of an observation at the SG site, then the AU034 and SEIS sites, finishing again at the SG site (Fig. 4.23). The SG gravity observation

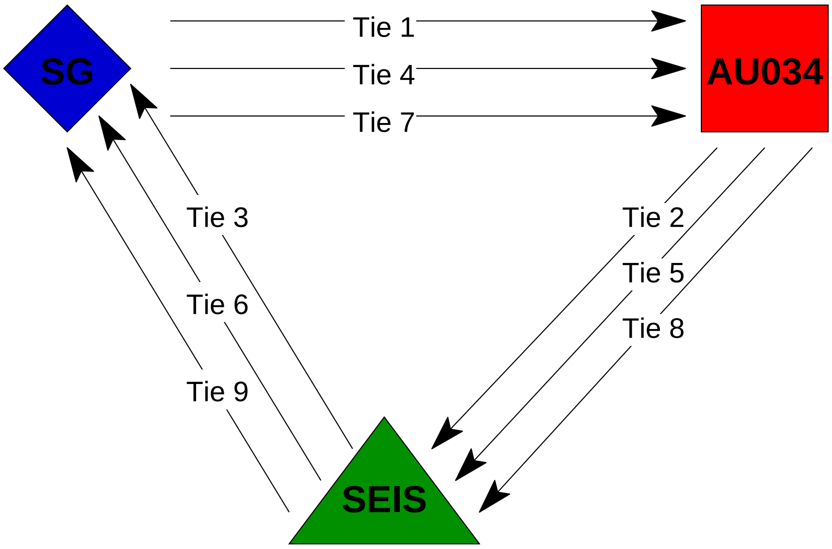

Fig. 4.23 Gravity network around Mt Stromlo, established on 5 October 2005 with a Scintrex CG-3M relative gravimeter. SG is a room adjacent to the superconducting gravimeter, AU034 is a geodetic benchmark approximately 30 m from the SG building, and SEIS is a seismic vault.

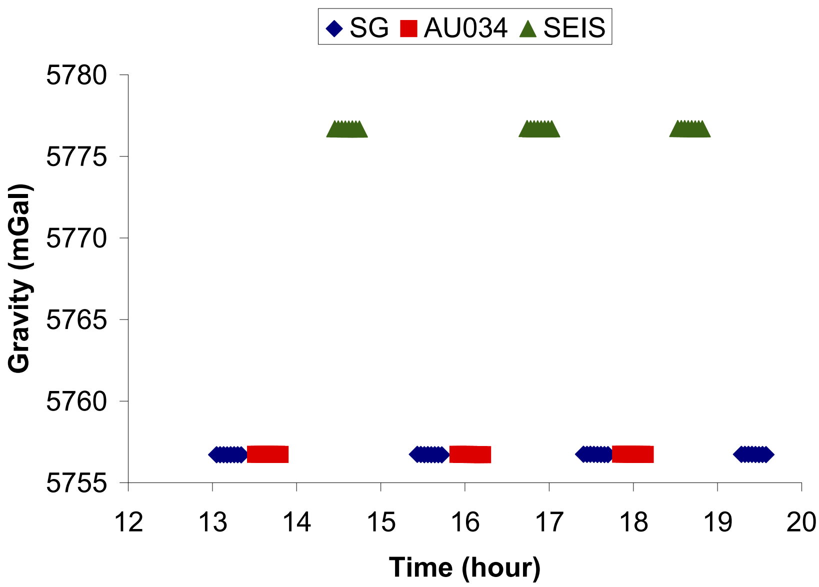

Fig. 4.24 As for Fig. 4.23 but showing a time series of gravity measurements.

was taken over an absolute gravity benchmark in a room next to the Canberra superconducting gravimeter (SG). For the AU034 gravity observation the Scintrex CG-3M gravimeter was carried by hand up a small hill (the crest of Mt Stromlo) to make the observation approximately 30 m from the SG on a rock (Geoscience Australia geodetic benchmark AU034). Next the gravimeter was packed in the transportation case in the back of a vehicle (Fig. 3.14) and driven over a rough track to a seismic vault. Similar to the SG site, at the SEIS site an observation was taken over an absolute gravity benchmark. The gravimeter was repacked and driven back to the SG where a final observation was made, thereby closing the loop (Fig. 4.23). The loop (SG-AU034-SEIS) was repeated three times (Fig. 4.23), with 6.5 hours needed to complete the ten relative gravity observations (Fig. 4.24).

Gravity Corrections

The Geoscience Australia earthquake monitoring service (`http://www.ga.gov.au/earthquakes`) did not report any significant earthquakes for 5 October 2005. An inspection of the Canberra SG one minute uncorrected gravity data (from `http://ggp.gfz-potsdam.de`) also shows the period to be free of earthquakes (Fig. 4.25), as indicated by the smoothness of both the gravity data and its numerical derivative.

The geophysical and meteorological corrections used for the Scintrex CG-3M gravity data (Table 4.8) are assessed by evaluating the magnitude of the SG gravity residual for 5 October 2005 after the corrections are applied (Fig. 4.26). After correcting for Earth tides, ocean tide loading, polar motion, and atmospheric pressure, the SG gravity residual for 5 October 2005 is smooth with a quadratic shape and range of 1.5 μGal, and a standard deviation of 0.38 μGal that is an improvement to the standard deviation of 0.65 μGal for the year 2005 (Table 4.9).

To assess the instrumental artefacts in the Scintrex CG-3M gravity data the relative gravity observations at the SG, AU034 and SEIS sites are offset by 5756.707, 5754.950, and 5776.671 mGal respectively (Fig. 4.27). During the gravity survey day there is a positive drift of around 4 μGal/h and a negative post transport stabilisation of about 50 μGal/h (Fig. 4.27), although the post transport stabilisation only occurs after the gravimeter is first transported by vehicle (after the first two gravity observations). This is because the CG-3M was in the SG location running

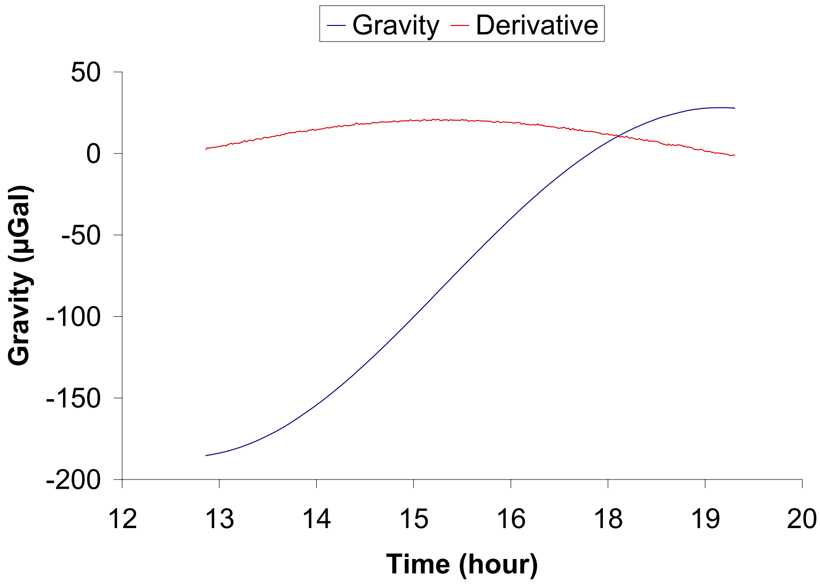

Fig. 4.25 Canberra SG gravity time series (and numerical derivative) during 5 October 2005. The SG relative gravity is 1 minute uncorrected data from `http://ggp.gfz-potsdam.de`.

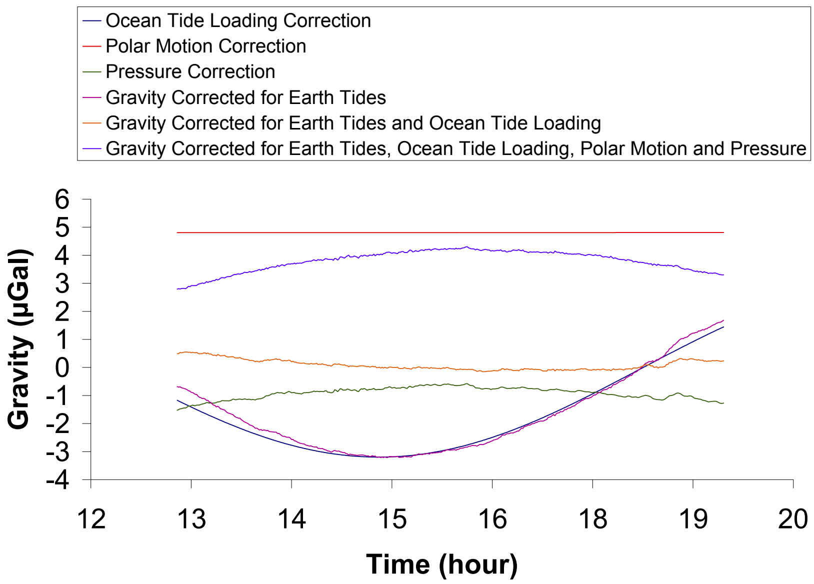

Fig. 4.26 Gravity as for Fig. 4.25 but corrected for Earth tides, ocean tide loading, polar motion and atmospheric pressure using methods in Table 4.8.

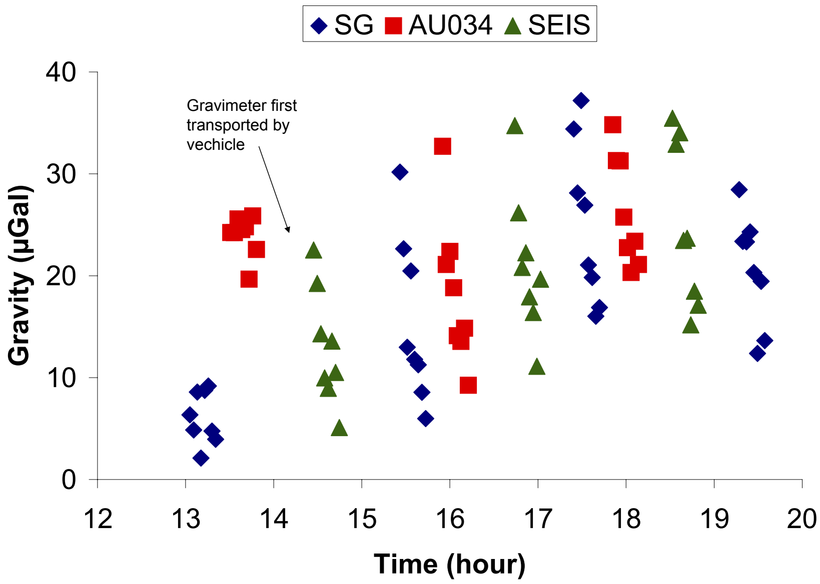

Fig. 4.27 As for Fig. 4.24 but the relative gravity observations at the SG, AU034 and SEIS sites are offset by 5756.707, 5754.950, and 5776.671 mGal respectively. Gravity corrections from Fig. 4.26 are also applied.

on AC power for 14 hours before the first observation. The gravimeter was then transported by hand to AU034.

The post transport stabilisation is plotted relative to the first measurement of each observation (Fig. 4.28), and is similar regardless of transportation method (by hand to AU034, and vehicle to SG and SEIS), with the exception of the first SG observation and the first observation at AU034. There is no post transport stabilisation for the first observation at SG and AU034 (Fig. 4.28), with the average gravity reduction over 20 minutes only 0.3 μGal. As post transport stabilisation is evident in the later gravity observations at both SG and AU034 (after vehicular transportation to and from SEIS) it is likely that the post transport effect lasts well after the gravimeter has been unpacked and relevelled at SG, through to the AU034 observations approximately half an hour after the travel from SEIS to SG (Fig. 4.27). After vehicular transportation is used the post transport stabilisation of all observations is very similar (Fig. 4.28), with the average post transport stabilisation over all sites and observations corresponding extremely well to the predicted post transport stabilisation using the natural logarithm fitted to the average September 2005 data

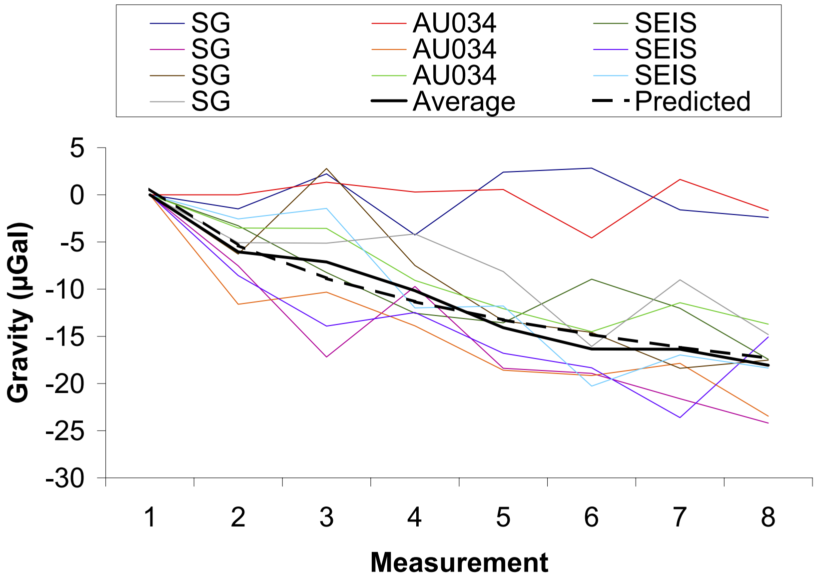

Fig. 4.28 As for Fig. 4.27 but the relative gravity measurements at the SG, AU034 and SEIS sites are each offset so that the first measurement is 0 µGal. Blue and red lines centred on 0 µGal are the first observations at SG and AU034 (Fig. 4.27) before vehicular transportation was used. Solid line is an average of observations excluding the first SG and AU034; dashed line is predicted using a logarithm fitted to the average of observations at different sites a month previous (see Fig. 4.20).

(Fig. 4.20). After applying the post stabilisation correction using the logarithmic function in Fig. 4.20 the scatter of the (2.5 minute) gravity measurements is reduced significantly (Fig. 4.29).

The scatter of the 8 measurements during the first SG and AU034 observations (Fig. 4.27) can be used as an estimate of the precision of the CG-3M in the field if vehicular transportation was not necessary. The standard error of the twenty minute gravity observation indoors at SG is 0.91 µGal while at AU034 in exposed conditions is 0.70 µGal. In contrast, after vehicular transportation (and without post transport stabilisation correction) the standard error at SG is 1.93-2.90 µGal, and at AU034 is 1.92-2.56 µGal, while at SEIS (also indoors) it varies from 2.01-2.86 µGal. After applying the predicted post transport stabilisation curve (Fig. 4.20 and 4.28) the standard error of the gravity observations at each of the sites following vehicular transportation ranges from 0.74 µGal (at AU034) to 1.58 µGal (at SG).

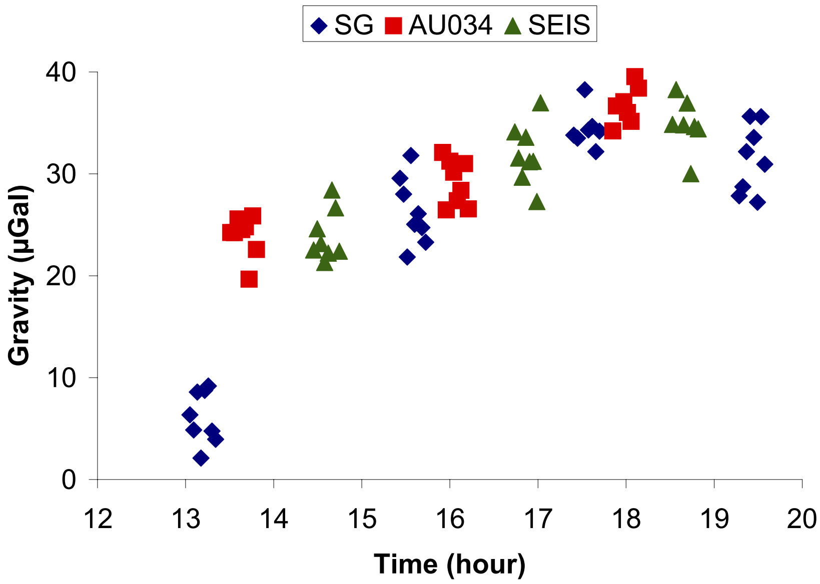

Fig. 4.29 As for Fig. 4.27 but corrected for post transport stabilisation using the logarithmic function in Fig. 4.20.

Site Gravity Differences

An estimate of the site gravity differences (and standard error) is produced by performing a network adjustment using the gravity ties (Fig. 4.23) and code of Hwang et al. (2002), with a number of different scenarios considered to assess the robustness of the network adjustment to outliers, and whether there is an optimal way of removing drift (Table 4.11). Case I uses raw gravity data as recorded by the Scintrex CG-3M (using the automatic Earth tide and linear drift corrections). Case II uses gravity data with corrections from Table 4.8 applied. The precision of the gravity estimates at each of the sites for both cases I and II is 1.9 µGal (Table 4.11), but the corrected gravity data (case II) results in more precise site gravity differences (Table 4.12), with an error of 2.6 µGal for each site difference. After network adjustment the site differences around the network sum to 0 µGal (Table 4.12) and the (gravity) network loop is closed. Moreover, the gravity estimates for each site also sum to 0 µGal (Table 4.11), due to the free network constraint. The gravity data precision at each of the sites after network adjustment is uniform (Table 4.11), because the network consists of a single loop with the same number of ties between

Table 4.11 Estimated gravity at sites around Mt Stromlo after network adjustment (μGal), standard error is shown in brackets. Cases I-IV use all the data (gravity ties), while Cases V-IX remove different portions of the data set.

Case	Gravity Data Processing	SG	AU034	SEIS
I	Uncorrected	-6071.0 (1.9)	-7822.7 (1.9)	13893.7 (1.9)
II	Corrected	-6071.2 (1.9)	-7823.6 (1.9)	13894.8 (1.9)
III	Corrected and Drift Removed	-6071.3 (1.7)	-7823.1 (1.7)	13894.4 (1.7)
IV	Corrected and Drift Estimated	-6071.7 (1.7)	-7823.1 (1.7)	13894.8 (1.7)
V	Corrected and Drift Removed with first Observation Removed	-6069.5 (1.0)	-7824.9 (1.0)	13894.4 (0.9)
VI	Corrected and Drift Estimated with first Observation Removed	-6069.6 (1.0)	-7825.2 (1.0)	13894.8 (0.8)
VII	Corrected and Drift Removed with first Loop Removed	-6070.0 (1.3)	-7824.9 (1.3)	13894.8 (1.3)
VIII	Corrected and Drift Removed with second Loop Removed	-6072.5 (2.2)	-7822.1 (2.2)	13894.6 (2.2)
IX	Corrected and Drift Removed with third Loop Removed	-6071.4 (2.6)	-7822.4 (2.6)	13893.7 (2.6)

Table 4.12 As for Table 4.11 but for site gravity differences.

Case	SG–AU034	AU034–SEIS	SEIS–SG
I	-1751.7 (2.7)	21716.4 (2.7)	-19964.8 (2.7)
II	-1752.4 (2.6)	21718.4 (2.6)	-19966.0 (2.6)
III	-1751.8 (2.4)	21717.5 (2.4)	-19965.7 (2.4)
IV	-1751.4 (2.5)	21717.9 (2.4)	-19966.5 (2.4)
V	-1755.3 (1.4)	21719.3 (1.4)	-19963.9 (1.4)
VI	-1755.7 (1.4)	21720.1 (1.3)	-19964.4 (1.3)
VII	-1754.9 (1.8)	21719.7 (1.8)	-19964.8 (1.8)
VIII	-1749.6 (3.1)	21716.7 (3.1)	-19967.1 (3.1)
IX	-1751.0 (3.7)	21716.1 (3.7)	-19965.1 (3.7)

each site. While the gravity corrections make a modest improvement to the gravity precision for a site gravity difference (Table 4.12) this may be due to both the short duration of the field campaign (only 6.5 hours) and the simplicity of the 3 site network in this case study. The corrections are expected to be more significant for longer field campaigns and larger networks. Consequently, the remaining cases all use corrected gravity data, and it is recommended that all field gravity data has the corrections of Table 4.8 applied.

While the Scintrex CG-3M automatically applies a linear drift correction (of 344 μGal/day during 5 October 2005) a residual linear drift is evident in Fig. 4.29, that was fit as 3.4 μGal/h to the three gravity observations at SEIS (with an R^2 of 0.99). Case III is as case II but with the gravity data also corrected for this residual linear drift. While case IV again uses the same data as case II but estimates the residual linear drift with the network adjustment (together with the site gravity). As for cases I and II, the results for case III and IV are also almost identical (Table 4.11 and 4.12) Additionally, the network adjustment estimates the residual linear drift as 2.7±1.7 μGal/h, which is in agreement with the drift of 3.4 μGal/h fit to the observations at SEIS. Therefore, the residual linear drift can either be removed prior to network adjustment or during network adjustment, with similar results obtained. While removing the residual drift increased the precision at each of the sites (Table 4.11) from 1.9 μGal (cases I and II) to 1.7 μGal (cases III and IV), it is unlikely that the drift for a field campaign longer than 6.5 hours could be adequately approximated by a single linear estimate. Consequently it is recommended the drift is simply removed by the automatic linear drift correction and differencing gravity data (over approximately 1 hour) between sites.

The first gravity observation (at SG) appears to be an outlier (Fig. 4.29), therefore a number of cases are investigated to assess the impact of removing suspected outliers, or entire portions of the gravity dataset prior to network adjustment. Cases V and VI are the same as III and IV (respectively) but with the first (SG) gravity observation removed from the data set. While cases VII, VIII, and IX are as case III but with the first, second, and third (respectively) loop of SG, AU034 and SEIS gravity observations removed from the data set. Removing the first gravity observation reduces the standard error for each of the site gravity estimates (Table 4.11) from 1.7 μGal (cases III and IV) to 0.8-1.0 μGal (cases V and VI), or from 2.4-2.5 μGal (cases III and IV) to 1.3-1.4 μGal (cases V and VI) for a site gravity difference (Table 4.12). While removing the first gravity loop (case VII) rather than just the first gravity observation (case V) degrades the precision of both the site gravity estimates (from 0.9-1.0 μGal (case V) to 1.3 μGal (case VII)) and site differences (from 1.4 to 1.8 μGal), but still improves the precision (from 1.7 μGal for a site estimate, or 2.4 μGal for a site difference) compared to the case when the suspected outlier is not removed (case III). In contrast, removing either the second or third gravity loop (cases VIII and IX), where outliers where not suspected, degrades the precision for a site estimate to 2.2 or 2.6 μGal (Table 4.11) and for a site difference to 3.1 or 3.7 μGal (Table 4.12). Therefore removing gravity data can either increase, or significantly decrease the precision of the gravity estimates at a site and the gravity difference between sites, depending on the portion of the data set removed. Consequently, due to the difficulty of identifying outliers in relative gravity data, it is recommended that gravity data is not removed prior to network adjustment.

Using the preferred method (of case II) a precision of 1.9 μGal was achieved for the site gravity estimates (Table 4.11), and 2.6 μGal for the site gravity differences Table 4.12. The SG–SEIS site gravity difference of 19966 μGal is close to the 19999 μGal site difference computed from two absolute gravity determinations at SG (979549592 μGal) and SEIS (979569591 μGal) on 4 June and 26 March 2004 (respectively). The absolute gravity measurements were translated to a 1 m datum using a vertical gravity gradient computed with a relative LaCoste and Romberg gravimeter, whereas the CG-3M measures gravity approximately 30 cm above the ground surface. The 30 μGal discrepancy between the SG–SEIS gravity difference measured by the Micro-g FG5 absolute gravimeters and the Scintrex CG-3M relative gravimeter is attributed to a large solid brick and concrete prism (approximately 50 cm high and wide, and 2 m deep) directly behind the SEIS benchmark that would increase the gravity observed at 1 m and decrease the gravity at 30 cm.

4.6.2 Kyeamba Creek Catchment

For the second case study a network of three sites in the Kyeamba Creek Catchment is observed. All three sites are outdoors, with the gravimeter transported by vehicle to the two soil moisture monitoring sites (K4 and K5), and the assumed hydrologically stable bedrock reference site BED (Fig. 4.30). Prior to the first observation at BED the gravimeter is transported for 3 hours by vehicle from the SG site at Mt Stromlo (the CG-3M is also returned to Mt Stromlo after the last observation at BED). The network is observed twice over 8 days, with the change in terrestrial water storage (TWS) at the soil moisture monitoring sites negligible over the 8 days. This case study is used as a null case to assess the power of monitoring TWS with

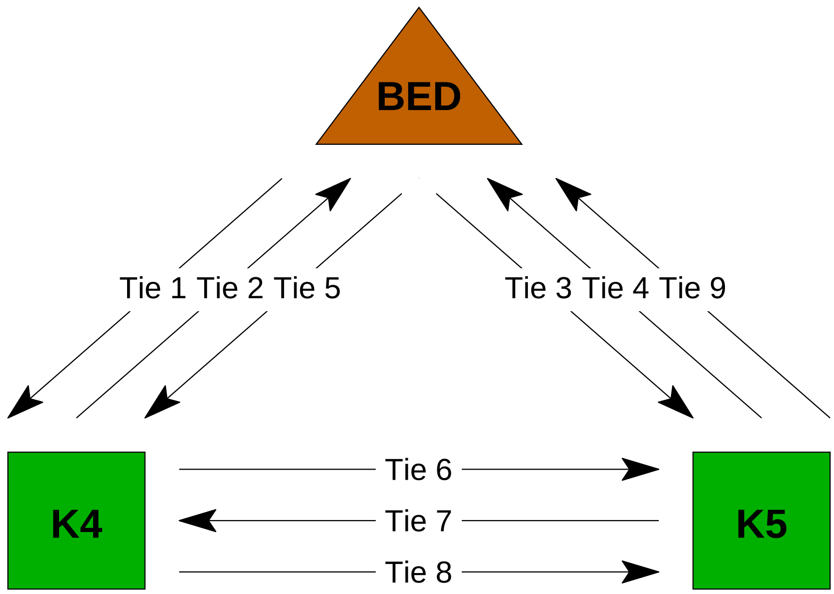

Fig. 4.30 Small gravity network around Kyeamba Creek Catchment, established on 25 February 2004 with a Scintrex CG-3M relative gravimeter, and resampled on 4 March 2004. BED is an assumed hydrologically stable bedrock reference site, and K4 and K5 are nearby soil moisture monitoring sites.

gravity data, and assess whether the methods will report a false positive change in gravity when there is no corresponding change in TWS. This case study again uses the simplest gravity network possible of only three sites, but the three sites are in a far less controlled environment than Mt Stromlo, with all three sites outdoors and travel by vehicle required between all sites. Again this case study seeks to determine the gravity data precision achievable in the field, in particular at the soil moisture monitoring sites.

Repeatability of Gravity Observations

The field campaign on 25 February 2004 was repeated eight days later on 4 March. For the two campaigns gravity observations were made at the same sites, in the same order, with approximately the same timing between sites (Fig. 4.31). Similar to the previous case study at Mt Stromlo (subsection 4.6.1), the 10 gravity observations at the three sites take around 6.5 hours to complete, but for the Kyeamba Creek Catchment network the sites are connected by ties in both directions (Fig. 4.30).

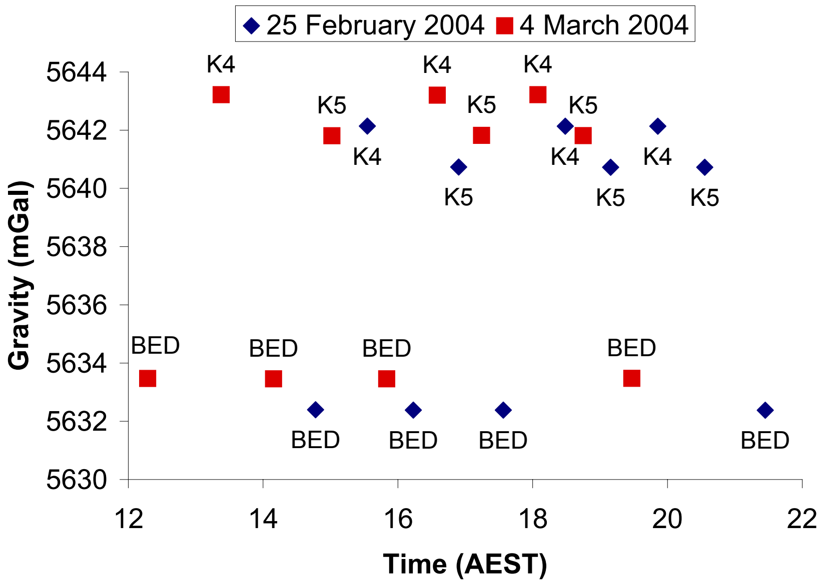

Fig. 4.31 Gravity observations at three sites during 25 February and 4 March 2004 with a Scintrex CG-3M gravimeter.

No significant earthquakes were recorded for 25 February or 4 March 2004 (`http://www.ga.gov.au/earthquakes`). The post transport stabilisation behaviour of the CG-3M during each of the gravity observations was analysed to assess the repeatability of the gravity measurements. A plot of each of the sets of 8 gravity measurements (that are averaged for an observation) for both surveys is shown in Fig. 4.32 where the relative gravity measurements are offset so the first measurement is 0 μGal. The post transport stabilisation of the gravimeter is consistent between both sites and field campaigns with only two sites (one from February and March) showing some deviations during the second half of the observation.

To assess the repeatability of the gravity observations the individual March observations are differenced with their February counterpart both before and after applying the corrections from Table 4.8. The observation to observation differences are shown in Fig. 4.33. The differences are mostly around 1080 μGal which implies roughly a 135 μGal/day drift during the intervening 8 days. The drift constant for 25 February was 435 μGal, and was reset the following day (to 392 μGal). After accounting for the resetting of the (automatic linear) drift correction, a 592 μGal difference is evident between the gravity observations separated by 8 days. This

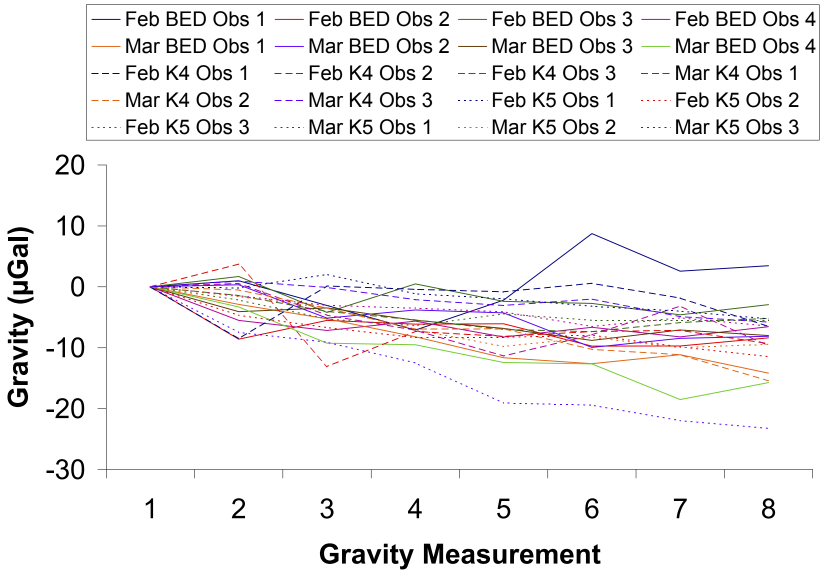

Fig. 4.32 Post transport stabilisation during 25 February and 4 March 2004 gravity observations.

corresponds to an additional 74 μGal/day residual drift, that is comparable to the residual linear drift of around 3 μGal/h found around the Mt Stromlo network (subsection 4.6.1).

The difference between the raw and corrected observation differences is generally small (Fig. 4.33), with the largest correction of 7 μGal for the first BED observation where site coordinates for the internal CG-3M Earth tide correction were accidentally left as the SG site coordinates (0.11 ° latitude and 1.4 ° longitude difference). However, the next gravity observation (at site K4) also has a correction of 5 μGal with the correct coordinates set, this is due to the pressure correction. While the corrections are generally small (Fig. 4.33) they reduce both the range and variability of the gravity observation differences (from 33 to 29 μGal, and 11.5 to 9.5 μGal respectively). The first six gravity observation differences are fairly consistent (standard deviation of 3.3 μGal for the corrected differences) but the seventh (i.e. the second K5 observation) appears to be an outlier. A gravity observation outlier also causes an outlier in the tie calculated with that observation. This is shown in Fig. 4.34 for gravity tie difference 6 (the first K4–K5 tie).

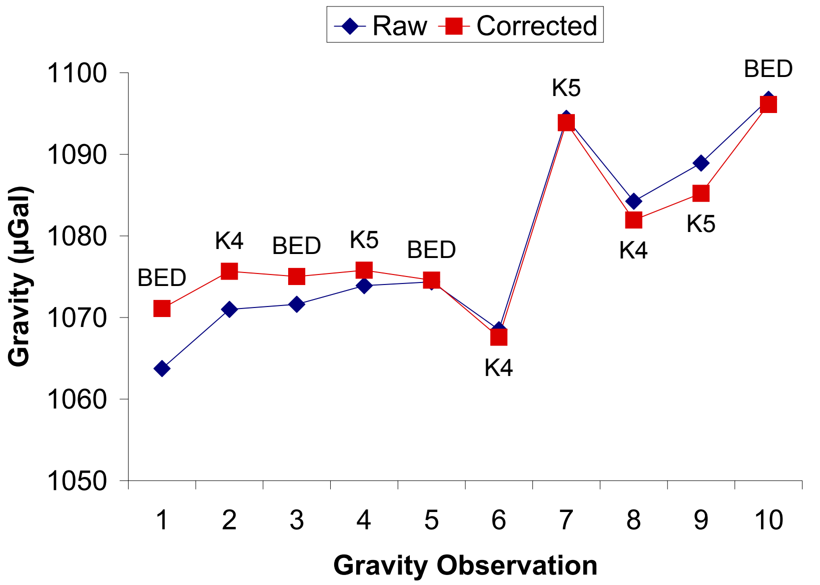

Fig. 4.33 Gravity change at each site (for a gravity observation) over 8 days.

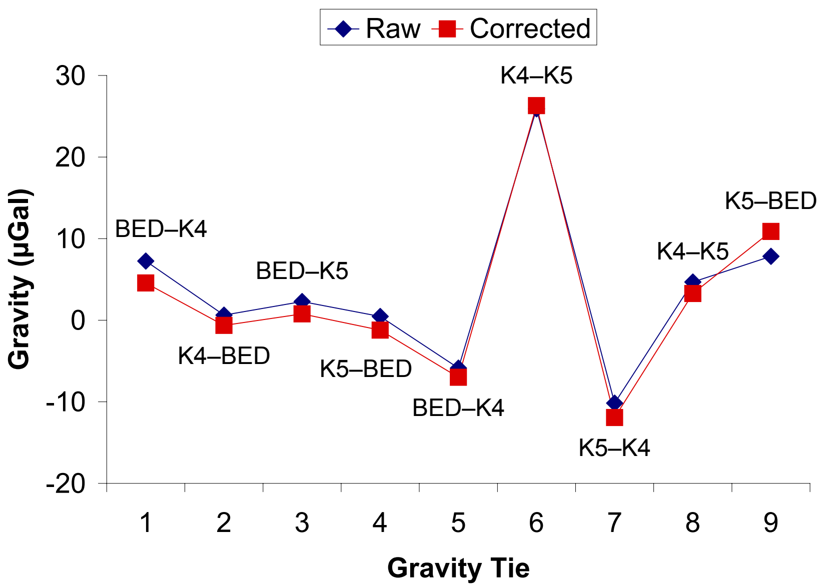

Fig. 4.34 Gravity change between sites (for a gravity tie) over 8 days.

Gravity Changes

The average and standard error of the three ties, for each site difference (Fig. 4.30) are shown in Table 4.13 for each field campaign, together with the gravity change over the intervening 8 days. The loop misclosure for both campaigns is 8 μGal (calculated by subtracting the average BED–K5 and K4–K5 site differences from the average BED–K4 difference). However, the error on the gravity differences between sites is consistently higher for the second campaign (4 March), and significantly more so for the BED–K5 and K4–K5 differences. Assuming the gravity at the bedrock reference site (BED) is constant, the average site differences indicate a small decrease in gravity at both K4 and K5 of 0.6 μGal and 3.0 μGal respectively, in the 8 days from 25 February to 4 March 2004 (Table 4.13). However the standard errors of 6.0 and 4.3 μGal associated with these gravity changes indicate they are not statistically significant.

To use the additional information from the K4–K5 site difference (Table 4.13) network adjustment is performed for each of the campaigns using the code of Hwang et al. (2002) and the nine gravity ties (Fig. 4.30) together with the (free) constraint that the site differences across the network sum to 0 μGal (i.e. the network loop closes). The network adjustment is also performed with the previously identified outlier removed, and using just the five gravity ties before the outlier (Fig. 4.34). The network adjustment calculates the gravity and standard error for the three sites with all three cases shown in Table 4.14 and 4.15. The gravity data precision achievable at the field sites is 1.4 μGal for 25 February 2004 (Table 4.14), this is better than the 1.9 μGal precision achieved at the Mt Stromlo sites (two of which are indoors) on 5 October 2005. However, the precision at the Kyeamba Creek Catchment field sites for 4 March 2004 is lower at 2.3 μGal (Table 4.15), despite no earthquakes

Table 4.13 Average gravity difference between sites (μGal), standard error is shown in brackets.

Site Difference	25 February 2004	4 March 2004	Gravity Change
BED–K4	9750.4 (4.2)	9749.8 (4.3)	-0.6 (6.0)
BED–K5	8348.1 (0.4)	8345.1 (4.3)	-3.0 (4.3)
K4–K5	1410.3 (0.8)	1396.5 (6.0)	-13.8 (6.1)

Table 4.14 Site gravity and standard error after network adjustment for 25 February 2004. The initial adjustment uses all 9 gravity differences, the next adjustment removes the K4-K5 tie that is an outlier (Fig. 4.34), and the final adjustment uses only the 5 ties before the outlier.

Site	All data (9 ties)	No K4-K5 Outlier (8 ties)	Ties before outlier (5 ties)
BED	-6032.8 (1.4)	-6032.8 (1.4)	-6033.0 (1.8)
K4	3720.2 (1.4)	3719.7 (1.5)	3717.5 (2.7)
K5	2312.6 (1.4)	2313.1 (1.5)	2315.5 (3.0)

Table 4.15 As for Table 4.14 but for 4 March 2004.

Site	All data (9 ties)	No K4-K5 Outlier (8 ties)	Ties before outlier (5 ties)
BED	-6031.6 (2.3)	-6031.6 (1.8)	-6033.1 (1.8)
K4	3715.4 (2.3)	3717.5 (1.9)	3716.7 (2.7)
K5	2316.2 (2.3)	2314.2 (1.9)	2316.4 (3.1)

being reported. As was found for the case study at Mt Stromlo (subsection 4.6.1) the site gravity estimate precision is generally reduced when gravity data is removed (Table 4.14 and 4.15), even if the data is suspect. However, when the outlier K4-K5 gravity tie is removed from the data for the February field campaign, the precision is degraded by 0.1 μGal for the K4 and K5 gravity estimates (Table 4.14), whereas when the outlier is removed from the data for March the precision of the gravity estimates at all 3 sites are improved by 0.4-0.5 μGal. This strongly suggests the outlier K4-K5 tie was on 4 March 2004. It is interesting that the precision at each site is almost the same for both February and March when only the 5 ties before the outlier are used (Table 4.14 and 4.15).

Site differences are calculated from the gravity estimates for each site (Table 4.16 and 4.17). The network adjustment has resulted in more precise site differences for the March field campaign with the BED-K4 and BED-K5 site difference error reduced from 4.3 to 3.3 μGal (Table 4.13 and 4.17). However, the March errors are still larger than the corresponding site difference errors for February (Table 4.16 and 4.17). For the February field campaign the network adjustment has increased the precision of the BED-K4 site difference from 4.2 to 1.9 μGal (Table 4.13 and4.16), but degraded the precision of the BED-K5 site difference from 0.4 to 1.9 μGal. After network adjustment the precision is equivalent for all site differences in the

Table 4.16 As for Table 4.14 but for site differences.

Site Difference	All data	No K4-K5 Outlier	Ties before outlier
BED–K4	9753.1 (1.9)	9752.5 (2.1)	9750.4 (3.2)
BED–K5	8345.4 (1.9)	8346.0 (2.1)	8348.4 (3.5)
K4–K5	1407.7 (1.9)	1406.6 (2.2)	1402.0 (4.1)

Table 4.17 As for Table 4.16 but for 4 March 2004.

Site Difference	All data	No K4-K5 Outlier	Ties before outlier
BED–K4	9747.1 (3.3)	9749.1 (2.6)	9749.8 (3.3)
BED–K5	8347.9 (3.3)	8345.8 (2.6)	8349.4 (3.6)
K4–K5	1399.2 (3.3)	1403.3 (2.7)	1400.4 (4.1)

network (Table 4.16 and4.17). While increasing the precision of most of the gravity differences between sites, the network adjustment has also adjusted the estimates of the site differences (in comparison with the average site differences in Table 4.13) to make the network consistent.

The gravity differences between sites for the 25 February and 4 March 2004 field campaigns (after network adjustment) are used to determine the gravity change (over 8 days) for each site relative to the bedrock reference site (Table 4.18). The statistical significance of the gravity change at each soil moisture monitoring site relative to the assumed hydrologically stable bedrock reference site is assessed with a t-test, where a significance level of 0.05 was chosen and the degrees of freedom (*df*) are the sum of the *df* for February (7) and March (7). The degrees of freedom for each campaign are calculated as the number of gravity ties (9) minus the number of gravity sites (3) plus one for the free network constraint that the site differences across the network sum to 0 μGal (i.e. the network loop closes). The large decrease in gravity at K4 (relative to the bedrock site) of 6.0 μGal is not statistically significant (Table 4.18). Similarly, there is a statistically insignificant increase of 2.4 μGal at K5 after network adjustment. Removing the K4-K5 outlier results in a reduction in significance of the gravity changes at K4 and K5, coupled with much smaller changes (Table 4.19). While using only the first five ties of each field campaign results in a further reduction in the significance of the gravity changes at K4 and K5 (Table 4.20), together with much smaller (less than 1 μGal) changes.

Removing the outlier gravity tie, or the outlier and all subsequent ties, progres-

Table 4.18 Gravity changes between 25 February and 4 March 2004 field campaigns after network adjustment (μGal), standard error is shown in brackets. Test statistic and critical t value for a significance level of 0.05 and 14 degrees of freedom (9 ties each for February and March, that is the first case of Table 4.14 and 4.15) are shown.

Site	Gravity Change	Test Statistic	Critical t Value
K4	-6.0 (3.8)	1.8	2.1
K5	2.4 (3.8)	1.4	2.1

Table 4.19 As for Table 4.18 but with the K4-K5 outlier removed, and 12 degrees of freedom (8 ties each for February and March, that is the second case of Table 4.14 and 4.15).

Site	Gravity Change	Test Statistic	Critical t Value
K4	-3.5 (3.3)	0.9	2.2
K5	-0.1 (3.3)	0.4	2.2

Table 4.20 As for Table 4.18 but only using ties before the K4-K5 outlier, and 6 degrees of freedom (5 ties each for February and March, that is the third case of Table 4.14 and 4.15).

Site	Gravity Change	Test Statistic	Critical t Value
K4	-0.6 (4.6)	0.2	2.4
K5	1.0 (5.0)	0.2	2.4

sively decreases the magnitude of the observed gravity changes, while also reducing the value of the test statistic and increasing the critical t value, thereby making the gravity changes both smaller and less statistically significant (Table 4.18- 4.20). It is expected that in a real field application with campaigns taking multiple days or weeks, and involving many more ties and loops (and sites) that the effects of an outlier tie on the gravity network adjustment should be negligible. However, the case study does highlight the usefulness of observing the same gravity sites in the same sequence for each field campaign, so direct differencing of gravity observations at each site (or ties between sites) can be used to detect outliers prior to network adjustment.

A gravity data precision of 1.4 μGal was achieved at the soil moisture monitoring and bedrock field sites in the Kyeamba Creek Catchment (for a field campaign that consisted of 9 gravity ties and took 6.5 hours to complete). Consequently a precision of 1.9 μGal was achieved for the site gravity differences, in particular between the soil moisture monitoring sites and assumed hydrologically stable bedrock reference site. Similarly, a precision of 2.3 μGal was achieved at all sites for the second field campaign 8 days later, and a precision of 3.3 μGal for the site differences. This resulted in a precision of 3.8 μGal on the gravity change for each of the soil moisture monitoring sites (relative to the bedrock site). Consequently, both a positive gravity increase of 2.4 μGal at one soil moisture site (K5) and a negative gravity change of 6.0 μGal at the other (K4) were found to be statistically insignificant (at the 0.05 level). Examining the hydrological data from the soil moisture monitoring sites it was expected that the gravity at these sites would not change over the 8 days as there had been little to no precipitation (0.8 mm at K4 and 0 mm at K5) and minimal changes in soil moisture (2.6 % vol/vol decrease over the top 90 cm of soil at K4 and 1.8 % vol/vol decrease over the top 90 cm at K5). The changes in soil moisture over 8 days at the monitoring sites are presumably due to evapotranspiration in late summer and correspond to an estimated TWS change of -23.4 mm at K4 and -16.5 mm at K5, or using the Bouguer slab approximation, a gravity change of -1.0 μGal at K4 and -0.7 μGal at K5, that is in agreement with the statistically insignificant changes of -6.0±3.8 μGal at K4 and 2.4±3.8 μGal at K5 determined from gravity observations (Table 4.18). Therefore, the observed gravity change from the Scintrex CG-3M relative gravimeter and gravity monitoring method corresponds well with the expected gravity change from independently observed TWS changes using soil moisture observations. The method of monitoring TWS with ground-based gravity data appears repeatable, robust and reliable and will be applied in the next chapter to additional soil moisture monitoring sites, covering a longer time period when significant terrestrial water storage changes are expected.

4.6.3 Section Summary

This section investigated the gravity data precision achievable in the field via two case studies. The first case study involved three sites around the Canberra SG at Mt Stromlo observed in 6.5 hours with absolute gravity benchmarks at two of the sites. The second case study also involved three sites observed in 6.5 hours, but the gravimeter was first transported for 3 hours by vehicle from the SG site at Canberra. These two soil moisture monitoring sites and one assumed hydrologically stable bedrock reference site were also observed a second time eight days later with negligible rainfall or observed TWS change in the intervening 8 days.

Checking the gravity corrections of Earth tides, ocean tide loading, polar motion and pressure against the SG data during the first case study, it was found that the range of the residual is small at approximately 1.5 μGal, showing that the corrections worked very well under these conditions.

Case study I showed that the post transport stabilisation is around -50 μGal/h, being much greater than the residual daily drift that is around 4 μGal/h. However it was found that the post transport behaviour is similar for all gravity observations, and a logarithmic curve derived from different sites predicted the effect well. Moreover, it was found that the vehicular transport duration was irrelevant. It was also found that the gravity corrections make only a small difference to the final network adjustment results (1 to 2 μGal changes to the gravity ties). The ability to remove drift using the network adjustment when determining the site gravity was assessed against the alternative approach of removing the residual drift before the network adjustment. It was found that the approach only slightly effects the results. Removing gravity data from the network adjustment was found to affect the results more than gravity corrections, but quite often degraded the precision of the gravity estimate, depending on the portion of data removed. Due to the difficulty of detecting outliers in relative gravity data, it is recommended that gravity data is not removed prior to network adjustment. The estimated gravity difference from the network adjustment compared well with the difference between two sites computed from absolute gravity observations at those sites (on different dates) with the network adjusted differences about 30 μGal less than the absolute gravity differences of around 20000 μGal. It is hypothesised that the discrepancy is due to a combination of local effects and the difference in observing heights between the absolute and relative gravimeters. Overall the precision achievable for the first case study is 1.9 μGal for a site gravity estimate, and 2.6 μGal for the difference in gravity between two sites. For the difference of 20000 μGal between the two absolute gravity benchmark sites this is a relative precision of 0.01 % indicating the high precision of current portable relative gravimeters.

Case study II showed that the post transport stabilisation behaviour was consistent over twenty observations at three sites on two different days, with observations made between three hours and half an hour of transportation. By differencing the respective gravity observations for each day, the residual drift was calculated to be around 3 μGal/h, similar to the residual drift of 4 μGal/h found in case study I when examining successive observations at the same site on one day. The gravity data corrections were again found to make only a small change, but reduced both the range (by 4 μGal) and variability (by 2 μGal) of the gravity observation differences. Even though the same sites were observed (in the same order), the error on the gravity observations was found to be higher for the second campaign with a minimum error of 4.3 μGal on the gravity ties (compared to a minimum error of 0.4 μGal eight days previous). For the first field campaign a gravity precision of 1.4 μGal was achieved at the soil moisture monitoring sites, and consequent precision of 1.9 μGal for the gravity difference between the soil moisture monitoring sites and the assumed hydrologically stable bedrock reference site in the Kyeamba Creek Catchment. For the second noisier field campaign a precision of 2.3 μGal was achieved for the gravity estimate at each site, and 3.3 μGal for the difference between sites. Consequently a precision of 3.8 μGal was achieved for the gravity change at each soil moisture monitoring site (relative to the bedrock site). The gravity change over 8 days at two sites was not statistically significant, and corresponded with the expected change based on hydrological observations.

4.7 Chapter Summary

This chapter developed methods to achieve high precision gravity data with a portable gravimeter to enable monitoring of terrestrial water storage, in particular soil moisture. The most precise portable gravimeter (available at the time of the study) a Scintrex CG-3M relative gravimeter was calibrated using the highly precise superconducting gravimeter (SG) at Mt Stromlo, Canberra. The SG was calibrated with a FG5 absolute gravimeter. Both SG and Scintrex CG-3M calibration factors were shown to be temporally stable.

Methods to correct the geophysical signals in gravity data were tested using the Canberra SG. The following methods are selected to remove significant geophysical signals (Earth tides, ocean tide loading, and polar motion):

- Tsoft Earth tide program (Van Camp and Vauterin, 2005) using the Tamura (1987) tidal potential catalogue and Dehant et al. (1999) Love numbers;
- GOTIC2 ocean tide loading software (Matsumoto et al., 2001) using the CSR4.0 ocean tide model (Watkins and Eanes, 1997);
- Tsoft using the EOP C04 series of Earth orientation parameters from the International Earth Rotation Service website `http://www.iers.org`.

Additionally earthquakes are monitored using the Geoscience Australia earthquake monitoring service `http://www.ga.gov.au/earthquakes`.

Based on laboratory analysis in Melbourne and Canberra with the Scintrex CG-3M and adjacent meteorological observations (air temperature, air pressure and relative humidity) the following correction is selected to remove all significant meteorological signals from gravity data:

- a linear pressure admittance of -0.394 μGal/mbar applied to atmospheric pressure measured with a portable barometer adjacent to the gravimeter.

Additionally the gravimeter is shaded when gravity measurements are made.

From laboratory and field analysis of the Scintrex CG-3M the following corrections are proposed to remove the significant instrumental artefacts (drift, post transport stabilisation and battery voltage response) in (field) gravity data:

- difference gravity observations at successive sites (i.e. form gravity ties), and use the ties in the gravity network adjustment of Hwang et al. (2002);
- average post transport stabilisation at a site and remove from all observations at that site;
- apply a gravimeter battery voltage admittance of 4.6 μGal/V to data at the time of each gravity observation.

Additionally the gravimeter is transported by vehicle in a custom built suspension based device.

The gravity corrections and field procedures were assessed with two field based case studies. The case studies involved two networks of three sites. One network was adjacent to the SG in Canberra, and the other used two soil moisture monitoring sites and the assumed hydrologically stable bedrock reference site in the Kyeamba Creek Catchment, 100 km west of Canberra. The gravity data precision achieved in the field was:

- 1.4-2.3 μGal for a gravity estimate at a site;
- 1.9-3.3 μGal for the estimate of the gravity difference between sites; and
- 3.8 μGal for the gravity change over time at a site.

This chapter presented material to achieve precise gravity estimates at soil moisture monitoring sites. The precise gravity estimates were used to determine the statistical significance of a gravity change at a site between two field campaigns 8 days apart when the terrestrial water storage (TWS) change was known to be negligible. A precision of 3.8 μGal (90 mm TWS) was achieved on the gravity change, and a statistically significant change was not detected. Therefore the methods can be used with confidence that a statistically significant change in gravity will not be detected without a corresponding change in TWS. The methods developed in this chapter will be applied in the following chapter to gravity observations from two field campaigns six months apart to assess if there is a detectable terrestrial water storage signal in ground-based gravity data.

Chapter 5

Detecting a Terrestrial Water Storage Signal in Gravity Data

The previous chapter presented methods to achieve high precision ground-based gravity data at a network of soil moisture monitoring sites. This chapter applies the methods from Chapter 4 to detect a terrestrial water storage (TWS) signal at four soil moisture monitoring sites in the Kyeamba Creek Catchment, over 6 months corresponding approximately to the minimum and maximum observed TWS.[1]

5.1 Experimental Design

A number of soil moisture and groundwater monitoring sites were installed in the Kyeamba Creek Catchment (part of the Murray Darling Basin) in the year 2003 to complement an existing network (Smith et al., 2012). Additionally, one location (on a granite outcrop) was selected as a stable bedrock reference site at which minimal hydrological changes were anticipated (Fig. 5.1). The Kyeamba Creek Catchment is small to medium (approximately 600 km^2) with topography dominated by gentle slopes. Land use is predominantly sheep and beef grazing with some dairy. The climate is temperate with average annual precipitation of around 600 mm. The catchment is approximately 20 km south east of the town Wagga Wagga, and about

[1] The soil particle size analysis in this chapter contributed to the validation of the general soil moisture sensor calibration approach in the published peer-reviewed journal paper Rüdiger et al. (2010).

120 km west of Australia's capital city Canberra.

At each of the second generation soil moisture monitoring sites commissioned in 2003, three Campbell Scientific CS616 water content reflectometers were vertically installed to cover the depths 0-30, 30-60 and 60-90 cm. The first generation sites are similar, except the older CS615 water content reflectometer was used (Fig. 5.2). Time domain reflectometry (TDR) probes were inserted nearby to verify (or field calibrate) the water content reflectometers (in addition to gravimetric sampling). At the first generation sites, 20 cm buriable type TDR probes were inserted horizontally at 45 and 75 cm depth, with a 30 cm (removable) connector type TDR probe (rods connected to a balun) used for the surface 0-30 cm soil moisture (Fig. 5.2 (a)). At the second generation sites 30, 60 and 90 cm long (connector type) TDR rods were permanently inserted (Fig. 5.2 (b)). The TDR probes were read using a portable Trase TDR unit, primarily to verify the CS615 and CS616 water content reflectometer soil moisture calibrations (see Appendix D). A shallow piezometer and capacitance probe were installed at all sites to monitor groundwater level. The piezometer (a PVC tube with a closed top, open bottom and slots near the bottom) doubled as an access tube for neutron moisture meter (NMM) measurements that were made periodically to the bottom of the shallow piezometer or the water table. Each site also had a tipping bucket raingauge installed, together with soil temperature probes (used for temperature correction as part of the water content reflectometer calibrations, see Appendix C).

Ground-based gravity may be measured by a variety of gravity meters manufactured by a small number of companies. These gravity meters (or gravimeters) can be distinctly classified as taking either a relative or absolute measurement of gravity. Absolute gravimeters operate by measuring the time taken for an object to free fall over a fixed distance. Absolute measurements of gravity are desirable, but the gravity meters have low precision and are not field portable. A portable gravimeter is the preferred choice to maximise the possibility of observing subsurface hydrological variations. Specifically, the gravimeter does not require a permanent enclosure that may prevent recharge of the soil moisture (and groundwater) from rainfall. Additionally, power requirements (and cost) for a permanently installed gravimeter are prohibitive and the permanent installation limits the number of field sites that can be investigated for hydrological changes. Relative gravimeters operate

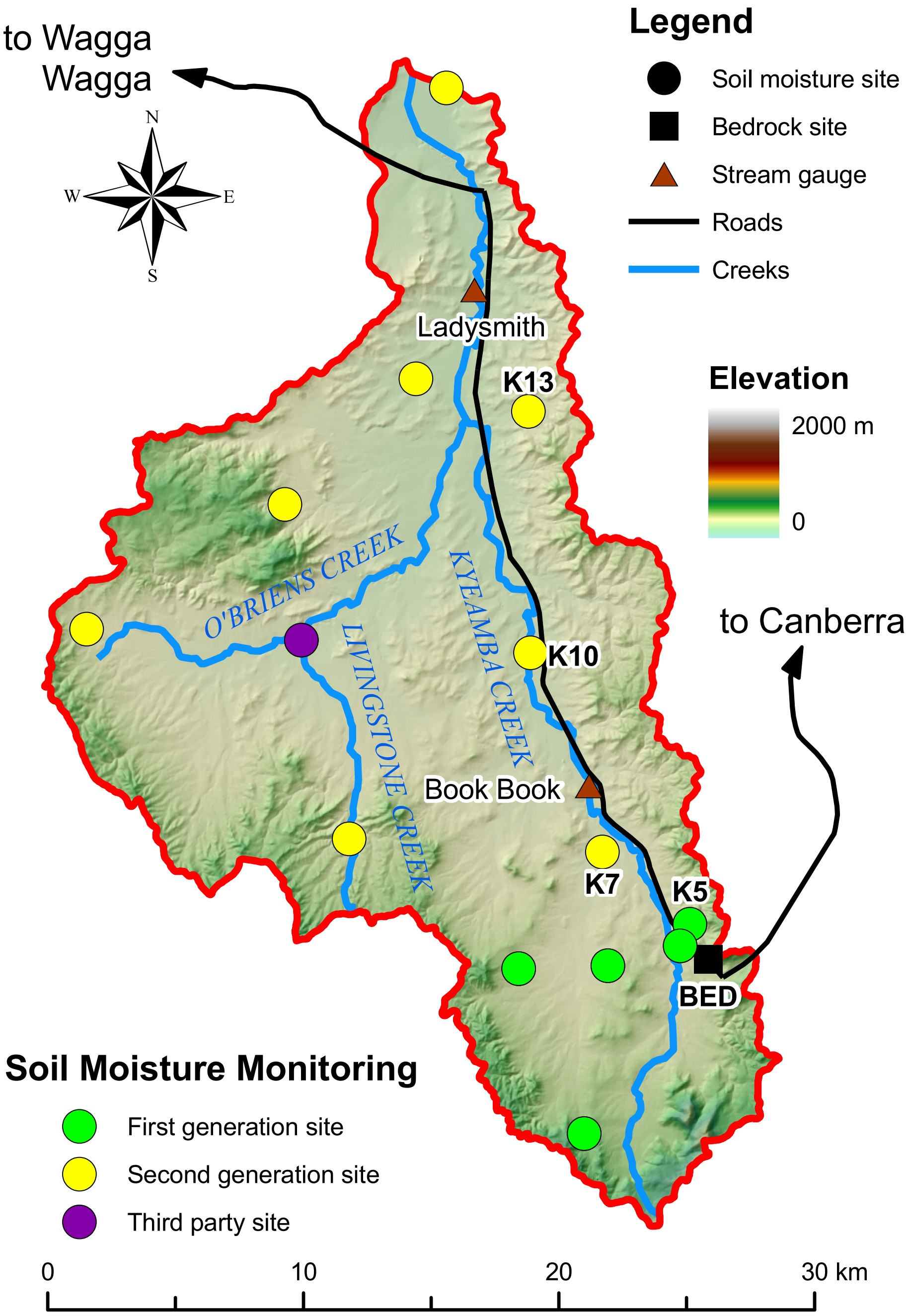

Fig. 5.1 Kyeamba Creek Catchment soil moisture monitoring. Sites are shown on a DEM with hillshading, together with creeks, stream gauges, major access road, and bedrock reference site. Four sites are selected for gravity observations (K5, K7, K10 and K13) based on ease of access and proximity to the bedrock site.

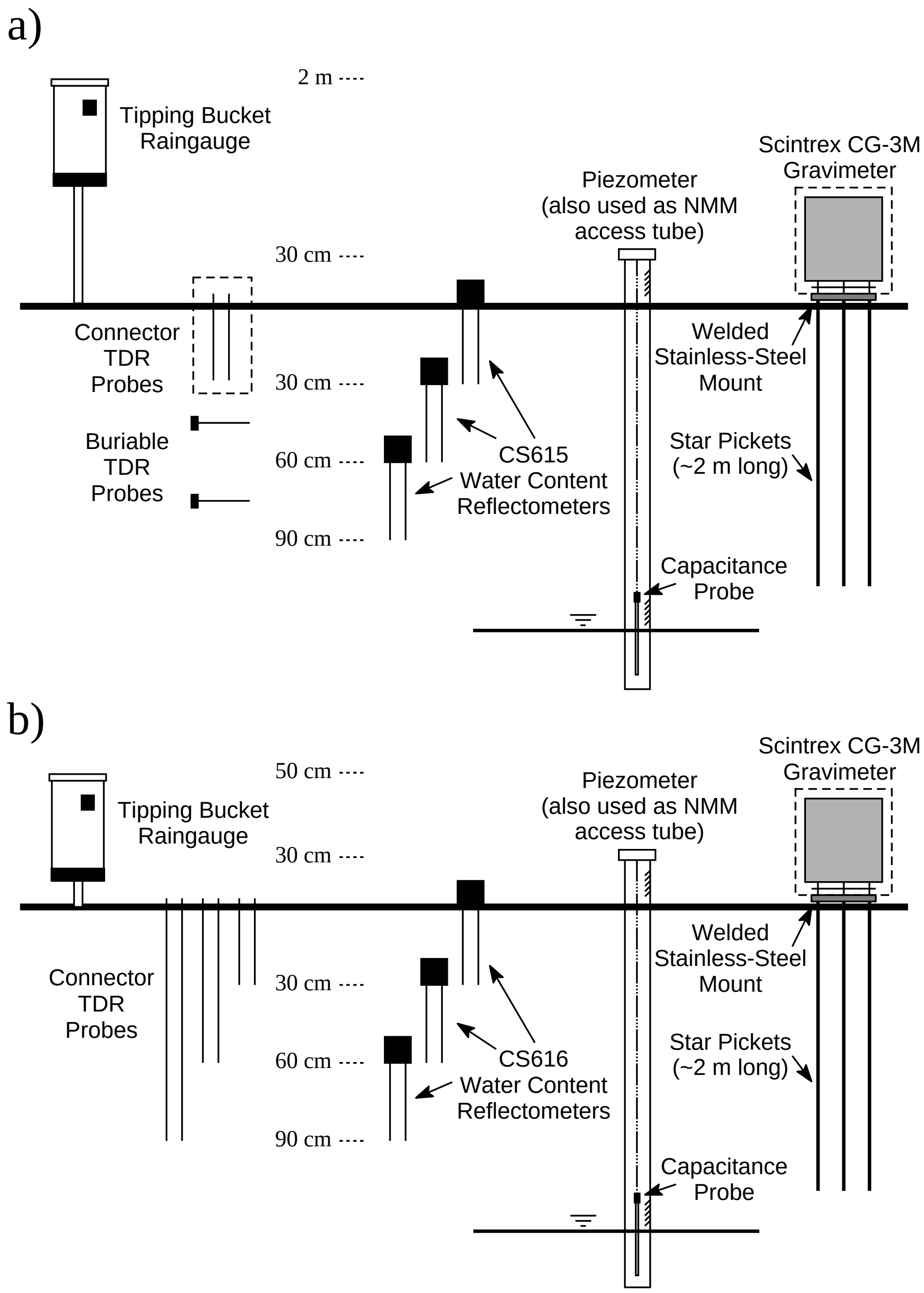

Fig. 5.2 Schematic of the soil moisture monitoring sites: a) first generation (K5), and b) second generation (K7, K10 and K13). Each site measures soil moisture in the upper 90 cm of the profile with three vertically installed water content reflectometers. Deeper vadose zone soil moisture is measured every 30 cm by NMM, and groundwater level is measured with a capacitance probe.

by measuring the extension of a spring (that has a fixed mass attached). Relative gravimeters are field portable and precise but the sensor suffers from a large drift in apparent gravity value (due to permanent stretching of the spring). Therefore when relative meters are used for high precision microgravimetry, the drift needs to be accurately accounted for and the calibration of the meter is crucial. The Scintrex CG-3M was chosen because it was the most accurate field portable, rugged gravimeter at the time (Smith et al., 2005). The Scintrex CG-3M was calibrated to an accurate, precise, GWR superconducting gravimeter (SG) located in Canberra at Mt Stromlo (see section 4.1).

As shown in Chapter 4, the gravity observation at a site is a function of both gravimeter behaviour and gravity. The gravity values reported by the gravimeter vary linearly with time due to drift (extension) of the spring sensor. Additionally there is a short term post transport stabilisation period where the gravity changes nonlinearly with time. Both of these effects are corrected by differencing gravity observations between sites. Reported gravity values also tend to decrease as the gravimeter battery is discharged, this battery voltage effect is corrected using a laboratory determined relationship. In addition to changes in water storage, temporal changes of gravity occur due to variations in Earth and ocean tides, polar motion, atmospheric pressure and earthquakes. Tide, polar motion and pressure effects can be corrected however, earthquakes must be screened for by keeping a log of all earthquakes during the gravity survey that can be obtained from `http://www.ga.gov.au/earthquakes`.

Gravity is observed at the soil moisture monitoring sites during dry (autumn) and wet (spring) conditions later in the same year to determine if a terrestrial water storage signal is detectable in ground-based gravity. Steel pads for the gravimeter are installed as close to the soil surface as possible but on vertically stable 2 m star pickets inserted to depth of refusal (Fig. 5.2). The pad was designed as a cut out triangle to allow as much precipitation and evapotranspiration to pass as possible while maintaining maximum rigidity (Fig. 3.6). As well as observing gravity at a number of soil moisture monitoring sites, one hydrologically stable bedrock reference site is observed to allow a simple analysis of the (relative) gravity changes at the sites between field campaigns. The gravity at the soil moisture sites is differenced with the gravity at the bedrock reference site to give site gravity differences (relative to the bedrock site) that can be analysed for a change between field campaigns (dry and wet conditions). It is assumed there is no change in gravity at the bedrock site. The gravity sampling strategy is designed to control the relative gravimeter drift, with the soil moisture monitoring sites selected based on ease of access and proximity to the bedrock site. The gravimeter is stored in Wagga Wagga overnight (a 0.5 hour drive from the bedrock site, see Fig. 5.1) to recharge the battery, with the bedrock reference site observed at the beginning and end of each survey day. The gravimeter is also run adjacent to the SG in Canberra (a 3 hour drive from the field sites) at the start and end of the field campaigns to check the gravimeter drift.

A sampling strategy was developed to construct a complete homogeneous network using (relative) gravity ties. A tie is formed by measuring gravity at one site and then another in quick succession, and taking a gravity difference. A network is complete if each site is connected to every other site; if by the same number of ties then it is also homogeneous (Lambert and Beaumont, 1977). Each line in Fig. 5.3 represents one set of ties (for both campaigns a set consists of 8 ties) that equates to about a day of observations. Thus, increasing the size of the gravity network from four to five sites results in an additional 4 sets of ties (for a complete network such as in Fig 5.3), extending the field campaign by at least four days. This increases

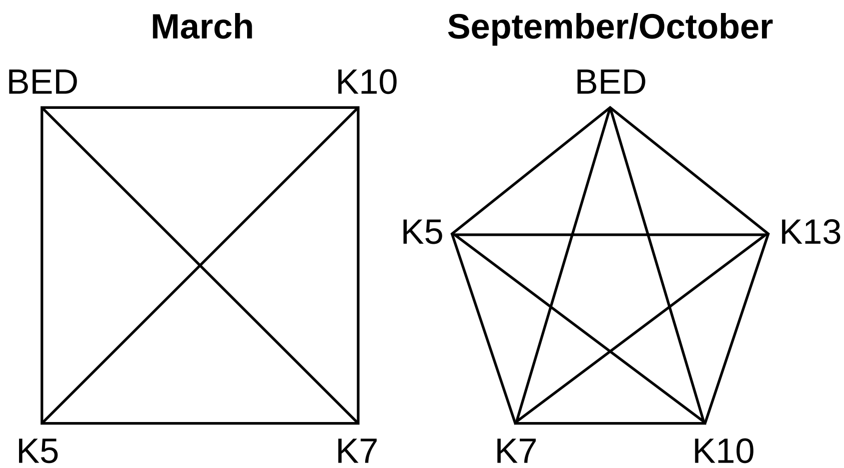

Fig. 5.3 Gravity networks for March and September/October 2005 field campaigns. A tie is formed by observing gravity at one site then another in quick succession and taking a gravity difference. Each line represents a set of ties (8 for both campaigns).

the chance of detrimental effects impinging on the precision of the gravity data, such as earthquakes, gravimeter drift or changing environmental conditions (both meteorological and hydrological). Therefore, there is a definite trade off between the precision of the data and the number of sites observed. For this reason, no more than four soil moisture monitoring sites were selected for gravity observations.

The ties with the bedrock site (BED) can be used directly to determine the gravity at a soil moisture monitoring site relative to the hydrologically stable reference site, but the other ties (e.g. K5–K7) can also be used in conjunction with the BED ties to form closed loops (BED–K5–K7). The site gravity differences in these closed loops should sum to zero. By enforcing this zero sum condition, outliers can be detected and the network strengthened by distributing the standard error of weak ties (e.g. BED–K5, where both sites do not have good wind protection) throughout the network. This procedure is referred to as network adjustment (Hwang et al., 2002), see section 4.6.

After network adjustment the observed gravity changes are tested for significance using a t-test. Finally, observed terrestrial water storage changes (soil moisture and groundwater) are converted to a predicted gravity change via the Bouguer slab approximation (Telford et al., 1990) and compared to the observed gravity changes.

5.2 Terrestrial Water Storage Observations

A high resolution soil survey of the Kyeamba Creek Catchment (John Gallant, pers. comm., 2002, CSIRO Land and Water) is shown in Fig. 5.4. Soils in the Kyeamba Creek Catchment are alluvial along the valley floor (where K7 and K10 are located), transferal on the valley gutters, erosional on the mid hillslopes (where K5 and K13 are located) and colluvial on the upper hillslopes, with some other vestigial and residual soil types also present. The four soil moisture monitoring sites are situated on only two soil units, both K5 and K13 are on the Lloyd (ld) unit (a member of the erosional group), while K7 and K10 are located on the O'Briens Creek (ob) unit (part of the alluvial soil group).

Soil samples were taken approximately 2 m from the soil moisture monitoring sites (at the same elevation if on a hillslope). The samples were sieved and the material passing a 2 mm sieve analysed using laser diffraction. The laser diffraction

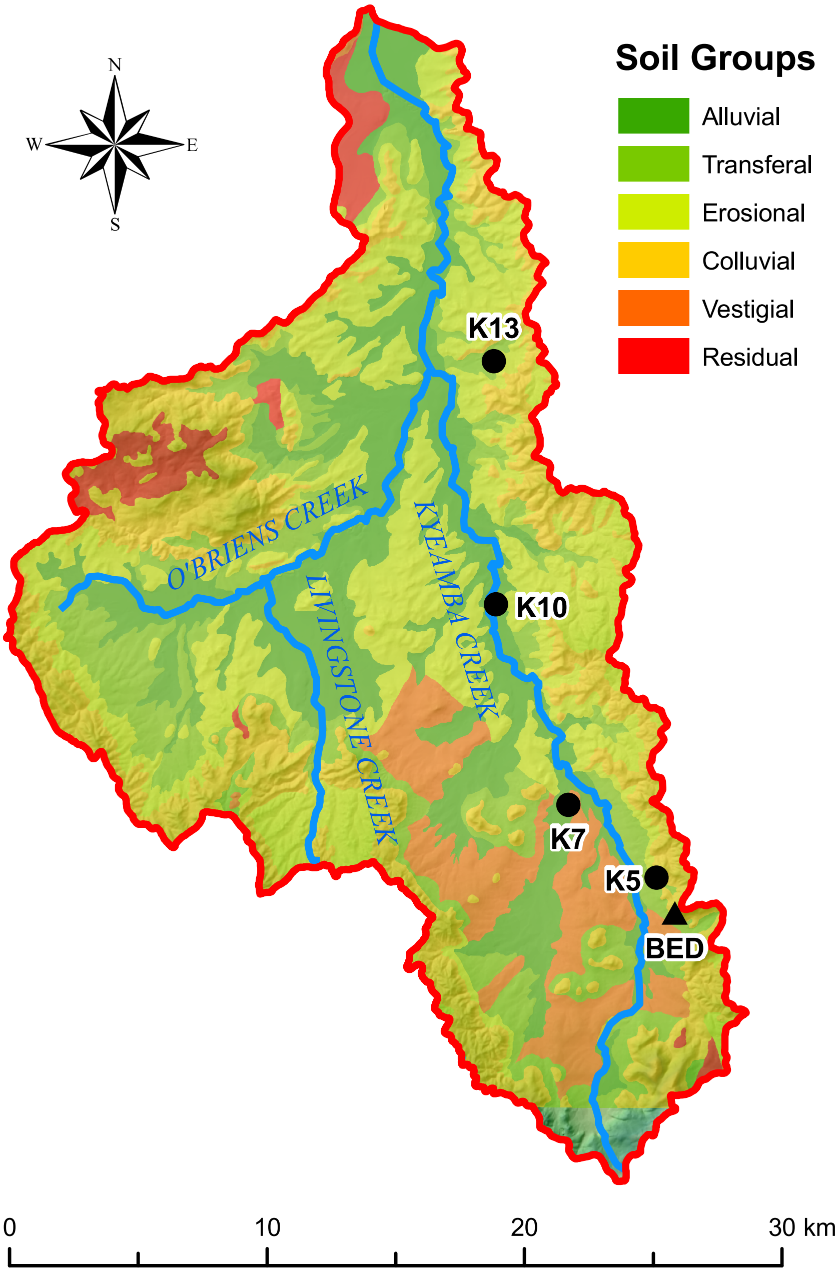

Fig. 5.4 Kyeamba Creek Catchment soil groups. Soil groups are overlain on a DEM with hillshading, together with creeks, soil moisture monitoring sites and bedrock reference site.

Table 5.1 Particle size distribution of soil at the soil moisture monitoring sites for depths at which soil moisture sensors are installed. Data is not available for K5.

Site	Depth	Sand	Silt	Clay	Soil Type
	0 – 30 cm	58.0	31.8	10.2	Silt Loam
K7	30 – 60 cm	36.2	45.1	18.8	Silt Loam
	60 – 90 cm	31.1	48.7	20.2	Silt Loam
	0 – 30 cm	42.4	49.5	8.1	Silt Loam
K10	30 – 60 cm	45.1	45.2	9.7	Silt Loam
	60 – 90 cm	39.7	49.9	10.4	Silt Loam
	0 – 30 cm	75.0	21.0	4.0	Loamy Sand
K13	30 – 60 cm	61.5	29.7	8.8	Silt Loam
	60 – 90 cm	50.3	43.1	6.6	Silt Loam

analysis was conducted by CSIRO Minerals using a Malvern Mastersizer 2000 which gives particle size distribution in the range 0.02 μm – 2 mm (results are shown in Appendix B). The laser diffraction and sieving results were combined to give the soil texture for K7, K0 and K13 (Table 5.1). Soil samples were not taken at K5, but on the basis of Fig. 5.4 could be expected to be similar to those from K13 (both erosional soils). Soil type at all depths (to 90 cm) at all sites is silt loam, except for the surface soil (0-30 cm) at K13 that contains less silt and more sand (being on a hillslope and comprised of erosional soil). Clay content increases (likewise sand content decreases) at all sites with depth, except at K13 the 30-60 cm soil contains slightly more clay than that at 60-90 cm (Table 5.1). The K10 soil profile (to 90 cm) is more homogeneous than that at K7 (also an alluvial soil) with the K7 surface soil (0-30 cm) quite different (more sand and less silt and clay) to the soils below (that contain double the clay content).

The soil samples were used to calibrate the soil moisture probes (Campbell Scientific CS616 water content reflectometers) at K7, K10, and K13 using the calibration procedure of Rüdiger et al. (2010); see also Appendix C. The Campbell Scientific CS615 water content reflectometers at K5 had already been calibrated (Western and Seyfried, 2005; Western et al., 2005).

Neutron moisture meter (NMM) measurements were used to quantify terrestrial water storage changes below the soil moisture probes; that is between 90 cm and the water table (between 2 and 4 m depth at K7 and K10), or the bottom of the access tube (approximately 2 m at K5 and K13 due to coarse erosional material and deep groundwater level). Field operation of the NMM consists of a background radiation measurement (thermalised neutron count) followed by a measurement every 30 cm down the access tube (beginning 12 cm below the surface), and finishing with another background measurement. The two background measurements are averaged and used to calculate count ratios for the NMM measurements. The count ratios at 12, 42 and 72 cm depth are calibrated to the soil moisture from the 0-30, 30-60 and 60-90 cm water content reflectometers (see Appendix E). The three individual NMM calibrations at each site are then grouped into a surface and a deeper calibration (which is used to convert the NMM count ratios below 1 m to volumetric soil moisture). The NMM data can be seen (together with the water content reflectometer soil moisture and capacitance probe groundwater level data) as point observations in Fig. 5.5 and as profile soil moisture in Fig. 5.6.

The same general soil moisture trend is observed at all four soil moisture monitoring sites with dry soil moisture conditions in the first half of the year (January to June) and wet conditions in the second half, but starting to dry out in October and returning to dry conditions again in November (Fig. 5.5). There are four isolated large rainfall events (in January, February, April and December) that are observed at all sites during the dry conditions, these events result in changes to the 0-30 cm soil moisture that sometimes propagates to the 30-60 cm soil moisture (particularly noticeable for the February event). Except for the February event, 60-90 cm soil moisture changes are only observed during the second half of the year when potential evapotranspiration is reduced. The increase in the 60-90 cm soil moisture in the second half of the year also corresponds to an increase in groundwater (reduction in water table depth). This increase in groundwater level is gradual at K7 but sudden at K10 and K13 (Fig. 5.5); note that during 2005 groundwater was never observed within the piezometer at K5, and a capacitance probe was only installed at K13 after groundwater (less than 1 m below the surface) was observed in the piezometer in September. The measurable piezometer depth at K5 and K13 is 2 m whereas at K7 and K10 it is greater than 5 m. This can be seen clearly in Fig. 5.6 where NMM measurements at K5 and K13 stop at 162 cm but at K7 and K10 continue to the water table (that varies between 4 m in May and 2 or 3 m in October, at K7 and K10 respectively); note the K13 NMM measurements for September and

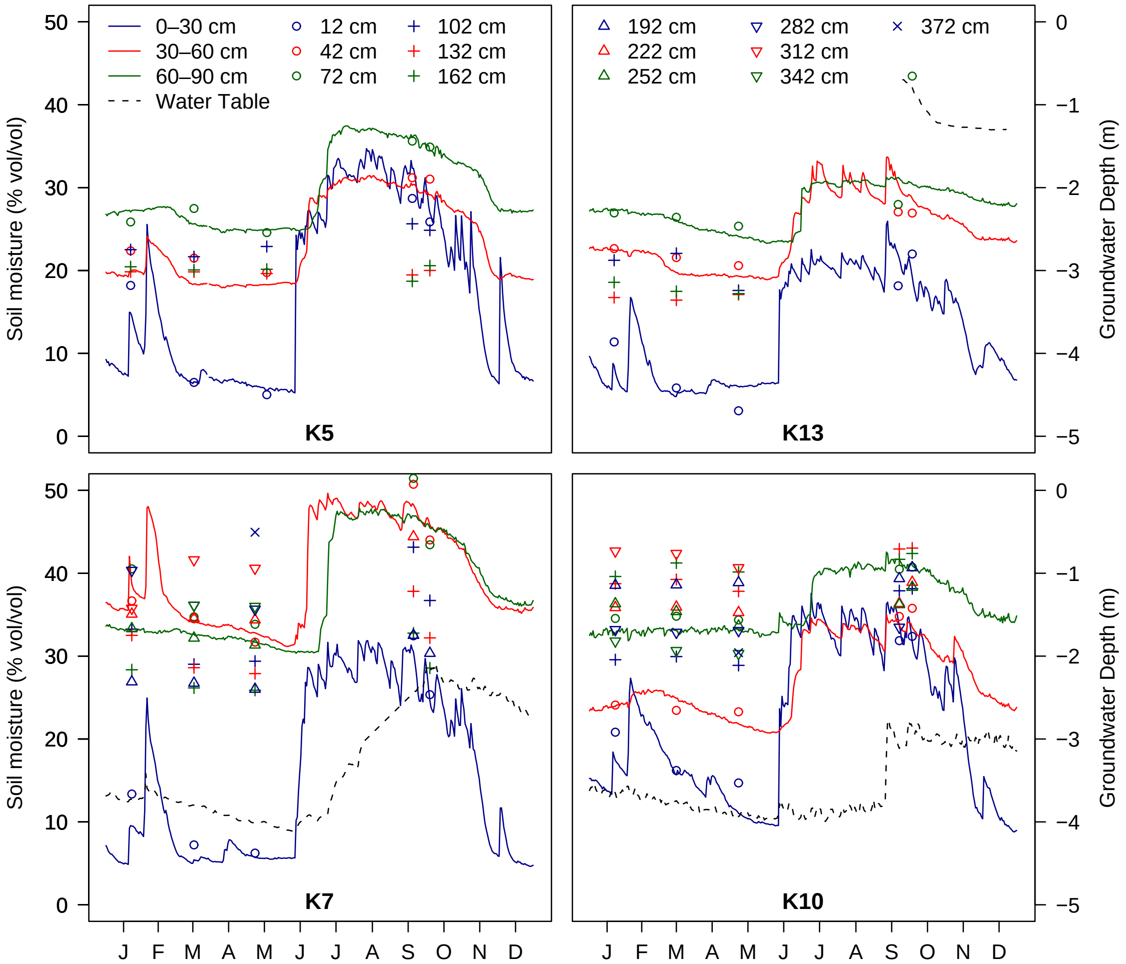

Fig. 5.5 Observed soil moisture and groundwater level at four sites (K5, K7, K10 and K13) in the Kyeamba Creek Catchment for the year 2005. Soil moisture points were from neutron moisture measurement, while continuous soil moisture was observed with water content reflectometers. Groundwater level was measured with capacitance probes, but the water table was below the bottom of the piezometer at K5 and at K13 (until September).

October stop at 72 cm depth due to the water table. The profile soil moisture from the NMM measurements is greatest in the top 1 m at all sites except K10 where soil moisture is slightly higher between 1 and 2 m depth. For the valley sites (K7 and K10) in the drier conditions (January, March and May) the NMM measurements show the profile soil moisture trend is to increase with depth with maximum soil moisture near the water table. The profile measurements are also shown as points

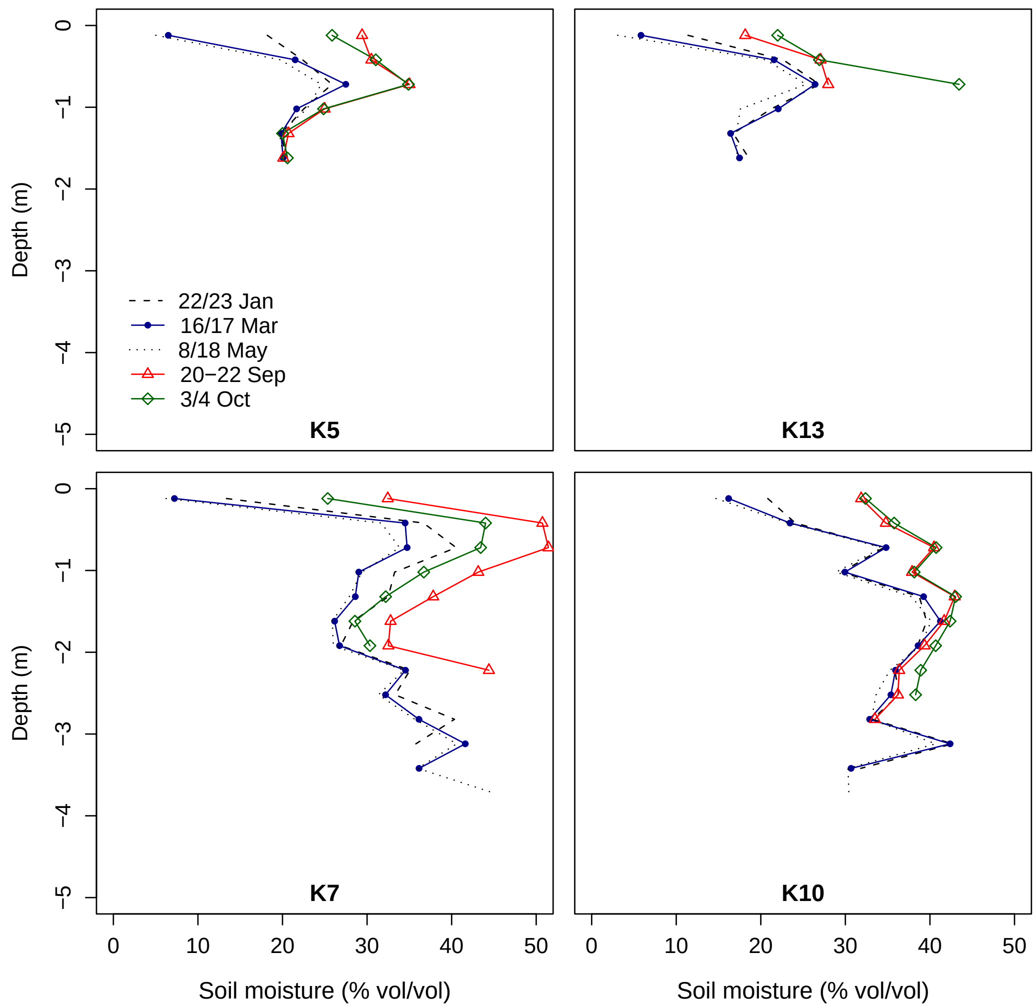

Fig. 5.6 Observed profile soil moisture at four sites (K5, K7, K10 and K13) in the Kyeamba Creek Catchment for the year 2005. Soil moisture points are from neutron moisture measurement.

in Fig. 5.5 where the 12, 42 and 72 cm NMM measurements are close to the 0-30, 30-60 and 60-90 cm continuous soil moisture measurements (from the water content reflectometers) except for the October and May deepest NMM measurements at K13 and K7 respectively (the 72 and 372 cm NMM measurements respectively) where the NMM measurement is spuriously high due to probe contact with groundwater. These spuriously high soil moisture points are also clear in the profile soil moisture plots for K13 in October and K7 in May (Fig. 5.6).

5.3 Gravity Observations

Gravity observations made at each site with the Scintrex CG-3M relative gravity meter consist of eight consecutive measurements averaged to improve precision. The gravity measurements are represented as

$$\begin{aligned} z = g + B + P \\ +E + O + A \\ +D + V + S + \epsilon \end{aligned} \tag{5.1}$$

where z is gravity reported by the (calibrated) gravity meter (μGal), g desired gravity that is dependent on elevation (static) and hydrological (dynamic) changes, B a bias constant across all sites (due to the relative gravimeter), P atmospheric pressure, E Earth tides, O ocean tide loading, A (annual) polar motion, D gravimeter drift, V gravimeter battery voltage, S post transport stabilisation, and ϵ a random error (assumed Gaussian).

The pressure correction is calculated as

$$P = C\left(p - p_n\right), \tag{5.2}$$

where p is measured barometric pressure (mbar) and p_n is normal atmospheric pressure modelled by

$$p_n = 1013.25\left(1 - \frac{0.0065H}{288.15}\right)^{5.2559}, \tag{5.3}$$

where H (m) is station elevation (Torge, 1989) and C an admittance constant, theoretically between -0.3 and -0.4 μGal/mbar but both site and instrument specific. The admittance constant (C) for this instrument was calculated from a laboratory analysis of gravity and pressure and found to be -0.394 (±0.045) (see section 4.3).

Earth tides were predicted with Tsoft (Van Camp and Vauterin, 2005) using parameters (Love numbers) for the site (Dehant et al., 1999) and the Tamura (1987) tidal potential catalogue (see section 4.2.2). Ocean tide loading was calculated using the ocean tide model CSR4.0 (Watkins and Eanes, 1997) and the ocean tide loading model GOTIC2 (Matsumoto et al., 2001) (see section 4.2.4). Polar motion was calculated with Tsoft using the EOP C04 series of Earth orientation parameters from

Table 5.2 Average post transport gravity reduction (μGal) at each site for the March and September/October 2005 field campaigns, and differences between the campaigns. See Fig. 5.7 for the individual measurements at each site.

Tie	March 2005	September/October 2005	Post Transport Differences
BED	-20.78	-16.53	4.25
K5	-16.48	-15.31	1.17
K7	-13.47	-12.08	1.39
K10	-15.13	-11.90	3.23
K13		-13.40	

the International Earth Rotation Service (IERS) website `http://www.iers.org` (see section 4.2.3).

Gravimeter drift was removed by a linear correction applied within the gravimeter as this accurately represents the drift behaviour (see Fig. 4.12). The drift constant was determined (in a laboratory next to the superconducting gravimeter in Canberra) over a 24 hour time period (corresponding to the principal Earth tides) prior to each field deployment. The March campaign used a linear drift rate of 430 μGal/day set on 6/1/2005 (that replaced the previous correction rate of 392 μGal/day set on 8/10/2004), the September/October 2005 campaign used 344 μGal/day (set on 19/9/2005). No additional drift removal was performed prior to (or during) network adjustment as this was found to have marginal impact on results (see section 4.6.1).

A voltage correction was calculated (-4.6 μGal/V) using gravimeter battery voltage data recorded at the time of the gravity observations (see section 4.5.4). While the post transport stabilisation could be corrected using a natural logarithm (see section 4.5.3), instead it was corrected by removing the average observed post transport stabilisation at each site for each field campaign (Fig. 5.7). This resulted in the largest correction (over the two campaigns) for the bedrock (BED) and K10 sites (Table 5.2). The post transport stabilisation was lower (and more consistent) for the September/October 2005 field campaign when a custom designed, suspension based transportation device was used (Fig. 3.14). The transportation device was not available for the March field campaign due to logistical issues.

For site i (and observation j) the eight (2.5 minute duration) gravity measure-

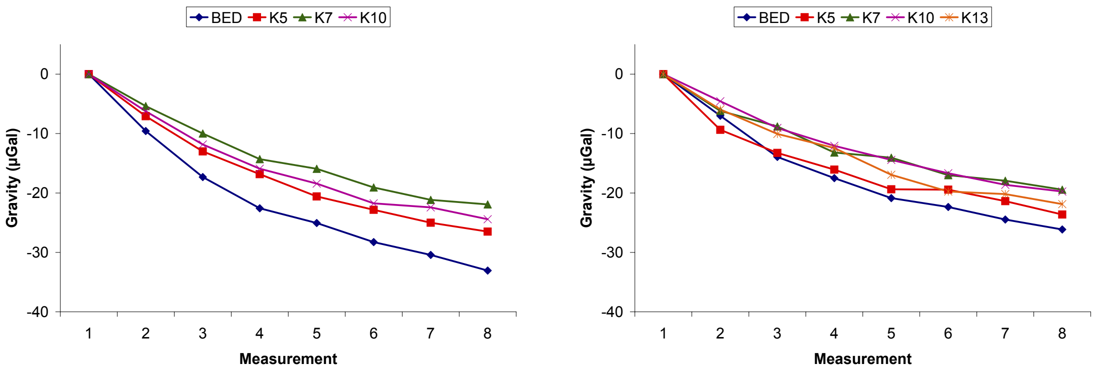

Fig. 5.7 Post transport stabilisation of the gravimeter for the March (left) and September/October (right) field campaigns. The first gravity measurement at each site is set to 0 µGal and the average of the following seven measurements (relative to the first measurement) are shown (for each site and field campaign).

ments were averaged to give a 20 minute gravity observation

$$\begin{aligned} z_{i,j} + v_{i,j} = g_{i,j} + B_{i,j} + P_{i,j} \\ +E_{i,j} + O_{i,j} + A_{i,j} \\ +D_{i,j} + V_{i,j} + S_{i,j}, \end{aligned} \tag{5.4}$$

where $v_{i,j}$ is the gravity observation residual. Differencing successive gravity observations (j and $j+1$), that are always at different sites (i and k) gives a gravity tie

$$\Delta z_{ik} + v_{ik} = \Delta g_{ik}, \tag{5.5}$$

where $\Delta z_{ik} = z_{k,j+1} - z_{i,j}$, and v_{ik} is the gravity tie residual. The components P, E, O, A, and V are removed through modelling (together with pressure, polar motion and battery voltage observations), S is removed using average behaviour (determined from gravity observations), B is removed through differencing, and D is removed by the in built gravimeter linear drift correction.

A field campaign at three soil moisture monitoring sites (K5, K7, K10) and the bedrock site (BED) was conducted on 10-16 March 2005 (the dry autumn campaign). Nineteen gravity observations were made at BED (over all seven days), twelve at K5 and K10, and thirteen at K7 (Table 5.3 and Fig. 5.8) resulting in four ties each way

Table 5.3 Gravity observations during the March and September/October 2005 field campaigns. See Fig. 5.8 for the individual measurements at each site.

	March							
Site	10	11	12	13	14	15	16	Total
BED	2	2	5	5	2	1	2	19
K5	2	4		2		4		12
K7				2	5	5	1	13
K10	1	3	4		4			12
Total	5	9	9	9	11	10	3	56

	September											October			
Site	19	20	21	22	23	24	25	26	27	28	29	30	1	2	3	Total
BED	2	2	2	2	2	2	2	2	3	1	2	2	2	2	1	29
K5	1	2		1	1	1	1	1		2	3	1	1	1		16
K7		1		2	2	1	1	1	1	1		1	4	1		16
K10			2	2		3		1	1		1	4	1	1		16
K13			1				3	4			2	1	1	4	1	17
Total	3	5	5	7	5	7	7	9	5	4	8	9	9	9	2	94

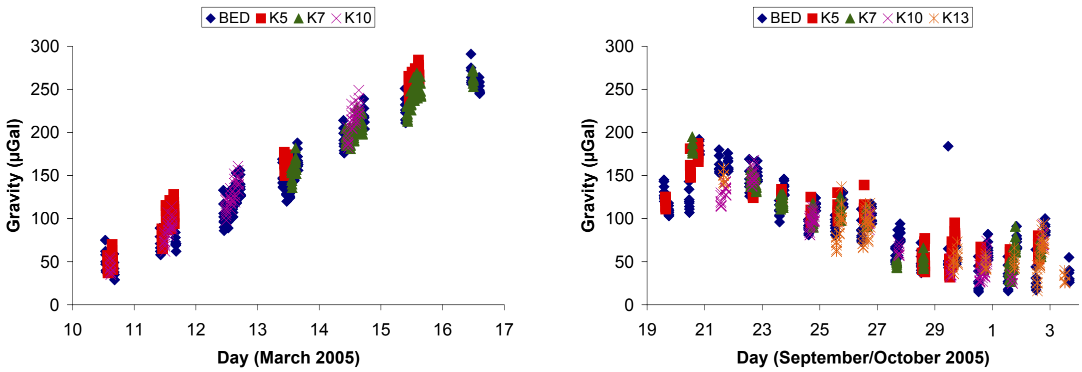

Fig. 5.8 Gravity measurements during the March (left) and September/October (right) field campaigns. Measurements are relative to the first measurement at each site, which is set close to the interpolated BED value for that time.

between any two sites (and an additional BED–K7 tie). There were extremely few earthquakes during this campaign, with only one (Southeastern Iran) over magnitude 6 (Table 5.4).

A second field campaign at four soil moisture monitoring sites (K5, K7, K10, K13) and the bedrock site (BED) was conducted from 19 September to 3 October

2005 (the wet spring campaign). Twenty nine gravity observations were made at BED (over all fifteen days of the field campaign), sixteen at K5, K7, and K10, and seventeen at K13 (Table 5.3 and Fig. 5.8) resulting in four ties each way between any two sites except K5–BED which had only three ties. There were many earthquakes during this field campaign (Table 5.4), with five between magnitude 6 and 7 and one (halfway into the campaign) over magnitude 7.

5.4 Gravity Changes

The eight gravity ties between any two sites are averaged to give gravity differences between the four sites observed in both the March and September/October 2005 field campaigns (Table 5.5), together with the change in site gravity (between campaigns) and standard error. Except for the K7–K10 site difference, the error is consistently higher for the second campaign (September/October 2005), and significantly more so for all site differences involving K5. Assuming the gravity at the stable bedrock reference site BED is constant, the change in site differences relative to BED indicate a small decrease in gravity at both K5 and K10 of 1.2 μGal and 2.8 μGal between the March and September/October campaigns. However, the large standard errors of 8.8 μGal and 5.6 μGal associated with these changes indicate they are not statistically significant. A large (positive) change is also observed at K7 (8.6 μGal), that while also having a large uncertainty (5.4 μGal), has a much larger signal to noise ratio.

Network adjustment increases the precision of the site gravity difference estimates for each of the campaigns by using the data from all gravity ties in the network (Hwang et al., 2002). Using six sets of ties (49 individual ties) between four sites for the March campaign and ten sets (79 individual ties) between five sites for the September/October campaign (Fig. 5.3), together with the (free) constraint that the site differences across the network sum to 0 μGal (i.e. the network loop closes), the network adjustment calculates the gravity and standard error for each site (for each campaign). These are shown in Table 5.6 (note the gravity values sum to zero due to the free network constraint). After network adjustment the misclosure of any of the closed loops (such as K5–K7–K10) is 0 μGal (compared to a K5–K7–K10 loop misclosure of 8.6 and 0.6 μGal for the March and Septem-

Table 5.4 Earthquakes during the March (above the line) and September/October (below the line) 2005 field campaigns (from `http://www.ga.gov.au/earthquakes`). Field sites (BED, K5, K7, K10 and K13) are at latitude 35 ° S and longitude 148 ° W.

Date	Time (UTC)	Lat.	Long.	Depth	Mag.	Location
12/03/05	15:55	-30.7	117.4	0	2.9	Koorda, WA
13/03/05	2:10	-26.2	131.6	5	4.6	W of Ernabella SA
13/03/05	3:31	27.2	61.9	55	6	Southeastern Iran
13/03/05	10:57	-20.0	130.4	20	2.1	Tanami Desert, NT
15/03/05	12:50	-32.5	116.8	0	2.7	SW of Brookton, WA
16/03/05	1:27	-30.6	117.5	3	4.2	N Koorda WA
20/09/05	4:50	-30.1	117.2	2	2.5	Kalannie WA
21/09/05	2:25	43.9	146.1	95	6.2	Kuril Island
21/09/05	21:39	-30.1	117.2	2	2.7	N of Kalannie WA
21/09/05	22:47	-30.1	117.2	2	4	N of Kalannie WA
21/09/05	22:59	-30.2	117.2	1	3.7	N of Kalannie WA
21/09/05	23:04	-30.1	117.2	2	2.6	N of Kalannie WA
22/09/05	0:29	-30.2	117.2	3	3	N of Kalannie WA
22/09/05	3:53	-30.1	117.2	3	4.1	NE of Kalannie WA
22/09/05	4:29	-30.1	117.2	2	2.1	N of Kalannie WA
22/09/05	18:35	-30.1	117.2	5	3.9	N of Kalannie WA
23/09/05	9:57	-30.1	117.2	2	2.7	N of Kalannie WA
23/09/05	11:43	-30.1	117.2	0	2.9	N of Kalannie WA
23/09/05	13:49	16.1	-87.5	31	6	Offshore Honduras
24/09/05	6:56	-30.2	117.2	2	2.2	N of Kalannie WA
25/09/05	12:56	-17.6	167.8	30	6.1	Vanuatu
25/09/05	13:18	-25.9	137.5	0	2.4	Simpson Desert NT
26/09/05	1:56	-5.7	-76.4	85	7.5	Northern Peru
28/09/05	21:38	-38.6	146.0	10	2.7	SW of Tarwin Vic
29/09/05	15:50	-5.5	151.8	35	6.5	New Britain region PNG
29/09/05	18:23	-5.6	151.8	35	6.1	New Britain region PNG
29/09/05	21:50	-31.8	138.8	10	2.5	Hawker SA
2/10/05	17:50	-30.0	150.7	0	2.5	Bingara area NSW
3/10/05	7:22	-30.5	117.1	0	2.7	W of Burakin WA

ber/October campaigns prior to adjustment) and the K5–K7 site gravity difference (Table 5.7) is now simply the difference of the K5 and K7 gravity values (Table 5.6). The network adjustment has significantly reduced the error for all site differences (Table 5.7) to 2 μGal for March and 3 μGal for September/October 2005, compared to errors ranging from 2 to 5 μGal and 4 to 7 μGal respectively for the March and

Table 5.5 Average gravity difference between sites (μGal), standard error is shown in brackets.

Site Difference	March 2005	September/October 2005	Gravity Change
BED–K5	8354.9 (5.0)	8353.7 (7.2)	-1.2 (8.8)
BED–K7	11264.1 (3.8)	11272.6 (3.9)	8.6 (5.4)
BED–K10	16546.8 (2.2)	16544.0 (5.2)	-2.8 (5.6)
K5–K7	2915.6 (2.4)	2925.3 (6.2)	9.7 (6.6)
K5–K10	8191.3 (2.8)	8204.6 (5.7)	13.3 (6.4)
K7–K10	5284.4 (3.9)	5278.6 (3.7)	-5.8 (5.4)

September/October average site differences (Table 5.5). While network adjustment has reduced the error for all of the site differences, it has also changed the gravity value (in comparison with the average site differences in Table 5.5), reducing all site gravity differences (except K5–K10 in March which increases by 0.9 μGal) by 0.3 to 10.6 μGal (for BED–K10 and K5–K10 in September/October respectively). After network adjustment the error on the relative gravity changes is much smaller (3.6 μGal) than for the average tie differences (up to 8.8 μGal for BED–K5), but

Table 5.6 Site gravity (μGal) after network adjustment, standard error is shown in brackets.

Site	March 2005	September/October 2005
BED	-9037.2 (1.4)	-9714.9 (2.1)
K5	-688.1 (1.5)	-1365.1 (2.1)
K7	2221.2 (1.4)	1553.4 (2.1)
K10	7504.1 (1.5)	6828.8 (2.1)
K13		2697.8 (2.1)

Table 5.7 As for Table 5.6 but for site differences. Compare to Table 5.5 for average site differences before network adjustment.

Site Difference	March 2005	September/October 2005	Gravity Change
BED–K5	8349.1 (2.0)	8349.8 (3.0)	0.7 (3.6)
BED–K7	11258.3 (2.0)	11268.3 (3.0)	9.9 (3.6)
BED–K10	16541.3 (2.0)	16543.8 (3.0)	2.4 (3.6)
K5–K7	2909.3 (2.0)	2918.5 (3.0)	9.2 (3.6)
K5–K10	8192.2 (2.1)	8193.9 (3.0)	1.7 (3.6)
K7–K10	5283.0 (2.0)	5275.5 (3.0)	-7.5 (3.6)

Table 5.8 Gravity changes between March and September/October 2005 field campaigns after network adjustment (μGal). Test statistic and critical t value for a significance level of 0.05 and 121 degrees of freedom are shown.

Site	Gravity Change	Test Statistic	Critical t Value
K5	0.7	0.28	1.98
K7	9.9	3.93	1.98
K10	2.4	0.95	1.98

the gravity changes before and after network adjustment are quite similar (compare Table 5.5 and 5.7) with the largest change for the K5–K10 site difference (from 13.3 to 1.7 μGal). After network adjustment the gravity changes relative to the bedrock reference site are all positive (Table 5.7), that is the gravity increases at all soil moisture monitoring sites between the (dry) March and (wet) September/October 2005 field campaigns. Also, after network adjustment the BED–K7 change is still the only tie difference that is significant (compared to the magnitude of the error).

The statistical significance of a change in gravity at K5, K7 and K10 (relative to BED) between the March and September/October campaigns is assessed using a t-test (Table 5.8). A significance level of 0.05 is selected and the degrees of freedom (*df*) are the sum of the *df* for the March (46) and September/October campaigns (75), calculated as the number of gravity ties (49 or 79) minus the number of gravity sites (4 or 5) plus one for the free network constraint. The gravity increases at all soil moisture sites between the March and September/October 2005 field campaigns (Table 5.8). However, the changes are smaller (0.7 and 2.4 μGal) and not significant at K5 and K10. The gravity change at K7 of 9.9 μGal is statistically significant (at the 0.05 level).

5.5 Analysis of Terrestrial Water Storage and Gravity Changes

The only significant streamflow event for January 2003 to September 2008 occurred during the September/October 2005 field campaign (Fig. 5.9). Furthermore, this campaign corresponds to the maximum observed soil moisture and groundwater level

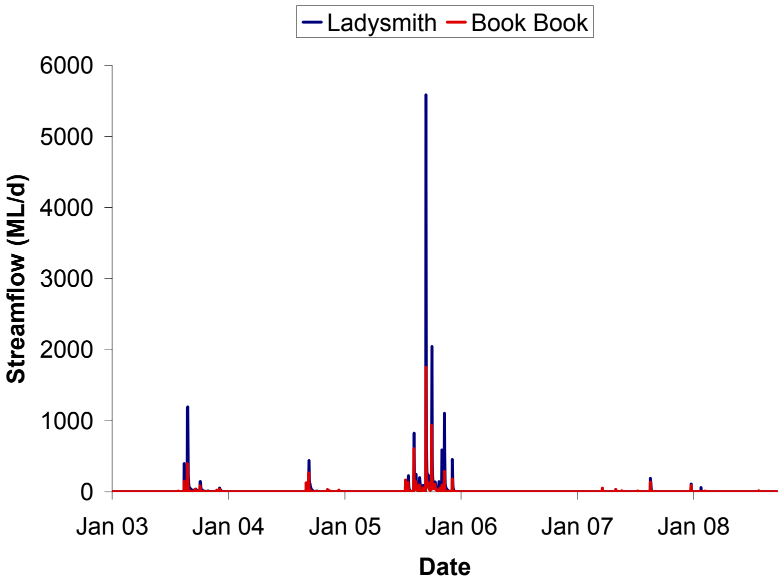

Fig. 5.9 Kyeamba Creek Catchment daily streamflow for two locations within the catchment (Book Book and Ladysmith). Book Book is upstream of Ladysmith; both streamgauges are on Kyeamba Creek (see Fig. 5.1).

during 2005 (Fig. 5.5 and 5.6). Likewise the March 2005 campaign corresponds to near minimum observed soil moisture and groundwater level, with both slightly lower during May 2005 (Fig. 5.5 and 5.6). Consequently, observed changes in terrestrial water storage (soil moisture and groundwater) and gravity at each site between the March and September/October 2005 field campaigns are as large as can reasonably be expected for this catchment.

The hydrological observations (precipitation, soil moisture and groundwater level) are shown in Table 5.9 for the two field campaigns. Almost 400 mm of precipitation is observed at K7 and K10 (and almost 270 mm at K5) between the March and September/October 2005 field campaigns. This corresponds to a large increase in soil moisture at all sites (particularly at 0-30 cm depth). The groundwater level also rises in response to the rainfall (by almost 140 cm at K7 and 70 cm at K10). While precipitation is observed (at all sites) between the start and end of the September/October field campaign (with up to 45.8 mm observed at K10), the soil moisture decreases at all sites (although an initial rise in response to the rainfall is evident in Fig. 5.5). The falling tendency of the soil moisture at all sites during the

Table 5.9 Hydrological observations for the March and September/October 2005 field campaigns. See Fig. 5.5 for a full timeseries at each site. Soil moisture, groundwater level and cumulative precipitation is shown for each soil moisture monitoring site. The three observation times correspond to the NMM measurements for 16/17 March, 20-22 September and 3/4 October (see Fig. 5.6).

Hydrological observations	March	September	October
(K5) Cumulative precipitation (mm)	0	268.6	10.0
0-30 cm soil moisture (% vol/vol)	6.0	32.1	26.2
30-60 cm soil moisture (% vol/vol)	18.3	30.4	29.3
60-90 cm soil moisture (% vol/vol)	25.6	36.1	34.5
Water table depth (of groundwater) (cm)	Nil observed		
(K7) Cumulative precipitation (mm)	0	398.8	38.6
0-30 cm soil moisture (% vol/vol)	5.6	30.8	24.8
30-60 cm soil moisture (% vol/vol)	34.2	48.6	45.9
60-90 cm soil moisture (% vol/vol)	32.6	47.4	45.8
Water table depth (of groundwater) (cm)	380	243	215
(K10) Cumulative precipitation (mm)	0	396.6	45.8
0-30 cm soil moisture (% vol/vol)	15.9	33.2	31.5
30-60 cm soil moisture (% vol/vol)	24.8	33.7	33.5
60-90 cm soil moisture (% vol/vol)	32.7	41.7	41.1
Water table depth (of groundwater) (cm)	376	308	285

September/October field campaign is due to the onset of spring (and corresponding increase in potential evapotranspiration). While the soil moisture is falling during the September/October field campaign the groundwater shows more delay in its response to atmospheric forcing and continues to rise at K7 and K10 (Table 5.9).

The soil moisture and groundwater level observations at each site (Table 5.9) are used to calculate terrestrial water storage (TWS). The water content reflectometers (0-90 cm soil moisture), neutron moisture meter measurements (from 102 cm depth), and water table (at K7 and K10) are used to calculate TWS to a nominal depth of 5 m. Estimates of the TWS corresponding to the observation times in Table 5.9 are shown in Table 5.10, where TWS is partitioned into root zone (RZ), intermediate vadose zone (IVZ), deeper vadose zone (DVZ), and groundwater (GW).

The root zone (RZ) terrestrial water storage is calculated using the 0-30, 30-60 and 60-90 cm water content reflectometers. While 0-90 cm is nominally denoted the root zone, there is no rooting depth data to support this naming convention.

Terrestrial water storage in the intermediate vadose zone (IVZ) is calculated using the NMM measurements at 102, 132, and 162 cm together with an estimate of the NMM "sphere of influence" (Hignett and Evett, 2002) to calculate (roughly) 90-120, 120-150 and 150-180 cm soil moisture. Where the sphere of influence of a deeper NMM measurement overlaps with that of one higher in the profile, the soil moisture from the NMM measurement higher in the profile is used, in this way there is no double counting of soil moisture when calculating TWS.

The deeper vadose zone (DVZ) terrestrial water storage (Table 5.10) is calculated using NMM measurements from 192 cm to the water table (at K7 and K10), again using NMM measurement higher in the profile together with the sphere of influence to ensure NMM measurements do not overlap. Groundwater was not observed at K5, and the access tube is only 2 m deep (due to coarse material preventing further drilling). Consequently the NMM measurement of soil moisture at 162 cm is assumed constant to 5m depth. This assumption appears reasonable as both the 132 and 162 cm NMM measurements are constant at about 21 % vol/vol over five different observations throughout the year (Fig. 5.6).

The groundwater (GW) terrestrial water storage is calculated from the water table to 5 m using the maximum observed soil moisture (from the 60-90 cm water content reflectometer) as an estimate of saturation. A terrestrial water storage component for groundwater is not calculated at K5.

Terrestrial water storage in the root zone almost doubles from March to September at K5 (Table 5.10). However, TWS in the intermediate and deeper vadose zone both decrease. This results in total terrestrial water storage at K5 increasing slightly (over 5 m depth). At K7, TWS for the root zone almost doubles between March and September, TWS for the intermediate vadose zone increases, and the groundwater TWS more than doubles. The TWS for the deeper vadose zone decreases, but this is due to TWS from this portion of the profile being counted as TWS for GW as the water table rises (see Table 5.9). This is particularly clear for the September and October TWS where the TWS for the deeper vadose zone decreased by 14.4 cm but the TWS for the groundwater increases by 13.3 cm (the water table also increases by 28 cm in this period, see Table 5.9). Again at K10 the TWS for the deeper vadose zone decreased while the TWS for groundwater increased (Table 5.10). More modest increases in the TWS for the root zone and (particularly) the intermediate vadose

Table 5.10 Terrestrial water storage (TWS) for the March and September/October 2005 field campaigns. The three observation times correspond to the NMM measurements for 16/17 March, 19-22 September and 3/4 October (see Fig. 5.6). Estimates of TWS (cm) are given for root zone (RZ), intermediate vadose zone (IVZ), deeper vadose zone (DVZ), and groundwater (GW). See Table 5.9 for groundwater level (WT) at time of field campaigns.

Terrestrial water storage	March	September	October
RZ (CS615 0-90 cm)	15.0	29.6	27.0
IVZ (NMM 102-162 cm)	20.8	20.1	20.3
DVZ (NMM 162 cm assumed constant to 5 m)	72.8	59.8	65.6
Total (K5)	108.5	109.5	112.8
RZ (CS616 0-90 cm)	21.7	38.0	35.0
IVZ (NMM 102-162 cm)	25.8	34.1	29.6
DVZ (NMM 192 cm to WT)	67.9	24.1	9.7
GW (WT to 5 m)	58.4	124.8	138.1
Total (K7)	173.9	221.1	212.5
RZ (CS616 0-90 cm)	22.0	32.6	31.8
IVZ (NMM 102-162 cm)	33.7	37.4	37.8
DVZ (NMM 192 cm to WT)	66.8	43.5	35.4
GW (WT to 5 m)	53.1	82.5	92.0
Total (K10)	175.6	196.0	197.0

zone are seen at K10. The total terrestrial water storage at K5 and K10 increased between the start and end of the September/October field campaign, whereas at K7 a decrease was seen. This is mostly due to a loss of TWS in the root and vadose zones, presumably due to evapotranspiration as the K7 valley site is mostly flat (see Fig. 5.1) and there is a decrease in TWS below the intermediate vadose zone (when the DVZ and GW terrestrial water storages are combined).

Terrestrial water storage changes can be converted to (predicted) gravity changes using a simple Bouguer slab model (Telford et al., 1990), where mass changes are converted to gravity changes under the assumption that the mass is distributed as a horizontal sheet with infinite extent. This assumption is well suited to soil moisture and groundwater at flat valley sites, but the horizontal assumption is not met for hillslope sites. The terrestrial water storage at each site (Table 5.10) is used together with the Bouguer slab approximation (1 μGal equates to about 23.85 mm of water) to calculate predicted gravity (Table 5.11). Similar features to Table 5.10 can be

Table 5.11 Predicted gravity (from TWS) for the March and September/October 2005 field campaigns. Gravity predictions (μGal) are calculated using Table 5.10 and the Bouguer slab approximation.

Predicted gravity	March	September	October
RZ (CS615 0-90 cm)	6.3	12.4	11.3
IVZ (NMM 102-162 cm)	8.7	8.4	8.5
DVZ (NMM 162 cm constant to 5 m)	30.5	25.1	27.5
Total (K5)	45.5	45.9	47.3
RZ (CS616 0-90 cm)	9.1	15.9	14.7
IVZ (NMM 102-162 cm)	10.8	14.3	12.4
DVZ (NMM 192 cm to WT)	28.5	10.1	4.1
GW (WT to 5 m)	24.5	52.3	57.9
Total (K7)	72.9	92.7	89.1
RZ (CS616 0-90 cm)	9.2	13.7	13.3
IVZ (NMM 102-162 cm)	14.1	15.7	15.8
DVZ (NMM 192 cm to WT)	28.0	18.2	14.8
GW (WT to 5 m)	22.2	34.6	38.6
Total (K10)	73.6	82.1	82.6

seen in Table 5.11 (but in units of μGal). In addition, it is clear that the change at K10 between the start and end of the September/October field campaign is only 0.5 μGal, whereas at K5 it is only 0.4 μGal between March and September. At K7 a large gravity change of almost 20 μGal is predicted between March and September with the change decreasing by 3.6 μGal by the end of the September/October field campaign. The large predicted gravity change at K7 between March and September is primarily due to soil moisture with 6.8 μGal from the upper 90 cm of the profile (root zone) and 3.5 μGal from the next 90 cm (intermediate vadose zone).

Both TWS and predicted gravity (Table 5.10 and 5.11) are shown in Fig. 5.10, where the September and October predicted gravity is averaged to give a September/October field campaign prediction. The terrestrial water storage for the root zone (RZ) is shown as 0-0.9 m profile depth while the TWS for the intermediate vadose zone (IVZ) is shown as 0.9-1.8 m profile depth, and TWS below the vadose zone (DVZ and GW) is shown as 1.8-5 m profile depth (Fig. 5.10).

The changes in (total) predicted gravity (to 5 m depth) at each site (from Fig. 5.10) are shown in Fig. 5.11 together with the observed gravity changes after network adjustment (Table 5.8). Vertical error bars (from Table 5.8) are shown

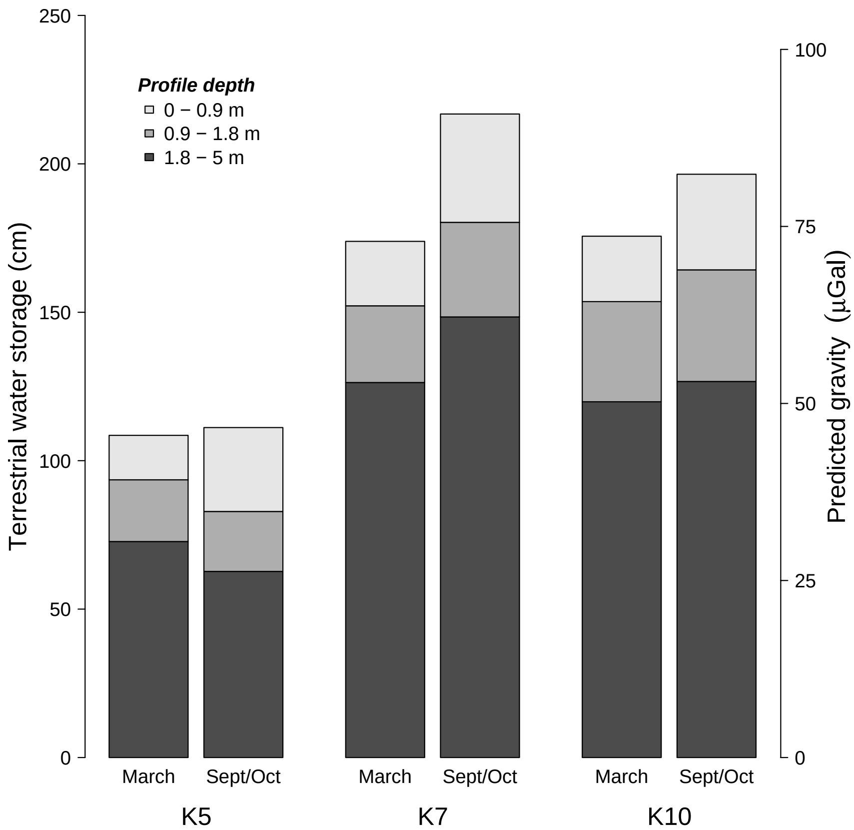

Fig. 5.10 Terrestrial water storage and predicted gravity for the March and September/October 2005 field campaigns. Gravity predictions (μGal) are calculated from TWS (cm) using the Bouguer slab approximation (approximately 1 μGal for each 2.385 cm of TWS). See Table 5.10 and 5.11 for a textual summary of the TWS components (and associated gravity predictions) at each site for each campaign.

for observed gravity, where the horizontal endpoints of the error bar caps correspond to the September and October predicted gravity (see Table 5.11).

A positive gravity change (due to increased terrestrial water storage) was expected at all sites, except perhaps K5 (the hillslope site), where the gravitational effect of upslope moisture (a reduction) could cancel the gravitational effect of moisture underneath the gravity meter (an increase). Indeed a positive gravity change is observed at all soil moisture monitoring sites (see Table 5.8 and Fig. 5.11) with the K5 change close to 0 μGal, particularly when the error of the K5 change is considered (see the BED–K5 gravity change in Table 5.7 and error bar for K5 in Fig. 5.11). However, the K7 (positive) change of 9.9 μGal is the only statistically

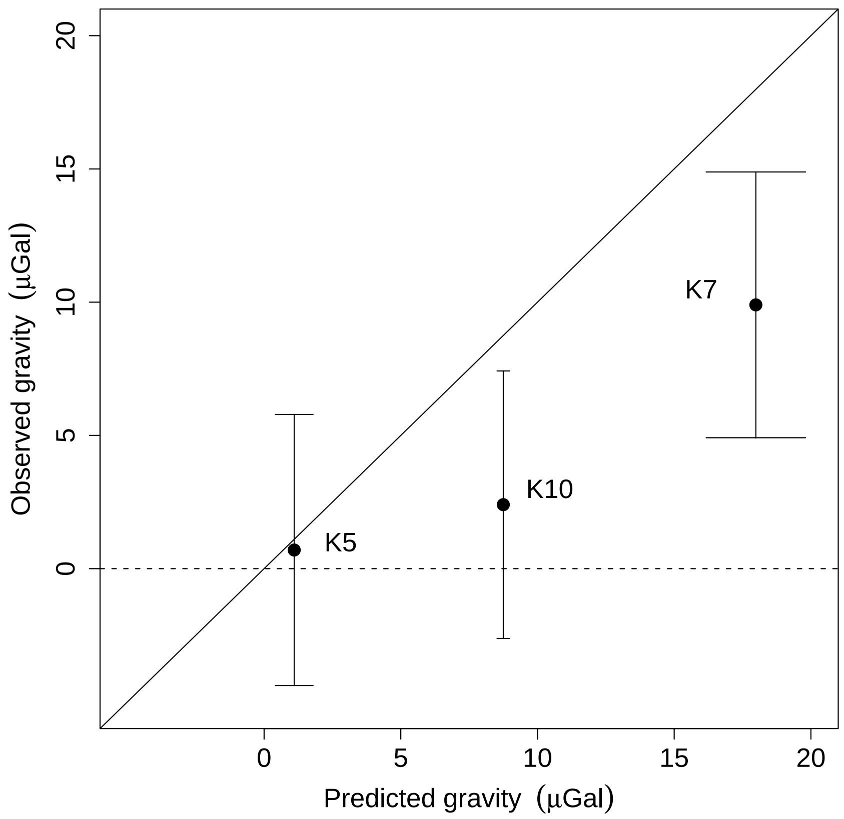

Fig. 5.11 Gravity changes (observed and predicted) between the March and September/October 2005 field campaigns. The predicted gravity is calculated with a Bouguer slab approximation using soil moisture and groundwater data (see Fig. 5.5 and 5.10, also Table 5.11). Observed gravity is the difference after network adjustment, a significant change of 9.9 µGal is observed at K7 (see Table 5.8). Error bars are calculated from Table 5.8 with the endpoints of the caps corresponding to the September and October predictions (see Table 5.11).

significant (observed) gravity change at the soil moisture monitoring sites between the two field campaigns (see Table 5.8 and Fig. 5.11). The predicted gravity change at each site is also positive, with the largest (and smallest) predicted gravity change corresponding to the largest (and smallest) gravity change at K7 (and K5), see Fig. 5.11. The predicted gravity change at K5 is particularly similar to the observed gravity change (after network adjustment) with the point lying close to the 1:1 line in Fig. 5.11. While the predicted gravity changes at all sites are greater than the observed gravity changes (Fig. 5.11), the error bar of the observed gravity is close to crossing the 1:1 line for both K10 and K7, particularly when the error bar cap widths (that represent the difference in predicted gravity from the start to the end of the September/October field campaign) are taken into consideration.

5.6 Chapter Summary

A field based experiment was used to determine if a terrestrial water storage signal can be detected in ground-based gravity data. Soil moisture and groundwater monitoring equipment and gravity pads were installed throughout the Murrumbidgee River Catchment in NSW, Australia. Gravity observations were made with a Scintrex CG-3M relative gravimeter in March (autumn) and September (spring) of 2005 (dry and wet conditions) at four sites in the Kyeamba Creek Catchment (a sub-catchment of the Murrumbidgee River Catchment). The sites were selected to have contrasting site characteristics (e.g. hillslope and valley, shallow groundwater and deep groundwater). Two gravity field campaigns were undertaken with many gravity observations at all sites, as well as at a hydrologically stable bedrock reference site at the beginning and end of each survey day to control the gravity meter drift. The gravity at each location was differenced with the gravity observation at the preceding location to form a series of gravity ties (i.e. gravity differences between sites) that were statistically adjusted to ensure gravity estimates at each site are consistent and precise.

A t-test was conducted to establish whether a statistically significant change in gravity had occurred. A significant increase in gravity of 9.9±3.6 μGal was found at one site, K7, a valley site with silt loam soil and a shallow water table. This corresponded to an estimated gravity change of 18±1.8 μGal based on observed TWS and the Bouguer slab approximation. Of the 18 μGal gravity change at K7, approximately 8.7 μGal is due to soil moisture changes with 6.2 μGal in the top 90 cm of the soil profile. While a statistically significant change in ground-based gravity was not detected at the other two sites (K5 and K10), the observed gravity change of 0.7 μGal) at the hillslope site K5 was close to 0 μGal as expected due to upslope and downslope soil moisture signals in ground based gravity cancelling with opposite signs. Likewise, the observed and predicted gravity at K10 were quite similar, with an observed change of 2.4 μGal and a change of 8.8 μGal estimated from TWS observations. The estimated gravity change at both of the valley sites is larger than the observed gravity change, while at the hillslope site with no observed groundwater level the estimated and observed gravity changes are very similar. This indicates the water storage change from the increase in the groundwater level at the valley sites may be overestimated.

Extensive analysis to achieve a high precision gravity change (Chapter 4), and a combined 22 days of field observations was not able to reduce the error of the gravity change (at a site) below 3.6 μGal (or 86 mm TWS). Consequently for the technique to be applied the change in TWS must be around 100 mm or greater. Therefore the method is applicable to seasonal monitoring of sites with large TWS changes, such as the alluvial sites monitored in this thesis. For the technique to be more widely applicable an increase in gravimeter precision is required.

Chapter 6

Retrieving the Soil Moisture Profile from Gravity Data

Based on the assumption that a terrestrial water storage signal can be observed using ground-based gravity measurements (Chapter 5), this chapter tests the hypothesis that this signal can be used to derive the soil moisture profile.[1] A case study is investigated that uses a controlled scenario with a known soil moisture profile and groundwater evolution, at a grass covered valley site (K10) with silt loam soil in a temperate climate that was previously shown to contain a terrestrial water storage (TWS) signal in ground-based gravity data. To provide a long time series of gravity data, a gravity signal is modelled from the TWS measurements at the field site (soil moisture and groundwater level) using the Bouguer slab approximation.

The approach taken is to assimilate the gravity data into the CABLE land surface model using a variational data assimilation method. The model independent parameter estimation software PEST is used to adjust the modelled state value of soil moisture at the start of moving assimilation windows by minimising the gravity residual. The gravity residual is the difference of gravity predicted by CABLE (using modelled TWS) and gravity observations generated from the (field) observations of TWS. Consideration is given to the size of the assimilation window, the type (and frequency) of gravity observation, and the benefit of additional near-surface soil moisture observations (that could be provided by a hand-held probe or remotely

[1] Parts of this chapter have been published in the peer-reviewed conference paper Smith et al. (2011).

sensed soil moisture). The case studies are compared to an open loop model run with degraded atmospheric forcing (such as may be provided by NWP data) illustrating a worst case scenario. The success of the soil moisture retrieval is assessed against the field observations of soil moisture and groundwater level used to derive the gravity signal.

6.1 Land Surface Model

The CSIRO Atmosphere Biosphere Land Exchange (CABLE) land surface model is a third generation model in the classification of Pitman (2003); that is leaf conductance and carbon assimilation is modelled. CABLE has six layers for representing the soil moisture and temperature, using Richard's and the heat equation respectively (with layer depths from the surface of 2.2, 8, 23.4, 64.3, 172.8 and 460 cm). Additionally, there is a 3 layer snowpack module that solves for albedo at the surface, as well as temperature, density and thickness of each layer. Permafrost (frozen soil) is also modelled (Kowalczyk et al., 2006). CABLE has a single (above ground) canopy consisting of two "big" leaves (shaded and sun-lit) for calculation of stomatal conductance, photosynthesis and leaf temperature for each "big" leaf (Wang and Leuning, 1998; Wang, 2000), and a turbulence model to calculate within canopy air temperature and humidity (Raupach et al., 1997).

CABLE uses the Clapp and Hornberger (1978) soil water retention curve

$$\psi = \psi_S \left(\frac{\theta}{\theta_S} \right)^{-b} \tag{6.1}$$

and corresponding hydraulic conductivity (Campbell, 1974)

$$K = K_S \left(\frac{\theta}{\theta_S} \right)^{2b+3} \tag{6.2}$$

to model soil moisture movement in the profile, where ψ, θ, and K are soil suction, moisture and hydraulic conductivity, and ψ_S, θ_S, and K_S are the same variables at soil saturation. After the moisture based form of Richard's equation has been split into its advective and diffusive parts, CABLE uses the total variation diminishing

(TVD) method (Durran, 1999) with a Superbee flux limiter (Roe, 1985) to solve the advective equation (Kowalczyk et al., 2006). This solution is used as an initial condition for the diffusion equation that is solved using an implicit finite difference method.

CABLE uses a moisture based formulation of the Richard's equation. Consequently groundwater level is not explicitly modelled, but represented by saturation of the soil layers. Furthermore CABLE is only able to accept a single set of soil parameters for the profile.

6.2 Data

The data requirements for soil moisture retrieval from ground-based gravity data using a land surface model and data assimilation include:

- atmospheric forcing data to drive the land surface model;
- perturbed forcing data to create degraded model runs representing the forcing data quality typically available (e.g. from a NWP model);
- data sets to provide soil and vegetation parameters to the land surface model;
- initial conditions for the land surface model states (soil moisture and soil temperature amongst other prognostic variables);
- soil moisture and TWS data to assess the soil moisture retrieval; and finally
- gravity (and near-surface soil moisture) data to assimilate.

6.2.1 Forcing

CABLE requires atmospheric forcing data including: precipitation, air temperature and pressure, relative humidity, wind speed, and downward short and long wave radiation at hourly (or finer) temporal resolution. This data could be obtained for any soil moisture monitoring site by using the output of an NWP model (e.g. ECMWF or ACCESS). If available, ground-based atmospheric observations should provide more accurate forcing for the land surface model. For this study half-hourly forcing data is derived primarily from an automatic weather station (AWS) at the Wagga Wagga airport, located approximately 20 km north of the study site. The AWS data includes precipitation, air and dew point temperature, mean sea level pressure, wind speed and direction, and is complemented by cloud cover and radiation observations. Relative humidity is calculated from air and dew point temperature data. Screen level (2 m) wind speed is calculated from 10 m observations assuming a logarithmic wind profile (Richter et al., 2004). Further details on data checking, infilling and processing can be found in Siriwardena et al. (2003). Downward long wave radiation is calculated from air temperature, emissivity (set at 0.96), relative humidity, and fraction of cloud cover. Downward short wave radiation is measured with a pyranometer. The Wagga Wagga airport AWS data from January 2000 (earliest available) to December 2004 is used as land surface model forcing.

Local forcing data (within 200 m) is available for 2005 from an eddy correlation flux station (Pipunic et al., 2013). This data consists of half-hourly long and short wave radiation measured with a net radiometer, air temperature and relative humidity, barometric pressure, and wind speed.

Precipitation from the AWS is used for 1 January 2000 to 14 November 2001, when a soil moisture monitoring site (K4) was installed approximately 12 km to the south of the study area. The rainfall from that site is used from 14 November 2001 until 5 December 2003, at which time the soil moisture monitoring site used for this study (K10) was commissioned. The precipitation from K10 is used from 5 December 2003 to the end of December 2004. Precipitation from the flux station is used for the year 2005. Rainfall was measured at all locations (AWS, two soil moisture sites, and flux station) with a 0.2 mm resolution tipping bucket raingauge.

6.2.2 Perturbed Forcing

Two open loop scenarios are considered, both using perturbed forcing from Pipunic et al. (2013), generated using the Turner et al. (2008) method that (stochastically) assigns a prescribed error to each individual forcing variable. Error ranges for each forcing variable, based on recommendations of an expert (John Gorman, pers. comm., 2006, Australian Bureau of Meteorology), are used to generate an ensemble of forcing data (Pipunic et al., 2008). From twenty ensemble members two extreme cases are selected for the year 2005, one with 243 mm of annual rainfall (denoted DRY) the other with 1219 mm (denoted WET) these compare to average annual observed rainfall of 595 mm.

6.2.3 Parameters

Soil and vegetation parameters provided with the land surface model are based on the 2 ° resolution global datasets used by Potter et al. (1993). Soil parameters are derived from the FAO/UNESCO soil map of the world for 9 soil types (Zobler, 1999). Similarly, vegetation parameters are provided for 13 vegetation classes (Dorman and Sellers, 1989). The default soil and vegetation parameters were augmented with leaf area index (LAI), calculated from remotely sensed (AVHRR) 0.05 ° resolution monthly average woody and herbaceous fractional cover for the period 1981-1994 (Lu et al., 2003).

The model (soil) parameters that affect soil moisture prediction are tuned for the site, to improve predictive capacity (Table 6.1). Soil type is the dominant 0-90 cm soil type from Table 5.1 (see also Fig. B.2) determined from 0-30, 30-60 and 60-90 cm soil samples and particle size analysis. Clay, silt and sand fractions are an average of 0-30, 30-60 and 60-90 cm fractions observed at K10 (Table 5.1). Soil hydraulic properties are sourced from a high resolution soil survey (Fig. 5.4) of the Kyeamba Creek catchment (John Gallant, pers. comm., 2002, CSIRO Land and Water) and are average A horizon parameters for the O'Briens Creek soil unit (ob), as the B horizon parameters are sparse and unreliable (Smith and Zhang, 2007). The soil parameters sourced from the high resolution map include bulk density,

Table 6.1 Land surface model soil parameters (default and tuned) at K10.

Parameter	Default	Tuned
Soil type	Sandy Loam	Silt Loam
Clay, silt, and sand fraction (%)	20, 20, 60	9.4, 48.2, 42.4
Bulk density (g/cm^3)	1.60	1.56
Specific heat (J/kg/K)	850	871
Thermal conductivity (W/m/K)	0.283	0.278
Albedo	0.1	0.1
Wilting point (% vol/vol)	13.5	6.9
Field capacity (% vol/vol)	21.8	35.6
Saturation (% vol/vol)	44.3	38.3
Saturated hydraulic conductivity (mm/h)	75.6	30
Saturated soil suction (m)	-0.348	-0.802
Campbell's b parameter	5.15	3.05
Root fraction (%) for model layer 1, 2, 3, 4, 5, 6	5, 15, 34, 38, 6, 2	5, 15, 34, 38, 6, 2

saturated hydraulic conductivity, field capacity (soil moisture at 0.1 bar soil suction) and wilting point (soil moisture at 15 bar soil suction). Saturation θ_S is calculated from bulk density ρ_b using

$$\rho_b = 2.65 \left(1 - \frac{\theta_S}{0.93}\right) \tag{6.3}$$

where 2.65 is the particle density and 0.93 is an air-entrapment factor (Williams et al., 1992). Campbell's b parameter is given by the soil water retention curve (Eq. 6.1) after solving simultaneous equations for field capacity and wilting point. Similarly soil suction at saturation is calculated from the soil water retention curve using Campbell's b, saturation and field capacity. The specific heat capacity of silt loam is taken from Ochsner et al. (2001). Thermal conductivity is calculated (by the model) from clay, silt and sand fraction. Bare soil albedo and root fraction in each model layer are left unchanged due to an absence of data.

6.2.4 Initialisation and Evaluation

Soil moisture and soil temperature of the land surface model are seeded from output of the global (coupled) Conformal-Cubic Atmospheric Model (C-CAM) (McGregor, 2005). CABLE is then initialised by spinning up ten times over the year 2000 and run through to the end of the year 2005. The forcing of Siriwardena et al. (2003) is used for 2000 to the end of 2004 and that of Pipunic et al. (2013) for 2005.

The land surface model (and later the soil moisture retrieval) is assessed against 0-30, 30-60 and 60-90 cm soil moisture data (Smith et al., 2012) for a valley site (K10) in the temperate Kyeamba creek catchment (part of the Murray Darling Basin) Australia (Fig. 3.1 and fig:MurrumStack). While a consistent bias is present (more severe in the deeper layers), the model simulates the variability of the soil moisture well (Fig. 6.1). Furthermore, the observations (with the exception of the wetter portion of the 60-90 cm soil moisture) fall within the model parameter limits (of wilting point, field capacity and saturation). The bias in the deeper layers is a result of using A horizon (average depth of 30 cm) soil parameters throughout the soil column (to a depth of 4.6 m). This is necessary as the model uses a moisture based formulation of Richard's equation and consequently is limited to a single set of

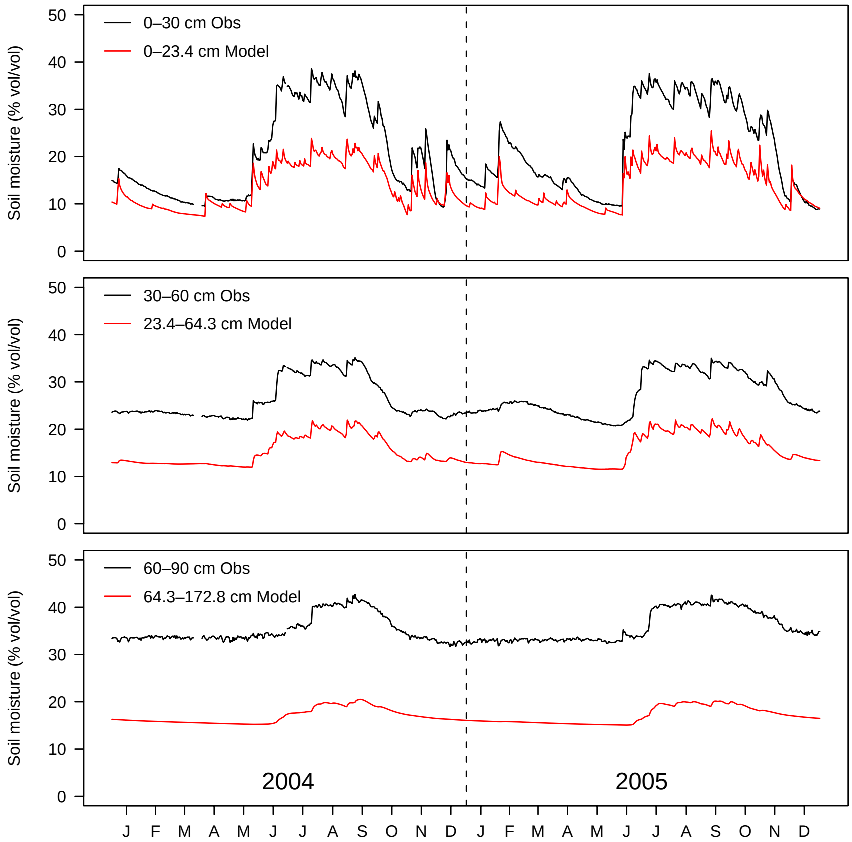

Fig. 6.1 Evaluation of CABLE soil moisture prediction at K10 for 2004 and 2005. The three panels are 0-30, 30-60, and 60-90 cm soil moisture, with the top three model layers aggregated (to 0-23.4 cm) for the top panel, while the second and third panel use the fourth (23.4-64.3 cm) and fifth (64.3-172.8 cm) model layers respectively. Model predictions (Model) are in red, observations (Obs) in black. The model predictions use the tuned parameters from Table 6.1.

soil parameters (Talbot et al., 2004), and the B horizon soil parameters are unreliable (Smith and Zhang, 2007).

6.2.5 Gravity

Gravity is synthetically generated from TWS observations using the Bouguer slab approximation. This approximation is derived by calculating the gravitational attraction of a vertical cylinder (below the surface) and extending the radius to infinity (Telford et al., 1990). The gravitational attraction of a slab is proportional to its density and thickness. There is a change in gravity if density is held constant with a change in height (i.e. water table fluctuations), or if thickness is maintained and density varied (i.e. vertical soil moisture changes).

Specifically, gravity due to soil moisture g_{SM} (μGal) is

$$g_{\mathrm{SM}} = 41.92\theta H, \tag{6.4}$$

where θ is volumetric water content and H is thickness of the soil profile (m). Gravity due to groundwater g_{GW} (μGal) is

$$g_{\mathrm{GW}} = 41.92 S_y H, \tag{6.5}$$

where S_y is specific yield and H is height (above bedrock) of the water table (m). Both Eq. 6.4 and 6.5 simply state that change in gravity is proportional to change in (hydrological) mass (section 2.1).

Gravity varies both temporally and spatially, and is a function of: (i) latitude and elevation; (ii) Earth and oceanic tides; (iii) subsurface, surface and atmospheric mass distribution and density (Chapter 2 and 4). It is assumed in this study that the gravity data has been corrected for all other effects (Chapter 4) and therefore is a measure of subsurface hydrological mass (or TWS) only (Chapter 5).

A few types of synthetic gravity observations are generated. One is a difference of monthly averages representing repeated field campaigns with a relative gravimeter (Chapter 5) or expected GRACE observations (Swenson and Wahr, 2002), another is an anomaly representing repeated field campaigns with an absolute gravimeter (e.g. Jacob et al. (2008, 2009, 2010)) or the product actually generated by each GRACE data centre (e.g. Zaitchik et al. (2008)). A ten day anomaly is also generated representing a permanently installed absolute gravimeter (e.g. Kazama and Okubo (2009)) or SG (e.g. Wilson et al. (2012)) or the newer increased temporal resolution GRACE product of Bruinsma et al. (2010).

Gravity is generated using 0-30, 30-60 and 60-90 cm soil moisture and groundwater level observations. The 0-30 and 30-60 cm soil moisture is converted to a 0-60 cm (water) mass by multiplying the volumetric soil moisture with the depth of measurement. The 60-90 cm soil moisture observation is converted to a 60 cm to water table hydrological mass, assuming that the 60-90 cm soil moisture represents moisture from 60 cm to the water table. The water table above an arbitrary datum of 4.6 m is converted to hydrological mass using specific yield equal to the maximum observed 60-90 cm soil moisture (an estimate of soil saturation). The 0-60 cm, 60 cm to water table, and groundwater hydrological masses are summed to give TWS. The TWS is converted to gravity using the Bouguer slab approximation constant of proportionality (see Eq. 6.4 and 6.5). Half-hourly absolute gravity values are averaged over a month (or ten days) and the averages used to create gravity anomaly and difference products, these are assimilated as gravity observations.

As the CABLE land surface model implicitly models groundwater through saturated soil layers, the predicted gravity (and TWS) is calculated by summing soil moisture over the model depth (4.6 m)

$$g_{\text{mod}} = 41.92 \sum_{i=1}^{6} \theta_i z_i, \tag{6.6}$$

where θ_i is modelled (volumetric) soil moisture for CABLE layer i and z_i is thickness of that layer. Similarly, gravity observations are calculated from observed soil moisture and groundwater by

$$g_{\text{obs}} = 41.92 \left[(\theta_{0-30} + \theta_{30-60})\, 30 + \theta_{60-90} (WT - 60) + \theta_{60-90}^{max} (460 - WT) \right], \tag{6.7}$$

where θ_{k-l} is observed soil moisture from k to l cm and WT is the observed water table depth (positive downwards). Note the observed WT is always less than 4.6 m.

6.2.6 Near-Surface Soil Moisture

It is hypothesised that additional near-surface soil moisture observations may improve the soil moisture retrieval from ground-based gravity data. The near-surface soil moisture observations could easily be measured with a hand held probe at the same time as the ground-based gravity observation, or alternatively provided by a remotely sensed soil moisture product such as from AMSR-E (Njoku et al., 2003). The near-surface soil moisture observations assimilated are 0-8 cm soil moisture from the flux tower site used for forcing (section 6.2.1). The soil moisture observations are an instantaneous observation (actually thirty minute average) every three days (at 1:30 AM local time), chosen to coincide with the worst case repeat time (and descending overpass) of the AMSR-E satellite (Njoku et al., 2003).

6.3 Data Assimilation

Variational data assimilation is a natural choice for observations that are temporal averages, as this method adjusts all predictions in the assimilation (or averaging) window to minimise the difference between predictions and observations at the times of the observations (see Fig. 6.2 (a)). Change in model predictions is achieved by adjusting the model states at the **start** of the assimilation window, allowing the state updating to propagate through the window via model dynamics. In contrast, sequential assimilation updates the model states at the time of observation, or in the case of an observation that is a temporal average, at the **end** of the assimilation window (see Fig. 6.2 (b)). This causes a problem in that, unlike variational assimilation, there is no control over almost all of the model prediction that is creating

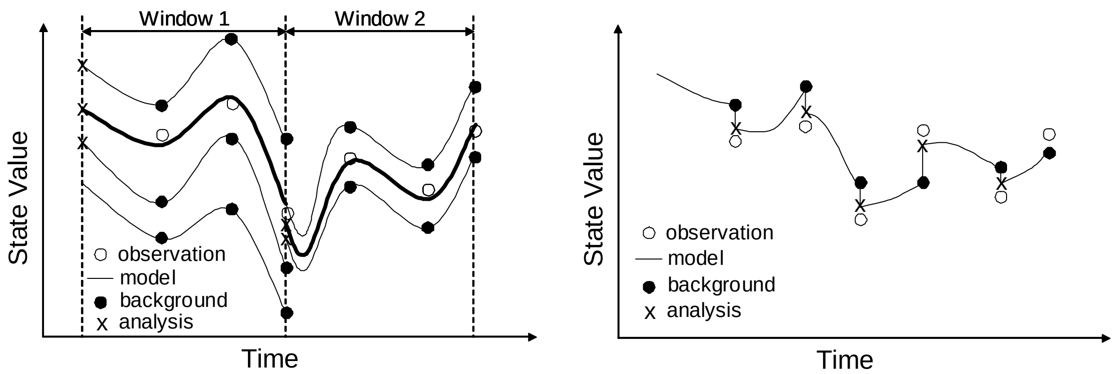

(a) Variational assimilation. (b) Sequential assimilation.

Fig. 6.2 Variational and sequential assimilation (from Walker and Houser (2005)). For variational assimilation (a) the model predictions are adjusted over an assimilation window until the residual between predictions and observations is minimised (the bold line) giving new initial conditions (analysis) for the forecast. In sequential assimilation (b) the model predicts deterministically until encountering an observation, at which point the observation is assimilated, giving an analysis that is used as a starting point (initial conditions) for further model predictions.

the modelled observation (or background) to compare with the real observation. The only point adjusted by sequential assimilation is the last point of the averaging window (assuming of course that the temporal average is associated with the end time of the averaging window). Zaitchik et al. (2008) minimised this problem when assimilating remotely sensed (GRACE) gravity data by updating the fifth, fifteenth and twenty-fifth day of the month (assimilation window) simultaneously using the Ensemble Kalman Smoother. However, this method is heuristic with no theoretical basis on which to choose the proportion of the innovation (assimilation adjustment) that is partitioned between the three pseudo-observation times.

6.3.1 Variational Assimilation

The approach used for the data assimilation is a brute force variational method similar to Calvet and Noilhan (2000), Sabater et al. (2007) and Rüdiger (2007), using the model independent parameter estimation software PEST (Doherty, 2010). PEST adjusts user specified parameters to minimise the sum of squares of differences between model predictions and observations over a fixed window using the Levenberg-Marquardt algorithm.

To coincide with the observation duration (a monthly gravity average), the assimilation window is one month. The retrieved parameters are initial soil moisture conditions for the window. The assimilation window moves through one year (2005) retrieving soil moisture at the beginning of each month that best corresponds to gravity observations for that month.

6.4 Soil Moisture Retrieval

Soil moisture retrieval from ground-based gravity is investigated through a series of case studies at one site during the year 2005. The case studies use gravity anomalies computed from TWS with 2004 as the background mean, and/or near-surface soil moisture. The TWS is computed from 0-30, 30-60 and 60-90 cm soil moisture observations together with water table height (groundwater depth) observations at the site for 2004 and 2005. Near-surface soil moisture is simply observed 0-8 cm soil moisture at the flux station (used for the 2005 forcing) within 200 m of the site. The case studies include:

a) gravity anomalies;

b) both gravity anomalies and near-surface soil moisture observations;

c) near-surface soil moisture only;

d) differencing gravity anomalies to obtain a change in gravity;

e) absolute gravity observations; and

f) gravity anomalies with a bias.

All case studies are investigated using a monthly (sliding) assimilation window. In addition, cases (a) though (c) are investigated using a two month window and a higher resolution ten day gravity anomaly with a narrower ten day assimilation window.

The land surface model parameters, initial conditions and forcing of the open loop and assimilation runs are identical. The only difference between open loop and assimilation runs is that gravity and/or near-surface soil moisture observations are assimilated (according to the cases above). The optimisation scheme of the variational assimilation adjusts the (log of) soil moisture for the first time step of the assimilation window. The "initial" soil moisture is adjusted for model layers 1, 4, 5 and 6, with the initial soil moisture of the second and third model layers computed as a fixed ratio of the (adjusted) soil moisture of the first layer. This ratio is that observed at the end (last timestep) of the previous assimilation window.

The second and third model layers are tied to the first due to a strong correlation that results in very similar monthly averages for all three layers over the assimilation period. In addition to ratios of soil moisture from the end of the previous assimilation window (for layer 1 and layer 2, and layer 1 and layer 3), the four soil moisture states (model layers 1, 4, 5, and 6) are also used as a prior (effectively assimilated as additional observations). The previous soil moisture is used as a prior to make the assimilation smoother, both temporally and vertically throughout the profile. Both using a prior (increasing the number of observations) and tying the top three model layers (reducing the number of estimated model states) improves the identifiability of the states and consequently the performance of the soil moisture retrieval.

6.4.1 1 Month Assimilation Window

Gravity Anomaly Data

The first soil moisture retrieval experiment investigated the use of (monthly) gravity anomalies with a one month assimilation window. Both observed and model predicted anomalies use the average gravity of 2004 as a background mean. Average gravity for a month is differenced with the background mean to generate a gravity anomaly. Gravity is calculated from TWS using Eq. 6.6 for the model and Eq. 6.7 for observations. Results of the gravity anomaly assimilation using a monthly window are shown in Fig. 6.3. The gravity anomaly assimilation consistently improved soil moisture (over all depths) and also TWS estimates. There is modest improvement in soil moisture estimates in the drier first half of the year (January to June) with larger improvements evident in the wetter portion of the year (July through to December). It should be noted that the improvement in soil moisture estimates at the end of the year (last timestep) are larger than at the beginning (due to the assimilation and open loop starting with the same initial conditions) therefore larger improvements in the soil moisture retrieval would be expected in the following (and subsequent years) if the assimilation period were to be extended. The bias evident in open loop predictions is reduced, though still present, in the assimilation runs with gravity anomaly assimilation clearly unable to significantly improve bias. However, variability of the observations is well retrieved particularly for TWS and 60-90 cm soil moisture.

Gravity Change Data

Next gravity changes (from one month to the next) are assimilated using a one month assimilation window. When using gravity changes there are only eleven observations for the year (rather than twelve for the anomalies), so it is expected that soil moisture retrieval will be slightly worse, and this is indeed shown to be the case (Table 6.2-6.5). Gravity change results are not plotted as they are very similar to the anomaly results, although for the gravity change results the open loop and assimilation runs are identical in January (Appendix G). A change in gravity can be used without knowledge of the background mean used as the datum for the anomalies.

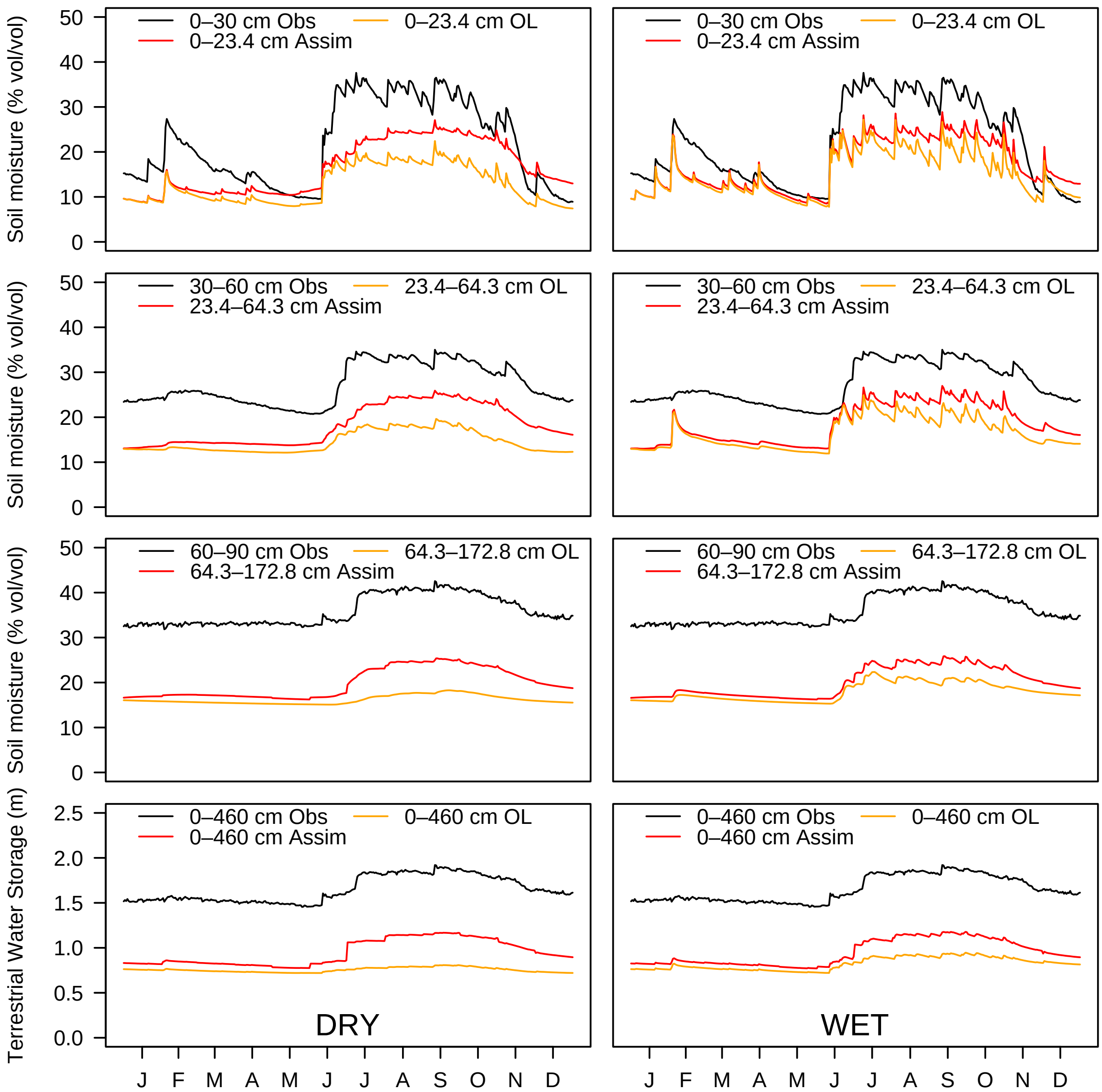

Fig. 6.3 K10 gravity anomaly assimilation results for 2005 using a one month assimilation window (case 1Ma in Table 6.2-6.5) with dry and wet forcing (left and right columns). Top three panels are 0-30, 30-60, and 60-90 cm soil moisture. The top three model layers are aggregated (to 0-23.4 cm) for the first panel. The second and third panels use the fourth (23.4-64.3 cm) and fifth (64.3-172.8 cm) model layers respectively. Bottom panel is terrestrial water storage (TWS) that is an aggregate of soil moisture and groundwater to 4.6 m. Assimilation (Assim) and open loop (OL) runs are in red and orange, observations (Obs) in black.

Gravity Anomaly Data with Model Bias

To investigate the effect of model bias on gravity data assimilation an experiment was conducted that assimilated the same gravity anomalies as above (generated using 2004 as the background mean), but the model predicted gravity anomalies with respect to a (lower) background mean (generated using the average gravity from 2002). This year was chosen as it is a period of severe drought. Consequently, the TWS (and gravity) is much lower than for the correct year of the background mean (2004). Results for this experiment are again visually similar to the first case and are subsequently not plotted (but see Table 6.2-6.5). A distinction is that the bias in deeper soil moisture layers and TWS is made worse. That is, data assimilation of gravity anomalies when the background mean predicted by the model is incorrect no longer improves the soil moisture retrieval (or TWS) for all depths at all times. The dry bias in the background mean introduced a dry bias in the soil moisture retrieval.

Absolute Gravity Data

An experiment was conducted in which anomalies were added to the background (open loop) mean for the assimilation period (2005). This experiment uses an observation type similar to that used in Zaitchik et al. (2008). Again results for this case are not plotted, being similar to cases discussed previously (a, d, and f). The results are particularly similar to those from gravity anomaly assimilation when an incorrect background mean is used by the model (i.e. a modelled TWS bias). This was expected as the absolute gravity assimilation case is essentially equivalent to assimilating an anomaly that uses 2004 as the background mean, but with model predicted anomalies using the average gravity from 2005 as a background mean. The performance of the absolute gravity assimilation is somewhat better than that of gravity anomaly assimilation when the wrong period is used for the background mean (Table 6.2-6.5). This is primarily due to the background means for 2004 and 2005 being very similar, as the soil moisture (and precipitation) is almost the same for both years (Fig. 6.1).

Table 6.2 Soil moisture retrieval bias using dry open loop forcing. Different cases are one, two month and ten day assimilation windows (1M, 2M, and 10D respectively) using: gravity anomalies (a); both gravity anomalies and near-surface soil moisture (b); near-surface soil moisture (c); gravity change (d); absolute gravity computed like Zaitchik et al. (2008) with anomalies added to the open loop background mean (e); and gravity anomalies with incorrect background mean (f). Results are assessed against 0-30, 30-60 and 60-90 cm soil moisture observations (% vol/vol), and total terrestrial water storage (m). Open loop values are given as case 0OL.

Case	0-30 cm	30-60 cm	60-90 cm	TWS
0OL	-9.4	-12.8	-19.8	-0.90
1Ma	-5.5	-9.1	-16.1	-0.71
1Mb	-1.2	-5.0	-12.2	-0.60
1Mc	-0.9	-4.7	-11.3	-0.50
1Md	-7.0	-10.5	-17.5	-0.77
1Me	-8.4	-12.2	-19.2	-0.87
1Mf	-8.5	-12.3	-19.3	-0.87
2Ma	-6.9	-11.7	-17.7	-0.71
2Mb	-1.6	-5.3	-12.3	-0.54
2Mc	-0.6	-4.2	-11.7	-0.43
10Da	-5.5	-9.1	-16.2	-0.71
10Db	-1.9	-5.8	-12.5	-0.67
10Dc	-0.6	-4.4	-10.8	-0.49

Table 6.3 Same as Table 6.2 but using wet open loop forcing.

Case	0-30 cm	30-60 cm	60-90 cm	TWS
0OL	-7.0	-10.7	-18.1	-0.83
1Ma	-5.0	-8.7	-15.9	-0.71
1Mb	-0.5	-4.4	-11.4	-0.56
1Mc	0.0	-3.7	-10.6	-0.41
1Md	-5.9	-9.7	-17.0	-0.77
1Me	-6.2	-10.1	-17.5	-0.80
1Mf	-6.9	-11.0	-18.6	-0.87
2Ma	-5.6	-10.1	-17.4	-0.71
2Mb	-0.8	-4.6	-12.0	-0.54
2Mc	0.2	-3.4	-10.7	-0.42
10Da	-5.0	-8.7	-15.9	-0.71
10Db	-1.1	-4.8	-11.8	-0.67
10Dc	0.4	-3.1	-10.2	-0.41

Table 6.4 Same as Table 6.2 but for variance rather than bias.

Case	0-30 cm	30-60 cm	60-90 cm	TWS
0Obs	87.0	20.6	11.1	0.02
0OL	17.5	5.8	0.9	0.00
1Ma	33.9	19.5	10.8	0.02
1Mb	51.7	38.0	31.3	0.08
1Mc	60.0	46.3	34.9	0.08
1Md	33.0	18.2	9.9	0.02
1Me	26.2	15.2	8.1	0.02
1Mf	25.8	14.9	8.0	0.02
2Ma	30.2	31.5	19.1	0.02
2Mb	53.8	40.2	30.0	0.07
2Mc	64.8	49.1	50.2	0.07
10Da	34.6	20.1	11.3	0.02
10Db	43.1	33.9	18.8	0.04
10Dc	62.6	50.8	33.5	0.09

Table 6.5 Same as Table 6.4 but using wet open loop forcing.

Case	0-30 cm	30-60 cm	60-90 cm	TWS
0Obs	87.0	20.6	11.1	0.02
0OL	23.6	12.1	4.3	0.00
1Ma	32.9	19.7	10.9	0.02
1Mb	46.0	34.5	27.0	0.08
1Mc	49.1	36.5	28.8	0.05
1Md	30.9	18.9	10.4	0.02
1Me	29.8	18.4	10.1	0.02
1Mf	26.8	17.0	9.4	0.02
2Ma	29.5	26.1	19.0	0.02
2Mb	47.7	34.4	28.6	0.07
2Mc	51.6	36.6	33.0	0.06
10Da	33.2	20.0	11.2	0.02
10Db	35.2	23.7	19.5	0.04
10Dc	50.0	35.7	31.6	0.07

Gravity Anomaly and Near-Surface Soil Moisture Data

As gravity anomaly assimilation gives the best results, this is used in conjunction with near-surface soil moisture (observed every three days) to see if using both data sets gives further improvement in soil moisture retrieval. Assimilating both gravity anomalies and near-surface soil moisture dramatically increases the performance of the soil moisture retrieval (Fig. 6.4 and Table 6.2-6.5).

When using both gravity anomalies and near-surface soil moisture the retrieved soil moisture is very close to the 0-30 and 30-60 cm soil moisture observations (more so in the wet half of the year for the 30-60 cm observations). The retrieved 60-90 cm soil moisture and TWS are also quite close to observations in the second (wetter) half of the year (Fig. 6.4).

Bias is reduced over all depths (Table 6.2 and 6.3) and the 0-30 cm variability is improved (Table 6.4 and 6.5). However, variability for 30-60 and 60-90 cm soil moisture and TWS is significantly degraded (Table 6.4 and 6.5), and the soil moisture retrieval is no longer as smooth (temporally) as the open loop or observed (Fig. 6.4).

The rapid reduction in assimilated soil moisture for February and March (particularly evident at 60-90 cm) indicates that the data assimilation of gravity anomalies and near-surface soil moisture is successfully retrieving observed soil moisture, but the model is quickly restoring its preferred states as it dynamically evolves through the assimilation window. This appears to be a result of model parameters and may be due to saturated hydraulic conductivity (and possibly also Campbell's b parameter) being set too high. In the wetter part (second half) of the year there is enough precipitation (and evapotranspiration has reduced sufficiently) that the model can no longer dry out the soil moisture states, and the retrieved TWS increases as well.

There remains a consistent (negative) bias in the 60-90 cm soil moisture and TWS for July, August and September (Fig. 6.4), due to the bias between the observed and modelled background mean. This bias in the background mean is a result of the bias in the land surface model (Fig. 6.1), again indicating that improving soil moisture prediction of the model (possibly by using more accurate model parameters) will improve the soil moisture retrieval of the gravity data assimilation.

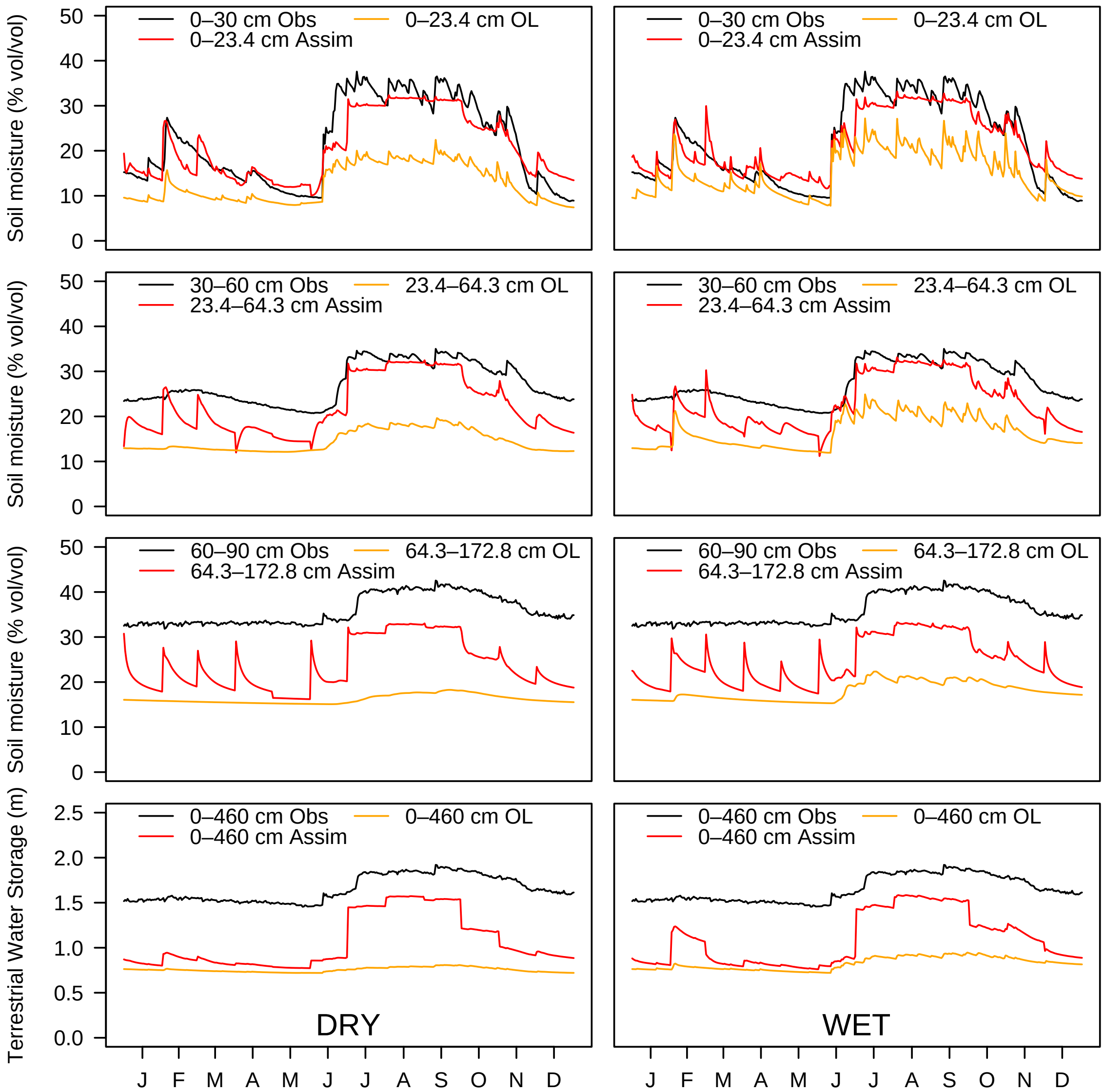

Fig. 6.4 As for Fig. 6.3 but using both gravity anomalies and near-surface soil moisture observations (case 1Mb in Table 6.2-6.5).

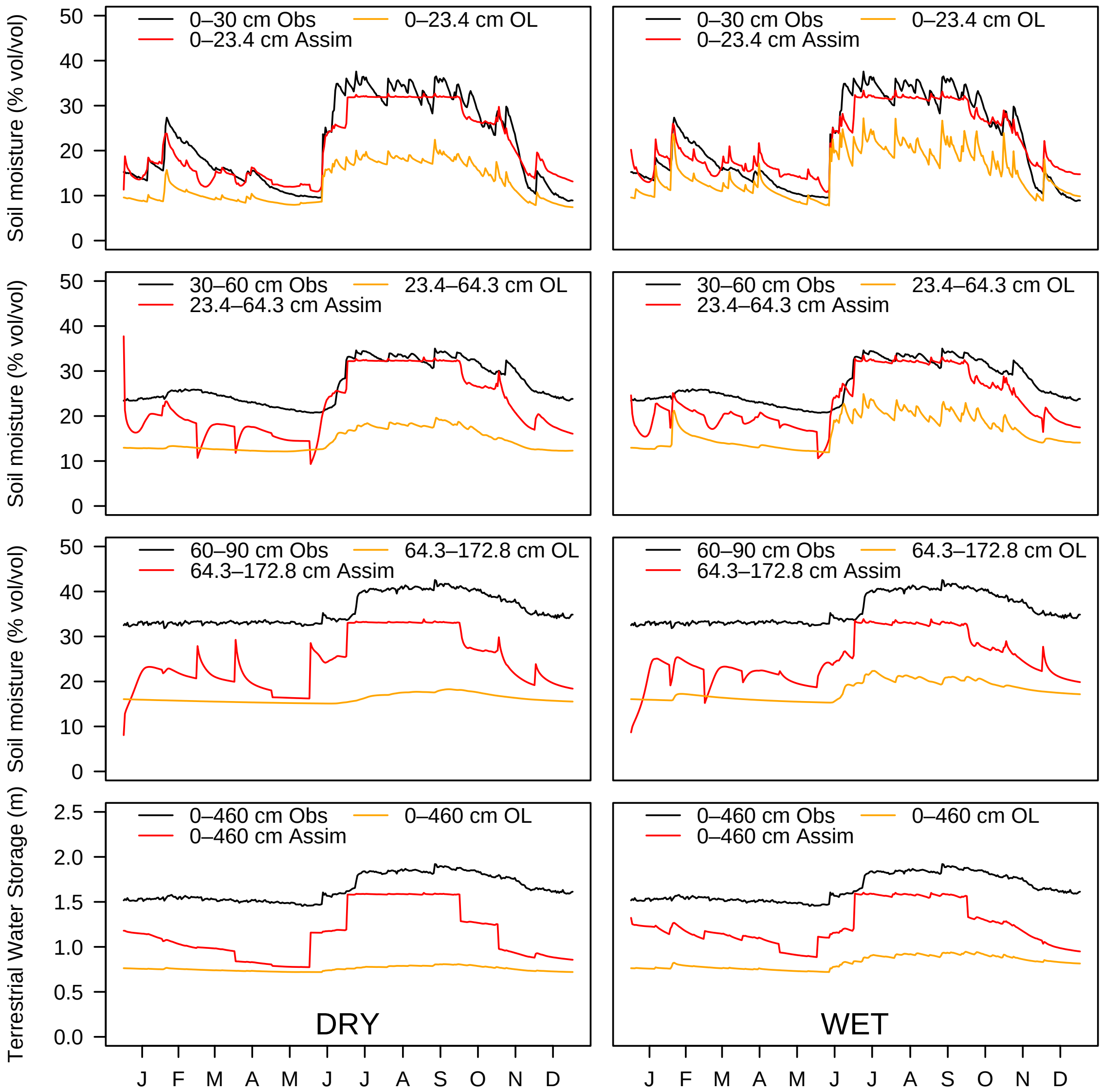

Fig. 6.5 As for Fig. 6.3 but using near-surface soil moisture observations instead of gravity anomalies (case 1Mc in Table 6.2-6.5).

Near-Surface Soil Moisture Data

For completeness, only near-surface soil moisture is also assimilated to see if assimilating both gravity anomalies and near-surface soil moisture gives a better soil moisture retrieval than assimilating either data type individually. Near-surface soil moisture assimilation appears to give the best results visually (Fig. 6.5) and this is reflected in the bias reduction (Table 6.2 and 6.3) and lowest RMSE of all six cases (RMSE is not shown as it is dominated by the large bias and shows the same trends as Table 6.2 and 6.3). However (except for 0-30 cm soil moisture) variance is further degraded compared to the open loop and gravity assimilation cases (Table 6.4 and 6.5). Assimilation of near-surface soil moisture gives the best result (smallest RMSE and bias) of all cases (a) through (f) due to the model using A horizon (average depth of 30 cm) soil parameters throughout the soil profile to a depth of 4.6 m. These A horizon parameters are not suitable below 30 cm and introduce a (negative) bias in the modelled TWS (and gravity) and consequent underperformance in the gravity assimilation. The A horizon parameters are however suitable for modelled soil moisture near the surface and this results in good performance of the near-surface soil moisture data assimilation, particularly for 0-30 cm soil moisture (Fig. 6.4 and 6.5).

6.4.2 2 Month Assimilation Window

Gravity Anomaly Data

The gravity anomaly assimilation is performed again using a two month assimilation window to assess if increasing the number of observations in the window improves results. While the retrieved TWS still shows a consistent improvement (reduced bias, and variance similar to observed TWS) for the whole assimilation period, variance of the retrieved soil moisture is significantly degraded and the bias is quite often larger than for the open loop (Fig. 6.6 and Table 6.2-6.5). The retrieved 30-60 and 60-90 cm soil moisture oscillates for the first three (two month) assimilation windows showing the prior (soil moisture states from the end of the previous assimilation window) is not an effective constraint when a two month window is used. Further, soil moisture retrieval is poor in the wet part (second half) of the year, significantly underestimating soil moisture at all depths for July and August (Fig. 6.6).

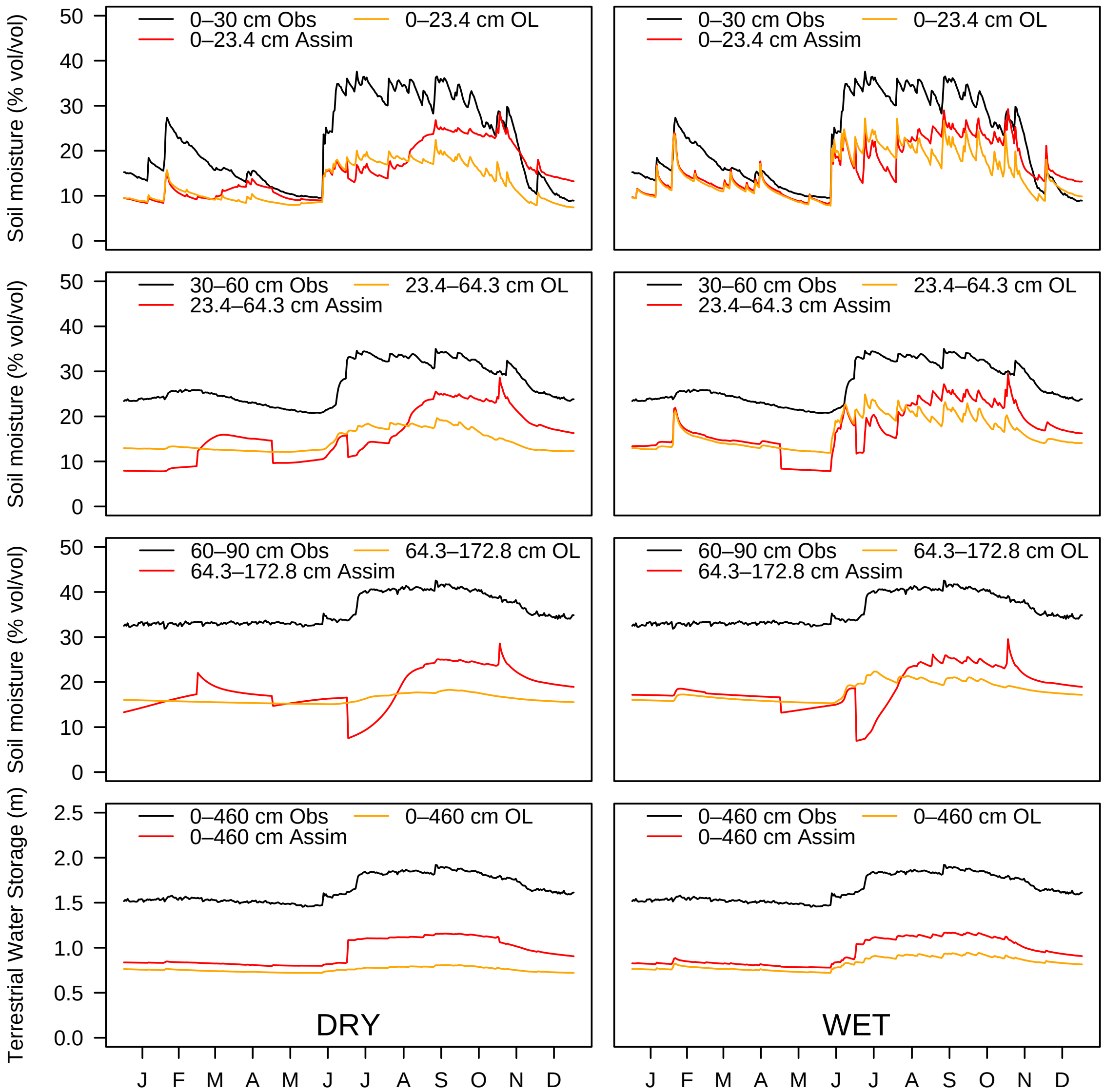

Fig. 6.6 As for Fig. 6.3 but using a two month assimilation window (case 2Ma in Table 6.2-6.5).

Gravity Anomaly and Near-Surface Soil Moisture Data

When near-surface soil moisture observations augment gravity anomalies the assimilation results for a two month window are good (Fig. 6.7) and comparable to results when using both data sets and a one month window (Table 6.2-6.5). Retrieved soil moisture bias is marginally smaller at all depths for the one month window, although retrieved TWS bias is smaller when using a two month assimilation window.

6.4.3 10 Day Assimilation Window

Gravity Anomaly Data

Finally, gravity anomalies are generated over ten day intervals and assimilated using a ten day window to see if the higher temporal resolution of the gravity anomalies and narrower assimilation window improves soil moisture retrieval. Results for the ten day window are quite similar to the one month window with ten day retrievals somewhat smoother for TWS (Fig. 6.8). Variance is marginally better (closer to that of the observations) for the ten day anomaly assimilation compared to the one month assimilation (Table 6.4 and 6.5). Retrieved soil moisture bias for one month and ten day gravity anomaly assimilation is almost identical (Table 6.2 and 6.3) with the ten day assimilation bias marginally worse for 60-90 cm soil moisture retrieval.

Gravity Anomaly and Near-Surface Soil Moisture Data

Lastly the ten day assimilation is run using both gravity anomalies and near-surface soil moisture. The soil moisture retrieval is fairly smooth except for one (ten day) window near the start of June for 30-60 cm soil moisture and one window near the end of August for TWS (Fig. 6.9). The rapid 60-90 cm soil moisture drainage evident in the one month assimilation results is again seen for 60-90 but also 0-30 and 30-60 cm soil moisture retrievals. The retrieved soil moisture and TWS bias is low but still larger than for the one month window (Table 6.2 and 6.3). Variability of the retrieved soil moisture and TWS is good and only 0-30 cm soil moisture variance is degraded compared to the one month window.

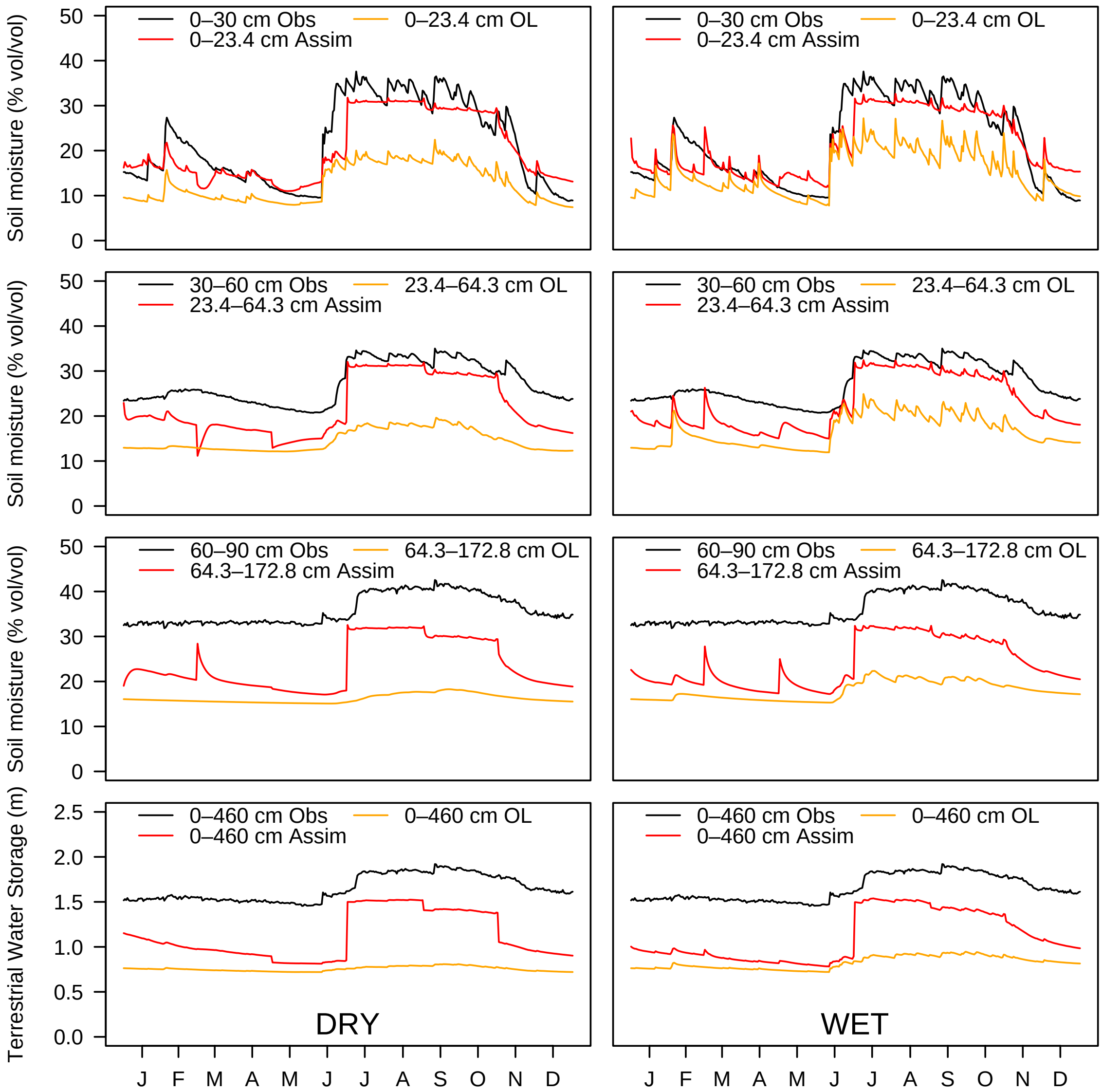

Fig. 6.7 As for Fig. 6.4 but using a two month assimilation window (case 2Mb in Table 6.2-6.5).

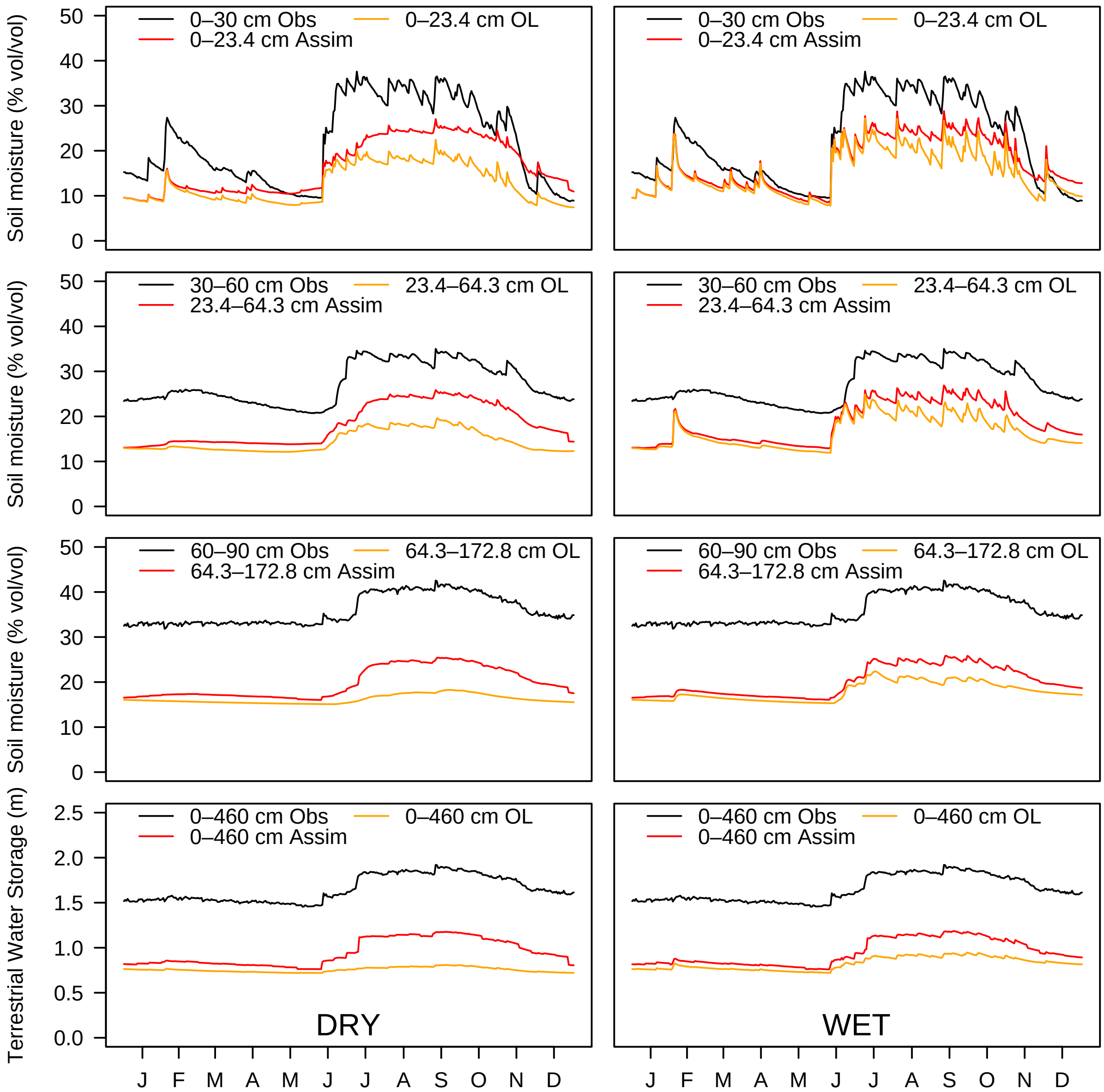

Fig. 6.8 As for Fig. 6.3 but using a ten day assimilation window and ten day anomalies (case 10Da in Table 6.2-6.5).

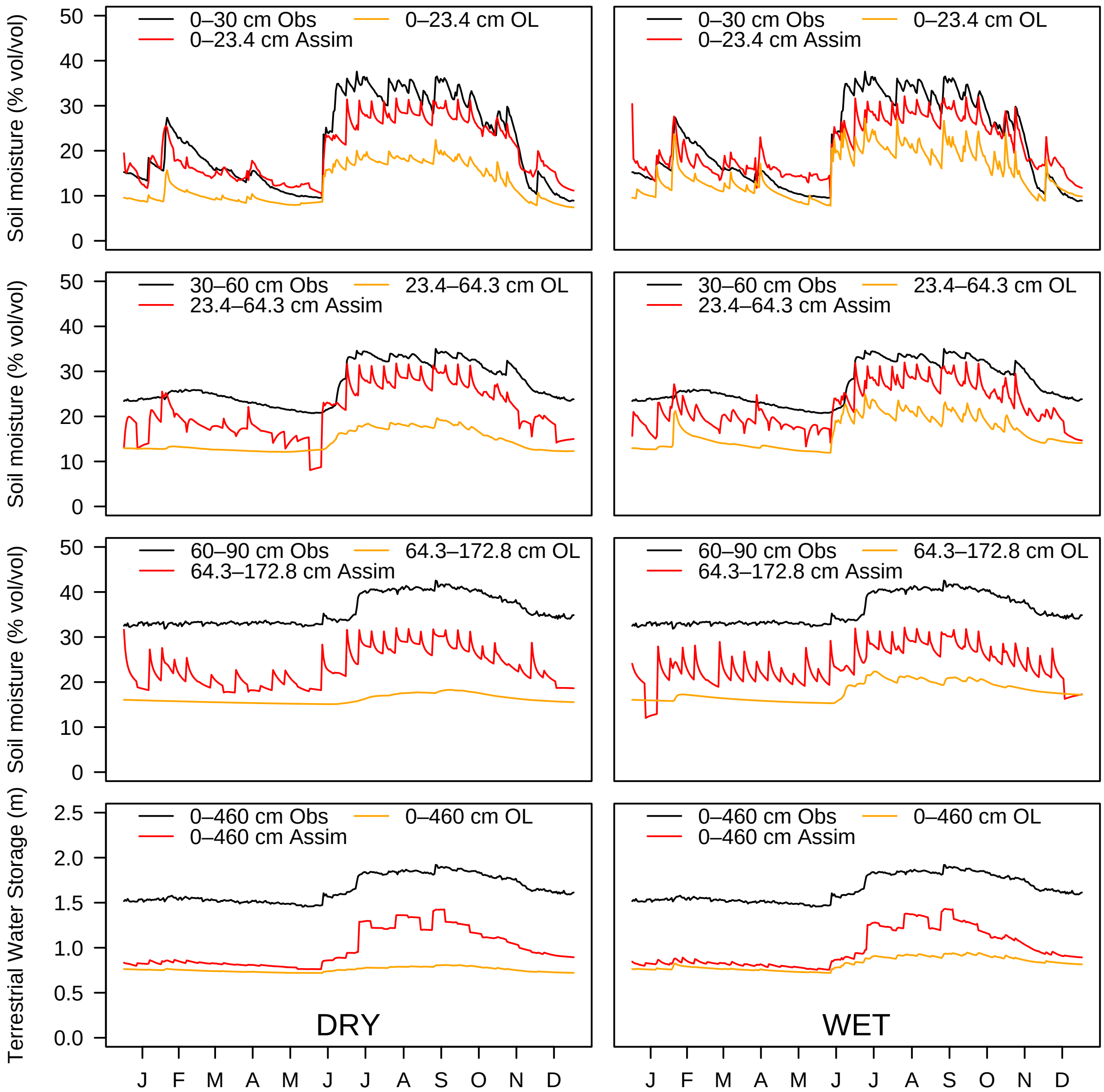

Fig. 6.9 As for Fig. 6.4 but using a ten day assimilation window and ten day anomalies (case 10Db in Table 6.2-6.5).

6.5 Chapter Summary

The feasibility of retrieving the soil moisture profile from ground-based gravity data was investigated through a series of case studies at a temperate valley site (in south-east Australia), using variational data assimilation and a land surface model. Model hydraulic parameters were tuned to the site, forcing was compiled from atmospheric observations, soil moisture and groundwater were observed to evaluate the performance of the retrieval, and various types of gravity observations were generated from the soil moisture and groundwater data. Assimilation experiments were conducted to assess the best type of gravity observation for assimilation, and whether the addition of near-surface soil moisture observations would improve soil moisture retrieval from the gravity data.

All assimilation case studies using gravity (and/or near-surface soil moisture) observations reduced soil moisture and terrestrial water storage (TWS) bias and improved temporal variability compared to an open loop simulation. Only when using a ten day window and gravity anomaly did assimilating both gravity and near-surface soil moisture improve soil moisture and TWS variability estimation over use of gravity data alone.

In general, near-surface soil moisture assimilation improves the soil moisture bias from the top of the profile down, while gravity assimilation improves the soil moisture variability from the bottom of the profile up. In summary assimilating both ten day gravity anomalies and near-surface soil moisture (every three days) over a ten day assimilation window provided the best compromise of bias reduction, variance similarity to observations, and smoothness of retrieved soil moisture. While assimilating both monthly gravity anomalies and near-surface soil moisture (every three days) over a one month window also gave very good results. An obvious extension of the research is to use GRACE and AMSR-E data. Additionally, more work needs to be done in a spatial setting, where the gravity observations integrate a lateral area orders of magnitude larger than the near-surface soil moisture measurements.

Chapter 7

Conclusions and Future Directions

Ground-based gravity data offers an unparalleled opportunity to non-invasively monitor depth integrated soil moisture and total terrestrial water storage (TWS). However it remains to be conclusively shown that a soil moisture and TWS signal can be routinely detected in ground-based gravity data from field sites. Moreover, well developed techniques are required to achieve the gravity data precision necessary to monitor soil moisture and there are currently no techniques to disaggregate the lumped TWS observation to its component soil moisture and groundwater level signals. This thesis developed transferable methods to monitor soil moisture (and TWS) with gravity data, and subsequently retrieve the soil moisture profile from the ground-based gravity data.

7.1 Conclusions

Conclusions from this thesis address the three main research questions:

1) What gravity precision is achievable in the field? i.e. What factors are important for monitoring soil moisture with ground-based gravity data, and what is required to obtain a sufficiently precise measurement to detect TWS changes (soil moisture in particular)?
2) Is there a detectable TWS signal (particularly soil moisture) in ground-based gravity data? i.e. Can ground-based gravity data be used to monitor soil moisture with current technology?

3) Can the TWS signal (particularly soil moisture) be retrieved from ground-based gravity data? i.e. Can the TWS signal be extracted from gravity changes and can TWS be disaggregated into profile soil moisture and groundwater components?

7.1.1 Achieving high precision gravity data

The gravity data precision achievable in the field using a single Scintrex CG-3M relative gravimeter at a number of sites, under different conditions was 1.4-2.3 μGal (32-55 mm TWS) for a gravity estimate at a site. This translated to a precision of 1.9-3.3 μGal (46-78 mm TWS) for the gravity difference between sites, and 3.8 μGal (90 mm TWS) for the gravity change over time at a site.

The factors that are important for monitoring soil moisture at a network of sites are different to the factors that are important for stationary monitoring at a single site (e.g. using an SG from the GGP network). At a single site the geophysical and meteorological signals can be analysed and precisely removed from the gravity data, leaving a residual (time series) that can be compared to hydrological observations or theory. Conversely monitoring soil moisture at field sites requires a precise prediction of the geophysical signals, without the benefit or convenience of a long time series of gravity data to analyse. Furthermore, while the geophysical and meteorological signals in ground-based gravity data are the cause of nearly all temporal variability at a site, when monitoring soil moisture at a network of sites (particularly with a relative gravimeter), the gravity observations from two nearby sites are differenced. This forming of gravity ties removes most of the geophysical and meteorological signals without the need for additional corrections. However, there is still a need to understand the spatial and temporal support of the signals, and consequently the limiting site separation in the gravity network. Moreover, in a field setting the response of the gravimeter to transportation is paramount. There is a clear need for further research on this important topic to guide field practice, survey and network design, and statistical analysis of gravity changes. Previous studies that have achieved high precision gravity data have limited the size of the network and transported the gravimeter by hand (Naujoks et al., 2008, 2010; Christiansen et al., 2011a,b,c). In the future, larger networks may be observed through the use of hybrid gravity surveys (Hinderer et al., 2009; Jacob et al., 2010) using both precise absolute and relative gravimeters. One day a field portable absolute gravimeter may be as easily used as a portable relative gravimeter and able to make an accurate gravity determination at a soil moisture monitoring site (Faller and Vitouchkine, 2005).

Recommendations to detect TWS changes (in particular soil moisture) using ground-based gravity data

Together with corrections for the geophysical signals, meteorological signals, and instrumental artefacts in gravity data, further field and statistical methods are recommended from the work conducted in this thesis. These include:

- Install a stable platform allowing precipitation and evapotranspiration to pass.
- Use a portable gravimeter that does not require a permanent installation and can be used to monitor many sites.
- Select a hydrologically stable reference site as part of the gravity network.
- Fix one leg of the gravimeter to control elevation changes.
- Transport the gravimeter with a custom designed suspension case to reduce shock and vibration, and post transport stabilisation of the gravity data.
- Shade the gravimeter at all times when taking a field measurement.
- Measure atmospheric pressure adjacent to the gravimeter.
- Average 120 one second samples over 2.5 minutes for a gravity measurement at a site.
- Average eight (2.5 minute) gravity measurements over 20 minutes for a gravity observation at each site.
- Apply corrections to the gravity observations at each site for geophysical signals, meteorological signals, and instrumental artefacts.
- Difference gravity observations at successive sites to remove drift (and bias) and form a gravity tie (over about 1 hour).
- Form eight gravity ties between each site.
- Connect every site in the network to every other site with a gravity tie to form a complete gravity network.
- Connect every pair of sites in the network with the same number of gravity ties to form a homogeneous gravity network.

- Use the gravity ties in a gravity network adjustment to statistically adjust the site gravity differences, increase precision of the gravity estimates, ensure a consistent network, and distribute random error.
- Use a t-test to determine the statistical significance of a gravity change at a site over time.

7.1.2 Detecting a TWS Signal in Gravity Data

A soil moisture signal was detected in ground-based gravity at a valley site with silt loam soil and a groundwater level within 4 m of the surface. This corresponds with the findings of Mäkinen and Tattari (1988) and Peter et al. (1994), who also detected a soil moisture signal in ground based gravity at flat sites with a shallow water table. However at another valley site with silt loam soil and a groundwater level within 4 m of the surface, a statistically significant change of gravity was not detected. The reasons for this are not clear, although this also corresponds to the findings of Mäkinen and Tattari (1991a,b), who did not detect a TWS signal at a second site. A small change in ground-based gravity at a hillslope soil moisture monitoring site without an observed groundwater level, while not statistically significant, corresponded well with the expected result of upslope and downslope soil moisture signals in ground-based gravity cancelling, and also corresponded well with the observed TWS (soil moisture) changes.

While a statistically significant change in gravity was detected at one site, no significant change was detected at the other two sites. A total of 22 days of field work was required to obtain a single gravity change estimate at three sites. While there is potential to monitor soil moisture with current generation gravimeters the technique will not blossom until new technology is available that minimises the need to consistently repeat gravity observations throughout a network. With an accurate field portable absolute gravimeter (i.e. that from Faller and Vitouchkine (2003) or Schmidt et al. (2011)), a soil moisture monitoring network could be as large as the 38 sites in the MSMMN, with each site observed only once during each field campaign.

The conclusions from this study are limited by the number of field campaigns and soil moisture monitoring sites that could be observed, which in turn is limited by the precision of the current gravimeters. The limitations of current instrumentation, including the precision of field portable gravimeters, and the durability and transportability of more precise laboratory based gravimeters, make current day field based monitoring of soil moisture with ground-based gravity data a continuing challenge. However a new era of gravimeter technology is dawning with the advent of the atom based absolute gravimeter (Peters et al., 1999; Schmidt et al., 2011), that is both more accurate and smaller than current absolute gravimeters, and the development of a field portable superconducting gravimeter (Wilson et al., 2012) that is much more precise than current relative gravimeters.

7.1.3 Retrieving the Soil Moisture Profile from Gravity Data

A method was developed to retrieve the soil moisture profile using a land surface model and gravity data assimilation, and tested at one of the soil moisture monitoring sites. Variational data assimilation was used with sliding (non-overlapping) assimilation windows, with the initial soil moisture for each window retrieved. The soil moisture retrieval was not sensitive to the land surface model forcing data, or the size of the assimilation window, with similar results obtained using 1 month or 10 day windows, and 200 or 1200 mm of annual rainfall. However the gravity data assimilation was not able to correct the severe model bias (in simulated soil moisture). This makes sense as the developed method assimilated gravity changes. Creating synthetic absolute gravity observations using the annual mean modelled TWS (as done by Zaitchik et al. (2008)) reduced the assimilation performance, with the assimilation of gravity anomalies (or changes) giving better results. However, assimilating near-surface soil moisture together with gravity data improved the results, with the gravity data assimilation retrieving the soil moisture variance from the bottom of the profile up, and the near-surface assimilation reducing the soil moisture bias from the top of the profile down. The best results were obtained using an assimilation window of 1 month or 10 days and assimilating both gravity data (as an anomaly or gravity change) and near-surface soil moisture.

The main limitation of the soil moisture retrieval is the accuracy of the predictive model. To further improve the gravity data assimilation performance, the model physics need improving. In particular, the model needs to accurately represent the soil moisture profile and use realistic soil parameters that vary with depth.

7.1.4 Concluding Summary

This thesis developed a new method to non-invasively monitor profile soil moisture with ground-based gravity data. A significant finding in this thesis is that the soil moisture profile can be retrieved from ground-based gravity observations using a land surface model and variational data assimilation. This is the first ever study to assimilate ground-based gravity data into a land surface model, or conversely retrieve a soil moisture signal from ground-based gravity data. Also of significance are novel contributions including a determination of the gravity data precision achievable in the field, and recommendations on how to achieve the precision required to monitor soil moisture and TWS with ground-based gravity data. For the first time ever total TWS was independently observed and compared to gravity observations at a number of field sites, with a statistically significant observed gravity change corresponding to the change in TWS. A significant legacy of this thesis is the large network of soil moisture monitoring sites established in the Murrumbidgee River Catchment, that is now part of the International Soil Moisture Network. This publicly available dataset (Smith et al., 2012) has contributed to numerous studies and will continue to contribute to scientific knowledge for many years to come.

7.2 Further Research

Recommendations for further research on each of the research questions investigated in this thesis follow.

7.2.1 Achieving precise field gravity data

The transferability of the geophysical corrections selected in this thesis (using gravity data from the Canberra SG) should be assessed using SG gravity data from other sites in the GGP network (Crossley et al., 1999; Crossley and Hinderer, 2009). The ocean tide loading correction method warrants particular analysis at a number of sites on multiple continents at different elevations and distances from the coast. Similarly, the temporal stability of the atmospheric pressure correction should be investigated at more sites in different climate zones. The spatial and temporal variability of geophysical and meteorological corrections should be further analysed. A worldwide spatio-temporal map of geophysical gravity corrections (combined Earth tides, polar motion and ocean tide loading) could be produced.

Accurate recording of the time and location of a gravity observation is required to effectively correct the geophysical or meteorological signals. All gravity observations should be complemented by simultaneous GPS observations of time and location. Future gravimeter design should incorporate a GPS antenna and barometer.

To further improve the precision of gravity data a knowledge (and understanding) of the elevation variation is critical. All gravity observations should be done simultaneously with differential GPS observations (similar to Ferguson et al. (2008)) to achieve an elevation observation precision greater than 1 mm. Remotely sensed elevation from Interferometric Synthetic Aperture Radar (inSAR) data could also be investigated for this purpose.

The nature and cause of variations in surface elevation needs further investigation using a loading model, physical process model, and observations. Further research is needed using dynamic ocean models that respond to wind forcing, and which can model storm surges together with ocean tides. Hydrodynamic models with accurate bathymetry should be used for coastal areas. Moreover, the coastal grids should be refined for the ocean tide loading correction. The utility of 2D and 3D atmospheric pressure and loading corrections needs further investigation, in particular using NWP data. Similarly the impact of soil moisture and groundwater loading needs further investigation using a variety of land surface models and forcing data. Using a GCM or Earth system model like ACCESS to consistently model the attraction and loading of ocean, atmosphere, and land surface mass variations (i.e. TWS) appears to have great potential.

The presence of instrumental artefacts in gravity data is an important and often neglected issue that needs much more research. In particular, the response of gravimeters to transportation requires further analysis. Similarly, the nature and cause of drift in gravity data should be much better understood. The affect of the gravimeter power supply on gravity data should not be ignored and needs to be investigated thoroughly. Multiple gravimeters should be used simultaneously to identify any instrumental artefacts, particularly in relative gravity data (that is subject to drift). A variety of gravimeter models and manufacturers should be used (e.g. Scintrex, LaCoste and Romberg, and ZLS). Absolute gravimeters should be used in conjunction with relative gravimeters, again using multiple gravimeters and models from Micro-g LaCoste (e.g. FG5 and A-10).

Future studies should utilise hybrid gravity networks (such as Naujoks (2009)) with both absolute and relative gravity observations. Gravity network sites should be observed in the same order in each campaign, and if possible on each day within a campaign. Gravity networks could contain a continuously operating base station to screen for earthquakes and determine the Earth tide and ocean tide loading signal in the field. Future work should investigate the utility of field based SG and also the newer atomic absolute gravimeter presented by Schmidt et al. (2011).

7.2.2 Detecting a Soil Moisture Signal in Gravity Data

Further investigation is required to determine the conditions best suited to monitor soil moisture with ground-based gravity. The investigation in this thesis should be extended to more sites in differing climates, with different soil types, land cover and topography. A combination of relative gravimeters produced by different manufacturers (e.g. Scintrex, LaCoste and Romberg, ZLS) and also absolute gravimeters (A-10 and FG5) should be used to observe the gravity at each soil moisture monitoring site. Using a combination of gravimeters will improve reliability of the gravity data and help identify any instrumental artefacts present in the data. A large, catchment scale experiment using the portable A-10 absolute gravimeter at multiple sites should be considered. More research on the impact of surface water (river height and farm dams) is needed. At large scales the impact of soil moisture and groundwater loading should be further investigated.

At a smaller scale, further studies should investigate a gravity network around an SG, similar to Naujoks et al. (2008). However, each site in the network should observe precipitation and total TWS (snow, soil moisture, groundwater) from the surface to groundwater level. Detailed information on soil properties, specific yield, and groundwater flow paths is also required.

Further gravity experiments in controlled environments (laboratories and lysimeters) such as Christiansen et al. (2011c) and Creutzfeldt et al. (2010c) are essential to verify the theory with current instrumentation (in particular gravimeters). More work needs to be done in determining a general gravimeter "footprint". Similarly, more research is required to usefully use 2D or 3D gravity forward models (such as Nagy (1966) or Leirião et al. (2009)). Future research should focus on accurately representing the spatial distribution of soil moisture and soil depth to be used in the 2D or 3D gravity forward model.

New gravimeters such as the atomic absolute gravimeter (Peters et al., 1999, 2001; de Angelis et al., 2009; Schmidt et al., 2011) offer the opportunity to precisely measure absolute gravity at a site, and not require time consuming gravity ties between sites. Further research should investigate the use of the atomic gravimeter in the field. The impact of the area immediately surrounding the gravimeter (within a 2 m radius) needs to be further assessed, in particular the presence of the gravimeter operator, and the type and construction of gravimeter platform. This will become even more significant as gravimeter precision increases.

7.2.3 Soil Moisture Retrieval from Gravity Data Assimilation into a Land Surface Model

Application of the method developed in this thesis to retrieve the profile soil moisture should be extended to using AMSR-E and GRACE satellite data. Other remotely sensed near-surface soil moisture data could also be used (e.g. ASCAT, AMSR2, SMOS, SMAP). The presented method should also be used with real ground-based gravity data, such as the data from the Moxa SG in Germany presented by Naujoks (2009). Other possibilities are the data of Wilson et al. (2012) using a field installation of an SG, or the current GHYRAF experiment using the FG5 absolute gravimeter (Hinderer et al., 2009; Pfeffer et al., 2011). At these remote field sites the use of modelled (NWP) atmospheric forcing data (e.g. ECMWF) should be tested. The method developed in this thesis (using the Bouguer slab approximation) should also be extended to use a 3D gravity forward model (i.e. Nagy (1966) or Leirião et al. (2009)). Most importantly, the method needs to be used with a land surface model that explicitly models groundwater, and if one is not available a groundwater modelling capability (e.g. Niu et al. (2007)) needs to be added to an existing land surface model (e.g. Kowalczyk et al. (2006)).

More generally, the method needs to be extended spatially. The approach in this thesis was to use a 1D column, which is an important development for interpreting the ground-based gravity data at a point. However gridded assimilation of surface soil moisture and 3D gravity is a far more interesting (and challenging) research proposition, particularly if surface water (rivers and farm dams) are incorporated. Gridded near-surface soil moisture and gravity are currently available from remotely sensed data. However, airborne microwave radiometer data over an SG, or gridded soil moisture around an SG obtained from TDR or other manual sampling methods, could also be used. What is presented in this thesis should also be tested with other land surface models, and at other sites.

References

Abd El-Gelil, M., S. Pagiatakis, and A. El-Rabbany, 2008: Frequency-dependent atmospheric pressure admittance of superconducting gravimeter records using least squares response method. *Physics of the Earth and Planetary Interiors*, **170**, 24–33.

Abe, M., C. Kroner, J. Neumeyer, and X. Chen, 2010: Assessment of atmospheric reductions for terrestrial gravity observations. *Bulletin d'Informations Marées Terrestres*, **146**, 11 825–11 845.

Abe, M., et al., 2006: Hydrological effects on the superconducting gravimeter observation in Bandung. *Journal of Geodynamics*, **41**, 288–295.

Achilli, V., P. Baldi, G. Casula, M. Errani, S. Focardi, M. Guerzoni, F. Palmonari, and G. Raguní, 1995: A calibration system for superconducting gravimeters. *Bulletin Géodésique*, **69**, 73–80.

Agnew, D., 2007: Earth tides. *Treatise on Geophysics, Volume 3 - Geodesy*, T. Herring, Ed., Elsevier, 163–195.

Agnew, D. C., 1996: SPOTL: Some programs for ocean-tide loading. SIO Ref. Ser. 96-8, Scripps Institution of Oceanography, 35 pp., La Jolla, CA.

Agnew, D. C., 1997: NLOADF: A program for computing ocean-tide loading. *Journal of Geophysical Research*, **102**, 5109–5110.

Akaike, H., 1974: A new look at the statistical model identification. *IEEE Transactions on Automatic Control*, **19**, 716–723.

Almalvict, M., H. McQueen, and R. Govind, 2001: Absolute gravity measurements and calibration of SG-CT031 at Canberra, 1999-2000. *Journal of the Geodetic Society of Japan*, **47**, 410–416.

Amalvict, M., J. Hinderer, J. Mäkinen, S. Rosat, and Y. Rogister, 2004: Long-term and seasonal gravity changes at the Strasbourg station and their relation to crustal deformation and hydrology. *Journal of Geodynamics*, **38**, 343–353.

Amalvict, M., J. Hinderer, and S. Rózsa, 2006: Crustal vertical motion along a profile crossing the Rhine graben from the Vosges to the Black Forest Mountains: Results from absolute gravity, GPS and levelling observations. *Journal of Geodynamics*, **41**, 358–368.

Andersen, O., 1995a: Global ocean tides from ERS1 and TOPEX/POSEIDON altimetry. *Journal of Geophysical Research*, **100**, 25 249–25 259.

Andersen, O., 1995b: New ocean tide models for loading computations. *Bulletin d'Informations Marées Terrestres*, **102**, 256–259.

Andersen, O., G. Egbert, L. Erofeeva, and R. Ray, 2006: Non-linear tides in shallow water regions from multi-mission satellite altimetry and the Andersen 06 global ocean tide model. *EOS Trans., Beijing, China, July*, AGU.

Andersen, O., P. Woodworth, and R. Flather, 1995: Intercomparison of recent ocean tide models. *Journal of Geophysical Research*, **100**, 25 261–25 282.

Arnoso, J., M. Benavent, B. Ducarme, and F. Montesinos, 2006: A new ocean tide loading model in the Canary Islands region. *Journal of Geodynamics*, **41**, 100–111.

Arnoso, J., B. Ducarme, A. Venedikov, and R. Vieira, 2002: Time variations and anomalies in the air pressure admittance of superconducting tidal gravity data. *Bulletin d'Informations Marées Terrestres*, **136**, 10 793–10 808.

Arnoso, J., J. Fernández, R. Vieira, E. J. Vélez, and A. P. Venedikov, 2000: Results of tidal gravity observations in Tenerife, Canary Islands. *Bulletin d'Informations Marées Terrestres*, **132**, 10 283–10 290.

Australian Bureau of Statistics, 2010: Experimental estimates of the gross value of irrigated agricultural production, 2000–01 - 2008–09 (cat. no. 4610.0.55.008).

Badell, C., H. Drewes, and W. Torge, 1982: Gravimetric Earth tide observations in western Venezuela. *Bulletin d'Informations Marées Terrestres*, **87**, 5603–5614.

Baker, T. F. and M. S. Bos, 2003: Validating Earth and ocean tide models using tidal gravity measurements. *Geophysical Journal International*, **152**, 468–485.

Baldi, P. and G. Casula, 1997: The gravimetric station of Brasimone. *Bulletin d'Informations Marées Terrestres*, **127**, 9816–9825.

Bastien, R. and A. Goodacre, 1989: The effect of humidity variations on long-term tidal gravity recordings. *Bulletin d'Informations Marées Terrestres*, **106**, 7506–7510.

Becker, M., X. Gao, and E. Groten, 1986: First results of precise gravity measurements on the "A-B-C" profile. *Tectonophysics*, **130**, 33–47.

Becker, M., E. Groten, A. Lambert, J. Liard, and S. Nakai, 1987: An intercomparison of LaCoste and Romberg Model D gravimeters: Results of the international D-meter campaign 1983. *Geophysical Journal of the Royal Astronomical Society*, **89**, 499–526.

Becker, M., et al., 1995: Microgravimetric measurements at the 1994 international comparison of absolute gravimeters. *Metrologia*, **32**, 145–152.

Bi, D., et al., 2013: The ACCESS coupled model: Description, control climate and evaluation. *Australian Meteorological and Oceanographic Journal*, **63**, 41–64.

Bich, W., G. D'Agostino, F. Pennecchi, and A. Germak, 2011: Uncertainty due to parasitic accelerations in absolute gravimetry. *Metrologia*, **48**, 212–218.

Blainey, J. B., T. P. A. Ferré, and J. T. Cordova, 2007: Assessing the likely value of gravity and drawdown measurements to constrain estimates of hydraulic conductivity and specific yield during unconfined aquifer testing. *Water Resources Research*, **43**, W12408, doi:10.1029/2006WR005678.

Bolster, C. H., D. P. Genereux, and J. E. Saiers, 2001: Determination of specific yield for the Biscayne Aquifer with a canal-drawdown test. *Ground Water*, **39**, 768–777.

Bonatz, M., 1967: Der gravitationseinfluß der bodenfeuchtigkeit. *Zeitschrift für Vermessungswesen*, **92**, 135–139.

Bonatz, M., 1987: Multichannel analysis and instrumental drift of spring gravimeters. *Bulletin d'Informations Marées Terrestres*, **99**, 6753–6755.

Bonvalot, S., M. Diament, and G. Gabalda, 1998: Continuous gravity recording with Scintrex CG-3M meters: A promising tool for monitoring active zones. *Geophysical Journal International*, **135**, 470–494.

Bower, D. and N. Courtier, 1998: Precipitation effects on gravity measurements at the Canadian absolute gravity site. *Physics of the Earth and Planetary Interiors*, **106**, 353–369.

Boy, J.-P. and B. F. Chao, 2005: Precise evaluation of atmospheric loading effects on Earth's time-variable gravity field. *Journal of Geophysical Research*, **110**, B08412, doi:10.1029/2002JB002333.

Boy, J.-P., P. Gegout, and J. Hinderer, 2002: Reduction of surface gravity data from global atmospheric pressure loading. *Geophysical Journal International*, **149**, 534–545.

Boy, J.-P., J. Hinderer, and P. Gégout, 1998a: The effect of atmospheric loading on gravity. *13th International Symposium on Earth Tides*, B. Ducarme and P. Paquet, Eds., Brussels, 439–446.

Boy, J.-P., J. Hinderer, and P. Gegout, 1998b: Global atmospheric loading and gravity. *Physics of the Earth and Planetary Interiors*, **109**, 161–177.

Boy, J.-P., J. Hinderer, and P. Gegout, 2001: Gravity variations and global pressure loading. *Journal of the Geodetic Society of Japan*, **47**, 267–272.

Boy, J.-P., L. Longuevergne, F. Boudin, T. Jacob, F. Lyard, M. Llubes, N. Florsch, and M.-F. Esnoult, 2009: Modelling atmospheric and induced non-tidal oceanic loading contributions to surface gravity and tilt measurements. *Journal of Geodynamics*, **48**, 182–188.

Boy, J. P. and F. Lyard, 2008: High-frequency non-tidal ocean loading effects on surface gravity measurements. *Geophysical Journal International*, **175**, 35–45.

Breili, K. and B. R. Pettersen, 2009: Effects of surface snow cover on gravimetric observations. *Journal of Geodynamics*, **48**, 16–22.

Bretagnon, P., 1982: Théorie du mouvement de l'ensemble des planètes. Solution VSOP82. *Astronomy and Astrophysics*, **114**, 278–288.

Brocca, L., T. Tullo, F. Melone, T. Moramarco, and R. Morbidelli, 2012: Catchment scale soil moisture spatial-temporal variability. *Journal of Hydrology*, **422-423**, 63–75.

Bronstert, A. and A. Bárdossy, 1999: The role of spatial variability of soil moisture for modelling surface runoff generation at the small catchment scale. *Hydrology and Earth System Sciences*, **3**, 505–516.

Brown, E., 1905: Theory of the motion of the Moon Part IV. *Memoirs of the Royal Astronomical Society*, **57**, 136–141.

Bruinsma, S., J.-M. Lemoine, R. Biancale, and N. Valès, 2010: CNES/GRGS 10-day gravity field models (release 2) and their evaluation. *Advances in Space Research*, **45**, 587–601.

Brzezinski, A. and J. Nastula, 2000: Oceanic excitation of the Chandler wobble. *Advances in Space Research*, **30**, 195–200.

Büllesfeld, F.-J., 1985: Ein beitrag zur harmonischen darstellung des gezeitenerzeugenden potentials. *Deutsche Geodätische Kommission*, **C 314**, 1–103.

Calvet, J.-C. and J. Noilhan, 2000: From near-surface to root-zone soil moisture using year-round data. *Journal of Hydrometeorology*, **1**, 393–411.

Campbell, G., 1974: A simple method for determining unsaturated conductivity from moisture retention data. *Soil Science*, **117**, 311–314.

Campbell Scientific, 1996: *CS615 Water Content Reflectometer: Instruction Manual.* Campbell Scientific, Inc., Logan, UT.

Campbell Scientific, 2002: *CS616 Water Content Reflectometer Instruction Manual.* Campbell Scientific, Inc., Logan, UT.

Carrera-Hernández, J., B. Smerdon, and C. Mendoza, 2012: Estimating groundwater recharge through unsaturated flow modelling: Sensitivity to boundary conditions and vertical discretization. *Journal of Hydrology*, **452-453**, 90–101.

Cartwright, D. and A. C. Edden, 1973: Corrected tables of tidal harmonics. *Geophysical Journal of the Royal Astronomical Society*, **33**, 253–264.

Cartwright, D. and R. Tayler, 1971: New computations of the tide-generating potential. *Geophysical Journal of the Royal Astronomical Society*, **23**, 45–74.

Chandler, S., 1891: On the variation of latitude I-IV. *The Astronomical Journal*, **11**, 59–61, 65–70, 75–79, 83–86.

Chandler, S., 1892: On the variation of latitude V-VII. *The Astronomical Journal*, **12**, 17–22, 57–72, 97–101.

Chapman, D. S., E. Sahm, and P. Gettings, 2008: Monitoring aquifer recharge using repeated high-precision gravity measurements: A pilot study in South Weber, Utah. *Geophysics*, **73**, WA83–WA93.

Chapront-Touzé, M. and J. Chapront, 1983: The lunar ephemeris ELP-2000. *Astronomy and Astrophysics*, **124**, 50–62.

Christiansen, L., P. J. Binning, D. Rosbjerg, O. B. Andersen, and P. Bauer-Gottwein, 2011a: Using time-lapse gravity for groundwater model calibration: An application to alluvial aquifer storage. *Water Resources Research*, **47**, W06503, doi:10.1029/2010WR009859.

Christiansen, L., E. B. Haarder, A. B. Hansen, M. C. Looms, P. J. Binning, D. Rosbjerg, O. B. Andersen, and P. Bauer-Gottwein, 2011b: Calibrating vadose zone models with time-lapse gravity data. *Vadose Zone Journal*, **10**, 1034–1044.

Christiansen, L., S. Lund, O. B. Andersen, P. J. Binning, D. Rosbjerg, and P. Bauer-Gottwein, 2011c: Measuring gravity change caused by water storage variations: Performance assessment under controlled conditions. *Journal of Hydrology*, **402**, 60–70.

Clapp, R. and G. Hornberger, 1978: Empirical equations for some soil hydraulic properties. *Water Resources Research*, **14**, 601–604.

Cook, A., 1953: Adjustment of the principal gravity observations in Great Britain. *Monthly Notices of the Royal Astronomical Society, Geophysical Supplement*, **6**, 494–534.

Cosh, M. H., J. R. Stedinger, and W. Brutsaert, 2004: Variability of surface soil moisture at the watershed scale. *Water Resources Research*, **40**, W12513, doi: 10.1029/2004WR003487.

Cresswell, R. G., W. R. Dawes, G. K. Summerell, G. T. Beale, N. K. Tuteja, and G. R. Walker, 2003: Assessment of salinity management options for Kyeamba Creek, New South Wales: Data analysis and groundwater modelling. Murray Darling Basin Commission Publication 12/03, 30 pp.

Creutzfeldt, B., 2010: The effect of water storages on temporal gravity measurements and the benefits for hydrology. Ph.D. thesis, University of Potsdam.

Creutzfeldt, B., T. Ferré, P. Troch, B. Merz, H. Wziontek, and A. Güntner, 2012: Total water storage dynamics in response to climate variability and extremes: Inference from long-term terrestrial gravity measurement. *Journal of Geophysical Research*, **117**, D08112, doi:10.1029/2011JD016472.

Creutzfeldt, B., A. Güntner, T. Klügel, and H. Wziontek, 2008: Simulating the influence of water storage changes on the superconducting gravimeter of the Geodetic Observatory Wettzell, Germany. *Geophysics*, **73**, WA95–WA104, doi: 10.1190/1.2992508.

Creutzfeldt, B., A. Güntner, H. Thoss, B. Merz, and H. Wziontek, 2010a: Measuring the effect of local water storage changes on in situ gravity observations: Case study of the Geodetic Observatory Wettzell, Germany. *Water Resources Research*, **46**, W08531, doi:10.1029/2009WR008359.

Creutzfeldt, B., A. Güntner, S. Vorogushyn, and B. Merz, 2010b: The benefits of gravimeter observations for modelling water storage changes at the field scale. *Hydrology and Earth System Sciences*, **14**, 1715–1730.

Creutzfeldt, B., A. Güntner, H. Wziontek, and B. Merz, 2010c: Reducing local hydrology from high-precision gravity measurements: A lysimeter-based approach. *Geophysical Journal International*, **183**, 178–187.

Crossley, D., C. de Linage, J. Hinderer, J.-P. Boy, and J. Famiglietti, 2012: A comparison of the gravity field over Central Europe from superconducting gravimeters, GRACE and global hydrological models, using EOF analysis. *Geophysical Journal International*, **189**, 877–897, doi:10.1111/j.1365-246X.2012.05404.x.

Crossley, D. and J. Hinderer, 2009: A review of the GGP network and scientific challenges. *Journal of Geodynamics*, **48**, 299–304.

Crossley, D., J. Hinderer, J.-P. Boy, and C. de Linnage, 2006: Status of the GGP satellite project. *Bulletin d'Informations Marées Terrestres*, **142**, 11 423–11 432.

Crossley, D., J. Hinderer, and S. Rosat, 2002: Using atmosphere-gravity correlation to derive a time-dependent admittance. *Bulletin d'Informations Marées Terrestres*, **136**, 10 809–10 820.

Crossley, D., O. Jensen, and J. Hinderer, 1995: Effective barometric admittance and gravity residuals. *Physics of the Earth and Planetary Interiors*, **90**, 221–241.

Crossley, D., X. Su, and T. van Dam, 1998: Comprehensive analysis of 2 years of SG data from Table Mountain, Colorado. *13th International Symposium on Earth Tides*, B. Ducarme and P. Paquet, Eds., Brussels, 659–668.

Crossley, D., et al., 1999: Network of superconducting gravimeters benefits a number of disciplines. *EOS*, **80**, 121–132.

Csapó, G. and G. Szatmári, 1995: Apparatus for moving mass calibration of LaCoste-Romberg feedback gravimeters. *Metrologia*, **32**, 225–230.

Damiata, B. N. and T.-C. Lee, 2006: Simulated gravitational response to hydraulic testing of unconfined aquifers. *Journal of Hydrology*, **318**, 348–359.

Davis, K., Y. Li, and M. Batzle, 2008: Time-lapse gravity monitoring: A systematic 4D approach with application to aquifer storage and recovery. *Geophysics*, **73**, WA61–WA69.

de Angelis, M., et al., 2009: Precision gravimetry with atomic sensors. *Measurement Science and Technology*, **20**, 022001, doi:10.1088/0957-0233/20/2/022001.

Debeglia, N. and F. Dupont, 2002: Some critical factors for engineering and environmental microgravity investigations. *Journal of Applied Geophysics*, **50**, 435–454.

Dehant, V., 1987: Tidal parameters for an inelastic Earth. *Physics of the Earth and Planetary Interiors*, **49**, 97–116.

Dehant, V., P. Defraigne, and J. Wahr, 1999: Tides for a convective Earth. *Journal of Geophysical Research*, **104**, 1035–1058.

Desilets, D., M. Zreda, and T. P. A. Ferré, 2010: Nature's neutron probe: Land surface hydrology at an elusive scale with cosmic rays. *Water Resources Research*, **46**, W11505, doi:10.1029/2009WR008726.

Dick, W. R. and B. Richter, 2008: IERS annual report 2006. Tech. rep., 187 pp.

Dierks, O. and J. Neumeyer, 2002: Comparison of Earth tides analysis programs. *Bulletin d'Informations Marées Terrestres*, **135**, 10 669–10 688.

Dittfeld, H.-J., 2000: Final results of the SG-registration in Potsdam. *Bulletin d'Informations Marées Terrestres*, **132**, 10 355–10 368.

Dittfeld, H.-J., 2001: On the validity of environmental parameters in gravimetric tidal analyses. *Journal of the Geodetic Society of Japan*, **47**, 287–293.

Doherty, J., 2010: *Manual and Addendum for PEST: Model Independent Parameter Estimation*. Brisbane, Australia.

Doodson, A., 1921: The harmonic development of the tide generating potential. *Proceedings of the Royal Society of London*, **A 100**, 306–328.

Dorigo, W., P. Van Oevelen, W. Wagner, M. Drusch, S. Mecklenburg, A. Robock, and T. Jackson, 2011a: A new international network for in situ soil moisture data. *EOS*, **92**, 141–148.

Dorigo, W., et al., 2011b: The international soil moisture network: A data hosting facility for global in situ soil moisture measurements. *Hydrology and Earth System Sciences*, **15**, 1675–1698.

Dorman, J. and P. Sellers, 1989: A global climatology of albedo, roughness length and stomatal resistance for atmospheric general circulation models as represented by the simple biosphere model (SiB). *Journal of Applied Meteorology*, **28**, 833–855.

Dragert, H., A. Lambert, and J. Liard, 1981: Repeated precise gravity measurements on Vancouver Island, British-Columbia. *Journal of Geophysical Research*, **86**, 6097–6106.

Draper, C. S., J. P. Walker, P. J. Steinle, R. A. de Jeu, and T. R. Holmes, 2009: An evaluation of AMSR-E derived soil moisture over Australia. *Remote Sensing of Environment*, **113**, 703–710, doi:10.1016/j.rse.2008.11.011.

Ducarme, B., 1979: Calibration problems for TRG-1 Earth tides meters. *Bulletin d'Informations Marées Terrestres*, **82**, 5103–5108.

Ducarme, B., 2009: Limitations of high precision tidal prediction. *Bulletin d'Informations Marées Terrestres*, **145**, 11 663–11 677.

Ducarme, B. and A. Somerhausen, 1997: Tidal gravity recording at Brussels with a Scintrex CG-3M gravity meter. *Bulletin d'Informations Marées Terrestres*, **126**, 9611–9634.

Ducarme, B., L. Vandercoilden, and A. Venedikov, 2006: Estimation of the precision by the tidal analysis programs ETERNA and VAV. *Bulletin d'Informations Marées Terrestres*, **141**, 11 189–11 200.

Ducharne, A. and K. Laval, 2000: Influence of the realistic description of soil water-holding capacity on the global water cycle in a GCM. *Journal of Climate*, **13**, 4393–4413.

Durran, D. R., 1999: *Numerical Methods for Wave Equations in Geophysical Fluid Dynamics*. Springer Verlag, New York, pp. 465.

Dziewonski, A. and D. Anderson, 1981: Preliminary reference Earth model. *Physics of the Earth and Planetary Interiors*, **25**, 297–356.

Eanes, R. and S. Bettadpur, 1995: The CSR 3.0 global ocean tide model. Technical Memorandum CSR-TM-95-06, Center for Space Research.

Eanes, R. J. and S. V. Bettadpur, 1994a: Diurnal and semidiurnal tides from TOPEX/POSEIDON altimetry. *EOS Trans.*, AGU, Vol. 75, 108.

Eanes, R. J. and S. V. Bettadpur, 1994b: Ocean tides from two year of TOPEX/POSEIDON altimetry. *EOS Trans., Fall Meet., Suppl.*, AGU, Vol. 75, 61.

Egbert, G. and L. Erofeeva, 2002: Efficient inverse modeling of barotropic ocean tides. *Journal of Atmospheric and Oceanic Technolgy*, **19**, 183–204.

Egbert, G. D., A. F. Bennett, and M. G. Foreman, 1994: TOPEX/POSEIDON tides estimated using a global inverse model. *Journal of Geophysical Research*, **99**, 24 821–24 852.

El Wahabi, A., H.-J. Dittfeld, and Z. Simon, 2000: Meteorological influence on tidal gravimeter drift. *Bulletin d'Informations Marées Terrestres*, **133**, 10 403–10 414.

El Wahabi, A., B. Ducarme, and M. Van Ruymbeke, 2001: Humidity and temperature effects on LaCoste & Romberg gravimeters. *Journal of the Geodetic Society of Japan*, **47**, 10–15.

Ellett, K. M., J. P. Walker, A. W. Western, and M. Rodell, 2006: A framework for assessing the potential of remote-sensed gravity to provide new insight on the hydrology of the Murray-Darling Basin. *Australian Journal of Water Resources*, **10**, 89–101.

Entekhabi, D., et al., 2010: The Soil Moisture Active Passive (SMAP) mission. *Proceedings of the IEEE*, **98**, 704–716.

Faller, J. and A. Vitouchkine, 2005: A new small cam-driven absolute gravimeter. *Gravity, Geoid and Space Missions*, C. Jekeli, L. Bastos, and J. Fernandes, Eds., Springer-Verlag, Berlin, 276–279.

Faller, J. E., 2002: Thirty years of progress in absolute gravimetry: A scientific capability implemented by technological advances. *Metrologia*, **39**, 425–428.

Faller, J. E. and A. L. Vitouchkine, 2003: Prospects for a truly portable absolute gravimeter. *Journal of Geodynamics*, **35**, 567–572.

Farrell, W., 1972: Deformation of the Earth by surface loads. *Reviews of Geophysics and Space Physics*, **10**, 761.

Ferguson, J., T. Chen, J. Brady, C. Aiken, and J. Seibert, 2007: The 4D microgravity method for waterflood surveillance II – Gravity measurements for the Prudhoe Bay reservoir, Alaska. *Geophysics*, **72**, 133–143.

Ferguson, J. F., F. Klopping, T. Chen, J. E. Seibert, J. L. Hare, and J. L. Brady, 2008: The 4D microgravity method for waterflood surveillance: Part 3 – 4D absolute microgravity surveys at Prudhoe Bay, Alaska. *Geophysics*, **73**, WA163–WA171.

Ferré, T., et al., 2009: Critical steps for the continuing advancement of hydrogeophysics. *EOS*, **90**, 200.

Flach, D., G. Gommlich, and G. Jetzsch, 1993: Three years of experiences with a movable superconducting gravimeter at the underground installation site in the salt mine ASSE in Northern Germany. *Bulletin d'Informations Marées Terrestres*, **117**, 8639–8648.

Francis, O. and M. Hendrickx, 2001: Calibration of the LaCoste-Romberg 906 by comparison with the superconducting gravimeter C021 in Membach (Belgium). *Journal of the Geodetic Society of Japan*, **47**, 16–21.

Francis, O. and P. Melchior, 1996: Tidal loading in south western Europe: A test area. *Geophysical Research Letters*, **23**, 2251–2254.

Francis, O., T. Niebauer, G. Sasagawa, F. Klopping, and J. Gschwind, 1998: Calibration of a superconducting gravimeter by comparison with an absolute gravimeter FG5 in Boulder. *Geophysical Research Letters*, **25**, 1075–1078.

Francis, O., M. Van Camp, T. van Dam, R. Warnant, and M. Hendrickx, 2004: Indication of the uplift of the Ardenne in long-term gravity variations in Membach (Belgium). *Geophysical Journal International*, **158**, 346–352.

Francis, O., et al., 2005: Results of the international comparison of absolute gravimeters in Walferdange (Luxembourg) of November 2003. *Gravity, Geoid and Space Missions*, C. Jekeli, L. Bastos, and J. Fernandes, Eds., Springer-Verlag, Berlin, 272–275.

Franz, T., M. Zreda, T. Ferré, R. Rosolem, C. Zweck, S. Stillman, X. Zeng, and W. Shuttleworth, 2012: Measurement depth of the cosmic-ray soil moisture probe affected by hydrogen from various sources. *Water Resources Research*, **48**, W08515, doi:10.1029/2012WR011871.

Fu, G. and W. Sun, 2007: Effects of lateral inhomogeneity in a spherical Earth on gravity Earth tides. *Journal of Geophysical Research*, **112**, B06409, doi:10.1029/2006JB004512.

Fukuda, Y., et al., 2004: The first absolute gravity measurements in Indonesia. *Journal of Geodynamics*, **38**, 489–501.

Gabalda, G., S. Bonvalot, and R. Hipkin, 2003: CG3TOOL: An interactive computer program to process Scintrex CG-3/3M gravity data for high-resolution applications. *Computers & Geosciences*, **29**, 155–171.

Garland, G. D. and A. H. Cook, 1955: A determination of the differences in gravity between the National Physical Laboratory, Teddington, the Dominion Observatory, Ottawa, and the National Bureau of Standards, Washington. *Proceedings of the Royal Society of London*, **A 229**, 445–458.

Gehman, C. L., D. L. Harry, W. E. Sanford, J. D. Stednick, and N. A. Beckman, 2009: Estimating specific yield and storage change in an unconfined aquifer using temporal gravity surveys. *Water Resources Research*, **45**, W00D21, doi:10.1029/2007WR006096.

Geller, R. J., 1997: Earthquake prediction: A critical review. *Geophysical Journal International*, **131**, 425–450.

Gettings, P., D. S. Chapman, and R. Allis, 2008: Techniques, analysis, and noise in a Salt Lake Valley 4D gravity experiment. *Geophysics*, **73**, WA71–WA82.

Gilbert, F. and A. Dziewonski, 1975: An application of normal mode theory to the retrieval of structure parameters and source mechanisms for seismic spectra. *Philosophical Transactions of the Royal Society Series A*, **278**, 187–269.

Gilbert, R., 1958: An investigation into the calibration of gravity meters. *Geophysical Journal of the Royal Astronomical Society*, **1**, 330–340.

Gitlein, O. and L. Timmen, 2007: Atmospheric mass flow reduction for terrestrial absolute gravimetry in the Fennoscandian land uplift network. *Dynamic Planet*, P. Tregoning and C. Rizos, Eds., Springer Berlin Heidelberg, International Association of Geodesy Symposia, Vol. 130, 461–466.

Gladwin, M., C. Smith, M. Murakami, B. Murphy, and M. Morse, 1997: An absolute gravimeter comparison in Australia towards establishment of a precise reference frame for mean sea level change monitoring in South-Western Pacific. Tech. rep., Mine Scale Geophysics, CSIRO - Exploration and Mining, 4 pp.

Goodkind, J., 1986: Continuous measurement of nontidal variations of gravity. *Journal of Geophysical Research*, **91**, 9125–9134.

Goodkind, J., 1999: The superconducting gravimeter. *Review of Scientific Instruments*, **70**, 4131–4152.

Goodkind, J. M., 1979: Continuous measurement with the superconducting gravimeter. *Tectonophysics*, **52**, 99–105.

Grayson, R. B. and A. W. Western, 1998: Towards areal estimation of soil water content from point measurements: Time and space stability of mean response. *Journal of Hydrology*, **207**, 68–82.

Gross, R., 2000: The excitation of the Chandler wobble. *Geophysical Research Letters*, **27**, 2329–2332.

Gross, R., I. Fukumori, and D. Menemenlis, 2003: Atmospheric and oceanic excitations of the Earth's wobbles during 1980-2000. *Journal of Geophysical Research*, **108**, 2370–2386.

Guerschman, J. P., A. I. Van Dijk, G. Mattersdorf, J. Beringer, L. B. Hutley, R. Leuning, R. C. Pipunic, and B. S. Sherman, 2009: Scaling of potential evapotranspiration with MODIS data reproduces flux observations and catchment water balance observations across Australia. *Journal of Hydrology*, **369**, 107–119.

Hackney, R. I., 2001: A gravity-based study of the Pilbara–Yilgarn proterozoic continental collision zone and the south-eastern Hamersley province, Western Australia. Ph.D. thesis, The University of Western Australia.

Hamilton, A. C. and B. G. Brulé, 1967: Vibration-induced drift in LaCoste and Romberg geodetic gravimeters. *Journal of Geophysical Research*, **72**, 2187–2197.

Hanada, H., T. Tsubokawa, and S. Tsuruta, 1996: Possible large systematic error source in absolute gravimetry. *Metrologia*, **33**, 155–160.

Hare, J. L., J. F. Ferguson, C. L. V. Aiken, and J. L. Brady, 1999: The 4-D microgravity method for waterflood surveillance: A model study for the Prudhoe Bay reservoir, Alaska. *Geophysics*, **64**, 78–87.

Hare, J. L., J. F. Ferguson, and J. L. Brady, 2008: The 4D microgravity method for waterflood surveillance: Part IV – Modeling and interpretation of early epoch 4D gravity surveys at Prudhoe Bay, Alaska. *Geophysics*, **73**, WA173–WA180.

Harnisch, G. and M. Harnisch, 2006a: Hydrological influences in long gravimetric data series. *Journal of Geodynamics*, **41**, 276–287.

Harnisch, M. and G. Harnisch, 1995: Processing of the data from two superconducting gravimeters, recorded in 1990 - 1991 at Richmond (Miami, Florida). Some problems and results. *Bulletin d'Informations Marées Terrestres*, **122**, 9141–9147.

Harnisch, M. and G. Harnisch, 1999: Hydrological influences in the registrations of superconducting gravimeters and ways to their elimination. *Bulletin d'Informations Marées Terrestres*, **131**, 10 161–10 170.

Harnisch, M. and G. Harnisch, 2002: Seasonal variations of hydrological influences on gravity measurements at Wettzell. *Bulletin d'Informations Marées Terrestres*, **137**, 10 849–10 861.

Harnisch, M. and G. Harnisch, 2006b: Study of long-term gravity variations, based on data of the GGP co-operation. *Journal of Geodynamics*, **41**, 318–325.

Harnisch, M., G. Harnisch, and R. Falk, 2006: Hydrological influences on the gravity variations recorded at Bad Homburg. *Bulletin d'Informations Marées Terrestres*, **142**, 11 331–11 342.

Harnisch, M., G. Harnisch, I. Nowak, B. Richter, and P. Wolf, 2000: The dual sphere superconducting gravimeter CD029 at Frankfurt a.M. and Wettzell. First results and calibration. *Bulletin d'Informations Marées Terrestres*, **132**, 10 323–10 340.

Harrison, J. C., 1971: New computer programs for the calculation of Earth tides. Internal report, Cooperative Institute for Research in Environmental Sciences, University of Colorado.

Hartmann, T. and H.-G. Wenzel, 1995a: Catalogue HW95 of the tide generating potential. *Marées Terrestres Bulletin d'Informations*, **123**, 9278–9301.

Hartmann, T. and H.-G. Wenzel, 1995b: The HW95 tidal potential catalogue. *Geophysical Research Letters*, **22**, 3553–3556.

Hasan, S., P. A. Troch, P. W. Bogaart, and C. Kroner, 2008: Evaluating catchment-scale hydrological modeling by means of terrestrial gravity observations. *Water Resources Research*, **44**, W08416, doi:10.1029/2007WR006321.

Hasan, S., P. A. Troch, J. Boll, and C. Kroner, 2006: Modeling the hydrological effect on local gravity at Moxa, Germany. *Journal of Hydrometeorology*, **7**, 346–354.

Haynes, B. A., 1999: Establishment of a gravity calibration network on the Bentley campus of the Curtin University of Technology. Honours thesis, Curtin University of Technology.

Herckenrath, D., E. Auken, L. Christiansen, A. A. Behroozmand, and P. Bauer-Gottwein, 2012: Coupled hydrogeophysical inversion using time-lapse magnetic resonance sounding and time-lapse gravity data for hydraulic aquifer testing: Will it work in practice? *Water Resources Research*, **48**, W01539, doi: 10.1029/2011WR010411.

Hignett, C. and S. R. Evett, 2002: Neutron thermalization. *Methods of Soil Analysis: Part 4. Physical Methods*, J. H. Dane and G. C. Topp, Eds., Soil Science Society of America, 501–521.

Hinderer, J., M. Almavict, N. Florsch, O. Francis, and J. Mäkinen, 1998: On the calibration of superconducting gravimeters with the help of absolute gravity measurements. *Thirteenth International Symposium on Earth Tides*, Royal Observatory of Belgium, Brussels, 557–564.

Hinderer, J., D. Crossley, and R. Warburton, 2007: Gravimetric methods - Superconducting gravity meters. *Treatise on Geophysics, Volume 3 - Geodesy*, T. Herring, Ed., Elsevier, 65–122.

Hinderer, J., N. Florsch, J. Mäkinen, H. Legros, and J. Faller, 1991: On the calibration of a superconducting gravimeter using absolute gravity measurements. *Geophysical Journal International*, **106**, 491–497.

Hinderer, J., et al., 2009: The GHYRAF (Gravity and Hydrology in Africa) experiment: Description and first results. *Journal of Geodynamics*, **48**, 172–181.

Hinnell, A. C., T. Ferré, J. Vrugt, J. Huisman, S. Moysey, J. Rings, and M. Kowalsky, 2010: Improved extraction of hydrologic information from geophysical data through coupled hydrogeophysical inversion. *Water Resources Research*, **46**, W00D40, doi:10.1029/2008WR007060.

Hipkin, R., 1978: A microgravimetric network for secular gravity studies in Scotland. *Geophysical Journal of the Royal Astronomical Society*, **52**, 383–396.

Hipkin, R., E. Lagios, D. Lyness, and P. Jones, 1988: Reference gravity stations on the IGSN71 standard in Britain and Greece. *Geophysical Journal*, **92**, 143–148.

Hokkanen, T., K. Korhoven, and H. Virtanen, 2006: Hydrogeological effects on superconducting gravimeter measurements at Metsähovi in Finland. *Journal of Environmental and Engineering Geophysics*, **11**, 261–267.

Hokkanen, T., K. Korhoven, H. Virtanen, and E. L. Laine, 2007a: Effects of the fracture water of bedrock on superconducting gravimeter data. *Near Surface Geophysics*, **5**, 145–151.

Hokkanen, T., H. Virtanen, and M. Pirttivaara, 2007b: Hydrogeological effects on superconducting gravimeter measurements at Metsähovi in Finland. *Near Surface Geophysics*, **5**, 137–143.

Howle, J., S. Philips, R. Denlinger, and L. Metzger, 2003: Determination of specific yield and water-table changes using temporal microgravity surveys collected during the second injection, storage, and recovery test at Lancaster, Antelope Valley, California, November 1996 through April 1997. U.S. Geol. Surv. Water Resour. Invest. Rep. 03-4019, United States Geological Survey.

Hu, X.-G., L. Liu, B. Ducarme, H. Hsu, and H.-P. Sun, 2006: Wavelet filter analysis of local atmospheric pressure effects in the long-period tidal bands. *Physics of the Earth and Planetary Interiors*, **159**, 59–70.

Hu, X.-G., L. Liu, J. Hinderer, and H.-P. Sun, 2005: Wavelet filter analysis of local atmospheric pressure effects on gravity variations. *Journal of Geodesy*, **79**, 447–459.

Hwang, C., T.-C. Cheng, C. Cheng, and W. Hung, 2010: Land subsidence using absolute and relative gravimetry: A case study in Central Taiwan. *Survey Review*, **42**, 27–39.

Hwang, C., C.-G. Wang, and L.-H. Lee, 2002: Adjustment of relative gravity measurements using weighted and datum-free constraints. *Computers & Geosciences*, **28**, 1005–1015.

Imanishi, Y., T. Higashi, and Y. Fukuda, 2002: Calibration of the superconducting gravimeter T011 by parallel observation with the absolute gravimeter FG5 #210—A Bayesian approach. *Geophysical Journal International*, **151**, 867–878.

Imanishi, Y., K. Kokubo, and H. Tatehata, 2006: Effect of underground water on gravity observation at Matsushiro, Japan. *Journal of Geodynamics*, **41**, 221–226.

Imanishi, Y., K. Nawa, and H. Takayama, 2013: Local hydrological processes in a fractured bedrock and the short-term effect on gravity at Matsushiro, Japan. *Journal of Geodynamics*, **63**, 62–68.

Imanishi, Y., T. Sato, T. Higashi, W. Sun, and S. Okubo, 2004: A network of superconducting gravimeters detects submicrogal coseismic gravity changes. *Science*, **306**, 476–478, doi:10.1126/science.1101875.

Jacob, T., R. Bayer, J. Chery, and N. Le Moigne, 2010: Time-lapse microgravity surveys reveal water storage heterogeneity of a karst aquifer. *Journal of Geophysical Research*, **115**, B06402, doi:10.1029/2009JB006616.

Jacob, T., J. Chery, R. Bayer, N. Le Moigne, J.-P. Boy, P. Vernant, and F. Boudin, 2009: Time-lapse surface to depth gravity measurements on a karst system reveal the dominant role of the epikarst as a water storage entity. *Geophysical Journal International*, **177**, 347–360.

Jacob, T., et al., 2008: Absolute gravity monitoring of water storage variation in a karst aquifer on the larzac plateau (Southern France). *Journal of Hydrology*, **359**, 105–117.

Jahr, T., G. Jentzsch, and C. Kroner, 2001: The geodynamic observatory Moxa/Germany: Instrumentation and purposes. *Journal of the Geodetic Society of Japan*, **47**, 34–39.

Jeffreys, H., 1962: Who named the milligal? *Geophysical Journal of the Royal Astronomical Society*, **6**, 553.

Jentzsch, G., C. Kroner, D. Flach, and G. Gommlich, 1995: Underground SG-gravity record at the Asse/Northern Germany: Air pressure effects and long-term drift. *Bulletin d'Informations Marées Terrestres*, **122**, 9180–9181.

Jentzsch, G. and J. Melzer, 1989: Calibration and stability of the gravimeter LCR ET 18. *Bulletin d'Informations Marées Terrestres*, **104**, 7283–7289.

Jiang, Z., et al., 2009: Relative gravity measurement campaign during the 7th international comparison of absolute gravimeters (2005). *Metrologia*, **46**, 214–226.

Jiang, Z., et al., 2011: Final report on the seventh international comparison of absolute gravimeters (ICAG 2005). *Metrologia*, **48**, 246–260.

Jiang, Z., et al., 2012a: The 8th international comparison of absolute gravimeters 2009: The first key comparison (CCM.G-K1) in the field of absolute gravimetry. *Metrologia*, **49**, 666–684.

Jiang, Z., et al., 2012b: Relative gravity measurement campaign during the 8th international comparison of absolute gravimeters (2009). *Metrologia*, **49**, 95–107.

Jousset, P., M. Van Ruymbeke, S. Bonvalot, and M. Diament, 1995: Performance of two Scintrex CG3M instruments at the fourth international comparison of absolute gravimeters. *Metrologia*, **32**, 231–244.

Kang, K., H. Li, P. Peng, H. Hao, and J. Wei, 2011: Seasonal variations in hydrological influences on gravity measurements using gPhones. *Terrestrial Atmospheric and Oceanic Sciences*, **22**, 157–168.

Kazama, T. and S. Okubo, 2009: Hydrological modeling of groundwater disturbances to observed gravity: Theory and application to Asama Volcano, Central Japan. *Journal of Geophysical Research*, **114**, B08402, doi:10.1029/2009JB006391.

Kim, J. W., J. Neumeyer, T. H. Kim, I. Woo, H.-J. Park, J.-S. Jeon, and K.-D. Kim, 2009: Analysis of superconducting gravimeter measurements at MunGyung station, Korea. *Journal of Geodynamics*, **47**, 180–190.

Klügel, T., 2002: Tilt variations at shallow depth: Implications for the installation of a laser gyroscope at the geodetic observatory Wettzell. *Bulletin d'Informations Marées Terrestres*, **137**, 10 927–10 930.

Klügel, T., G. Harnisch, and M. Harnisch, 2006: Measuring integral soil moisture variations using a geoelectrical resistivity meter. *Bulletin d'Informations Marées Terrestres*, **142**, 11 369–11 375.

Klügel, T. and H. Wziontek, 2009: Correcting gravimeters and tiltmeters for atmospheric mass attraction using operational weather models. *Journal of Geodynamics*, **48**, 204–210.

Kowalczyk, E., Y. Wang, R. Law, H. Davies, J. McGregor, and G. Abramowitz, 2006: The CSIRO atmosphere biosphere land exchange (CABLE) model for use in climate models and as an offline model. CSIRO Marine and Atmospheric Research Paper 013, 37 pp.

Kowalczyk, E., et al., 2013: The land surface model component of ACCESS: Description and impact on the simulated surface climatology. *Australian Meteorological and Oceanographic Journal*, **63**, 65–82.

Krasinsky, G., E. Pitjeva, M. Sveshnikov, and L. Chunajeva, 1993: The motion of major planets from observations 1769-1988 and some astronomical constants. *Celestial Mechanics and Dynamical Astronomy*, **55**, 1–23.

Krause, P., M. Fink, and C. Kroner, 2006: Soil moisture measurement and simulation and their impact on gravimetric measurements. *Bulletin d'Informations Marées Terrestres*, **142**, 11 377–11 386.

Krause, P., M. Naujoks, M. Fink, and C. Kroner, 2009: The impact of soil moisture changes on gravity residuals obtained with a superconducting gravimeter. *Journal of Hydrology*, **373**, 151–163.

Kroner, C., 2001: Hydrological effects on gravity at the geodynamic observatory Moxa. *Journal of the Geodetic Society of Japan*, **47**, 353–358.

Kroner, C., 2006: Hydrological signals in the SG records at Moxa – A follow-up. *Bulletin d'Informations Marées Terrestres*, **142**, 11 353–11 357.

Kroner, C. and T. Jahr, 2006: Hydrological experiments around the superconducting gravimeter at Moxa Observatory. *Journal of Geodynamics*, **41**, 268–275.

Kroner, C., T. Jahr, and G. Jentzsch, 2001: Comparison of data sets recorded with the dual sphere superconducting gravimeter CD 034 at the geodynamic observatory Moxa. *Journal of the Geodetic Society of Japan*, **47**, 398–403.

Kroner, C., T. Jahr, and G. Jentzsch, 2002: Comparison of results obtained with a dual sensor superconducting gravimeter. *Bulletin d'Informations Marées Terrestres*, **135**, 10 617–10 620.

Kroner, C., T. Jahr, and G. Jentzsch, 2004: Results from 44 months of observations with a superconducting gravimeter at Moxa/Germany. *Journal of Geodynamics*, **38**, 263–280.

Kroner, C., T. Jahr, M. Naujoks, and A. Weise, 2007: Hydrological signals in gravity - Foe or friend? *Dynamic Planet*, P. Tregoning and C. Rizos, Eds., Springer Berlin Heidelberg, International Association of Geodesy Symposia, Vol. 130, 504–510.

Kroner, C. and G. Jentzsch, 1997: Methods of air pressure reduction tested on Potsdam station. *Bulletin d'Informations Marées Terrestres*, **127**, 9834–9842.

Kroner, C. and G. Jentzsch, 1998: Comparison of air pressure reducing methods and discussion of other influences on gravity. *13th International Symposium on Earth Tides*, B. Ducarme and P. Paquet, Eds., Brussels, 423–430.

Kroner, C. and G. Jentzsch, 1999: Comparison of different barometric pressure reductions for gravity data and resulting consequences. *Physics of the Earth and Planetary Interiors*, **115**, 205–218.

Lagios, E., 1984: A FORTRAN IV program for a least-squares gravity base-station network adjustment. *Computers & Geosciences*, **10**, 263–276.

Lambert, A. and C. Beaumont, 1977: Nano variations in gravity due to seasonal groundwater movements - Implications for gravitational detection of tectonic movements. *Journal of Geophysical Research*, **82**, 297–306.

Lambert, A., N. Courtier, and T. James, 2006: Long-term monitoring by absolute gravimetry: Tides to postglacial rebound. *Journal of Geodynamics*, **41**, 307–317.

Lambert, A., N. Courtier, G. Sasagawa, F. Klopping, D. Winester, T. James, and J. Liard, 2001: New constraints on Laurentide postglacial rebound from absolute gravity measurements. *Geophysical Research Letters*, **28**, 2109–2112.

Lampitelli, C. and O. Francis, 2010: Hydrological effects on gravity and correlations between gravitational variations and level of the Alzette River at the station of Walferdange, Luxembourg. *Journal of Geodynamics*, **49**, 31–38.

Le Provost, C., M. Genco, F. Lyard, P. Vincent, and P. Canceil, 1994: Spectroscopy of the world ocean tides from a finite-element hydrodynamic model. *Journal of Geophysical Research*, **99**, 24 777–24 797.

Le Provost, C., F. Lyard, J. Molines, M. Genco, and F. Rabilloud, 1998: A hydrodynamic ocean tide model improved by assimilating a satellite altimeter-derived data set. *Journal of Geophysical Research*, **103**, 5513–5529.

Lefèvre, F., F. Lyard, and C. Le Provost, 2002: FES99: A global tide finite element solution assimilating tide gauge and altimetric information. *Journal of Atmospheric and Oceanic Technology*, **19**, 1345–1356.

Lefèvre, F., F. H. Lyard, and C. Le Provost, 2000: FES98: A new global tide finite element solution independent of altimetry. *Geophysical Research Letters*, **27**, 2717–2720.

Leirião, S., X. He, L. Christiansen, O. B. Andersen, and P. Bauer-Gottwein, 2009: Calculation of the temporal gravity variation from spatially variable water storage change in soils and aquifers. *Journal of Hydrology*, **365**, 302–309.

Letellier, T., 2004: Etude des ondes de marée sur les plateux continentaux. Ph.D. thesis, University of Toulouse III.

Levine, J., J. Harrison, and W. Dewhurst, 1986: Gravity tide measurements with a feedback gravity meter. *Journal of Geophysical Research*, **91**, 12 835–12 841.

Liard, J. and C. Gagnon, 2002: The new A-10 absolute gravimeter at the 2001 international comparison of absolute gravimeters. *Metrologia*, **39**, 477–483.

Liard, J., C. Gagnon, and N. Courtier, 1995: Absolute gravity observations on BIPM site A3 during the 1989 and 1994 international comparisons of absolute gravimeters. *Metrologia*, **32**, 153–157.

Llubes, M., N. Florsch, J. Hinderer, L. Longuevergne, and M. Amalvict, 2004: Local hydrology, the Global Geodynamics Project and CHAMP/GRACE perspective: Some case studies. *Journal of Geodynamics*, **38**, 355–374.

Longman, I., 1959: Formulas for computing the tidal accelerations due to the Moon and the Sun. *Journal of Geophysical Research*, **64**, 2351–2355.

Longman, I., 1961: Corrigenda. *Journal of Geophysical Research*, **66**, 3082.

Longuevergne, L., J. Boy, N. Florsch, D. Viville, G. Ferhat, P. Ulrich, B. Luck, and J. Hinderer, 2009: Local and global hydrological contributions to gravity variations observed in Strasbourg. *Journal of Geodynamics*, **48**, 189–194.

Love, A., 1909: The yielding of the Earth to disturbing forces. *Proceedings of the Royal Society of London*, **A 82**, 73–88.

Lu, H., M. R. Raupach, T. R. McVicar, and D. J. Barrett, 2003: Decomposition of vegetation cover into woody and herbaceous components using AVHRR NDVI time series. *Remote Sensing of Environment*, **86**, 1–18.

Lyard, F., F. Lefevre, T. Letellier, and O. Francis, 2006: Modelling the global ocean tides: Modern insights from FES2004. *Ocean Dynamics*, **56**, 394–415.

Lyness, D. and E. Lagios, 1984: A microgravimetric network in East Central Greece – An area of potential seismic hazard. *Geophysical Journal of the Royal Astronomical Society*, **77**, 875–882.

Mäkinen, J. and S. Tattari, 1988: Soil moisture and groundwater: Two sources of gravity variations. *BGI Bull. Inf.*, **62**, 103–110.

Mäkinen, J. and S. Tattari, 1991a: The influence of variation in subsurface water storage on observed gravity. *Proc. of the XI International Symposium on Earth Tides, July 3-August 5, 1989*, J. Kakkuri, Ed., E. Schweitzerbart'sche Verlagsbuchhandlung, Stuttgart, Helsinki, Finland, 457–471.

Mäkinen, J. and S. Tattari, 1991b: Subsurface water and gravity. *Proc. of the Workshop: Nontidal Gravity Changes Intercomparison between Absolute and Superconducting Gravimeters*, Conseil de L'Europe Cahiers du Centre Européen de Géodynamique et de Séismologie, Walferdange, Luxembourg, Vol. 3, 235–240.

Marson, I., 2012: A short walk along the gravimeters path. *International Journal of Geophysics*, **2012**, 687813, doi:10.1155/2012/687813.

Marson, I., et al., 1995: Fourth international comparison of absolute gravimeters. *Metrologia*, **32**, 137–144.

Mathews, P. M., 2001: Love numbers and gravimetric factor for diurnal tides. *Journal of the Geodetic Society of Japan*, **46**, 231–236.

Matsumoto, K., T. Sato, T. Takanezawa, and M. Ooe, 2001: GOTIC2: A program for computation of oceanic tidal loading effect. *Journal of the Geodetic Society of Japan*, **47**, 243–248.

Matsumoto, K., T. Takanezawa, and M. Ooe, 2000: Ocean tide models developed by assimilating TOPEX/POSEIDON altimeter data into hydrodynamical model: A global model and a regional model around Japan. *Journal of Oceanography*, **56**, 567–581.

McCarthy, D. D. and G. Petit, 2004: IERS conventions (2003). IERS Technical Note 32, 127 pp.

McClymont, A., M. Hayashi, L. Bentley, and J. Liard, 2012: Locating and characterising groundwater storage areas within an alpine watershed using time-lapse gravity, GPR and seismic refraction methods. *Hydrological Processes*, **26**, 1792–1804.

McGregor, J. L., 2005: C-CAM: Geometric aspects and dynamical formulation. CSIRO Atmospheric Research Technical Paper 70, 43 pp.

McQueen, H., 2003: Phoenix rises from the ashes. *ANU Reporter*, **34**, 5.

Melchior, P., B. Barlow, M. Delcourt, and B. Ducarme, 1982: Discussion of a long series of gravity tide measurements at Alice Springs in the centre Australia. *Bulletin d'Informations Marées Terrestres*, **87**, 5568–5589.

Merlin, O., J. Walker, R. Panciera, R. Young, J. Kalma, and E. Kim, 2007: Soil moisture measurements in heterogeneous terrain. *MODSIM07: International Congress on Modelling and Simulation*, L. Oxley and D. Kulasiri, Eds., Canberra, Australia, MSSANZ, 2604–2610.

Merlin, O., et al., 2008: The NAFE'06 data set: Towards soil moisture retrieval at intermediate resolution. *Advances in Water Resources*, **31**, 1444–1455, doi: 10.1016/j.advwatres.2008.01.018.

Merriam, J., 1981: An investigation of dispersive effects on tidal gravity measurements at Alice-Springs. *Physics of the Earth and Planetary Interiors*, **27**, 187–193.

Merriam, J., 1992a: Atmospheric pressure and gravity. *Geophysical Journal International*, **109**, 488–500.

Merriam, J., 1992b: An ephemeris for gravity tide predictions at the nanogal level. *Geophysical Journal International*, **108**, 415–422.

Métivier, L. and C. P. Conrad, 2008: Body tides of a convecting, laterally heterogeneous, and aspherical Earth. *Journal of Geophysical Research*, **113**, B11405, doi:10.1029/2007JB005448.

Metzger, L. F., M. E. Ikehara, and J. F. Howle, 2002: Vertical-deformation, water-level, microgravity, geodetic, water-chemistry, and flow-rate data collected during injection, storage, and recovery tests at Lancaster, Antelope Valley, California, September 1995 through September 1998. U.S. Geol. Surv. Water Resour. Open-File Rep. 01-414, United States Geological Survey.

Meurers, B., 2000: Gravitational effects of atmospheric processes in SG gravity data. *Bulletin d'Informations Marées Terrestres*, **133**, 10 395–10 402.

Meurers, B., 2001a: Superconducting gravimetry in geophysical research today. *Journal of the Geodetic Society of Japan*, **47**, 300–307.

Meurers, B., 2001b: Tidal and non-tidal gravity variations in Vienna - A five years' SG record. *Journal of the Geodetic Society of Japan*, **47**, 392–397.

Meurers, B., 2002: Aspects of gravimeter calibration by time domain comparison of gravity records. *Bulletin d'Informations Marées Terrestres*, **135**, 10 643–10 650.

Meurers, B., 2004: Investigation of temporal gravity variations in SG-records. *Journal of Geodynamics*, **38**, 423–435.

Meurers, B., 2006: Long and short term hydrological effects on gravity in Vienna. *Bulletin d'Informations Marées Terrestres*, **142**, 11 343–11 351.

Meurers, B., M. Van Camp, and T. Petermans, 2007: Correcting superconducting gravity time-series using rainfall modelling at the Vienna and Membach stations and application to Earth tide analysis. *Journal of Geodesy*, **81**, 703–712.

Milly, P. and K. Dunne, 1994: Sensitivity of the global water cycle to the water-holding capacity of land. *Journal of Climate*, **7**, 506–526.

Milne, G. and J. Mitrovica, 1998: Postglacial sea-level change on a rotating Earth. *Geophysical Journal International*, **133**, 1–19.

Montgomery, E., 1971: Determination of coefficient of storage by use of gravity measurements. Ph.D. thesis, University of Arizona, Tucson.

Moore, R. and W. Farrell, 1970: Linearization and calibration of electrostatically fedback gravity meters. *Journal of Geophysical Research*, **75**, 928–932.

Moritz, H., 1980: Geodetic reference system 1980. *Bulletin Géodésique*, **54**, 388–398.

Mualem, Y., 1976: A new model for predicting the hydraulic conductivity of unsaturated porous media. *Water Resources Research*, **12**, 513–522.

Mukai, A., 1997: Effects of groundwater on gravity observation at Kyoto. *Gravity, Geoid, and Marine Geodesy*, J. Segawa, H. Fujimoto, and S. Okubo, Eds., Springer Berlin Heidelberg, International Association of Geodesy Symposia, Vol. 117, 123–130.

Mukai, A., T. Higashi, S. Takemoto, I. Nakagawa, and I. Naito, 1995: Accurate estimation of atmospheric effects on gravity observations made with a superconducting gravity meter at Kyoto. *Physics of the Earth and Planetary Interiors*, **91**, 149–159.

Müller, T. and W. Zürn, 1983: Observation of gravity changes during the passage of cold fronts. *Journal of Geophysics*, **53**, 155–162.

Munk, W. and D. Cartwright, 1966: Tidal spectroscopy and prediction. *Philosophical Transactions of the Royal Society Series A*, **259**, 533–581.

Nabighian, M., et al., 2005: Historical development of the gravity method in exploration. *Geophysics*, **70**, 63ND–89ND.

Nagy, D., 1966: Gravitational attraction of a right rectangular prism. *Geophysics*, **31**, 362–371.

Naujoks, M., 2009: Hydrological information in gravity: Observation and modelling. Ph.D. thesis, Friedrich-Schiller-University Jena.

Naujoks, M., C. Kroner, T. Jahr, and A. Weise, 2006: From a disturbing influence to a desired signal: Hydrological effects in gravity observations. *Bulletin d'Informations Marées Terrestres*, **142**, 11 359.

Naujoks, M., C. Kroner, A. Weise, T. Jahr, P. Krause, and S. Eisner, 2010: Evaluating local hydrological modelling by temporal gravity observations and a gravimetric three-dimensional model. *Geophysical Journal International*, **182**, 233–249.

Naujoks, M., A. Weise, C. Kroner, and T. Jahr, 2008: Detection of small hydrological variations in gravity by repeated observations with relative gravimeters. *Journal of Geodynamics*, **82**, 543–553.

Nawa, K., N. Suda, I. Yamada, R. Miyajima, and S. Okubo, 2009: Coseismic change and precipitation effect in temporal gravity variation at Inuyama, Japan: A case of the 2004 off the Kii peninsula earthquakes observed with a superconducting gravimeter. *Journal of Geodynamics*, **48**, 1–5.

Neumeyer, J., 1994: Acquisition, preprocessing and evaluation of GFZ Potsdam SCG data. *Bulletin d'Informations Marées Terrestres*, **120**, 8938–8945.

Neumeyer, J., 1995: Frequency dependent atmospheric pressure correction on gravity variations by means of cross spectral analysis. *Bulletin d'Informations Marées Terrestres*, **122**, 9212–9220.

Neumeyer, J., 2010: Superconducting gravimetry. *Sciences of Geodesy - I Advances and Future Directions*, G. Xu, Ed., Springer, Berlin Heidelberg, 339–413.

Neumeyer, J., F. Barthelmes, C. Kroner, S. Petrovic, R. Schmidt, H. Virtanen, and H. Wilmes, 2008: Analysis of gravity field variations derived from superconducting gravimeter recordings, the GRACE satellite and hydrological models at selected European sites. *Earth, Planets and Space*, **60**, 505–518.

Neumeyer, J., F. Barthelmes, and D. Wolf, 1998: Atmospheric pressure correction for gravity data using different methods. *13th International Symposium on Earth Tides*, B. Ducarme and P. Paquet, Eds., Brussels, 431–438.

Neumeyer, J., F. Barthelmes, and D. Wolf, 1999: Estimates of environmental effects in superconducting gravimeter data. *Bulletin d'Informations Marées Terrestres*, **131**, 10 153–10 159.

Neumeyer, J., E. Brinton, P. Fourie, H.-J. Dittfeld, H. Pflug, and B. Ritschel, 2001: Installation and first data analysis of the dual sphere superconducting gravimeter at the South African geodynamic observatory Sutherland. *Journal of the Geodetic Society of Japan*, **47**, 316–321.

Neumeyer, J. and H.-J. Dittfeld, 1997: Results of three year observation with a superconducting gravimeter at the GeoForschungsZentrum Potsdam. *Journal of Geodesy*, **71**, 97–102.

Neumeyer, J., J. Hagedoorn, J. Leitloff, and T. Schmidt, 2004: Gravity reduction with three-dimensional atmospheric pressure data for precise ground gravity measurements. *Journal of Geodynamics*, **38**, 437–450.

Neumeyer, J., T. Schmidt, and C. Stoeber, 2007: Improved determination of the atmospheric attraction with 3D air density data and its reduction on ground gravity measurements. *Dynamic Planet*, P. Tregoning and C. Rizos, Eds., Springer Berlin Heidelberg, International Association of Geodesy Symposia, Vol. 130, 541–548.

Neumeyer, J., et al., 2006: Combination of temporal gravity variations resulting from superconducting gravimeter (SG) recordings, GRACE satellite observations and global hydrology models. *Journal of Geodesy*, **79**, 573–585.

Niebauer, T., 1988: Correcting gravity measurements for the effects of local air pressure. *Journal of Geophysical Research*, **93**, 7989–7991.

Niebauer, T., 1989: The effective measurement height of free-fall absolute gravimeters. *Metrologia*, **26**, 115–118.

Niebauer, T., 2007: Gravimetric methods - Absolute gravimeter: Instruments concepts and implementation. *Treatise on Geophysics, Volume 3 - Geodesy*, T. Herring, Ed., Elsevier, 43–64.

Niebauer, T., G. Sasagawa, J. Faller, R. Hilt, and F. Klopping, 1995: A new generation of absolute gravimeters. *Metrologia*, **32**, 159–180.

Nied, M., Y. Hundecha, and B. Merz, 2013: Flood-initiating catchment conditions: A spatio-temporal analysis of large-scale soil moisture patterns in the Elbe River basin. *Hydrology and Earth System Sciences*, **17**, 1401–1414.

Niu, G.-Y., Z.-L. Yang, R. E. Dickinson, L. E. Gulden, and H. Su, 2007: Development of a simple groundwater model for use in climate models and evaluation with Gravity Recovery and Climate Experiment data. *Journal of Geophysical Research*, **112**, D07103, doi:10.1029/2006JD007522.

Njoku, E., T. Jackson, V. Lakshmi, T. Chan, and S. Nghiem, 2003: Soil moisture retrieval from AMSR-E. *IEEE Transactions on Geoscience and Remote Sensing*, **41**, 215–229.

Ochsner, T. E., R. Horton, and T. Ren, 2001: A new perspective on soil thermal properties. *Soil Science Society of America Journal*, **65**, 1641–1647.

Pagiatakis, S. and P. Salib, 2003: Historical relative gravity observations and the time rate of change of gravity due to postglacial rebound and other tectonic movements in Canada. *Journal of Geophysical Research*, **108**, 2406, doi: 10.1029/2001JB001676.

Pálinkáš, V., 2006: Precise tidal measurements by spring gravimeters at the station Pecný. *Journal of Geodynamics*, **41**, 14–22.

Park, J., et al., 2005: Earth's free oscillations excited by the 26 December 2004 Sumatra-Andaman earthquake. *Science*, **308**, 1139–1144, doi:10.1126/science.1112305.

Paulson, A., S. Zhong, and J. Wahr, 2007: Inference of mantle viscosity from GRACE and relative sea level data. *Geophysical Journal International*, **171**, 497–508.

Peischl, S., J. Walker, C. Rüdiger, N. Ye, Y. Kerr, E. Kim, R. Bandara, and M. Allahmoradi, 2012: The AACES field experiments: SMOS calibration and validation across the Murrumbidgee River catchment. *Hydrology and Earth System Sciences*, **16**, 1697–1708.

Peltier, W. R., 1994: Ice-age paleotopography. *Science*, **265**, 195–201.

Peter, G., F. Klopping, and K. Berstis, 1994: Observing and modelling gravity changes caused by soil moisture and groundwater table variations with superconducting gravimeters in Richmond, Florida, U.S.A. *Proc. of the 2nd Workshop: Nontidal Gravity Changes Intercomparison between Absolute and Superconducting Gravimeters*, Conseil de L'Europe Cahiers du Centre Européen de Géodynamique et de Séismologie, Walferdange, Luxembourg, Vol. 11, 147–159.

Peters, A., K. Chung, and S. Chu, 1999: Measurement of gravitational acceleration by dropping atoms. *Nature*, **400**, 849–852.

Peters, A., K. Chung, and S. Chu, 2001: High-precision gravity measurements using atom interferometry. *Metrologia*, **38**, 25–61.

Petit, J., 1954: Tables for the computation of the tidal accelerations of the Sun and Moon. *Transactions of the American Geophysical Union*, **35**, 193.

Pfeffer, J., et al., 2011: Local and global hydrological contributions to time-variable gravity in Southwest Niger. *Geophysical Journal International*, **184**, 661–672.

Pipunic, R., J. Walker, and A. Western, 2008: Assimilation of remotely sensed data for improved latent and sensible heat flux prediction: A comparative synthetic study. *Remote Sensing of Environment*, **112**, 1295–1305.

Pipunic, R., J. Walker, A. Western, and C. Trudinger, 2013: Assimilation of multiple data types for improved heat flux prediction: A one-dimensional field study. *Remote Sensing of Environment*, **136**, 315–329.

Pitman, A., 2003: The evolution of, and revolution in, land surface schemes designed for climate models. *International Journal of Climatology*, **23**, 479–510.

Pool, D. and J. Eychaner, 1995: Measurements of aquifer-storage change and specific yield using gravity surveys. *Ground Water*, **33**, 425–432.

Pool, D. and W. Schmidt, 1997: Measurement of ground-water storage change and specific yield using the temporal-gravity method near Rillito Creek, Tucson, Arizona. U.S. Geol. Surv. Water Resour. Invest. Rep. 97-4125, United States Geological Survey.

Pool, D. R., 2008: The utility of gravity and water-level monitoring at alluvial aquifer wells in southern Arizona. *Geophysics*, **73**, WA49–WA59.

Potter, C. S., J. T. Randerson, C. B. Field, P. A. Matson, P. M. Vitousek, H. A. Mooney, and S. A. Klooster, 1993: Terrestrial ecosystem production: A process model based on global satellite and surface data. *Global Biogeochemical Cycles*, **7**, 811–841.

Prothero, W. and J. Goodkind, 1968: A superconducting gravimeter. *Review of Scientific Instruments*, **39**, 1257–1262.

Puri, K., et al., 2013: Implementation of the initial ACCESS numerical weather prediction system. *Australian Meteorological and Oceanographic Journal*, **63**, in press.

Raupach, M., K. Finkele, and L. Zhang, 1997: SCAM (Soil-Canopy-Atmosphere Model): Description and comparison with field data. CSIRO Centre for Environmental Mechanics Technical Report 132, 81 pp.

Ray, R. D., 1999: A global ocean tide model from TOPEX/POSEIDON altimetry: GOT99.2. NASA Technical Memorandum 209478, Goddard Space Flight Center, 108 pp.

Riccardi, U., S. Rosat, and J. Hinderer, 2011: Comparison of the Micro-g LaCoste gPhone-054 spring gravimeter and the GWR-C026 superconducting gravimeter in Strasbourg (France) using a 300-day time series. *Metrologia*, **48**, 28–39.

Richter, B. and R. Warburton, 1998: A new generation of superconducting gravimeters. *Proceedings of the Thirteenth International Symposium on Earth Tides*, B. Ducarme and P. Pâquet, Eds., Brussels, 545–555.

Richter, B., H. Wenzel, W. Zurn, and F. Klopping, 1995a: From Chandler-wobble to free oscillations - Comparison of cryogenic gravimeters and other instruments in a wide period range. *Physics of the Earth and Planetary Interiors*, **91**, 131–148.

Richter, B., H. Wilmes, and I. Nowak, 1995b: The Frankfurt calibration system for relative gravimeters. *Metrologia*, **32**, 217–224.

Richter, H., A. Western, and F. Chiew, 2004: The effect of soil and vegetation parameters in the ECMWF land surface scheme. *Journal of Hydrometeorology*, **5**, 1131–114.

Robertsson, L., 2007: On the diffraction correction in absolute gravimetry. *Metrologia*, **44**, 35–39.

Robertsson, L., et al., 2001: Results from the fifth international comparison of absolute gravimeters, ICAG97. *Metrologia*, **38**, 71–78.

Roe, P. L., 1985: Some contributions to the modelling of discontinuous flows. *Large-Scale Computations In Fluid Mechanics*, Vol. 22, 163–194.

Romagnoli, C., S. Zerbini, L. Lago, B. Richter, D. Simon, F. Domenichini, C. Elmi, and M. Ghirotti, 2003: Influence of soil consolidation and thermal expansion effects on height and gravity variations. *Journal of Geodynamics*, **35**, 521–539.

Roosbeek, F., 1996: RATGP95: A harmonic development of the tide generating potential using an analytical method. *Geophysical Journal International*, **126**, 197–204.

Rothleitner, C. and O. Francis, 2010: On the influence of the rotation of a corner cube reflector in absolute gravimetry. *Metrologia*, **47**, 567–574.

Rothleitner, C., S. Svitlov, H. Mérimèche, and L. J. Wang, 2007: A method for adjusting the centre of mass of a freely falling body in absolute gravimetry. *Metrologia*, **44**, 234–241.

Rüdiger, C., 2007: Streamflow data assimilation for soil moisture prediction. Ph.D. thesis, The University of Melbourne.

Rüdiger, C., A. W. Western, J. P. Walker, A. B. Smith, J. D. Kalma, and G. R. Willgoose, 2010: Towards a general equation for frequency domain reflectometers. *Journal of Hydrology*, **383**, 319–329.

Rymer, H., 1989: A contribution to precision microgravity data analysis using Lacoste and Romberg gravity meters. *Geophysical Journal International*, **97**, 311–322.

Sabater, J. M., L. Jarlan, J.-C. Calvet, F. Bouyssel, and P. D. Rosnay, 2007: From near-surface to root-zone soil moisture using different assimilation techniques. *Journal of Hydrometeorology*, **8**, 194–206.

Sato, T., H. McQueen, B. Murphy, K. Lambeck, Y. Hamano, K. Asari, Y. Tamura, and M. Ooe, 1998: On the observations of gravity tides and Earth's free oscillations with a superconducting gravimeter CT#031 at Mt. Stromlo, Australia. *13th International Symposium on Earth Tides*, B. Ducarme and P. Paquet, Eds., Brussels.

Savcenko, R. and W. Bosch, 2008: EOT08a - A new global ocean tide model derived by empirical analysis of multi-mission altimetry data. *Geophysical Research Abstracts*, European Geosciences Union, Vol. 10.

Scherneck, H.-G., 1991: A parametrized solid Earth tide model and ocean tide loading effects for global geodetic baseline measurements. *Geophysical Journal International*, **106**, 677–694.

Schmerge, D. and O. Francis, 2006: Set standard deviation, repeatability and offset of absolute gravimeter A10-008. *Metrologia*, **43**, 414–418.

Schmidt, M., A. Senger, M. Hauth, C. Freier, V. Schkolnik, and A. Peters, 2011: A mobile high-precision absolute gravimeter based on atom interferometry. *Gyroscopy and Navigation*, **2**, 170–177.

Schrama, E. and R. Ray, 1994: A preliminary tidal analysis of TOPEX/POSEIDON altimetry. *Journal of Geophysical Research*, **99**, 24 799–24 808.

Schwahn, W., T. Baker, R. Falk, G. Jeffries, A. Lothhammer, B. Richter, H. Wilmes, and P. Wolf, 2000: Long-term increase of gravity at the Medicina station (Northern Italy) confirmed by absolute and superconducting gravimetric time series. *Bulletin d'Informations Marées Terrestres*, **132**, 10 299–10 322.

Schwank, M., T. R. Green, C. Mätzler, H. Benedickter, and H. Flühler, 2006: Laboratory characterization of a commercial capacitance sensor for estimating permittivity and inferring soil water content. *Vadose Zone Journal*, **5**, 1048–1064.

Schwiderski, E., 1980a: Ocean tides: A hydrodynamic interpolation model. *Marine Geodesy*, **3**, 219–255.

Schwiderski, E. W., 1980b: On charting global ocean tides. *Reviews of Geophysics and Space Physics*, **18**, 243–268.

Scintrex, 1995: *CG-3/3M Autograv Automated Gravity Meter Operator Manual.* Scintrex Limited, Concord, Ontario, Canada.

Seitz, F. and M. Schmidt, 2005: Atmospheric and oceanic contributions to Chandler wobble excitation determined by wavelet filtering. *Journal of Geophysical Research*, **110**, doi:10.1029/2005JB003826.

Seitz, F. and H. Schuh, 2010: Earth rotation. *Sciences of Geodesy - I Advances and Future Directions*, G. Xu, Ed., Springer, Berlin Heidelberg, 185–227.

Seyfried, M., L. Grant, E. Du, and K. Kumes, 2005: Dielectric loss and calibration of the Hydra Probe soil water sensor. *Vadose Zone Journal*, **4**, 1070–1079.

Simon, D., 2002: Modelling of the field of gravity variations induced by the seasonal air mass warming during 1998-2000. *Bulletin d'Informations Marées Terrestres*, **136**, 10 821–10 836.

Siriwardena, L., F. Chiew, H. Richter, and A. Western, 2003: Preparation of a climate data set for the Murrumbidgee River catchment. Cooperative Research Centre for Catchment Hydrology Working Document 03/1, 57 pp.

Smith, A., J. Walker, and A. Western, 2006: Detection of a soil moisture and groundwater signal in ground-based gravity observations. *30th Hydrology and Water Resources Symposium*, Launceston, Tasmania, Australia, I.E. Aust., [CD-ROM], 6 pp.

Smith, A., J. Walker, and A. Western, 2011: Variational gravity data assimilation to improve soil moisture prediction in a land surface model. *MODSIM2011, 19th International Congress on Modelling and Simulation*, F. Chan, D. Marinova, and R. Anderssen, Eds., Perth, Australia, Modelling and Simulation Society of Australia and New Zealand, 3391–3397.

Smith, A. and H. Zhang, 2007: Evaluating CABLE soil moisture predictions in the Murray Darling Basin. *'Physical processes and modelling of the water and carbon cycle': Extended abstracts of presentations at the first annual CAWCR Modelling Workshop 27-29 November 2007*, A. Hollis and V. Jemmeson, Eds., Melbourne, Australia, Bureau of Meteorology Research Centre, 15–18, BMRC Research Report 133.

Smith, A., et al., 2012: The Murrumbidgee soil moisture monitoring network data set. *Water Resources Research*, **48**, W07701, doi:10.1029/2012WR011976.

Smith, A. B., J. P. Walker, A. W. Western, and K. M. Ellett, 2005: Using ground-based gravity measurements to monitor changes in terrestrial water storage. *29th Hydrology and Water Resources Symposium*, Canberra, Australian Capital Territory, Australia, I.E. Aust., [CD-ROM], 8 pp.

Spratt, R., 1982: Modeling the effect of atmospheric pressure variations on gravity. *Geophysical Journal of the Royal Astronomical Society*, **71**, 173–186.

Standish, E. M. J., 1982: The JPL planetary ephemerides. *Celestial Mechanics*, **26**, 181–186.

Sun, H.-P., B. Ducarme, and V. Dehant, 1993: Preliminary investigations of the atmospheric pressure effect on vertical displacement and gravity observations. *Bulletin d'Informations Marées Terrestres*, **114**, 8334–8362.

Sun, H.-P., B. Ducarme, and V. Dehant, 1995: Correction of the atmospheric pressure on gravity measurements recorded by a superconducting gravimeter at Brussels. *Proc. of the XII International Symposium on Earth Tides, Beijing, 1993*, H.-T. Hsu, Ed., Science Press, Beijing, 317–330.

Swenson, S. and J. Wahr, 2002: Methods for inferring regional surface-mass anomalies from Gravity Recovery and Climate Experiment (GRACE) measurements of time-variable gravity. *Journal of Geophysical Research*, **107**, 2193, doi: 10.1029/2001JB000576.

Takemoto, S., Y. Fukuda, T. Higashi, M. Abe, S. Ogasawara, S. Dwipa, D. Kusuma, and A. Andan, 2002: Effect of groundwater changes on SG observations in Kyoto and Bandung. *Bulletin d'Informations Marées Terrestres*, **136**, 10 839–10 848.

Talbot, C. A., F. L. Ogden, and D. Or, 2004: Comment on "Layer averaged Richard's equation with lateral flow" by Praveen Kumar. *Advances in Water Resources*, **27**, 1041–1042.

Tamura, Y., 1987: A harmonic development of the tide-generating potential. *Bulletin d'Informations Marées Terrestres*, **99**, 6813–6855.

Tamura, Y., 1994: Additional terms to the tidal harmonic tables. *Proc. of the XII International Symposium on Earth Tides, Beijing, 1993*, H.-T. Hsu, Ed., Science Press, Beijing, 345–350.

Tamura, Y., 1999: Analysis of Earth tides data. *The Practice of Time Series Analysis*, H. Akaike and G. Kitagawa, Eds., Springer, New York, 327–339.

Tamura, Y., T. Sato, Y. Fukuda, and T. Higashi, 2005: Scale factor calibration of a superconducting gravimeter at Esashi station, Japan, using absolute gravity measurements. *Journal of Geodesy*, **78**, 481–488.

Tamura, Y., T. Sato, M. Ooe, and M. Ishiguro, 1991: A procedure for tidal analysis with a Bayesian information criterion. *Geophysical Journal International*, **104**, 507–516.

Telford, W., L. Geldart, and R. Sheriff, 1990: *Applied Geophysics.* 2d ed., Cambridge University Press, Cambridge, 770 pp.

Tikku, A., D. McAdoo, M. Schenewerk, and E. Willoughby, 2006: Temporal fluctuations of microseismic noise in Yellowstone's Upper Geyser Basin from a continuous gravity observation. *Geophysical Research Letters*, **33**, L11306, doi: 10.1029/2006GL026113.

Timmen, L., 2010: Absolute and relative gravimetry. *Sciences of Geodesy - I Advances and Future Directions*, G. Xu, Ed., Springer, Berlin Heidelberg, 1–48.

Timmen, L. and H.-G. Wenzel, 1994: Improved gravimetric Earth tide parameters for station Hannover. *Bulletin d'Informations Marées Terrestres*, **119**, 8834–8846.

Timofeev, V. Y., M. van Ruymbeke, G. Woppelmann, M. Everaerts, E. Zapreeva, P. Y. Gornov, and B. Ducarme, 2006: Tidal gravity observations in Eastern Siberia and along the Atlantic coast of France. *Journal of Geodynamics*, **41**, 30–38.

Topp, G., J. Davis, and A. Annan, 1980: Electromagnetic determination of soil water content: Measurements in coaxial transmission lines. *Water Resources Research*, **16**, 574–582.

Torge, W., 1989: *Gravimetry.* de Gruyter, Berlin, pp. 465.

Torge, W. and H. Wenzel, 1974: Gravimetric Earth tide observations in Iceland. *Bulletin d'Informations Marées Terrestres*, **74**, 4312–4318.

Turner, M., J. Walker, and P. Oke, 2008: Ensemble member generation for sequential data assimilation. *Remote Sensing of Environment*, **112**, 1421–1433.

Valliant, H., 1969a: The effect of humidity on the length of invariable pendulums. *Geophysical Journal of the Royal Astronomical Society*, **17**, 327–332.

Valliant, H., 1969b: Gravity measurements on the North American calibration line with the Candadian pendulum apparatus. *Geophysical Journal of the Royal Astronomical Society*, **17**, 489–505.

Valliant, H., 1973: A technique for the precise calibration of continuously recording gravimeters. *Philisophical Transactions of the Royal Society of London. Series A, Mathematical and Physical Sciences*, **274**, 227–230.

Van Camp, M., 2003: Efficiency of tidal corrections on absolute gravity measurements at the Membach station. *Proc. of the workshop: IMG-2002 Instrumentation and Metrology in Gravimetry*, Conseil de L'Europe Cahiers du Centre Européen de Géodynamique et de Séismologie, Walferdange, Luxembourg, Vol. 22, 99–103.

Van Camp, M., T. Camelbeeck, and O. Francis, 2002: Experiment to evaluate crustal motions across the Ardenne and the Roer Graben (north-western Europe) using absolute gravity measurements. *Metrologia*, **39**, 503–508.

Van Camp, M., O. de Viron, H.-G. Scherneck, K.-G. Hinzen, S. D. Williams, T. Lecocq, Y. Quinif, and T. Camelbeeck, 2011: Repeated absolute gravity measurements for monitoring slow intraplate vertical deformation in western Europe. *Journal of Geophysical Research*, **116**, B08402, doi:10.1029/2010JB008174.

Van Camp, M. and O. Francis, 2007: Is the drift of superconducting gravimeters a linear or exponential function of time? *Journal of Geodesy*, **81**, 337–344.

Van Camp, M., L. Métivier, O. de Viron, B. Meurers, and S. Williams, 2010: Characterizing long-time scale hydrological effects on gravity for improved distinction of tectonic signals. *Journal of Geophysical Research*, **115**, B07407, doi: 10.1029/2009JB006615.

Van Camp, M., P. Meus, Y. Quinif, O. Kaufman, M. Van Ruymbeke, M. Vandiepenbeeck, and T. Camelbeeck, 2006a: Karst aquifer investigation using absolute gravity. *EOS*, **87**, 298.

Van Camp, M., M. Vanclooster, O. Crommen, T. Petermans, K. Verbeeck, B. Meurers, T. van Dam, and A. Dassargues, 2006b: Hydrogeological investigations at the Membach station, Belgium, and application to correct long periodic gravity variations. *Journal of Geophysical Research*, **111**, B10403, doi:10.1029/2006JB004405.

Van Camp, M. and P. Vauterin, 2005: Tsoft: Graphical and interactive software for the analysis of time series and Earth tides. *Computers & Geosciences*, **31**, 631–640.

van Dam, T. and O. Francis, 1998: Two years of continuous measurements of tidal and nontidal variations of gravity in Boulder, Colorado. *Geophysical Research Letters*, **25**, 393–396.

van Dam, T., K. Larson, J. Wahr, S. Gross, and O. Francis, 2000: Using GPS and gravity to infer ice mass changes in Greenland. *EOS*, **81**, 421,426–427.

van Dam, T. and J. Wahr, 1987: Displacements of the Earth's surface due to atmospheric loading: Effects on gravity and baseline measurements. *Journal of Geophysical Research*, **92**, 1281–1286.

Van Genuchten, M. T., 1980: A closed-form equation for predicting the hydraulic conductivity of unsaturated soils. *Soil Science Society of America Journal*, **44**, 892–898.

Van Ruymbeke, M., A. Somerhausen, and N. Grammatica, 1995: Calibration of gravimeters with the VRR 8601 calibration platform. *Metrologia*, **32**, 209–216.

Varga, P., 1995: Gravimeter calibration device with the use of a heavy cylindrical ring. A state of the art report. *Bulletin d'Informations Marées Terrestres*, **121**, 9049–9060.

Varga, P., A. Hajósy, and G. Csapó, 1995: Laboratory calibration of Lacoste-Romberg type gravimeters by using a heavy cylindrical ring. *Geophysical Journal International*, **120**, 745–757.

Vauterin, P., 1998: The correction of the pressure effects for the superconducting gravimeter in Membach (Belgium). *13th International Symposium on Earth Tides*, B. Ducarme and P. Paquet, Eds., Brussels, 447–454.

Venedikov, A. P., J. Arnoso, and R. Vieira, 2003: VAV: A program for tidal data processing. *Computers & Geosciences*, **29**, 487–502.

Venedikov, A. P., J. Arnoso, and R. Vieira, 2005: New version of program VAV for tidal data processing. *Computers & Geosciences*, **31**, 667–669.

Virtanen, H., 2000: On the observed hydrological environmental effects on gravity at the Metsähovi station, Finland. *Bulletin d'Informations Marées Terrestres*, **133**, 10 369–10 375.

Virtanen, H., 2001: Hydrological studies at the gravity station Metsähovi in Finland. *Journal of the Geodetic Society of Japan*, **47**, 328–333.

Virtanen, H., 2002: Summary of observations in Metsähovi 1994 - 2001 with T020. *Bulletin d'Informations Marées Terrestres*, **135**, 10 605–10 606.

Virtanen, H. and J. Kääriäinen, 1998: One thousand days of superconducting gravimetry in Finland. *Thirteenth International Symposium on Earth Tides*, Royal Observatory of Belgium, Brussels, 591–598.

Virtanen, H., M. Tervo, and M. Bilker-Koivula, 2006: Comparison of superconducting gravimeter observations with hydrological models of various spatial extents. *Bulletin d'Informations Marées Terrestres*, **142**, 11 361–11 368.

Vitouchkine, A. and J. Faller, 2002: Measurement results with a small cam-driven absolute gravimeter. *Metrologia*, **39**, 465–469.

Vitushkin, L., et al., 2002: Results of the sixth international comparison of absolute gravimeters, ICAG-2001. *Metrologia*, **39**, 407–424.

Wahr, J., 1981: Body tides on an elliptical, rotating, elastic and oceanless Earth. *Geophysical Journal of the Royal Astronomical Society*, **64**, 677–703.

Wahr, J., M. Molenaar, and F. Bryan, 1998: Time variability of the Earth's gravity field: Hydrological and oceanic effects and their possible detection using GRACE. *Journal of Geophysical Research*, **103**, 30,205–30,229.

Wahr, J. M., 1985: Deformation induced by polar motion. *Journal of Geophysical Research*, **90**, 9363–9368.

Walker, J. P. and P. R. Houser, 2005: Hydrologic data assimilation. *Advances in Water Science Methodologies*, U. Aswathanarayana, Ed., A.A. Balkema, The Netherlands, 25–48.

Walker, J. P., G. R. Willgoose, and J. D. Kalma, 2004: In situ measurement of soil moisture: A comparison of techniques. *Journal of Hydrology*, **293**, 85–99.

Wang, T., V. A. Zlotnik, J. Šimunek, and M. G. Schaap, 2009: Using pedotransfer functions in vadose zone models for estimating groundwater recharge in semiarid regions. *Water Resources Research*, **45**, W04412, doi:10.1029/2008WR006903.

Wang, Y., 2000: A refinement to the two-leaf model for calculating canopy photosynthesis. *Agricultural and Forest Meteorology*, **101**, 143–150.

Wang, Y. and R. Leuning, 1998: A two-leaf model for canopy conductance, photosynthesis and partitioning of available energy I. Model description and comparison with a multilayered model. *Agricultural and Forest Meteorology*, **91**, 89–111.

Warburton, R. and J. Goodkind, 1977: The influence of barometric-pressure variations on gravity. *Geophysical Journal of the Royal Astronomical Society*, **48**, 281–292.

Watkins, M. and R. Eanes, 1997: Observations of tidally coherent diurnal and semidiurnal variations in the geocenter. *Geophysical Research Letters*, **24**, 2231–2234.

Weiss, R. and B. Block, 1970: A gravimeter to monitor the ${}_0S_0$ dilational mode of the Earth. *Journal of Geophysical Research*, **75**, 928–932.

Wenzel, H.-G., 1996: The nanogal software: Earth tide data processing package ETERNA 3.30. *Bulletin d'Informations Marées Terrestres*, **124**, 9425–9439.

Wenzel, H.-G., 1997: Tide-generating potential for the Earth. *Tidal Phenomena*, H. Wilhelm, W. Zürn, and H.-G. Wenzel, Eds., Springer, Berlin Heidelberg, 9–26.

Western, A., R. Grayson, G. Bloschl, G. Willgoose, and T. McMahon, 1999: Observed spatial organization of soil moisture and its relation to terrain indices. *Water Resources Research*, **35**, 797–810.

Western, A., R. Young, and F. Chiew, 2005: Murrumbidgee soil moisture monitoring network field calibration. Cooperative Research Centre for Catchment Hydrology, 16 pp.

Western, A. W. and M. S. Seyfried, 2005: A calibration and temperature correction procedure for the water-content reflectometer. *Hydrological Processes*, **19**, 3785–3793.

Williams, J., P. Ross, and K. Bristow, 1992: Prediction of the Campbell water retention function from texture, structure and organic matter. *Proceedings of the International Workshop on Indirect Methods for Estimating the Hydraulic Properties of Unsaturated Soils*, M. van Genuchten, F. Leij, and L. Lund, Eds., University of California, Riverside, CA, 427–441.

Wilmes, H., A. Boer, B. Richter, M. Harnisch, G. Harnisch, H. Hase, and G. Engelhard, 2006: A new data series observed with the remote superconducting gravimeter GWR R038 at the geodetic fundamental station TIGO in Cóncepcion (Chile). *Journal of Geodynamics*, **41**, 5–13.

Wilson, C. R., B. Scanlon, J. Sharp, L. Longuevergne, and H. Wu, 2012: Field test of the superconducting gravimeter as a hydrologic sensor. *Ground Water*, **50**, 442–449.

Wünsch, J., C. Kroner, C. Förste, and B. Fersch, 2011: Investigations to improve the signal-to-noise-ratio in data from superconducting gravimeters in the short-period spectral range. *Bulletin d'Informations Marées Terrestres*, **147**, 11 869–11 880.

Xi, Q., 1989: The precision of the development of the tidal generating and some explanatory notes. *Bulletin d'Informations Marées Terrestres*, **105**, 7396–7404.

Xu, J., H. Sun, and B. Ducarme, 2004a: A global experimental model for gravity tides of the Earth. *Journal of Geodynamics*, **38**, 293–306.

Xu, J.-Q., H.-P. Sun, and X.-F. Yang, 2004b: A study of gravity variations caused by polar motion using superconducting gravimeter data from the GGP network. *Journal of Geodesy*, **78**, 201–209.

Yeh, P. J.-F. and E. A. Eltahir, 2005a: Representation of water table dynamics in a land surface scheme. Part I: Model development. *Journal of Climate*, **18**, 1861–1880.

Yeh, P. J.-F. and E. A. Eltahir, 2005b: Representation of water table dynamics in a land surface scheme. Part II: Subgrid variability. *Journal of Climate*, **18**, 1881–1901.

Yeoh, N., J. Walker, R. Young, C. Rüdiger, A. Smith, K. Ellett, R. Pipunic, and A. Western, 2008: Calibration of the Murrumbidgee monitoring network CS616 soil moisture sensors. Department of Civil and Environmental Engineering, The University of Melbourne, 19 pp.

York, J., M. Person, W. Gutowski, and T. Winter, 2002: Putting aquifers into atmospheric simulation models: An example from the Mill Creek watershed, northeastern Kansas. *Advances in Water Resources*, **25**, 221–238.

Zaitchik, B. F., M. Rodell, and R. H. Reichle, 2008: Assimilation of GRACE terrestrial water storage data into a land surface model: Results for the Mississippi river basin. *Journal of Hydrometeorology*, **9**, 535–548.

Zerbini, S., M. Negusini, C. Romagnoli, F. Domenichini, B. Richter, and D. Simon, 2002: Multi-parameter continuous observations to detect ground deformation and to study environmental variability impacts. *Global and Planetary Change*, **34**, 37–58.

Zerbini, S., B. Richter, M. Negusini, C. Romagnoli, D. Simon, F. Domenichini, and W. Schwahn, 2001: Height and gravity variations by continuous GPS, gravity and environmental parameter observations in the southern Po Plain, near Bologna, Italy. *Earth and Planetary Science Letters*, **192**, 267–279.

Zhou, J., H. Sun, and J. Xu, 2009a: Validating global hydrological models by ground and space gravimetry. *Chinese Science Bulletin*, **54**, 1534–1542.

Zhou, J.-C., J.-Q. Xu, and H.-P. Sun, 2009b: Accurate correction models for tidal gravity in Chinese continent. *Chinese Journal of Geophysics*, **52**, 575–584.

Zobler, L., 1999: Global soil types, 1-degree grid (Zobler). Data set. Available online [http://www.daac.ornl.gov] from Oak Ridge National Laboratory Distributed Active Archive Center, Oak Ridge, Tennessee, U.S.A.

Zreda, M., D. Desilets, T. P. A. Ferré, and R. L. Scott, 2008: Measuring soil moisture content non-invasively at intermediate spatial scale using cosmic-ray neutrons. *Geophysical Research Letters*, **35**, L21402, doi:10.1029/2008GL035655.

Appendix A

Barometer Calibration

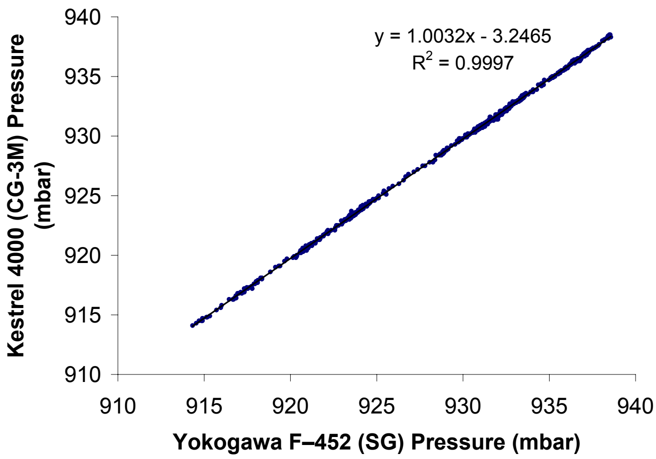

Fig. A.1 Kestrel 4000 barometer calibration.

Appendix B

Soil Particle Size Analysis

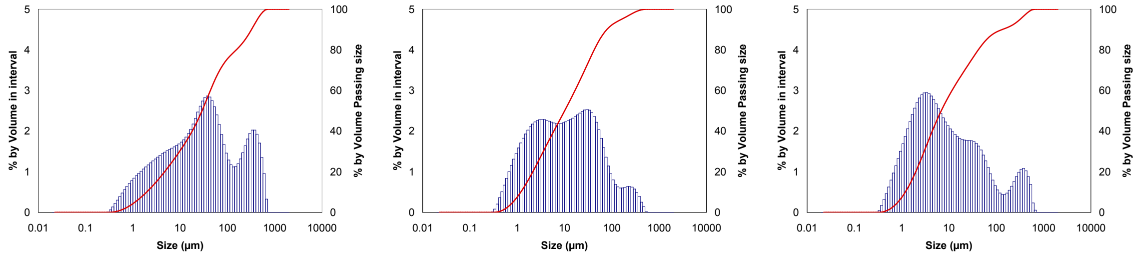

(a) K7 0-30 cm. (b) K7 30-60 cm. (c) K7 60-90 cm.

Fig. B.1 K7 soil particle size distribution for the range 0.02 – 2000 µm calculated by laser diffraction.

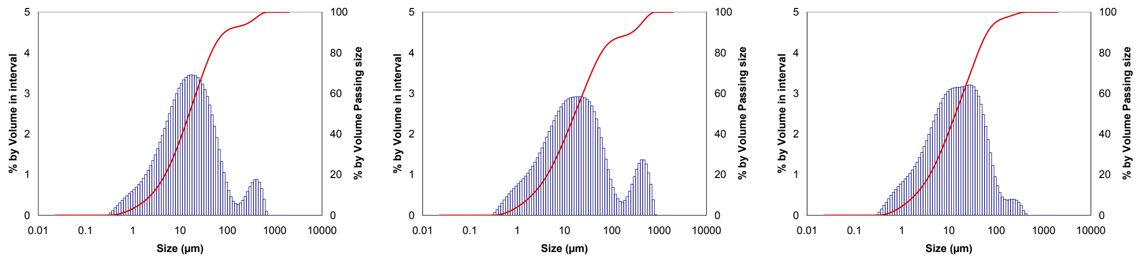

(a) K10 0-30 cm. (b) K10 30-60 cm. (c) K10 60-90 cm.

Fig. B.2 As for Fig. B.1 but for K10.

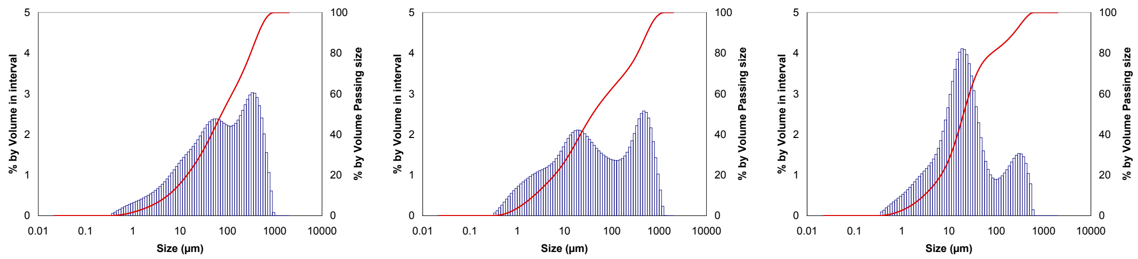

(a) K13 0-30 cm. (b) K13 30-60 cm. (c) K13 60-90 cm.

Fig. B.3 As for Fig. B.1 but for K13.

Appendix C

Soil Moisture Sensor Calibration

Both Campbell Scientific CS615 and CS616 water content reflectometers are used to measure soil moisture in the top 90 cm of the profile (CS615 at the older K5 site and CS616 at the newer K7, K10, and K13 sites). The two sensors differ slightly, with the CS615 (a discontinued model) operating at a lower frequency. Default calibrations provided by the manufacturer (Campbell Scientific, 1996, 2002) are quadratic (Table C.1) in the period (ms for the CS615 and µs for the CS616) with an additional quadratic calibration for the temperature dependence (Table C.2), temperature must be provided by a separate sensor. For soils with a low soil solution electrical conductivity, clay content and bulk density the default manufacturers calibrations are suitable, otherwise soil specific calibration is necessary (Campbell Scientific, 2002).

The default calibration is assessed against time domain reflectometry (TDR) measurements at K5, K7, K10 and K13. The 30-60 and 60-90 cm TDR measurements are obtained using a weighted difference of 0-30 and 0-60 cm measurements (respectively). The agreement between the default calibration and the field TDR measurements is reasonable for the 0-30 cm soil moisture at K5, K7, K10 and K13 (Fig. D.1–D.4), but degrades significantly at deeper depths, particularly at K7 where the default CS616 calibration predicts soil moisture in the range of 40-80 % vol/vol. Consequently water content reflectometer calibration is essential for K7 (this is probably due to high clay content at deeper depths at this site, Table 5.1), however the accuracy of soil moisture measurement will be improved considerably at all sites (and

Table C.1 Campbell Scientific CS615 and CS616 water content reflectometer calibration provided by the manufacturer (Campbell Scientific, 1996, 2002).

Sensor	Salinity	CS615/CS616 Calibration
CS615	< 1 dS/m	$SM = 0.335P^2 + 0.037P - 0.187$
	$1 - 1.8$ dS/m	$SM = 0.288P^2 + 0.097P - 0.207$
	$1.8 - 3$ dS/m	$SM = 0.096P^2 + 0.361P - 0.298$
CS616	< 0.5 dS/m	$SM = -0.0663 - 0.0063P_{20} + 0.0007P_{20}^2$
	≈ 0.4 dS/m	$SM = 0.0950 - 0.0211P_{20} + 0.0010P_{20}^2$
	≈ 0.75 dS/m	$SM = -0.0180 - 0.0070P_{20} + 0.0006P_{20}^2$

Table C.2 As for Table C.1 but for temperature correction.

Sensor	Temperature Correction
CS615	$SM_{20} = SM - (T - 20)(-0.045SM^2 + 0.019SM - 0.000346)$
CS616	$P_{20} = P + (20 - T)(0.526 - 0.052P + 0.00136P^2)$

depths) by using a site (or soil) specific calibration. As the soil moisture monitoring sites need to be undisturbed (no change of mass) for the period of the gravity experiment, a laboratory based calibration is performed on soil samples extracted from the sites before gravity measurements begin. Further, laboratory calibration allows field TDR observations to be used as evaluation data for the calibration (Fig. D.1–D.4).

The laboratory method of Rüdiger et al. (2010) is used for calibration of the Campbell Scientific CS616 water content reflectometers at K7, K10 and K13. This method uses a known volume and mass of soil and water to determine the volumetric soil moisture of the soil that the CS616 probes are inserted in and is based on the Western and Seyfried (2005) method of calibration for the earlier model CS615 that is used at K5. The main difference between the two approaches (beside the slightly different sensors) is the use of load cells to facilitate continuous logging as water is added to the soil column and infiltrates. For the calibration approach of Western and Seyfried (2005) water is thoroughly mixed through the soil before packing into the tubes, thus creating a homogeneous profile. It is thought that the infiltration approach of Rüdiger et al. (2010) simulates field soil moisture conditions more accurately, and also results in many more different moisture levels being observed (after equilibrium in the profile is reached).

In the calibration approaches of Western and Seyfried (2005) and Rüdiger et al.

(2010) the temperature is changed while moisture is held at a constant level allowing temperature dependence of the water content reflectometer (in that soil water mixture) to be assessed and corrected with,

$$P_{25} = P_{obs} - C_T(T - 25) \tag{C.1}$$

where P_{25} is water content reflectometer period corrected to 25 °C, P_{obs} is observed period, C_T (linear) temperature correction coefficient, and T (soil) temperature. However the temperature correction C_T is also moisture dependant (Western and Seyfried, 2005), hence C_T is determined at a number of moisture levels (by regression of P_{obs} on T, e.g. Fig. C.1 (a)). These regression lines are used to predict period at 25 °C (P_{25}), and this is plotted against the slope (C_T) from the fitted linear equation (Fig. C.1 (b)). Another linear regression is then performed on the calculated temperature corrected period P_{25} (Fig. C.1 (b)) to determine the temperature correction moisture dependence at a range of soil moisture levels (not just the three or four that were measured). This regression is

$$C_T = sP_{25} + o \tag{C.2}$$

Eq. (C.2) is then substituted back into Eq. (C.1) to remove the moisture dependence (P_{25} term) in the temperature correction (C_T). After rearrangement Eq. (C.1) be-

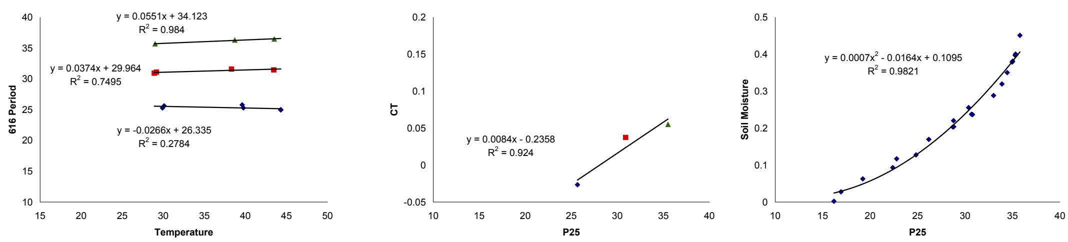

(a) Temperature dependence at three soil moisture levels.

(b) Temperature correction.

(c) CS616 calibration (temperature corrected to 25 °C).

Fig. C.1 K7 60 − 90 cm CS616 calibration and temperature correction. For (b) the points are the 616 period value at a temperature of 25 °C and the slope from the fitted linear equation (P25 and CT respectively) from (a).

comes

$$P_{25} = \frac{P_{obs} - o(T - 25)}{1 + s(T - 25)} \tag{C.3}$$

In Rüdiger et al. (2010) and Western and Seyfried (2005) P_{25} is used together with the period for oven dried soil $P_{0.0}$ and nominal soil saturation (40 % vol/vol) $P_{0.4}$ to calculate normalised soil moisture

$$N = \frac{P_{25} - P_{0.0}}{P_{0.4} - P_{0.0}} \tag{C.4}$$

that is used in a power equation

$$\theta = 0.4N^{\beta} \tag{C.5}$$

where $P_{0.0}$ is observed while $P_{0.4}$ and β are jointly optimised using laboratory data. In the case of Rüdiger et al. (2010) the final calibration equation is a generalised version of Eq. C.5, a piecewise linear-power function that has additional parameters α (slope of linear portion) and γ (transition point from linear to power) to calibrate (together with β and $P_{0.4}$).

The appeal of the normalised equation is that from previous analysis of a range of soils the parameters may be prescribed (Rüdiger et al., 2010), for example $P_{0.0}$ as 0.76 and β as 0.7 for the CS615 (Western and Seyfried, 2005). With all but one parameter prescribed the remaining parameter can be calibrated by as little as one field TDR measurement (Western and Seyfried, 2005). While appealing in a data scarce situation, for the highest accuracy in the calibration a normalisation is not necessary (as a "universal" calibration for all soil types is not sought), therefore a polynomial was simply fit to P_{25} and volumetric soil moisture data (Fig. C.1 (c)). The calibration for each sensor is given in Table C.3 and shown graphically in Fig. C.2-C.10. For K13 a linear calibration is sufficient (Fig. C.10), however for K7 and K10 a quadratic is necessary to obtain an adequate fit. While a calibration is fitted to all laboratory data (after essential cleaning) the observed CS616 period range in the field is considerably smaller than the laboratory range, and further is not very well covered by laboratory observations. Therefore it is essential that the laboratory calibrations are evaluated with field TDR measurements.

The TDR derived soil moisture is calculated from field measurements of apparent soil dielectric constant (K_a) and the "universal" TDR calibration (Topp et al., 1980). At K5 0-30 cm TDR measurements are made using a balun and 30 cm connector type probes that are randomly inserted close to the soil moisture station when a measurement is made, whereas 30-60 cm and 60-90 cm TDR measurements are made using permanently installed, horizontally oriented 20 cm buriable type probes located 45 and 75 cm below the soil surface. At the newer K7, K10, and K13 sites 30, 60 and 90 cm connector type TDR probes are permanently installed (Fig. 3.3). The 30-60 and 60-90 cm TDR measurements are obtained using a weighted difference of 0-30 and 0-60 cm measurements (respectively).

From Fig. D.1–D.4 it can be seen that the high EC manufacturers calibration (pink crosses) gives reasonable agreement with the field TDR (at all sites and depths), however the laboratory calibrations (blue diamonds) give consistently better agreement with field TDR, and hence a more accurate absolute soil moisture measurement. The laboratory calibration was repeated for 0-30 cm and 60-90 cm at K13 (as the temperature correction procedure was not performed for the initial

Table C.3 Campbell Scientific CS616 water content reflectometer calibration and temperature correction. Determined by laboratory analysis on soil from depths at which soil moisture sensors are installed. K5 has a CS615 calibration as CS615 probes are installed at this site. CS615 probes were also calibrated for the other sites but are not shown as only CS616 probes are installed at those sites. As a 30-60 cm temperature correction was not determined for K13 the 60-90 cm laboratory determined temperature correction is used.

Site	Depth	Temperature Correction	CS615/CS616 Calibration
K5	0-30 cm	$C_T = 0.0134P_{25} - 0.0114$	$SM = 0.4[(P_{25} - 0.76)/(1.468 - 0.76)]^{0.7}$
	30-60 cm	$C_T = 0.0134P_{25} - 0.0114$	$SM = 0.4[(P_{25} - 0.76)/(1.731 - 0.76)]^{0.7}$
	60-90 cm	$C_T = 0.0134P_{25} - 0.0114$	$SM = 0.4[(P_{25} - 0.76)/(1.675 - 0.76)]^{0.7}$
K7	0-30 cm	$C_T = 0.0116P_{25} - 0.1783$	$SM = 0.0007P_{25}^2 - 0.0069P_{25} - 0.059$
	30-60 cm	$C_T = 0.0082P_{25} - 0.2305$	$SM = 0.0008P_{25}^2 - 0.0171P_{25} + 0.0922$
	60-90 cm	$C_T = 0.0084P_{25} - 0.2358$	$SM = 0.0007P_{25}^2 - 0.0164P_{25} + 0.1095$
K10	0-30 cm	$C_T = 0.0081P_{25} - 0.1267$	$SM = 0.0006P_{25}^2 + 0.0013P_{25} - 0.1939$
	30-60 cm	$C_T = 0.0038P_{25} - 0.0507$	$SM = 0.0009P_{25}^2 - 0.0187P_{25} + 0.0884$
	60-90 cm	$C_T = 0.006P_{25} - 0.0873$	$SM = 0.0005P_{25}^2 - 0.0026P_{25} - 0.0825$
K13	0-30 cm	$C_T = -0.001P_{25} + 0.0689$	$SM = 0.0233P_{25} - 0.3552$
	30-60 cm	$C_T = 0.0029P_{25} - 0.0364$	$SM = 0.0253P_{25} - 0.4645$
	60-90 cm	$C_T = 0.0029P_{25} - 0.0364$	$SM = 0.0235P_{25} - 0.4247$

calibration). This allows a check on the repeatability of the laboratory calibrations (Fig. D.4). Consistent with the other sites, the 0-30 cm calibrations at K13 are all very similar (the two laboratory calibrations and the three default manufacturers calibrations). When the 60-90 cm calibration at K13 was redone the load cell (used to calculate volumetric soil moisture) was faulty, hence some laboratory TDR measurements also had to be used to calibrate the CS616, therefore the initial calibration is deemed more reliable. However, even with the added uncertainty the redone calibration is still comparable to the best (high EC) manufacturers calibration in terms of agreement with the field TDR measurements (Fig. D.4). K5 is a first generation site in the Murrumbidgee Soil Moisture Monitoring Network (Fig. 3.1) and has CS615 water content reflectometers installed that were field calibrated using buriable type TDR measurements. The K5 CS615 calibration is evaluated, both with the measurements used for the calibration and with later TDR data (Fig. D.1). Similar to the laboratory based calibrations of the CS616 water content reflectometers, Fig. D.1 shows an improvement in the accuracy of absolute soil moisture measurement when using a site specific calibration compared to the manufacturers calibration provided with the instrument.

K7

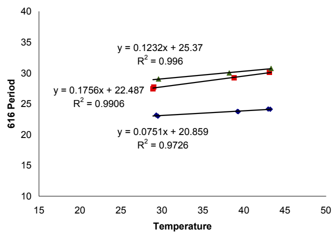

(a) K7 0-30 cm.

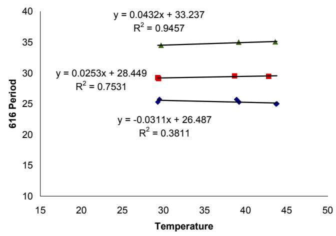

(b) K7 30-60 cm.

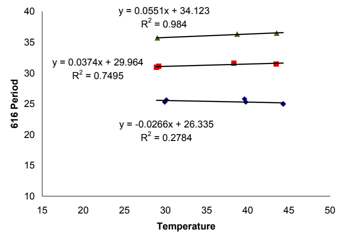

(c) K7 60-90 cm.

Fig. C.2 K7 CS616 temperature dependence at three soil moisture levels.

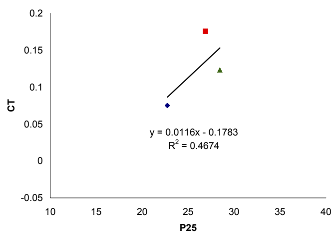

(a) K7 0-30 cm.

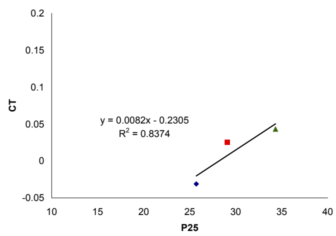

(b) K7 30-60 cm.

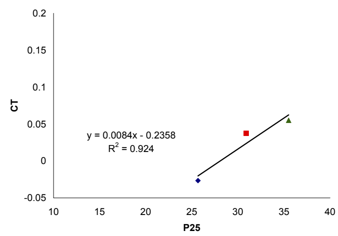

(c) K7 60-90 cm.

Fig. C.3 K7 CS616 temperature correction. Points are from figure above (Fig. C.2), the 616 period value at a temperature of 25 °C and the slope from the fitted linear equation (P25 and CT respectively).

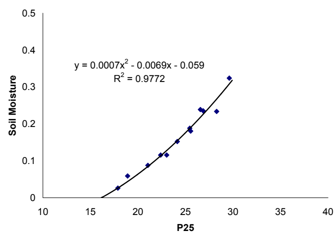

(a) K7 0-30 cm.

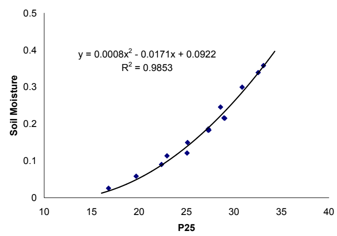

(b) K7 30-60 cm.

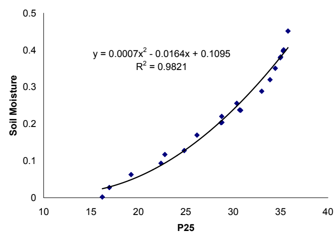

(c) K7 60-90 cm.

Fig. C.4 K7 CS616 calibration (temperature corrected to 25 °C).

K10

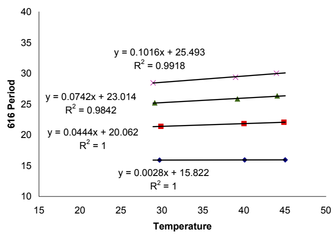

(a) K10 0-30 cm.

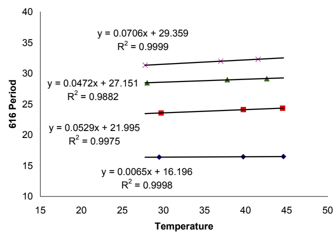

(b) K10 30-60 cm.

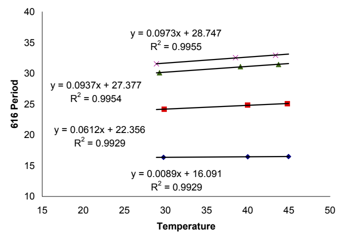

(c) K10 60-90 cm.

Fig. C.5 K10 CS616 temperature dependence at four soil moisture levels.

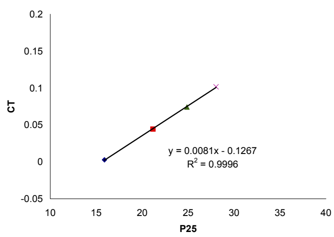

(a) K10 0-30 cm.

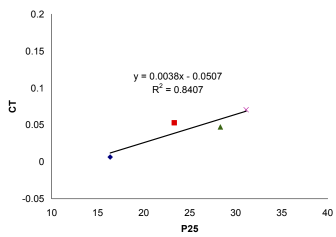

(b) K10 30-60 cm.

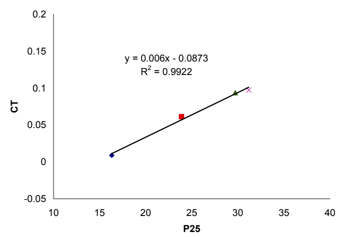

(c) K10 60-90 cm.

Fig. C.6 K10 CS616 temperature correction. Points are from figure above (Fig. C.5), the 616 period value at a temperature of 25 °C and the slope from the fitted linear equation (P25 and CT respectively).

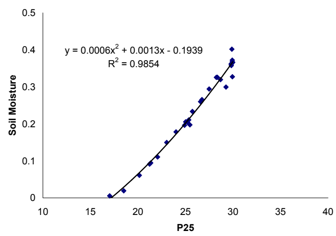

(a) K10 0-30 cm.

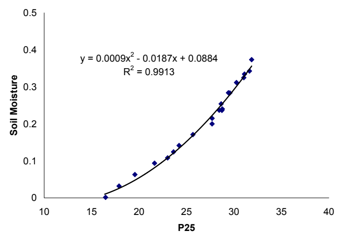

(b) K10 30-60 cm.

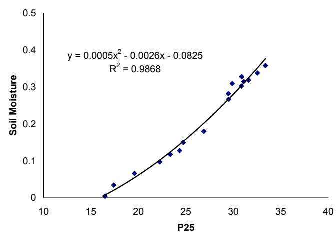

(c) K10 60-90 cm.

Fig. C.7 K10 CS616 calibration (temperature corrected to 25 °C).

K13

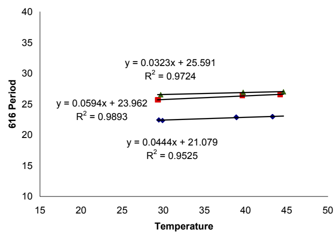

(a) K13 0-30 cm.

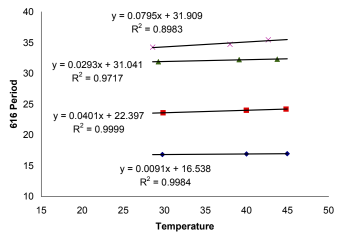

(b) K13 60-90 cm.

Fig. C.8 K13 CS616 temperature dependence at different soil moisture levels.

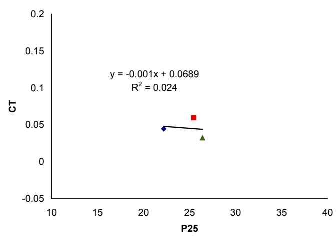

(a) K13 0-30 cm.

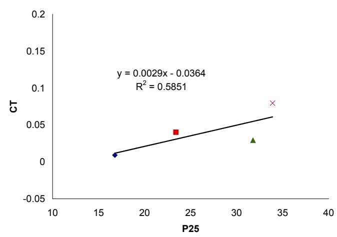

(b) K13 60-90 cm.

Fig. C.9 K13 CS616 temperature correction. Points are from figure above (Fig. C.8), the 616 period value at a temperature of 25 °C and the slope from the fitted linear equation (P25 and CT respectively).

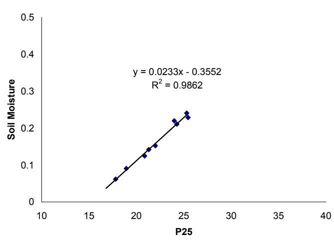

(a) K13 0-30 cm.

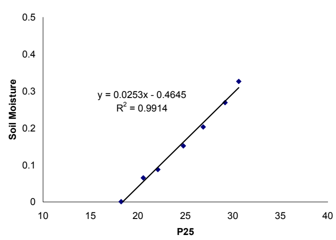

(b) K13 30-60 cm.

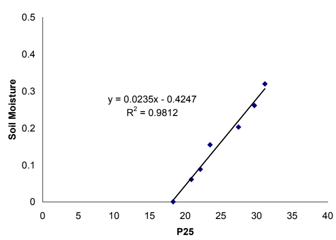

(c) K13 60-90 cm.

Fig. C.10 K13 CS616 calibration (temperature corrected to 25 °C).

Appendix D

Soil Moisture Sensor Validation

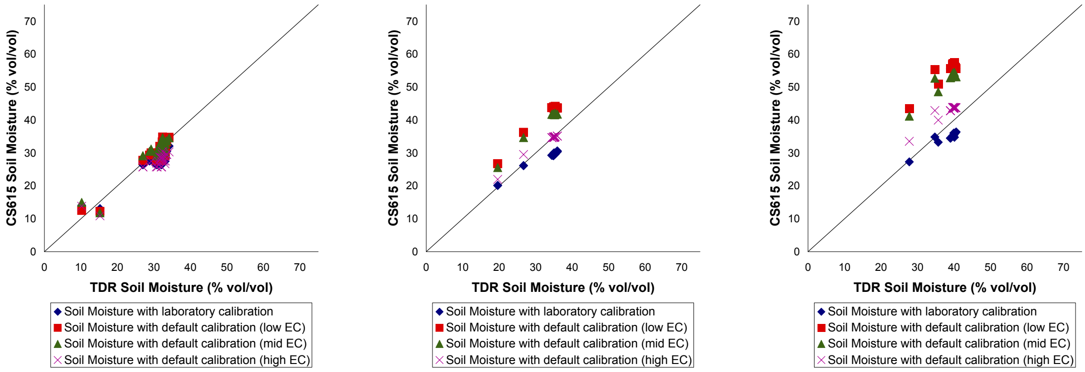

(a) K5 0-30 cm. (b) K5 30-60 cm. (c) K5 60-90 cm.

Fig. D.1 K5 in-situ verification of CS615 calibration (Table C.3). Blue diamonds are soil moisture using site-specific calibration of the CS615 water content reflectometer, whereas red squares are using the default (low EC) manufacturers calibration (Table C.1 and C.2). Green triangles and pink crosses are mid and high EC (respectively) manufacturers calibrations.

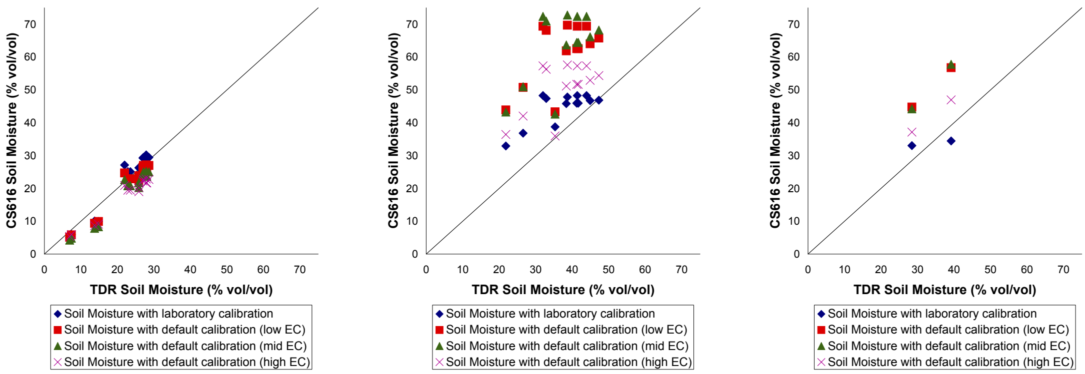

(a) K7 0-30 cm. (b) K7 30-60 cm. (c) K7 60-90 cm.

Fig. D.2 K7 in-situ verification of laboratory CS616 calibration.

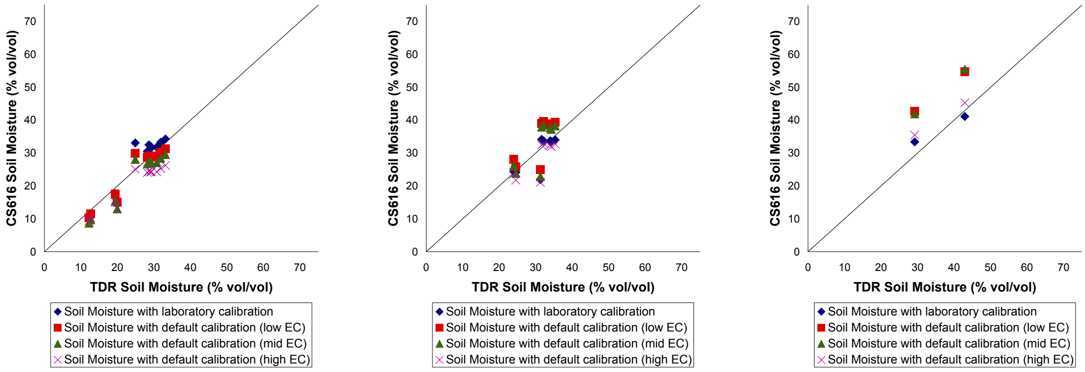

(a) K10 0-30 cm. (b) K10 30-60 cm. (c) K10 60-90 cm.

Fig. D.3 K10 in-situ verification of laboratory CS616 calibration.

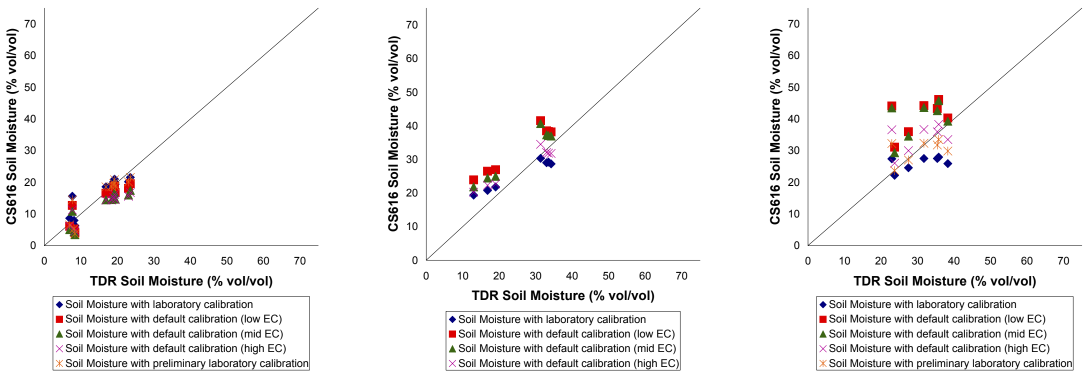

(a) K13 0-30 cm. (b) K13 30-60 cm. (c) K13 60-90 cm.

Fig. D.4 K13 in-situ verification of laboratory CS616 calibration. The K13 preliminary calibrations use the default temperature correction (Table C.2).

Appendix E

Neutron Moisture Meter Calibration

K5

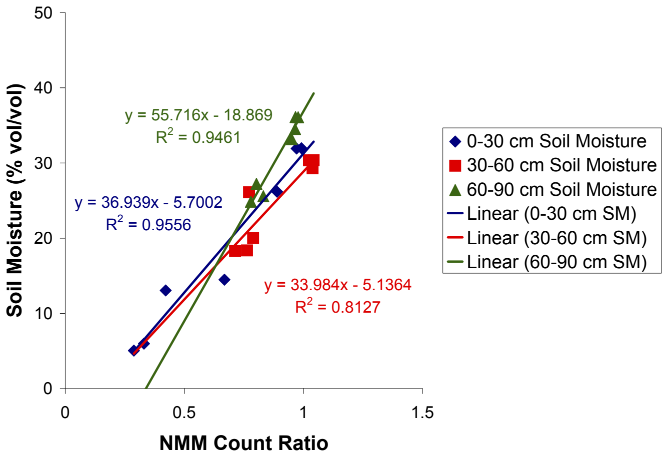

Fig. E.1 K5 initial neutron moisture meter calibration.

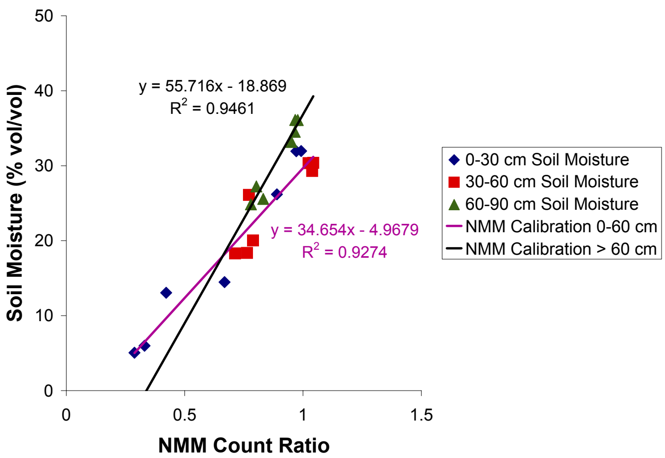

Fig. E.2 K5 neutron moisture meter calibration.

K7

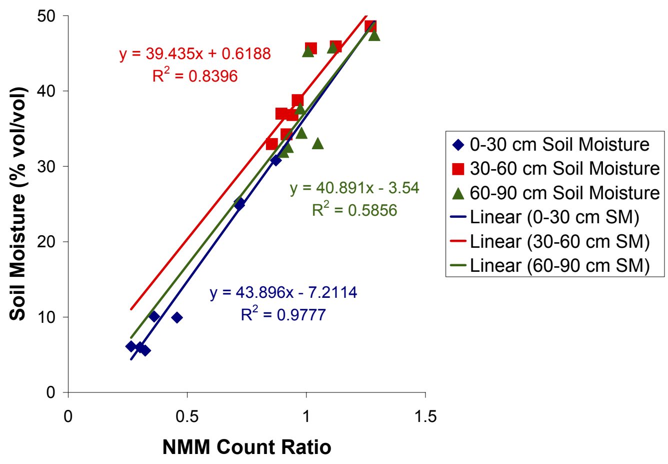

Fig. E.3 K7 initial neutron moisture meter calibration.

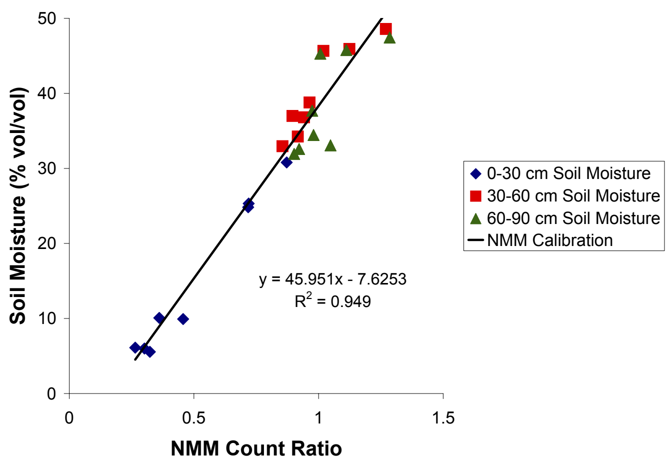

Fig. E.4 K7 neutron moisture meter calibration.

K10

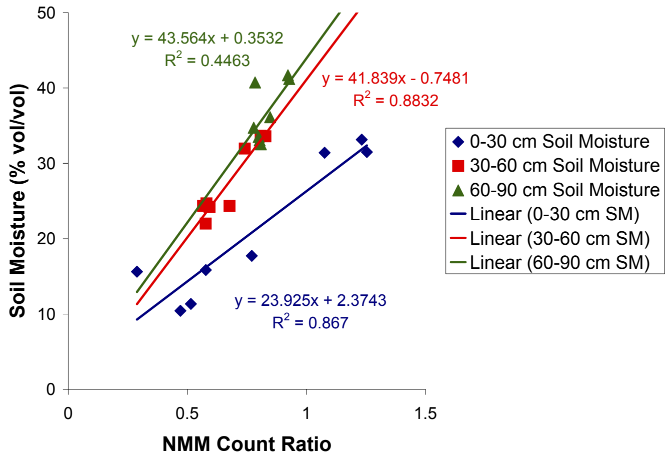

Fig. E.5 K10 initial neutron moisture meter calibration.

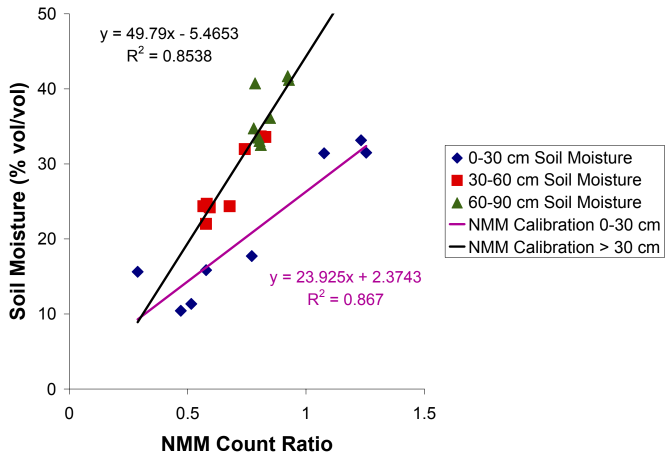

Fig. E.6 K10 neutron moisture meter calibration.

K13

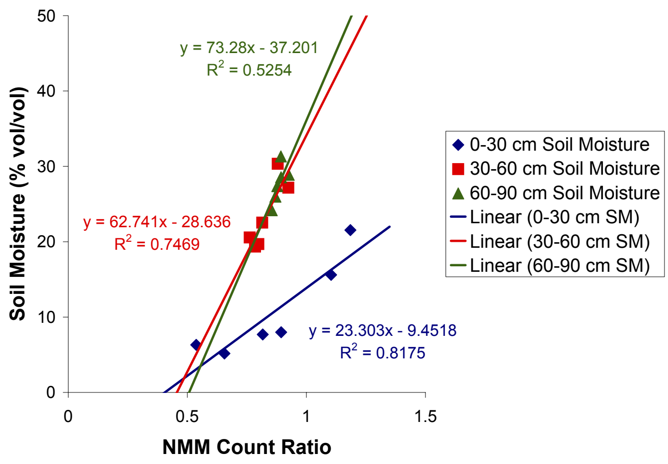

Fig. E.7 K13 initial neutron moisture meter calibration.

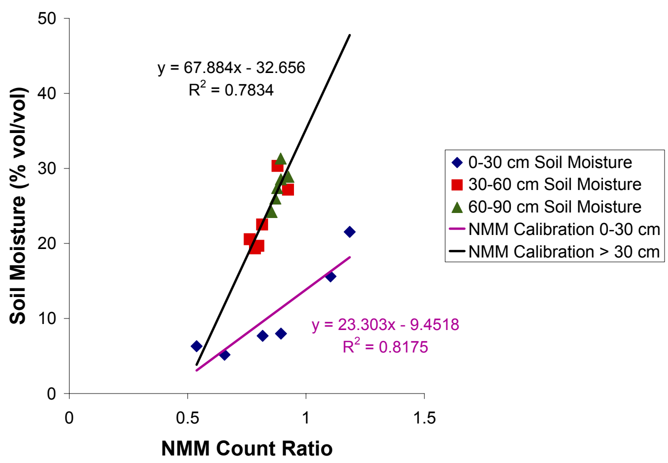

Fig. E.8 K13 neutron moisture meter calibration.

Appendix F

Ground Water Probe Calibration

K7

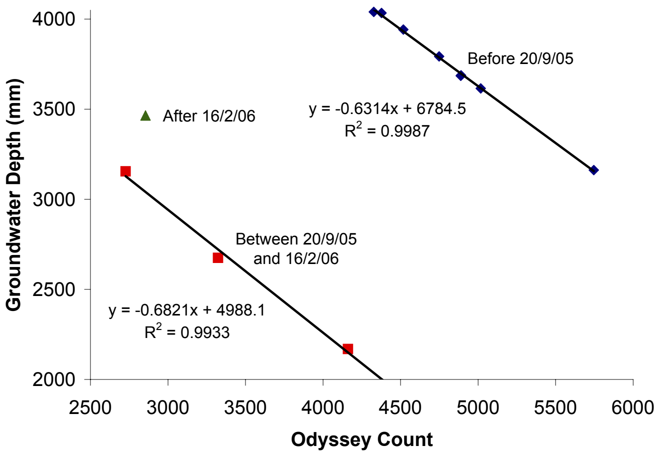

Fig. F.1 K7 capacitance probe calibration.

K10

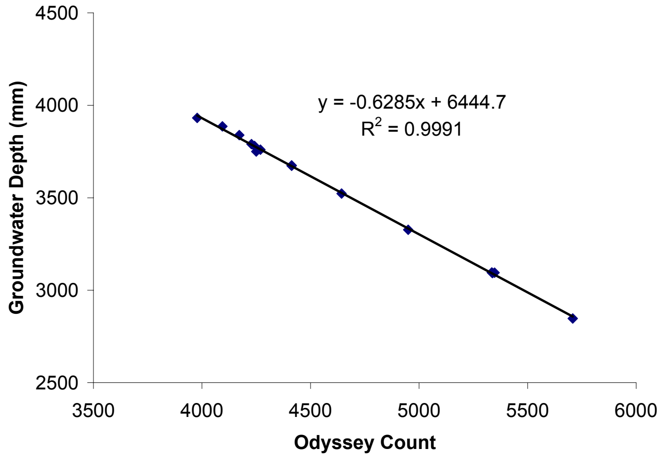

Fig. F.2 K10 capacitance probe calibration.

K13

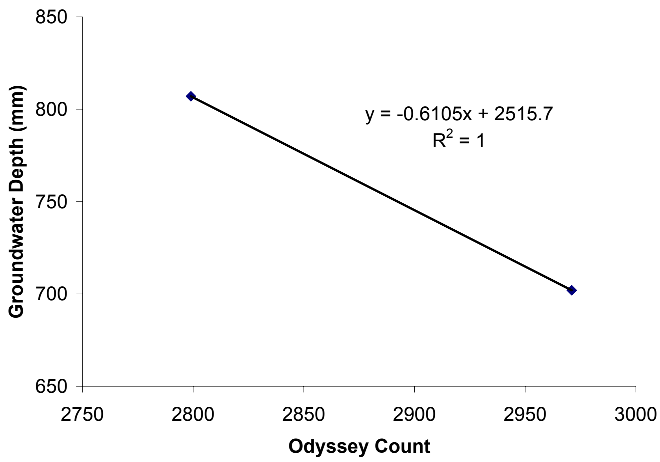

Fig. F.3 K13 capacitance probe calibration.

Appendix G

Soil Moisture Retrieval

1 Month Assimilation Window

Gravity Anomaly

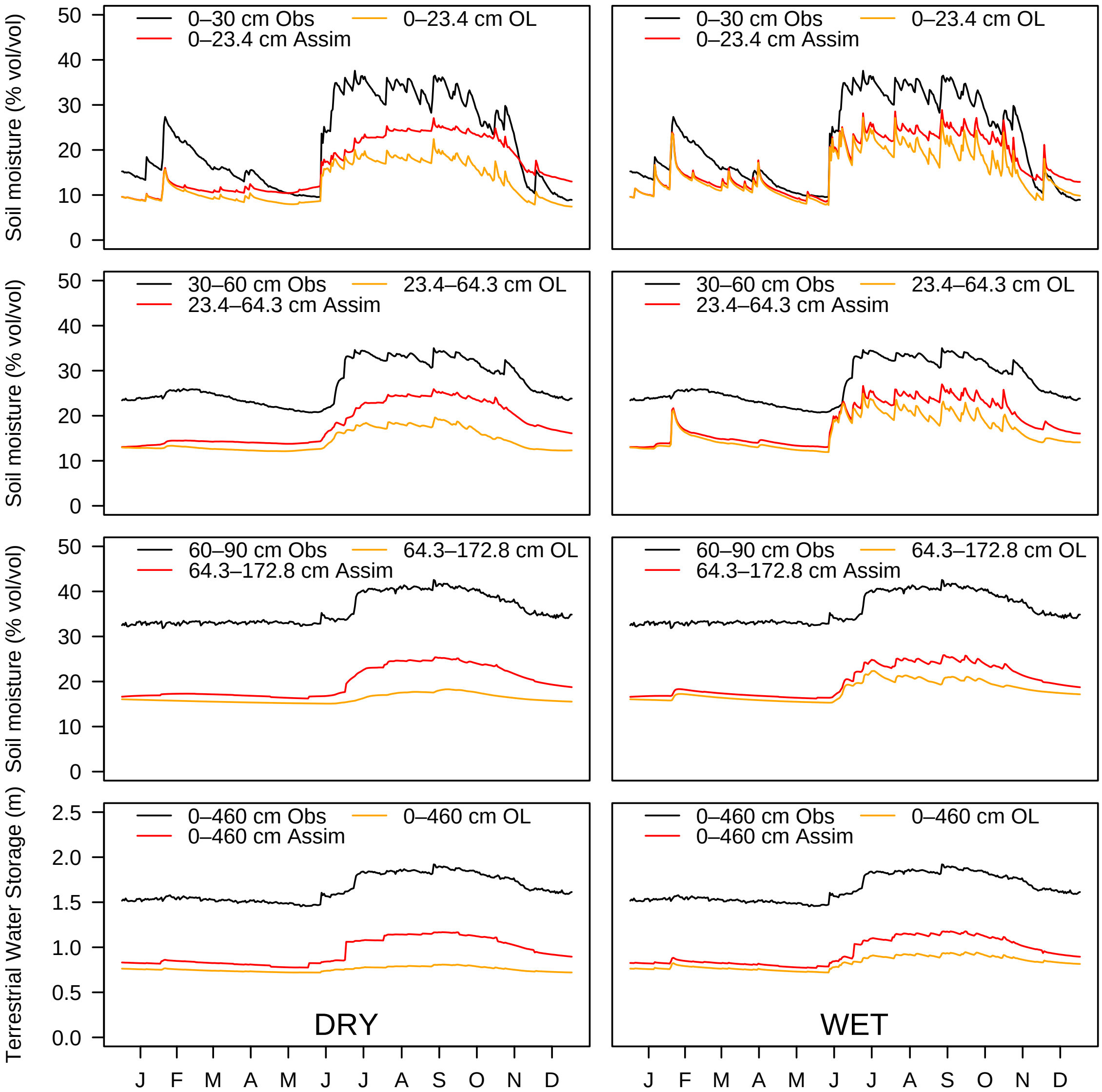

Fig. G.1 K10 gravity anomaly assimilation results for 2005 (with correct 2004 OL mean as background) using a one month assimilation window (case 1Ma in Table 6.2-6.5) with dry and wet open loop forcing (left and right columns). Assimilation (Assim) and open loop (OL) runs are in red and orange, observations (Obs) in black.

Gravity Change

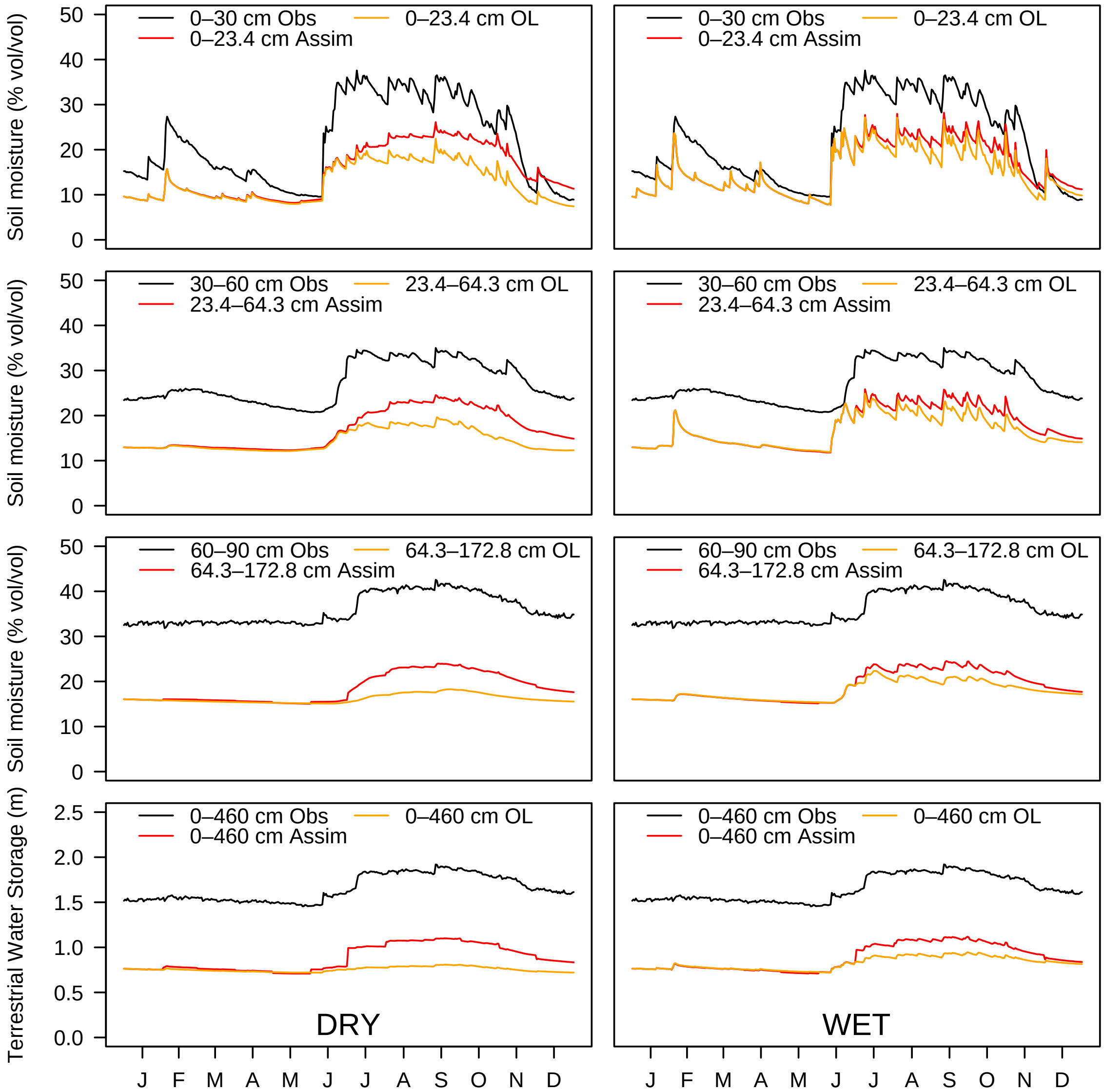

Fig. G.2 K10 gravity change results for 2005 using a one month assimilation window (case 1Md in Table 6.2-6.5) with dry and wet open loop forcing (left and right columns). Assimilation (Assim) and open loop (OL) runs are in red and orange, observations (Obs) in black.

Absolute Gravity (using Open Loop Background)

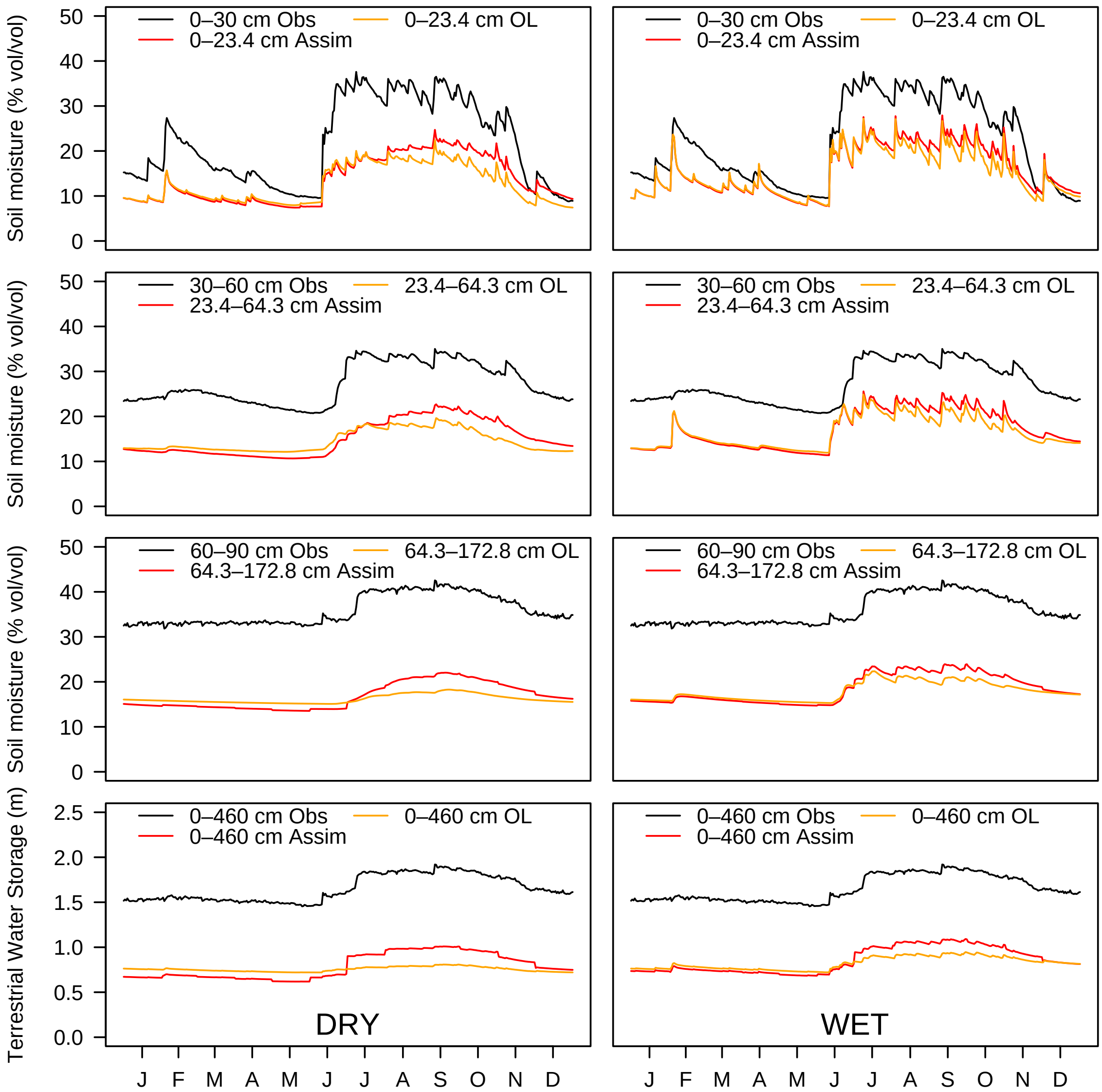

Fig. G.3 K10 absolute gravity assimilation results for 2005 (with 2005 OL mean as background) using a one month assimilation window (case 1Me in Table 6.2-6.5) with dry and wet open loop forcing (left and right columns). Assimilation (Assim) and open loop (OL) runs are in red and orange, observations (Obs) in black.

Gravity Anomaly (Background Incorrect)

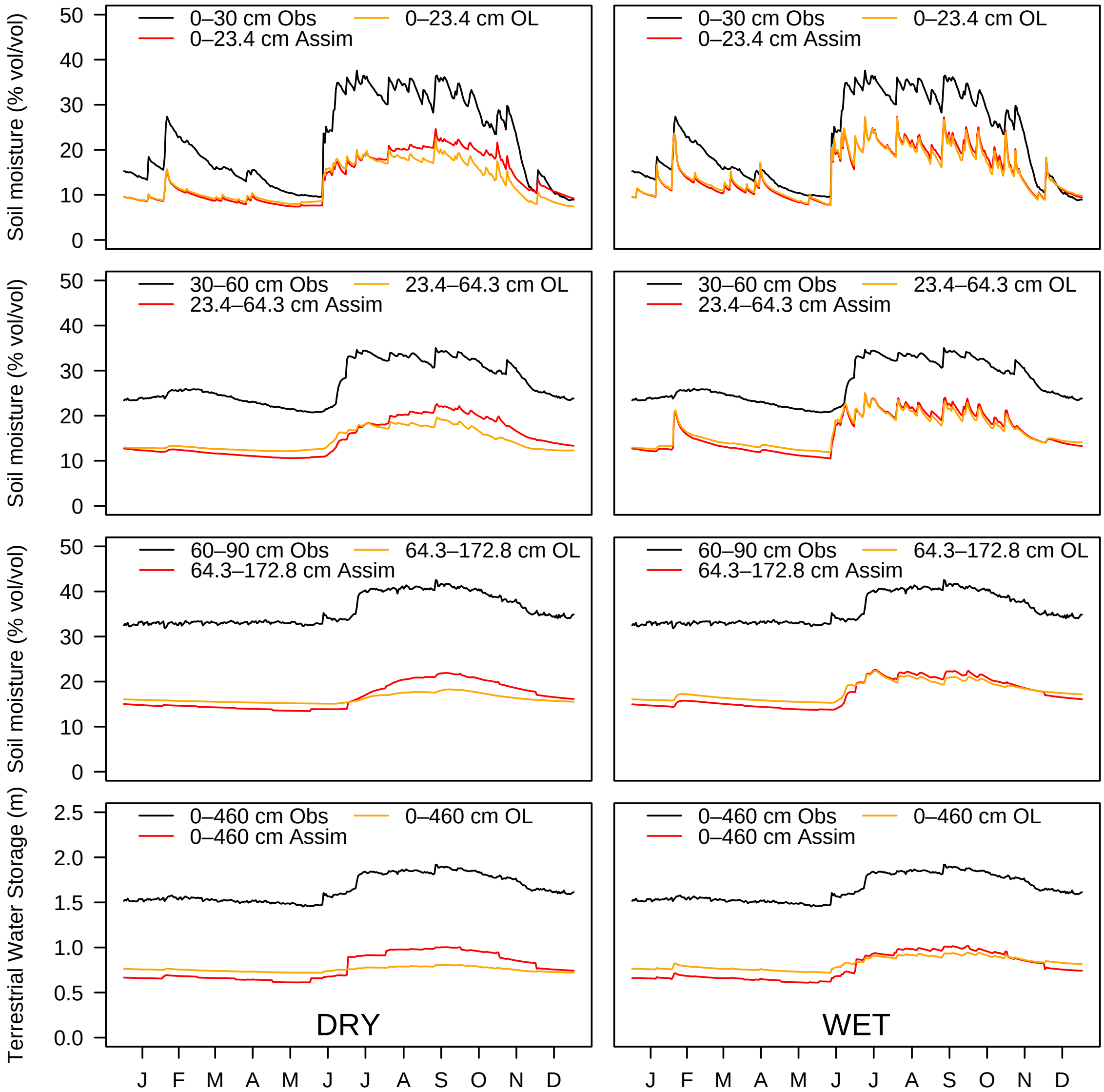

Fig. G.4 K10 gravity anomaly assimilation results for 2005 (with incorrect 2002 OL mean as background) using a one month assimilation window (case 1Mf in Table 6.2-6.5) with dry and wet open loop forcing (left and right columns). Assimilation (Assim) and open loop (OL) runs are in red and orange, observations (Obs) in black.

Gravity Anomaly and Near-surface Soil Moisture

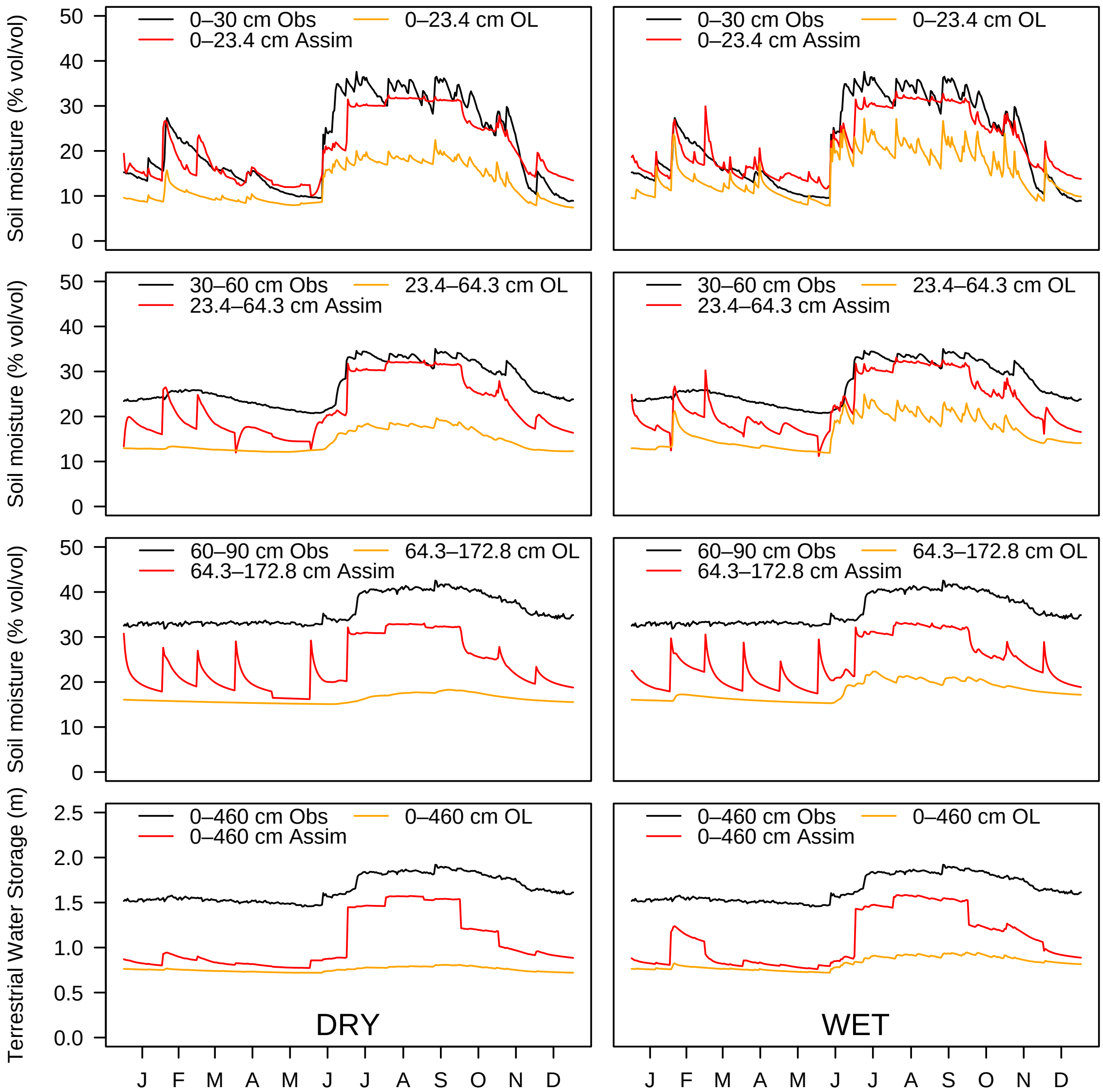

Fig. G.5 K10 gravity anomaly and near-surface soil moisture assimilation results for 2005 (with correct 2004 OL mean as background) using a one month assimilation results for 2005 using a one month assimilation window (case 1Mb in Table 6.2-6.5) with dry and wet open loop forcing (left and right columns). Assimilation (Assim) and open loop (OL) runs are in red and orange, observations (Obs) in black.

Near-surface Soil Moisture

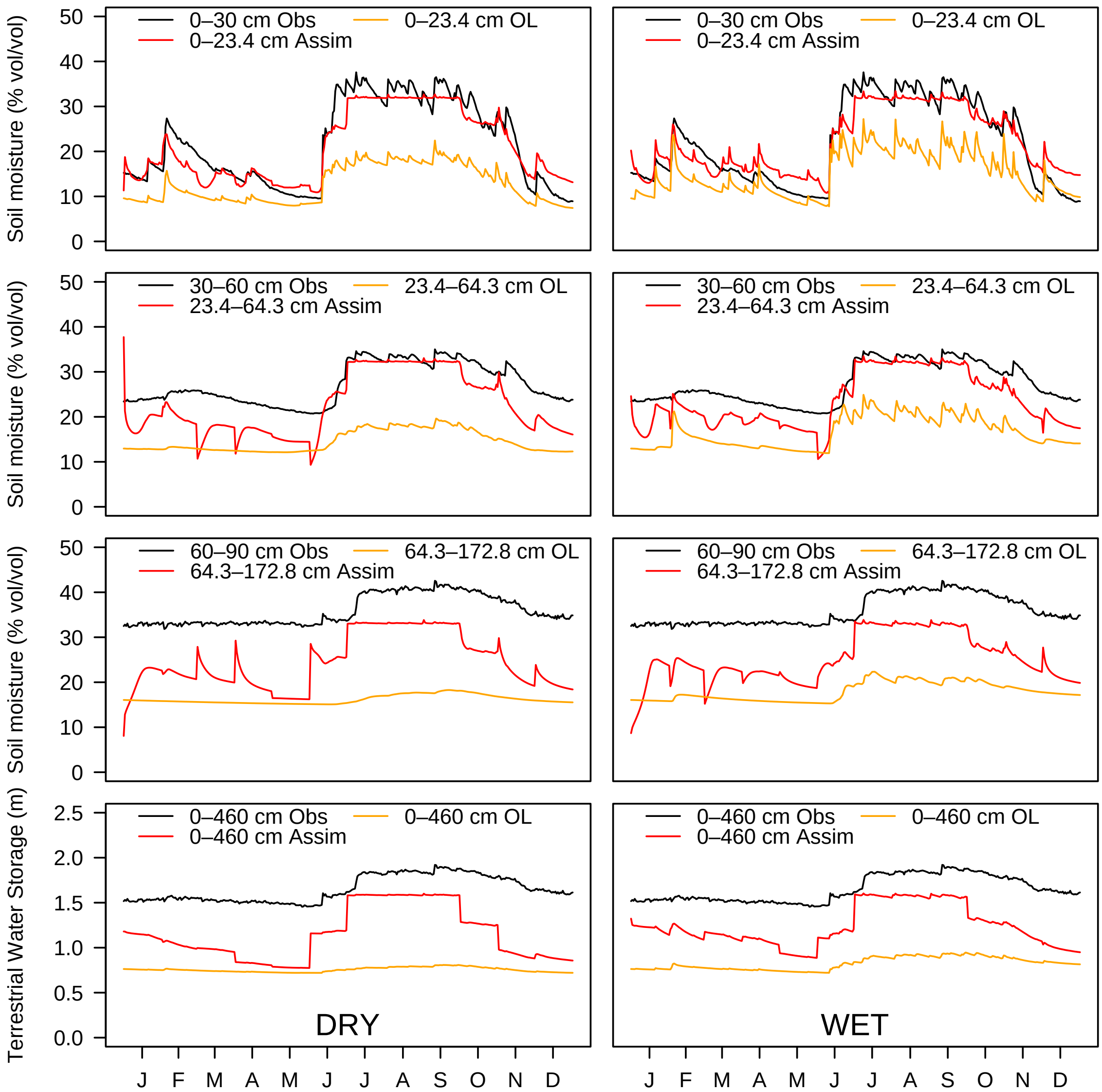

Fig. G.6 K10 near-surface soil moisture assimilation results for 2005 using a one month assimilation window (case 1Mc in Table 6.2-6.5) with dry and wet open loop forcing (left and right columns). Assimilation (Assim) and open loop (OL) runs are in red and orange, observations (Obs) in black.

2 Month Assimilation Window

Gravity Anomaly

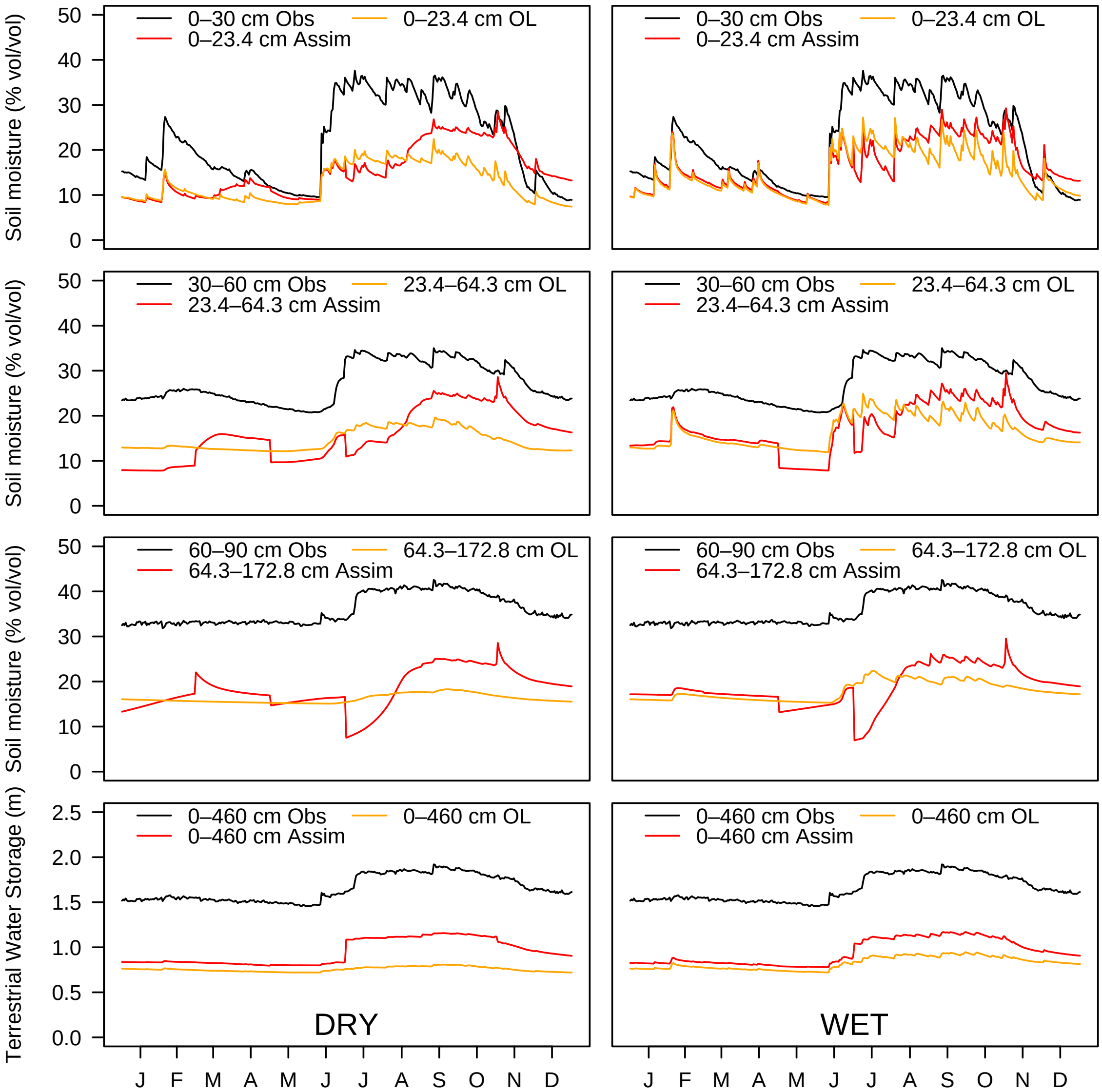

Fig. G.7 K10 gravity anomaly assimilation results for 2005 (with correct 2004 OL mean as background) using a two month assimilation window (case 2Ma in Table 6.2-6.5) with dry and wet open loop forcing (left and right columns). Assimilation (Assim) and open loop (OL) runs are in red and orange, observations (Obs) in black.

Gravity Anomaly and Near-surface Soil Moisture

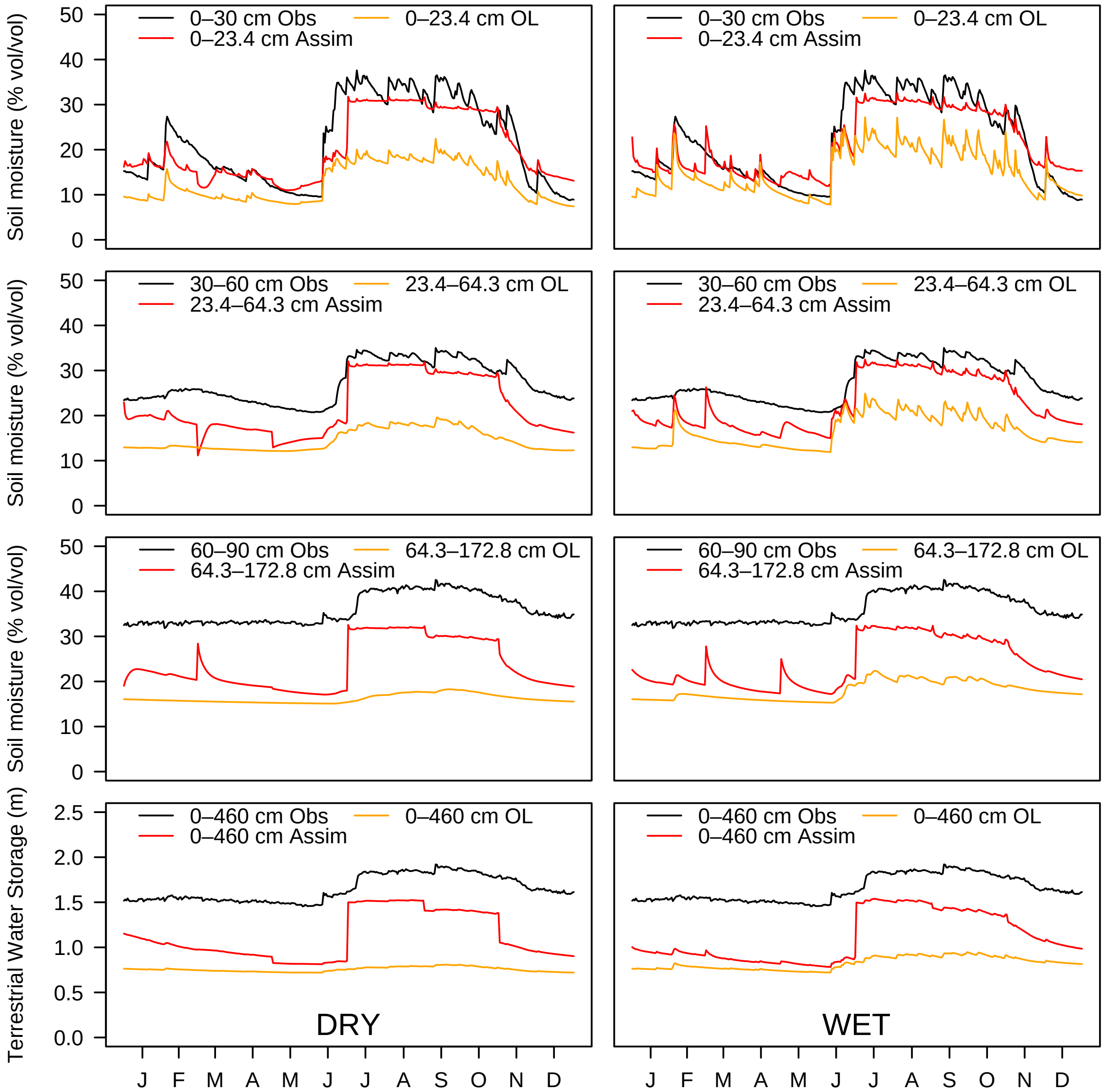

Fig. G.8 K10 gravity anomaly and near-surface soil moisture assimilation results for 2005 (with correct 2004 OL mean as background) using a two month assimilation results for 2005 using a two month assimilation window (case 2Mb in Table 6.2-6.5) with dry and wet open loop forcing (left and right columns). Assimilation (Assim) and open loop (OL) runs are in red and orange, observations (Obs) in black.

Near-surface Soil Moisture

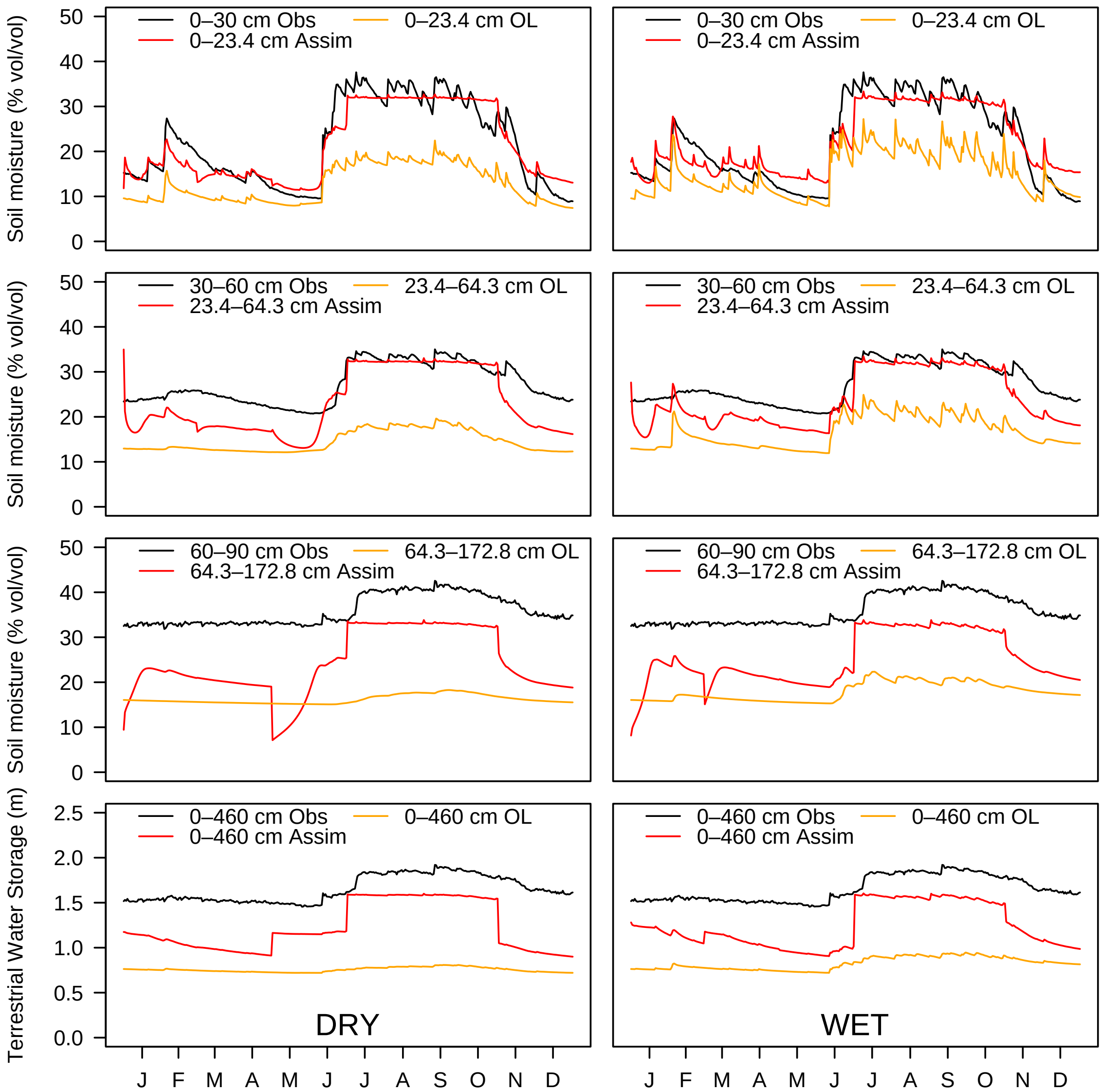

Fig. G.9 K10 near-surface soil moisture assimilation results for 2005 using a two month assimilation window (case 2Mc in Table 6.2-6.5) with dry and wet open loop forcing (left and right columns). Assimilation (Assim) and open loop (OL) runs are in red and orange, observations (Obs) in black.

10 Day Assimilation Window

Gravity Anomaly

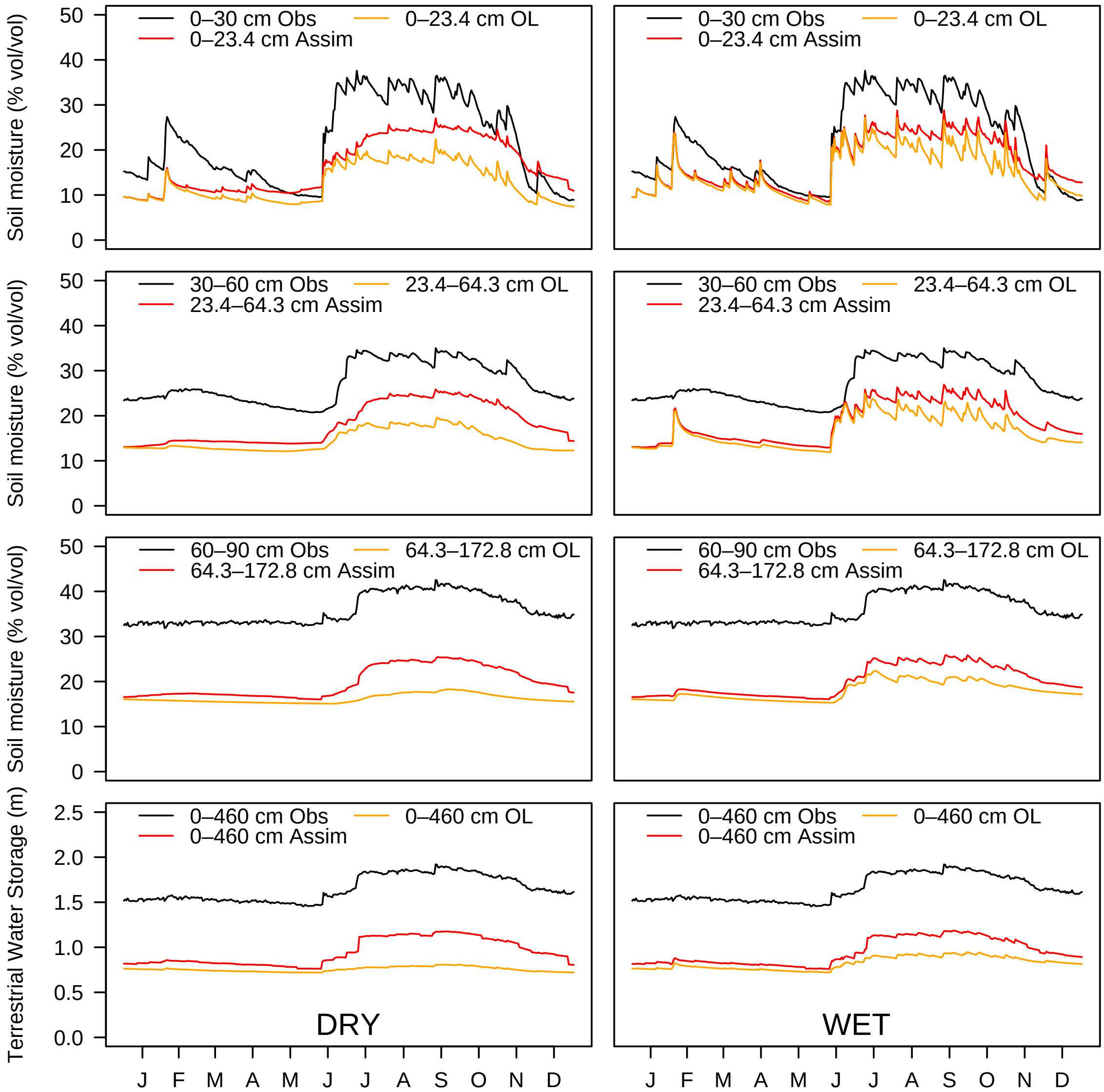

Fig. G.10 K10 gravity anomaly assimilation results for 2005 (with correct 2004 OL mean as background) using a ten day assimilation window (case 10Da in Table 6.2-6.5) with dry and wet open loop forcing (left and right columns). Assimilation (Assim) and open loop (OL) runs are in red and orange, observations (Obs) in black.

Gravity Anomaly and Near-surface Soil Moisture

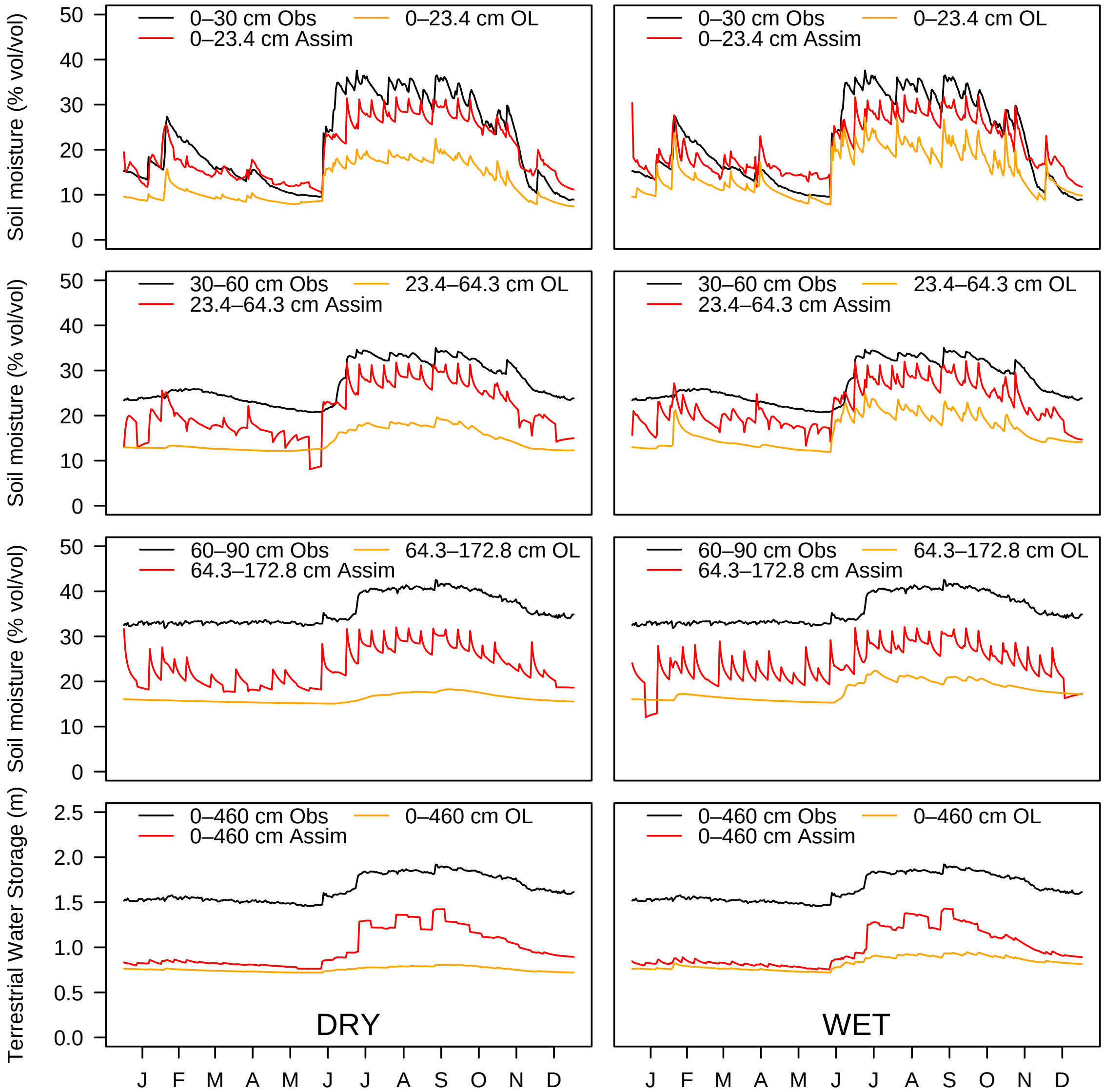

Fig. G.11 K10 gravity anomaly and near-surface soil moisture assimilation results for 2005 (with correct 2004 OL mean as background) using a ten day assimilation results for 2005 using a one month assimilation window (case 10Db in Table 6.2-6.5) with dry and wet open loop forcing (left and right columns). Assimilation (Assim) and open loop (OL) runs are in red and orange, observations (Obs) in black.

Near-surface Soil Moisture

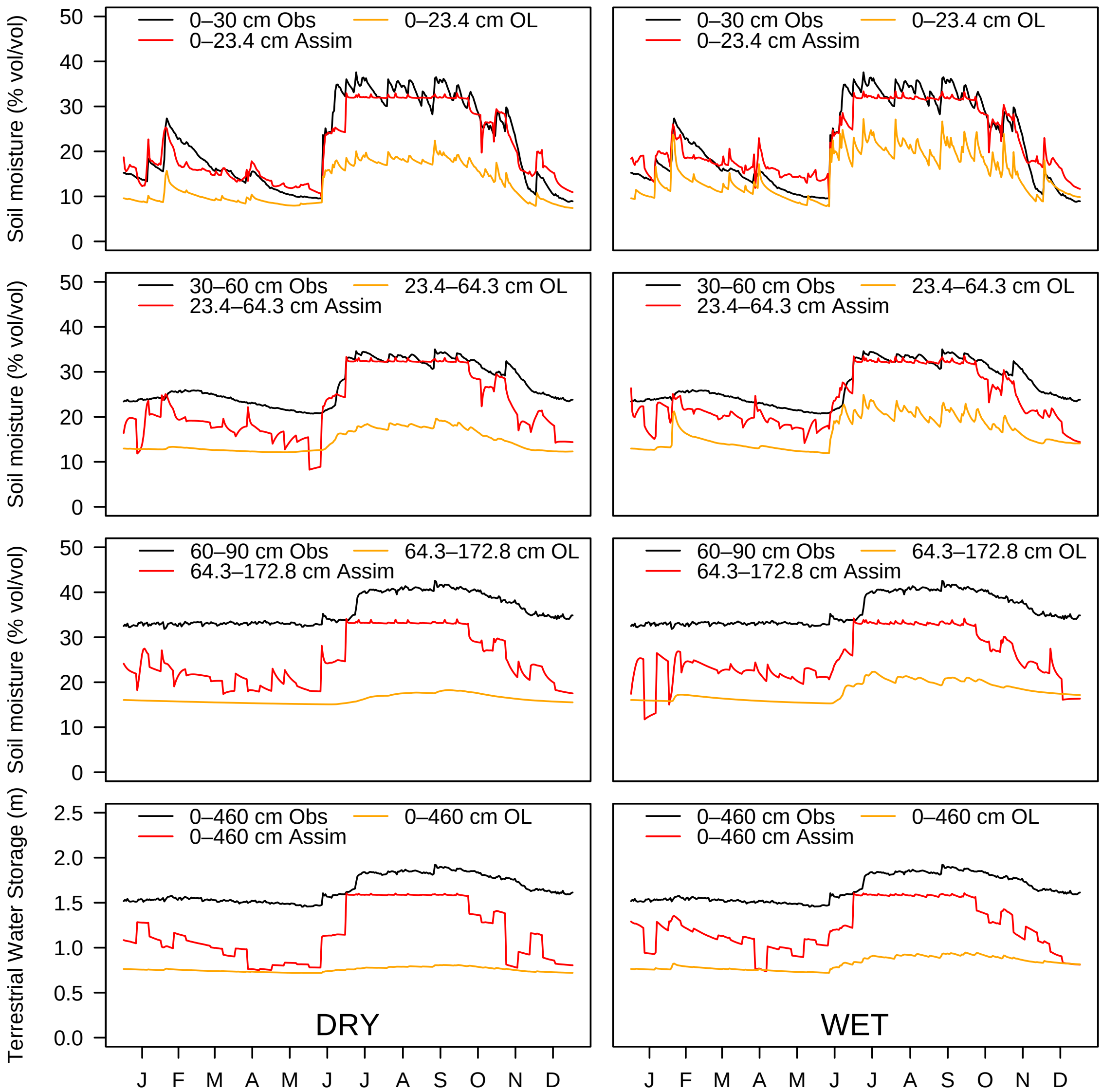

Fig. G.12 K10 near-surface soil moisture assimilation results for 2005 using a ten day assimilation window (case 10Dc in Table 6.2-6.5) with dry and wet open loop forcing (left and right columns). Assimilation (Assim) and open loop (OL) runs are in red and orange, observations (Obs) in black.